The genetic regulation and subcellular dynamics of secretory and endolysosomal organelles of *Drosophila* secondary cells.



Benjamin Robert Kroeger

Oriel College

University of Oxford

Trinity Term 2017

Wellcome Trust D.Phil. in Chromosome and Developmental Biology

Supervisor: Professor Clive Wilson

Department of Physiology, Anatomy and Genetics

i. Declaration

The work presented in this thesis is my own, except where collaborative studies were presented, which are duly acknowledged in the text. Notably amongst these, Dr. S-J. Fan contributed significantly to the experiments using human cancer cells (Section 4.2.4), and F. Castellanos drove much of the work into the roles of AP-1 and Arf79F in secondary cells (Section 5.2.2.3). Figure 5.16 presents data that will be included in his thesis, but is reported here to help place other data I present into context.

ii. Acknowledgements

First and foremost I would like to thank my supervisor, Dr Clive Wilson for his help and guidance throughout my DPhil. His insights and enthusiasm for experiments truly enriched my experience as a new researcher. I also thank him for encouraging me to collaborate with other researchers using different model systems, and to think 'beyond the fly', to engage a wider context of biomedical research.

I would also like to thank Dr Deborah Goberdhan for her mentorship. Special thanks go to Dr Shih-Jung Fan, Dr Sumeth Perera, and Dr Cleidson Alves with whom I have worked closely on my first paper, and also to Felix Castellanos, for collaborating with me on the dense-core granule project. Working together with these researchers was honestly one of the best aspects of my DPhil.

I extend my thanks to the numerous other members of the Wilson and Goberdhan labs, both past and present, with whom I have made several long-lasting friendships. I thank Dr Laura Corrigan and Dr Arron Leiblich, who first introduced me to the world of *Drosophila*. I am extremely grateful to Dr Mark Wainwright, whose wealth of fly experience and generosity in sharing it has been invaluable. I thank Josephine Hellberg, for the enjoyable discussions on many aspects of science. I also thank Kristie McCormick for her insightful comments during lab meetings, and Carina Gandy for her management of the lab. I also thank Rosie Marshall, an undergraduate student that I mentored in the lab, for her hard work. I've also received invaluable support and mentoring, particularly with microscopy, from many other members of the Oxford community. In particular, I thank the Micron imaging team including Dr Ian Dobbie, Dr Andrew Jefferson, Dr Maryam Qurashi and Dr Richard Parton. I also thank Dr Errin Johnson and Dr Anna Pielach from the Dunn School of Pathology. My thanks also go to my sponsors, the Wellcome Trust, for giving me the opportunity to carry out a DPhil with generous financial support.

I thank my close friends from the CDB programme, Tomek Dobrzycki, Anne Turberfield and George Ronson. I count myself very lucky to have gone through this DPhil with you all.

Most importantly, I thank my partner, Mana Ryuba, who has shared this DPhil experience with me and kept me going through the ups and the downs. Truly, spending this time in Oxford with her has been one of the most enjoyable times of my life.

iii. Abstract

Secretory processes underpin the emergence of cellular diversity in complex multicellular organisms. However, our understanding of the basic mechanisms controlling the different secretory and endosomal compartments involved remains surprisingly incomplete. During my DPhil I have studied a specialised epithelial cell type in the male *Drosophila* accessory glands, the secondary cell, which contains unusually large intracellular compartments that are accessible to detailed morphological study. I characterise the organisation, ultrastructure and molecular composition of this cell's secretory and endosomal compartments, and I employ specific Rab GTPases, conserved coordinators of membrane trafficking and identity, to define multiple compartmental subtypes.

By developing super-resolution and time-lapse microscopy approaches in these cells, I show that numerous intraluminal vesicles (ILVs) are formed within Rab11-labelled secretory compartments and released into the accessory gland lumen as exosomes, the first clear demonstration in eukaryotic cells of exosome biogenesis within a non-late endosomal compartment. Biogenesis of these ILVs is dependent on evolutionarily conserved *Endosomal Sorting Complexes Required for Transport (ESCRT) 0-III* genes and involves loading of compartment-specific cargoes. Work by others, some in collaboration with me, has shown that these novel mechanisms are conserved in human cells.

I show that dense-core granules, the structures employed to package proteins and other molecules destined for regulated secretion, form within large non-cored Rab6-positive compartments, in a process that seems to involve inputs from both the Golgi and recycling endosomal pathways. Further analysis has revealed roles for specific Rabs, for ILVs and for the conserved fibrillar protein Mfas/TGFBI in different aspects of DCG formation. I also show that DCGs are not only secreted, but can also be degraded by fusion to acidic endosomal compartments. Remarkably, there is evidence that mammalian cells may employ all of these mechanisms and defects in these processes may be linked to diseases like cancer, diabetes and neurodegenerative disorders.

Hence my work has established a new system to study complex secretory mechanisms, which can now be developed to model specific disease processes in the future.

In summary, I have discovered several novel cell biological mechanisms controlling exosome biology, dense-core granule biogenesis, regulated secretion, and endolysosomal trafficking. Some of these already appear relevant to human health and disease, suggesting that the secondary cell system has considerable further potential for unravelling the fundamental processes underlying eukaryotic secretion in the future.

iv. List of abbreviations

Abbreviation	Description
3D-SIM	**3**-**d**imensional **S**tructured **I**llumination **M**icroscopy
Acp	**Ac**cessory gland **p**rotein
Arf	**A**DP-**r**ibosylation **f**actor
ANCE	**An**giotensin **c**onverting **e**nzyme
ALiX	**A**poptosis **l**inked factor **X** or **AL**G-2 **i**nteracting protein **X**
BDSC	**B**loomington ***D****rosophila* **S**tock **C**enter
Bnl	**B**ra**n**ch**l**ess
Btl	**B**rea**th**l**e**ss
Chp	**Ch**ao**p**tin
Chc	**C**lathrin **h**eavy **c**hain
Clc	**C**lathrin **l**ight **c**hain
CFP	**C**yan **F**luorescent **P**rotein
dsx	**d**ouble**s**e**x**
DGRC	***D****rosophila* **G**enomics **R**esource **C**enter
ESCRT	**E**ndosomal **S**orting **C**omplexes **R**equired for **T**ransport
fas	**fas**ciclin
FGF	**F**ibroblast **G**rowth **F**actor
FGFR	**F**ibroblast **G**rowth **F**actor **R**eceptor
GDI	**G**DP **d**issociation **i**nhibitor
GDF	**G**DP dissociation inhibitor **d**issociation **f**actor
GPI	**G**lycosyl**p**hosphatidyl **i**nositol
GFP	**G**reen **F**luorescent **P**rotein
GAP	**G**TPase **a**ccelerating **p**rotein
GEF	**G**uanine nucleotide **e**xchange **f**actor
GTPase	**G**uanosine **t**ri**p**hosphat**ase**
Hrs	**H**epatocyte **r**eceptor tyrosine kinase **s**ubstrate
HPF	**H**igh **P**ressure **F**reezing
ILV	**I**ntra**l**uminal **v**esicle
mTORC1	**m**echanistic **T**arget **O**f **R**apamycin **C**omplex **1**
mfas	**m**idline **fas**ciclin
mCherry	**m**onomeric **Cherry**
MVB	**M**ulti**v**esicular **b**ody
REP	**R**ab **e**scort **p**rotein
RabGGT	**R**ab **g**erenylgeranyl **t**ransferase
RNAi	**RNA i**nterference
SNAP	**S**oluble **N**SF **A**ttachment **P**rotein
SNARE	**S**oluble **N**SF **A**ttachment **P**rotein **R**eceptor
spi	**spi**tz
syx	**sy**nta**x**in

t-SNARE	**t**arget-associated **SNARE**
TfR	**T**rans**f**errin **r**eceptor
TGF-βI	**T**ransforming **G**rowth **F**actor-**B**eta **I**nduced
TEM	**T**ransmission **E**lectron **M**icroscopy
Tsg101	**T**umour **s**usceptibility **g**ene **101**
UAS	**U**pstream **A**ctivating **S**equence
Vps	**V**acuolar **p**rotein **s**orting
v-SNARE	**v**esicle-associated **SNARE**
VDRC	**V**ienna ***D****rosophila* **R**NAi **C**enter
YFP	**Y**ellow **F**luorescent **P**rotein

v. Table of contents

i. Declaration **2**
ii. Acknowledgements **3**
iii. Abstract **4**
iv. List of abbreviations **5**
v. Table of contents **7**

1.0 Introduction **12**
1.1 Cell organisation and compartmentalisation **13**
1.1.1 Organelles 13
1.1.2 Cell polarity 15
1.2 The endolysosomal system **16**
1.2.1 Overview of trafficking pathways in the endolysosomal system 16
1.2.1.1 Early and recycling endosomes 18
1.2.1.2 Late endosomes 19
1.2.1.3 Lysosomes 19
1.2.2 Pathologies related to the endolysosomal system 21
1.3 Rab GTPases **23**
1.3.1 Overview of Rab biology 23
1.3.1.1 Rab structure 23
1.3.1.2 Rab activation 24
1.3.1.3 Rab targeting 26
1.3.2 Rabs regulate secretory and endolysosomal pathways 26
1.3.2.1 Secretory Rabs 26
1.3.2.2 Endolysosomal Rabs 27
1.4 Exosome biology **28**
1.4.1 Exosomes mediate cell signalling 28
1.4.2 Mechanisms of exosome biogenesis and secretion 30
1.4.3 The ESCRT complexes 33
1.4.4 Rab GTPases regulate exosome secretion 36
1.4.5 Functions of exosomes in health and disease 36
1.4.6 Limitations in our understanding of exosome biology 37
1.5 Protein secretion and dense-core granule biology **38**
1.5.1 Protein secretion by constitutive, regulated and unconventional pathways 38
1.5.2 Functions of regulated secretion 40
1.5.3 Regulation of dense-core granule biogenesis 41
1.6 The *Drosophila melanogaster* male accessory glands as a model genetic system to study the secretory and endolysosomal pathways **43**
1.6.1 Brief historical overview of research using *Drosophila* 43
1.6.2 The *Drosophila* male accessory glands 44
1.6.2.1 Structure and organisation of the accessory glands 44
1.6.2.2 Functions of the accessory glands 47
1.6.3 The *Drosophila* female post-mating response 47
1.6.4 Secondary cells 48
1.6.4.1 Secondary cell organelles 48
1.6.4.2 Analysing the genetic regulation of growth, exosome biogenesis, endolysosomal trafficking and dense-core granule secretion in the secondary cell model 50
1.6.4.3 Secondary cells regulate the female post-mating response 52
1.7 Aims and objectives **53**

2.0 Methods **56**
2.1 Fly Stocks **57**

2.1.1 GAL4 and GAL80 combination lines ... 57
2.1.2 Fluorescently tagged protein lines ... 58
2.1.3 RNAi lines and controls ... 60
2.2 Fly husbandry ... 61
2.3 Control of transgene expression in secondary cells ... 61
2.4 Micro-dissection of accessory glands ... 62
2.5 LysoTracker™ staining of living accessory glands ... 63
2.6 Mounting of living accessory glands ... 64
2.7 Fixation of accessory glands for light microscopy ... 64
2.8 Immunostaining of fixed accessory glands ... 64
2.8.1 Primary antibodies ... 66
2.8.2 Secondary antibodies ... 67
2.9 Phalloidin staining of fixed accessory glands ... 67
2.10 Mounting of fixed accessory glands for light microscopy ... 68
2.11 Super-resolution 3D-SIM ... 68
2.12 Wide-field ... 69
2.13 Confocal ... 70
2.14 Image analysis and figure presentation ... 70
2.15 Subcellular compartment analysis ... 70
2.16 Exosome secretion assay ... 71
2.17 Measuring ILV fluorescence ... 72
2.18 ILV diameter ... 72
2.19 Sample preparation for electron microscopy ... 73
2.19.1 Chemically fixed accessory glands for ultrastructural analysis ... 73
2.19.2 High Pressure Freezing (HPF) and freeze substitution of accessory glands for ultrastructural analysis ... 75
2.20 Ultramicrotomy ... 78
2.20.1 Semi-thin sections ... 78
2.20.2 Ultra-thin sections ... 78
2.21 Transmission Electron Microscopy (TEM) ... 80
2.22 Cloning and generation of new transgenic lines ... 80
2.23 Statistical Analysis ... 81

3.0 Characterisation of secondary cells by light and electron microscopy ... **82**
3.1 Introduction ... 83
3.1.1 Secondary cells contain extremely large subcellular compartments with different morphological features and physiological properties ... 83
3.1.2 Rab GTPases help define different types of subcellular compartments in secondary cells ... 84
3.1.3 Novel imaging techniques are revolutionising our ability to study secondary cell biology ... 85
3.1.4 Chapter aims ... 87
3.2 Results ... 88
3.2.1 Defining the organisation and ultrastructure of secondary cell intracellular compartments ... 88
3.2.1.1 Secondary cells are specialised, polarised secretory epithelial cells in the male accessory glands ... 88
3.2.1.2 Electron microscopy of accessory glands highlights the compartmental organisation and diversity in secondary cells ... 91
3.2.1.3 Cryo-electron microscopy of accessory glands identifies novel intracellular compartments and ultrastructural characteristics ... 96
3.2.1.4 The large subcellular compartments of living secondary cells are differentially localised along the apical-basal axis ... 101
3.2.1.5 Super-resolution imaging reveals the structure of the Golgi apparatus in living secondary cells ... 104

3.2.1.6 Microtubules form a network running between secondary cell organelles.....107
3.2.1.7 Secondary cells contain plentiful mitochondria that provide the energy to drive cell biological processes.....111
3.2.1.8 Junctions between neighbouring secondary and main cells.....113
3.2.2 Characterisation of Rab localisation in secondary cells using a library of fluorescently tagged Rab gene trap fly lines.....115
3.2.2.1 Rab1 and Rab2 localise to cis-Golgi cisternae and adjacent vesicles.....115
3.2.2.2 Rab6 localises to the surface of the large non-cored compartments and also on vesicles in close proximity to the Rab1/ Rab2-marked Golgi.....122
3.2.2.3 Rab8, Rab10, Rab11, Rab19 and Rab30 localise to the centrally located, Golgi-rich subcellular region surrounding the large Rab6-positive compartment.....135
3.2.2.4 Rab11 localises to the surface of the secretory dense-core granule compartments, subsets of which can carry Rab6, Rab7, Rab10, Rab19, Rab21 and Rab30.....153
3.2.2.5 Rab6 co-localises with Rab11 on some dense-core compartments, but does not overlap with Rab7, Rab19, Rab21 or Rab30.....162
3.2.2.6 Rab4, Rab5, Rab21 and Rab35 localisation is consistent with their roles on early or recycling endosomes.....171
3.2.2.7 Rab7 and Rab39 are enriched on the surface of acidic late endosomal and lysosomal compartments.....183
3.2.2.8 Rab23 localises to the secondary cell plasma membrane.....188
3.2.2.9 Rab3, Rab14, Rab26, Rab27, Rab32 and Rab40 are not detectable in secondary cells.....190
3.2.2.10 Acknowledgements to important contributors to the analysis of the fluorescently tagged Rab GTPase in secondary cells.....190
3.2.3 Super-resolution imaging enables more detailed analyses of secondary cell biology.....192
3.3 Discussion.....200
3.3.1 The diverse subcellular compartments of secondary cells have distinctive ultrastructural features and molecular cargos.....200
3.3.2 Rabs localise to specific subcellular compartments in secondary cells.....204

4.0 Novel exosome subtypes, their origins and regulation in both secondary cells and human cells.....209
4.1 Introduction.....210
4.1.1 Exosomes are a subtype of extracellular vesicle that mediate communication between cells.....210
4.1.2 Mechanisms of exosome biogenesis.....211
4.1.3 Exosome biogenesis in secondary cells.....212
4.1.4 Chapter aims.....214
4.2 Results.....215
4.2.1 Rab11-positive compartments are a novel source of exosomes produced by secondary cells.....215
4.2.1.1 Secondary cells secrete exosomes from a non-late endosomal compartment.....215
4.2.1.2 Non-acidic Rab11-positive compartments are a novel source of exosomes in secondary cells.....219
4.2.1.3 Rab11 is a specific exosome cargo found on ILVs within Rab11-positive compartments.....224
4.2.1.4 Chaoptin is a novel marker of native extracellular vesicles secreted secondary cells.....232
4.2.1.5 breathless and branchless gene products are putative exosome cargos, specifically loaded onto ILVs within Rab11-positive compartments.....235
4.2.1.6 The effect of transgene expression on secondary cell biology.....249
4.2.2 Regulatory mechanisms of ILV formation in Rab11-positive compartments.....252
4.2.2.1 ESCRTs localise onto the limiting membranes of Rab11-positive compartments.....252

4.2.2.2 Exosome biogenesis in Rab11-positive compartments is ESCRT-dependent 262
4.2.3 Mechanisms of cargo selection for incorporation into ILVs within Rab11-positive compartments 270
4.2.4 Rab11-positive endosomal compartments are a novel source of exosomes in human cancer cells 275
4.2.4.1 Rab11a-positive endosomes contain ILVs labelled by Rab11a in human colorectal cancer cells 275
4.2.4.2 Endosomal compartments in human cancer cells can produce ILVs carrying different Rab GTPases 278
4.3 Discussion 281
4.3.1 Rab11-positive compartments contain ILVs, which can be secreted as exosomes, in both *Drosophila* and human cells 281
4.3.2 Rab GTPases may be useful markers of the subcellular compartments from which exosomes originate 285
4.3.3 Differential loading of exosome cargos within the same subcellular compartment 287
4.3.4 ESCRTs regulate ILV formation in Rab11-positive compartments 288
5.0 Regulation of dense-core granule compartment biogenesis and endolysosomal maturation in secondary Cells 291
5.1 Introduction 292
5.1.1 Dense-core granules are characteristic of regulated secretion 292
5.1.2 The biology of dense-core granule compartments in secondary cells 293
5.1.3 Lysosomal growth in secondary cells 295
5.1.4 Chapter aims 297
5.2 Results 298
5.2.1 Formation, maturation and secretion of dense-core granule-containing compartments 298
5.2.1.1 Dynamics of dense-core granule compartment formation and maturation in secondary cells 298
5.2.1.2 A novel Rab6 to Rab11 switch occurs during dense-core granule biogenesis 306
5.2.1.3 Secretion of dense-core granule compartments by secondary cells 309
5.2.1.4 Secreted dense-core granule compartments in secondary cells appear to carry Rab19 on their limiting membrane 314
5.2.1.5 Novel molecular markers of dense-core granules in secondary cells 316
5.2.2 Characterisation of the genetic regulation of dense-core granule biogenesis in secondary cells 325
5.2.2.1 Roles for Rab GTPases in dense-core granule biology 325
5.2.2.2 SNAREs regulate large dense-core granule compartment biogenesis in secondary cells 336
5.2.2.3 Conserved regulators of granule biogenesis, the AP-1 complex and the Arf79F GTPase regulate the maturation of dense-core granules 338
5.2.2.4 Clathrin may regulate the trafficking of GFP-GPI in secondary cells 349
5.2.2.5 A novel role for the ESCRT components in dense-core granule biogenesis 353
5.2.2.6 Mfas regulates dense-core granule morphogenesis in secondary cells 356
5.2.3 Formation and maturation of large acidic compartments 360
5.2.3.1 Rab GTPases regulate the formation and maturation of large acidic compartments 360
5.2.3.2 ILVs may function as platforms for the acidification of endolysosomal compartments 363
5.3 Discussion 367
5.3.1 Dense-core granules are formed within large Rab6-positive precursor compartments that undergo morphological and positional changes 368
5.3.2 Novel dense-core granule cargos in secondary cells 370
5.3.3 Dense-core granules are secreted by more than one mechanism 373

5.3.4 Rab GTPases play novel roles in dense-core granule maturation and may co-operate to perform different functions 374
5.3.5 Subcellular compartments undergo novel Rab transitions as they mature and interact with other compartments 377
5.3.6 The conserved trafficking regulators, AP-1 and Arf79F block different steps of dense-core granule formation in secondary cells 379
5.3.7 Mfas, Syx5 and the ESCRT-III component shrb are novel regulators of dense-core granule formation and maturation 381
5.3.8 Rab-regulated trafficking pathways drive lysosome growth 383
5.3.9 ILVs function as platforms for the acidification of large lysosomal compartments 385

6.0 Concluding remarks **388**
6.1 Summary of findings **390**
6.2 Overall perspectives and future directions **392**
6.2.1 Advantages of the secondary cell model to study membrane trafficking and secretion 392
6.2.2 Implications for exosome biology 393
6.2.3 Implications for dense-core granule biology 395
6.2.4 Potential for the study of zymophagy 397
6.2.5 Open questions and problems 397

7.0 Bibliography **400**

8.0 Appendix **425**
8.1.1 Characterisation of non-transgenic w^{1118} secondary cells using novel antibody markers for intracellular compartments 426
8.1.2 Characterisation of secondary cells overexpressing CD63-GFP and GFP-GPI by co-staining with compartment-specific antibodies 430

1.0 Introduction

1.1 Cell organisation and compartmentalisation

1.1.1 Organelles

Eukaryotic cells are distinguished from prokaryotic cells by their numerous lipid-bound subcellular compartments, or organelles (Barr, 2013). The main types of organelles present in all eukaryotic cells consist of the nucleus, endoplasmic reticulum, Golgi apparatus, mitochondria, lysosomes, endosomes, and peroxisomes (Alberts *et al*., 2002; Figure 1.1). By compartmentalising different activities within distinct organelles, eukaryotic cells create specific aqueous environments optimised for particular functions. The lipid membranes also provide additional surface area for membrane-localised enzymes, for example those involved in ATP production through oxidative phosphorylation (Hatefi *et al*., 1985). In general, each organelle performs the same set of basic functions in all cell types. But to serve the specialized functions of different cells, these organelles vary in abundance and can have additional properties that differ from cell type to cell type.

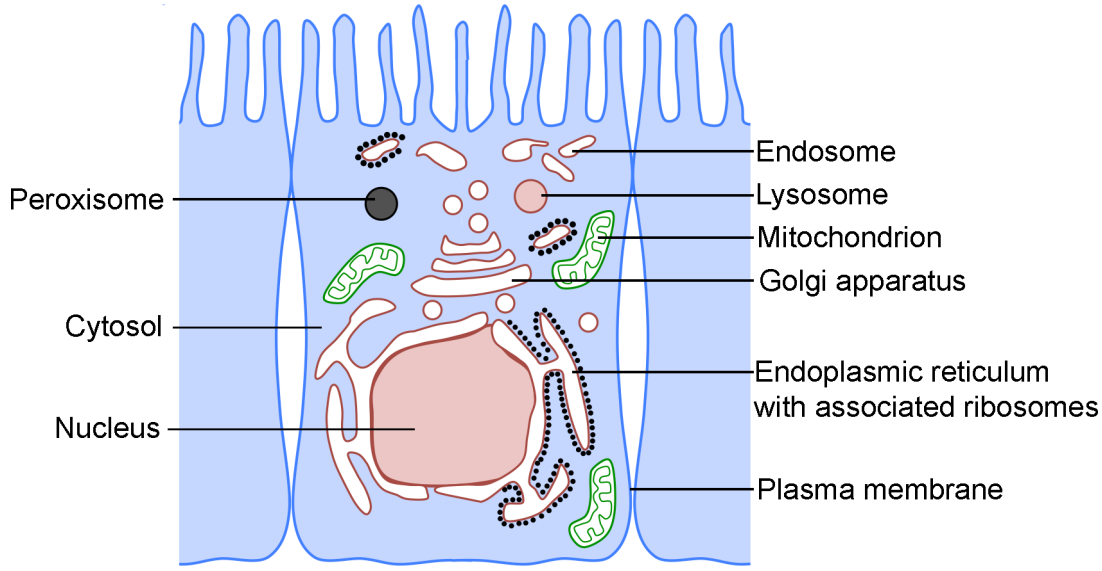


Figure 1.1 Schematic representation of the major intracellular compartments in a eukaryotic cell. Adapted from Alberts *et al*. (2002).

The nucleus, endoplasmic reticulum, Golgi apparatus, mitochondria, lysosomes, endosomes, peroxisomes and cytosol are distinct intracellular compartments separated by lipid bilayers.

Each organelle has its own discovery story. The nucleus was the first organelle to be identified; it was reported by one of the fathers of optical microscopy, Antony van Leeuwenhoeck, in amphibian and avian erythrocytes in 1710 (Pederson, 2011). Many of the smaller organelles were described much later, enabled by the advent of cell fractionation and electron microscopy techniques in the mid-twentieth century. For example, lysosomes were first identified through biochemical analysis of fractionated subcellular structures, and later characterised with electron microscopic observations (Bainton, 1981; de Duve *et al*., 1955; Novikoff *et al*., 1956). In recognition of this, and the work of others who identified different subcellular organelles, the 1974 Nobel Prize in Physiology or Medicine was awarded to Albert Claude, Christian de Duve and George E. Palade “for their discoveries concerning the structural and functional organization of the cell” (de Duve, 1975).

1.1.2 Cell polarity

Most eukaryotic cells are polarised, which is manifested in differences in protein localisation and also in the distribution of subcellular organelles along a particular (often apical-basal) axis (Cao *et al*., 2012). Not only does polarity play important roles in individual cell physiology, it is also essential for tissue homeostasis. For example, loss of cell polarity in tissues is often considered a hallmark of cancer progression (Royer and Lu, 2011).

In tissues such as glands, epithelial cell polarity involves the generation of distinct domains in the plasma membrane: an apical domain and a basolateral domain, separated by tight junctions and other junctional complexes (Rodriguez-Boulan & Macara, 2014). This organisation is required to ensure directionality of particular secretions. Furthermore, the tight junctions prevent

glandular contents leaking into the body cavity. The polarised sorting of different proteins to the apical or basolateral plasma membrane is thought to involve sorting motifs, which can be intrinsic to the protein itself, or result from modifications such as glycosylation or GPI-anchoring (Mellman & Nelson, 2008). The polarisation of subcellular organelles is demonstrated by secretory pancreatic acinar cells, where the nucleus and rough endoplasmic reticulum are found basally, Golgi cisternae in a supranuclear position, and secretory zymogen granules at the cell apex (Chang & Jamieson, 1989).

1.2 The endolysosomal system

1.2.1 Overview of trafficking pathways in the endolysosomal system

Endocytosis describes the basic conserved cellular process used by cells to internalise a variety of molecules including fluid, solutes, macromolecules, and plasma membrane components (Huotari & Helenius, 2011; Mayor & Pagano, 2007). The endolysosomal system comprises a complex assortment of compartments that were classically defined by their roles in the sorting, recycling and degradation of endocytosed cargo (Gould & Lippincott-Schwartz, 2009). The numerous types of endolysosomal compartments, including early and recycling endosomes, late endosomes, also often referred to as multivesicular bodies (MVBs), and lysosomes, interact with one another, the Golgi apparatus and the plasma membrane through tightly regulated trafficking pathways (Figure 1.2).

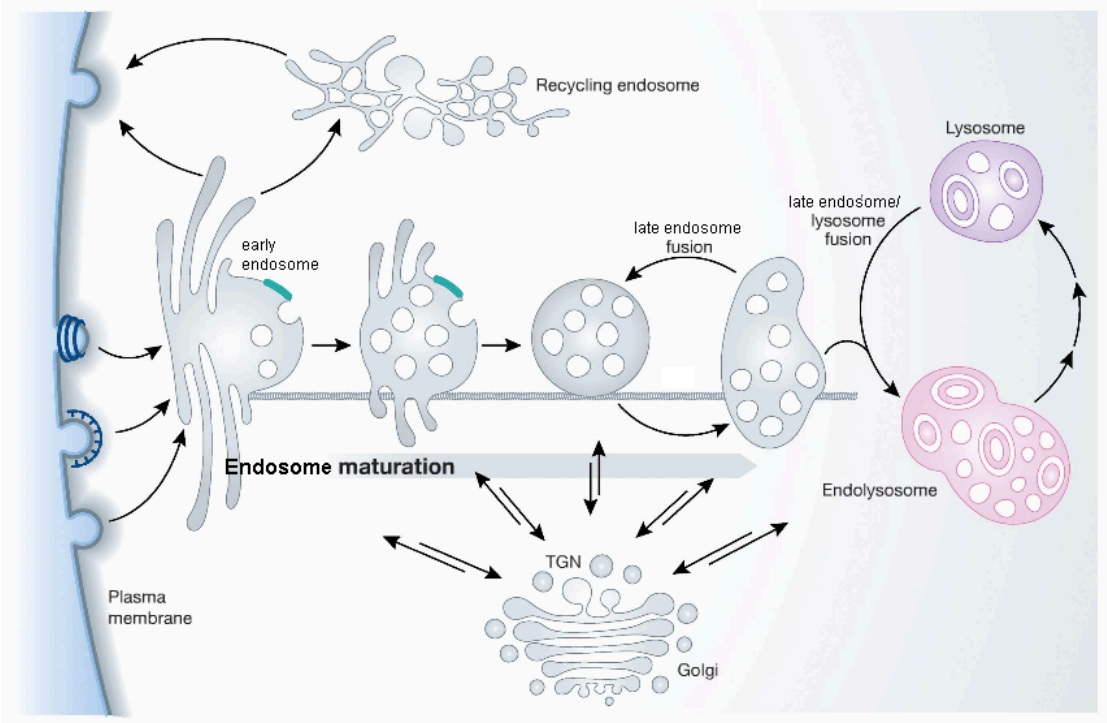


Figure 1.2 Schematic representation of the endolysosomal system. Adapted from Huotari & Helenius (2011). Endocytic vesicles budding from the plasma membrane deliver their contents to early endosomes, where sorting of endocytic cargos takes place. Some cargos are recycled back to the plasma membrane either directly, or indirectly via recycling endosomes, and others cargos are targeted for degradation by retention within the early endosome. This compartment matures into a late endosomes, which grows through homotypic fusions and with other late endosomes and subsequently fuses with lysosomes, forming endolysosomes. Here, endocytosed macromolecules are degraded. The Golgi apparatus interacts with all of these compartments via small vesicles that shuttle important proteins required for the endolysosomal system to function.

1.2.1.1 Early and recycling endosomes

Small endocytic vesicles budding from the plasma membrane are trafficked towards a network of early endosomes, where they deliver their contents through fusion. The early endosomes are heterogeneous in their morphology, subcellular localisation and contents (Klumperman & Raposo, 2014). Electron microscopy has revealed that they contain a vacuolar domain, from which tubules extend (Tooze & Hollinshead, 2001). The vacuolar region is often referred to as a sorting endosome, as this is where endocytosed cargos are sorted for either degradation or recycling. The extending tubules, on the other hand, are referred to as recycling endosomes, as they mediate the recycling of cargos back to the plasma membrane or Golgi apparatus (Bonifacino & Rojas, 2006; Geuze *et al.*, 1983).

Early endosomes are highly dynamic and have been observed to undergo homotypic fusion (Gorvel *et al*., 1991; Rybin *et al*., 1996) and fission between their vacuolar and tubular domains (Mesaki *et al*., 2011). Once separated, the tubular domains are thought to form distinct endosomal recycling compartments, which are often localised either peripherally or next to the nucleus (Yamashiro *et al*., 1984; Ullrich *et al*., 1996). The generation of these distinct compartments creates further diversity in the recycling pathway. Certain recycled cargos, such as Transferrin and the Transferrin receptor, are trafficked back to the plasma membrane at different rates due to their passage through the distinct recycling organelles: a fast-recycling pathway is mediated by tubules emanating from the vacuolar sorting endosome, and a slow-recycling pathway, which involves passage through the endosomal recycling compartment (Klumperman & Raposo, 2014).

1.2.1.2 Late endosomes

The separated early endosome vacuolar domain is thought to mature by conversion into a late endosome (Stoorvogel *et al*., 1991). Late endosomal compartments are heterogeneous by electron microscopy, consisting of a vacuolar domain and a few extending tubules, from which proteins are mostly recycled back to the trans-Golgi network (Rojas *et al*., 2008). Numerous changes have been reported during early-late endosome maturation (reviewed in detail by Huotari & Helenius, 2011), including the acidification of the compartment's lumen, due the activity of V-type ATPases carried at their surface, changes in the concentrations of lumenal ions such as Cl^- and Ca^{2+}, and the acquisition of lysosomal hydrolases and membrane proteins (Maxfield & Yamashiro, 1987; Beyenbach & Wieczorek, 2006). One well-established feature of late endosomes is their numerous intraluminal vesicles (ILVs), hence their other name, multivesicular bodies (MVBs). Specific endocytosed cargos, such as active transmembrane signalling receptors, like EGFR, are packaged within these ILVs to deprive them of contact with the cytosol (Appelqvist *et al*., 2013). Recently, late endosomes have been identified as important secretory compartments that facilitate inter-cellular communication. They can fuse to the plasma membrane, releasing their ILVs, loaded up with bioactive molecules, as so-called exosomes into the extracellular space (discussed in detail in Section 1.5; Raposo & Stoorvogel, 2013).

1.2.1.3 Lysosomes

Late endosomes are known to deliver their contents to lysosomes via both kiss-and-run and complete fusion, forming compartments known as secondary lysosomes, or endolysosomes (Luzio *et al*., 2014; Bright *et al*.,

2005). These compartments are considered the terminal degradative compartment of the endocytic pathway; they contain numerous acidic hydrolases involved in the degradation of macromolecules, including proteins, lipids, nucleic acids and carbohydrates. Lysosomes are highly acidic organelles, which provide the optimal environment for their lumenal hydrolases to function. The transferred late endosomal ILVs contain membrane proteins that are accessible to lysosomal hydrolases (Huotari & Helenius, 2011).

Lysosomal shape, size and number vary greatly depending on cell and organism type, but in many animal cells they range between 0.1 and 1 μm in diameter (Perera & Zoncu, 2016). However, yeast and plant cells often contain just one lysosome-like organelle called a vacuole (Baba *et al*., 1994). Lysosomes are partly characterised by their morphological characteristics, as visualised by electron microscopy, which include electron-dense content and multilamellar membrane whorls (Klumperman & Raposo, 2014). They are also classically defined by an absence of mannose-6-phosphate receptors (Brown *et al*., 1986), which ferry many lysosomal hydrolases to the late endosomal system from the Golgi (Gan *et al*., 2009).

In addition to fusing with late endosomes, lysosomes are also known to fuse with both phagosomes and autophagosomes, in order to facilitate intracellular killing of microorganisms, and the degradation of cytosolic proteins or organelles, respectively (Tooze *et al*., 2014). The classical electron-dense lysosome stores hydrolases at high concentrations, ready to fuse to late endosomes or other subcellular compartments to enable macromolecule degradation (Luzio *et al*., 2014). In some cells, particularly in specific blood

cell types and osteoclasts, lysosomes have been reported to secrete their contents by fusing to the plasma membrane (Blott *et al*., 2002). Lysosome secretion has been observed in other cell types too, and may be involved in plasma membrane repair (Reddy *et al*., 2001). Lysosomes have also recently been highlighted as one of the key subcellular sites for nutrient sensing and metabolic regulation through the control of mechanistic Target Of Rapamycin Complex 1 (mTORC1) activity (Settembre *et al*., 2013; Zoncu *et al*., 2011; Sancak *et al*., 2010). The conserved serine-threonine kinase mTOR, the key enzyme in this complex, is localised to the surface of lysosomes, where it is activated by growth factors and nutrients such as amino acids, to regulate cell growth and proliferation (Perera & Zoncu, 2016).

1.2.2 Pathologies related to the endolysosomal system

The misregulation of endolysosomal activities is central to the pathophysiology of numerous human diseases. Some of the best characterised are the lysosomal storage diseases, a family of disorders resulting from mutations in lysosomal enzymes or other proteins that cause abnormal storage of macromolecular substrates within the endolysosomal and autophagic systems (Platt *et al*., 2012). Most of these disorders are caused by defective lysosomal hydrolases (Winchester, 2004), such as β-Glucocerebrosidase (GBA), which causes Gaucher type 1, 2 and 3. A diverse, but less common set of lysosomal storage diseases are caused by defective soluble non-enzymatic proteins, lysosomal membrane proteins, or through the mislocalisation of lysosomal enzymes (Platt *et al*., 2012).

Impairment of lysosome-autophagy pathways are increasingly recognised as key pathogenic events in neurodegenerative diseases, such as Parkinson's

(Dehay *et al*., 2013). The build-up of neurotoxic α-Synuclein, which has been genetically and neuropathologically linked to Parkinson's (Stefanis, 2012), is associated with defective lysosome-autophagy trafficking and degradation. Recently, genetic studies have implicated the lysosomal type 5 P-type ATPase (*ATP13A2*), which is required for normal lysosome physiology, in familial autosomal recessive Parkinson's (Ramirez *et al*., 2006), further supporting an important role for the lysosome in this disease.

Lysosome-mediated catabolism has also been identified as having key roles during cancer progression (Perera and Zoncu, 2016). In order to satisfy the catabolic requirements of rapidly dividing cancer cells, especially under micro-environmental stresses such as nutrient starvation, endocytic and autophagic delivery to the lysosome are essential pathways that provide the building blocks, including amino acids and membrane lipids, required for survival and proliferation (DeNicola & Cantley, 2015). Furthermore, the released amino acids can activate lysosome-localised mTORC1 signalling to further promote cancer growth (Zoncu *et al*., 2011).

A model has therefore emerged in which the lysosome and its associated membrane trafficking acts as a central regulatory hub in the cell that is susceptible to multiple pathological disturbances and can participate in secretion and cell-cell communication. Untangling the functions of this system form the classical secretory pathway, while also determining how they interact, is a major challenge in modern cell biology.

1.3 Rab GTPases

1.3.1 Overview of Rab biology

Rab GTPases (Rabs) are the largest family of conserved small Ras-like GTPases, with 11 identified members in yeast, 27 in *Drosophila* and almost 70 in humans (Hutagalung & Novick, 2011; Dunst *et al*., 2015). Distinct Rabs associate with specific membrane-bound subcellular compartments, where they regulate the specificity of membrane trafficking pathways (Zhen & Stenmark, 2015). Rabs perform their regulatory functions by recruiting specific effectors. Several themes of effector function have been identified and include vesicle budding, transport, tethering and fusion (Hutagalung & Novick, 2011). Rabs are important contributors to membrane identity, and have been widely used as markers for specific compartments (Stenmark, 2009; Barr & Lambright, 2010; Zerial & McBride, 2001). The diverse, but conserved, functions of related Rabs suggests that they evolved alongside the core set of membrane organelles in the endocytic and secretory pathways (Barr, 2013; Stenmark, 2012; Diekmann *et al*., 2011).

1.3.1.1 Rab structure

The crystal structures of several Rabs have been obtained, helping to define some of their common features (Pfeffer, 2005). Rabs possess the GTPase fold found in all members of the Ras superfamily, including a GTP binding and hydrolysis domain, linked to a hypervariable region of 35-40 amino acids on the C-terminal side of the fold, followed by CAAX boxes that normally contain two cysteine residues, to which gerenylgeranyl moieties, required for

membrane incorporation, are covalently attached (Pfeffer, 2013; Hutagalung & Novick, 2011), one possible form of so-called prenylation.

1.3.1.2 Rab activation

Following their synthesis, Rabs are chaperoned by the Rab escort protein (REP) to the Rab gerenylgeranyl transferase (RabGGT), which catalyses the addition of one, or in most cases, two geranylgeranyl lipid groups to its COOH terminus (Alexandrov *et al*., 1994; Andres *et al*., 1993). The modified Rabs are then inserted into a target membrane in their inactive GDP-bound state with the assistance of a GDP dissociation inhibitor (GDI) dissociation factor (GDF; Collins, 2003). The membrane-inserted Rab is converted to its GTP-bound 'active' state, which has greater stability within the membrane, through the activity of a guanine nucleotide exchange factor (GEF). Once activated, the Rab interacts with effector proteins that facilitate a wide variety of trafficking processes. A GTPase accelerating protein (GAP) inactivates the Rab GTPase by catalysing its hydrolysis of bound GTP to GDP. Once inactive, the Rab is a substrate for GDI, which is able to extract the Rab in its GDP-bound conformation from the membrane. The cycle then begins again as the Rab is inserted into its target membrane in a GDF-mediated manner, which releases the Rab from GDI (Hutagalung & Novick, 2011). This cycle of activation and inactivation is summarised in Figure 1.3.

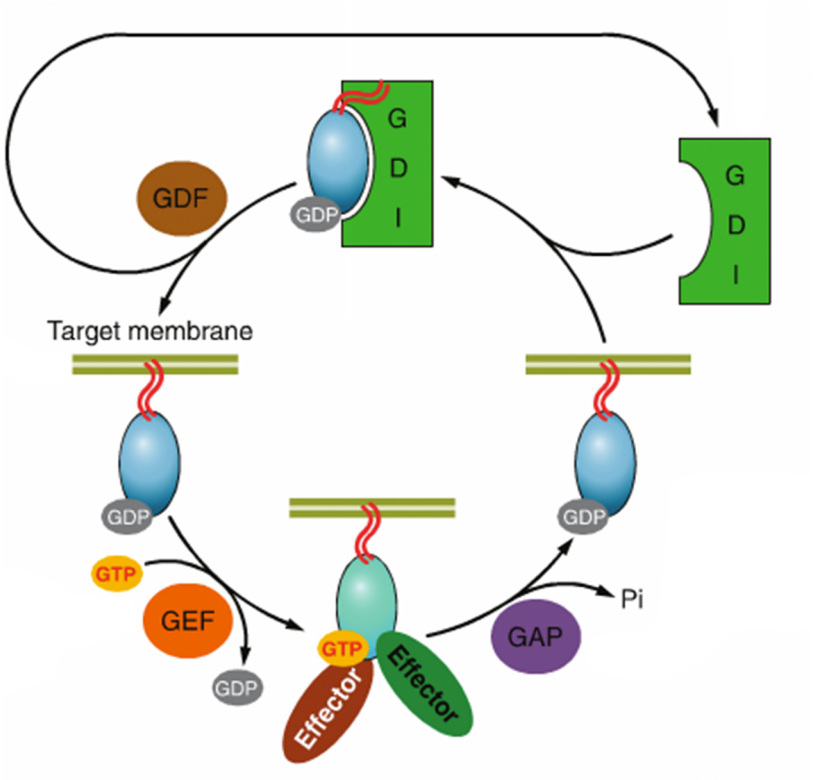


Figure 1.3 Schematic showing the Rab cycle of recruitment, activation, inactivation, and removal. Adapted from Hutagalung & Novick (2011). Following the insertion of nascent Rab proteins into their target membranes (not shown), the GDP-bound Rab is converted into the GTP-bound 'active' form through the catalytic activity of a guanine nucleotide exchange factor (GEF). This results in a conformational change in the Rab protein that is recognised by multiple 'effector' proteins, which in turn mediate membrane trafficking pathways. The GTP-bound 'active' Rab is subsequently converted back to the GDP-bound 'inactive' form through the activity of a GTPase-activating protein (GAP), which releases an inorganic phosphate (P_i). The GDP-bound Rab is then removed from the membrane by a guanine nucleotide dissociation inhibitor (GDI). The cycle begins again when a GDI dissociation factor (GDF) releases the Rab from GDI, and facilitates its insertion back into the target membrane.

1.3.1.3 Rab targeting

Initial work using chimaeric Rabs suggested that the hypervariable region of different Rabs provided a targeting mechanism to particular compartments (Chavrier *et al*., 1991), however, subsequent work indicated that this was not a general mechanism (Ali *et al*., 2004). Emerging evidence suggests that the structurally diverse Rab GEFs play a major role in targeting Rabs to specific membranes (Barr, 2013). This was clearly demonstrated through experiments by Blümer *et al*., (2013), who mistargeted the Rab1 GEF, DrrA, the Rab5 GEF, Rabex-5, and the Rab8 GEF, Rabin8, to the outer mitochondrial membrane, resulting in the re-localisation of their cognate Rabs onto the membrane surface. Several examples of GEF-mediated Rab targeting to particular compartments within cells have now been identified, and include the Rabex-5-rabaptin complex, which functions as a Rab5 GEF, and also an effector for Rab4 and Rab5 (Horiuchi *et al*., 1997). Rabex-5 binds to ubiquitin via a specific domain, which regulates its recruitment to early endosomes, where it activates Rab5 (Mattera *et al*., 2008).

1.3.2 Rabs regulate secretory and endolysosomal pathways

1.3.2.1 Secretory Rabs

Rabs were first linked to vesicle transport during yeast screens for mutants defective in protein secretion (Novick *et al*., 1980; Salminen & Novick, 1987). Since these important studies, it has become clear that specific Rab-mediated regulation of intracellular membrane transport is often conserved to humans. Rabs can mediate secretion by regulating the sorting of vesicular cargos, vesicle budding, vesicular uncoating, vesicle mobility through interaction with

the cytoskeleton, and finally vesicle tethering and fusion with the plasma membrane (Stenmark, 2009). For example, Rab6 localises to exocytotic vesicles in human cells and directs trafficking to the cortical plasma membrane (Grigoriev *et al*., 2007). An interesting study in yeast showed how different Rabs control different steps in the same secretory pathway by controlling their activation on the surface of the compartment. For example, the Rab11 homologue, Ytp32, associates with secretory compartments within the late Golgi, but it recruits Sec2, a GEF for Rab8 (Sec4) that in turn mediates Rab8 recruitment and activation. Rab8 then facilitates the delivery of these compartments to and fusion with the plasma membrane (Ortiz *et al*., 2002). Over the years, a complex network of Rab GTPases has emerged with Rabs regulating numerous different secretory trafficking steps (for a good overview, see Hutagalung & Novick, 2011).

1.3.2.2 Endolysosomal Rabs

Rab5 plays key roles in the formation, functioning and fusion of early endosomes (see Section 1.3.1.1; Klumperman & Raposo, 2014). When murine hepatocytes were depleted of Rab5 *in vivo* by targeted siRNA, the whole endolysosomal system completely collapsed (Zeigerer *et al*., 2012). Rab5, Rab4 and Rab11 have all been observed on the surface of early endosomes, but in distinct domains (Sönnichsen *et al*., 2000). It is now thought that Rab4 mediates the fast-recycling pathway, whilst Rab11 facilitates the slow-recycling pathway (Hutagalung & Novick, 2011).
A groundbreaking study in the field showed that Rab5-positive endosomes matured to Rab7-positive late endosomes through a process of conversion (Rink *et al*., 2005). The molecular mechanisms underpinning this Rab switch

were identified in *C. elegans* and conserved to human cells (Poteryaev *et al*., 2010; Kinchen & Ravichandran, 2010). SAND-1 (Mon1 in humans) functions in a complex with CCZ to displace the Rab5 GEF, Rabex-5, from the endosomal surface, and simultaneously functions as a GEF for Rab7, recruiting and activating it on the limiting membrane of the compartment. Rab7 has been shown to mediate numerous aspects of late endosome biology, including a role in promoting the fusion between late endosomes and lysosomes (Bucci *et al*., 2000).

1.4 Exosome biology

1.4.1 Exosomes mediate cell signalling

The secretion of extracellular vesicles by cells appears to be a conserved process throughout evolution (Colombo *et al*., 2014). Exosomes are a type of extracellular vesicle that can mediate intercellular communication. Loaded up with ligands, receptors, intracellular signalling molecules, lipids and nucleic acids, exosomes can trigger a variety of responses in their target cells (Figure 4). These events can be elicited directly at the cell surface, or when their contents are released into target cells by fusion or endocytosis (Raposo & Stoorvogel, 2013; Théry, 2011).

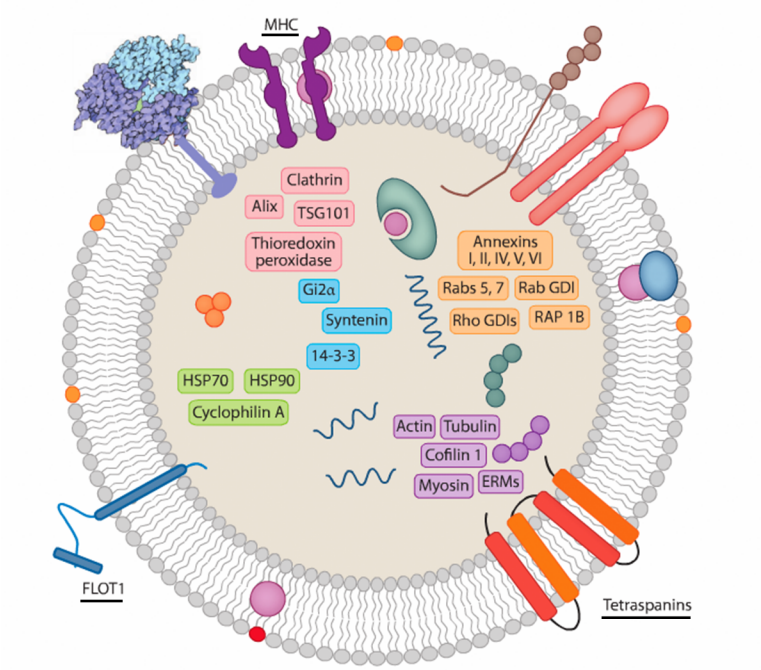


Figure 1.4 Typical exosome structure and contents. Adapted from Kourembanas (2015).

Exosomes contain a large variety of molecules including families of proteins, lipids and nucleic acids, which facilitate their functions in target cells. They are often characterised by the presence of endosomal proteins including tetraspanins, but they contain numerous other proteins including ESCRT components, such as TSG101, which are involved in their formation. They also contain miRNAs, mRNAs and other non-coding RNAs, which are encapsulated by a sphingomyelin and ceramide enriched membrane.

1.4.2 Mechanisms of exosome biogenesis and secretion

Exosomes constitute just a fraction of the population of extracellular vesicles. They are often defined by a combination of their size (30-150 nm diameter), the particular cargoes that they carry, and their origin within the cell (Kowal *et al*., 2014). Exosomes are classically proposed to originate as ILVs inside late endosomal MVBs, which fuse to the plasma membrane, releasing the ILVs as exosomes. These contrast with ectosomes (or microvesicles), which are shed directly from the plasma membrane (Figure 1.5). Endosomal cargoes, including the transmembrane tetraspanins CD9, CD63 and CD81, are commonly used to identify exosomes (Kowal *et al*., 2016; Tkach & Théry, 2016).

In yeast, ILV formation is dependent on four large multi-protein complexes known as the Endosomal Sorting Complex Required for Transport (ESCRT) 0-III alongside the accessory proteins ALIX, Eps15B and Vps4 (Christ *et al*., 2017; Wollert & Hurley, 2010; Bissig & Gruenberg, 2014; Babst *et al*., 2011). Together with the ESCRT complexes, these proteins target and localise ubiquitinated membrane proteins on the late endosome surface, then co-ordinate the membrane deformation of budding vesicles as well as the scission of the vesicle neck (Hanson & Cashikar, 2012). However, mammalian cells can still form ILVs in the absence of key subunits of all four ESCRT complexes, suggesting that alternative formation processes exist (Stuffers *et al*., 2009). Some have been described: for example, lipid rafts containing the sphingolipid ceramide have been shown to trigger spontaneous ILV formation in oligodendroglial cells (Trajkovic *et al*., 2008). Additionally, the tetraspanin CD63 is reported to participate in an ESCRT-independent form of

ILV formation in some mammalian cell types (Edgar *et al*., 2014; van Niel *et al*., 2011).

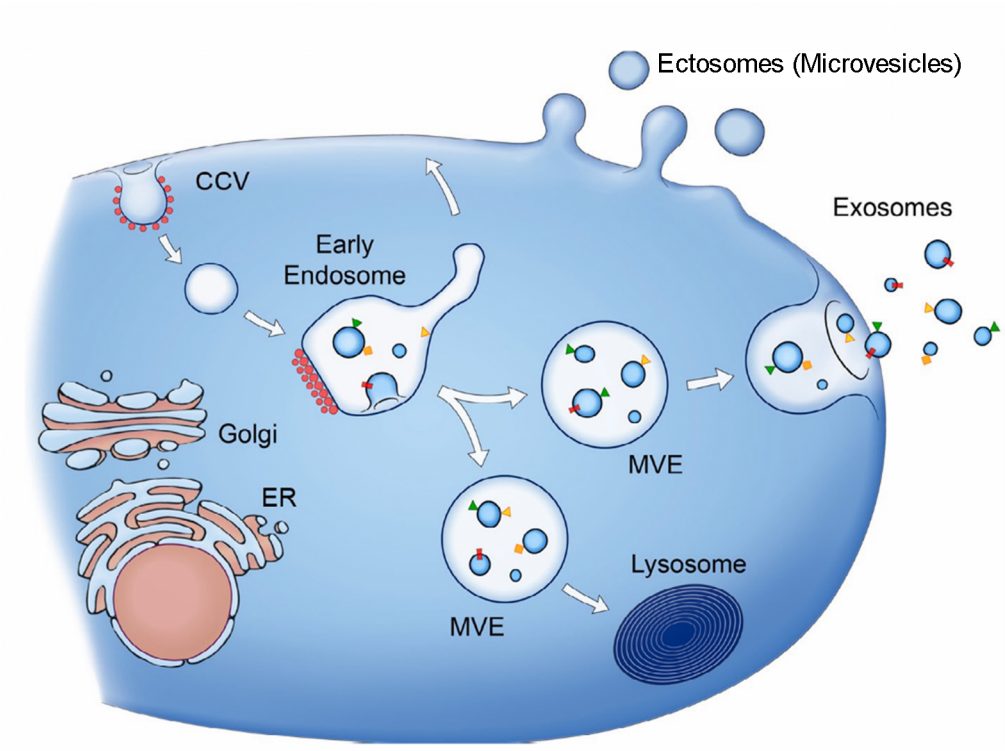


Figure 1.5 Secretion of extracellular vesicles. Adapted from Raposo & Stoorvogel (2013).

Following clathrin-mediated (CCV) endocytosis, membrane-associated cargos are sorted into budding ILVs within the endosomal system, forming multivesicular endosomes (MVEs). These compartments can either fuse to the lysosome, resulting in the degradation of their contents, or fuse to the plasma membrane, releasing their ILVs as exosomes. Other small vesicles are shed directly from the plasma membrane, releasing a population of extracellular vesicles called ectosomes (also known as microvesicles). Arrows represent proposed direction of protein and lipid transport between subcellular organelles and between MVEs and the plasma membrane to highlight exosome secretion.

Exosome secretion can be stimulated by Ca^{2+} ionophores, as has been demonstrated in K562 cells (Savina *et al*., 2003), oligodendroglial cells (Krämer-Albers *et al*., 2007), dendritic cells (Montecalvo *et al*., 2012), and mast cells (Valadi *et al*., 2007). However, it remains unclear what cellular and molecular mechanisms are triggered by the Ca^{2+} influx that would result in this secretion (Colombo *et al*., 2014). Trafficking regulators, including SNAREs and Rab GTPases have been implicated in regulating secretion, and are discussed later (Section 1.5.4).

1.4.3 The ESCRT complexes

The ESCRT machinery was first identified for its roles in vacuolar protein sorting in yeast (Raymond *et al*., 1992). These complexes were subsequently established as evolutionarily conserved membrane-remodelling assemblies involved in the formation of endosomal ILVs. Recently, however, ESCRTs have been implicated in a very diverse set of cellular functions including HIV release, scission during cytokinesis, plasma membrane repair, nuclear envelope reformation and repair, neural pruning, ectovesicle shedding and unconventional protein secretion (Christ *et al*., 2017; Hurley *et al*., 2015). Within the endosomal pathway, the ESCRTs play key roles in cargo sorting and also in the generation of MVBs. The complexes are recruited in a sequential manner to perform specific functions on the appropriate membranes. Firstly, the heterodimeric ESCRT-0 complex is targeted to endosomes through Hrs-mediated binding to the endosomal lipid, phosphatidylinositol 3-phosphate (PI3P), via its FYVE domain (Raiborg *et al*., 2001). Together with STAM and the accessory protein Eps15B, Hrs also binds ubiquitinated cargo and clathrin, which helps to concentrate ESCRT-0 in

subdomains of the endosomal membrane (Christ *et al*., 2017; Bache *et al*., 2003; Raiborg *et al*., 2001). Hrs also binds to the heterotetrameric ESCRT-I subunit TSG101 to facilitate the complex's recruitment (Lu *et al*., 2003). In turn, the Vps28 subunit of ESCRT-I binds to the Y-shaped ESCRT-II complex through interactions with its EAP45 subunit (Gill *et al*., 2007). ESCRT-I and -II are thought to initiate ILV budding by inducing membrane invagination (Wollert *et al*., 2009). The two EAP20 subunits of ESCRT-II directly interact with CHMP6, an ESCRT-III component (Henne *et al*., 2011). Additional direct interactions between the ESCRT-I component Vps28 and CHMP6 have also been reported (Pineda-Molina *et al*., 2006).

Recruitment of CHMP6 drives the polymerisation of ESCRT-III filaments, which mostly consist of CHMP4, together with CHMP2 and CHMP3 (Teis *et al*., 2008). CHMP4 also recruits the adaptor protein ALIX, a Bro1 domain protein family member, which stabilises the filaments and recruits the deubiquitinating enzyme Doa4. The latter de-ubiquitinates transmembrane cargos (Luhtala *et al*., 2004; Odorizzi *et al*., 2003). Together, the ESCRT-III complex is thought to constrict the invaginated membrane and catalyse scission that detaches the ILV buds (Wollert *et al*., 2009). The conserved ATPase, Vps4, regulates ESCRT-III by catalysing disassembly (Babst et al., 1998). However, recent studies suggest that Vps4 carries out other roles in actively controlling vesicle neck constriction and scission (Adell *et al*., 2014). The process of ESCRT-mediated ILV formation is summarised in Figure 1.6.

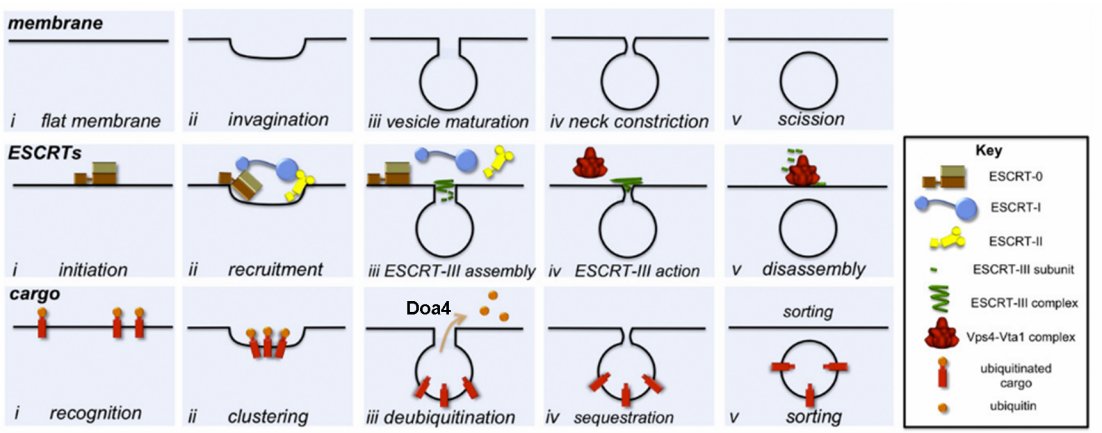


Figure 1.6 ESCRT complexes mediate ILV formation. Adapted from Henne *et al.* (2011).

This schematic recognises five distinct recognised stages of ILV budding. The flat membrane (i) is invaginated (ii) and matures into a vesicle (iii) whose neck is constricted (iv) to enable scission (v). The ESCRT complexes mediate distinct steps in this process. ESCRT-0 is targeted to endosomal membranes where it binds ubiquitinated cargos and ESCRT-I, which in turn recruits ESCRT-II, cargos are clustered into subdomains of the membrane. ESCRT-II then facilitates ESCRT-III assembly. Cargos are deubiquitinated by Doa4. The ESCRT-III complex then constricts the neck of the ILV, catalysing scission, and is subsequently dissessembled by the Vps4-Vta complex.

1.4.4 Rab GTPases regulate exosome secretion

The trafficking of multivesicular endosomes to the plasma membrane is at least partly regulated by Rabs. The first Rab demonstrated to regulate exosome secretion was Rab11 in K562 cells (Savina *et al*., 2005). A seminal paper in the field later showed that Rab27a and Rab27b, alongside their effectors Slp4 and Slac2b, regulate the secretion step in HeLa cells (Ostrowski *et al*., 2010). In *Drosophila* S2 cells, however, Rab27 does not affect exosome secretion. Similar to K562 cells, Rab11 was found to be important for their exosome release (Becket *et al*., 2013). In the oligodendroglial precursor cell line, Oli-neu, Rab35 is implicated in exosome secretion (Hsu *et al*., 2010), and in MCF-7 cells, Rab7 is required (Baietti *et al*., 2012). Both Rab7 and Rab27 are closely associated with late endosomal compartments, consistent with the current model of exosome biogenesis (Section 1.5.2), but Rab35 and Rab11 are associated with recycling pathways. These and other findings have led several authors to recently postulate the existence of multiple subtypes of exosomes that exist in different compartments, though no publications to date directly demonstrate this idea (Colombo *et al*., 2014; Kowal *et al*., 2014).

1.4.5 Functions of exosomes in health and disease

The reported roles of exosomes in normal physiological processes and disease are expanding year on year (Yáñez-Mó *et al*., 2015; Kalluri *et al*., 2016). There are numerous contexts in which exosomes appear to play important roles. Cancer cells take advantage of exosomes to manipulate their microenvironment in favour of immune escape, therapy resistance, tumour growth and metastasis (Miller & Gunewald, 2015; Costa-Silva *et al*., 2015;

Azmi *et al*., 2013). During *Drosophila* wing disc development, Wnt morphogens are secreted on exosomes (Gros *et al*., 2012). Exosomes also play roles in the mammalian immune system; the first description showed that B cells release exosomes that carry MHC class II, co-stimulatory and adhesion molecules and can activate CD4+ T cells (Raposo *et al*., 1996). This discovery led to the development of an exosome-based cancer vaccine that reduced tumour growth in mice by activating T cells (Zitvogel *et al*., 1998). Exosomes also hold potential in the clinic as biomarkers of disease, because they are released into accessible bodily fluids such as plasma and urine, and they are also potential delivery systems for drugs (Properzi *et al*., 2013; Johnsen *et al*., 2014).

1.4.6 Limitations in our understanding of exosome biology

In recent years, it has become clear that the functional properties ascribed to exosomes may have been often overstated. Sometimes they may be confused with ectosomes (membrane shedding), because of the difficulty in distinguishing between these subtypes of extracellular vesicles (Juan & Fürthauer, 2017). For example, exosomes are often separated on the basis of their small size, but recent findings have shown that small ectosomes can be comparable (Maas *et al*., 2017). Furthermore, the endosomal ESCRTs, previously thought to specifically regulate exosome formation, are now known to also mediate ectosome release (Hurley *et al*., 2015). Association of vesicle preparations with soluble extracellular molecules that stick to them during isolation may also affect compositional and functional analysis. Evidence to prove the subcellular origins of exosomes is challenging, because MVBs are very small compartments (<1 μm) in most cell types, and so require electron

microscopic analysis for detailed analysis (Colombo *et al*., 2014). Given the remarkable complexity and heterogeneity of exosome preparations, better understanding of exosome biogenesis is essential in order to unravel their physiological relevance.

1.5 Protein secretion and dense-core granule biology

1.5.1 Protein secretion by constitutive, regulated and unconventional pathways

Most cells secrete proteins, which are folded, assembled and glycosylated as they traffic through the endoplasmic reticulum and Golgi apparatus, and are released at the plasma membrane through either regulated or constitutive secretory trafficking pathways. During regulated secretion, proteins are often highly concentrated as dense-core granules inside specialised organelles, and are released upon stimulation by a secretagogue. In contrast, during constitutive secretion, proteins are trafficked to the plasma membrane without the formation of dense core granules, and secretagogue stimulation is not required for their release (Burgess & Kelly, 1987; Palade, 1975; Figure 1.7). These two secretory pathways are considered to be the conventional forms of exocytosis in eukaryotic cells. However, unconventional protein secretion has also been observed when cells are placed under stress, where proteins reach the plasma membrane, or are secreted, despite bypassing the Golgi apparatus (Rabouille *et al*., 2017).

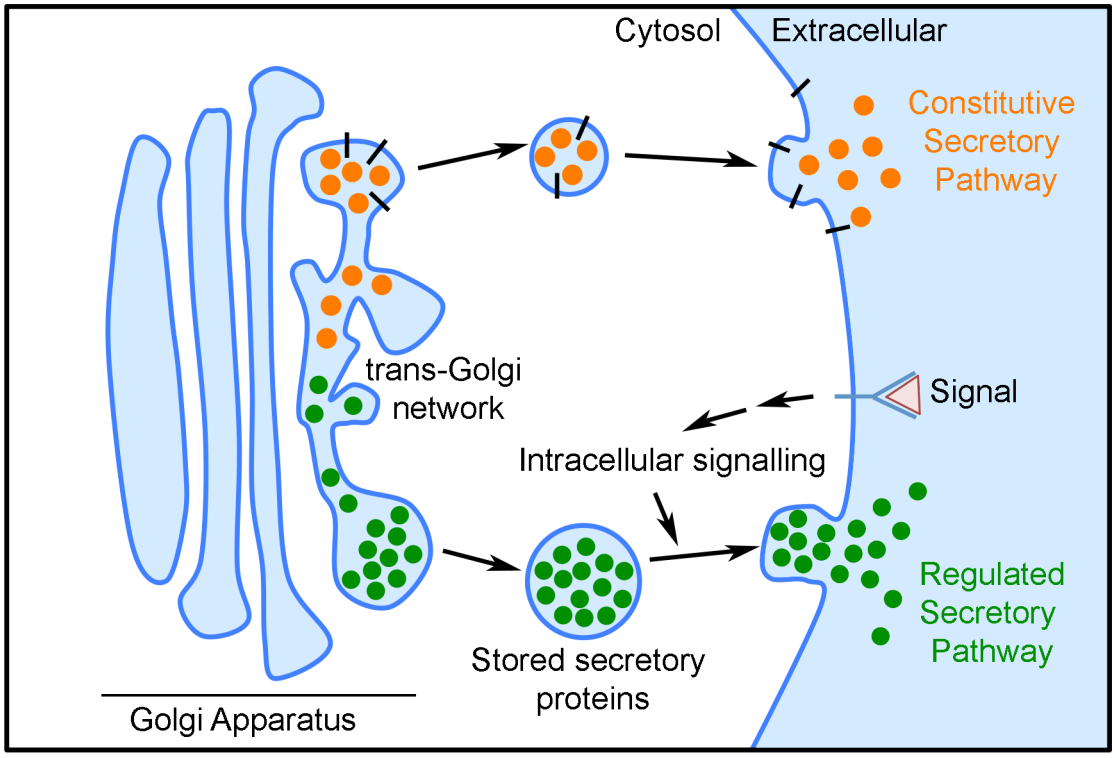


Figure 1.7 Constitutive and regulated secretion. Adapted from Alberts *et al*. (2002).

Two secretory pathways diverge at the trans-Golgi network. Constitutive secretion occurs in a continual manner, releasing soluble molecules and delivering plasma membrane components including lipids and proteins. Regulated secretion, on the other hand, is stimulated by a signal, and involves the release of stored secretory proteins that are maintained in specialised subcellular vesicles.

1.5.2 Functions of regulated secretion

The regulated secretion pathway plays essential roles in human physiology (Burgoyne & Morgan, 2003). For example, at neuronal synapses, regulated secretion controls the release of neurotransmitters from synaptic vesicles that mediate neurotransmission (Kelly, 1993). This process is essential in mammals for the development of the motor neuron system, as impairment of regulated secretion results in disorganisation of nerve terminal branches and reduced stabilisation of synapses (Heeroma *et al*., 2003). Certain neurons also contain dense-core granules that are regulated independently of the synaptic vesicles, and release different neuroactive molecules (Bartfai *et al*., 1988). Many non-neuronal cell types also possess dense-core granules that are secreted by regulated exocytosis, for example neuroendocrine chromaffin cells, endocrine pancreatic β-cells and exocrine pancreatic acinar cells (Burgoyne & Morgan, 2003). The adrenal medullary chromaffin cells contain dense-core granules rich in catecholamines, such as adrenaline, noradrenaline, and dopamine, which are released in response to acute stress (Crivellato *et al*., 2008). The regulated secretion of insulin granules by β-cells within the pancreatic islets of Langerhans plays important physiological roles maintaining normal blood glucose levels by facilitating cellular glucose uptake (Wilcox 2005). Misregulation of this process is often associated with the highly prevalent disease, diabetes type 2, although altered sensitivity to circulating insulin is also thought to be involved (Ashcroft & Rorsman, 2012). Regulated secretion of digestive enzymes by the pancreatic acinar cells is essential for digestion in the small intestine (Williams, 2010). In addition to these secretory cell types, regulated secretion plays specialised roles during fertilisation

events involving sperm and egg cells (Burgoyne & Morgan, 2003). The sperm cell acrosome, a specialised lysosome-derived dense-core granule in the head of the sperm, is released during fertilisation, whilst cortical granules are released by the egg cell to prevent polyspermy (Mayorga *et al*., 2007; Masumoto *et al*., 1996).

1.5.3 Regulation of dense-core granule biogenesis

The important functions of dense-core granules in human physiology and disease have driven numerous studies into their biogenesis. Primarily, using primary cultured cells and specific secretory cell lines, specific aspects of this process have now been characterised in some detail. The sorting of proteins targeted towards the regulated secretory pathway begins in the trans-Golgi network (Tooze et al., 2001; Tooze *et al*., 1991). Protein cargos are clustered into budding immature secretory granule compartments through interactions between lipid rafts and protein components (Montero-Hadjadje *et al*., 2009). The key constituent of lipid rafts, cholesterol, has been shown to play important roles in in dense-core granule formation in both neuroendocrine and pancreatic β-cells (Tsuchiya *et al*., 2010; Wang *et al*., 2000). Together with other lipids, such as diacylglycerol and phosphatidic acids, cholesterol-rich lipid rafts are thought to promote the budding of immature secretory granule compartments (Siddhanta & Shields, 1998; Asp *et al*., 2009; Kim *et al*., 2006). Furthermore, diacylglycerol is known to recruit protein kinase D (PKD) to the trans-Golgi network, where it facilitates scission of budding vesicles by downregulating Arfaptin-1, an inhibitor of the protein scission machinery, through phosphorylation (Gehart *et al*., 2012). The lipid rafts also contain specific raft-associated proteins, including carboxypeptidase E (Cool *et al*.,

1997; Zhang *et al*., 1999), prohormone convertase PC2 (Blázquez *et al*., 2000) and secretogranin III (Hosaka *et al*., 2004), which are thought to act as chaperones, tethering soluble or aggregated proteins and prohormones inside the budding immature secretory granule compartments (Tanguy *et al*., 2016; Kim *et al*., 2006). For example, cholesterol-bound secretogranin III recruits chromogranin A into the secretory granules of both pituitary and pancreatic endocrine cells (Hosaka *et al*., 2002). Chromogranin A itself plays key roles in dense core formation in neuroendocrine cells, and has been shown to promote hormone sorting into dense-core granules of pituitary AtT20 cells (Montero-Hadjadje *et al*., 2009; Day & Gorr, 2003).

By electron microscopy the immature secretory granule compartments that bud from the trans-Golgi network often contain electron-lucent lumens, but these gradually convert into mature electron-dense granules (Tooze et al., 2001). In some cells, such as neuroendocrine PC12 cells, maturation involves homotypic fusion of immature secretory granule vesicles (Urbe *et al*., 1998; Tooze *et al.,* 1991), in a process that requires the fusion-mediating Qc-SNARE protein, syntaxin 6 (Wendler *et al*., 2001). Maturation is also thought to involve a reduction in pH levels, which activates hormone-processing enzymes (Tanaka *et al*., 1997; Orci *et al*., 1986), and an increase in the level of intralumenal Ca^{2+}, which is required for the aggregation of granule constituents such as chromogranin A (Yoo *et al*., 1996). In addition, non-specifically packaged proteins are removed from the lumen of the immature secretory granule compartment through interactions with the clathrin adaptor protein complex, AP-1, which is recruited to the membrane of the immature secretory granule compartments by the Arf1 GTPase (Bonnemaison *et al*.,

2013). The lipid raft-rich membranes of these compartments are also thought to accumulate aquaporins, which are involved in the removal of water from the maturing compartment, resulting in the condensation of its interior proteins (Tanguy *et al*., 2016).

These complex interactions are thought to drive the biogenesis of mature dense-core granules, which are then trafficked to the plasma membrane through the activity of Rab GTPases such as Rab8 (Faust *et al*., 2008), and released in a Ca^{2+}-regulated manner, involving several SNARE proteins (Gaisano, 2017). However, the requirement for electron microscopy to investigate the dynamics of this process means that the real-time events that underlie dense-core granule biogenesis are not well characterised. Furthermore, our current knowledge is almost entirely based on analysis in cultured cells, where many of the normal control mechanisms will be absent.

1.6 The *Drosophila melanogaster* male accessory glands as a model genetic system to study the secretory and endolysosomal pathways

1.6.1 Brief historical overview of research using *Drosophila*

The common fruit fly, *Drosophila melanogaster*, has proven to be an invaluable tool in genetic research (Bellen, 2010). It was first used as a genetic system in the lab of Thomas Hunt Morgan (Morgan, 1910) to develop the theory of genetic inheritance and the roles of chromosomes in this process (Muller, 1946). The significance of these findings resulted in Morgan

being awarded the Nobel Prize in Physiology or Medicine in 1933. The work not only laid the foundations of our current understanding of genetics, but it also established the fruit fly as a powerful research tool that has been embraced ever since. One of the most significant studies using *Drosophila* was a set of large-scale forward genetic screens to discover the genes controlling embryonic patterning and development (Johnston, 2002; Nüsslein-Volhard & Wieschaus, 1980; Nüsslein-Volhard *et al*., 1984). Many of the genes identified during these screens, and their functions, are now known to be conserved across the animal kingdom. Numerous other influential studies have followed, establishing *Drosophila* as an important model system that can be used to examine the genetic regulation of many biological processes.

1.6.2 The *Drosophila* male accessory glands

1.6.2.1 Structure and organisation of the accessory glands

The accessory glands are an essential part of the male *Drosophila* reproductive system, which also includes the testes, seminal vesicles, ejaculatory duct and ejaculatory bulb (Figure 1.8). Each male possesses two glands that feed into the anterior ejaculatory duct via independent connections to a papilla region (Bairati, 1968). Each accessory gland is composed of a monolayered epithelium sat on a basement membrane and surrounded by a layer of striated muscle (Leiblich *et al*., 2012; Susic-Jung *et al*., 2012). The epithelial cells secrete apically into the lumen of the gland, filling it with contents that cause the gland to swell during periods of no sexual activity. The contents of the lumen are expelled during mating through the activity of peristaltic muscle contractions in the gland and the ejaculatory duct (Bairati

1968). Mating also stimulates both RNA and protein synthesis in the accessory glands, presumably to replenish the lumen following depletion (Schmidt *et al*., 1985; DiBenedetto *et al*., 1990)

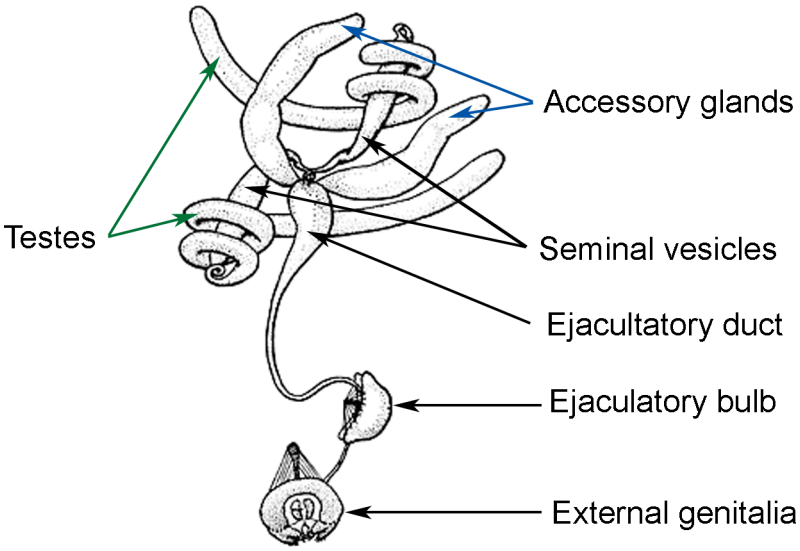


Figure 1.8 The *Drosophila* male reproductive tissues. Adapted from Miller (1950).

The main reproductive tissues of the Drosophila melanogaster male include the testes, seminal vesicles, accessory glands, ejaculatory duct, ejaculatory bulb and external genitalia. The accessory glands produce most of the seminal fluid, which is transferred to the female during mating with the mature sperm, that are stored in the seminal vesicles.

Two morphologically and biochemically distinct types of epithelial cell populate the accessory gland epithelial layer (Bertram *et al*., 1992). These include main cells, ~1000 of which populate the entire length of the epithelium, and secondary cells, ~40 of which are generally restricted to the distal tips of each gland. Both cell types are binucleate, which, it has been argued, helps to maintain the integrity of the epithelium during the shape changes that occur during mating as a consequence of muscle contraction (Taniguchi *et al*., 2012). Other work in the Wilson lab has recently demonstrated that both cell types undergo quite dramatic morphological changes from columnar to squamous to accommodate for the amount of secretory contents in the lumen (Hellberg, 2017).

1.6.2.2 Functions of the accessory glands

The *Drosophila* male accessory glands share functional similarities with the mammalian prostate and seminal vesicles, as they secrete many components of the seminal fluid that are transferred to the female during mating alongside the sperm (Corrigan, 2014). Interestingly, male flies lacking accessory glands, due to a mutation in *paired*, are sterile, suggesting that the secretions from these tissues likely play important roles in normal reproductive physiology (Xue & Noll, 2000). The secreted accessory gland proteins (Acps) are now known to induce a variety of physiological and behavioural responses in females after mating, known as the post-mating response (described in more detail in Section 1.6.3; Wolfner, 1997; Wolfner, 2007).

1.6.3 The *Drosophila* female post-mating response

The post-mating response is characterised by numerous changes in the female, evoked primarily by peptide signals derived from the male accessory

glands (Wolfner, 2002). Some of the effects include: increased egg laying, resulting from increased oogenesis and ovulation, increased immunosuppression, due to the reduced release of anti-microbial peptides, and reduced receptivity to re-mating. The types of effects on physiology and behaviour can be divided into short- and long-term responses (Kalb *et al*., 1993; Manning, 1962) and these depend on different molecules. Main cells secrete many of the most important Acps identified so far. One of the most important and well characterised is Sex Peptide (Acp70; Chen *et al*., 1988), as it regulates all aspects of the post-mating response. Other accessory gland products, including ovulin (Monsma *et al*, 1990) and CG33943 (Ram & Wolfner, 2007), which play roles in the short-term response, by stimulating ovulation and egg laying. Many of the Acps are proteases and anti-proteases, which process key proteins and peptides required for inducing the post-mating response, for example by promoting their activation in the female. Furthermore, some of these Acps contribute to the formation and integrity of the mating plug, an important physical structure that is deposited in the female after copulation to retain ejaculate (Ram & Wolfner, 2007).

1.6.4 Secondary cells

1.6.4.1 Secondary cell organelles

The unusually large subcellular organelles of secondary cells have captured the attention of numerous researchers studying the accessory glands. During their original characterisation by electron microscopy (Bairati, 1968), one organelle in particular stood out – the large dense-core granules surrounded by tubular filaments, called ‘filamentous bodies’. It has remained unclear how

exactly these organelles are formed, though it has been speculated that the core must be pre-existent to the filaments. Based on further ultrastructural observations, it was suggested that the tubular filaments were microtubules, a novel secretory product (Perotti, 1972). Furthermore, it has been reported that their release correlated with a degeneration of cellular structures, suggesting that secondary cells likely secrete in a holocrine manner. Currently, the only confirmed molecular cargo within the dense-core granule is the Angiotensin Converting Enzyme (AnCE), a peptidase thought to process biologically active peptides once secreted into the lumen (Rylett *et al*., 2007). However, other studies have suggested that the Bone Morphogenic Protein (BMP) ligand, Decapentaplegic (Dpp), is also packaged into the dense-core granules and is released to regulate autocrine growth signalling (Redhai *et al*., 2016).

Recent studies have mostly used light microscopy to study the organelles within living secondary cells. By expressing fluorescently tagged proteins, such as YFP-tagged Rab GTPases, and staining with dyes such as pH sensitive Lysotracker-Red, researchers in the Wilson lab have defined several subtypes of organelles, including both early and late endosomes (Corrigan *et al*., 2014; Redhai, 2016). These studies identified the presence of extremely large Rab7-positive acidic compartments found in secondary cells, corresponding to late endosomal MVBs or lysosomes. However, electron microscopic characterisation of these compartments has proven challenging, so little is currently known about their morphology.

1.6.4.2 Analysing the genetic regulation of growth, exosome biogenesis, endolysosomal trafficking and dense-core granule secretion in the secondary cell model

Secondary cells were first developed in the Wilson lab as a model to study the genetic regulation of cancer-related functions, including cell growth and migration (Leiblich *et al*., 2012). Interestingly, Leiblich et al., (2012) found BMP signalling was active in secondary cells, and that it promoted nuclear growth and a process of delamination, where cells migrated along the apical surface of the gland to the proximal end, and were even transferred to females, in an age- and mating-dependent manner. These findings led to other researchers using similar methods to screen for genes involved in prostate cancer progression (Ito *et al*., 2014).

Subsequently, Corrigan *et al*., (2014) characterised secondary cells as a novel *in vivo* system to study the genetic regulation of exosome secretion and membrane trafficking. This built on observations that secondary cells expressing a commonly used exosome marker, the human tetraspanin CD63 tagged with GFP, secreted thousands of small fluorescent extracellular vesicles into the lumen of the gland. These secretions were regulated by many of the molecules implicated in exosome secretion by mammalian cells, such as the ESCRT-0 component Hrs, the ESCRT-III accessory protein ALIX, as well as Rabs 7, 11 and 27, supporting the hypothesis that secretions were primarily exosomes, rather than ectosomes. Furthermore, BMPs were shown to regulate exosome secretion, suggesting that signalling pathways may control membrane trafficking to control secretion. In order to better understand how exactly they regulated secretion, these observations were combined with

quantitative analyses of the endolysosomal compartments of secondary cells in the absence of these regulatory molecules. The numerous secreted exosomes were transferred to the female during mating, where they fused to sperm and interacted with epithelial cells in the female reproductive tract. Interestingly, these exosomes may be functional, as reducing exosome secretion, by RNAi silencing of ALIX, or overexpressing a dominant negative Rab11, impacted on the normal post-mating response; specifically, the females receiving exosomes were less receptive to new mates.

Redhai *et al.* (2016) recently established secondary cells as an *in vivo* model to study dense-core granule secretion in a physiological setting, and also furthered our understanding of how BMP signalling mediates secondary cell growth after mating (Leiblich *et al*., 2012). In accord with previous observations, BMP signalling was upregulated in a subset of secondary cells following mating, suggesting that BMP ligands may be released during mating. Of the two BMP ligands in *Drosophila*, Dpp was required for this process, and, evidence suggested it was packaged into secondary cell dense-core granules. Subsequent experiments found that dense-core granules were released during mating in a manner dependent on the Soluble NSF Attachment Protein, SNAP24. Interestingly, BMP signalling was also shown to be required for dense-core granule biogenesis. This led to the model that Dpp secreted from dense-core granules during mating activated autocrine signalling in secondary cells to drive growth and *de novo* dense-core granule formation.

1.6.4.3 Secondary cells regulate the female post-mating response

Several studies have now provided insight into the roles of secondary cells in the post-mating response. Firstly, work in the Wilson lab revealed that BMP signalling in secondary cells is required for males to induce the full post-mating response in females (Leiblich *et al*., 2012). Specifically, BMP signalling is required for females to reject advances of other males post-mating, though other aspects, such as egg laying and fecundity are unaffected. Interestingly, similar effects were observed when exosome secretion was blocked by knockdown of ALIX, suggesting that BMP-mediated exosome secretion may mediate this particular aspect of the post-mating response (Corrigan *et al*., 2014).

Secondary cells have recently been implicated in a wider variety of post-mating responses in females (Gligorov *et al*., 2013). Deletion of a specific enhancer element in the *Hox* gene, *Abdominal B* (*Abd-B)*, caused secondary cells to develop without any of their large subcellular compartments. When these mutant flies were mated, several aspects of the post-mating response were altered, including reduced egg laying and increased receptivity to re-mating. Further analysis revealed that important main cell secretions, known to mediate different aspects of the post-mating response, were abnormally glycosylated. Building on these observations, Sitnik *et al*., (2016) performed RNA-seq on the same mutant flies in order to to identify genes that may be involved in the post-mating functions. Of the top 20 candidate genes, 9 were required in secondary cells to facilitate the true post-mating response, including egg laying and female receptivity. Although some analyses of these

genes was undertaken, detailed cell biological characterisations is still required to understand the mechanisms of their activity.

1.7 Aims and objectives

Over the past few years, secondary cells have been developed as useful models to study a variety of cell biological processes including membrane trafficking, secretion and nuclear growth. This has been greatly facilitated by their natural characteristics, including their very large subcellular organelles and amenability to *ex vivo* live imaging. I have focussed my attention on the underlying mechanisms of cellular secretion and membrane trafficking, highly conserved processes that play essential roles in human health and disease. Throughout my DPhil, I have tried to use secondary cell strengths to my advantage in order to visualise processes that are extremely challenging to observe, let alone genetically manipulate, using other cell types. Whenever possible, I have also tried to collaborate with other researchers using different systems, in order to clarify the relevance and potential conservation of my findings. With an interest in using new technologies, such as super-resolution microscopy, I hoped to answer important biological problems that could not previously be addressed. In chapter 3, I demonstrate the efficacy of this approach and characterise the subcellular organisation of secondary cell compartments at a new level of detail. In chapter 4, I describe how I have used secondary cells to uncover mechanisms of exosome biogenesis, and collaborated with researchers in the Goberdhan lab to test the conservation of these findings in human cancer cells. In chapter 5, I discuss the characterisation of the mechanisms underlying the formation of the large

subcellular compartments in secondary cells. This work benefited greatly from collaborating with another DPhil student in the Wilson lab, F. Castellanos, who was studying related mechanisms.

Briefly, the overall aims of this thesis were to:

- Establish new light and electron microscopic imaging methods for secondary cells
- Characterise the organisation and identity of subcellular compartments within secondary cells and characterise new tools for live imaging
- Identify the mechanisms underlying exosome biogenesis in secondary cells
- Determine the pathways of compartment formation and maturation in secondary cells
- Through collaboration, determine whether novel insights made in secondary cells are conserved with human cells

The work presented within my thesis has provided several fundamental new insights into secondary cell biology, some of which are likely to be directly relevant to the cell biology of other higher eukaryotic cell types. Furthermore, the new microscopic techniques and practices that I developed, such as super-resolution microscopy and time-lapse imaging, will continue to be used by secondary cell researchers going forward. Parts of chapters 3 and 4 have contributed significantly to a paper (Perera *et al*., in preparation), which highlights a novel conserved mechanism of exosome biogenesis and its

functions. Chapter 5 will be developed over the following months into a second paper characterising the roles of Rab GTPases during dense-core granule formation (Kroeger *et al*., in preparation), which we believe also involves evolutionarily conserved mechanisms. Finally, additional aspects of my work are already feeding into other projects currently being undertaken in the Wilson lab. They suggest unexpected mechanisms in dense-core granule assembly that could be relevant to several human diseases affecting secretion or the endolysosomal pathway. My studies have therefore not only added to our understanding of exosome and dense-core granule biology, but also provided the foundation for future work that may ultimately have a direct impact on treatments and diagnosis of common human diseases.

2.0 Methods

2.1 Fly Stocks

2.1.1 GAL4 and GAL80 combination lines

Genotype	Source ID	Reference	Description
w; dsx-GAL4/TM6B	S. Goodwin	Rideout *et al*., 2010	Secondary cell specific GAL4 line
w; spi-GAL4/Cyo (NP0261)	Kyoto DGRC 112114	Hayashi *et al*., 2002	Secondary cell specific GAL4 line
tubulin-GAL80^{ts}	BDSC 7108	McGuire *et al*., 2003	Ubiquitously expressed temperature sensitive GAL80
w; spi-GAL4, tubGAL80^{ts}/CyO	L. Corrigan	Corrigan *et al*., 2014	Temperature sensitive secondary cell specific GAL4 line
w; tub-GAL80ts; dsx-GAL4/ SM5.TM6	L. Corrigan	Corrigan *et al*., 2014	Temperature sensitive secondary cell specific GAL4 line
w; UAS-GFP-CD63, tubulin-GAL80ts; dsx-GAL4/ SM5.TM6	L. Corrigan	Corrigan *et al*., 2014	Temperature sensitive secondary cell specific GAL4 line driving GFP-CD63
w; spi-GAL4, tubGAL80^{ts}; UAS-GFP-GPI/ SM5.TM6	L. Corrigan	Redhai *et al*., 2016	Temperature sensitive secondary cell specific GAL4 line driving GFP-GPI
w; spi-GAL4, tubGAL80^{ts}; UAS-CD63-mCherry/ SM5.TM6	B. Kroeger		Temperature sensitive secondary cell specific GAL4 line driving CD63-mCherry
w; spi-GAL4, tubGAL80^{ts}; YFP^{Myc}-Rab1/ SM5.TM6	B. Kroeger		Temperature sensitive secondary cell specific GAL4 line with YFP-Rab1 from endogenous promoter
w; spi-GAL4, tubGAL80^{ts}; YFP^{Myc}-Rab6/ SM5.TM6	B. Kroeger		Temperature sensitive secondary cell specific GAL4 line with YFP-Rab6 from endogenous promoter
w; spi-GAL4, tubGAL80^{ts}; YFP^{Myc}-Rab11/ SM5.TM6	I. Stefana		Temperature sensitive secondary cell specific GAL4 line with YFP-Rab11 from endogenous promoter
w; bnl-GAL4 (NP2211)	Kyoto DGRC	Hayashi *et al*., 2002	GAL4 line drives expression in secondary cells
w; btl-GAL4 (NP6593)	Kyoto DGRC	Hayashi *et al*., 2002	GAL4 line drives expression in secondary cells

2.1.2 Fluorescently tagged protein lines

Genotype	Source ID	Reference	Description
w; UAS-Bnl-GFP	M. Affolter		Bnl-GFP under UAS control
y, w; UAS-Btl-GFP	BDSC 41802	Sato & Kornberg, 2002	Btl-GFP under UAS control
w; UAS-GFP-CD63	S. Eaton	Panáková *et al*., 2005	CD63-GFP under UAS control
w; UAS-GFP-GPI	S. Eaton	Greco *et al*., 2001	GFP-GPI under UAS control
w; UAS-myr-mRFP	BDSC 7118	Medina et al., 2008	myr-mRFP under UAS control
w; UAS-alphatub84B.Dendra2/TM3, Sb	BDSC 51316		alphatub84B.Dendra2 under UAS control
w; UAS-ChRFP-Tub	BDSC 25774		mCherry-alpha-tubulin under UAS control
w; UAS-nod.GFP	BDSC 9282		Nod-GFP under UAS control
w; sqh-EYFP-Mito	BDSC 7194		eYFP-Mito under ubiquitous (*sqh*) control
w; UAS-GFP-FP4mito	BDSC 25747		GFP-FP4-mito under UAS control
y, w; DE-Cadherin-GFP	Schweisguth		E-Cadherin gene trap
w; UAS-Galtase-GFP	BDSC 31422	Snapp *et al*., 2004	Galtase-GFP under UAS control
w; UAS-shrb-GFP	BDSC 32559	Sweeney *et al*., 2006	shrb-GFP under UAS control
w; UAS-GFP-Hrs	S-J. Fan/ B. Kroeger		GFP-Hrs under UAS control
w; UAS-GFP^{NLS}	BDSC 4775	Corrigan *et al*., 2014	Nuclear localised GFP under UAS control
w; UAS-hTFR-GFP	BDSC 36858	Henthorn et al., 2011	Wild type human transferrin receptor tagged to GFP under UAS control
w; UAS- hTFRΔC-GFP	BDSC 36859	Henthorn et al., 2011	Mutant human transferrin receptor tagged to GFP under UAS control
w; UAS-GFP-Clc	BDSC 7107	Chang *et al*., 2002	Clathrin light chain tagged with GFP under UAS control
w; TI{TI}Rab1[EYFP]	BDSC 62539	Dunst *et al*., 2015	*YFP^{Myc}-Rab1* gene trap
w; TI{TI}Rab2[EYFP]/CyO	BDSC 62540	Dunst *et al*., 2015	*YFP^{Myc}-Rab2* gene trap
w; TI{TI}Rab3[EYFP]	BDSC 62541	Dunst *et al*., 2015	*YFP^{Myc}-Rab3* gene trap
y, w; TI{TI}Rab4[EYFP]	BDSC 62542	Dunst *et al*., 2015	*YFP^{Myc}-Rab4* gene trap
w; TI{TI}Rab5[EYFP]	BDSC 62543	Dunst *et al*., 2015	*YFP^{Myc}-Rab5* gene trap
w; TI{TI}Rab6[EYFP]	BDSC 62544	Dunst *et al*., 2015	*YFP^{Myc}-Rab6* gene trap
w; TI{TI}Rab7[EYFP]	BDSC 62545	Dunst *et al*., 2015	*YFP^{Myc}-Rab7* gene trap

w; TI{TI}Rab8[EYFP]	BDSC 62546	Dunst *et al*., 2015	*YFP^{Myc}-Rab8* gene trap
w; TI{TI}Rab10[EYFP]	BDSC 62548	Dunst *et al*., 2015	*YFP^{Myc}-Rab10* gene trap
w; TI{TI}Rab11[EYFP]	BDSC 62549	Dunst *et al*., 2015	*YFP^{Myc}-Rab11* gene trap
w; TI{TI}Rab14[EYFP]/CyO, P{w[+mC]=hs-hid}4	BDSC 62550	Dunst *et al*., 2015	*YFP^{Myc}-Rab14* gene trap
y, w; TI{TI}Rab18[EYFP]	BDSC 62550	Dunst *et al*., 2015	*YFP^{Myc}-Rab18* gene trap
w; TI{TI}Rab19[EYFP]	BDSC 62552	Dunst *et al*., 2015	*YFP^{Myc}-Rab19* gene trap
y, w; TI{TI}Rab21[EYFP]	BDSC 62553	Dunst *et al*., 2015	*YFP^{Myc}-Rab21* gene trap
y, w; TI{TI}Rab23[EYFP]	BDSC 62554	Dunst *et al*., 2015	*YFP^{Myc}-Rab23* gene trap
y, w; TI{TI}Rab26[EYFP]	BDSC 62555	Dunst *et al*., 2015	*YFP^{Myc}-Rab26* gene trap
y; TI{TI}Rab27[EYFP] w[1118]	BDSC 62556	Dunst *et al*., 2015	*YFP^{Myc}-Rab27* gene trap
w; TI{TI}Rab30[EYFP]	BDSC 62557	Dunst *et al*., 2015	*YFP^{Myc}-Rab30* gene trap
w; TI{TI}Rab32[EYFP]	BDSC 62558	Dunst *et al*., 2015	*YFP^{Myc}-Rab32* gene trap
w; TI{TI}Rab35[EYFP]	BDSC 62559	Dunst *et al*., 2015	*YFP^{Myc}-Rab35* gene trap
w; TI{TI}Rab39[EYFP]	BDSC 62560	Dunst *et al*., 2015	*YFP^{Myc}-Rab39* gene trap
y, w; TI{TI}Rab40[EYFP]	BDSC 62561	Dunst *et al*., 2015	*YFP^{Myc}-Rab40* gene trap
y, w; CFP-Rab6	F. Karch/ S. Eaton		*CFP^{Myc}-Rab6* gene trap
y, w; ANCE-GFP (MI05748-GFSTF.1)	BDSC 59828	Nagarkar-Jaiswal *et al*., 2015	*ANCE-GFP* gene trap
w; Cts-B1-GFP (CPTI003407)	Kyoto DGRC 115404		*cathepsin B1*-GFP gene trap
w; Trol-GFP (CPTI003621)	Kyoto DGRC 115429		*trol-GFP* gene trap
w; mfas-GFP	VDRC 318000	Sarov *et al*., 2016	*mfas-GFP* third copy insertion
w; mfas-GFP (MI11275-GFSTF.2)	BDSC 63204		*mfas-GFP* gene trap
w; Vha55-GFP (CPTI002645)	Kyoto DGRC 115558		Vha55-GFP gene trap
y, w; UAS-YFP-Rab11	BDSC 9790	Zhang *et al*., 2007	YFP-tagged Rab11 under UAS control

2.1.3 RNAi lines and controls

Genotype	Source ID	Reference	Description
w; UAS-shrb-RNAi	VDRC 106823	Matusek *et al*., 2014	RNAi targeting *shrb* under UAS control
y, v; UAS-shrb-RNAi (HMS01767)	BDSC 38305	Matias *et al*., 2015	RNAi targeting *shrb* under UAS control
UAS-Vps28-RNAi	VDRC 31894	Matusek et al., 2014	RNAi targeting *Vps28* under UAS control
y, v; UAS-Rab6-RNAi (JF02640)	BDSC 27490		RNAi targeting *Rab6* under UAS control
y, sc, v; UAS-Rab6-RNAi (HMS01486)	BDSC 35744		RNAi targeting *Rab6* under UAS control
y, v; UAS-Rab11-RNAi (JF02812)	BDSC 27730		RNAi targeting *Rab11* under UAS control
y, v; UAS-Rab7-RNAi (JF02377)	BDSC 27051		RNAi targeting *Rab7* under UAS control
y, v; UAS-Rab10-RNAi (JF02058)	BDSC 26289		RNAi targeting *Rab10* under UAS control
y, sc, v; UAS-Rab19-RNAi (HMS00592)	BDSC 34607		RNAi targeting *Rab19* under UAS control
y, v; UAS-Rab21-RNAi (JF03338)	BDSC 29403		RNAi targeting *Rab21* under UAS control
y, v; UAS-Syx6-RNAi (JF03125)	BDSC 28505		RNAi targeting *Syx6* under UAS control
w; UAS-Syx5-RNAi	VDRC 3859		RNAi targeting *Syx5* under UAS control
y, v; UAS-AP-1γ-RNAi (JF02684)	BDSC 27533		RNAi targeting *AP-1γ* under UAS control
w; UAS-AP-1μ1-RNAi	VDRC 24017		RNAi targeting *AP-1μ1* under UAS control
w; UAS-Arf79F-RNAi	VDRC 23082		RNAi targeting *Arf79F* under UAS control
y, v; UAS-Chc-RNAi (JF02681)	BDSC 27530		RNAi targeting *Chc* under UAS control
y, sc, v; UAS-Chc-RNAi (HMS01222)	BDSC 34742		RNAi targeting *Chc* under UAS control
y, sc, v; UAS-mfas-RNAi (HMC03645)	BDSC 52905		RNAi targeting *mfas* under UAS control
w; UAS-mfas-RNAi	VDRC 103621		RNAi targeting *mfas* under UAS control
w; UAS-VhaSFD-RNAi	VDRC 47471		RNAi targeting *VhaSFD* under UAS control
w; UAS-Vha100-1-RNAi (JF02059)	BDSC 26290		RNAi targeting *Vha100-1* under UAS control
w^{1118}	L. Partridge	Redhai *et al*., 2016	Non-transgenic control line

2.2 Fly husbandry

Flies were reared at 18°C on standard cornmeal agar medium containing, per litre, 12.5 g agar (F Gutkind & Co. Ltd), 75 g cornmeal (BTP Drewitt), 93 g D-(+)-glucose (Sigma-Aldrich®, a subsidiary of Merck) 31.5 g inactivated yeast (Fermipan Red, Lallemand Baking), 8.6 g potassium sodium tartrate tetrahydrate (Sigma-Aldrich®), 0.7 g calcium chloride dihydrate (Sigma-Aldrich®), and 2.5 g methyl 4-hydroxybenzoate (Sigma-Aldrich®) dissolved in 12 ml ethanol (Sigma-Aldrich®). Flies were raised in plastic vials (BTP Drewitt) plugged with cotton balls (Fisherbrand®, a subsidiary of Thermo Fisher Scientific), or larger plastic bottles (F-L Plastics Ltd) plugged with cotton. They were transferred onto fresh medium every 3-4 days. During transfers, water was added to rehydrate dry medium. No additional dried yeast was added to the vials.

2.3 Control of transgene expression in secondary cells

Secondary cell-specific transgene expression was achieved using the yeast GAL4-UAS transcriptional regulatory system, previously adapted for use in *Drosophila* (Brand and Perrimon, 1993). This method relies on a powerful transcription activator, GAL4, which induces the expression of transgenes (including RNAis, overexpression constructs and fluorescently-tagged proteins) with a UAS (Upstream Activating Sequence) enhancer sequence. Several different *GAL4* lines were used (see Section 2.1.1), all of which specifically expressed *GAL4* in secondary cells within the male accessory

glands (Leiblich *et al*., 2012; Corrigan *et al*., 2014). However, the levels of GAL4 expression, and the other types of cells within the fly that also expressed GAL4, depended on the enhancer element driving GAL4. Temporal regulation of transgene expression was achieved by combining GAL4-UAS with *tubulin-GAL80^{ts},* a ubiquitously expressed, temperature-sensitive transcriptional repressor (McGuire *et al*., 2003). Flies carrying this combination were kept at 18°C during developmental stages, a temperature at which GAL80^{ts} stably prevents GAL4 from driving transcription of the *UAS-transgene*. At eclosion, the flies were transferred to 28.5°C, inactivating GAL80^{ts} and relieving its repression of GAL4, which could then activate transcription of the *UAS-transgene*. This genetic method, known as temporal and regional gene expression targeting (TARGET; McGuire *et al*., 2004), enabled dissection of secondary cell-specific phenotypes and the study of transgenic flies that give lethal phenotypes when expressed during development.

2.4 Micro-dissection of accessory glands

Adult male flies were anaesthetised using CO_2 gas and micro-dissection was performed using forceps (5-Dumostar®-B, Dumont) under a dissection microscope (EMZ stereo microscope mounted on a 'P' type pole stand, Meiji Techno) with an LED light source (LED F1, Photonics). To prevent damage to the forceps, micro-dissection was carried out on a silicone cushion (Sylgard® 184 Silicone Elastomer, Dow Corning) in a plastic petri dish (Greiner Bio-One International).

During the micro-dissection procedure, anaesthetised flies were submerged in a pool of ice-cold 1× PBS (pH 7.4, Gibco®, Thermo Fisher Scientific) for living samples, or alternatively in 4% w/v paraformaldehyde (Sigma-Aldrich®) dissolved in 1× PBS at room temperature (~22°C) for fixed samples. The whole male reproductive tract was carefully pulled out of the fly body cavity. The testes were removed by scission close to the seminal vesicles, as they often folded over the accessory glands, obscuring imaging. Care was taken to prevent damage to the papilla of the anterior ejaculatory duct by keeping the seminal vesicles and vas deferens attached. The accessory gland epithelium can be stressed by damage to this valve-like papilla, through which the spermatozoa and accessory gland contents are transferred during mating (Bairati, 1968). Finally, the remaining reproductive tissues, including the accessory glands, were isolated by separation of the ejaculatory bulb from the external genitalia, fat tissues and gut.

2.5 LysoTracker™ staining of living accessory glands

The isolated accessory glands were transferred using glass Pasteur pipettes (Fisherbrand®) to clear 1.7 ml microtubes (Axygen®) containing 1× PBS and kept on ice until sufficient numbers had been obtained. Glands were then incubated with either ice-cold 200 nM LysoTracker™ Red DND-99 (Invitrogen™, Thermo Fisher Scientific) or ice-cold 100nM Lysotracker™ Deep Red (Invitrogen™) in 1× PBS for 5 minutes. Finally, the glands were washed in ice-cold 1× PBS for 1 minute before mounting.

2.6 Mounting of living accessory glands

Glands were mounted onto High Precision microscope cover glasses thickness No. 1.5H (Marienfeld-Superior). A custom-built holder secured the cover glasses in place during imaging with both the super-resolution 3D-SIM and wide-field systems. To avoid dehydration and hypoxia, the glands were carefully maintained in a small drop of 1× PBS, surrounded by 10S Voltalef® (VWR), an oxygen-diffusible hydrocarbon oil (Parton *et al*., 2010), and kept stably in place by the application of a round 13 mm cover glass (VWR).

2.7 Fixation of accessory glands for light microscopy

Following micro-dissection, the isolated accessory glands were transferred using glass Pasteur pipettes to clear 1.7 ml microtubes containing 4% w/v paraformaldehyde in 1× PBS. They were incubated for 20 minutes in the fixative solution at room temperature (~22°C) before being processed for immuno/phalloidin staining (see later sections), or if they did not require staining, they were washed in 1× PBS for 5 minutes prior to mounting.

2.8 Immunostaining of fixed accessory glands

Immunostaining was performed as previously reported (Corrigan *et al*., 2014). Following fixation, the isolated accessory glands were transferred to PBST, consisting of 1× PBS with 0.3% v/v Triton X-100 (Sigma-Aldrich®). Unless otherwise stated, all steps were performed on an orbital shaker (IKA® Labortechnik) at room temperature. Samples were protected from bleaching during the protocol by covering with aluminium foil. Solution changes were

made using Pipetman pipettes (Gilson®) with graduated tips (TipOne®, Star Lab). This initial permeabilisation step was followed by 30 minutes in a blocking solution, PBSTG, which consists of PBST with 10% v/v Goat serum (Sigma-Aldrich®). The glands were then incubated overnight at 4°C with primary antibody solutions of appropriate concentrations in PBSTG (see Section 2.8.1). After this incubation, the glands were washed six times in PBST, with each wash lasting 10 minutes. Glands were then incubated for 2 hours with secondary antibodies conjugated with fluorescent dyes in PBSTG (see Section 2.8.2). This was followed by a further five washes in PBST, for 10 minutes each, and a final wash with 1× PBS for 10 minutes prior to mounting.

2.8.1 Primary antibodies

Antigen	Host species	Source	Reference	Dilution
ANCE	Rabbit	Gift from Prof. E. Isaac, University of Leeds, UK	Rylett *et al*., 2007	1:2000
Fas3	Mouse	Developmental Studies Hybridoma Bank (DSHB), Iowa, USA.	Narasimha *et al*., 2008	1:10
GM130	Rabbit	Abcam #ab30637	Sinka *et al*., 2008	1:100
Rab11	Rabbit	Gift from A. Nakamura, RIKEN Center for Developmental Biology, Kobe, Japan	Tanaka & Nakamura, 2008	1:8000
Chp	Mouse	Developmental Studies Hybridoma Bank (DSHB), Iowa, USA.	Van Vactor *et al*., 1988	1:10
Rab6	Rabbit	Gift from A. Satoh, Hiroshima University, Japan	Iwanami *et al*., 2016	1:2000
Arl8	Rabbit	Developmental Studies Hybridoma Bank (DSHB), Iowa, USA.	Hofmann & Munro, 2006	1:500
Rab7	Mouse	Developmental Studies Hybridoma Bank (DSHB), Iowa, USA.	Riedel *et al*., 2016	1:10
AP-1γ	Mouse	Gift from R. Le Borgne, University of Rennes, France.	Benhra *et al*., 2011	1:150
GFP	Goat	Abcam #ab6673	Shakya et al., 2005)	1:500
Golgin-84	Mouse	Developmental Studies Hybridoma Bank (DSHB), Iowa, USA	Riedel *et al*., 2016	1:10
Golgin-245	Goat	Developmental Studies Hybridoma Bank (DSHB), Iowa, USA	Sinka *et al*., 2008	1:4000

2.8.2 Secondary antibodies

Antigen	Host species	Conjugate	Source	Dilution
Rabbit	Donkey	Alexa Fluor 555	Abcam #ab150062	1:400
Mouse	Donkey	Alexa Fluor 555	Abcam #ab150110	1:400
Goat	Donkey	Alexa Fluor 555	Abcam #ab150134	1:400
Rabbit	Donkey	Alexa Fluor 647	Life Technologies #A-21245	1:400
Mouse	Donkey	Alexa Fluor 647	Life Technologies #A-31571	1:400
Rabbit	Donkey	Alexa Fluor 594	Abcam #ab150064	1:400
Mouse	Donkey	Alexa Fluor 594	Abcam #ab150136	1:400
Goat	Donkey	Alexa Fluor 594	Abcam #ab150112	1:400

2.9 Phalloidin staining of fixed accessory glands

Phalloidin staining was performed at room temperature on glands that had been previously immunostained, after the final five PBST washes of that procedure. The accessory glands were incubated for 30 minutes with Phalloidin-TRITC in PBST (diluted at 1:400 from a 1 mg/ml stock solution in methanol, Sigma-Aldrich®). The glands were then washed once in 1× PBS for 10 minutes prior to mounting.

2.10 Mounting of fixed accessory glands for light microscopy

Accessory glands were mounted onto SuperFrost® microscope slides (VWR). Excess liquid was removed using a lint-free tissue and glands were immersed in a drop of Vectashield with or without DAPI (Vector Laboratories). Finally, they were covered by a 22 x 22 mm, thickness No. 1 coverslip (Fisherbrand®), and sealed with nail varnish (Natural Collection, Boots UK). The prepared slides were stored at 4°C, but were brought to room temperature over 15 minutes prior to imaging.

2.11 Super-resolution 3D-SIM

For super-resolution 3D-SIM, fixed human cells or freshly prepared living *Drosophila* accessory glands were imaged on a DeltaVision OMX V3 system (GE Healthcare Life Sciences) equipped with a 60×, NA 1.42 Plan Apo oil objective (Olympus), sCMOS cameras (PCO), and 405, 488, 593 and 633 nm lasers. Objective immersion oil of RI 1.516 (Cargille Labs) was used to produce optimal reconstruction a few µm into the z-plane of the sample. The microscope was kept at ~20°C throughout experiments. Images were acquired in sequential imaging mode, with z-stacks typically spanning 8-12 µm being acquired with 15 images per plane (5 phases, 3 angles) and a z-distance of 0.125 µm. The raw data were computationally reconstructed in the softWoRx 6.0 software package (GE Healthcare Life Sciences), using a Weiner filter of 0.002 and wavelength-specific optical transfer functions (OTFs) to generate super-resolution images with two-fold improved resolution

in all three axes (Wegel *et al*., 2016). As the OMX system uses separate cameras for each colour, the originally produced images required careful re-alignment. To make the appropriate adjustments, reference z-stacks of 200 nm TetraSpeck Microspheres (T7280, Invitrogen™) were aligned using custom automated software (OMX Editor) that corrected for x, y and z shifts, magnification and rotation differences between channels. The resulting transformations were then applied to align the images of the test samples. SIMcheck (Ball *et al*., 2015) was used to analyse the quality of the reconstructed images.

2.12 Wide-field

For wide-field imaging, fixed or living accessory glands were imaged using a DeltaVision Elite wide-field fluorescence deconvolution microscope (GE Healthcare Life Sciences) equipped with a set of Olympus UPlanSApo objectives including a 100×, NA 1.4 oil objective, a 60×, NA 1.42 oil objective, a 20×, NA 0.75 objective, a 10×, NA 0.4 objective, and fitted with a CoolSNAP HQ2 CCD camera (Photometrics®) and a 7 colour illumination system (SPECTRA light engine®, Lumencor). A 1.6× auxiliary magnification lens and objective immersion oil with RI 1.514 (Cargille Labs) were used throughout. The microscope room was temperature-controlled at ~18°C. The images acquired were typically z-stacks spanning 8-12 µm height with a z-distance of 0.2 µm. Images were subsequently deconvolved using the Resolve 3D-constrained iterative deconvolution algorithm within the softWoRx 5.5 software package (GE Healthcare Life Sciences).

2.13 Confocal

Fixed accessory gland samples were imaged on an LSM510 Meta scanning confocal microscope (Axioplan 2, Carl Zeiss) equipped with a 63×, NA 1.4 Plan APO oil DIC objective (Carl Zeiss) and operated using LSM 510 Meta software. RI 1.518 objective immersion oil (Leica) was employed. Images were acquired at 1.7× zoom. The microscope was kept at ~20°C during experiments. The images acquired were typically z-stacks spanning 10 µm height with a z-distance of 5 µm.

2.14 Image analysis and figure presentation

All image analysis was undertaken using ImageJ2 (Schindelin *et al*., 2015), distributed by Fiji (Schindelin *et al*., 2012). Detailed accounts of particular analytical methods are given in separate sections. Global image brightness and contrast was regularly adjusted during image production. Figures were prepared using Powerpoint (Microsoft) and Photoshop CS6 (Adobe®).

2.15 Subcellular compartment analysis

Secondary cell compartment numbers were manually analysed in ImageJ2 using the 'Cell Counter' plugin. Complete z-stacks of individual cells were scored for the number of large non-acidic compartments (LysoTracker Red-negative, >2 µm in diameter) and the number of MVBLs (LysoTracker Red-positive, >2 µm in diameter). The diameter of the largest MVBL was measured manually at the z-plane where the diameter was at its greatest using the line tool (see Corrigan *et al*., 2014; Redhai *et al*., 2016). Both

fluorescently labelled and non-transgenic w^{1118} flies were analysed using a combination of fluorescence and DIC microscopy on the wide-field microscope. The mean measurement was calculated from 3 cells within each gland, and generally n=≥6 flies were used for each genotype. Detailed manual quantification of intracellular compartments was not undertaken for all the genotypes presented in this thesis. However, all the phenotypes observed were made over numerous replicates (n=≥6 individuals, with 5 cells imaged per gland), and a copy of this data has been deposited with the Wilson lab.

2.16 Exosome secretion assay

Exosome secretion was measured using a previously described approach (Corrigan *et al*., 2014, Redhai *et al*., 2016), in which three areas of lumenal *CD63-GFP* fluorescent puncta (exosomes or exosome aggregates) were sampled within the central third of each gland. Identical microscope settings and equipment were used throughout. At each sampling location, three different z-planes were analysed, spaced by 5 µm, with the first image in the z-stack located exactly 5 µm apical to the main cell nuclei. This helped to ensure similar levels of detectable fluorescence between glands.

The raw data from each lumenal area was thresholded in ImageJ2 using the Kapur-Sahoo-Wong (Maximum Entropy) method (Kapur *et al*., 1985) to determine the outlines of *CD63-GFP* fluorescent particles. The 'Analyse Particles' function was then used to determine the total fluorescent area per sample. This analytical method was chosen in preference to particle counting, which can underrepresent clusters of small vesicles. The mean fluorescent

area from the three independent sample areas was then calculated for each gland (n=10).

2.17 Measuring ILV fluorescence

Living secondary cells from 6-day-old *CD63-GFP*-expressing flies (± RNAis) were imaged using identical settings by wide-field microscopy. Prior to image analysis, the contrast of each image was enhanced in ImageJ2 using a 'Rolling-Ball background subtraction', with a radius set at 50 pixels. The ILVs within the largest ten non-acidic compartments of each cell were then analysed by manually drawing an ellipse approximately 250 nm inside their limiting membrane, and the fluorescence intensity profile within this ellipse was measured. To further account for background fluorescence, the same ellipse was then used to measure fluorescence in a 'dark' extracellular region (in which fluorescent puncta are highly dispersed and therefore produce minimal signal), which was subtracted from the compartment fluorescence. The mean ILV fluorescence per compartment was calculated from these data for three individual secondary cells from each gland (n=3).

2.18 ILV diameter

Super-resolution 3D-SIM images of living secondary cells expressing *CD63-GFP* were used to determine the diameter of individual ILVs within non-acidic compartments. Careful manual measurements were taken of the diameters of ILVs within individual compartments using the line tool in ImageJ2. Many ILVs were smaller than the resolution limits of 3D-SIM, and were visualised as

individual bright puncta (<100 nm diameter). The three largest compartments per secondary cell were analysed by this method and the mean calculated from three separate secondary cells in each gland (n=3).

2.19 Sample preparation for electron microscopy

All electron microscopy techniques were developed in collaboration with Dr Errin Johnson, with training and assistance from Dr Anna Pielach, at the Sir William Dunn School of Pathology's Electron Microscopy Facility. Broadly, two main forms of sample preparation were used: 1) a chemical fixation method and 2) a high pressure freezing (HPF) method.

2.19.1 Chemically fixed accessory glands for ultrastructural analysis

Micro-dissection was performed at room temperature (~22°C) in a fume cupboard (Fumair). The accessory glands were micro-dissected from anaesthetised flies submerged in a drop of fixative solution containing 2.5% w/v glutaraldehyde (Agar Scientific, a subsidiary of Elektron Technology), 4% w/v aqueous methanol-free EM grade paraformaldehyde (Agar Scientific) and 0.1M PIPES buffer (Sigma-Aldrich®) in filtered deionised water (Milli-Q®, Merck) at pH 7.2. It was necessary to remove the reproductive tissues from the body cavity in one motion and separate away the testes quickly; the physical hardening of the tissues, caused by the fixative, made accessory glands susceptible to damage or loss during micro-manipulations. The isolated glands were then transferred to fresh fixative solution in 2 ml

Eppendorf tubes using a glass Pasteur pipette and left at room temperature for 1 hour, before being incubated overnight at 4°C.

Samples were first washed three times in 0.1M PIPES buffer for 15 minutes each, before being transferred to a secondary fixative solution consisting of 1% w/v osmium tetroxide (TAAB Laboratories) in 0.1M PIPES buffer and incubated at 4°C on a rotator (Agar Scientific). The glands were then washed five times with Milli-Q® water for 15 minutes each before being incubated overnight with a tertiary fixative solution consisting of 0.5% w/v aqueous uranyl acetate (TAAB Laboratories) at 4°C in the dark. Samples were washed three time with Milli-Q® water for 10 minutes each and then taken through an ethanol (VWR Chemicals) dehydration series of 30%, 50%, 70%, 80%, 85%, 90%, 95% ethanol on ice for 15 min each step. A final set of three 30 minute long incubations in 100% dry ethanol on ice completed the dehydration steps. Samples were then gradually infiltrated with an epoxy resin, made from a Premix Kit of Medium Grade Low Viscosity Resin (TLV, TAAB). All of the resin infiltration steps were undertaken at room temperature using the rotator in a fume cupboard. Glands were first incubated with a 3:1 mix of 100% dry ethanol:resin for 2 hours, followed by a 1:1 mix for 3 hours, and then a 1:3 mix for 2 further hours. The samples were then left overnight in 100% resin, which was replaced with fresh 100% resin twice the next day, and then left overnight again. The resin was changed the following morning and 8 hours later the glands were carefully transferred to embedding capsules (BEEM®), topped with fresh 100% resin. Glands were manoeuvred to the bottom of the capsule using a toothpick. Finally, the resin was polymerised into hard blocks at 60°C in an oven (Shel Lab®) for 40 hours.

2.19.2 High Pressure Freezing (HPF) and freeze substitution of accessory glands for ultrastructural analysis

Accessory glands were micro-dissected in ice-cold 1× PBS (as described previously) and maintained on ice in a clear 1.7 ml microfuge tube containing 1× PBS until processed. Glands were transferred using a glass Pasteur pipette to a small drop of ice-cold 1× PBS on a plastic petri-dish lid. Using the EMZ dissection microscope (previously described; Meiji Techno) the glands were then carefully manoeuvred out of the 1× PBS drop into adjacent pools of cryo-protectant solutions by holding the ejaculatory bulb with forceps and dragging them through the solutions to coat them. We tested a range of cryo-protectants including bakers yeast mixed with 10% v/v methanol (Sigma-Aldrich®) in Milli-Q water to form a yeast paste, 1-hexadecane (Sigma-Aldrich®), and 1.5% w/v low melting point agarose (Thermo Fisher Scientific). Once each gland was coated with a cryo-protectant, it was transferred using forceps into the well of a membrane carrier (1.5 mm diameter, 100 µm deep, Leica), until the well contained 3-5 glands. Care was taken to not create any bubbles, nor to spill excess solution over the top of the well. The carriers for samples coated in 1-hexadecane were themselves pre-coated with the same material.

The sample-filled carriers were then loaded into bayonet pods (Leica) and transferred using a manual loading device (Leica) to the high pressure freezer (EM PACT2, Leica). The HPF unit froze samples automatically with liquid nitrogen at 2000 bar, to ensure that vitreous ice, and not ultrastructurally damaging crystalline ice, formed throughout the sample. After freezing, the pod containing the carrier was released into a bath of liquid nitrogen. The

sample carrier was separated out of the pod using pre-cooled metal tweezers, and transferred to a numbered well within the bath in preparation for freeze substitution.

Once several samples were frozen, the carriers were carefully moved into pre-cooled 2 ml screw top cryotubes within the sample chamber of an automatic freeze substitution unit (EM AFS2, Leica), which was set to -130 °C. The samples were freeze substituted in either of two different pre-cooled solutions: 1) 0.5% w/v uranyl acetate and 2% w/v osmium tetroxide in 100% dry acetone (Thermo Fisher Scientific), or 2) 0.5% w/v uranyl acetate, 2% w/v osmium tetroxide and 0.1% w/v tannic acid (Emscope) in 100% dry acetone. The protocol for freeze substitution is provided below. During freeze substitution, the acetone solvent caused dissolution of ice from the specimen, which allowed the samples to warm up without ice crystals growing and damaging the specimen (McDonald *et al*., 2007). The presence of stains such as uranyl acetate, osmium tetroxide and tannic acid in the solvent improved ultrastructural contrast in the tissue.

Freeze substitution protocol:

Step	Temperature 1	Temperature 2	Slope	Duration
1	-130 °C	-90 °C	20°C / h	2 h
2	-90 °C	-90 °C	-	6 h
3	-90 °C	-60 °C	5°C / h	6 h
4	-60 °C	-60 °C	-	2 h
5	-60 °C	-25 °C	5°C / h	7 h
6	-25 °C	-25 °C	-	12 h
7	-25 °C	0 °C	5°C / h	5 h

When the freeze substitution program was completed, samples were incubated at 4°C for 10 minutes, rinsed with ice-cold 100% dry acetone for 10 minutes at room temperature, then twice with room temperature 100% dry acetone for 15 min each. The carriers and acetone were then transferred into small aluminium dishes (Agar Scientific), wherein the samples were carefully prized out of the well in the carrier using fine forceps. The samples were then moved using a plastic Pasteur pipette into clear 2 ml tubes containing 100% dry acetone in preparation for resin infiltration. Samples were infiltrated with epoxy resin and embedded as described above, except that acetone was used, rather than ethanol, for the resin infiltration series.

2.20 Ultramicrotomy

Polymerised resin blocks containing the accessory gland samples were sectioned using an ultramicrotome (Ultracut 7, Leica).

2.20.1 Semi-thin sections

Blocks were manually trimmed to a rough trapezoid shaped pyramid using feather razor blades. Semi-thin sections of 0.5 µm were cut using a glass knife with a Milli-Q® water-filled boat. Sections were transferred onto a drop Milli-Q® water on a clean glass slide using a wire loop or eyelash brush. The slide was then heated on a hot plate set at 60°C to evaporate the water and to flatten the sections onto the slide. Sections were stained in a drop of filtered 1% w/v Toluidine blue (Sigma-Adrich®) and 1% w/v sodium borate (Sigma-Adrich®) on the hotplate for approximately 20 seconds. The excess staining solution was then rinsed off in a glass beaker of Milli-Q® water, and the slides were dried on the hot plate. Finally, the sections were checked under a light microscope (MS160, Carson) to help target an area of the sample for ultra-thin sectioning.

2.20.2 Ultra-thin sections

Once an area of interest had been identified from the semi-thin sections, the block was carefully trimmed using a razor blade to a small trapezoid shaped pyramid (roughly 0.5 x 0.5 mm). Ultrathin sections of 50-90 nm thickness were obtained using a 45° Ultra diamond knife (DiATOME) with a Milli-Q® water-filled boat. The floating sections were stretched out using chloroform (Sigma-Adrich®), which was absorbed into a piece of Whatman® filter paper and carefully hovered over the sections. A wire loop was then used to transfer

sections onto 200 square mesh copper grids (Agar Scientific), which were laid flat on a piece of filter paper. Alternatively, sections were collected directly on a formvar (TAAB Laboratories) coated copper slot grid (Agar Scientific) by using forceps to bring the grid up and under the floating sections and an eyelash brush to orient the sections appropriately. This method ensured grid lines did not obscure the specimen during imaging.

HPF sections were post-stained for 5 minutes in a 20 µl drop of filtered 2% w/v aqueous uranyl acetate protected from light exposure by an aluminium foil-covered petri dish lid. All solutions used during staining procedures were placed on strips of Parafilm M® (Bemis). After staining, the sections were washed seven times in 20 µl drops of warmed Milli-Q® water for 5 seconds each, before a final eighth wash for 1 minute. Both chemically fixed and HPF sections were post-stained for 5 minutes in a 20 µl drop of filtered lead citrate (Reynolds, 1963) surrounded by sodium hydroxide pellets (Thermo Fisher Scientific) and kept inside a closed petri dish. This helped to prevent the lead citrate reacting with atmospheric CO_2 and forming lead carbonate precipitates. The sections were then washed seven times in 20 µl drops of warmed Milli-Q® water for approximately 5 seconds each, before a final eighth wash lasting 1 minute. The warm Milli-Q® water had been previously boiled in a microwave for 1 minute to remove dissolved CO_2, which could react with the lead citrate. Finally, the grids were carefully transferred onto a piece of filter paper to dry and then stored in a grid box.

2.21 Transmission Electron Microscopy (TEM)

Samples were imaged using a Tecnai T12 Transmission Electron Microscope (FEI, a subsidiary of Thermo Fisher Scientific) operated at 120kV with a OneView CMOS digital camera (Gatan).

2.22 Cloning and generation of new transgenic lines

The cloning of two new fusion protein constructs under UAS control, *UAS-CD63-mCherry* and *UAS-eGFP-dHrs*, was performed by S-J. Fan, a postdoctoral scientist in the Goberdhan Lab. The pUAST vector (Flybase ID: FBmc0000383) was used in both cases to generate the transgenic flies.
For *UAS-CD63-mCherry*, pUAST-mCherry was generated first and then full length human *CD63* inserted into the vector. To generate pUAST-mCherry, a 5' primer bearing a KpnI site and a 3' primer bearing an XbaI site was used to amplify the mCherry coding sequence using PCR and the resulting PCR fragment was cloned into KpnI/XbaI digested pUAST plasmids. Then a 5' primer bearing an EcoRI site and a 3' primer bearing a BglII site was used to amplify the CD63 coding sequence using PCR, with the resulting PCR fragment was cloned into an EcoRI/BglII digested pUAST-mCherry plasmids.
For *UAS-eGFP-Hrs*, pUAST-eGFP was generated first and then full length *Drosophila Hrs* inserted into this vector. To generate pUAST-eGFP, a 5' primer bearing an EcoRI site and a 3' primer bearing a BglII site was used to amplify the eGFP coding sequence using PCR, and the resulting PCR fragment was cloned into EcoRI/BglII digested pUAST plasmids. Then a 5' primer bearing a NotI site and a 3' primer bearing a KpnI site was used to

amplify *Hrs* coding sequence using PCR and the PCR fragment formed was cloned into NotI/KpnI digested pUAST-eGFP plasmids.

Microinjection of the genetic constructs into embryos was performed by Bestgene®, and the resulting transformant lines mapped in the lab to the level of chromosome and maintained using appropriate balancers. M. Wainwright, a postdoctoral scientist in the Wilson lab, mapped the *UAS-CD63-mCherry* fly line used in this work. I performed the mapping of the *UAS-eGFP-dHrs* fly line.

2.23 Statistical Analysis

All data were collated using Excel (Microsoft) and subsequently analysed using SPSS Statistics (IBM). The Shapiro-Wilk Test was used to assess normality of the datasets, and Levene's Test was used to evaluate equality of variances. If the datasets were normally distributed and showed equal variance between groups, then a One-Way ANOVA Test was employed, with post-hoc Dunnett's Two Tailed T Tests used to directly compare control and experimental groups. If datasets were not normally distributed and/or showed unequal variance between groups, then a Kruskal-Wallis Test was performed, with post-hoc Bonferroni-adjusted pairwise Mann-Whitney-Wilcoxon Tests used to compare control and experimental groups.

3.0 Characterisation of secondary cells by light and electron microscopy

3.1 Introduction

Previous work in the Wilson lab had demonstrated that the unusual morphology of *Drosophila* secondary cells makes them ideal for the study of evolutionarily conserved secretory processes (Corrigan *et al*., 2014, Redhai *et al*., 2016). As a first step in advancing these studies, this chapter is focused on the characterisation of the organisation, structure and identity of the intracellular compartments in secondary cells, employing a range of advanced methods. I have undertaken an ultrastructural electron microscopic analysis of secondary cells. I have used a combination of immunological techniques and fluorescent fusion proteins to identify specific structures, and to determine the localisation of important regulatory molecules. I systematically describe the localisation of almost all of the *Drosophila* Rab GTPases in secondary cells using a collection of flies that express YFP-tagged Rab fusion proteins from their endogenous genetic elements. I have also developed the use of multiple imaging methods, including super-resolution light microscopy and differential interference contrast (DIC), to help improve our understanding of their underlying cell biology.

3.1.1 Secondary cells contain extremely large subcellular compartments with different morphological features and physiological properties

The accessory gland epithelium is composed of two binucleate cell types, main cells and secondary cells, which are morphologically distinct and have different gene expression profiles (Bairati, 1968; Bertram *et al*., 1992;

Corrigan, 2014; Leiblich, 2015). The first ultrastructural study of the epithelium noted some of the differences between the two cell types (Bairati, 1968). Secondary cells had a rich network of rough endoplasmic reticulum, numerous Golgi complexes and mitochondria, and contained 1-2 remarkably large vacuoles, in addition to several large oval shaped compartments that contained dense-core granules surrounded by tubular filaments, termed 'filamentous bodies'. The other cell type, main cells, contained extensive rough endoplasmic reticulum and abundant Golgi complexes, but no very large intracellular or dense-core granule compartments. Recent ultrastructural studies of secondary cells in the Wilson lab have confirmed some of these observations and extended the characterisation to large late endosomal or lysosomal compartments, visualised using the Lysotracker-Red dye, which concentrated within the acidic lumens of these compartments, and smaller organelles, such as early and putative recycling endosomes (Corrigan *et al*., 2014; Redhai *et al*., 2016, Redhai, 2016).

3.1.2 Rab GTPases help define different types of subcellular compartments in secondary cells

The Rab GTPases, as described in Section 1.3, are important regulators of membrane trafficking and compartment identity (Wandinger-Ness & Zerial, 2014). Particular Rabs associate with specific subcellular organelles, enabling the identification of different organelles using either immunofluorescent techniques or by expression of fluorescently tagged Rab fusion proteins (Riedel *et al*., 2016; Dunst *et al*., 2015). The first study to characterise secondary cell compartments by their association with different Rabs utilised

a set of overexpressed YFP-tagged Rabs (using both UAS and tubulin promoter sequences), including Rab5, Rab7 and Rab11 (Corrigan *et al*., 2014; Marois *et al*., 2006). This work identified YFP-Rab5 on several small non-acidic compartments, presumably early endosomes, whilst YFP-Rab7 primarily localised to the surface of large and small acidic compartments, marking late endosomes or lysosomes, and YFP-Rab11 was enriched on the surface of the large non-acidic dense-core granule compartments. However, un-physiological expression levels of these YFP-Rab fusion proteins may alter membrane trafficking. A comprehensive set of 27 individual YFP-tagged Rabs expressed under the control of their endogenous genetic elements has recently been developed (Dunst *et al*., 2015). Some of these valuable YFP-Rab gene trap lines have already been studied in secondary cells, including Rab1, Rab6 and Rab11 (Redhai, 2016). YFP-Rab1 was found in a Golgi-like region, whilst Rab6 and Rab11 localised on the large non-acidic compartments. However, the majority of *Drosophila* Rab GTPases have not yet been studied in secondary cells, even though many of them may be playing important roles in the secretory biology of these cells.

3.1.3 Novel imaging techniques are revolutionising our ability to study secondary cell biology

Fluorescence imaging is particularly well suited for the study of cell biology, as it is non-invasive, highly sensitive, and has powerful spatial and temporal resolution (Ball *et al*., 2012). These advantages help to explain why most of the recent studies of secondary cells relied heavily upon fluorescence microscopy (Redhai *et al*., 2016; Sitnik *et al*., 2016). This trend is likely to

continue, as new super-resolution imaging methods, such as 3-dimensional structured illumination microscopy (3D-SIM; Gustafsson *et al*., 2008; Gustafsson, 2000), have now improved the achievable resolution beyond the diffraction limit, bridging the resolution gap between light and electron microscopy (Cox, 2015). However, many super-resolution techniques require high levels of light, which can be toxic to cells and bleach weakly fluorescent specimens, so only specific techniques can be combined successfully with living cells. Given that the subcellular compartments of secondary cells are highly sensitive to fixation (Corrigan *et al*., 2014), I chose to apply 3D-SIM, one of the most amenable super-resolution methods for live-cell imaging, to further clarify their detailed cell biology at double the resolution in both lateral and axial dimensions (Demmerle *et al*., 2017).

Confocal microscopy has been a popular choice for live-cell imaging of secondary cells (Redhai *et al*., 2016; Corrigan *et al*., 2014), as it can produce high quality 3D images with relatively low background fluorescence. However, wide-field microscopy remained a good alternative because of its higher sensitivity (Ball *et al*., 2012). Furthermore, the combination of wide-field microscopy with 3D deconvolution algorithms, which use the out-of-focus light to reconstruct the in-focus object, has greatly improved the resulting image quality. Some studies have shown that deconvolved wide-field images can achieve greater contrast than confocal, especially when the out-of-focus background is low (Murray *et al*., 2007).

Despite these developments in light microscopy, the resolution power of electron microscopy for ultrastructural studies remains greater. As previously noted (Section 3.1.1), electron microscopy has been performed on the

accessory gland to study secondary cells (Bairati, 1968; Chen, 1984; Corrigan *et al*., 2014). All of these studies utilised conventional chemical-fixative based techniques to preserve the cell's ultrastructure, with mixed results, as these cells are extremely sensitive to fixative. However, technological advances in Cryo-fixation methods for electron microscopy are enabling larger samples of accessory gland size to be readily prepared. Given that cryo-fixation is known to produce the closest approximation of a cell's native state (McDonald, 2007), it was important to perform a comparative analysis between this and conventional chemical-fixative approaches.

3.1.4 Chapter aims

In this chapter, I aim to characterise the subcellular compartments of secondary cells in greater detail than has previously been undertaken, using new molecular markers and improved microscopy techniques. Furthermore, I hope to demonstrate that light and electron microscopy studies complement one another to improve our understanding of secondary cell biology.

- Describe new ultrastructural features of secondary cells using electron microscopy
- Define the organisation of subcellular compartments within secondary cells using novel immunological markers and DIC microscopy
- Characterise the association between Rab GTPases and the different subcellular compartments of secondary cells
- Demonstrate the utility of super-resolution light microscopy in the visualisation of sub-compartmental cell biology

3.2 Results

3.2.1 Defining the organisation and ultrastructure of secondary cell intracellular compartments

3.2.1.1 Secondary cells are specialised, polarised secretory epithelial cells in the male accessory glands

Secondary cells have been developed in the Wilson lab as a model system to study cell biological processes, including the signalling pathways that underlie regulatory mechanisms of cell growth, exosome biogenesis and other forms of secretory cell biology (Leiblich *et al*., 2012; Corrigan *et al*., 2014; Redhai *et al*., 2016). Previous work by the lab has included careful investigations into secondary cell subcellular biology, but I undertook a more detailed analysis, enabled by novel genetic, immuno and microscopy tools.

Most of the reproductive system from a non-transgenic 6-day-old w^{1118} male fly, including the two accessory glands, was visualised by DIC microscopy (Figure 3.1A). As previously reported, the glands consisted of a monolayered epithelium of binucleate cells surrounded by a layer of striated muscle cells (Leiblich *et al*., 2012; Susic-Jung *et al*., 2012). Immunofluorescent microscopy showed that the secretory epithelium was composed of two cell types: 1) the numerous prismatic main cells, which are distributed throughout the gland, and 2) the less populous, but larger, secondary cells, which cluster at the distal tips of the glands, and can be identified by their large subcellular compartments, many of which contain angiotensin I-converting enzyme (ANCE; Figure 3.1B-D; Rylett *et al*., 2007). A single layer of striated muscle cells surrounded the epithelium and was distinguished by its actin-rich

contractile filaments, which stained strongly with Phalloidin-TRITC. Most of the apical and lateral plasma membrane of the secondary cells appeared in direct contact with main cells. However, junctional contacts between the two cell types were only found apically, where the main cells spread out thinly over the secondary cells, and were observed by staining for the cell-cell adhesion molecule Fasciclin 3 (Fas3). Direct secretion from secondary cells can occur into the accessory gland lumen through a specialised region of the apical plasma membrane, which was identified by cortical actin and the absence of Fas3 (Figure 3.1E).

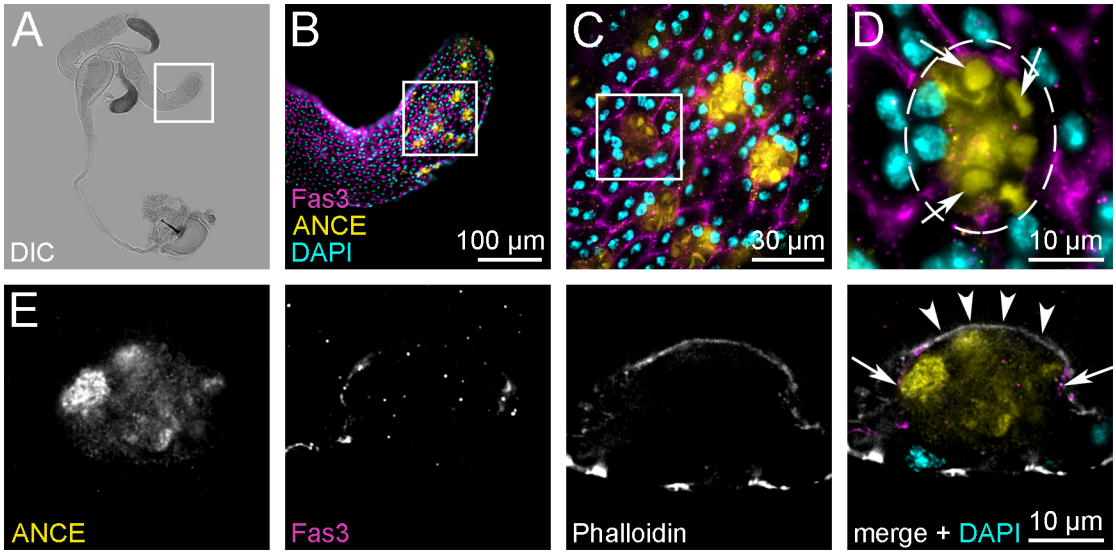


Figure 3.1 Secondary cells are a specialised epithelial cell type in *Drosophila melanogaster* male accessory glands

(A) Most of the *Drosophila* male reproductive tract, including the accessory glands, seminal vesicles, ejaculatory duct and ejaculatory bulb, but minus the testes, is shown here using DIC imaging. The box region highlights the tip of an accessory gland, magnified in B. During mating, the muscular layers surrounding these tissues contract to facilitate the transfer of sperm from the testes and accessory proteins (Acps) from the accessory glands to the female.
(B-D) The accessory gland epithelium is composed of two cell types. Secondary cells are specifically positioned at the distal tips of each accessory gland. They can be distinguished by immunostaining for the angiotensin I-converting enzyme (ANCE; yellow; arrow in D), which is stored in dense-core granules within specialised intracellular organelles. Main cells are found throughout the accessory gland length, and are shown by nuclear staining with DAPI (cyan). All of the cells in the accessory glands are bi-nucleate. The septate junctions between cells are immunolabelled here with a Fasciclin 3 antibody (Fas3; magenta). These junctions show that the numerous main cells have a characteristically hexagonal shape (C), and that they surround individual secondary cells.
(E) Secondary cells bulge out into the accessory gland lumen, but are surrounded by main cells along most of this surface. Their actin-rich apical cortex (arrowheads), with apical membrane in direct contact with the accessory gland lumen, is characterised by Phalloidin-TRITC staining (white), and the absence of cell-cell junctions (Fas3; arrows).

The accessory glands and secondary cells presented here are from six-day-old virgin non-transgenic w^{1118} flies incubated at 28.5°C since eclosion.

3.2.1.2 Electron microscopy of accessory glands highlights the compartmental organisation and diversity in secondary cells

Previous ultrastructural studies of the accessory glands have proven instrumental to our understanding of the cells in this secretory tissue (Bairati, 1968; Corrigan *et al*., 2014). However, limits to the quality of tissue preservation, particularly for secondary cells, have made it difficult to clearly link light and electron microscopy studies before. The ultrastructure of chemically fixed secondary cells was studied using electron microscopy, employing carefully developed and tested protocols for *Drosophila* tissue in collaboration with E. Johnson (Figure 3.2A-A''). The tissue preserved well, as demonstrated by the maintenance of cristae networks within the secondary cell's numerous mitochondria (Figure 3.2B-B'). However, some secondary cells had broken away from the underlying and neighbouring main cells, particularly at their basolateral surfaces (Figure 3.2A-A''). This may reflect the lack of cell-cell adhesion molecules, such as Fas3 and E-Cadherin, at the basolateral portions of these cells (Sections 3.2.1.1 and 3.2.1.8).

Each secondary cell contained extensive rough endoplasmic reticulum, indicative of high protein production. The basally localised nuclei were relatively heterochromatin-sparse (Figure 3.2C). Several large vesicular Golgi networks were observed, some centrally located, and others scattered throughout the cell, often in close proximity to large subcellular compartments (Figure 3.2D). Each Golgi cluster was composed of multiple layers of vesicles, with 2-3 medial tubular sacs separating the cis- and trans-vesicular networks (Figure 3.2B).

This ultrastructural study revealed for the first time the detailed internal structure of the large acidic compartments, which exhibited ‘secondary lysosome’ morphology (Figure 3.2E-E’’). These compartments contained many electron-dense degradative structures, large membranous whorls, small intraluminal vesicles (ILVs), and numerous autophagic structures, such as ribosomes and mitochondria. Much smaller, tubular-shaped endosomes, filled with ILVs, were also observed (Figure 3.2F).

A number of large electron-lucent compartments, some of which contained amorphous precipitates and a small number of fibre-like structures, were also characterised for the first time. They varied in size and shape – some were very large but irregular in morphology, and others smaller but more rounded (Figure 3.2G-G’), potentially equivalent to the different non-cored compartments observed with DIC. A strikingly different and previously reported population of large compartments, which contained electron-dense granules surrounded by a meshwork of fibres, were also observed (Figure 3.2H). The dense-core material was occasionally found in direct contact with the limiting membrane. The compartments contained a number of small ILVs, found in close proximity to the dense-core granule (Figure 3.2I). Between the fibrous regions of the compartments, electron-dense pathways connected the dense-core granule and the limiting membrane. However, the fibres were distanced away from each other by approximately 20 nm, and had an excluding electron-lucent ~15nm zone surrounding them (Figure 3.2J). Transverse sections though the fibres revealed that they were made of 10 subunits, which formed a tube-like structure with a ~30 nm diameter (Figure 3.2J’). Longitudinal sections revealed a repeating, striped pattern along the

length of these tubes (Figure 3.2J''). This banding pattern correlated well with previous observations (Perotti, 1972).

The fibrous dense-core granule compartments were found in both basal and apical portions of secondary cells, and in some cases in close proximity to the apical surface of the cell (Figure 3.2K). The apical surface of the secondary cell in direct contact with the lumen was relatively smooth, and had just a few small finger-like projections (Figure 3.2K).

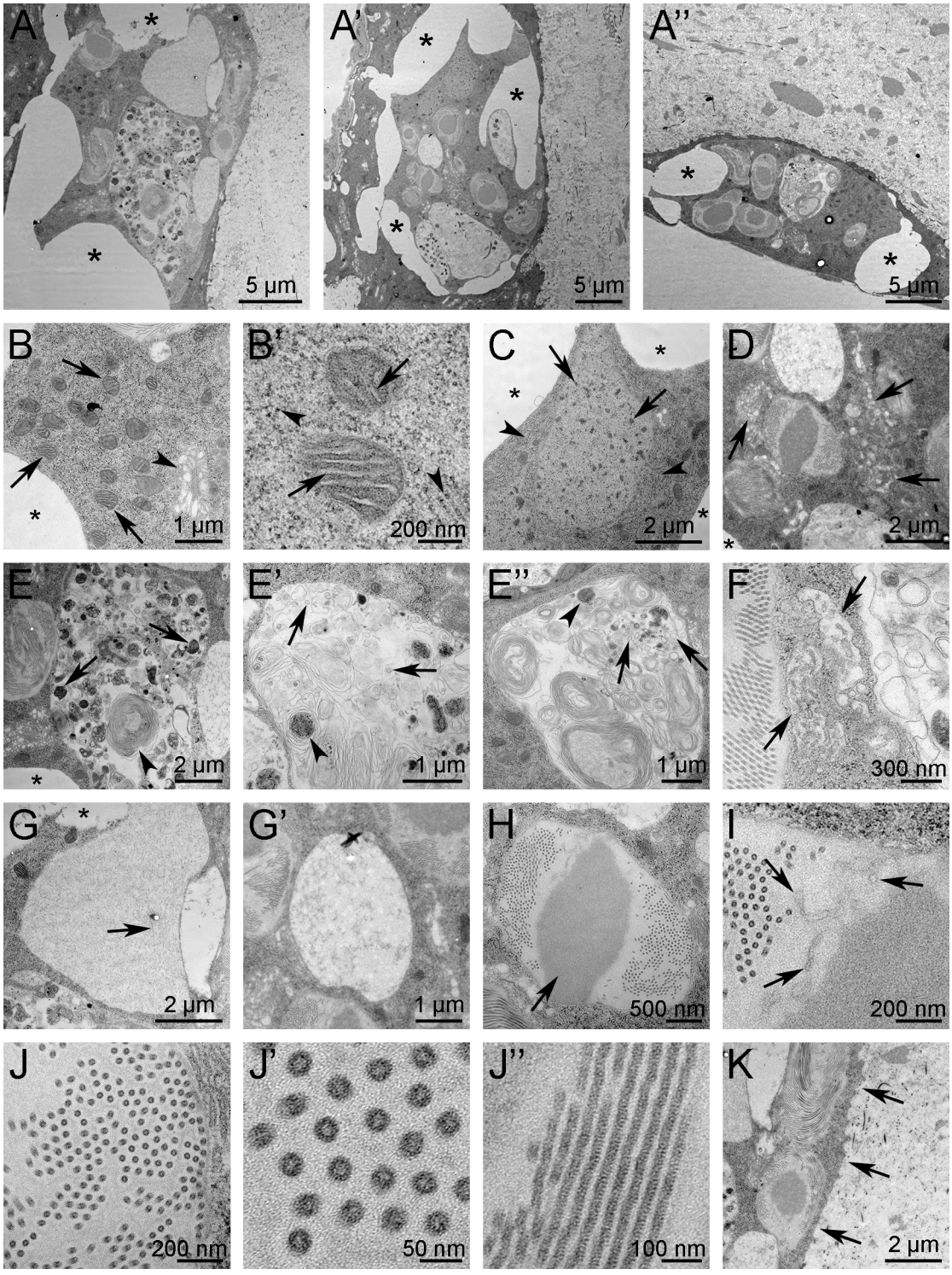

A
A'
A''
5 µm
5 µm
5 µm
B
B'
C
D
1 µm
200 nm
2 µm
2 µm
E
E'
E''
F
2 µm
1 µm
1 µm
300 nm
G
G'
H
I
2 µm
1 µm
500 nm
200 nm
J
J'
J''
K
200 nm
50 nm
100 nm
2 µm

Figure 3.2 Ultrastructural characterisation of secondary cells using chemically fixed specimens

Electron microscopy was undertaken in collaboration with E. Johnson. These panels show images of chemically fixed secondary cells from 6-day-old virgin transgenic males selectively overexpressing CD63-GFP. Flies were incubated at 28.5°C since eclosion to induce CD63-GFP expression using the GAL4-GAL80^{ts}-UAS system.
(A-A'') Secondary cells have detatched from their neighbouring main cells (areas marked with '*****').
(B) Numerous mitochondria (arrows) and organised Golgi compartments (arrowhead).
(B') Mitochondrial cristae are well preserved.
(C) Secondary cells contain extensive rough endoplasmic reticulum (arrowheads), and their nuclei (arrows) are relatively heterochromatin-poor.
(D) Numerous large vesiculated Golgi networks (D) are seen throughout the cell, in between different subcellular compartments.
(E) Several large compartments show morphological characteristics of secondary lysosomes, including membranous whorls (arrowheads), and electron-dense structures (arrows). (E') Some autophagic structures including ribosomes (arrowhead) are seen, in addition to numerous small ILVs (arrows).
(E'') More ILVs (arrows) and a mitochondria (arrowhead).
(F) Tubular endosomal compartment containing some ILVs (arrows)
(G-G') Morphologically heterogeneous non-cored compartments, some of which contain small fibers (arrow).
(H) Dense-core granule compartment, at higher magnification in (I), where numerous ILVs are observed (arrows).
(J-J'') The fibrous components of these compartments are banded and have electron-lucent exclusion zones.
(K) The apical surface the secondary cell is relatively smooth.

The specific genotype of these males is: *w; UAS-CD63-GFP, tub-GAL80ts / +; dsx-GAL4 / +*.

3.2.1.3 Cryo-electron microscopy of accessory glands identifies novel intracellular compartments and ultrastructural characteristics

In order to better understand the ultrastructure of secondary cells from wild type flies, the accessory glands from 6-day old non-transgenic w^{1118} flies were analysed by cryo-electron microscopy. Compared to the chemically fixed specimens (Figure 3.3), secondary cells did not stain notably differently to main cells using this technique, but were easily identified based on ultrastructural features (Figure 3.3A-A'). The secondary cells had separated away from their neighbouring main cells at the basolateral surfaces, but not to the same extent as in chemically fixed glands (Figure 3.3A-A'). In these separation sites, small finger-like protrusions from both cell types were observed (Figure 3.3A-A'). Although some tearing of the tissue was evident, likely due to incomplete resin infiltration, the cell morphologies and ultrastructure remained extremely well preserved, as demonstrated by the maintenance of cristae networks within the secondary cell's mitochondria (Figure 3.3J).

The secondary cells contained numerous dense-core granule compartments of differing morphologies (Figure 3.3B-B'). Some of the compartments appeared constrained by the fibrous network enwrapping them (Figure 3.3B). Interestingly, the dense-core granules were more electron-dense at their peripheries than at their central region, with the density particularly localised in subdomains, suggesting some subcompartmental heterogeneity in the dense-core granule's molecular nature (Figure 3.3B-C). Small ILVs (~100 nm diameter) were also observed within these dense-core granule compartments,

often adjacent to the dense-core granule, and also seen clustering closer to the limiting membrane of the compartment (Figure 3.3C-C').

These micrographs also clearly illustrated, for the first time, details about the centrally located, electron lucent non-cored (likely Rab6-positive) compartment (Figure 3.3D-D''). This large compartment appeared to be surrounded by Golgi cisternae, which consisted of numerous vesicular sacs, comparable to later observations using light microscopy (Section 3.2.1.5). The compartment contained highly invaginated regions in its limiting membrane (Figure 3.3D'). Although the interior of the compartment was mostly electron lucent, a small number of electron dense fibres were observed, of the same diameter (~30 nm) as those in the dense-core granule compartments (Figure 3.3D''). Given the evidence discussed later (Section 5.2.1) that these compartments are precursors of dense-core granule compartments, this suggest that some fibres form in advance of the dense-core granule.

Occasionally, a large compartment containing diffuse fibers was observed, with some electron-dense material in small subdomains (Figure 3.3E). This could potentially be a novel intermediate type of compartment between the non-cored and the dense-core granule compartments.

Some high power imaging of the Golgi apparatus showed that large vesicles were being formed in the trans-Golgi network, which contained some moderately electron-dense amorphous material inside (Figure 3.3H-H'').

The large secondary lysosome compartments showed some similarities to those seen using the chemical fixation approach: they contained numerous small ILVs, large concentric membranous whorls and electron-dense amorphous materials (Figure 3.3F-F'').

Several small multivesicular bodies were observed, again a novel finding (Figure 3.3G). These organelles were of a size similar to those observed in mammalian cells (300-400 nm diameter) and contained ILVs measuring <50 nm in diameter.

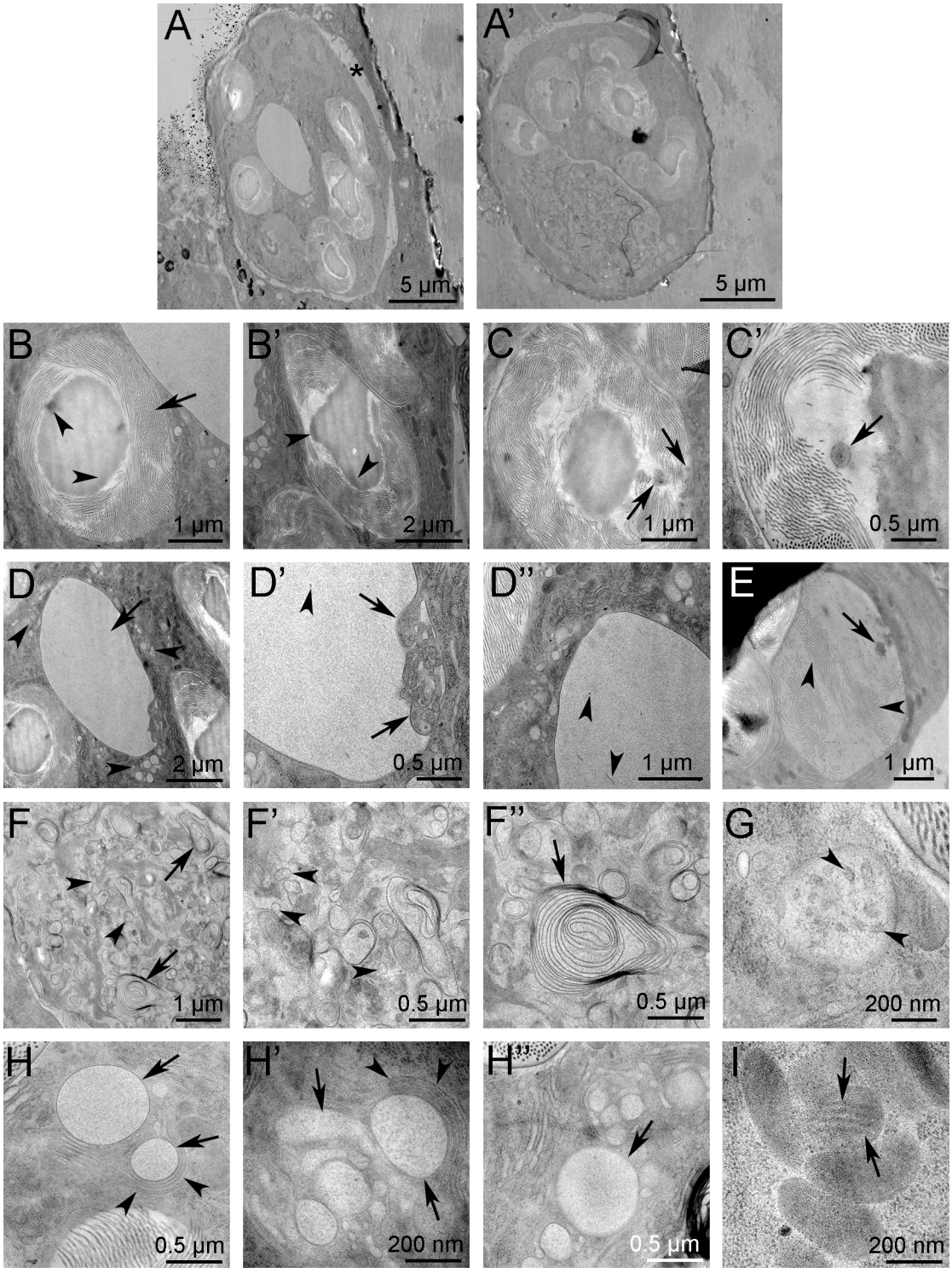

A
*
5 µm
A'
5 µm
B
1 µm
B'
2 µm
C
1 µm
C'
0.5 µm
D
2 µm
D'
0.5 µm
D''
1 µm
E
1 µm
F
1 µm
F'
0.5 µm
F''
0.5 µm
G
200 nm
H
0.5 µm
H'
200 nm
H''
0.5 µm
I
200 nm

Figure 3.3 Cryo-EM of non-transgenic *w*^{1118} characterises compartment subtypes in a more 'native' state

Cryo-EM was performed in collaboration with E. Johnson. These panels show images of the subcellular compartments in secondary cells from 6-day-old virgin non-transgenic *w*^{1118} males. Flies were incubated at 28.5°C following eclosion.
(A) Secondary cells have not separated much from their neighbouring main cells (region marked with a '*').
(B-B') Dense-core granules have electron-dense subdomains at their peripheries (arrowheads). Fibers wrap tightly around the dense-core granule (arrows).
(C-C') ILVs are observed within the dense-core granule compartments (arrows), some close to the limiting membrane and others further towards the dense-core granule.
(D) The large central non-cored compartment (arrow) is surrounded by small, possibly Golgi-associated, vesicles (arrowheads).
(D'-D'') Highly invaginated membrane extends into the lumen of the large non-cored compartment (arrows). Some small fibers are observed in the lumen (arrowheads).
(E) A large compartment with numerous diffuse fibers (arrowheads), and some clumps of electron-dense material (arrows).
(F-F'') The large acidic compartment contains numerous small ILVs (arrowheads), and large membranous whorls, which have an onion-like structure.
(G) A small MVB containing ILVs (arrowheads).
(H-H'') The Golgi complexes often have large vesicles budding off the trans face (arrows). The medial and cis Golgi cisternae are marked with arrowheads.
(I) Mitochondria with preserved cristae structure.

3.2.1.4 The large subcellular compartments of living secondary cells are differentially localised along the apical-basal axis

Polarity is an important feature of epithelial cells. The correct establishment and maintenance of cell polarity are crucial for normal cell physiology and tissue homeostasis, as it underlies the specialisation of cell function, for example ensuring directionality of secretion (Royer & Lu, 2011). Wide-field and DIC imaging of living non-transgenic 6-day-old w^{1118} secondary cells stained with Lysotracker-Red to mark acidic compartments, revealed the general apical-basal polarity, in relation to their large subcellular organelles (>2 μm diameter). Although each cell was organised slightly differently, a general set of observations was often made. The basal portion contained two nuclei, 4-6 non-acidic, dense-core granule compartments, and 1-2 acidic compartments that often extended apically through the cell (Figure 3.4A). The central region of the cell contained a further 2-3 non-acidic, dense-core granule compartments, and 1-2 non-acidic non-cored compartments, one of which was spherical and the other, usually more irregularly shaped (Figure 3.4B). The apical portion of the cell typically contained 1-2 large non-acidic, dense-core granule compartments, which were occasionally found in close proximity to several small acidic vesicles (<2 μm diameter), and 1-2 large acidic compartments (Figure 3.4C). A generalised schematic showing the different types of intracellular compartments that can be readily distinguished by DIC microscopy and Lysotracker Red staining is given in Figure 3.4D.

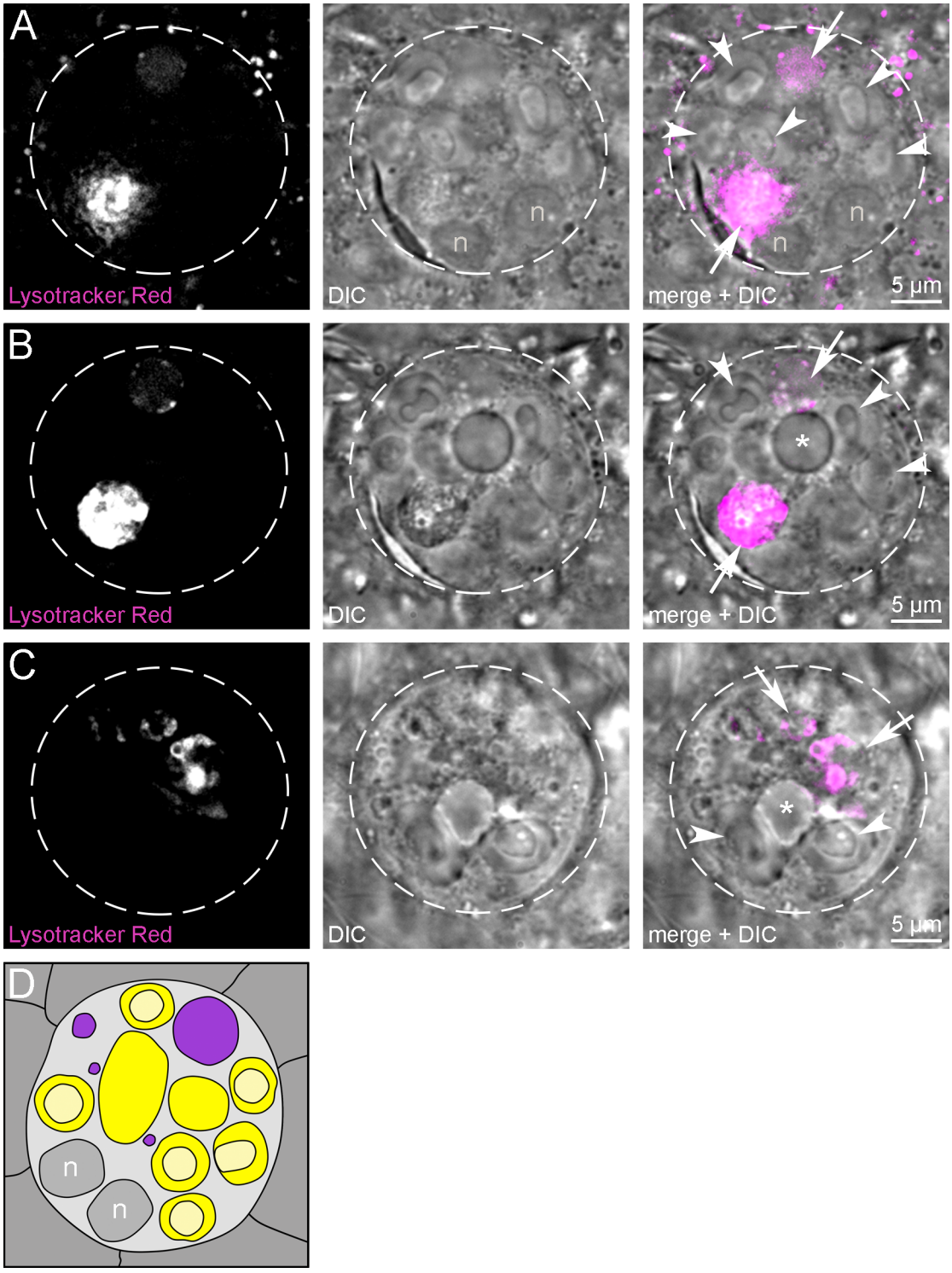

A
Lysotracker Red
DIC
n
n
merge + DIC
n
n
5 µm
B
Lysotracker Red
DIC
merge + DIC
*
5 µm
C
Lysotracker Red
DIC
merge + DIC
*
5 µm
D
n
n

Figure 3.4 Secondary cell organelles have a characteristic apical-basal organisation.

Figure shows three images from a Z stack of a single living secondary cell. (A) The basal portion of a secondary cell contains two nuclei, marked with 'n', several dense-core granule compartments (arrowheads), and 1-2 large acidic compartments, distinguished here using a Lysotracker Red vital dye (magenta; arrows). DIC imaging facilitates the characterisation of all of these organelles: the nuclei have a characteristically dark lumen, the dense-core granule compartments have a 'fried egg' morphology, and the acidic compartments often have a complex mottled lumen.
(B) The central region of the cell often contains a large non-cored compartment, marked with '*', which is surrounded by a 2-3 more dense-core granule compartments (arrowheads), and the large acidic compartments that extend from the basal portion of the cell (arrows). The non-cored compartments are distinguished using DIC imaging by their 'clear' lumen.
(C) The apical portion of the cell often contains 1-2 dense-core granule compartments (arrowheads), in addition to a non-cored compartment, again marked by '*', and a mixture of large and small acidic compartments (arrows).
(D) Schematic representation of a secondary cell's subcellular compartments. The large non-acidic compartments are colourised in yellow. Of these, the dense-core granule containing compartments (light yellow interior) are distinguished from non-cored compartments. The acidic compartments are labelled in magenta. Nuclei are marked with 'n'.

The secondary cells presented here are from six-day-old virgin non-transgenic w^{1118} flies incubated at 28.5°C since eclosion.

3.2.1.5 Super-resolution imaging reveals the structure of the Golgi apparatus in living secondary cells

The Golgi apparatus was visualised in living secondary cells by overexpression of the Golgi marker, *Galtase-GFP*, under UAS control. The marker consists of a truncated form of human β-1,4-galactosyltransferase, a resident enzyme of the Golgi complex, fused to GFP at its C-terminus (Snapp *et al*., 2004). In the *Drosophila* trachea this fusion protein has been used as a trans-Golgi marker (Armbruster & Luschnig, 2012). In secondary cells, *Galtase-GFP* localised to numerous small non-acidic vesicles, many of which surrounded a large non-acidic, non-cored compartment (Figure 3.5A-A'). Additional vesicles marked by *Galtase-GFP* were observed in other regions of secondary cells (Figures 3.5B-B'). Super-resolution imaging of this Golgi marker revealed that many of these regions consisted of collections of small vesicular sacs around the periphery of large compartments (Figure 3.5C-C'), similar to those observed using electron microscopy (Sections 3.2.1.2 and 3.2.1.3).

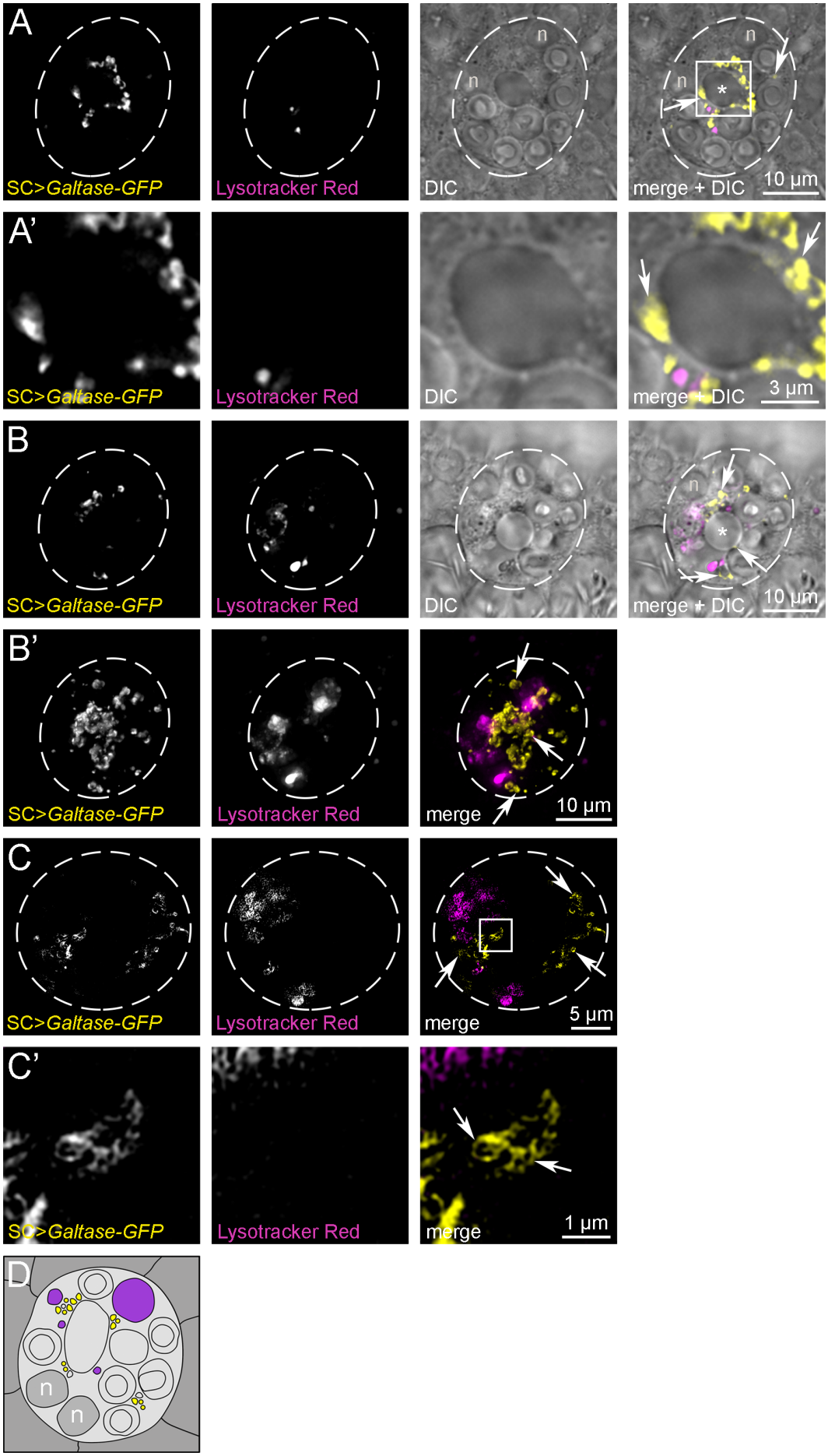

A
SC>Galtase-GFP
Lysotracker Red
DIC
n
n
merge + DIC
n
n
*
10 µm
A'
SC>Galtase-GFP
Lysotracker Red
DIC
merge + DIC
3 µm
B
SC>Galtase-GFP
Lysotracker Red
DIC
merge + DIC
n
*
10 µm
B'
SC>Galtase-GFP
Lysotracker Red
merge
10 µm
C
SC>Galtase-GFP
Lysotracker Red
merge
5 µm
C'
SC>Galtase-GFP
Lysotracker Red
merge
1 µm
D
n
n

Figure 3.5 Characterisation of the Golgi apparatus in living secondary cells

The structure of the Golgi apparatus was examined in living secondary cells from six-day-old virgin transgenic males selectively overexpressing Galtase-GFP, a Golgi-localised fusion protein, and that had been stained with Lysotracker Red. The flies were incubated at 28.5°C since eclosion to induce Galtase-GFP expression using the GAL4-GAL80^{ts}-UAS system. The images in panels A-B' were collected using wide-field fluorescence and DIC microscopy, whilst the images in panels C-C' were obtained using super-resolution 3D-SIM microscopy. Secondary cell nuclei, when distinguished by DIC morphology, are marked with 'n'. Approximate secondary cell outlines are marked with a dashed line.
(A) The Golgi marker Galtase-GFP (yellow) localises to a number of small non-acidic intracellular structures found in between the larger compartments (arrows), but heavily clustered around the large central non-cored compartment, marked with '*'. The box highlights the region magnified in (A')
(A') The Galtase-GFP-labelled Golgi structures (arrows) are clustered around the non-cored compartment.
(B) A more apical focal plane through a different secondary cell shows that Galtase-GFP localises to vesicles in other regions of the secondary cell.
(B') A maximum intensity projection image of both Galtase-GFP and Lysotracker Red through the secondary cell in (B) demonstrates the numerous Golgi structures throughout the depth of the cell.
(C) Super-resolution imaging provides higher contrast and resolution of Galtase-GFP localisation than wide-field fluorescence microscopy. Numerous vesicles labelled by Galtase-GFP are observed (arrows). Box area highlights region magnified in (C').
(C') High magnification image of Galtase-GFP shows vesicular Golgi domains (arrows), and other unresolved structures.
(D) Schematic representation of the Galtase-GFP-labelled Golgi (yellow) within an individual secondary cell. Acidic compartments are shown in magenta. Nuclei are marked with 'n'.

The specific genotype of the flies used in this figure is: *w; UAS-Galtase-GFP / tub-GAL80ts; dsx-GAL4 /* +.

3.2.1.6 Microtubules form a network running between secondary cell organelles

The actin cytoskeleton within secondary cells was previously visualised using a Phalloidin-TRITC stain, revealing a meshwork of actin filaments below the cell's plasma membrane (Figure 3.1E). The microtubule cytoskeleton of secondary cells is reported here for the first time. It was studied by overexpression of fluorescently tagged versions of alpha-tubulin, a core component of microtubules, and the kinesin motor protein Nod, which drives directional movement along microtubules. Overexpression of *alpha-tubulin-Dendra2* revealed a network of microtubule proteins throughout the cell, particularly in close proximity to the large compartments and underlying the plasma membrane (Figure 3.6A). In a specific focal plane, fluorescent puncta or short filaments were observed in these locations, because the microtubules extended outside the plane of focus. Some of the alpha-tubulin-Dendra2 protein was also found in the large acidic compartments.

To better visualise the microtubular network in the context of the subcellular compartments, overexpression of *mCherry-alpha-tubulin* was combined with *CD63-GFP*, which localised to the limiting membranes of many compartments (Figure 3.6B), and indicated that the mCherry fusion-protein surrounded each compartment. Again this fusion protein appeared to traffic to the large acidic compartments and individual z-planes only revealed short subsections of individual microtubules.

The fluorescently tagged kinesin, *Nod-GFP* was far brighter, and super-resolution imaging of the fusion protein confirmed previous observations with *alpha-tubulin-Dendra2*, but better illustrated the dense microtubule networks

throughout the cell, interweaving between both large and small subcellular organelles (Figure 3.6C-C''). When overexpressed in combination with *CD63-mCherry*, *Nod-GFP* was observed in very close association with the various subcellular compartments (Figure 3.6D). The CD63-mCherry fusion protein was generated in the lab (by S-J. Fan; see Methods) as a fluorescent alternative to CD63-GFP. It consisted of full length human CD63 fused to mCherry at its C-terminus, rather than its N-terminus, as was the case with CD63-GFP and it generally trafficked at much higher levels than CD63-GFP to large acidic compartments. These data showed that the organisation of the cytoskeleton in secondary cells bears some similarity to other post-mitotic cell types, with a dense microtubule network providing the primary cytoskeleton within the cells, and actin playing roles at the plasma membrane. There was no obvious microtubule organising centre (MTOC) structure, as is often seen, particularly in mitotic cells.

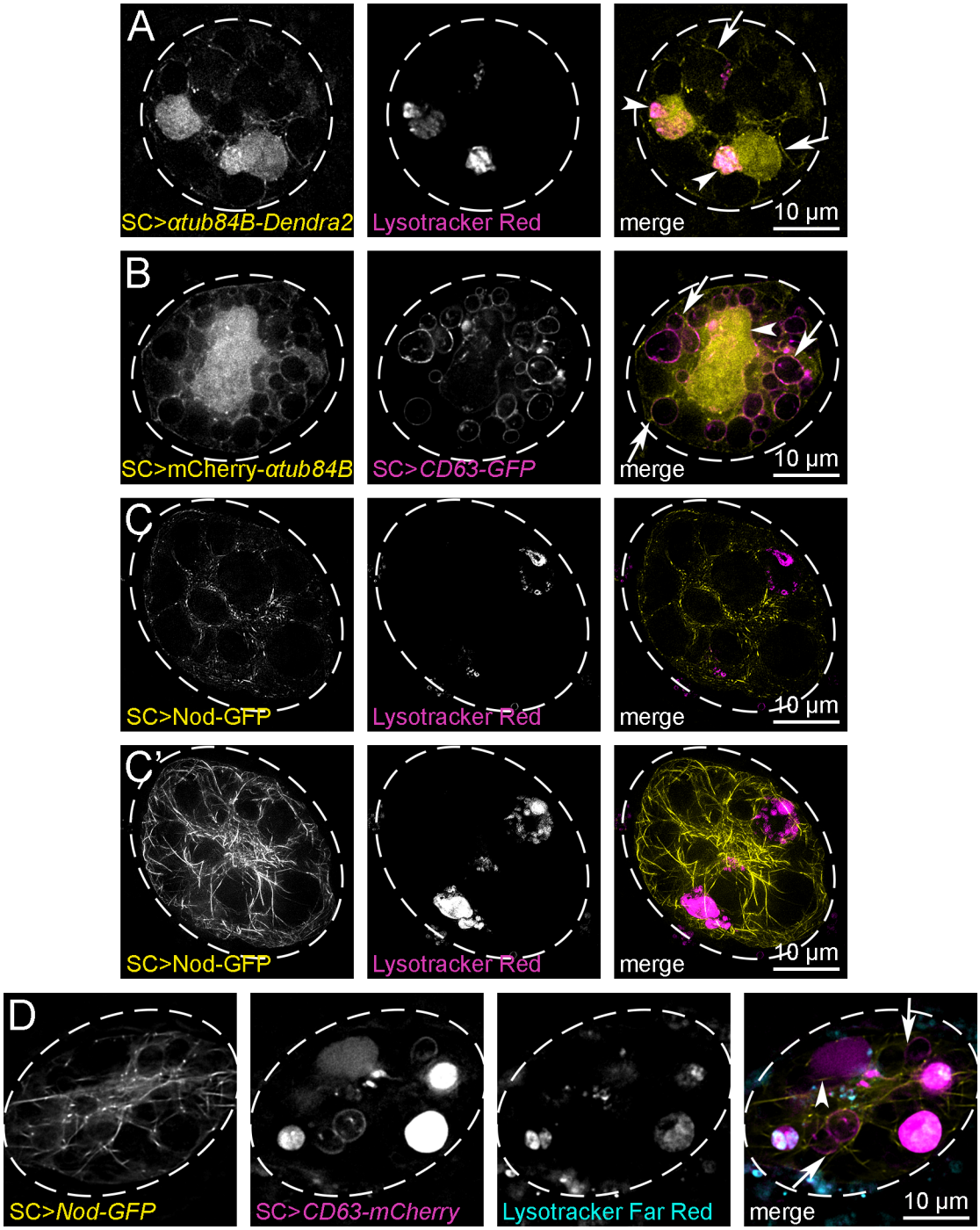

A
SC>αtub84B-Dendra2
Lysotracker Red
merge
10 μm
B
SC>mCherry-αtub84B
SC>CD63-GFP
merge
10 μm
C
SC>Nod-GFP
Lysotracker Red
merge
10 μm
C'
SC>Nod-GFP
Lysotracker Red
merge
10 μm
D
SC>Nod-GFP
SC>CD63-mCherry
Lysotracker Far Red
merge
10 μm

Figure 3.6 Fluorescent microtubule protein markers reveal an elaborate microtubule cytoskeleton in secondary cells

The organisation of the microtubule cytoskeleton in living secondary cells was visualised using cells specifically overexpressing a variety of different fluorescent fusion-protein constructs. Six-day-old virgin male flies were incubated at 28.5°C from eclosion to induce transgene expression using the GAL4-GAL80^{ts}-UAS system. The accessory glands were stained using Lysotracker dyes. The images in panels A, B and D are wide-field fluorescence images, and the images in panel C-C' are super-resolution 3D-SIM images.
(A) Overexpression of αtub84B-Dendra2 (yellow), a fluorescently tagged core component of microtubules, appeared to mark parts of numerous fibres that ran between the large intracellular compartments of secondary cells (arrows). It was also detected in the acidic compartments (arrowheads), marked by Lysotracker Red (magenta).
(B) The microtubule cytoskeleton, marked by overexpressed mCherry-αtub84B (yellow), associates very closely with the large subcellular compartments (arrows), the surface of which are clearly marked by GFP-CD63 (magenta). It is also incorporated into a large putative lysosomal compartment (arrowhead).
(C) Overexpression of a fluorescently tagged kinesin, Nod-GFP (yellow), permitted super-resolution imaging of the microtubule network. Lysotracker-Red (magenta) staining of this cell shows the large acidic compartments.
(C') Maximum intensity projection of the secondary cell from (C) better illustrates the 3-dimensionality of the microtubule cytoskeleton.
(D) A secondary cell overexpressing both Nod-GFP (yellow) and mCherry-CD63 (magenta) and stained with Lysotracker Far Red (cyan), shows that the microtubules tightly associate with the large acidic (arrowhead) and non-acidic compartments (arrows).

The specific genotypes of the flies used in this figure are: *w; tubGAL80ts / +; dsx-GAL4/ UAS-αtub84B-Dendra2* or *w; tubGAL80ts / UAS-mCherry-αtub84B; dsx-GAL4 /* + or *w; tubGAL80ts / Nod-GFP; dsx-GAL4 /* + or *w; UAS-CD63-GFP, tub-GAL80ts / Nod-GFP; dsx-GAL4 /* +.

3.2.1.7 Secondary cells contain plentiful mitochondria that provide the energy to drive cell biological processes

Numerous mitochondria, indicative of highly active cells, were visualised in living secondary cells by overexpression of *eYFP-mito* or *GFP-FP4-mito* (Lajeunesse *et al*., 2004; Gates *et al*., 2007) constructs. *eYFP-mito* consisted of a mitochondrial targeting sequence fused to eYFP at its N-terminus, and was expressed throughout the fly by a ubiquitous promoter (*sqh*). The other marker, *GFP-FP4-mito* marker was expressed specifically in secondary cells under UAS control, and consisted of four FPPPP (FP4) motifs (that sequester actin-capping Ena/VASP proteins), linked to GFP at its N-terminus, and fused to a mitochondrial anchoring sequence at its C-terminus. Both of these markers showed secondary cells contain many mitochondria, which were primarily localised basally and in between different subcellular compartments (Figure 3.7A-B).

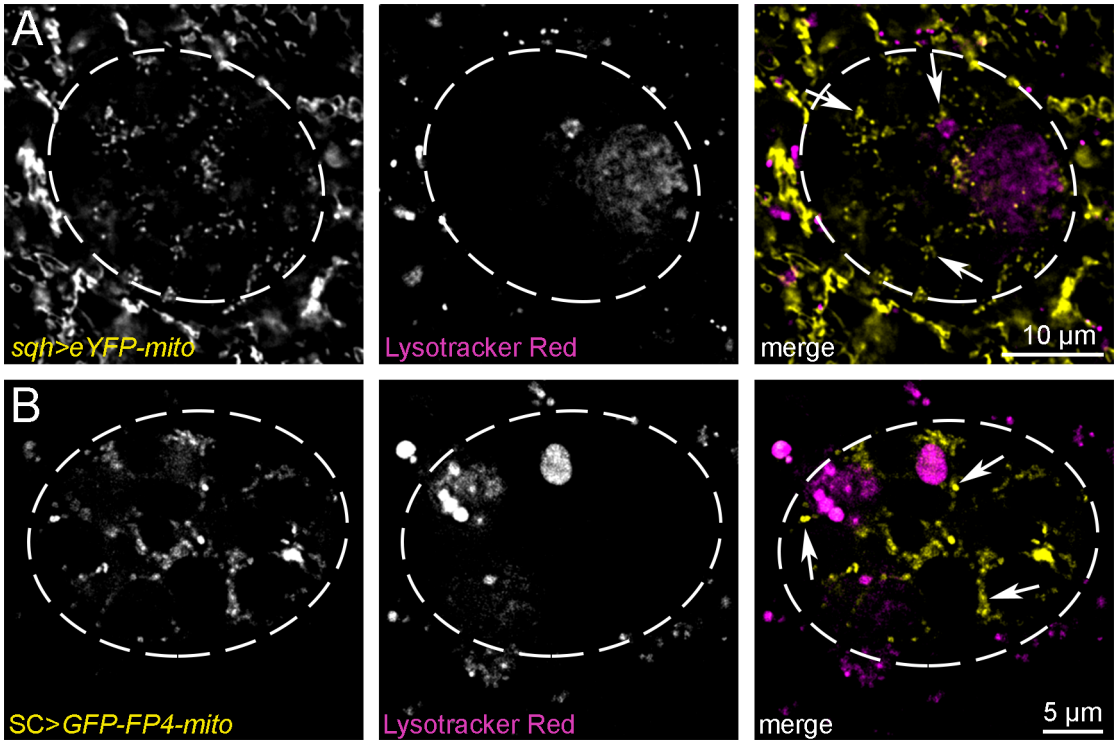


Figure 3.7 Numerous mitochondria are distributed throughout secondary cells

Wide-field fluorescence imaging was undertaken of living secondary cells overexpressing two different mitochondria-targeted fluorescent fusion proteins. Six-day-old virgin male flies were incubated at 28.5°C from eclosion, and were stained with Lysotracker Red (magenta).
(A) The ubiquitously expressed eYFP-mito (yellow) localise on numerous small non-acidic structures (arrows), presumably mitochondria, throughout the secondary cell, which are located in between the large subcellular compartments.
(B) GFP-FP4-mito, overexpressed specifically in secondary cells, localise on many small structures that are found throughout the cell (arrows), in between the different large compartments.

3.2.1.8 Junctions between neighbouring secondary and main cells

The close association between neighbouring main and secondary cells was previously reported in fixed tissue, using the localisation of the cell-cell adhesion molecule Fas3 (Section 3.2.1.1). These cell-cell interactions were further examined in living tissue through the localisation of an important cell-cell adhesion molecule, E-Cadherin, tagged with GFP and expressed throughout the fly from its endogenous genomic locus (*E-Cad-GFP* gene trap). E-Cadherin plays essential roles in adherens junctions (Walther & Pichaud, 2010). E-Cad-GFP was localised to the apical contact sites between main and secondary cells. Importantly, these junctions enabled the distinction between the apical and lateral plasma membrane of each cell (Figure 3.8A). The apical face of the secondary cell, in direct contact with the lumen of the gland, was easily visualised by the ring of apical E-Cad-GFP (Figure 3.8B). Similar to other epithelia, the interactions between neighbouring main and secondary cells did not involve E-cadherin in their basolateral portions (Figure 3.8C).

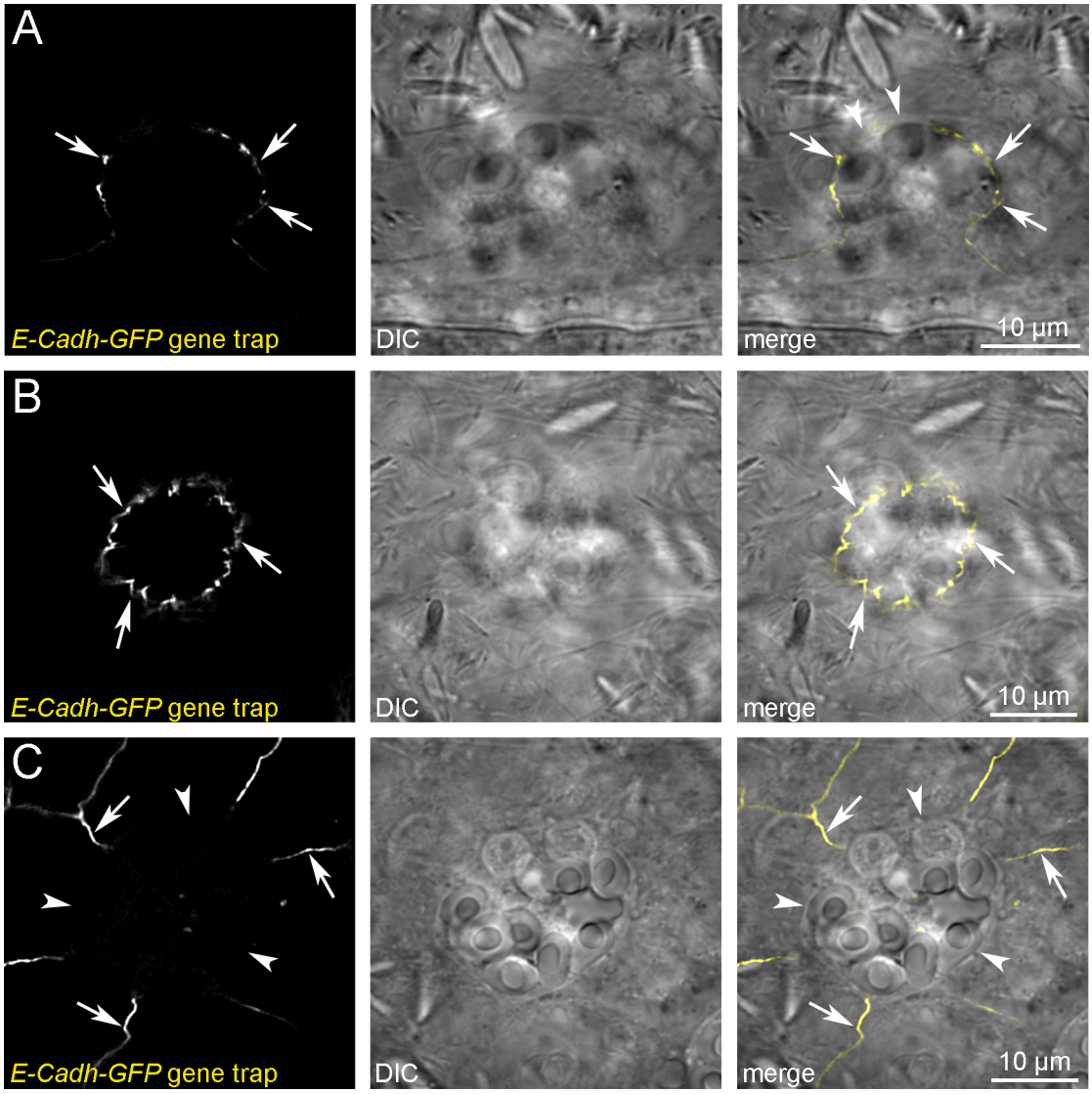


Figure 3.8 Adherens junctions in secondary cells

The adherens junctions between secondary cells and main cells were visualised using wide-field fluorescence and DIC imaging of E-Cadherin-GFP, expressed from its endogenous genomic locus. Nuclei were distinguished by. Nine-day-old virgin male flies were incubated at 17°C from eclosion.
(A) Transverse image showing a large secondary cell bulging into the lumen of the accessory gland, and illustrating the junctional complexes, marked by E-Cadherin-GFP (yellow, arrows), between it and its neighbouring main cells.
(B) The apical face of the secondary cell when viewed from above is characterised by a ring of E-Cadherin-marked junctional complexes (arrows) with its neighbouring main cells.
(C) The basolateral surfaces of the secondary cell do not carry E-Cadherin-GFP (arrowheads). Main cell-main cell junctions are marked (arrows).

Homozygous *E-Cadherin-GFP* gene trap flies were used.

3.2.2 Characterisation of Rab localisation in secondary cells using a library of fluorescently tagged Rab gene trap fly lines

Rab proteins are a highly conserved family of small GTPases that play essential cell biological roles in membrane trafficking and compartment identity (Zhen & Stenmark, 2015; Section 1.3). Secondary cells are potentially a powerful model system to study Rab protein localisation and function, due to the large size of many of their subcellular compartments, and their amenability to high-resolution imaging techniques. A collection of fly lines, which express YFP^{Myc} or CFP^{Myc} fused to Rab proteins at their N-terminus from their endogenous genomic loci (Dunst *et al*., 2015), was screened to characterise the Rab signatures of the different subcellular organelles within secondary cells. For all of these lines, a number of individual flies were analysed (n=>6 accessory glands, with at least 5 cells analysed in each gland), and a representative localisation pattern is reported here.

3.2.2.1 Rab1 and Rab2 localise to cis-Golgi cisternae and adjacent vesicles

Rab1 plays conserved roles in vesicular trafficking from the endoplasmic reticulum to the cis-Golgi network (Hutagulung & Novick, 2011; Moyer *et al*., 2001; Allan *et al*., 2000; Satoh *et al*., 1997). The YFP-Rab1 fusion protein from the *YFP-Rab1* gene trap localised at high levels on numerous small non-acidic vesicles that predominantly surrounded the large non-acidic, non-cored compartment in secondary cells, identified by its distinct irregular morphology and central location (Figure 3.9A-A'). The localisation was consistent between secondary cells (Figure 3.9B), with generally lower levels of expression observed in main cells. This expression pattern was similar to the

overexpressed Golgi marker Galtase-GFP (Section 3.2.1.5). Immunostaining showed that YFP-Rab1 also partially colocalised with the cis-Golgi matrix protein GM130 in secondary cells (Figure 3.9C). In addition, YFP-Rab1 was observed at high levels on a number of other small vesicles in close proximity to the cis-Golgi, possibly corresponding to medial- or trans-Golgi, or other vesicles mediating trafficking between the endoplasmic reticulum and the cis-Golgi, as would be expected given the previously identified locations for Rab1 in mammalian cells (Figure 3.9D; Plutner *et al*., 1991). Similarly, in main cells, YFP-Rab1 exhibited partial colocalisation with GM130, and localised on other small nearby vesicles, some of which likely corresponded to the concave medial- or trans-Golgi region (Figure 3.9E).

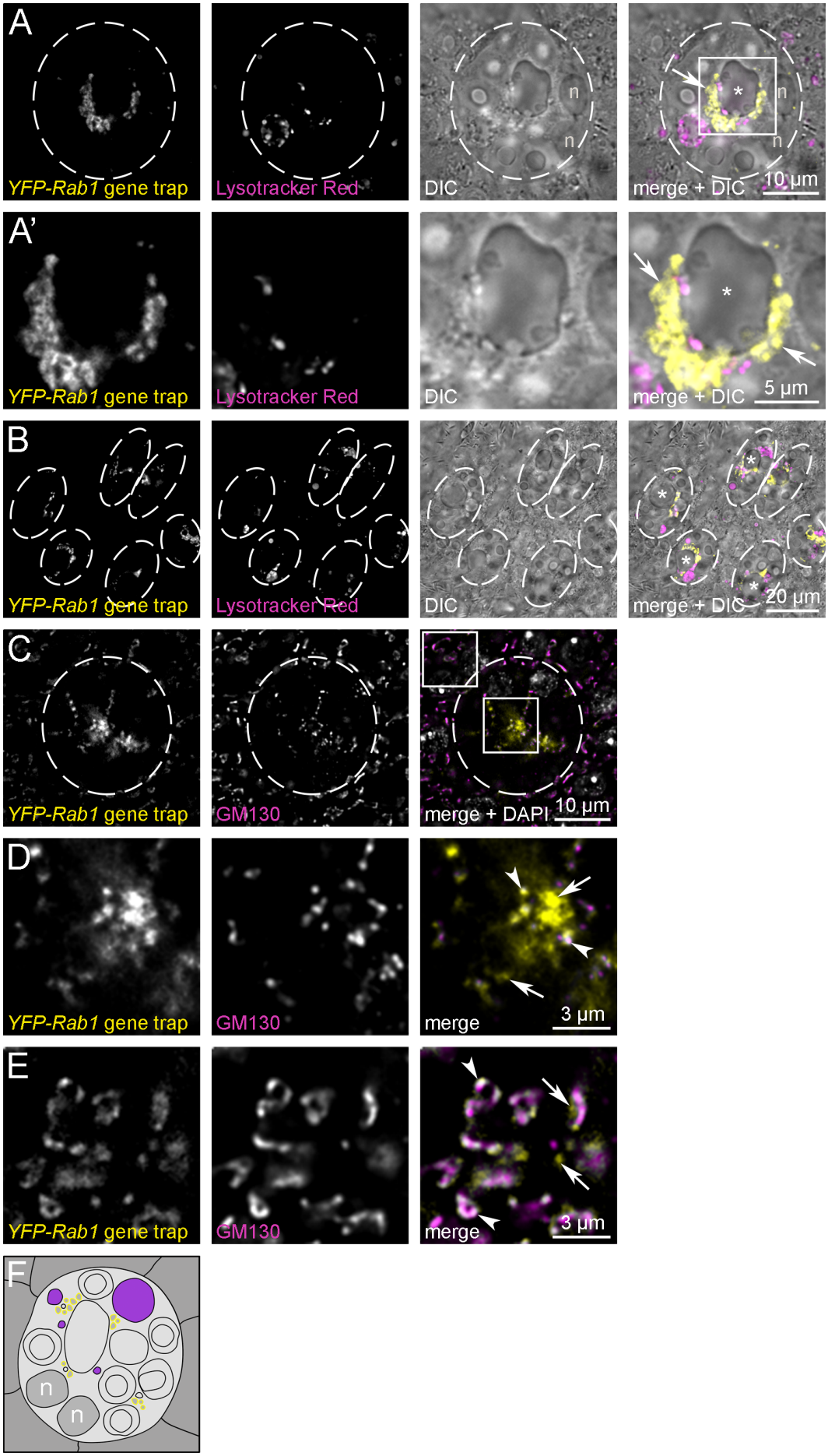

A
YFP-Rab1 gene trap
Lysotracker Red
DIC
merge + DIC
10 µm
A'
YFP-Rab1 gene trap
Lysotracker Red
DIC
merge + DIC
5 µm
B
YFP-Rab1 gene trap
Lysotracker Red
DIC
merge + DIC
20 µm
C
YFP-Rab1 gene trap
GM130
merge + DAPI
10 µm
D
YFP-Rab1 gene trap
GM130
merge
3 µm
E
YFP-Rab1 gene trap
GM130
merge
3 µm
F
n
n

Figure 3.9 YFP-Rab1 localises to the cis-Golgi and some adjacent structures, including around the large non-cored compartment

Wide-field fluorescence and DIC microscopy was performed on secondary cells from six-day-old virgin males expressing *YFP-Rab1* from the gene's endogenous locus. The flies were kept at 28.5°C since eclosion. Panels (A-B) present living secondary cells also stained for Lysotracker Red, and panels (C-E) display fixed cells immunostained with anti-GM130 antibody and stained with DAPI to mark nuclei. In living secondary cells, the nuclei of secondary cells were distinguished by DIC morphology and marked with 'n'. Approximate secondary cell outlines are marked with a dashed line.
(A) In secondary cells, YFP-Rab1 (yellow) localises to numerous small intracellular non-acidic vesicles and structures (arrow) found primarily clustering around the large central non-cored compartment (marked with '*'). The box highlights the region magnified in (A')
(A') Higher magnification image of YFP-Rab1-labelled vesicles (arrows) adjacent to the large non-cored compartment, marked with '*'.
(B) Lower magnification image shows consistency in the YFP-Rab1 localisation pattern characterised in (A-A') between different cells in the same accessory gland.
(C) YFP-Rab1 (yellow) in secondary cells localised within a region of the cell rich in cis-Golgi cisternae, as marked by anti-GM130 (magenta) staining. The boxes highlight regions in secondary cells and surrounding main cells that are magnified in (D) and (E), respectively.
(D) Secondary cell YFP-Rab1 puncta colocalise with GM130 (arrowheads), and also mark distinct structures at high levels (arrows).
(E) Main cell YFP-Rab1 co-localises primarily with the cis-Golgi marker GM130 (arrowheads), but is also in some nearby regions without GM130 staining (arrows).
(F) Schematic representation of YFP-Rab1 localisation (yellow) on small non-acidic vesicles within an individual secondary cell. Acidic compartments are shown in magenta. Nuclei are marked with 'n'.

Homozygous *YFP-Rab1* gene trap flies were used for all panels.

Rab2 is also known to function in the Golgi apparatus, mediating anterograde trafficking between the endoplasmic reticulum and cis-Golgi network, as well as inter-Golgi trafficking to the medial stack (Chavrier *et al*., 1990; Tisdale & Balch, 1996; Tisdale *et al*., 1992; Short *et al*., 2001). The fusion protein expressed from the YFP-Rab2 gene trap was detected at lower levels than YFP-Rab1 in secondary cells, but was localised to a similar group of small non-acidic vesicles surrounding the large non-acidic, non-cored compartment (Figure 3.10A-A'). It co-localised more closely with the cis-Golgi matrix protein GM130 (Figure 3.10B, C), as it also did in main cells (Figure 3.10D).

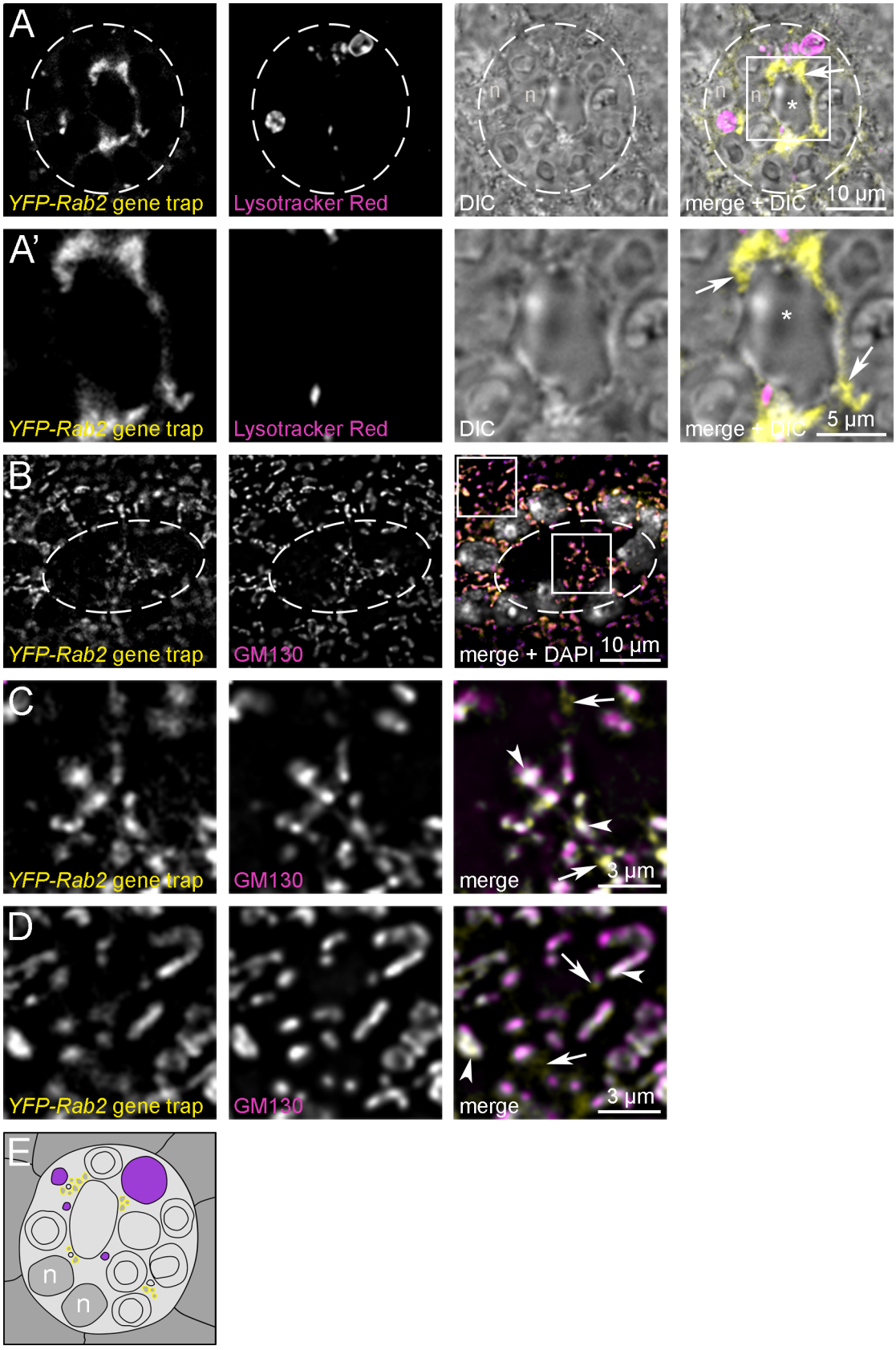

A
YFP-Rab2 gene trap
Lysotracker Red
DIC
merge + DIC
10 µm
n
n
*
A'
YFP-Rab2 gene trap
Lysotracker Red
DIC
merge + DIC
5 µm
B
YFP-Rab2 gene trap
GM130
merge + DAPI
10 µm
C
YFP-Rab2 gene trap
GM130
merge
3 µm
D
YFP-Rab2 gene trap
GM130
merge
3 µm
E
n
n

Figure 3.10 YFP-Rab2 localises to the cis-Golgi and some adjacent structures, including around the large non-cored compartment

Wide-field fluorescence and DIC microscopy was performed on secondary cells from six-day-old virgin males that expressed *YFP-Rab2* from the gene's endogenous locus. The flies were kept at 28.5°C since eclosion. Panels (A-A') present living secondary cells also stained with Lysotracker Red, and panels (B-D) display fixed cells immunostained with anti-GM130 antibody and stained with DAPI to mark nuclei. In living secondary cells, the nuclei of secondary cells were distinguished by DIC morphology and marked with 'n'. Approximate secondary cell outlines are marked with a dashed line.
(A) In secondary cells, YFP-Rab2 (yellow) localises primarily to the numerous small intracellular non-acidic vesicles and structures (arrow) that cluster around the large central non-cored compartment, marked with '*****'. The box highlights the region magnified in (A')
(A') Higher magnification image of YFP-Rab2-labelled structures (arrows) adjacent to the large non-cored compartment, marked with '*****'.
(B) YFP-Rab2 (yellow) in secondary cells co-localised well with the cis-Golgi matrix protein GM130 (magenta), in the central region of the cell. The boxes highlight regions in secondary cells and surrounding main cells that are magnified in (D) and (E), respectively.
(C) Secondary cell YFP-Rab2 puncta colocalise with GM130 (arrowheads), and also mark distinct vesicular structures at high levels (arrows).
(D) Main cell YFP-Rab2 co-localises heavily with the cis-Golgi marker GM130 (arrowheads), but is also in some nearby regions without GM130 staining (arrows).
(E) Schematic representation of YFP-Rab2 localisation (yellow) on small non-acidic vesicles within an individual secondary cell. Acidic compartments are shown in magenta. Nuclei are marked with 'n'.

Homozygous *YFP-Rab2* gene trap flies were used for all panels.

3.2.2.2 Rab6 localises to the surface of the large non-cored compartments and also on vesicles in close proximity to the Rab1/ Rab2-marked Golgi

Rab6 plays multiple roles in different cell types and has previously been reported to localise in the Golgi apparatus, where it regulates trafficking within the Golgi and from the Golgi to the plasma membrane, endosomes and the endoplasmic reticulum (Wandinger-Ness & Zerial, 2014; Martinez *et al*., 1994). Consistently, in secondary cells, fusion protein from the *YFP-Rab6* gene trap was observed in the region of the cell known to contain the Golgi complexes, such as the small non-acidic vesicles surrounding the large central non-cored compartment (Figure 3.11A-A'). However, much higher levels of *YFP-Rab6* gene trap were observed on the limiting membranes of several of the large subcellular compartments within secondary cells, some of which contained adjacent membranous structures, also enriched in YFP-Rab6 (Figure 3.11A-A'). Confirming previous immunostaining for Rab6 (Appendix 8.1.1, 8.1.2), the large centrally located, non-cored compartments carried the highest subcellular levels of YFP-Rab6 on their limiting membranes. In many cells these non-cored compartments consisted of one apical rounded compartment and one basal irregularly shaped compartment (Figure 3.11B-B''). The cells also contained several small basally located (<2 μm diameter) non-acidic compartments with high levels of YFP-Rab6 at their surface (Figure 3.11C). In their basal portions, most cells also contained 2-3 dense-core granule compartments that carried *YFP-Rab6* gene trap on their limiting membranes at lower levels (Figure 3.11C-C'). Many of the subcellular

compartments labelled with YFP-Rab6, and even some that were not, contained YFP-labelled intraluminal puncta (Figure 3.11D).

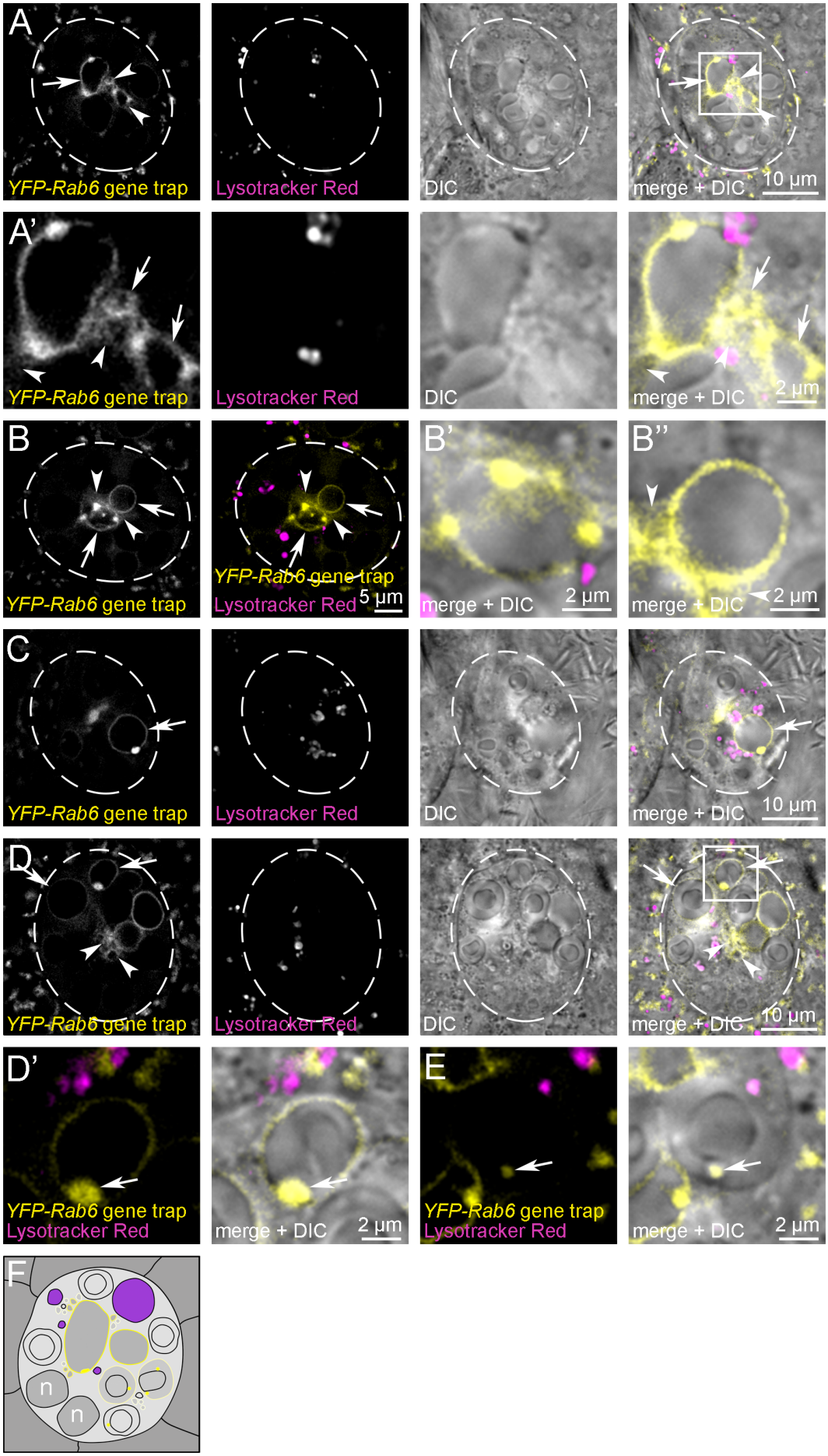

A
YFP-Rab6 gene trap
Lysotracker Red
DIC
merge + DIC
10 µm
A'
YFP-Rab6 gene trap
Lysotracker Red
DIC
merge + DIC
2 µm
B
YFP-Rab6 gene trap
YFP-Rab6 gene trap
Lysotracker Red
5 µm
B'
merge + DIC
2 µm
B''
merge + DIC
2 µm
C
YFP-Rab6 gene trap
Lysotracker Red
DIC
merge + DIC
10 µm
D
YFP-Rab6 gene trap
Lysotracker Red
DIC
merge + DIC
10 µm
D'
YFP-Rab6 gene trap
Lysotracker Red
merge + DIC
2 µm
E
YFP-Rab6 gene trap
Lysotracker Red
merge + DIC
2 µm
F
n
n

Figure 3.11 YFP-Rab6 concentrates on large non-cored compartments and some adjacent vesicles, and also localises to a subset of dense-core granule compartments and their intraluminal puncta

Wide-field fluorescence and DIC microscopy was performed on living secondary cells from six-day-old virgin males that expressed the *YFP-Rab6* gene trap. The flies were kept at 28.5°C since eclosion and accessory glands were stained with Lysotracker Red (magenta). Secondary cell nuclei were distinguished by DIC morphology and are marked with 'n'. Approximate secondary cell outlines are marked with a dashed line.
(A). YFP-Rab6 (yellow) localises at high levels on the surface of the large centrally located non-cored compartment, marked by '*' and some adjacent structures (arrows). The box highlights the region magnified in panel (A').
(A') The large compartment carries high levels of YFP-Rab6 fusion protein at its surface. Other moderately sized vesicles also carry YFP-Rab6 on their surface or are associated closely with smaller YFP-Rab6-marked vesicles (arrows). More diffuse YFP-Rab6 fusion protein is also found in other regions adjacent to the non-cored compartment (arrowheads).
(B) Both rounded and irregularly shaped non-cored compartments carry YFP-Rab6 at their surface (arrows), and diffuse YFP-Rab6 is observed in the region adjacent to these compartments (arrowheads). The boxes highlight regions magnified in (B') and (B'').
(B') The large irregularly shaped YFP-Rab6-marked compartment contains bright intraluminal puncta adjacent to its limiting membrane (arrows).
(B'') In addition to the rounded non-cored compartment, YFP-Rab6 localises to smaller adjacent structures (arrows)
(C) In the basal region of the secondary cell, several large dense-core granule compartments carry YFP-Rab6 on their surface (arrows), though at lower levels than the large non-cored compartment (arrowhead). Box highlights region magnified in (C')
(C') The large dense-core granule compartment contains intraluminal structures marked by YFP-Rab6 (arrow) that lie outside the dense-core granule.
(D) Some dense-core granule compartments lacking YFP-Rab6 staining at their limiting membrane contain intraluminal puncta labelled by YFP-Rab6 (arrows)
(F) Schematic representation of YFP-Rab6 localisation (yellow) on the surface of intracellular compartments within an individual secondary cell. The level of localisation is represented by intensity of yellow (i.e. large non-cored compartments is highest). Acidic compartments are shown in magenta. Nuclei are marked with 'n'.

Homozygous *YFP-Rab6* gene trap flies were used for all panels.

Rab6 localisation was also studied using a *CFP-Rab6* gene trap, which could be combined with other *YFP-Rab* gene trap lines. The *CFP-Rab6* gene trap line was characterised collaboratively with F. Castellanos, another DPhil student in the lab, and a detailed description of its localisation on large compartments is also reported in his thesis (Castellanos, 2017). Consistent with both the *YFP-Rab6* gene trap and immunofluorescent staining of w^{1118} cells (Appendix 8.1.1), the fusion protein expressed from the *CFP-Rab6* gene trap was most concentrated on the surface of the large non-acidic, non-cored compartments in secondary cells (Figure 3.12A-A'). It was also observed on small non-acidic vesicles scattered throughout the cell, but often in close proximity to the non-cored compartments, in the region known to include numerous Golgi cisternae (Figure 3.12A-A'). Lower levels of CFP-Rab6 were localised on the limiting membranes of some large dense-core granule compartments (Figure 3.12A). Similar to YFP-Rab6, it was often present on intraluminal puncta within these compartments (Figure 3.12B), and inside other compartments that lacked detectable CFP-Rab6 on their limiting membranes (Figure 3.12C).

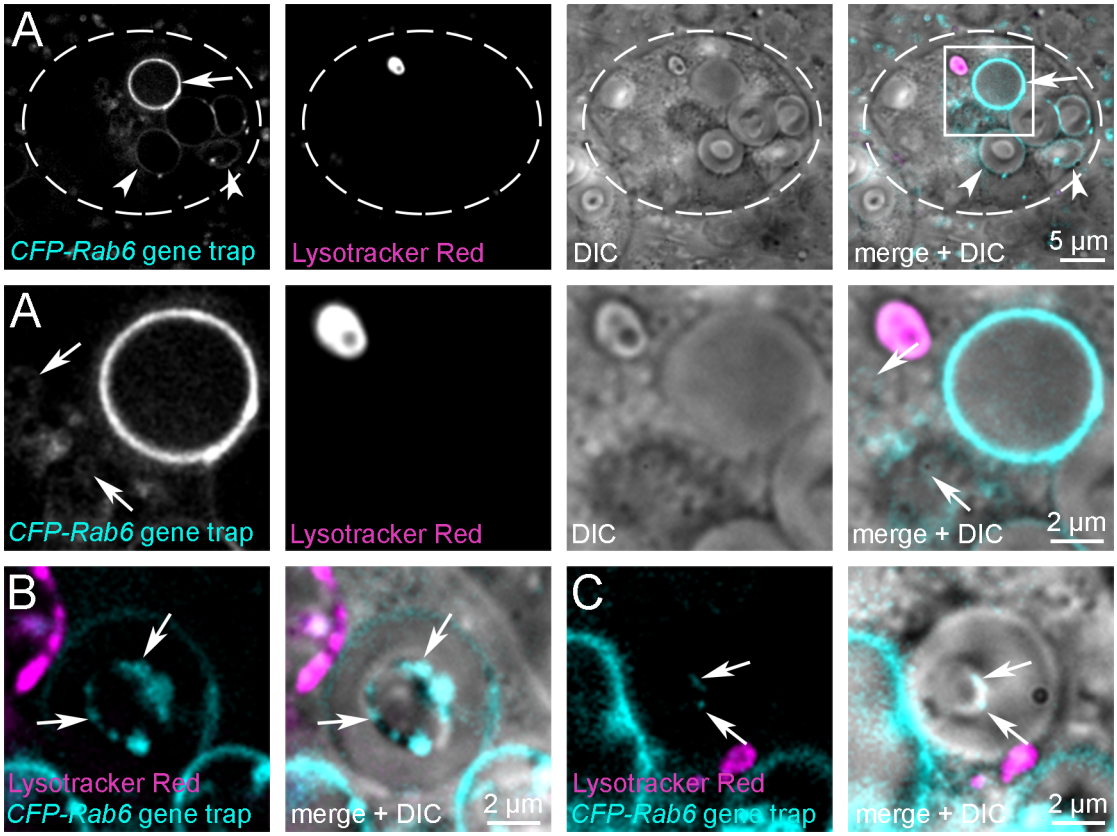


Figure 3.12 CFP-Rab6 localises to a similar set of secondary cell compartments as YFP-Rab6

Wide-field fluorescence and DIC microscopy was performed on living secondary cells from six-day-old virgin males that expressed the *CFP-Rab6* gene trap. The flies were kept at 28.5°C following eclosion and their accessory glands were stained with Lysotracker Red (magenta). Approximate secondary cell outlines are marked with a dashed line. These flies were analysed in collaboration with F. Castellanos.
(A) The large non-cored compartments (arrow) carry the highest level of CFP-Rab6 (cyan) in secondary cells; other large dense-core granule compartments carry more modest levels (arrowheads). The box highlights the non-cored compartment and surrounding region magnified in (A')
(A') In addition to the rounded non-cored compartment, CFP-Rab6 localises at relatively high levels on small adjacent non-acidic vesicles and structures (arrows)
(B) Some large dense-core granule compartments carry CFP-Rab6 on their surface, and on numerous intraluminal puncta (arrows), which surround the dense-core granule.
(C) CFP-Rab6 is also observed on intraluminal puncta (arrows) within large dense-core granule compartments that do not carry detectable levels of CFP-Rab6 at their limiting membrane.
Homozygous *CFP-Rab6* gene trap flies were used for all panels.

To determine whether the small vesicles marked by the *CFP-Rab6* gene trap were Golgi-associated, as is reported in mammalian cells (Goud *et al*., 1990), secondary cells were immunostained for the native cis-Golgi protein GM130. This protein was found in discrete puncta in close proximity to the small CFP-Rab6-positive vesicles, in the region around the large central Rab6-positive compartment (Figure 3.13A-A'). In main cells, CFP-Rab6 also mostly localised to small vesicles close to the cis-Golgi, in a region consistent with the trans-Golgi surface, or possibly an adjacent type of vesicle (Figure 3.13B). To determine whether the small vesicles corresponded to the trans-face of the Golgi, glands were stained for the native trans-Golgi protein Golgin245 (Riedel *et al*., 2016). Due to poor antibody penetration, co-localisation analyses were only possible in the muscle cell layer surrounding the epithelium. Here, the CFP-Rab6 partially co-localised with Golgin245, providing evidence that it partly resided within the trans-Golgi network (Figure 3.13C).

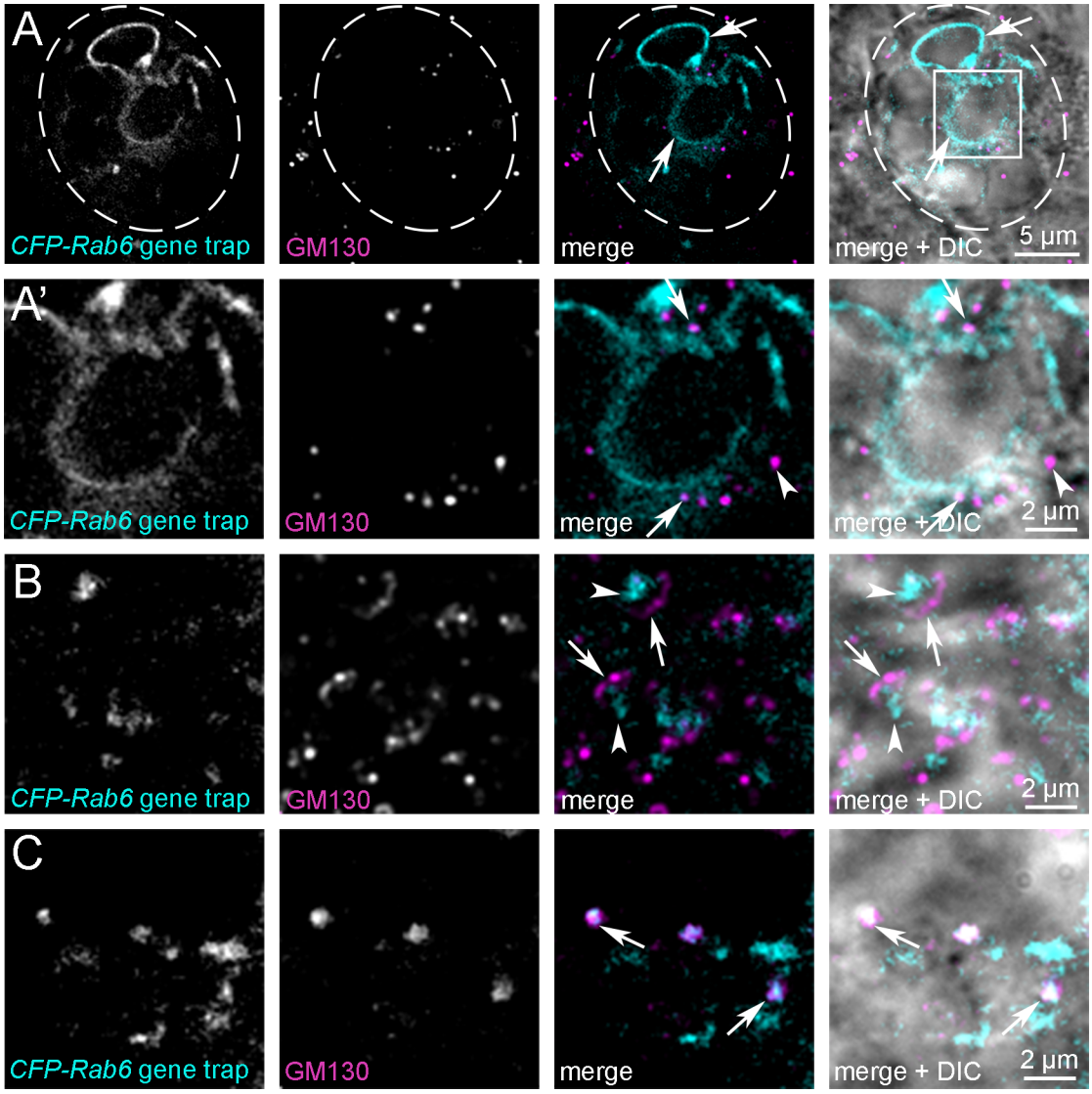

A
CFP-Rab6 gene trap
GM130
merge
merge + DIC
5 µm
A'
CFP-Rab6 gene trap
GM130
merge
merge + DIC
2 µm
B
CFP-Rab6 gene trap
GM130
merge
merge + DIC
2 µm
C
CFP-Rab6 gene trap
GM130
merge
merge + DIC
2 µm

Figure 3.13 The large CFP-Rab6 labelled compartments are surrounded by Golgi-localised proteins

Wide-field fluorescence and DIC microscopy was performed on accessory glands from six-day-old virgin males that expressed *CFP-Rab6* gene trap from its endogenous locus. The males were kept at 28.5°C since eclosion and immunostained using antibodies including anti-GM130 or anti-Golgin245 to visualise the Golgi apparatus. Approximate secondary cell outlines are marked with a dashed line.
(A) In secondary cells, CFP-Rab6 (cyan) localises on a subset of secondary cell compartments (arrows), some of which are centrally located and surrounded by cis-Golgi structures, labelled with GM130 (magenta). The box highlights the central region magnified in (A')
(A') Higher magnification shows that CFP-Rab6 localises to the surface of the large central compartment, and also diffusely throughout a region adjacent to this compartment. The cis-Golgi protein GM130 localises in puncta within this general region (arrows) and also on other separate structures (arrowhead).
(B) CFP-Rab6 likely marks the trans-Golgi network or closely associated vesicles in main cells, as the GM130-marked tubular cis-Golgi structures are closely associated with CFP-Rab6-labelled structures, which localise at its concave, or trans-face.
(C) The muscle cells surrounding the epithelium contained small trans-Golgi structures, marked by Golgin-245, which also contained CFP-Rab6.

Homozygous *CFP^{Myc}-Rab6* gene trap flies were used for all panels.

To further investigate the possible Golgi localisation of CFP-Rab6 in secondary cells, these flies were crossed to the *YFP-Rab1* gene trap line, which was previously shown to produce a fusion protein that resides at least partially in the cis-Golgi network (Figure 3.9). In secondary cells expressing both of these transgenes, some of the small vesicles surrounding the large non-cored compartment were marked by low levels of CFP-Rab6, and also contained YFP-Rab1 (Figure 3.14A-A'). However, other slightly larger vesicles (though still <2 μm in diameter) with higher levels of CFP-Rab6 did not (Figure 3.14A''). They might represent a specialised region of the trans-Golgi network or structures that have emerged from that network. The smaller double-labelled vesicles potentially correspond to the trans-Golgi network. Small YFP-Rab1-positive vesicles nearby were potentially cis-Golgi structures (Figure 3.14A''). Interestingly, this organisation resembled structures observed using electron microscopy (Section 3.2.1.3).

The *CFP-Rab6* gene trap was also crossed to the cis-Golgi localised *YFP-Rab2* gene trap (Figure 3.14B). In these cells, as in the combination with *YFP-Rab1* gene trap, very low levels of CFP-Rab6 co-localised with YFP-Rab2 in the unresolved vesicular region surrounding central non-cored compartment (Figure 3.14B'). However, the small non-acidic vesicles with high levels of CFP-Rab6 did not co-localise with YFP-Rab2, which was found on small vesicles in close proximity independently of CFP-Rab6 (Figure 3.14B'). Although the lower levels of YFP-Rab2 expressed by secondary cells did not facilitate the same level of detailed analysis achieved using the *YFP-Rab1* gene trap, it seems likely that these two small vesicle populations similarly belong to the cis- and trans-Golgi. In support of this, in main cells, CFP-Rab6

resembled the trans-Golgi, as it associated with the concave face of the YFP-Rab2-marked cis-Golgi.

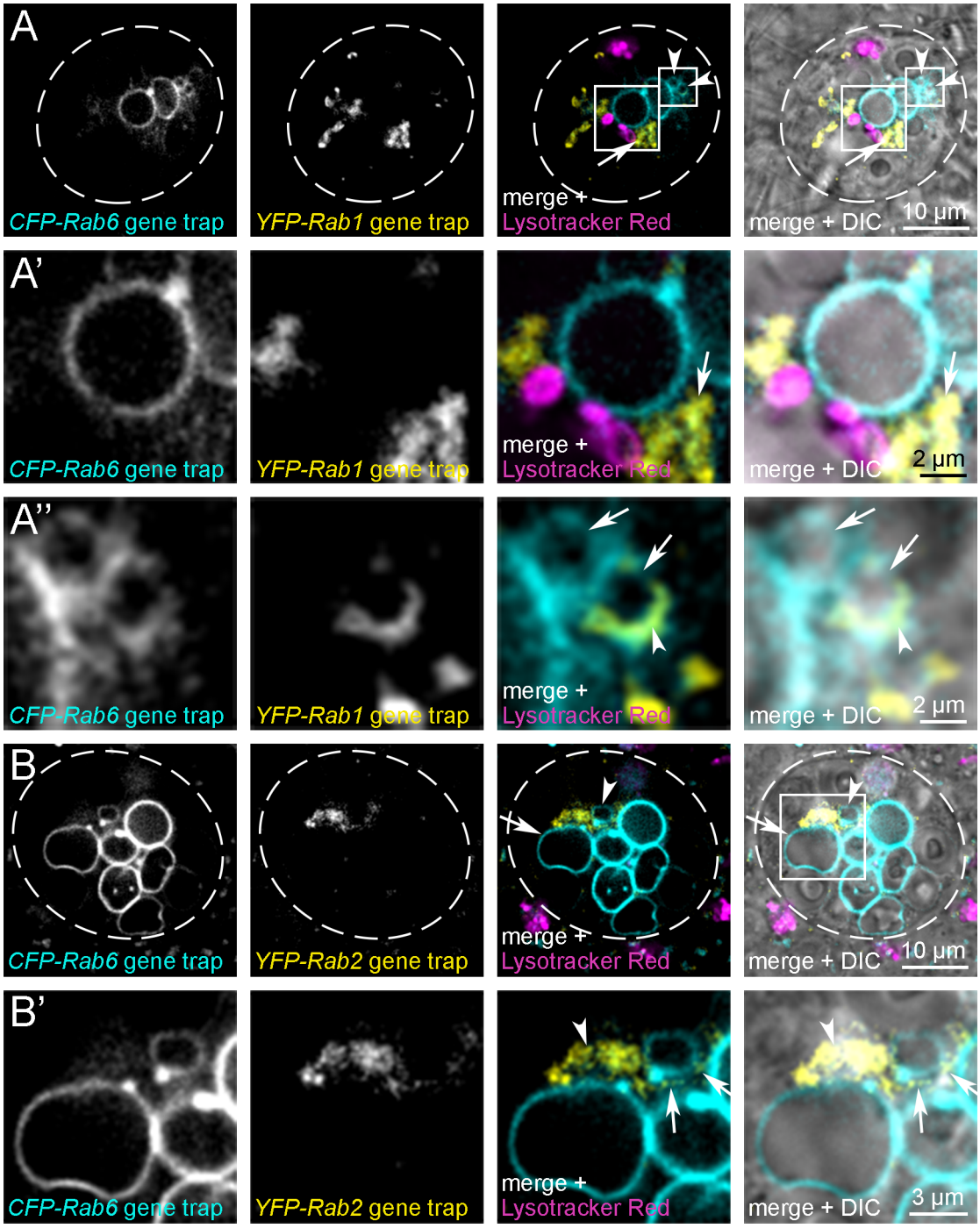

A
CFP-Rab6 gene trap
YFP-Rab1 gene trap
merge +
Lysotracker Red
merge + DIC
10 µm
A'
CFP-Rab6 gene trap
YFP-Rab1 gene trap
merge +
Lysotracker Red
merge + DIC
2 µm
A''
CFP-Rab6 gene trap
YFP-Rab1 gene trap
merge +
Lysotracker Red
merge + DIC
2 µm
B
CFP-Rab6 gene trap
YFP-Rab2 gene trap
merge +
Lysotracker Red
merge + DIC
10 µm
B'
CFP-Rab6 gene trap
YFP-Rab2 gene trap
merge +
Lysotracker Red
merge + DIC
3 µm

Figure 3.14 Small CFP-Rab6-marked vesicles are closely associated with cis-Golgi proteins YFP-Rab1 and YFP-Rab2

Wide-field fluorescence and DIC microscopy was performed on living secondary cells from six-day-old virgin males that expressed CFP-Rab6 in combination with either YFP-Rab1 or YFP-Rab2 from their endogenous loci. The flies were kept at 28.5°C since eclosion and accessory glands were stained with Lysotracker Red. Secondary cell nuclei were distinguished by DIC morphology and marked with 'n'. Approximate secondary cell outlines are marked with a dashed line.
(A) In secondary cells, CFP-Rab6 (cyan) localised at low levels to the region surrounding the large non-cored compartment, where it overlapped with YFP-Rab1-labelled (yellow) structures (arrows). Higher levels of CFP-Rab6 were found on a small number of other vesicles (arrowheads), which associated closely, but did not overlap with YFP-Rab1. Boxes highlight regions magnified in (A') and (A'') to better illustrate these distinct regions.
(A') CFP-Rab6 co-localises at low levels with YFP-Rab1 in the regions surrounding the central non-cored compartment (arrows).
(A'') Small intracellular vesicles with higher levels of CFP-Rab6 at their surface are closely associated with YFP-Rab1-marked tubular structures.
(B) YFP-Rab2 (yellow) co-localised with diffuse CFP-Rab6 (cyan) in the region surrounding the large non-cored compartments (arrows). Other small vesicles with higher levels of CFP-Rab6 associated closely with YFP-Rab2-structures. The boxed region highlighting this interaction is magnified in (B').
(B') Small CFP-Rab6-positive vesicles localise closely with tubular YFP-Rab2-labelled structures (arrows). Low levels of CFP-Rab6 also diffusely co-localised with YFP-Rab2-labelled vesicles (arrowheads).

The specific genotype of the flies used in this figure are: *w; CFP^{Myc}-Rab6 gene trap / +; YFP^{Myc}-Rab1 gene trap / +* and *w; CFP^{Myc}-Rab6 gene trap / YFP^{Myc}-Rab2 gene trap; + / +*.

3.2.2.3 Rab8, Rab10, Rab11, Rab19 and Rab30 localise to the centrally located, Golgi-rich subcellular region surrounding the large Rab6-positive compartment

Rab8 mediates constitutive secretory trafficking routes from the trans-Golgi network directly to the plasma membrane, and has been implicated in ciliogenesis and GLUT4 vesicle secretion (Huber *et al*., 1993; Knödler *et al*., 2010; Li *et al*., 2017). Consistent with these Golgi-related functions, in secondary cells, the fusion protein expressed from the *YFP-Rab8* gene trap was found on small non-acidic vesicles surrounding the large non-acidic, non-cored Rab6-positive compartment (Figure 3.15A-B), in the region known to include numerous Golgi sacs. Interestingly, secondary cells expressing the *YFP-Rab8* gene trap produced abnormal, diffusely packaged granules within their specialised secretory compartments (Figure 3.15C). This may be due to functional differences between the heterozygous YFP-Rab8 fusion protein and its wild type form, or alternatively because it interferes with the function of the wild-type copy. High levels of YFP-Rab8 were observed within acidic compartments (Figure 3.15A-B), perhaps reflecting clearance of a malfunctioning protein. Similarly, in main cells, YFP-Rab8 localised on small vesicles and within their acidic compartments (Figure 3.15D).

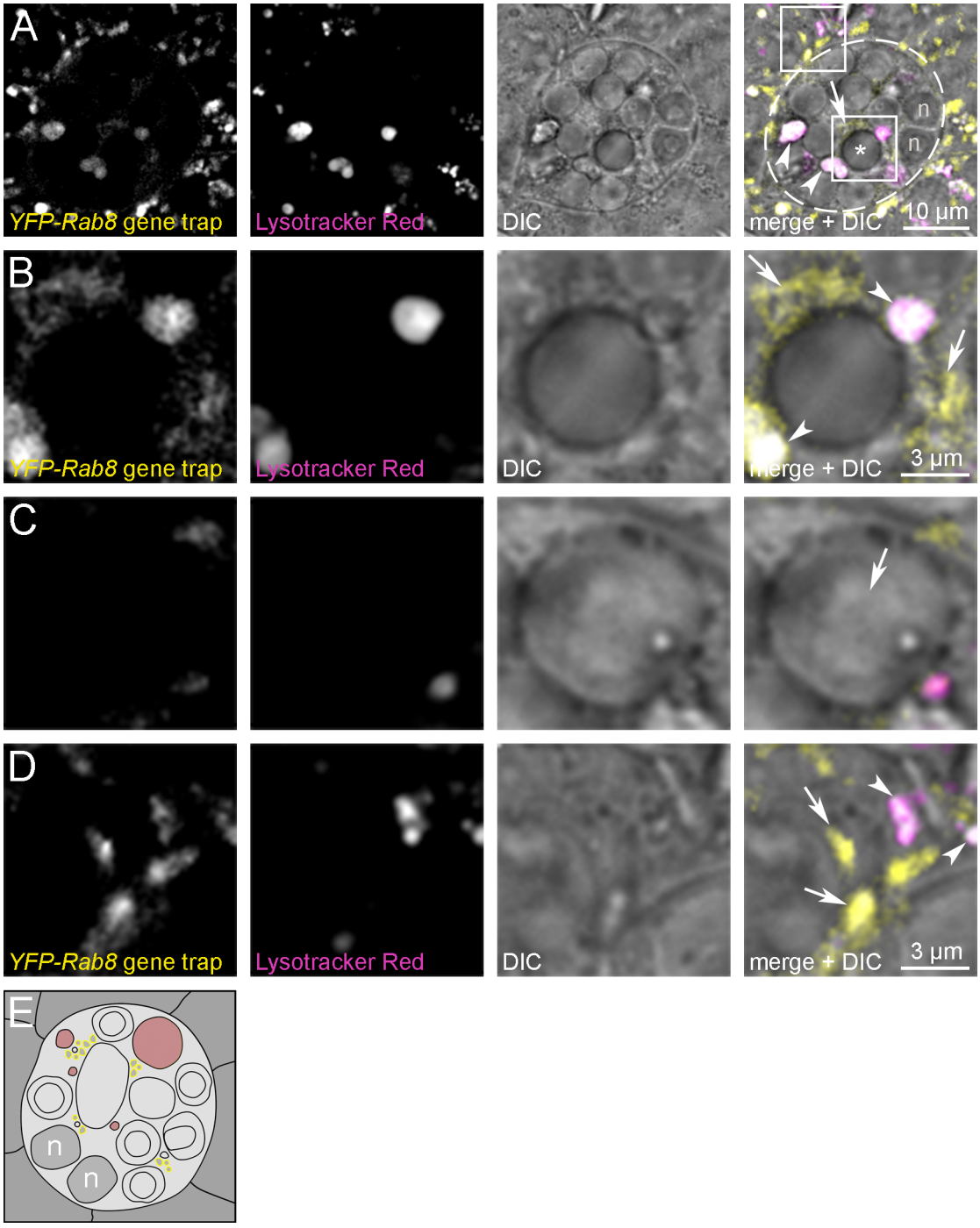

A
YFP-Rab8 gene trap
Lysotracker Red
DIC
merge + DIC
n
n
*
10 µm
B
YFP-Rab8 gene trap
Lysotracker Red
DIC
merge + DIC
3 µm
C
D
YFP-Rab8 gene trap
Lysotracker Red
DIC
merge + DIC
3 µm
E
n
n

Figure 3.15 YFP-Rab8 localises on intracellular vesicles adjacent to the large non-cored compartment and affects dense-core granule morphology

Wide-field fluorescence and DIC microscopy was performed on living secondary cells from six-day-old virgin males that expressed *YFP-Rab8* gene trap from its endogenous locus. The flies were kept at 28.5°C since eclosion and accessory glands were stained with Lysotracker Red. Secondary cell nuclei were distinguished by DIC morphology and marked with 'n'. Approximate secondary cell outlines are marked with a dashed line.
(A) YFP-Rab8 (yellow) localised to the small vesicular structures (arrow) adjacent to the central non-cored compartment, marked with '*', and also within their acidic compartments (magenta; arrowheads). The boxes highlight the regions magnified in panels (B) and (D).
(B) The vesicular structures in close contact with the non-cored compartment, are enriched in YFP-Rab8 (arrows), which is also packaged at high levels into the acidic compartments (arrowheads).
(C) The dense-core granules within YFP-Rab8 expressing secondary cells are uncharacteristically diffuse (arrow).
(D) Main cells contain small YFP-Rab8-labelled compartments (arrows). Some YFP-Rab8 also localises within acidic compartments (arrowheads).
(E) Schematic representation of YFP-Rab8 localisation (yellow) within an individual secondary cell. Small non-acidic vesicles carry YFP-Rab8 on their surface, and it is found within acidic compartments (magenta). Nuclei are marked with 'n'.

The specific genotype of the flies used is: *w; + / +; YFP^{Myc}-Rab8 gene trap / +*

Rab10 has been implicated in many of the same functions as Rab8, including exocytic trafficking pathways from the trans-Golgi network to the plasma membrane as well as GLUT4 vesicle translocation (Wandinger-Ness & Zerial, 2014; Schuck *et al*., 2007; Sano *et al*., 2008), and it is associated with recycling from sorting endosomes (Babbey *et al*., 2006). The fusion protein expressed from the *YFP-Rab10* gene trap was observed on a subset of dense-core granule compartments (see Section 3.2.2.4) and on small non-acidic vesicles, many of which surrounded the large non-acidic, non-cored Rab6-positive compartments (Figure 3.16A-A'), similar to other Golgi-localised molecules. In main cells, YFP-Rab10 was localised at high levels on numerous small non-acidic vesicles, and was found inside some small acidic compartments (Figure 3.16B).

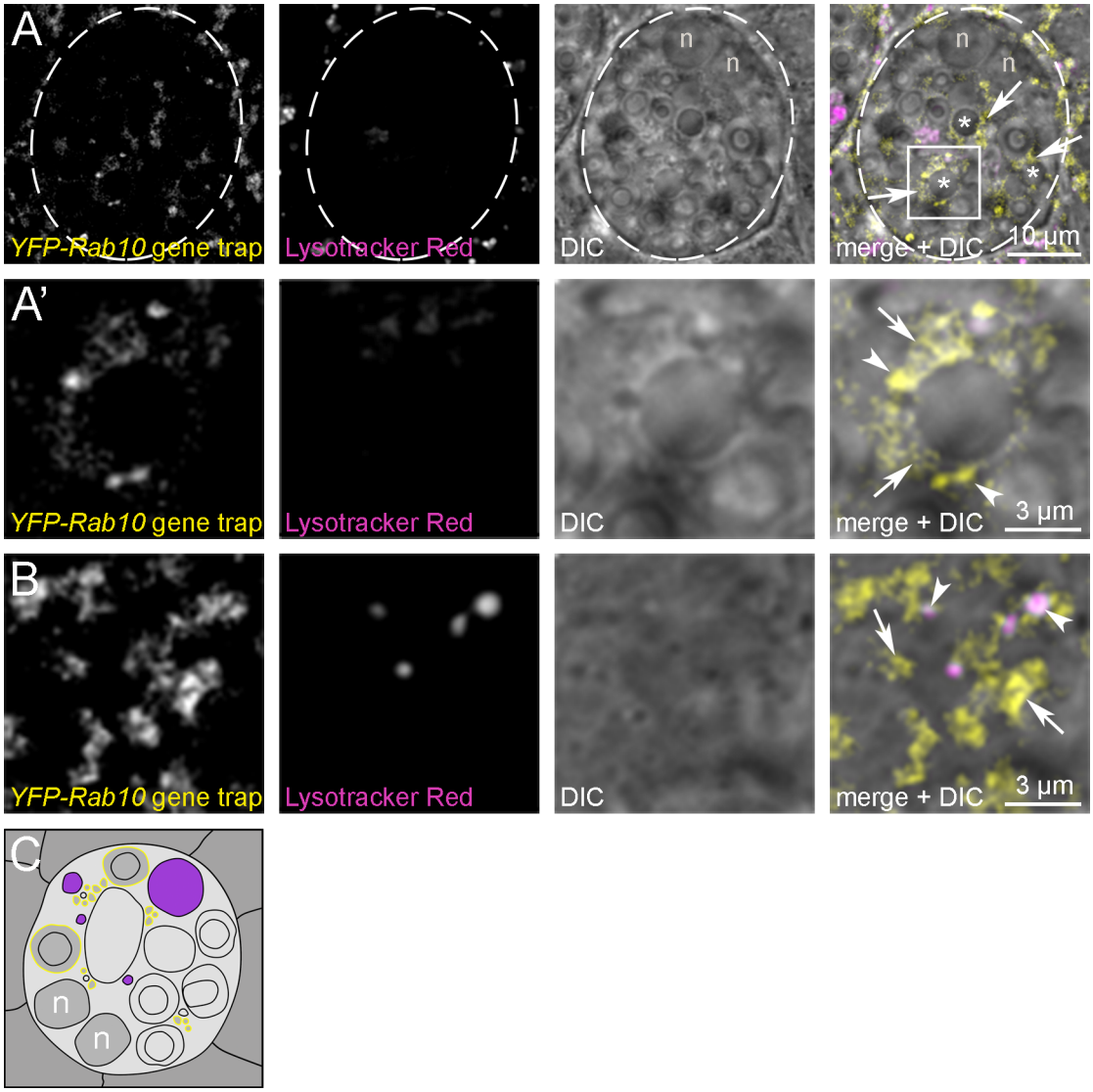

A
YFP-Rab10 gene trap
Lysotracker Red
DIC
n
n
merge + DIC
10 µm
A'
3 µm
B
C

Figure 3.16 YFP-Rab10 localises on intracellular vesicles adjacent to the large Rab6-positive non-cored compartment

Wide-field fluorescence and DIC microscopy was performed on living secondary cells from six-day-old virgin males that expressed *YFP-Rab10* gene trap from its endogenous locus. The flies were kept at 28.5°C since eclosion and accessory glands were stained with Lysotracker Red. Secondary cell nuclei were distinguished by DIC morphology and marked with 'n'. Approximate secondary cell outlines are marked with a dashed line.
(A) Within secondary cells, YFP-Rab10 (yellow) localised to the numerous small non-acidic vesicular structures (arrows) surrounding the Rab6-positive non-cored compartments, marked with '*'. The boxes highlight the region magnified in (A')
(A') Higher magnification image shows the close association between YFP-Rab10-labelled vesicles and the non-cored compartments (arrows). Particularly high levels of YFP-Rab10 were observed on a subset of these vesicles (arrowheads).
(B) In main cells, YFP-Rab10 localises to complex vesicular structures (arrows), some of which are closely contacting or possibly within small acidic compartments (arrowheads).
(C) Schematic representation of YFP-Rab10 localisation (yellow) on the surface of small non-acidic vesicles and a subset of dense-core granule compartments within an individual secondary cell. Acidic compartments are shown in magenta. Nuclei are marked with 'n'.

Homozygous *YFP^{Myc}-Rab10* gene trap flies were used for all panels.

Rab11 plays important roles in recycling endosomal pathways, and in some cell types, such as neuroendocrine PC12 cells, functions in both constitutive and regulated secretory pathways from the trans-Golgi network (Ullrich *et al*., 1996; Ren *et al*., 1998; Urbé *et al*., 1993). In secondary cells, in addition to marking dense-core granule compartments (see Section 3.2.2.4), YFP-Rab11 from the homozygous gene trap line also localised at low levels on numerous small vesicles in the region surrounding the non-cored, Rab6-positive compartment (Figure 3.17A). This localisation may correspond to the previously reported trans-Golgi localisation of Rab11 (Chen *et al*., 1998), or alternatively highlight compartments adjacent to the Golgi that cannot be distinguished in other cell types. Secondary cells carried low levels of YFP-Rab11 on or directly adjacent to the limiting membranes of some non-cored compartments, particularly the rounded compartments (Figure 3.17A''), rather than those that are irregularly shaped (Figure 3.17A'). The possibility that YFP-Rab11 can mark trans-Golgi vesicles was supported by immunofluorescent analysis in main cells, which showed YFP-Rab11-labelled vesicles adjacent to the cis-Golgi, marked by GM130, in a domain that potentially resembled the trans-Golgi (Figure 3.17B).

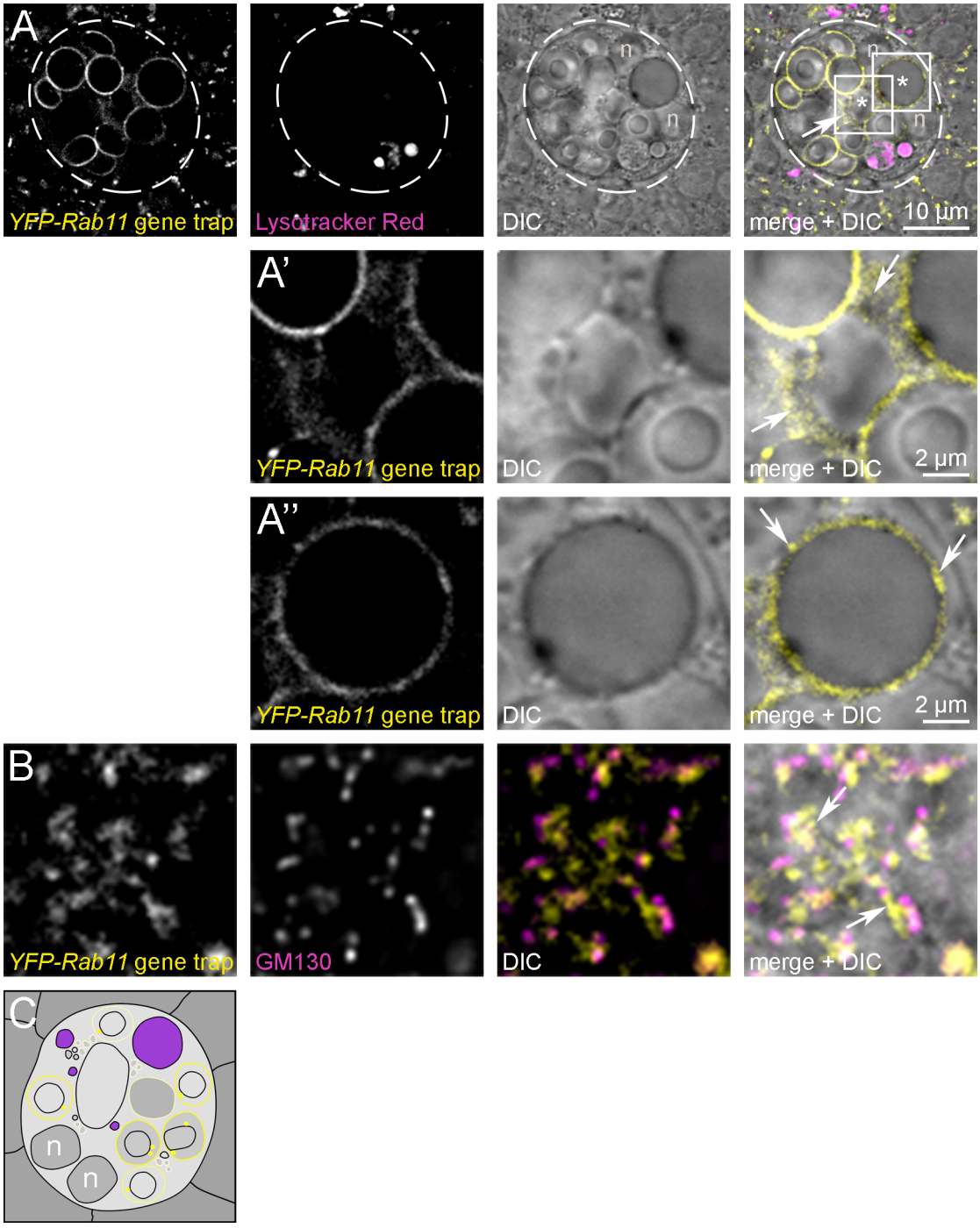

A
YFP-Rab11 gene trap
Lysotracker Red
DIC
merge + DIC
10 µm
n
*
A'
YFP-Rab11 gene trap
DIC
merge + DIC
2 µm
A''
YFP-Rab11 gene trap
DIC
merge + DIC
2 µm
B
YFP-Rab11 gene trap
GM130
DIC
merge + DIC
C
n

Figure 3.17 YFP-Rab11 localises to rounded non-cored compartments, and associated vesicles, in addition to dense-core granule compartments

All panels consist of wide-field fluorescence and DIC images of cells from six-day-old virgin males expressing the *YFP-Rab11* gene trap. The flies were kept at 28.5°C from eclosion. Panels A-A'' are living secondary cells from accessory glands stained with Lysotracker Red, and Panel B shows fixed main cells immunostained for GM130. Secondary cell nuclei were distinguished by DIC morphology and are marked with 'n'. Approximate secondary cell outlines are marked with a dashed line.
(A) Within secondary cells, YFP-Rab11 labels numerous large subcellular compartments, most of them containing a dense-core granule, and some small non-acidic vesicles (arrow) adjacent to the irregularly shaped non-cored compartment, marked with '*'. Boxes highlight the regions enlarged in panels A' and A''.
(A') The irregularly shaped non-cored compartment is surrounded by numerous vesicular structures marked by low levels of YFP-Rab11 (arrows).
(A'') YFP-Rab11 localises on or directly adjacent to the surface of rounded non-cored compartment, where it appears to be concentrated in subdomains of the membrane (arrows).
(B) In main cells, YFP-Rab11 (yellow) localises adjacent to the tubular cis-Golgi, labelled with GM130 (magenta), potentially at the concave trans-face (arrows).
(C) Schematic representation of YFP-Rab11 localisation (yellow) on the surface of diverse intracellular compartments within an individual secondary cell. The level of localisation is represented by the intensity of yellow (i.e. large dense-core granule compartments is highest). Acidic compartments are shown in magenta. Nuclei are marked with 'n'.

Homozygous *YFP^{Myc}-Rab11* gene trap flies were used for all panels.

To further clarify these observations, a homozygous line for both the *CFP-Rab6* gene trap and *YFP-Rab11* gene traps was analysed. The two fusion proteins co-localised at relatively low levels on numerous small non-acidic vesicles surrounding the central CFP-Rab6-positive compartment, in or near the Golgi-rich region (Figure 3.18A). Given that both Rab6 and Rab11 are associated with the trans-Golgi in mammalian cells (Goud *et al*., 1990; Chen *et al*., 1998), it is possible that some of these puncta corresponded to vesicles of the trans-Golgi network. Indeed, in main cells the two GTPases showed almost complete co-localisation adjacent to the cis-Golgi, marked by GM130, in a region that morphologically resembled the trans-Golgi (Figure 3.18B). Further, immunostaining for Golgin245, a trans-Golgi protein, showed colocalisation with both markers in the muscle cells surrounding the epithelium (Figure 3.18C). However, since *Rab1* and *Rab6* gene trap staining do not fully overlap in secondary cells (Section 3.2.2.2), it seems likely that Rab11 may localise to structures adjacent to the trans-Golgi that cannot be distinguished in cells with less clearly defined post-Golgi compartments.

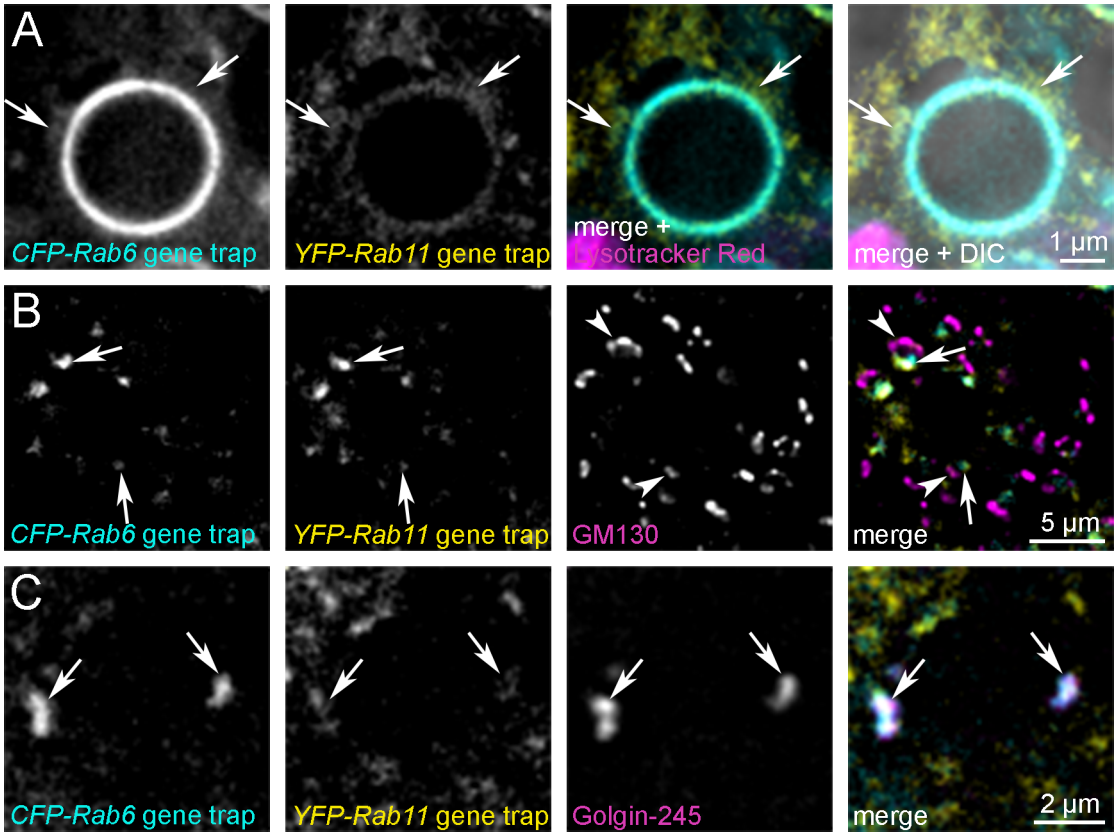


Figure 3.18 YFP-Rab11 localises in or near the trans-Golgi network in different accessory gland cells

All panels show wide-field fluorescence and DIC images from six-day-old virgin males, kept at 28.5°C since eclosion, and expressing CFP-Rab6 and YFP-Rab11 from their endogenous loci. Panel A shows a living secondary cell stained with Lysotracker Red. Panels B-C display main cells from accessory glands that were fixed and immunostained with either anti-GM130 or anti-Golgin-245.
(A) Some of the small CFP-Rab6-marked (cyan) vesicular structures (arrows) surrounding the large non-cored compartment colocalise with YFP-Rab11 (yellow).
(B) In main cells, CFP-Rab6 and YFP-Rab11 partially co-localise (arrows) close to the cis-Golgi, marked by GM130 (arrowheads), on the concave, trans-face of the Golgi.
(C) The trans-Golgi network of surrounding muscle cells, marked by Golgin-245 (magenta), co-localises with high levels of CFP-Rab6 (cyan) and relatively lower levels of YFP-Rab11 (yellow).

Homozygous *w; CFP^{Myc}-Rab6; YFP^{Myc}-Rab11* gene trap flies were used for all panels.

To date, no functional roles for mammalian Rab19 have been reported, though in *Drosophila* it has been shown to interact with Golgi-localised coiled-coil proteins, and to preferentially localise to synaptic boutons in neurons (Sinka *et al*., 2008; Gillingham *et al*., 2014; Chan *et al*., 2011). In secondary cells homozygous for the *YFP-Rab19* gene trap, the expressed fusion protein was predominantly observed on a subset of large apical dense-core granule compartments (see Section 3.2.2.4). It did not localise on the limiting membrane of the central non-core Rab6 compartment, but it was observed on the small non-acidic vesicles that surrounded it, suggesting that it may be positioned in or near the vesicular Golgi networks, as predicted by its structural binding partners (Figure 3.19A-A'; Sinka *et al*., 2008; Gillingham *et al*., 2014). Many other small non-acidic vesicles throughout the secondary cell, which were often in close proximity to the plasma membrane, also carried YFP-Rab19 at their surfaces, suggesting it may be involved in other vesicle trafficking functions at those locations (Figure 3.19A). Some secondary cells exhibited protrusions at their basolateral edges, which were also highly enriched in YFP-Rab19, though it is unclear whether this is artificial, as these structures are not readily seen in control cells (Figure 3.19A). When the *CFP-Rab6* gene trap and *YFP-Rab19* gene trap lines were crossed together, both GTPases co-localised at low levels on small vesicles in the poorly resolved region surrounding the central non-cored compartment (Figure 3.19B). This localisation likely corresponded to the trans-Golgi or adjacent compartments, as might be predicted by Rab19's known binding sites for Golgi-related proteins. However, the expression of YFP-Rab19 from this heterozygous *YFP-Rab19* gene trap line was particularly weak in fluorescence, making it

difficult to analyse the other small vesicles with reduced levels of YFP-Rab19. A combination homozygous line with both of these gene traps might improve the quality of this analysis.

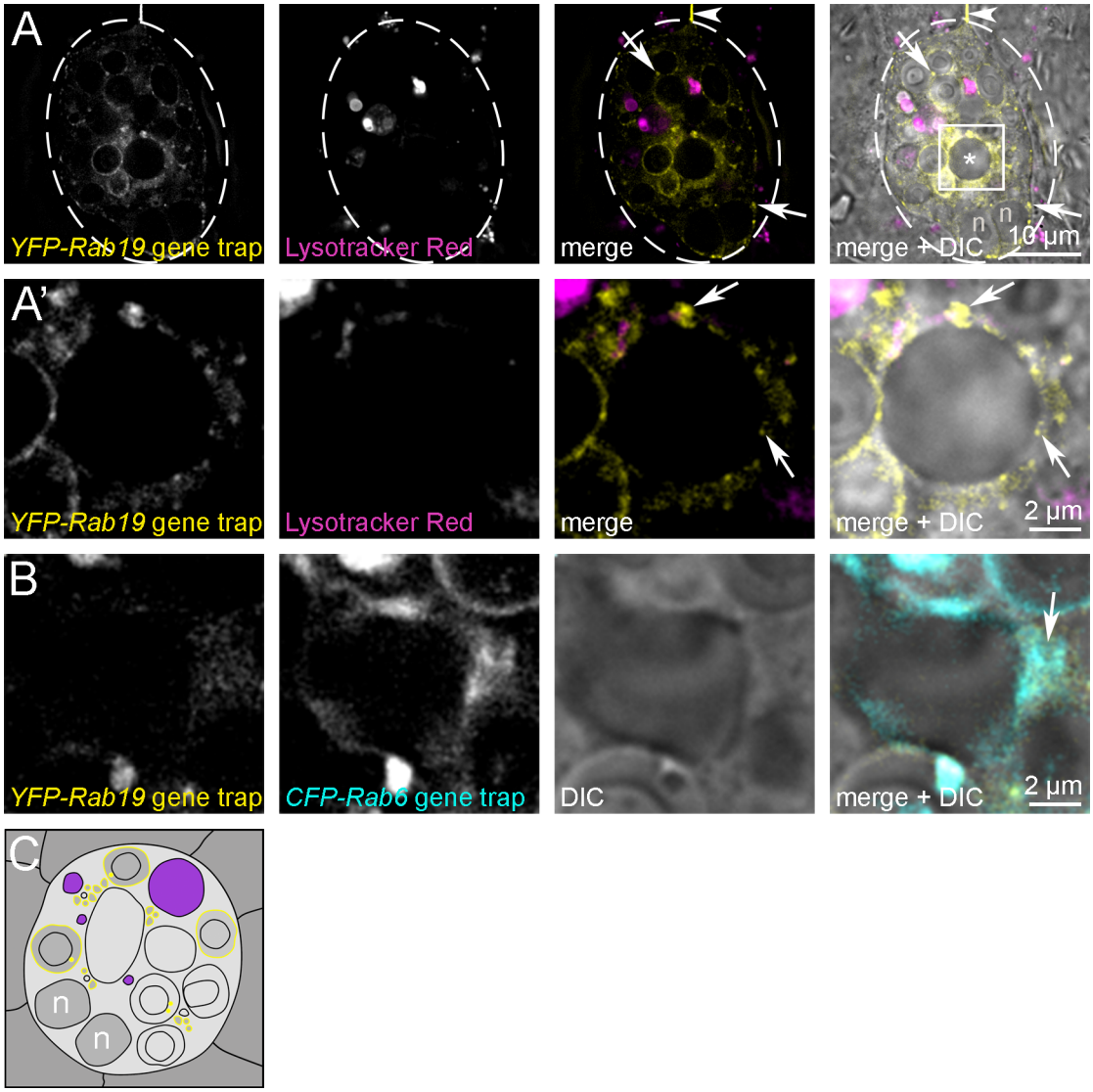

A
YFP-Rab19 gene trap
Lysotracker Red
merge
merge + DIC
10 µm
n
n
*
A'
YFP-Rab19 gene trap
Lysotracker Red
merge
merge + DIC
2 µm
B
YFP-Rab19 gene trap
CFP-Rab6 gene trap
DIC
merge + DIC
2 µm
C
n
n

Figure 3.19 YFP-Rab19 localises to numerous subcellular locations including the Golgi-rich region adjacent to the Rab6-positive non-cored compartment

All panels show wide-field fluorescence and DIC images of living secondary cells from six-day-old virgin males expressing YFP-Rab19 with and without CFP-Rab6 from their endogenous loci. The flies were kept at 28.5°C since eclosion and accessory glands were stained with Lysotracker Red. Secondary cell nuclei were distinguished by DIC morphology and are marked with 'n'. Approximate secondary cell outlines are marked with a dashed line.
(A) YFP-Rab19 (yellow) localises to a diverse range of subcellular structures including numerous small non-acidic intracellular vesicles, some of which are enriched in a region surrounding the large non-cored compartment, marked with '*****'. This region is highlighted with a box, and is enlarged in (A'). Other YFP-Rab19 vesicles localise on some other large compartments, between different subcellular compartments (arrows) and near the plasma membrane. In some cells, YFP-Rab19 is also seen enriched in basolateral cellular protrusions (arrowhead)
(A') Numerous small YFP-Rab19-labelled vesicles surround the central non-cored compartment (arrows).
(B) YFP-Rab19 (yellow) localises in a diffuse manner adjacent to the non-cored compartment, where it colocalises with diffuse CFP-Rab6 (cyan).
(C) Schematic representation of YFP-Rab19 localisation (yellow) on the surface of small non-acidic vesicles and a subset of dense-core granule compartments within an individual secondary cell. Acidic compartments are shown in magenta. Nuclei are marked with 'n'.

The specific genotypes of the flies used in this study were: homozygous *YFP^{Myc}-Rab19* gene trap flies and *w; CFP^{Myc}-Rab6 / +; YFP^{Myc}-Rab19 /* + gene trap flies.

Rab30 localises on the Golgi in cultured human and *Drosophila* cells, where it plays roles in maintaining Golgi integrity (Kelly *et al*., 2012; Sinka *et al*., 2008; Gillingham *et al*., 2014). Similarly, in secondary cells, fusion protein from the *YFP-Rab30* gene trap was observed on numerous small non-acidic vesicles surrounding the large non-cored compartment (Figure 3.20A-A'), where numerous Golgi vesicular networks are located. It was also found on a subset of large basally located dense-core granule compartments (see Section 3.2.2.4). However, like the YFP-Rab8 fusion protein, it was also trafficked into the acidic compartments at high levels. To clarify the Golgi-associated expression further, I crossed the *CFP-Rab6* gene trap to *YFP-Rab30* gene trap. Although difficult to resolve clearly due to weakly fluorescent specimens, YFP-Rab30 partially colocalised with CFP-Rab6 in the Golgi-rich region surrounding the central, large non-cored compartment (Figure 3.20B). Supporting this, in main cells the two GTPases also partially co-localised (Figure 3.20C).

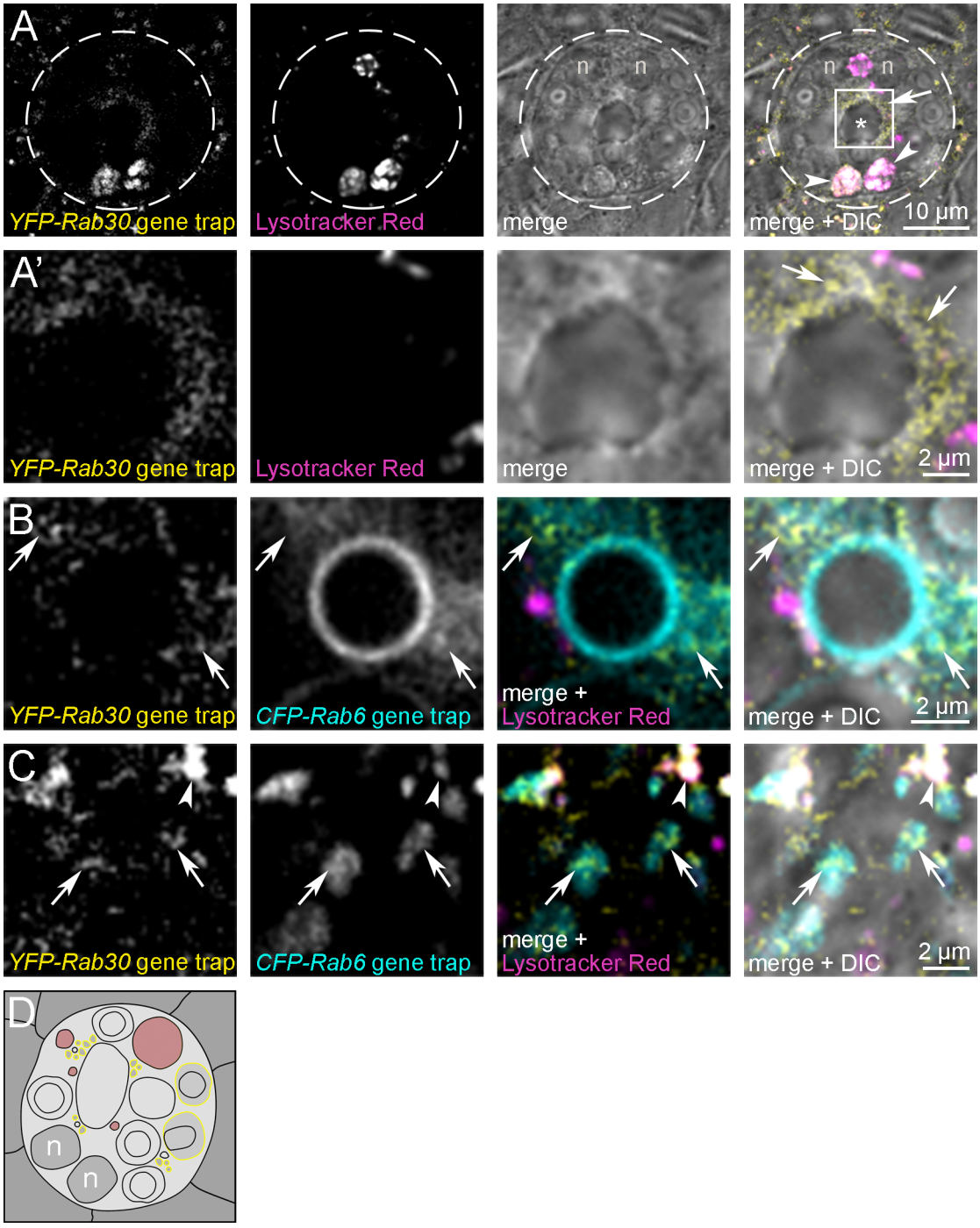

A
YFP-Rab30 gene trap
Lysotracker Red
merge
n
n
merge + DIC
*
10 µm
A'
YFP-Rab30 gene trap
Lysotracker Red
merge
merge + DIC
2 µm
B
YFP-Rab30 gene trap
CFP-Rab6 gene trap
merge +
Lysotracker Red
merge + DIC
2 µm
C
YFP-Rab30 gene trap
CFP-Rab6 gene trap
merge +
Lysotracker Red
merge + DIC
2 µm
D
n
n

Figure 3.20 YFP-Rab30 localises in the Golgi-rich region of secondary cells adjacent to the Rab6-positive non-cored compartment

All panels show wide-field fluorescence and DIC images of living cells from six-day-old virgin males expressing YFP-Rab30 with and without CFP-Rab6, from their endogenous loci. The flies were kept at 28.5°C since eclosion and accessory glands were stained with Lysotracker Red. Secondary cell nuclei were distinguished by DIC morphology and are marked with 'n'. Approximate secondary cell outlines are marked with a dashed line.
(A) In secondary cells, YFP-Rab30 (yellow) localised on the numerous non-acidic vesicular structures surrounding the large non-cored Rab6 compartment, marked with '*', and within the large acidic compartments (magenta). The box highlights the region enlarged in (A').
(A') YFP-Rab30 localises diffusely throughout the region surrounding the central non-cored compartment, but particularly on small vesicular structures (arrows).
(B) The YFP-Rab30-positive (yellow) region of small vesicles surrounding the non-cored compartment colocalises with diffuse CFP-Rab6 (cyan).
(C) In main cells YFP-Rab30 (yellow) and CFP-Rab6 (cyan) partially colocalise on subcellular structures (arrows), though CFP-Rab6 has a wider distribution in the cell. They are also both found within small acidic compartments (magenta; eg., arrowhead).
(D) Schematic representation of YFP-Rab30 localisation (yellow) within an individual secondary cell. A subset of the large dense-core granule compartments and numerous small non-acidic vesicles carry YFP-Rab30 on their surface, and it is found within acidic compartments (magenta). Nuclei are marked with 'n'.

The specific genotypes of the flies used in this study were: homozygous *YFP^{Myc}-Rab30* gene trap flies and *w; CFP^{Myc}-Rab6 / YFP^{Myc}-Rab30; + / +* gene trap flies.

3.2.2.4 Rab11 localises to the surface of the secretory dense-core granule compartments, subsets of which can carry Rab6, Rab7, Rab10, Rab19, Rab21 and Rab30

In secondary cells, the fusion protein synthesised from the *YFP-Rab11* gene trap was consistently found on the limiting membranes of all the large dense-core granule compartments, but not at consistent levels on all compartments (Figure 3.21A). These compartments also often contained intraluminal puncta marked by YFP-Rab11 (Figure 3.21A-B). On occasion, some cells contained one dense-core compartment that lacked YFP-Rab11 on its limiting membrane, and was often surrounded by small acidic compartments, or contained a small acidic microdomain within its lumen (Figure 3.21B'), suggesting that it might have been targeted for degradation (see Section 5.XX). YFP-Rab11 also occasionally marked thin projections from compartments towards the apical plasma membrane, potentially consistent with their known role in recycling some proteins to the cell surface (Figure 3.21C-C').

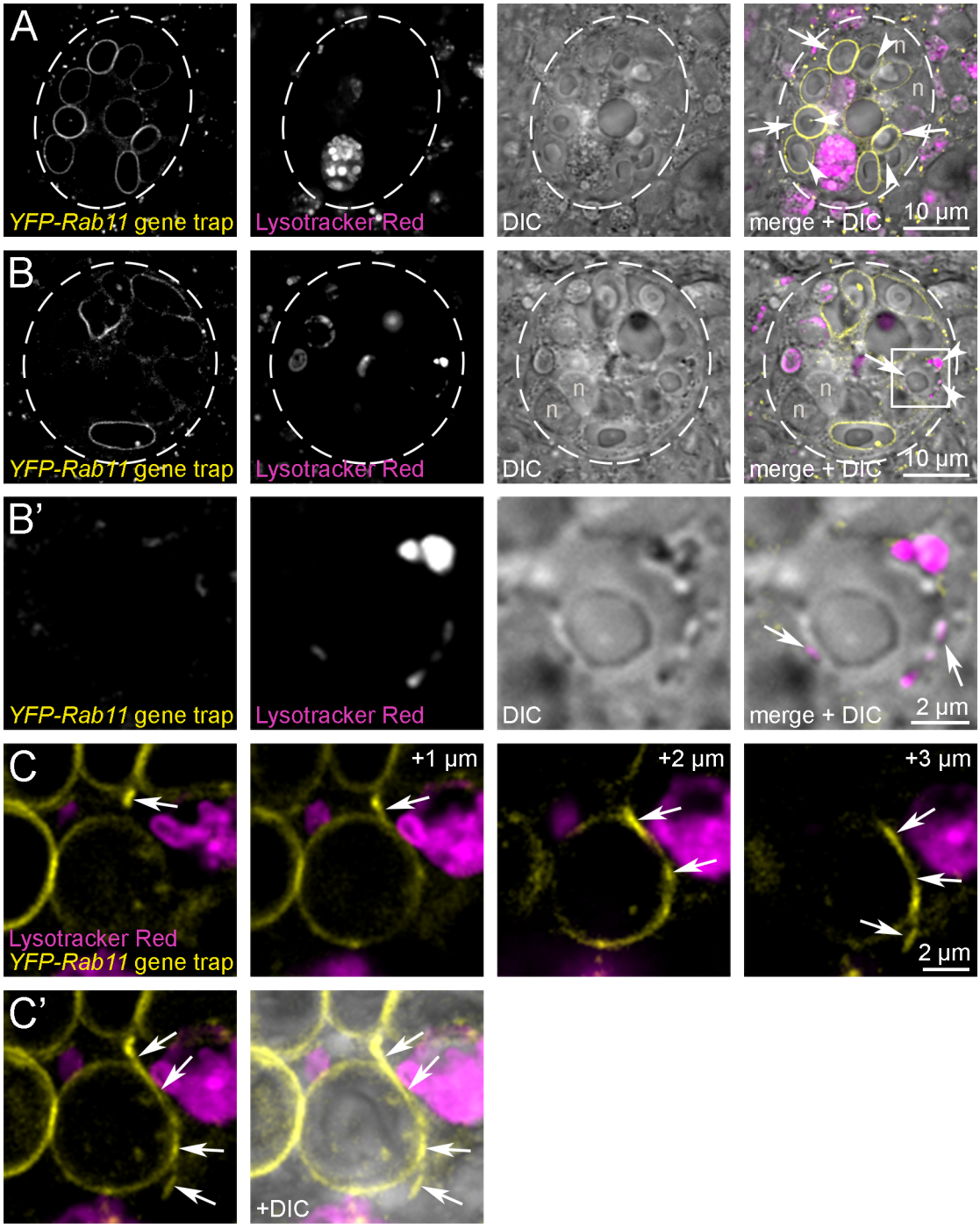

A
YFP-Rab11 gene trap
Lysotracker Red
DIC
merge + DIC
10 µm
n
B
YFP-Rab11 gene trap
Lysotracker Red
DIC
merge + DIC
10 µm
B'
YFP-Rab11 gene trap
Lysotracker Red
DIC
merge + DIC
2 µm
C
Lysotracker Red
YFP-Rab11 gene trap
+1 µm
+2 µm
+3 µm
2 µm
C'
+DIC

Figure 3.21 YFP-Rab11 localises on the surface of all of the non-acidic dense-core granule compartments in secondary cells

Wide-field fluorescence and DIC microscopy were performed on living secondary cells from six-day-old virgin males expressing the *YFP-Rab11* gene trap. The flies were kept at 28.5°C from eclosion and accessory glands were stained with Lysotracker Red (magenta). Secondary cell nuclei were distinguished by DIC morphology and marked with 'n'. Approximate secondary cell outlines are marked with a dashed line.
(A) YFP-Rab11 (yellow) localises to the surface of all the large dense-core granule compartments (arrows) within secondary cells. Intraluminal puncta labelled by YFP-Rab11 are also often observed inside these compartments (arrowheads).
(B) Occasionally, dense-core granule compartments in secondary cells do not carry YFP-Rab11 on their surface (arrow). These particular compartments normally closely associate with small acidic compartments (arrowheads; magenta). The box highlights this particular compartment and surrounding acidic vesicles, and is enlarged in (B').
(B') YFP-Rab11 is not observed on the surface of specific dense-core granule compartments that contain acidic microdomains in their lumen.
(C) Sequential maximum intensity projections of 1 μm depth steps demonstrate that long YFP-Rab11 tubulations (arrows) can project from non-acidic compartments towards the apical plasma membrane (positioned 3 μm above the initial plane of focus).
(C') The full-length 4 μm depth maximum intensity projection of the same compartment as in (C), with and without DIC.

Homozygous *YFP^{Myc}-Rab11* gene trap flies were used for all panels.

A range of other Rab GTPases, many of which are associated with secretory trafficking from the trans-Golgi, were also found on the surface of dense-core granule compartments in secondary cells. Firstly, YFP-Rab10 was detected at variable levels on the surface of several large dense-core granule compartments (Figure 3.22A-A'). There was no clear bias towards labelling of apical or basal compartments. However, it was noted that *YFP-Rab10* gene trap secondary cells contained many more large dense-core granule compartments than wild type non-transgenic cells (Section 3.2.2.3), suggesting the function of the YFP-Rab10 fusion protein is compromised. Interestingly, the *YFP-Rab19* gene trap was highly and specifically expressed by secondary cells within the accessory gland epithelium, where it marked several of the large non-acidic compartments (Figure 3.22B, C). Notably, 2-3 often apically located dense-core compartments displayed YFP-Rab19 at high levels on their limiting membranes (Figure 3.22B-B'), whilst a subset of basally located dense-core compartments carried it at more moderate levels (Figure 3.22C).

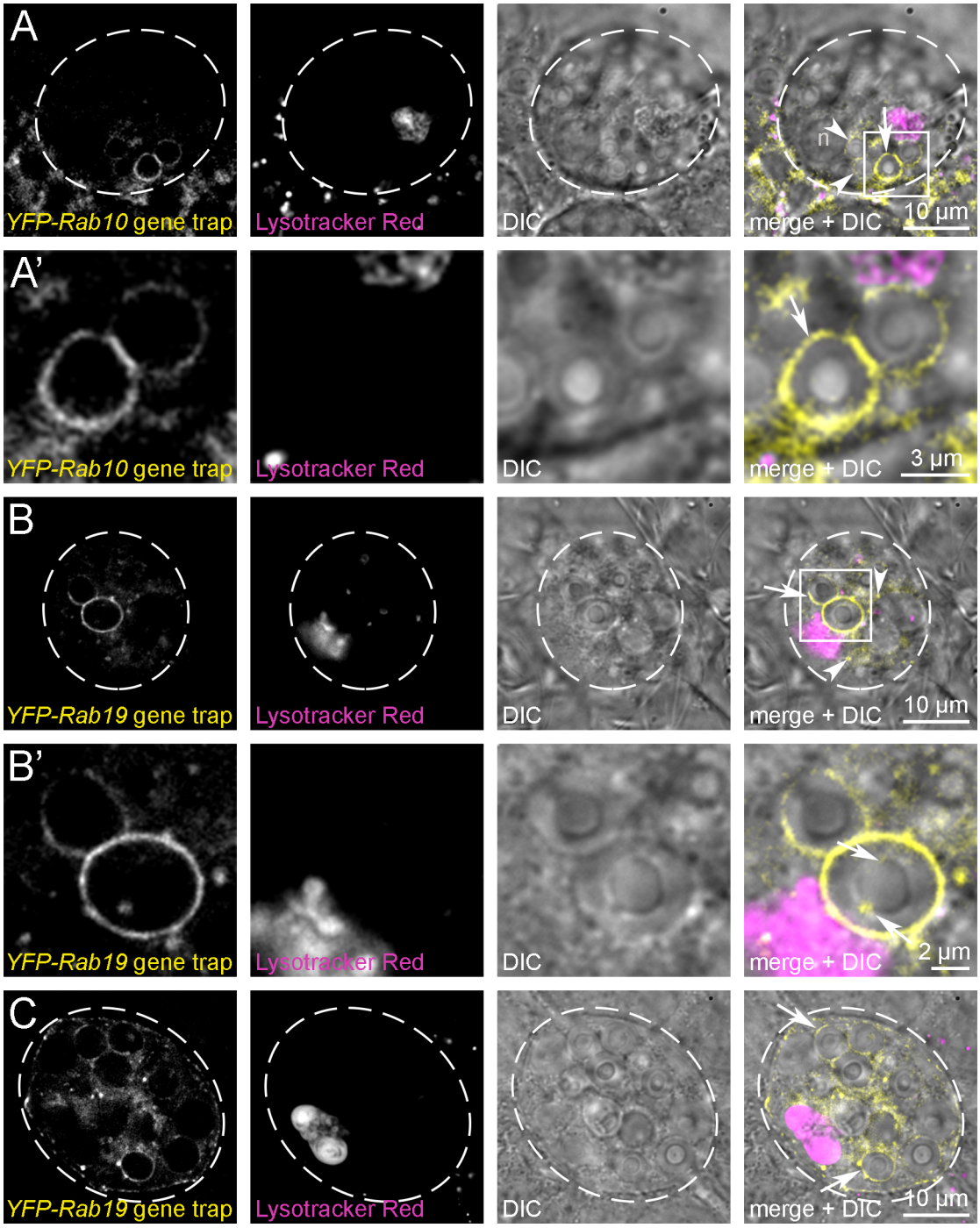

A
YFP-Rab10 gene trap
Lysotracker Red
DIC
n
merge + DIC
10 µm
A'
YFP-Rab10 gene trap
Lysotracker Red
DIC
merge + DIC
3 µm
B
YFP-Rab19 gene trap
Lysotracker Red
DIC
merge + DIC
10 µm
B'
YFP-Rab19 gene trap
Lysotracker Red
DIC
merge + DIC
2 µm
C
YFP-Rab19 gene trap
Lysotracker Red
DIC
merge + DIC
10 µm

Figure 3.22 YFP-Rab10 and YFP-Rab19 both localise to subsets of the large non-acidic dense-core granule compartments

These panels show wide-field fluorescence and DIC images of living secondary cells from six-day-old virgin males that expressing either YFP-Rab10 or YFP-Rab19 from the endogenous gene loci. The flies were kept at 28.5°C since eclosion and accessory glands were stained with Lysotracker Red. Secondary cell nuclei were distinguished by DIC morphology and are marked with 'n'. Approximate secondary cell outlines are marked with a dashed line.
(A) Variable levels of YFP-Rab10 (yellow) are observed on the surface of several dense-core granule compartments in secondary cells, with some compartments carrying high levels (arrow) and others relatively lower (arrowheads). The box highlights the region enlarged in (A')
(A') The surface of some dense-core granule compartments is marked by YFP-Rab10 (arrow).
(B) YFP-Rab19 (yellow) localises at high levels on the surface of 2-3 large dense-core granule compartments, which are typically apically located (arrows), and on numerous small non-acidic vesicles (arrowheads). The box highlights the region enlarged in (B').
(B') Intraluminal structures within the apical dense-core granule compartments are marked by YFP-Rab19 (arrows).
(C) A subset of basally located dense-core granule compartments in the same secondary cell as (B) carries surface YFP-Rab19 (yellow), but at more modest levels than the apical compartments.

Homozygous *YFP^{Myc}-Rab10* gene trap and homozygous *YFP^{Myc}-Rab19* gene trap flies were used for this figure.

The fusion protein from the *YFP-Rab21* gene trap, which is associated with early endosomal trafficking in human cells (Simpson *et al*., 2004), was found on the limiting membrane of 1-2 large, often apically located, non-acidic, dense-core granule compartments in about 50% of secondary cells imaged (Figure 3.23A-A'). YFP-Rab30 was also found at moderate levels on 3-4 basally located dense-core granule compartments (Figure 3.23B-B'). The basal location of those compartments marked by YFP-Rab30 suggested that it marked a different population of compartments to YFP-Rab21. Indeed, the differential patterns of localisation of several Rab proteins on dense-core granule compartments suggests that they might mark different maturation states or functions, an idea explored further below.

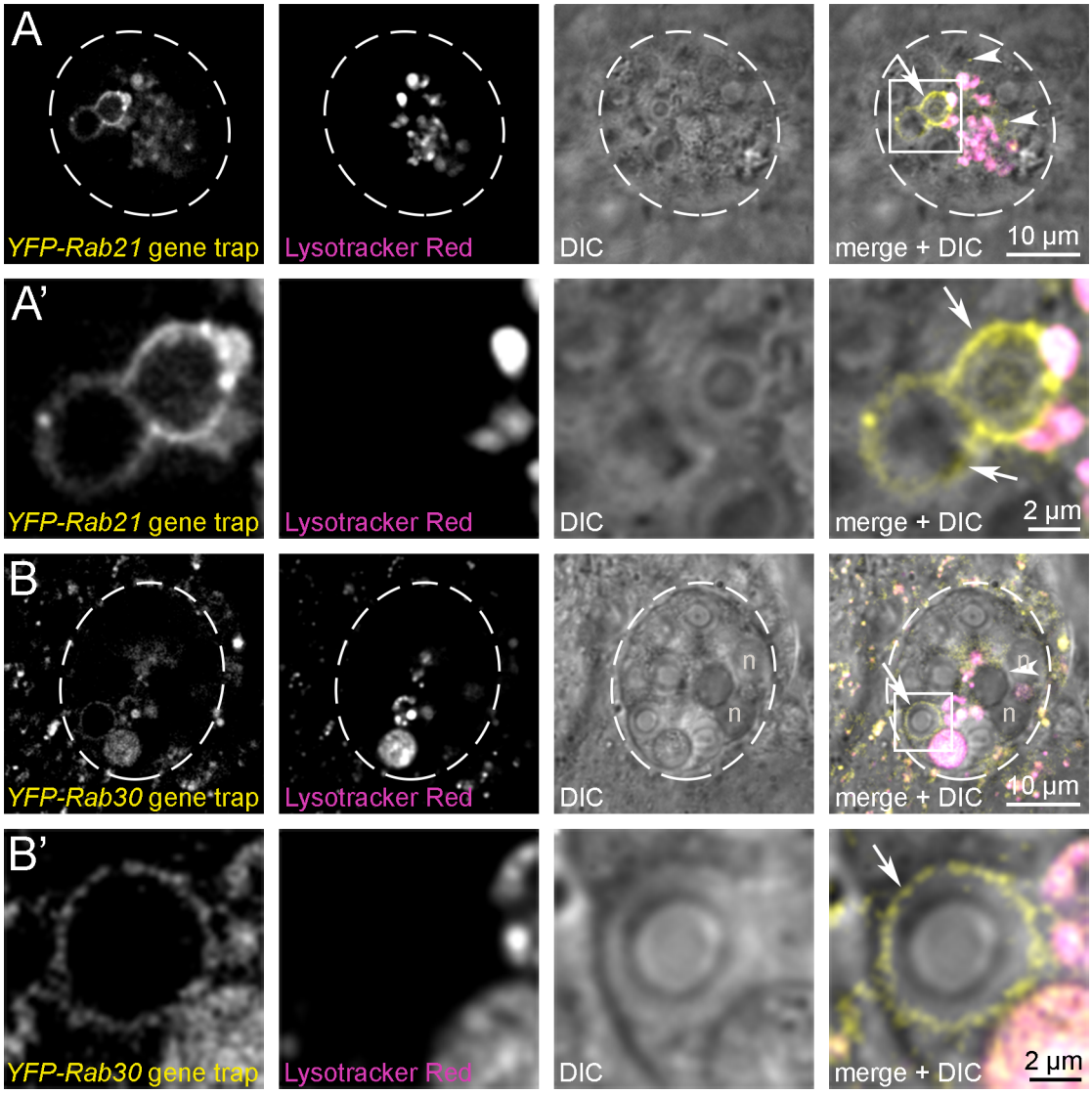

A
YFP-Rab21 gene trap
Lysotracker Red
DIC
merge + DIC
10 µm
A'
YFP-Rab21 gene trap
Lysotracker Red
DIC
merge + DIC
2 µm
B
YFP-Rab30 gene trap
Lysotracker Red
n
n
DIC
n
n
merge + DIC
10 µm
B'
YFP-Rab30 gene trap
Lysotracker Red
DIC
merge + DIC
2 µm

Figure 3.23 Rab21 and Rab30 localise on spatially distinct subsets of secondary cell dense-core granule compartments.

These panels display wide-field fluorescence and DIC images of living secondary cells from six-day-old virgin males expressing either YFP-Rab21 or YFP-Rab30 from their endogenous loci. The flies were kept at 28.5°C since eclosion and their accessory glands were stained with Lysotracker Red (magenta). Secondary cell nuclei were distinguished by DIC morphology and are marked with 'n'. Approximate secondary cell outlines are marked with a dashed line.
(A) In approximately half of secondary cells imaged, YFP-Rab21 (yellow) localised onto the surface of 1-2 apically located dense-core granule compartments (arrows). Small intracellular vesicles were also marked by YFP-Rab21. The box highlights the specific region that is enlarged in (A').
(A') YFP-Rab21 localises onto the surface of two apical dense-core granule compartments (arrows) at relatively high levels.
(B) A small subset of the basally located dense-core granule compartments in secondary cells carry low levels of YFP-Rab30 (yellow) on their surface (arrow). The box distinguishes the specific region enlarged in (B').
(B') YFP-Rab30 localises on the surface of a large non-acidic compartment (arrow) with a clear dense-core granule.

Homozygous *YFP^{Myc}-Rab21* gene trap and homozygous *YFP^{Myc}-Rab30* gene are presented in this figure.

3.2.2.5 Rab6 co-localises with Rab11 on some dense-core compartments, but does not overlap with Rab7, Rab19, Rab21 or Rab30

A homozygous line for both the *CFP-Rab6* gene trap and *YFP-Rab11* gene trap was examined extensively because the two proteins showed preferences for the limiting membranes of large non-cored and cored compartments, respectively (Figure 3.24A). Although the two GTPases overlapped on some compartments, the levels were inversely proportional, such that when CFP-Rab6 was observed at high levels, YFP-Rab11 was at low levels, and vice versa. Within the dense-core compartments, they co-localised on some intraluminal puncta or sometimes marked discrete puncta (Figure 3.24B-C). When the *CFP-Rab6* gene trap was crossed to the late endosomal and lysosomal *YFP-Rab7* gene trap (described in more detail in Section 3.2.2.7), the two respective fusion proteins marked distinct populations of large compartments and small vesicles (Figure 3.24D). Notably, however, the large non-acidic compartment marked by YFP-Rab7 often contained intraluminal puncta labelled with protein from the *CFP-Rab6* gene trap (Figure 3.24E). Some diffuse CFP-Rab6 was also detected inside the large acidic compartments marked by YFP-Rab7 (Figure 3.24D).

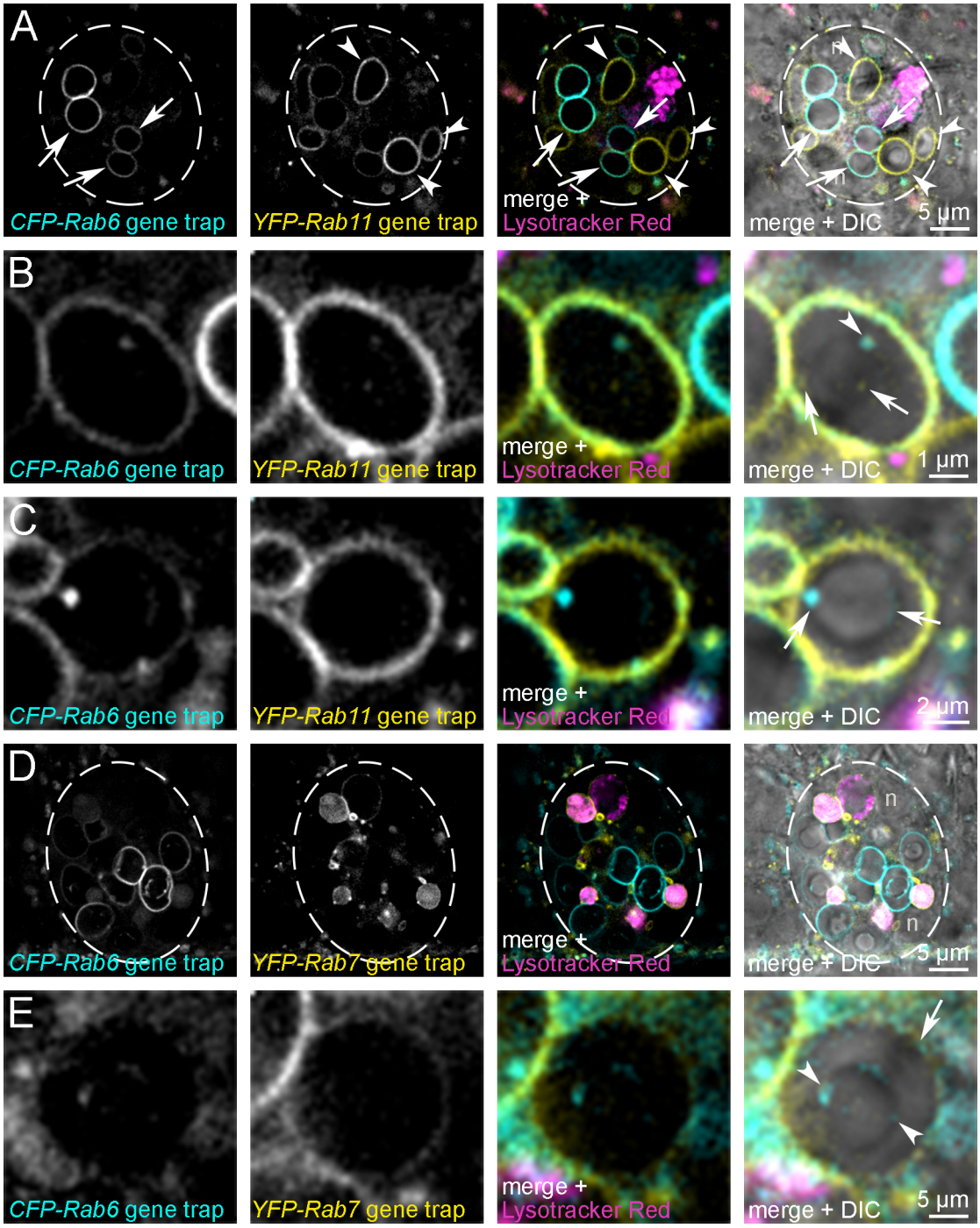

A
CFP-Rab6 gene trap
YFP-Rab11 gene trap
merge +
Lysotracker Red
n
n
merge + DIC
5 µm
B
CFP-Rab6 gene trap
YFP-Rab11 gene trap
merge +
Lysotracker Red
merge + DIC
1 µm
C
CFP-Rab6 gene trap
YFP-Rab11 gene trap
merge +
Lysotracker Red
merge + DIC
2 µm
D
CFP-Rab6 gene trap
YFP-Rab7 gene trap
merge +
Lysotracker Red
n
n
merge + DIC
5 µm
E
CFP-Rab6 gene trap
YFP-Rab7 gene trap
merge +
Lysotracker Red
merge + DIC
5 µm

Figure 3.24 Combinations of CFP-Rab6 with YFP-Rab11 and YFP-Rab7 highlight compartments containing more than one Rab

All panels present wide-field fluorescence and DIC images from six-day-old virgin males, kept at 28.5°C since eclosion, and expressing CFP-Rab6 in combination with either YFP-Rab11 or YFP-Rab7 from their endogenous loci. The accessory glands from these flies were stained with Lysotracker Red. Secondary cell nuclei were distinguished by DIC morphology and are marked with 'n'. Approximate secondary cell outlines are marked with a dashed line.
(A) In secondary cells, CFP-Rab6 (cyan) is localised at high levels on the surface of large non-acidic compartments (arrows), some containing dense-core granules, that carry lower levels of YFP-Rab11 (yellow) on their surface, whilst dense-core granule compartments with higher levels of YFP-Rab11 (arrowheads) carry lower levels of CFP-Rab6.
(B) Mixed Rab cargos are found on intraluminal puncta within dense-core granule compartments. Some intraluminal puncta within dense-core granule compartments carry only YFP-Rab11 (yellow; arrows), whilst others carry both CFP-Rab6 (cyan) and YFP-Rab11 (arrowhead).
(C) CFP-Rab6-marked (cyan; arrows) ILVs can be observed within dense-core granule compartments that primarily carry YFP-Rab11 (yellow) on their surface.
(D) Subcellular compartments labelled by CFP-Rab6 (cyan) are distinct from those that carry YFP-Rab7 (yellow).
(E) Non-acidic dense-core granule compartments labelled by YFP-Rab7 (yellow; arrow) can contain intraluminal puncta that carry CFP-Rab6 (arrowheads).

The specific lines used in this figure are: homozygous *w; CFP^{Myc}-Rab6; YFP^{Myc}-Rab11* gene trap flies, and *w; CFP^{Myc}-Rab6 / +; YFP^{Myc}-Rab11 / +* flies.

The *CFP-Rab6* gene trap was also crossed to the *YFP-Rab19* gene trap. Rab19 function is unclear, but is highly expressed in secondary cells, where it marks a variety of subcellular organelles. The two GTPases localised to the limiting membranes of distinct populations of large non-acidic compartments (Figure 3.25A). However, intraluminal puncta with high levels of YFP-Rab19 were observed inside dense-core compartments labelled by CFP-Rab6 (Figure 3.25B). Similarly, the YFP-Rab19-positive compartments contained some intraluminal puncta marked only by CFP-Rab6, suggesting either that Rab6- and Rab19-positive compartments communicate with each other or that these compartments can change their identity (Figure 3.25C).

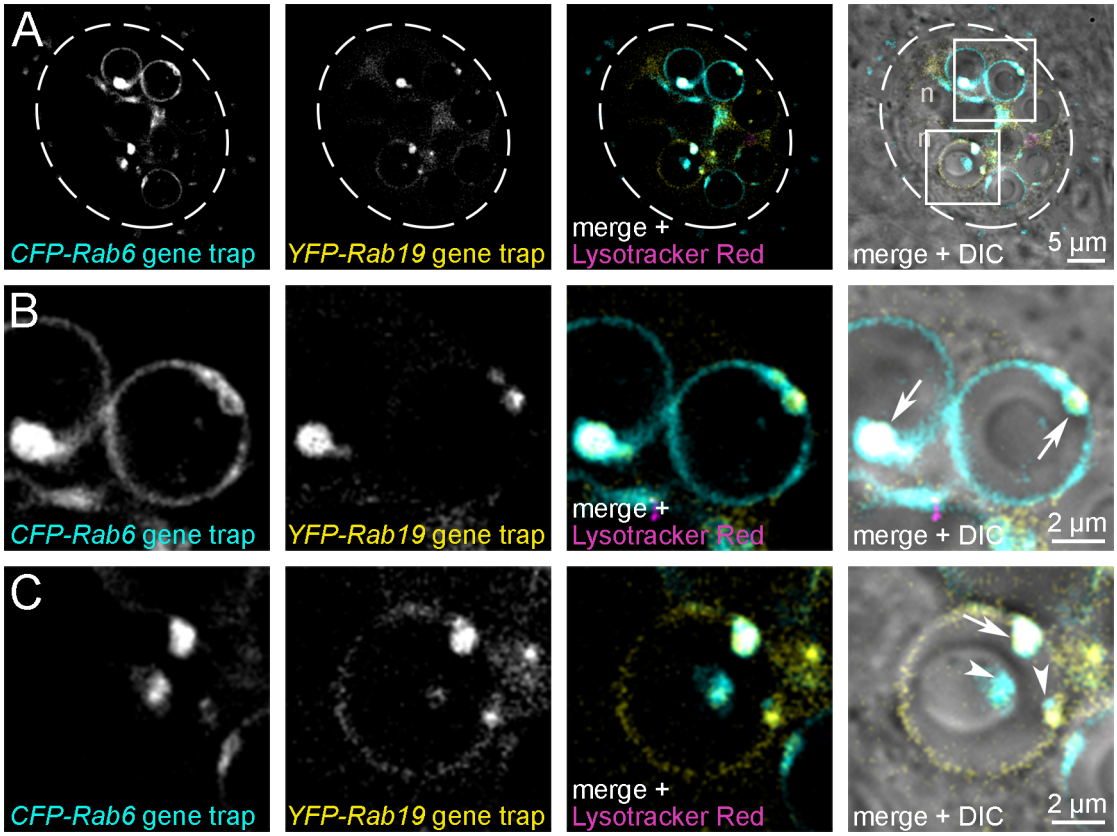


Figure 3.25 CFP-Rab6 and YFP-Rab19 localise to the limiting membranes of distinct dense-core granule compartments, but also localise as intraluminal puncta within compartments marked by the other Rab

All panels show wide-field fluorescence and DIC images of living secondary cells from three-day-old virgin males that expressed both CFP-Rab6 and YFP-Rab19 from their endogenous loci. The flies were kept at 28.5°C since eclosion and accessory glands were stained with Lysotracker Red. Secondary cell nuclei were distinguished by DIC morphology and are marked with 'n'. Approximate secondary cell outlines are marked with a dashed line.

(A) CFP-Rab6 (cyan) and YFP-Rab19 (yellow) localise onto distinct populations of non-acidic dense-core granule compartments in secondary cells. Boxes highlight specific regions that contain compartments carrying high levels of CFP-Rab6, which is enlarged in (B), and others that carry higher levels of YFP-Rab19, which is shown in (C).

(B) Large intraluminal puncta containing YFP-Rab19 (yellow, arrows) are observed within compartments specifically labelled with high levels of CFP-Rab6 (cyan).

(C) YFP-Rab19 (yellow) marked compartments contain CFP-Rab6-labelled (cyan) intraluminal puncta, some of which overlap with YFP-Rab19 (arrows), while others do not (arrowheads).

The specific genotype used in this figure is *w; CFP^{Myc}-Rab6 / +; YFP^{Myc}-Rab19 /* + gene trap flies

The cross between *CFP-Rab6* and *YFP-Rab21* gene traps similarly showed that the GTPases localised onto separate populations of large non-acidic compartments. YFP-Rab21 was observed exclusively on the limiting membrane of 1-2 apical dense-core compartments with no detectable CFP-Rab6 (Figure 3.26A-A'). The interior of these compartments contained a mixture of intraluminal puncta, some labelled only by CFP-Rab6, and others that showed co-localisation of the two GTPases (Figure 3.26A'). In a similar manner, despite not being present at the limiting membrane of CFP-Rab6-positive compartments, YFP-Rab21 was found on intraluminal puncta inside the compartments (Figure 3.26A').

A cross between *CFP-Rab6* and *YFP-Rab30* gene traps also revealed that the two GTPases localised on the surface of different populations of large non-acidic compartments. Specifically, 1-3 basally located dense-core compartments carried YFP-Rab30 on their limiting membranes, but not CFP-Rab6 (Figure 3.26B-B'). The interior of these compartments contained some intraluminal puncta marked by CFP-Rab6 (Figure 3.26B').

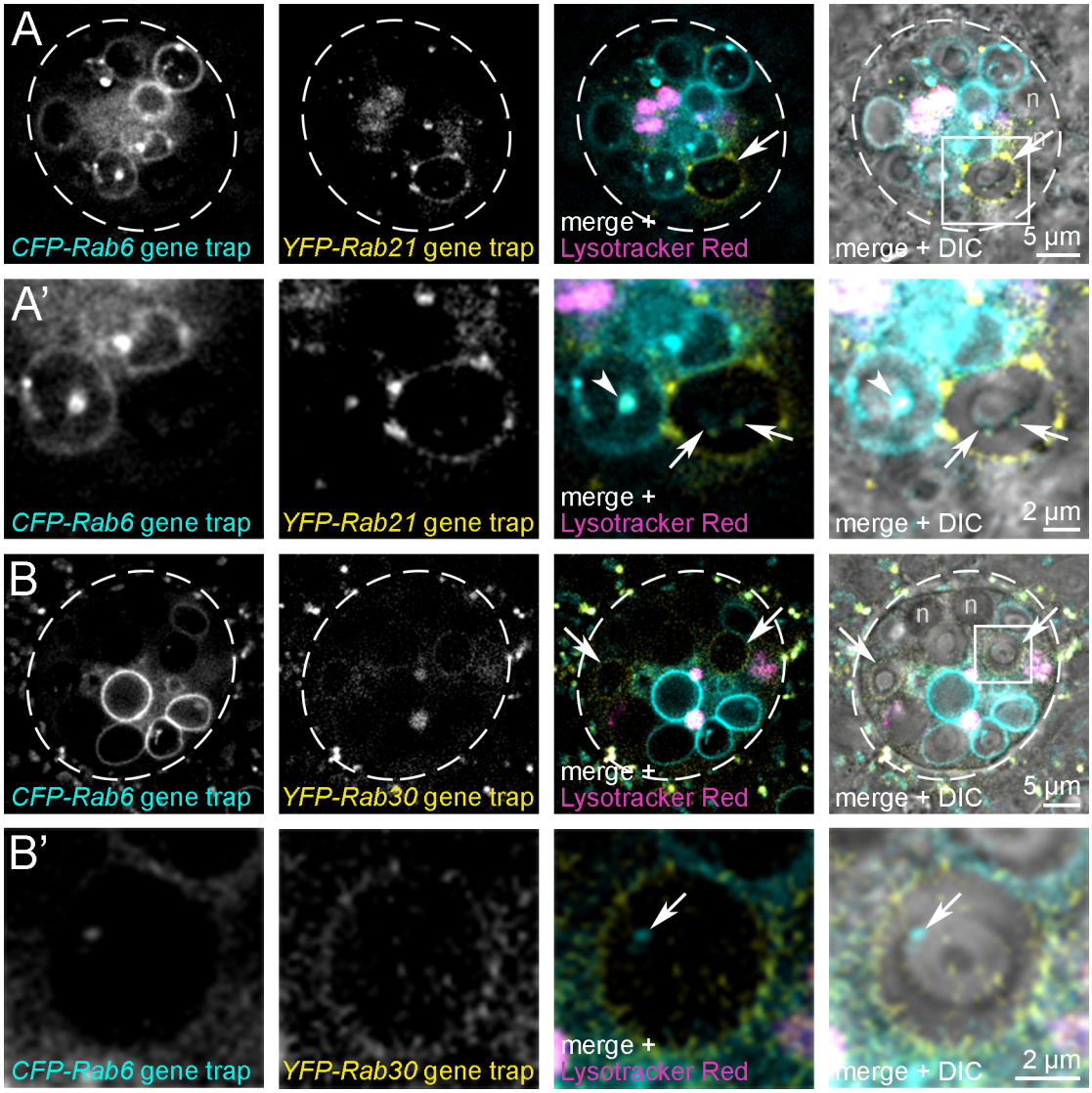

A
CFP-Rab6 gene trap
YFP-Rab21 gene trap
merge +
Lysotracker Red
n
n
merge + DIC
5 µm
A'
CFP-Rab6 gene trap
YFP-Rab21 gene trap
merge +
Lysotracker Red
merge + DIC
2 µm
B
CFP-Rab6 gene trap
YFP-Rab30 gene trap
merge +
Lysotracker Red
n
n
merge + DIC
5 µm
B'
CFP-Rab6 gene trap
YFP-Rab30 gene trap
merge +
Lysotracker Red
merge + DIC
2 µm

Figure 3.26 CFP-Rab6 localises on internal puncta within YFP-Rab21 and YFP-Rab30 compartments, despite being absent from their limiting membranes

All panels show wide-field fluorescence and DIC images of living secondary cells from six-day-old virgin males that expressed the *CFP-Rab6* gene trap in combination with either the *YFP-Rab21* or *YFP-Rab30* gene traps. The flies were kept at 28.5°C following eclosion and their accessory glands were stained with Lysotracker Red. Secondary cell nuclei were distinguished by DIC morphology and are marked with 'n'. Approximate secondary cell outlines are marked with a dashed line.
(A) YFP-Rab21 (yellow) localises on 1-2 apical dense-core granule compartments (arrow) that do not carry CFP-Rab6 (cyan) on their surface. The box highlights the subcellular region that is enlarged in (A').
(A') CFP-Rab6-marked intraluminal puncta within the YFP-Rab21-marked compartment (arrows). Some of these puncta are only labelled by CFP-Rab6, but other puncta colocalise with the YFP-Rab21 signal. Within the CFP-Rab6-labelled dense-core granule compartment, some YFP-Rab21-marked puncta are also observed (arrowhead).
(B) YFP-Rab30 (yellow) marks a small subset of basally-located dense-core granule compartments that do not carry CFP-Rab6 at their surface (cyan). A box highlights the region enlarged in (B')
(B') A higher magnified view of the YFP-Rab30 labelled dense-core granule compartment shows that it contains CFP-Rab6-postive intraluminal puncta (arrow).

The specific fly genotypes used in this figure are *w / YFP^{Myc}-Rab21; CFP^{Myc}-Rab6 / +; + / +* and *w; YFP^{Myc}-Rab30 / CFP^{Myc}-Rab6; + / +*.

In summary, these data suggest that Rab6 labels the limiting membrane of dense-core granule compartments that are distinct from compartments that carry Rab19, Rab21 and Rab30. Since compartments marked with these latter Rabs contain Rab6-positive intraluminal puncta, one possible explanation is that they are derived from Rab6-positive compartments, a hypothesis tested in Chapter 5.

3.2.2.6 Rab4, Rab5, Rab21 and Rab35 localisation is consistent with their roles on early or recycling endosomes

Rab5 has well-characterised roles in early endosome biogenesis and trafficking, as well as other endocytic processes such as macropinocytosis (Zeigerer *et al*., 2012; Wucherpfennig *et al*., 2003; Feliciano *et al*., 2011). The fusion protein from the *YFP-Rab5* gene trap was localised at high levels on dynamic small non-acidic vesicles, presumably early endosomes, found throughout secondary cells, but often in close proximity to large intracellular compartments (Figure 3.27A). For example, YFP-Rab5 was found on a few small vesicles adjacent to the large non-acidic, non-cored Rab6-positive compartment. It was also detected at lower levels in other vesicular structures surrounding that compartment (Figure 3.27A'), some of which are likely to overlap or be adjacent to the extensive Golgi networks. Several YFP-Rab5-positive small vesicles were observed close to the large acidic compartments (Figure 3.27B-B'), and also adjacent to numerous small acidic compartments at the apical plasma membrane (Figure 3.27C-C'), consistent with Rab5's roles in endocytosis, and with previous observations using an overexpressed YFP-tagged Rab5 (Corrigan *et al*., 2014). The close association of YFP-Rab5-positive vesicles with various other types of subcellular compartments may be indicative of interactions between early endosomes and these other compartments.

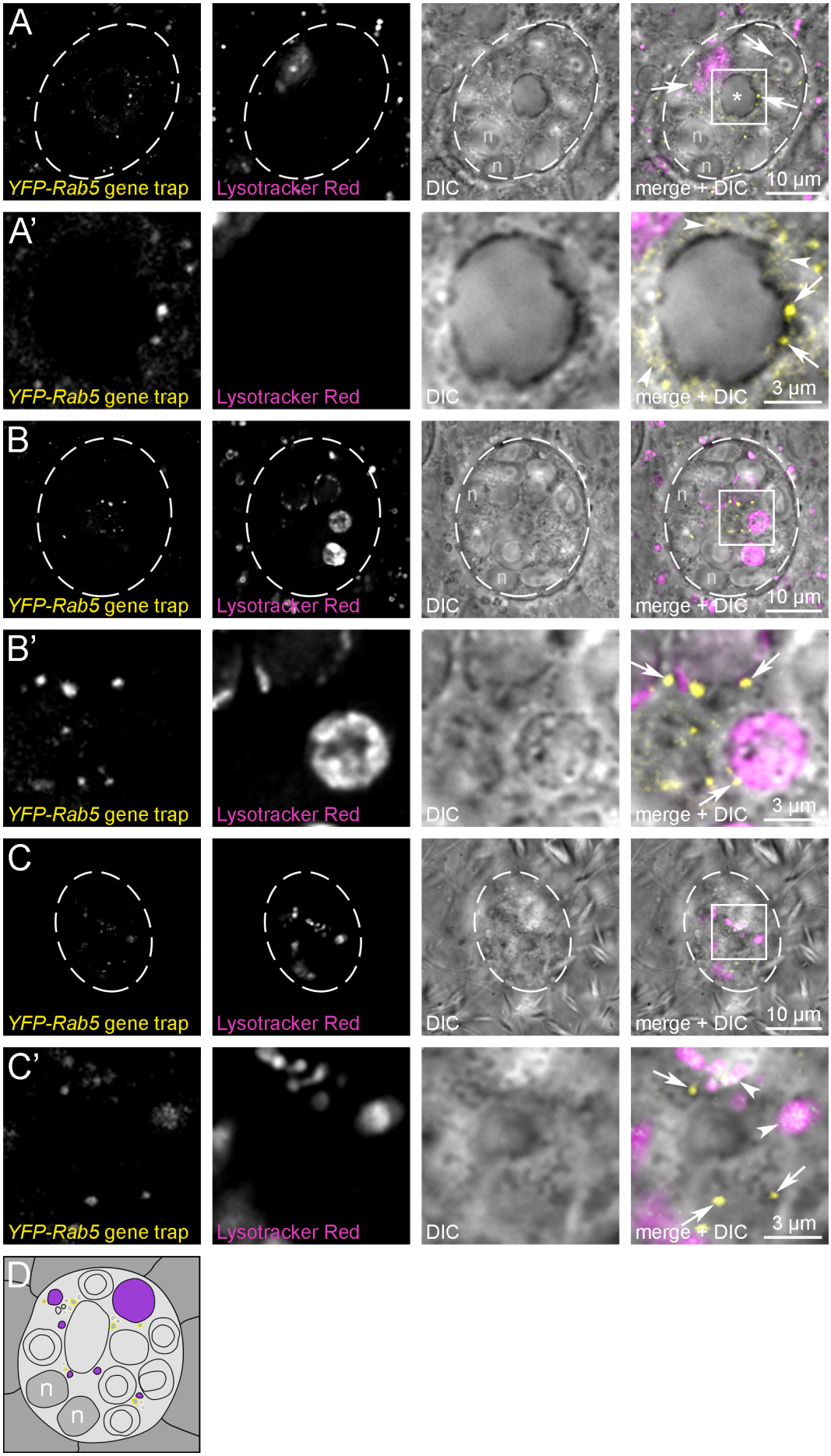

A
YFP-Rab5 gene trap
Lysotracker Red
DIC
merge + DIC
10 µm
A'
YFP-Rab5 gene trap
Lysotracker Red
DIC
merge + DIC
3 µm
B
YFP-Rab5 gene trap
Lysotracker Red
DIC
merge + DIC
10 µm
B'
YFP-Rab5 gene trap
Lysotracker Red
DIC
merge + DIC
3 µm
C
YFP-Rab5 gene trap
Lysotracker Red
DIC
merge + DIC
10 µm
C'
YFP-Rab5 gene trap
Lysotracker Red
DIC
merge + DIC
3 µm
D
n
n

Figure 3.27 YFP-Rab5 localises on small intracellular vesicles found adjacent to larger subcellular compartments and the plasma membrane

All panels show wide-field fluorescence and DIC images of living secondary cells from six-day-old virgin males expressing the *YFP-Rab5* gene trap. The flies were kept at 28.5°C following eclosion and their accessory glands were stained with Lysotracker Red (magenta). Secondary cell nuclei are distinguished by DIC morphology and are marked with 'n'. Approximate secondary cell outlines are marked with a dashed line.
(A) YFP-Rab5 (yellow) localises on numerous small non-acidic vesicles throughout the cell (arrows), several of which associate closely with the large non-cored Rab6-positive compartment, marked with '*'. This particular region is boxed and enlarged in (A')
(A') In addition to marking some specific vesicles at high levels (arrows), YFP-Rab5 also localises in a diffuse manner within the small vesicular structures adjacent to the large non-cored compartment (arrowheads).
(B) YFP-Rab5-labelled (yellow) small vesicles are often in close proximity to larger acidic compartments (magenta). An example region is boxed and enlarged in (B')
(B') Numerous small YFP-Rab5 vesicles associate closely with larger acidic compartments (arrows).
(C) This apical section shows that YFP-Rab5 (yellow) localises on small vesicles in close proximity to the plasma membrane. The box highlights a particular region that is enlarged in (C').
(C') Several YFP-Rab5-marked vesicles associate closely with small acidic compartments (magenta; arrows). Some diffuse YFP-Rab5 was found within these apical acidic compartments (arrowheads).
(D) Schematic representation of YFP-Rab5 localisation (yellow) on the surface small non-acidic vesicles within an individual secondary cell. The level of localisation is represented by the intensity of yellow. Acidic compartments are shown in magenta. Nuclei are marked with 'n'.

Homozygous *YFP^{Myc}-Rab5* gene trap flies were used throughout this figure.

Rab4 functions on early endosomes and has been implicated in the recycling of various cargoes, such as integrins and G-protein coupled receptors (Roberts et al., 2001; Li *et al*., 2008). In secondary cells, the fusion protein from the *YFP-Rab4* gene trap was observed on several small non-acidic vesicles scattered throughout the cell, presumably equivalent to early endosomes (Figure 3.28A). Several of these small non-acidic vesicles were very closely associated with both small and large Lysotracker-Red stained vesicles (Figure 3.28C). Other YFP-Rab4-labelled vesicles were found near the apical plasma membrane (data not shown). Furthermore, some of the small YFP-Rab4-labelled vesicles were located in close proximity to large compartments, possibly mediating traffic to or from these compartments. For example, a few small vesicles carrying this GTPase were adjacent to the large non-acidic, non-cored compartment (Figure 3.28A'). Other vesicles were found adjacent to large acidic compartments (Figure 3.28C), and non-acidic dense-core granule compartments (Figure 3.28B).

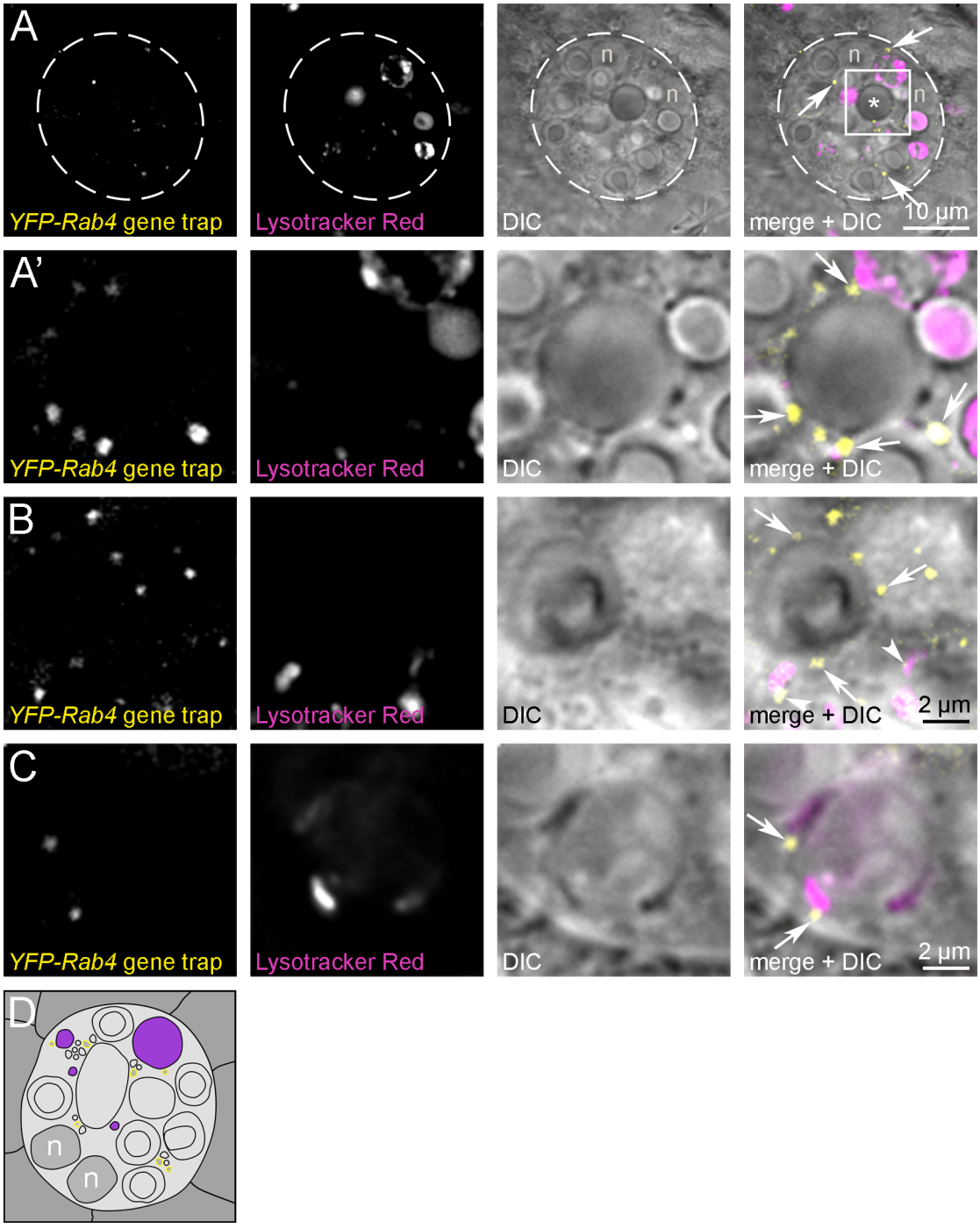

A
YFP-Rab4 gene trap
Lysotracker Red
DIC
n
n
merge + DIC
n
n
*
10 µm
A'
YFP-Rab4 gene trap
Lysotracker Red
DIC
merge + DIC
B
YFP-Rab4 gene trap
Lysotracker Red
DIC
merge + DIC
2 µm
C
YFP-Rab4 gene trap
Lysotracker Red
DIC
merge + DIC
2 µm
D
n
n

Figure 3.28 YFP-Rab4 localises on small intracellular vesicles that associate closely with different types of secondary cell compartments and the plasma membrane

All panels show wide-field fluorescence and DIC images of living secondary cells from six-day-old virgin males expressing the *YFP-Rab4* gene trap. The flies were kept at 28.5°C following eclosion and their accessory glands were stained with Lysotracker Red. Secondary cell nuclei were distinguished by DIC morphology and are marked with 'n'. Approximate secondary cell outlines are marked with a dashed line.
(A) In secondary cells YFP-Rab4 (yellow) localises on punctate non-acidic vesicles that are scattered throughout the cell, in between the larger subcellular compartments and also close to the plasma membrane (arrows). The box highlights a region surrounding the centrally located non-cored compartment, marked with '*', which is enlarged in (A').
(A') Several small YFP-Rab4-labelled vesicles are localised in the central region surrounding the non-cored Rab6-positive compartment (arrows).
(B) A more apical z-section of the same secondary cell shows that numerous YFP-Rab4 (yellow) vesicles associate closely with some dense-core granule compartments (arrows), and also with small acidic compartments (arrowheads; magenta).
(C) Some YFP-Rab4-labelled (yellow) vesicles are found adjacent to large acidic compartments (magenta; arrows).
(D) Schematic representation of YFP-Rab4 localisation (yellow) on small non-acidic vesicles within an individual secondary cell. Acidic compartments are shown in magenta. Nuclei are marked with 'n'.

Homozygous *YFP^{Myc}-Rab4* gene trap flies were used throughout this figure.

Rab21 is found on early endosomes in mammalian cells and is associated with the endocytic trafficking of integrins (Pellinen *et al*., 2006). Although the fusion protein from the *YFP-Rab21* gene trap was observed on the surface of 1-2 apical dense-core granule compartments (Section 3.2.2.4), it also localised to several small non-acidic vesicles scattered throughout the cell (Figure 3.29A-A''), in a manner similar to YFP-Rab5 and consistent with an early endosomal role.

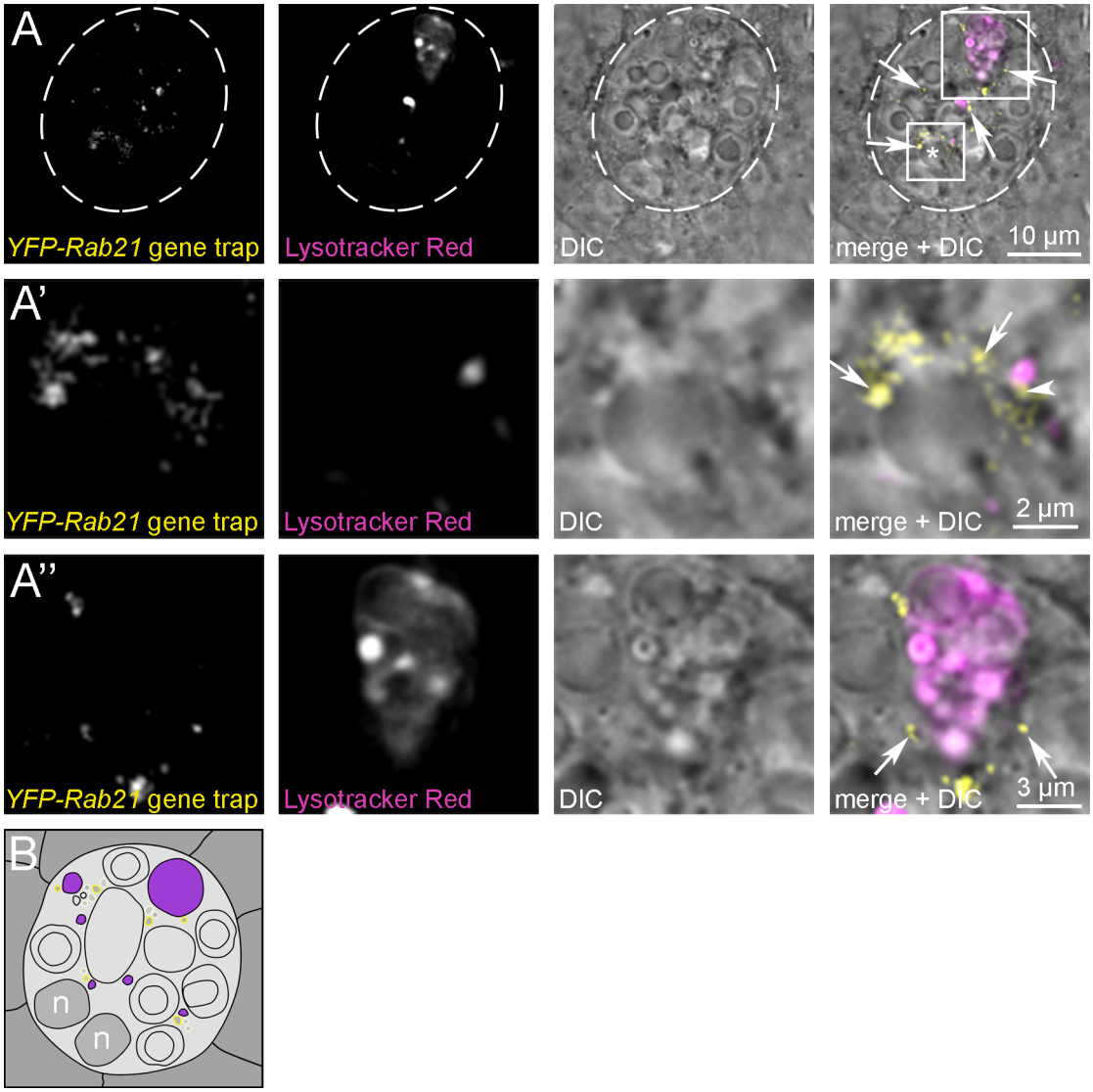

A
YFP-Rab21 gene trap
Lysotracker Red
DIC
merge + DIC
10 µm
A'
YFP-Rab21 gene trap
Lysotracker Red
DIC
merge + DIC
2 µm
A''
YFP-Rab21 gene trap
Lysotracker Red
DIC
merge + DIC
3 µm
B
n
n

Figure 3.29 YFP-Rab21 localises on small non-acidic vesicles that associate closely with the larger compartments in secondary cells

All panels show wide-field fluorescence and DIC images of a living secondary cell from a six-day-old virgin male expressing the *YFP-Rab21* gene trap. Flies were kept at 28.5°C following eclosion and accessory glands were stained with Lysotracker Red (magenta). Approximate secondary cell outlines are marked with a dashed line.
(A) In secondary cells YFP-Rab21 (yellow) localises on punctate non-acidic vesicles that are scattered throughout the cell, in between the larger subcellular compartments and also close to the plasma membrane (arrows). The boxes highlight regions that are enlarged in (A') and (A'').
(A') Several small YFP-Rab21-labelled vesicles are localised in the central region surrounding the non-cored Rab6-positive compartment (arrows), some of which localise in close proximity to a small acidic compartment (magenta; arrowhead).
(A'') YFP-Rab21 marks many small vesicular puncta in close association with the large acidic compartments.
(B) Schematic representation of YFP-Rab21 localisation (yellow) on the surface small non-acidic vesicles within an individual secondary cell. The level of localisation is represented by the intensity of yellow. Acidic compartments are shown in magenta. Nuclei are marked with 'n'.

Homozygous *YFP^{Myc}-Rab21* gene trap flies were used in this figure.

Rab35 localises to the plasma membrane and both early and recycling endosomes in mammalian cells, where it plays roles in fast recycling of varied molecules, including MHC Class I and II proteins (Klinkert & Echard, 2016; Kouranti *et al*., 2006). In secondary cells, the fusion protein expressed from the *YFP-Rab35* gene trap was localised at moderate levels on a several non-acidic vesicles, often apically located (Figure 3.30A), but also clustering between and in close proximity to different large subcellular compartments (Figure 3.30B-C) and the basolateral plasma membrane (Figure 3.30B). These locations were similar to those of other early endosomal *YFP-Rab* gene traps, including Rab4, Rab5 and Rab21. However, it localised to fewer vesicles, some of which were larger than those observed with other Rabs, suggesting that it may be associated with a specific endosomal subtype, potentially involved in recycling.

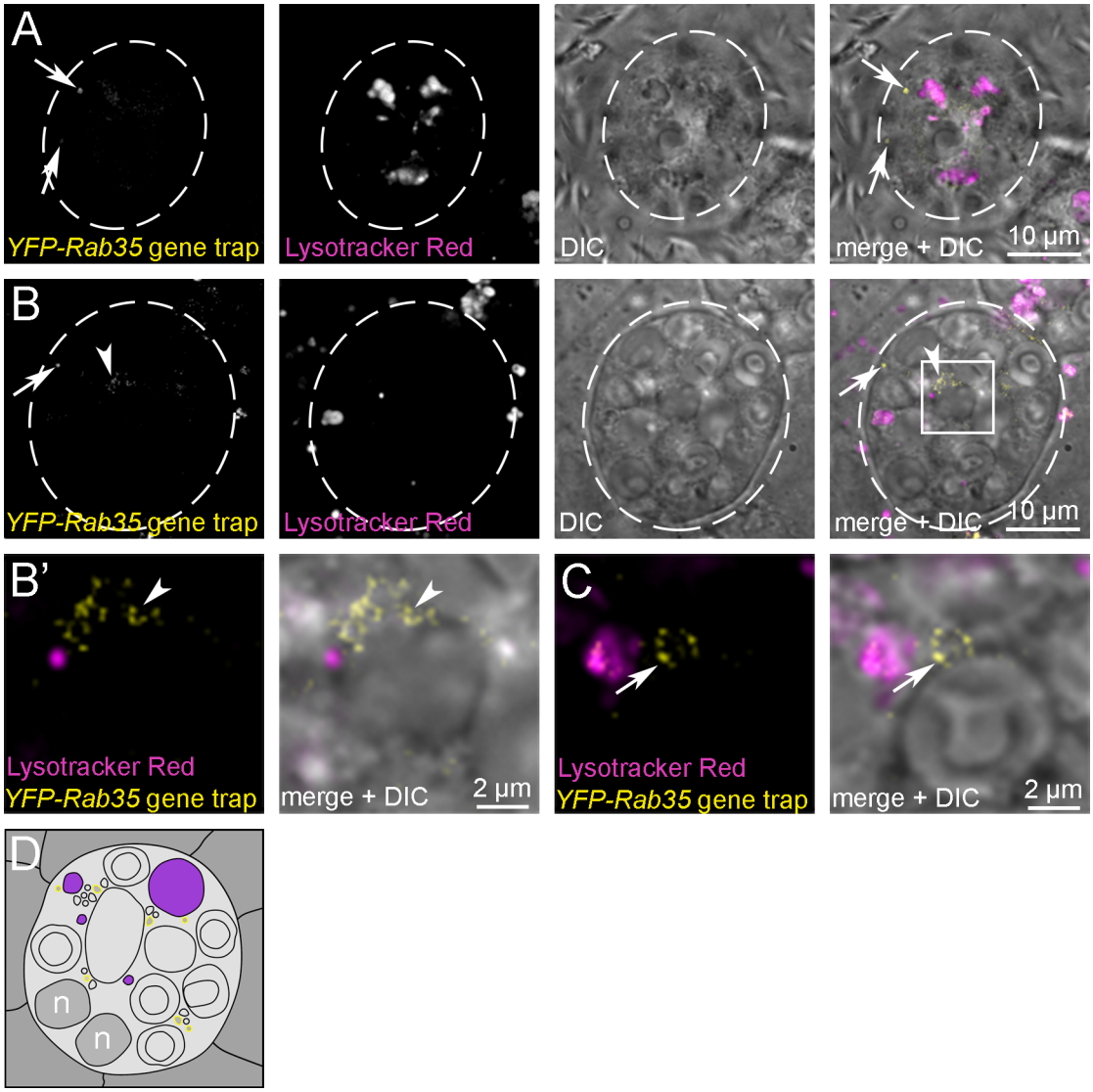

A
YFP-Rab35 gene trap
Lysotracker Red
DIC
merge + DIC
10 µm
B
YFP-Rab35 gene trap
Lysotracker Red
DIC
merge + DIC
10 µm
B'
Lysotracker Red
YFP-Rab35 gene trap
merge + DIC
2 µm
C
Lysotracker Red
YFP-Rab35 gene trap
merge + DIC
2 µm
D
n
n

Figure 3.30 YFP-Rab35 localises on a small number of non-acidic vesicles in secondary cells

All panels show wide-field fluorescence and DIC images of a living secondary cell from a six-day-old virgin male expressing the *YFP-Rab35* gene trap. The fly was kept at 28.5°C following eclosion and their accessory glands stained with Lysotracker Red (magenta). Approximate secondary cell outlines are marked with a dashed line.
(A) Apical view through a secondary cell shows YFP-Rab35 (yellow) localises on a few small non-acidic intracellular vesicles (arrows) in the region.
(B) Basolateral view through the same secondary cell shows YFP-Rab35-marked vesicles, some of which are close to the plasma membrane (arrow), and others are close to the large non-cored compartment (arrowhead). Box shows region enlarged in (B').
(B') The YFP-Rab35-labelled vesicles surrounding the non-cored compartment show an irregular, potentially tubular morphology (arrowhead).
(C) Alternative focal plane through the YFP-Rab35 marks a few larger non-acidic vesicles (arrow), which associate closely with different intracellular compartments.

Homozygous *YFP^{Myc}-Rab35* gene trap flies were used in this figure.

3.2.2.7 Rab7 and Rab39 are enriched on the surface of acidic late endosomal and lysosomal compartments

Rab7 is an important multifunctional Rab GTPase with roles in late endosome maturation, lysosome biogenesis and function, and the regulation of fusion between both autophagosomes and late endosomes with lysosomes (Hyttinen *et al*., 2013; Luzio *et al*., 2000). The localisation of the fusion protein from the *YFP-Rab7* gene trap on the limiting membranes of the large acidic compartments (Figure 3.31A-B) confirmed previous observations with overexpressed Rab7 and immunostaining (Corrigan *et al*., 2014; Appendix 8.1.1, 8.1.2). Because of the large size of these compartments, YFP-Rab7 could also be observed internally in small puncta (Figure 3.31A').

Many of the small acidic compartments (<2 μm diameter) carried YFP-Rab7 at more moderate levels on their surface (Figure 3.31B''). YFP-Rab7 was also observed on the limiting membranes of small non-acidic vesicles, which were scattered throughout the cell, but often clustered together (Figure 3.31B'').

The highest levels of YFP-Rab7 in secondary cells were observed on the limiting membranes of 1-3 non-acidic dense-core granule compartments (Figure 3.31B').

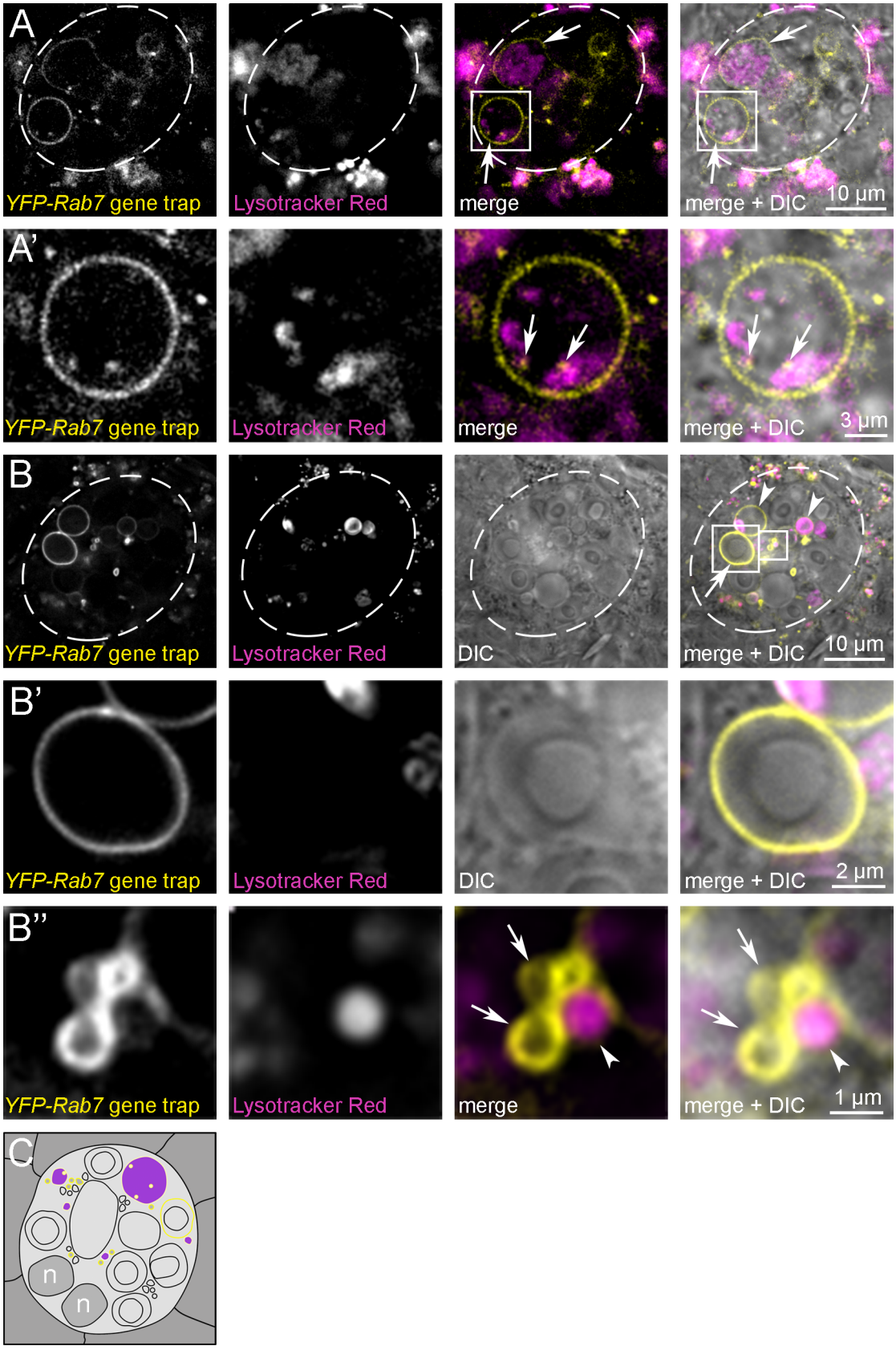

A
YFP-Rab7 gene trap
Lysotracker Red
merge
merge + DIC
10 µm
A'
YFP-Rab7 gene trap
Lysotracker Red
merge
merge + DIC
3 µm
B
YFP-Rab7 gene trap
Lysotracker Red
DIC
merge + DIC
10 µm
B'
YFP-Rab7 gene trap
Lysotracker Red
DIC
merge + DIC
2 µm
B''
YFP-Rab7 gene trap
Lysotracker Red
merge
merge + DIC
1 µm
C
n
n

Figure 3.31 YFP-Rab7 localises the surface of large acidic compartments and some intraluminal puncta, and is found on a subset of large and small non-acidic compartments

All panels show wide-field fluorescence and DIC images of living secondary cells from six-day-old virgin males expressing the *YFP-Rab7* gene trap. Flies were kept at 28.5°C following eclosion and their accessory glands stained with Lysotracker Red (magenta). Approximate secondary cell outlines are marked with a dashed line.
(A) YFP-Rab7 (yellow) localises on the surface of large acidic (magenta) compartments (arrows). Box region is enlarged in (A').
(A') Intraluminal puncta marked by YFP-Rab7 (arrows) are found within acidic compartments.
(B) A large non-acidic dense-core granule compartment carries high levels of YFP-Rab7 on its surface (arrow). Acidic compartments carrying YFP-Rab7 are marked with arrowheads. Boxes highlight regions enlarged in (B') and (B'')
(B') The YFP-Rab7-labelled non-acidic compartment has a clear dense-core granule at its interior.
(B'') Some small non-acidic vesicles are marked by YFP-Rab7 (arrows), which often cluster together. Neighbouring small acidic compartments are marked at lower levels (arrowhead).
(C) Schematic representation of YFP-Rab7 localisation (yellow) on the surface of diverse intracellular compartments within an individual secondary cell. The level of localisation is represented by the intensity of yellow. Acidic compartments are shown in magenta. Nuclei are marked with 'n'.

Homozygous *YFP^{Myc}-Rab7* gene trap flies were used in this figure.

Rab39 has been observed in the Golgi, endosomes and phagosomes of other cells, and has been implicated in phagosomal acidification (Gillingham *et al*., 2014; Chen *et al*., 2003; Chan et al., 2011; Seto *et al*., 2011). The fusion protein from the *YFP-Rab39* gene trap, strikingly, was localised on the surface of the large acidic compartments in secondary cells (Figure 3.32A). This was similar to, but more specific than the *Rab7-YFP* gene trap, which also localised on some non-acidic dense-core granule compartments. However, the level of expression of the *YFP-Rab39* gene trap was much lower than *YFP-Rab7*. YFP-Rab39 was observed inside some of the acidic compartments (Figure 3.32A'). This fusion protein also colocalised extensively with the acidic compartments in main cells (Figure 3.32B).

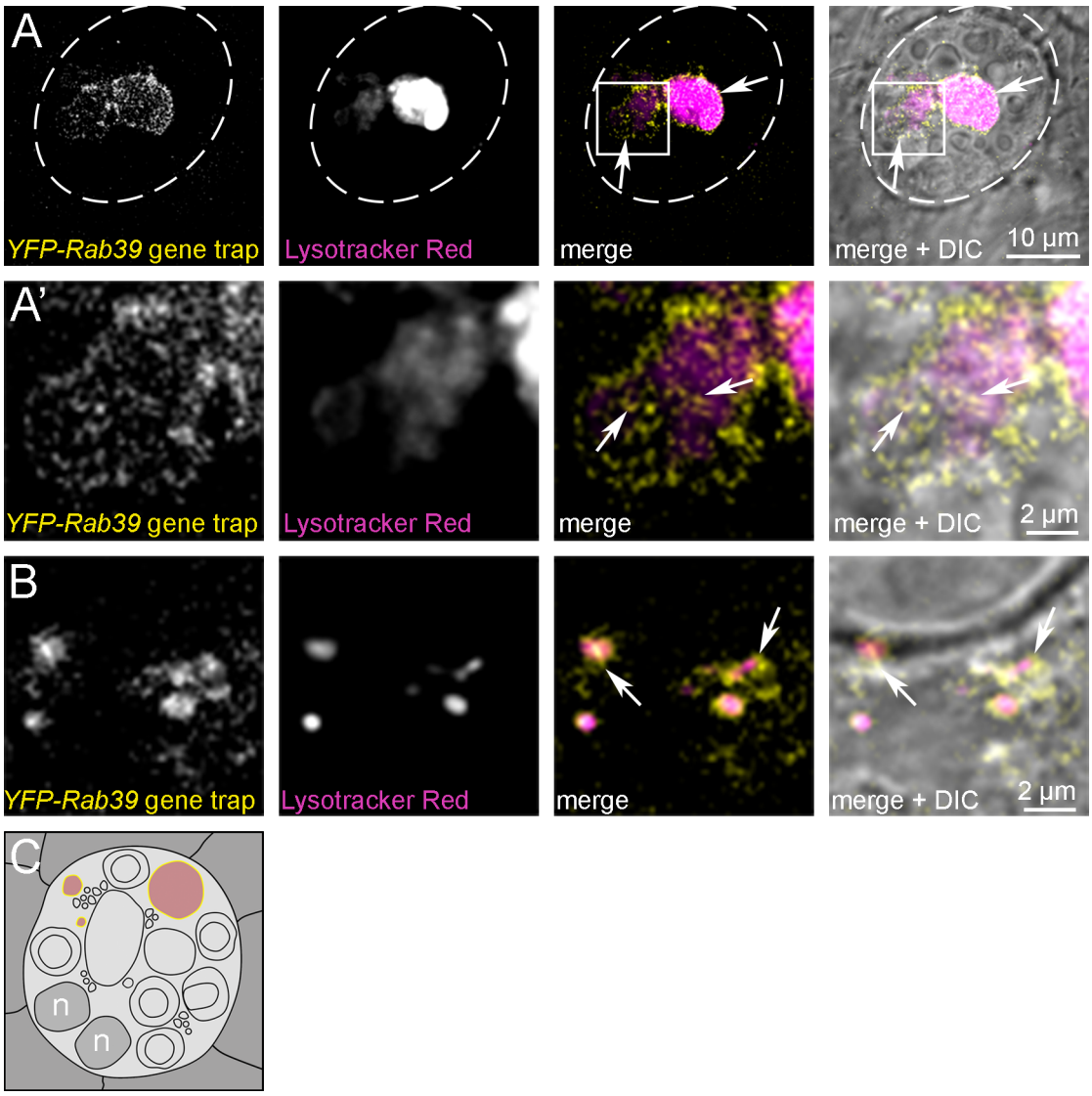


Figure 36. YFP-Rab39 specifically localises on the surface of acidic compartments in both secondary cells and main cells

All panels show wide-field fluorescence and DIC images living cells from six-day-old virgin males expressing the *YFP-Rab39* gene trap. Flies were kept at 28.5°C following eclosion and their accessory glands stained with Lysotracker Red (magenta). Approximate secondary cell outline in (A) is marked with a dashed line.

(A) YFP-Rab39 (yellow) localises on the surface of large acidic compartments (magenta; arrows). Intraluminal YFP-Rab39 fluorescence is also observed. The box highlights the region enlarged in (A'), which shows the YFP-Rab39-marked intraluminal puncta (arrows).

(B) In main cells, YFP-Rab39 localises on the surface of their acidic compartments (arrows), some of which have a tubular morphology.

(C) Schematic representation of YFP-Rab39 localisation (yellow) on the surface and interior of acidic compartments (magenta) within an individual secondary cell. Nuclei are marked with 'n'.

Homozygous *YFP^{Myc}-Rab39* gene trap flies were used in this figure.

3.2.2.8 Rab23 localises to the secondary cell plasma membrane

Rab23 has been observed on the plasma membrane of mammalian cells, where it mediates hedgehog signalling and primary ciliogenesis, but has also been found on early endosomes and implicated in phagosome-lysosome fusion (Evans *et al*., 2003; Wang *et al*., 2006; Yoshimura *et al*., 2007; Nozawa et al., 2012;). In secondary cells, the fusion protein from the *YFP-Rab23* gene trap specifically localised on the basolateral plasma membrane, albeit at low levels, the only Rab detected specifically in this region (Figure 3.33A). Within the accessory gland epithelium, only secondary cells, not main cells, expressed it at detectable levels.

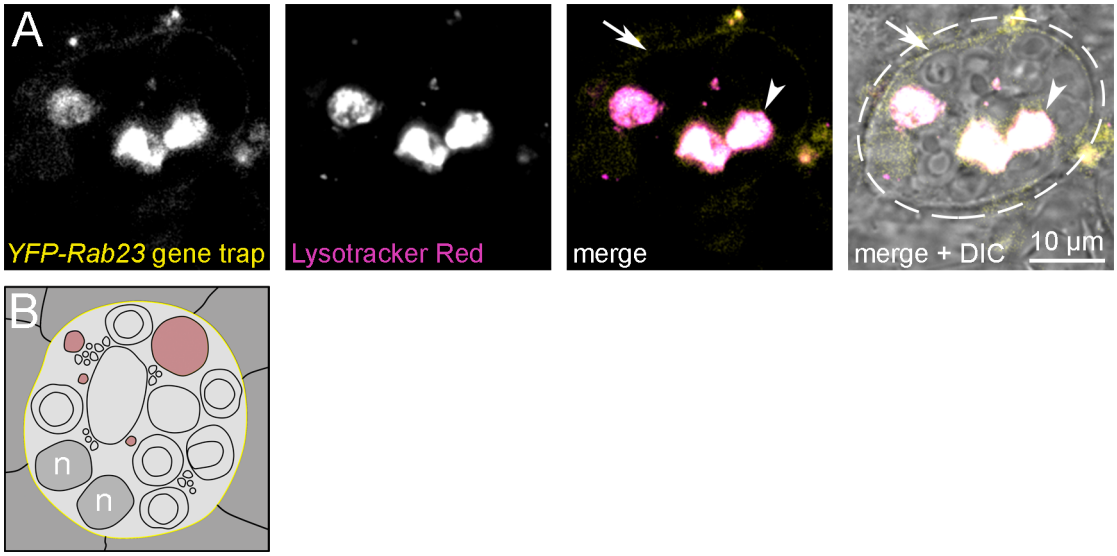


Figure 3.33 YFP-Rab23 localises to the basolateral plasma membrane of secondary cells

Panels show wide-field fluorescence and DIC images of a secondary cell from a six-day-old virgin male expressing the *YFP-Rab23* gene trap, which was kept at 28.5°C following eclosion and their accessory glands stained with Lysotracker Red (magenta). Approximate secondary cell outline is marked with a dashed line.
(A) YFP-Rab23 (yellow) specifically localises to the plasma membrane outline of the secondary cell (arrow), and some fluorescence is detected inside acidic compartments (arrowhead).
(B) Schematic representation of YFP-Rab23 localisation (yellow) on basolateral plasma membrane, and interior of acidic compartments (magenta) within an individual secondary cell. Nuclei are marked with ‘n’.

Homozygous *YFP^{Myc}-Rab23* gene trap flies were used in this figure.

3.2.2.9 Rab3, Rab14, Rab26, Rab27, Rab32 and Rab40 are not detectable in secondary cells

Several of the *YFP^{Myc}-Rab* gene trap flies were not expressed at detectable levels in secondary cells. A number of these, Rab3, Rab26, and Rab27 have been implicated in secretory trafficking pathways in mammalian cells (Geppert *et al*., 1997; Yoshie et al., 2000; Stenmark, 2009; Wandinger-Ness & Zerial, 2014). However, all of these Rabs have been detected in other tissues in the fly (Dunst *et al*., 2015), and I did observe them in the muscle layer surrounding the epithelium (data not shown). Rab14, Rab32 and Rab40, which play a diverse set of roles in other cell types, were also not detected on the membranes of subcellular compartments in secondary cells (see Stenmark, 2009 or Wandinger-Ness & Zerial, 2014 for good reviews on these Rabs).

3.2.2.10 Acknowledgements to important contributors to the analysis of the fluorescently tagged Rab GTPase in secondary cells

The first observations that proteins expressed from the *CFP-Rab6*, *YFP-Rab6* and *YFP-Rab19* gene traps localised to a subset of secondary cell compartments were made by our collaborator, E. Prince, on fixed tissues with some subsequent analyses of the compartmental properties in living tissue (e.g. staining for pH) done collaboratively (unpublished). S. Redhai, a previous DPhil student in the lab, reported the localisation of CFP-Rab6 and YFP-Rab6 in collaboration with E. Prince (Redhai, 2016). The further work on these gene traps reported here was pursued independently, utilising more sensitive wide-field imaging, and provides novel insights regarding the subcellular localisation of the fusion proteins and the compartments to which

they localise. Most notably, it establishes the presence of Rab6-positive non-cored, non-acidic compartments, including one surrounded by Golgi cisternae and small vesicles marked by many secretory and endosomal Rabs. It also identifies Rab-positive ILVs in multiple compartments and defines several types of dense-core compartment as defined by Rab signature. Furthermore, it highlights the effects of different *Rab* gene traps on the biology of secondary cells, which seem more sensitive to subtle modulations in Rab activity than other cell types.

The *CFP-Rab6* gene trap was studied collaboratively with F. Castellanos, another DPhil student in the lab, who undertook the detailed quantitative analysis of the effect of the transgene on overall secondary cell biology (Castellanos, 2017). However, working independently, I carried out further characterisation of *CFP-Rab6* gene trap-expressing secondary cells, including immunostaining and the analysis of combinations with other *YFP-Rab* gene trap lines.

S. Redhai previously reported the localisation of the fusion protein expressed from the *YFP-Rab1* gene trap in secondary cells (Redhai, 2016), describing a localisation pattern similar to the Golgi. My study used immunostaining to confirm its identity as a resident protein in different parts of the Golgi. The subcellular localisation of gene trap-expressed YFP-Rab35 in secondary cells was studied collaboratively with S. Redhai and reported previously (Redhai, 2016), using images that I had acquired.

I. Stefana made the initial observations that the *YFP-Rab21* gene trap marked a large non-acidic secondary cell compartment, and that gene trap-expressed YFP-Rab39 localised onto the large acidic compartments (unpublished). The

independent observations reported in this study included further analysis of these compartments, for example the cored nature and apical positioning of YFP-Rab21, the intraluminal localisation of YFP-Rab39, and the analysis of combinations with the *CFP-Rab6* gene trap.

3.2.3 Super-resolution imaging enables more detailed analyses of secondary cell biology

Super-resolution 3D-SIM was performed to overcome the resolution limits, imposed by diffraction, of using fluorescence microscopy to study the detailed cell biology of living secondary cells. The technique was only possible using samples with highly fluorescent markers, particularly those with strong signal-noise ratios, where it enabled the production of high contrast images with about 2-fold improved resolution in all axes. The difference in quality of images produced by this technique is demonstrated by a direct comparison between the original wide-field image and the reconstructed super-resolution image of the same secondary cell expressing CD63-GFP and stained with Lysotracker-Red (Figure 3.34A-B). CD63-GFP is a fusion protein composed of CD63, a human tetraspanin of the TM4 superfamily (Boucheix & Rubinstein, 2001) that is commonly used as an exosome marker because it is enriched on late endosomal compartments and their ILVs. It is linked at its N-terminus to eGFP (Panáková *et al*., 2005; Blott *et al*., 2001). The lab has used it extensively as a marker for the limiting membranes of most large secondary cell compartments, and because it is secreted on small nanovesicles into the gland lumen (Corrigan *et al*., 2014; Redhai *et al*., 2016).

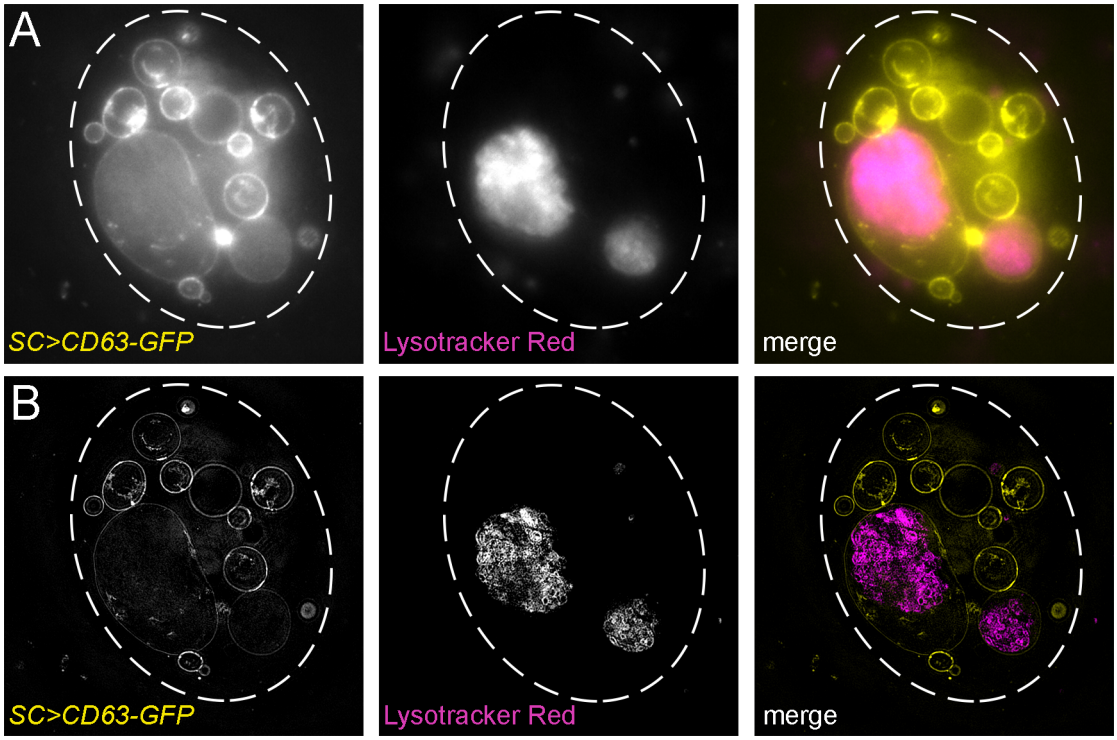


Figure 3.34 Super-resolution imaging of secondary cells overexpressing CD63-GFP dramatically improves image quality

These panels display wide-field fluorescence images before and after 3D-SIM super-resolution reconstruction. They display images of an individual secondary cell from a 6-day-old virgin transgenic male selectively overexpressing CD63-GFP. The fly was incubated at 28.5°C since eclosion to induce CD63-GFP expression using the GAL4-GAL80^{ts}-UAS system. Glands were stained with Lysotracker Red (magenta). Approximate secondary cell outline is marked with a dashed line.
(A) Unprocessed wide-field image of secondary cell.
(B) Super-resolution reconstruction of the same secondary cell. Improvements in contrast and resolution with both CD63-GFP (yellow) and Lysotracker-Red staining are observed.

The specific genotype of these males is: *w; UAS-CD63-GFP, tub-GAL80ts / +; dsx-GAL4 / +*.

Super-resolution images of *CD63-GFP*-expressing secondary cells resolved several novel cell biological details. For example, clusters of small non-acidic vesicles and tubular structures marked with high levels of CD63-GFP were observed, often in close proximity to, and possibly interacting with, other subcellular compartments, including both small non-acidic compartments and large acidic compartments (Figure 3.35A-A'').

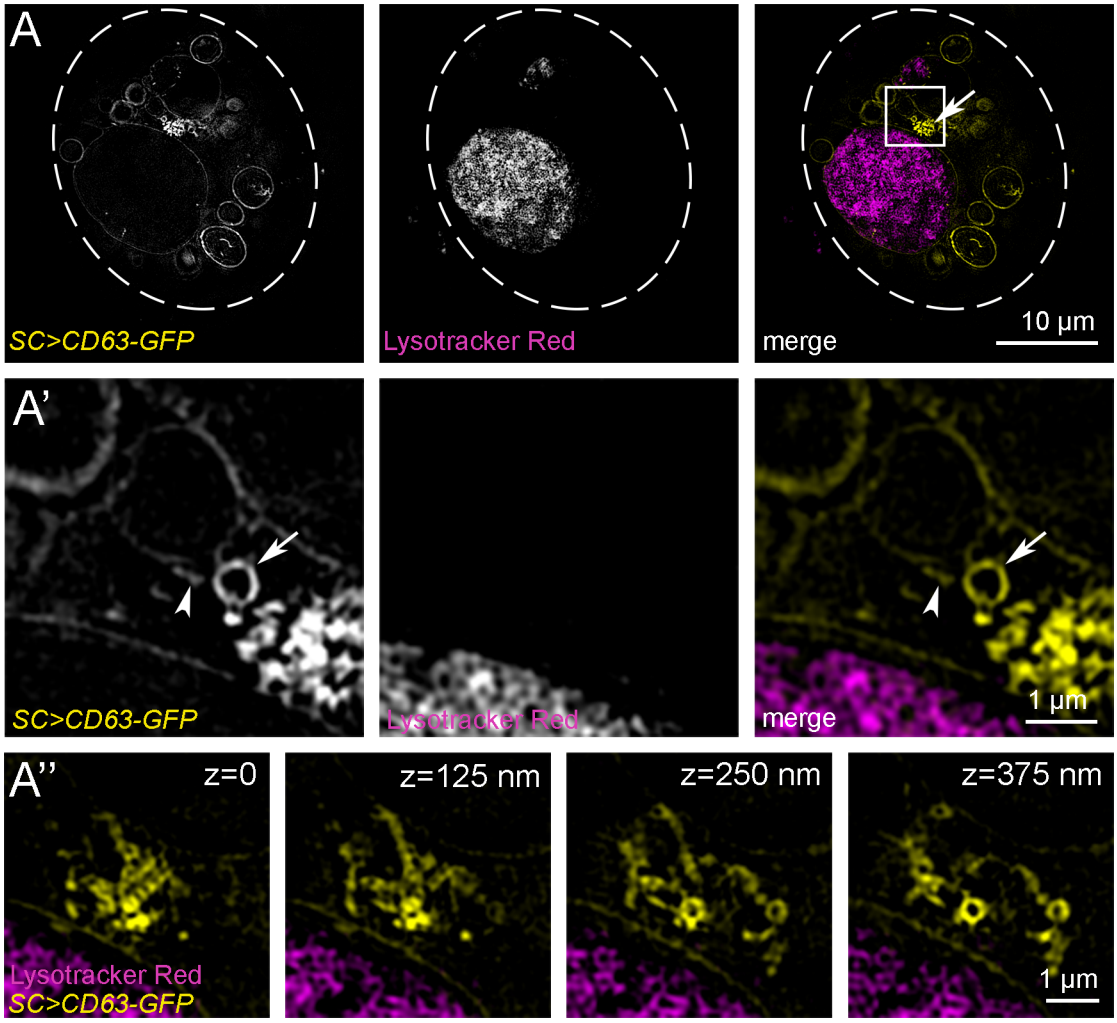

A
SC>CD63-GFP
Lysotracker Red
merge
10 µm
A'
SC>CD63-GFP
Lysotracker Red
merge
1 µm
A''
z=0
z=125 nm
z=250 nm
z=375 nm
Lysotracker Red
SC>CD63-GFP
1 µm

Figure 3.35 Super-resolution imaging of secondary cells overexpressing CD63-GFP identifies a previously unresolved multivesicular localisation in close contact other subcellular compartments

These panels show super-resolution images of an individual secondary cell from a 6-day-old virgin transgenic male selectively overexpressing CD63-GFP. The fly was incubated at 28.5°C since eclosion to induce CD63-GFP expression using the GAL4-GAL80^{ts}-UAS system. Glands were stained with Lysotracker Red (magenta). Approximate secondary cell outline is marked with a dashed line.
(A) In secondary cells overexpressing CD63-GFP (yellow), it localises on the surface of the numerous large compartments, as previously observed, and also onto some small vesicular structures (arrow). The Box highlights the region enlarged in (A').
(A') These vesicular structures (arrow) are closely associating with other intracellular compartments and may be interacting, potentially through fusion (arrowhead).
(A'') 4 different z-positions, over a total distance of 375 nm through the vesiculated region, demonstrate the presense of long tubular and vesicular structures labelled by CD63-GFP.

The specific genotype of these males is: *w; UAS-CD63-GFP, tub-GAL80ts / +; dsx-GAL4 /* +.

Long tubulations from the limiting membrane and small ILVs, labelled with CD63-GFP, were observed inside large acidic compartments (Figure 3.36A-A'). Many ILVs were also present within the large secretory non-acidic compartments, visualised as chains of vesicles surrounding the internal dense-core granule (Figure 3.36B,B''). Extremely fine projections of apical plasma membrane were observed at the apical surface of secondary cells (Figure 3.36C).

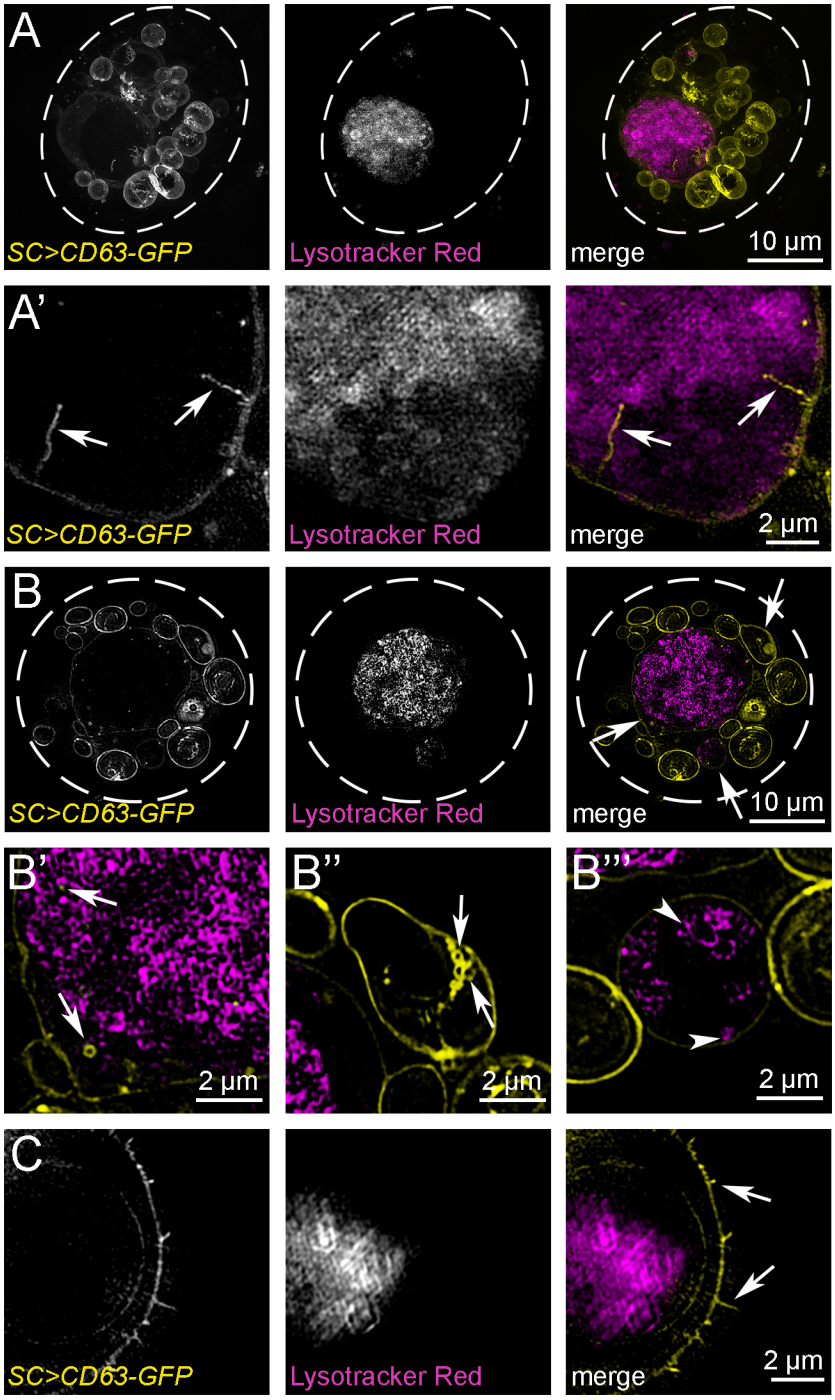

A
SC>CD63-GFP
Lysotracker Red
merge
10 µm
A'
SC>CD63-GFP
Lysotracker Red
merge
2 µm
B
SC>CD63-GFP
Lysotracker Red
merge
10 µm
B'
2 µm
B''
2 µm
B'''
2 µm
C
SC>CD63-GFP
Lysotracker Red
merge
2 µm

Figure 3.36. Super-resolution resolves that CD63-GFP localises on ILVs within different compartment subtypes, in addition to marking long intraluminal tubules and protrusions from the apical cell surface

These panels super-resolution images secondary cells from 6-day-old virgin transgenic males selectively overexpressing CD63-GFP. Flies were incubated at 28.5°C since eclosion to induce CD63-GFP expression using the GAL4-GAL80^{ts}-UAS system. Glands were stained with Lysotracker Red (magenta). Approximate secondary cell outlines are marked with a dashed line.
(A) Maximum intensity projection images (3 μm depth) of an individual secondary cell overexpressing CD63-GFP (yellow). Box shows region enlarged in (A')
(A') Maximum intensity projection images (1.125 μm depth) focus on the interior of the large acidic compartment (magenta). Long CD63-GFP-labelled tubulations extend from the limiting membrane into the interior of the compartment.
(B) CD63-GFP localises on the surface and within large compartments of secondary cells. Arrows point to compartments enlarged in (B'-B'''), though not always at the same focal plane as in (B).
(B') Small ILVs labelled with CD63-GFP are resolved within the large acidic compartments (arrows).
(B'') Numerous CD63-GFP-marked ILVs are also observed within non-acidic compartments (arrows).
(B''') Small acidic compartment has subdomains of Lysotracker staining (arrowheads).
(C) CD63-GFP localises on the apical plasma membrane, where it marks short protrusions (arrows) into the accessory gland lumen.

The specific genotype of these males is: *w; UAS-CD63-GFP, tub-GAL80ts / +; dsx-GAL4 / +*.

3.3 Discussion

In this results chapter, I have described secondary cell ultrastructure using electron microscopy, revealing novel types of subcellular compartments and providing insights into their subcompartmental organisation. I have used super-resolution, wide-field fluorescence and DIC microscopy to characterise the subcellular organisation and structure of secondary cell compartments. I have employed a variety of antibodies and fluorescently tagged proteins to visualise organelles and functionally important proteins. I have characterised the organisation of secondary cells in non-transgenic w^{1118} flies and transgenic lines that I have used throughout my research. I have also screened a large set of YFP-tagged *Rab* gene trap fly lines to identify their protein expression patterns within secondary cells. These findings reveal a complex network of Rabs localised to the surface of both distinct and sometimes overlapping organelles. I also highlighted the advantages of the new microscopic techniques that I have developed and applied to secondary cell research.

3.3.1 The diverse subcellular compartments of secondary cells have distinctive ultrastructural features and molecular cargos

The work described in this chapter has significantly developed our understanding of the intracellular compartments in secondary cells. Furthermore, the findings provided important insights that helped me to interpret numerous other experiments described later in this thesis. I have

shown that secondary cell compartments are polarised in a distinctive manner, similar to other secretory cell types (see Section 1.1.2; Chang & Jamieson, 1989). These polarised compartments have characteristic features and molecular contents, which I have identified using a number of different molecular markers and microscopy techniques.

I show that secondary cells contain numerous Golgi cisternae, many of which surround their large, centrally located non-cored compartments (Section 3.2.1.5). They also extend throughout and in between the other large intracellular compartments in these cells. Numerous vesicles of different morphologies were observed at the trans-face of the Golgi cisternae by electron microscopy, perhaps reflecting the functional activities of the range of Rab proteins that also cluster in this area (Sections 3.2.1.3, 3.2.2.1 and 3.2.2.3). This and other subcellular features, such as the numerous mitochondria and extensive rough endoplasmic reticulum are indicative of highly secretory cells. I show that the central non-cored compartments, corresponding to the large ‘vacuoles’ described by Bairati (1968), carry Rab6 on their surface (Section 3.2.2.2). The function of these compartments was unclear, but other recent studies in the lab have shown that molecular cargos traffic through these compartments en route to the other large dense-core granule compartments and acidic compartments in secondary cells (Castellanos, 2017). Furthermore, I have demonstrated that these compartments form fibres similar to dense-core granule compartments, suggesting that they are produced in advance of dense core condensation (Section 3.2.1.3). In chapter 5 of my thesis, I explore the function and biology of these compartments in more detail.

I report several novel findings about the ultrastructurally complex Rab11-positive dense-core granule compartments. I show that individual dense-core granule compartments have diverse levels of dense-core packaged proteins, marked by ANCE or GFP-GPI, despite containing a structurally similar 'dense-core' morphology (Appendix 8.1.1, 8.1.2). This could be due to further maturation events in the condensed dense-core granules within these compartments, a concept that could also apply to mammalian dense-core granules. The lysosomal GTPase, Arl8 (Hofmann & Munro, 2006), also appeared to be localised within dense-core granules by immunofluorescence, though its role there is unclear (Appendix 8.1.2). Using super-resolution microscopy, I have identified numerous ILVs within these compartments; a finding that was confirmed using electron microscopy in non-transgenic flies (Sections 3.2.1.3 and 3.2.3). The ILVs often occupy regions close to the limiting membrane of the compartment, or extend into the region between the dense-core granule and the numerous fibres that enwrap them. This observation raises the interesting possibility that these vesicles may be secreted alongside the dense-core granules (discussed in detail in Chapter 4). The identity of the fibres remains unclear, as the microtubule subunit alphatubulin did not incorporate into them, as was hypothesised in previous reports (Perotti, 1972; Section 3.2.1.6). Indeed the decameric subunit structure of these fibres (Section 3.2.1.2) is inconsistent with microtubule assembly. In the future, it will be important to identify the proteins that form these lumenal fibres, and to determine whether they contribute towards the formation of the dense-core granule, as is the case with pre-melanosomal protein (PMEL) fibrils during melanosome maturation in pigment cells

(Raposo & Marks, 2007). In this latter case, the melanosomes are thought to be derived from lysosomal structures, although they do appear to receive an input from Rab11 compartments during maturation (Delevoye *et al*., 2014).

I present several lines of evidence that suggest the large acidic compartments in secondary cells are a form of lysosome, or lysosome-like compartment. I show that Arl8, a small GTPase involved in lysosome positioning in mammalian cells and *Drosophila* (Pu *et al*., 2015; Tuli *et al*., 2013; Hofmann & Munro, 2006) localises to the surface of the large Rab7-positive compartments (Appendix 8.1.2). Importantly, electron microscopy revealed that these compartments are morphologically similar to secondary lysosomes, as they contained structures associated with late endosomes, lysosomes, and autophagosomes (Sections 3.2.1.2 and 3.2.1.3). Their ultrastructural morphology was not reported during previous studies, suggesting that the preservation techniques used here were key to their identification (Corrigan *et al*., 2014; Bairati, 1968). Although not widely reported, morphologically similar organelles are observed in stimulated B-cells (Klumperman & Raposo, 2014) and in reticulocytes during the final stages of their maturation. In reticulocytes, the formation of the compartments is thought to involve a complex interaction between endocytic and autophagic pathways, potentially consistent with my observations in secondary cells (Griffiths *et al*., 2012). Remarkably, similar enlarged lysosomes are associated with lysosome storage disorders, such as Niemann-Pick and Pombe disease (Lim *et al*., 2014), and have also been observed in neurodegenerative diseases such as Alzheimer's disease (Nixon, 2005). In these conditions, lysosome-mediated degradation of autophagic materials is often disrupted, resulting in inefficient degradation of certain

molecules. The continual growth of these large acidic compartments in secondary cells may therefore suggest that the catabolic lysosomal processes are unable to cope with the macromolecular turnover required in these highly secretory cells.

3.3.2 Rabs localise to specific subcellular compartments in secondary cells

In this chapter I have also reported in detail the localisation of most *Drosophila* Rab GTPases in secondary cells using a set of YFP^{Myc}- and CFP^{Myc}-tagged gene trap fly lines (Section 3.2.2). Together, these provided a more complete picture of the subcellular architecture of secondary cells. For example, I showed that Rab1 and Rab2, consistent with their localisations in mammalian cells, localised in the cis-Golgi and particularly for Rab1, in neighbouring vesicles that might be part of the meidal- and trans-Golgi (Section 3.2.2.1). This suggests they may play related roles in regulating membrane traffic associated with the Golgi, as predicted from their mammalian homologues (Hutagulung & Novick, 2011). The large non-cored compartments carried Rab6 at high levels on their surface, though Rab6 was also on smaller vesicles that closely associated with, but rarely overlapped, cis-Golgi markers (Section 3.2.2.2). Some of these Rab6-positive vesicles were also labelled by Rab1, but the most intensely fluorescent ones and the large Rab6-positive compartments were not. Given that Rab6 localises on the trans-Golgi in mammalian cells (Martinez *et al*., 1994), it seems likely that some of the vesicular staining marks the trans-Golgi, but other vesicles and the large non-cored compartments either represent a highly specialised part

of the trans-Golgi network or are separate post-Golgi compartments. The idea that the large compartment is not part of the Golgi is partly supported by the observations that several trans-Golgi-associated Rabs, including Rab8, Rab10 and Rab30 (Stenmark, 2009) all co-localised specifically with Rab6 on some of the small vesicles, but not on the large non-cored compartments (Section 3.2.2.3). Furthermore, the trans-Golgi marker, Galtase-GFP specifically marked small vesicles and cisternae, but did not localise within the large Rab6-positive compartment (Section 3.2.1.5).

In accord with previous work (Corrigan *et al*., 2014; Redhai, 2016), I have shown that Rab11 localises to the surface of all the dense-core granule compartments. Interestingly, I show that dense-core granule compartments can also carry a complex mixture of other Rabs on their surface, including Rab6, Rab7, Rab10, Rab19, Rab21 and Rab30 (Section 3.2.2.4). Given that Rab11 plays key roles in forming the appropriate number of non-acidic compartments (Redhai, 2016), it will be important to determine whether the other Rabs impact on dense-core granule compartment trafficking. Several of them likely co-inhabit the surface of these compartments with Rab11. However, one key observation is that Rab6-positive dense-core granule compartments typically do not carry other Rabs at their limiting membrane apart from Rab11. Since I will demonstrate in Chapter 5 that non-cored Rab6-positive compartments are precursor compartments for dense-core granule compartments, this strongly suggests that the other Rabs interact with these compartments only as they mature.

Although difficult to discern with light microscopy, it is also possible that different Rabs may separate into distinct micro-domains on the surface of the

same large dense-core granule compartments, in order to facilitate different functions. This would be analogous to Rab5, Rab4 and Rab11, which are found in distinct domains on early endosomes in mammalian cells (Sönnichsen *et al*., 2000), where they facilitate different aspects of endosome maturation and recycling (see Section 1.3.2.2).

I show that Rab7 likely marks a subset of dense-core granule compartments destined for degradation. Both Rab7 and Rab39 localised on the surface of the large acidic, lysosome-like compartments (Section 3.2.2.7). These two Rabs also colocalise in *Drosophila* neurons, suggesting that they may work on the same subcellular compartments in other cell types (Chan *et al*., 2011). Interestingly, both marked small acidic compartments, that could potentially correspond with the small MVBs observed here in secondary cells using electron microscopy. Finally, I show that Rab23 associates with the basolateral plasma membrane of secondary cells, similar to previous reports in *Drosophila* (Pataki *et al*., 2010; Section 3.2.2.8).

Several of the screened YFP-Rabs, with described roles in exocytosis, such as Rab3, Rab26 and Rab27 were not expressed at detectable levels in secondary cells, which suggests that the secretory mechanisms in secondary cells may not employ all the characterised set of Rab-GTPases involved in regulated secretion (Section 3.2.2.9). However, it has previously been reported that cell type-specific *Rab27* knockdown affects exosome secretion from secondary cells (Corrigan *et al*., 2014), albeit not strongly, so it may also be possible that expression levels are below the detection limit of the microscopic techniques employed here.

I have also identified that several of the fluorescently tagged Rab proteins localise in intraluminal puncta within the large non-acidic compartments. Interestingly, many of these compartments contain puncta labelled by Rabs that are not at their limiting membranes (Sections 3.2.2.4 and 3.2.2.5). This may be due to changes in the Rab association with the limiting membrane of a particular compartment, whilst the intraluminal puncta remain unchanged. Alternatively, the puncta may be formed through more stochastic means, where dynamically associating Rabs incorporate into a microdomain of the compartment's surface, and are delivered into the lumen, before they are recognised by a GAP or GDI, which would normally facilitate their extraction from the membrane (Hutagulung & Novick, 2011).

Several of the YFP-tagged Rabs affect the normal compartmental organisation of secondary cells. Most notably, YFP-Rab8 caused a number of effects in the secondary cells including defective dense-core granule formation (Section 3.2.2.3). Given that the *YFP-Rab8* gene trap was expressed as a heterozygote, it is possible that YFP-Rab8 protein interferes with the functions of the wild type molecule. I show in Chapter 4 that in other backgrounds, such as the homozygous *YFP-Rab11* gene trap, the effects on trafficking pathways, when compared with non-transgenic w^{1118} secondary cells, are likely due to differences in the capability of these molecules to recapitulate the normal wild type Rab protein. Overall, secondary cells appear extremely sensitive to transgenic constructs, even those associated with gene traps, possibly more than other cell types (Dunst *et al*., 2015), though it is also possible that it is only more noticeable in secondary cells due to their very large subcellular compartments.

Overall, these YFP^{Myc}- and CFP^{Myc}-tagged gene trap flies combined with the new microscopy approaches presented here, provided several novel insights into the organisation of secondary cells, and laid the foundation for further studies into Rab function within secondary cells. Furthermore, the localisation of several of the YFP-Rabs was consistent with the functions of their homologues in mammalian cells, suggesting that they are playing conserved roles, even in these morphologically distinct cells. Since the larger compartments in secondary cells therefore probably represent the equivalent of much smaller compartments in other cell types, my work opened up the possibility of studying subcellular processes that are challenging to see in other cell types, as discussed in the following two chapters.

4.0 Novel exosome subtypes, their origins and regulation in both secondary cells and human cells

4.1 Introduction

This chapter explores the subcellular basis and genetic regulation of exosome secretion by secondary cells. It builds on some of the observations presented in the previous chapter, which showed that many of the large non-acidic Rab11-positive compartments in secondary cells contained numerous intraluminal vesicles (ILVs). Here, I analyse whether this population of ILVs represents a major source of exosomes from secondary cells. This partly involved the identification and description of several novel population-specific exosome cargos. I also characterise the genetic regulation of ILV formation and exosome secretion directly in living secondary cells. Lastly, I worked collaboratively with researchers in the Goberdhan lab, who study exosome biology in human cells, to test the evolutionary conservation of some of the mechanisms I identified in flies.

4.1.1 Exosomes are a subtype of extracellular vesicle that mediate communication between cells

Extracellular vesicles are increasingly being recognised as important delivery systems carrying signals from one cell to another (Tkach & Théry, 2016). They consist of two main varieties, exosomes and ectosomes (also known as microvesicles), which are distinguished by their sites of origin. Exosomes are formed as ILVs within endosomal compartments and are released upon fusion of the compartment to the plasma membrane, whilst ectosomes are extracellular vesicles that have directly budded off the plasma membrane (Cocucci & Meldolesi, 2015).

Exosomes are small, typically 30-150 nm diameter, and carry endosomal tetraspanin cargos, such as CD9, CD63 and CD81, as evidence of their subcellular origins (Kowal *et al*., 2016). Proteomic and genomic studies have shown that they contain heterogeneous cargos including proteins, lipids, DNA and RNAs such as miRNA, which trigger a variety of responses in their target cells (Maas *et al*., 2017). The size and cargo profile of exosomes generated by a particular cell type can vary according to its condition or status, though the mechanisms behind these changes are currently unknown. The changes can have important pathological impact however, for example cancer cells take advantage of exosomes to manipulate their microenvironment in favour of immune escape, therapy resistance, tumour growth and metastasis (Becker *et al*., 2016). Therefore, further research into the packaging of exosome cargos and the molecular mechanisms that facilitate pathological exosome secretion may not just improve our understanding of this fundamental aspect of cell biology, but also impact on therapeutic approaches.

4.1.2 Mechanisms of exosome biogenesis

Exosomes are thought to originate as ILVs within late endosomal MVBs, which are released following fusion of these compartments to the plasma membrane (Maas *et al*., 2017). Generally, it is thought that the formation of ILVs and sorting of their cargos in most eukaryotic cells is at least partly dependent on members of the Endosomal Sorting Complexes Required for Transport (ESCRT) family and their accessory proteins (Schöneburg *et al*., 2017; MacDonald *et al*., 2015; Colombo *et al*., 2014; Henne *et al*., 2011). Alternative ESCRT-independent pathways of ILV formation have also been

identified, involving ceramide (Trajkovic *et al*., 2008) or tetraspanins (Edgar *et al*., 2014; van Niel *et al*., 2011).

Several members of the Rab family of small GTPases, including Rab11, Rab27a, Rab27b and Rab35, have also been implicated in secretion of exosomes from multivesicular endosomes (Juan & Fürthauer, 2017; Hsu *et al*., 2010; Ostrowski *et al*., 2010; Savina *et al*., 2005). Molecules involved in the fusion of lipid bilayers, such as the NSF-attachment protein receptor (SNARE) complexes, including VAMP7 and YKT6, have been implicated in exosome secretion (Kowal *et al*., 2014; Fader *et al*., 2009; Gros *et al*., 2012). Other studies have implicated the V0 subunit of the v-ATPase as a potential mediator of exosome release in *C. elegans* (Colombo *et al*., 2014; Liegeois *et al*., 2006).

The diversity of molecular mechanisms implicated in exosome formation and secretion may help to explain the heterogeneity in exosomes released by cells (Willms *et al*., 2016). Several models explaining this mechanistic diversity have been proposed in the literature; for example, Kowal *et al*., (2014) hypothesise that exosomes may be released from different types of endosomal compartments that contain and package different cargos. Furthermore, the same compartment may also form multiple different varieties of exosomes. However, clear examples that distinguish between these different mechanisms have yet to be reported.

4.1.3 Exosome biogenesis in secondary cells

Previous research in the Wilson lab has established secondary cells as an *in vivo* model for exosome secretion (Corrigan *et al*., 2014 reviewed in Wilson *et*

al., 2017; Section 1.6.4.2). Importantly, the genetic mechanisms underlying exosome secretion by secondary cells were found to be conserved with other described systems, requiring several Rab GTPases, the ESCRT-0 component Hrs, ESCRT-I member TSG101 and the accessory protein ALiX (Corrigan *et al*., 2014). However, this study relied heavily on the overexpression of the human exosome marker CD63 tagged with GFP, which is known to affect secondary cell membrane trafficking and promote ILV formation (Redhai *et al*., 2016; Edgar *et al*., 2014). Furthermore, the knockdown experiments targeted molecules that could be involved in exosome secretion indirectly, such as the Rabs. Additionally, the ESCRT-I member TSG101 and the accessory protein ALiX have also been identified in ectosome release (Christ *et al*., 2017), making it more important to demonstrate the exact mechanism of exosome secretion, a process that has never previously been directly observed in secondary cells. The development of new technologies, described in Chapter 3 (Section 3.2.3), provided the opportunity to better clarify the biogenesis of exosomes in secondary cells.

4.1.4 Chapter aims

In this chapter, I have used novel microscopy techniques to further investigate the subcellular and genetic mechanisms of exosome biogenesis in secondary cells. I have also collaborated with the Goberdhan lab, which studies human cancer cell lines, to determine whether mechanisms identified in secondary cells are conserved. My primary aims were to:

- Identify the subcellular basis of exosome biogenesis by secondary cells
- Identify and characterise new cargos as markers for exosome subtypes made by secondary cells
- Characterise the genetic mechanisms underlying exosome biogenesis in secondary cells and begin to search for potential subtype specificity
- Determine whether the cellular and genetic mechanisms behind exosome biogenesis in secondary cells are conserved

4.2 Results

4.2.1 Rab11-positive compartments are a novel source of exosomes produced by secondary cells

4.2.1.1 Secondary cells secrete exosomes from a non-late endosomal compartment

Previous characterisations of exosome biogenesis in secondary cells demonstrated that overexpressed CD63-GFP, a human endosomal tetraspanin tagged with GFP, localised to the limiting membranes of both acidic and non-acidic compartments, and the apical plasma membrane (Section 3.2.3 and Appendix 8.1.2; Corrigan *et al*., 2014; Redhai *et al*., 2016). The secondary cells secreted CD63-GFP at high levels into the lumen of the gland, detected as a mixture of large and small extracellular puncta. Further analysis of the subcellular origins of these puncta, using immunostaining, had shown that the highest levels of internal CD63-GFP were observed inside the large acidic Rab7-positive compartments, but the low pH environment quenched most of the GFP fluorescence in living cells (Appendix 8.1.2). Based on current models of exosome biogenesis, the lab previously concluded that the extracellular vesicles were presumably formed as ILVs inside these large acidic compartments. Upon fusion of the acidic compartments to the plasma membrane, the ILVs were released into the gland's lumen as exosomes, and the lumenal environment, more permissive to GFP fluorescence, might permit more vesicles to be detected.

However, as I analysed this process further, several observations suggested that the large acidic compartments were not readily releasing their contents

into the accessory gland lumen. Firstly, electron microscopy revealed that these compartments exhibited features of secondary lysosomes, rather than the classical MVBs, which are normally associated with exosome secretion in other cell types (Sections 3.2.1.2 and 3.2.1.3). Secondly, time-lapse imaging of secondary cells over 6 hour periods did not show any fusions of acidic compartments to the plasma membrane (data not shown). Rather, the large acidic compartment was only ever observed to grow in size, by fusions to both acidic and non-acidic compartments (Figure 4.1A-B). These data supported previous findings that the large acidic compartments grow in size as the cells age during adulthood (Redhai, 2016) and suggested that the CD63-GFP-positive puncta in the AG lumen were more likely to be secreted from an alternative source. Furthermore, the fusion protein from *YFP-Rab7* gene trap (Section 3.2.2.7) was detected at very low levels in the accessory gland lumen (data not shown).

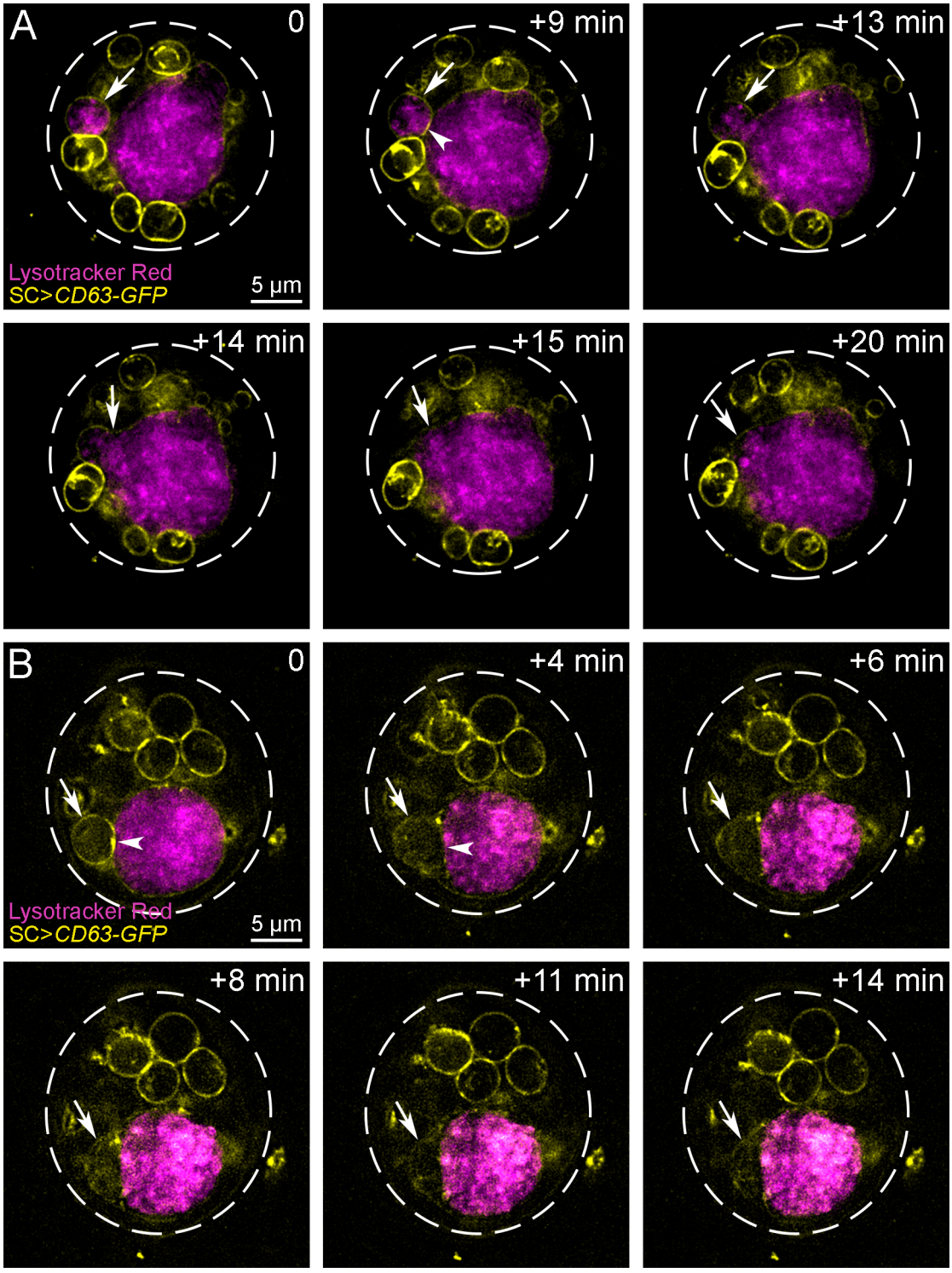

A
0
+9 min
+13 min
Lysotracker Red
SC>CD63-GFP
5 µm
+14 min
+15 min
+20 min
B
0
+4 min
+6 min
Lysotracker Red
SC>CD63-GFP
5 µm
+8 min
+11 min
+14 min

Figure 4.1 Large acidic compartments fuse together and with other non-acidic compartments

These panels display wide-field fluorescence images of living secondary cells from 6-day-old virgin transgenic males selectively overexpressing CD63-GFP. The flies were incubated at 28.5°C since eclosion to induce CD63-GFP expression using the GAL4-GAL80^{ts}-UAS system. Their accessory glands were stained with Lysotracker Red (magenta). Approximate cell outlines are shown using a dashed line.
(A) Time-lapse imaging shows two large acidic compartments fusing together and their contents mixing. Arrow points to the smaller acidic compartment. When the two compartments come into close contact (t=9 mins), there is a build up in CD63-GFP signal at the interacting site (arrowhead).
(B) Time-lapse imaging shows a large acidic compartment fusing to a large non-acidic compartment (arrow). The arrowhead at t=0 shows a bright CD63-GFP-positive signal between the two compartment's membranes, suggesting a close interaction, prior to fusion.

The specific genotype of these males is: *w; UAS-CD63-GFP, tub-GAL80ts / +; dsx-GAL4 /* +.

4.2.1.2 Non-acidic Rab11-positive compartments are a novel source of exosomes in secondary cells

These observations prompted me to investigate other potential sources of exosomes made in secondary cells using super-resolution 3D-SIM and wide-field imaging (Section 3.2.3). As the other prominent localisation sites of CD63-GFP, the extracellular vesicles could potentially derive from the large Rab11-positive non-acidic compartments or alternatively, via shedding from the apical plasma membrane (Section 3.2.3 and Appendix 8.1.2). In favour of the former, I showed using super-resolution 3D-SIM and electron microscopy that the non-acidic compartments contained numerous clustered ILVs that could be the source of exosomes (Figure 4.2A-B; Section 3.2.1.3). Most ILVs were within exosome size range (mostly <150nm diameter; Figure 4.2D), suggesting the existence of biogenesis mechanisms restricting their diameter. Super-resolution imaging also showed that vesicles of similar range of sizes were found in the lumen of the gland, often clumped together, but also individually (Figure 4.2C).

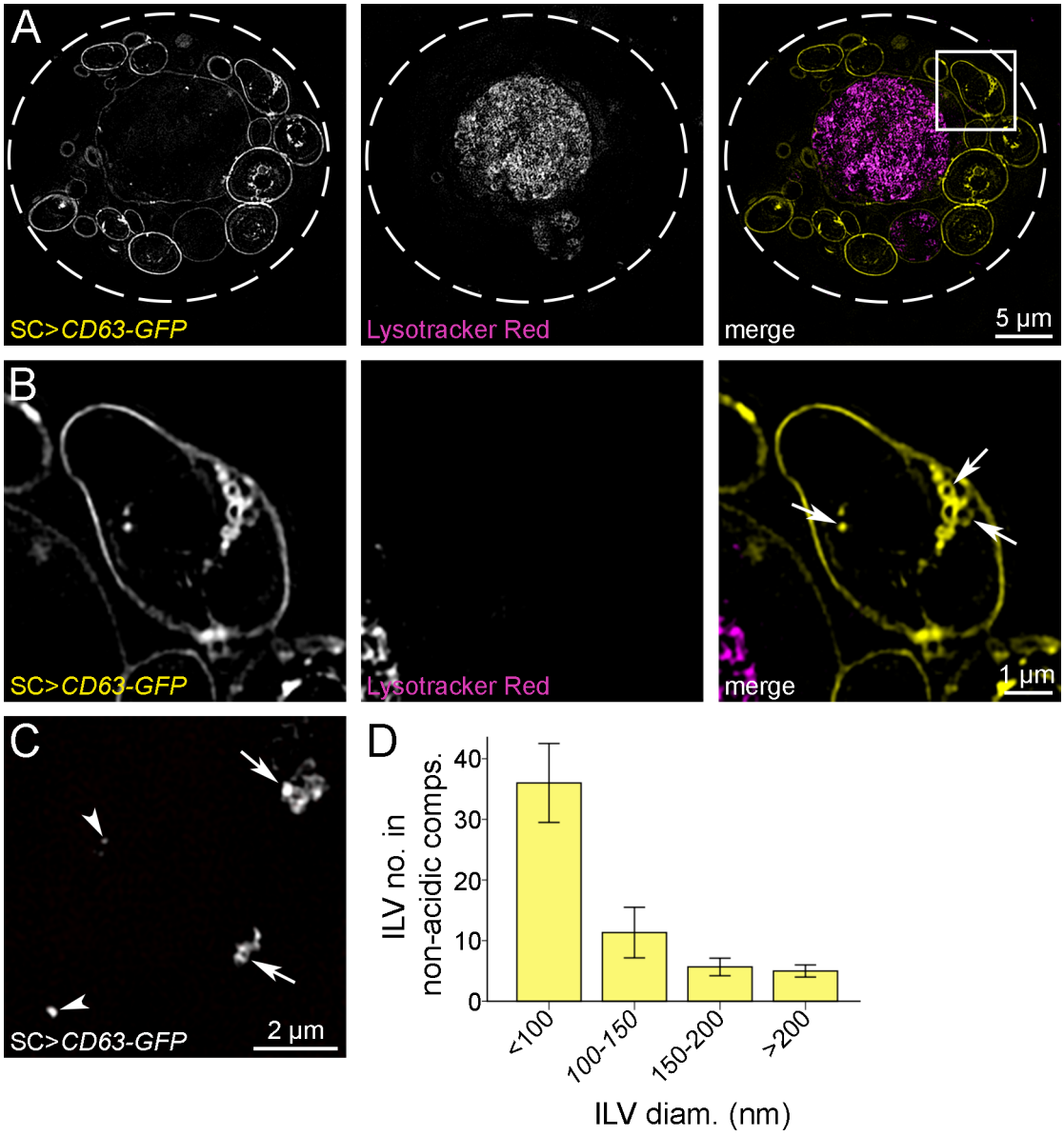

A
SC>CD63-GFP
Lysotracker Red
merge
5 µm
B
SC>CD63-GFP
Lysotracker Red
merge
1 µm
C
SC>CD63-GFP
2 µm
D
ILV no. in non-acidic comps.
40
30
20
10
0
<100
100-150
150-200
>200
ILV diam. (nm)

Figure 4.2 CD63-GFP is loaded onto exosome-sized ILVs within non-acidic compartments and secreted into the accessory gland lumen

Panels A-C display super-resolution 3D-SIM images of either secondary cells (A-B) or lumenal secretions (C) from 6-day-old virgin transgenic males selectively overexpressing CD63-GFP. The flies were incubated at 28.5°C following eclosion to induce CD63-GFP expression using the GAL4-GAL80^{ts}-UAS system. Their accessory glands were stained with Lysotracker Red (magenta). Approximate cell outlines are shown using a dashed line.
(A) CD63-GFP (yellow) localises on the limiting membranes and ILVs of both acidic and non-acidic compartments. The box region in (A) is enlarged in (B).
(B) High magnification image shows the CD63-GFP-labelled ILVs (arrows) within a large non-acidic compartment. Some structures are below the resolution limits of this microscopy technique, so appear as puncta.
(C) Imaging in the lumen of the accessory gland shows a mixture of small CD63-GFP-labelled puncta (arrowheads) and small vesicles (arrowheads), which are often clumped together.
(D) Bar chart showing the number of ILVs within specific size ranges in the non-acidic compartments of secondary cells overexpressing CD63-GFP. ILV size was measured in three compartments from three cells per gland, and using single glands from three independent animals.

The specific genotype of these males is: *w; UAS-CD63-GFP, tub-GAL80ts / +; dsx-GAL4 / +*.

Importantly, time-lapse imaging showed that secondary cells release the contents of the non-acidic compartments by direct fusion to the apical plasma membrane (Figure 4.3), supporting previous studies that suggested these compartments are secretory (Redhai *et al*., 2016). Together, these data suggest that non-acidic Rab11-positive compartments provide a source of exosomes for secretion in secondary cells. This prompted further characterisation of the origin, properties and cargos of the ILVs found in these compartments. To this end, I screened a variety of putative exosome cargos for their localisation in secondary cells.

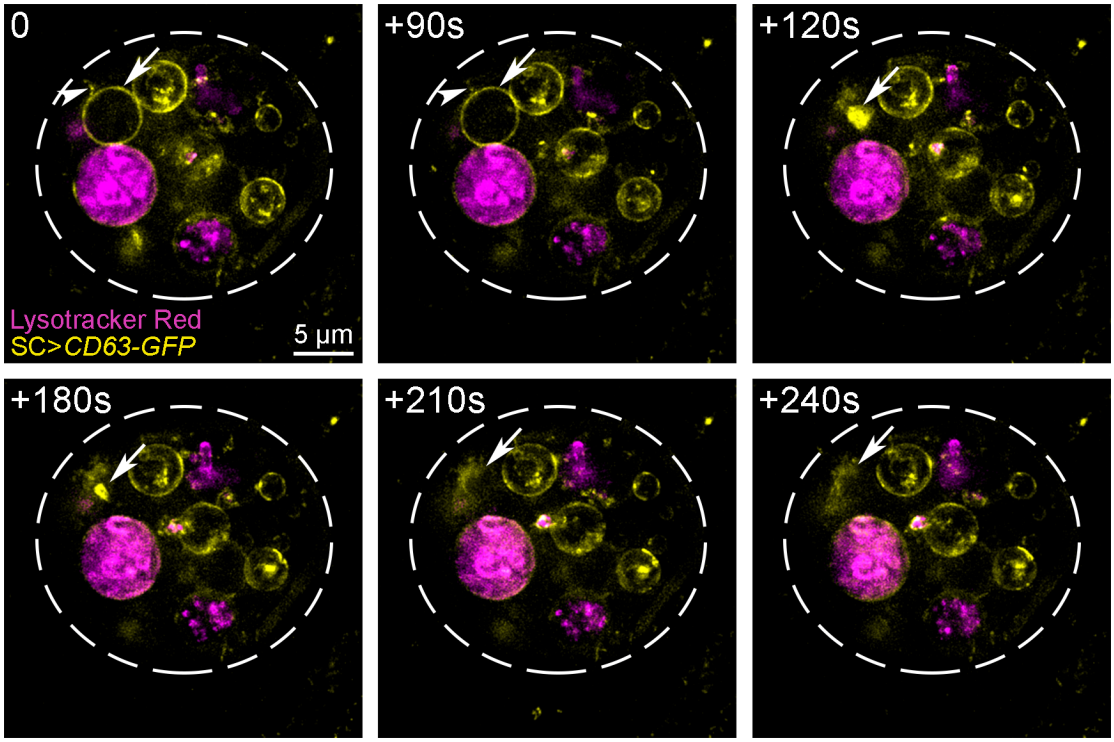


Figure 4.3 Secretion of large non-acidic compartments by secondary cells

These panels show wide-field fluorescence images of living secondary cells from 6-day-old virgin transgenic males selectively overexpressing CD63-GFP. The flies were incubated at 28.5°C following eclosion to induce CD63-GFP expression using the GAL4-GAL80^{ts}-UAS system. Their accessory glands were stained with Lysotracker Red to mark acidic compartments (magenta). Approximate cell outlines are shown using a dashed line. Maximum intensity projection images of 3.5 µm depth are shown.
Time-lapse images show a large non-acidic compartment (arrows), labelled with CD63-GFP (yellow), being secreted. The compartment first projects a tubule towards the plasma membrane (arrowhead, t=0), which is retracted prior to fusion. During fusion (t=120 secs), CD63-GFP fluorescence at the plasma membrane increases, but this gradually reduces over time.

The specific genotype of these males is: *w; UAS-CD63-GFP, tub-GAL80ts / +; dsx-GAL4 / +*.

4.2.1.3 Rab11 is a specific exosome cargo found on ILVs within Rab11-positive compartments

Several Rab GTPases play important roles in exosome secretion in both human cells and *Drosophila* (Colombo *et al*., 2014; Corrigan *et al*., 2014). They also have been observed as enriched cargo proteins inside exosomes derived from a variety of cell types (Haraszti *et al*., 2016; Colombo *et al*., 2014). The fusion protein from the *YFP-Rab11* gene trap, characterised in the previous chapter (Section 3.2.2.4), localised at high levels specifically on the limiting membrane of non-acidic compartments, and was also found on their intraluminal puncta, presumably localising within ILVs, given the cytosolic origin of this molecule (Figure 4.4A-A'). However, due to the low fluorescence levels of this fusion protein, I was unable to use super-resolution microscopy to resolve the structure of the puncta (data not shown).

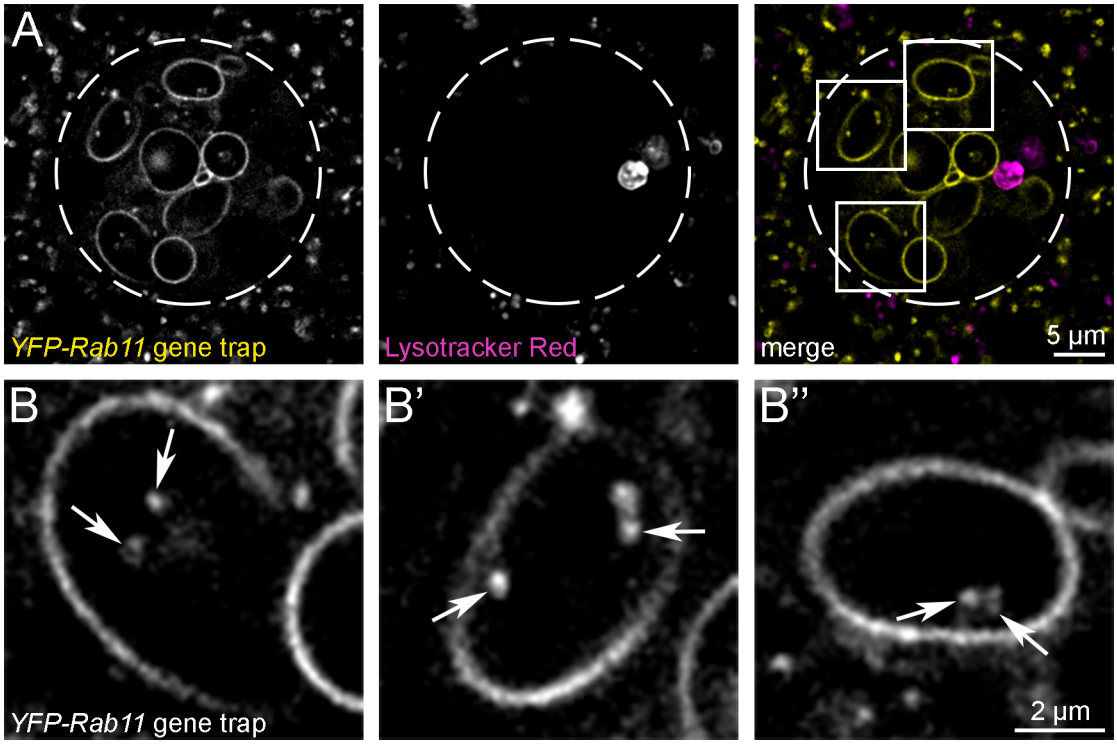


Figure 4.4 YFP-Rab11 marks intraluminal puncta within non-acidic compartments

These panels show wide-field fluorescence images of living secondary cells from 6-day-old virgin males expressing the fusion protein from *YFP-Rab11* gene trap. The flies were incubated at 28.5°C following eclosion. Their accessory glands were stained with Lysotracker Red to mark acidic compartments (magenta). Approximate cell outlines are shown using a dashed line.
(A) In secondary cells, YFP-Rab11 marks the large non-acidic compartments and their intraluminal puncta. Boxes highlight the regions enlarged in (B-B''). (B-B'') Higher magnification images of non-acidic compartments reveals intraluminal puncta marked with YFP-Rab11.

Homozygous *YFP^{Myc}-Rab11* gene trap male flies were used.

I analysed the *YFP-Rab11* gene trap in combination with overexpressed CD63-mCherry, and found that these markers co-localised on intraluminal puncta inside non-acidic compartments, supporting the hypothesis that YFP-Rab11 marks ILVs (Figure 4.5A-A'). Interestingly, YFP-Rab11 only localised on a subset of the CD63-mCherry marked intraluminal puncta within the compartments (Figure 4.5A'). This raised the possibility that heterogeneity in exosome cargo may in part be due to differential loading into ILVs, even when these vesicles are formed inside the same compartment.

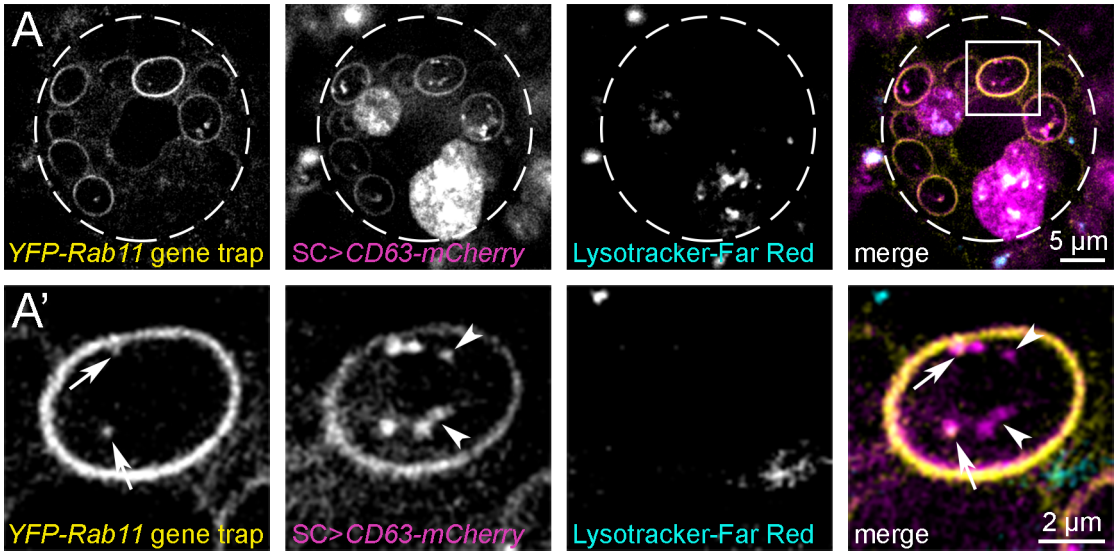


Figure 4.5 YFP-Rab11 localises in a subset of ILVs within non-acidic compartments

These panels show wide-field fluorescence images of living secondary cells from 6-day-old virgin transgenic males selectively overexpressing CD63-mCherry in combination with the *YFP-Rab11* gene trap. The flies were incubated at 28.5°C following eclosion to induce CD63-mCherry expression using the GAL4-GAL80^{ts}-UAS system. Their accessory glands were stained with Lysotracker Far Red to mark acidic compartments (cyan). Approximate cell outlines are shown using a dashed line.
(A) YFP-Rab11 (yellow) and CD63-mCherry (magenta) co-localise on the surface of numerous non-acidic compartments in secondary cells. The box highlights the region enlarged in (A').
(A') YFP-Rab11 co-localises with CD63-mCherry a subset of ILVs (arrows) within the non-acidic compartments. Other ILVs were marked with CD63-mCherry alone (arrowheads).

The specific genotype of these males is: *w; spi-GAL4, tubGAL80ts / +; UAS-CD63-mCherry / YFP^{Myc}-Rab11*

The accessory gland lumens from flies exclusively expressing *YFP-Rab11* gene trap contained puncta labelled with YFP-Rab11 protein, demonstrating that it is secreted, likely within extracellular vesicles (Figure 4.6A). Furthermore, in contrast to CD63-GFP, there was little YFP-Rab11 protein at the apical plasma membrane, suggesting that shedding of ectosomes was unlikely to be responsible for the secreted puncta (Figure 4.6E-E'). However, because both secondary and main cells in the accessory gland epithelium expressed the *YFP-Rab11* gene trap, it was unclear from which cell type the vesicles derived. When *YFP-Rab11* was overexpressed specifically by secondary cells under GAL4-UAS control, it localised on the intraluminal puncta within non-acidic compartments (Figure4.6F-F'), and on puncta in the lumen of the gland (Figure 4.6B), strongly suggesting that secondary cells are responsible for at least some of the secretions.

Notably, in contrast to overexpressed *CD63-GFP*, far fewer puncta were visualised in the lumens of *YFP-Rab11* glands (Figure 4.6C). It is possible that some of this difference in lumenal contents was due to additional plasma membrane shedding in *CD63-GFP*-overexpressing secondary cells, or alternatively, due to super-physiological intraluminal vesicle formation caused by overexpression of CD63 (Edgar *et al*., 2014; van Niel *et al*., 2011). It is also likely that the low level of YFP-Rab11 fluorescence, especially when imaging deeply into the lumen of the gland, contributed to this difference by making it difficult to detect all of the puncta.

Nonetheless, taken together these data demonstrate that Rab11 is a novel exosome cargo protein in *Drosophila*. Its identification raises the possibility that Rab GTPases may be used as markers for the subcellular origins of

exosomes, as they often specifically localise to particular compartments (Zhen & Stenmark, 2015). Other Rabs, such as Rab7 or Rab39, which localise specifically to late endosomal or lysosomal compartments, could be used to identify exosomes originating from those compartments (Section 3.2.2.7).

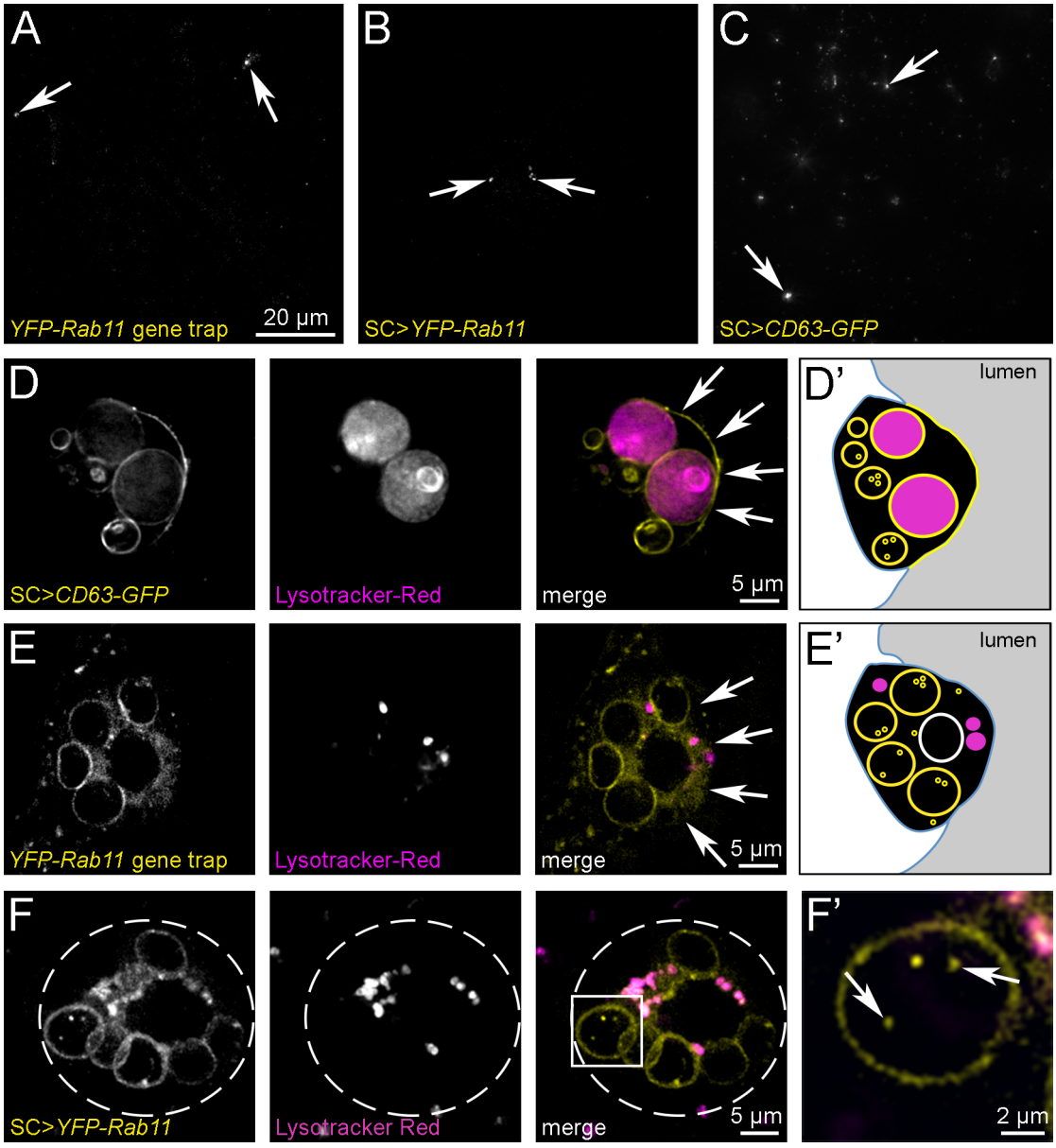

A
YFP-Rab11 gene trap
20 µm
B
SC>YFP-Rab11
C
SC>CD63-GFP
D
SC>CD63-GFP
Lysotracker-Red
merge
5 µm
D'
lumen
E
YFP-Rab11 gene trap
Lysotracker-Red
merge
5 µm
E'
lumen
F
SC>YFP-Rab11
Lysotracker Red
merge
5 µm
F'
2 µm

Figure 4.6 Secondary cells secrete YFP-Rab11 in exosomes

Wide-field fluorescence images of the accessory gland lumen from fixed glands (A-C) and of living secondary cells (D-F). All images are from 6-day-old virgin transgenic males incubated at 28.5°C following eclosion. This permissive temperature drove secondary cell specific overexpression of CD63-GFP or YFP-Rab11 using the GAL4-GAL80^{ts}-UAS system. The accessory glands in (D-F) were stained with Lysotracker Red (magenta). The approximate cell outline in (F) is shown with a dashed line.
(A-C) Accessory gland lumen from flies expressing the YFP-Rab11 gene trap, or secondary cell-specific overexpression of YFP-Rab11 and CD63-GFP. Arrows show the dispersed fluorescent puncta in the lumen.
(D) Transverse section from secondary cell overexpressing CD63-GFP (yellow). CD63-GFP is present on the large intracellular compartments and their ILVs, and also at the apical plasma membrane, illustrated by arrows in merge and in the schematic (D')
(E) Transverse section of a secondary cell expressing YFP-Rab11 from its endogenous locus, which marks large intracellular non-acidic compartments, and is also diffusely in the cytosol, but is not trafficked to the apical plasma membrane, indicated by arrows in merge and in schematic (E')
(F) In secondary cell selectively overexpressing YFP-Rab11, it lines the large non-acidic compartments and is loaded into ILVs within these compartments. The boxed region highlights an example compartment enlarged in (F').
(F') Arrows indicate the punctate YFP-Rab11-positive ILVs, which are secreted, as shown in (B).

The specific genotypes of the flies used here are: homozygous *YFP^{Myc}-Rab11* flies, *w; UAS-CD63-GFP, tub-GAL80ts / +; dsx-GAL4 /* + males and *w; tub-GAL80ts / +; dsx-GAL4 / UAS-YFP-Rab11*.

4.2.1.4 Chaoptin is a novel marker of native extracellular vesicles secreted secondary cells

The GPI-anchored adhesion molecule Chaoptin (Van Vactor *et al*., 1988) was first analysed by M. Wainwright, a postdoctoral researcher in the Wilson lab, who showed that it was specifically expressed at high levels by secondary cells within the male accessory glands, localising on the limiting membrane of several of their large subcellular compartments (unpublished). In my previous results chapter, I reported further analysis of its localisation, which showed that in addition to the limiting membrane, Chaoptin was also often observed on intraluminal puncta of the large Rab11-positive compartments and at the plasma membrane (Appendix 8.1.1, 8.1.2). However, it was excluded from the surface of the large acidic Rab7/Rab39-positive compartments (Appendix 8.1.2).

When CD63-GFP was overexpressed specifically in secondary cells and the glands immunostained for Chaoptin, the AG lumen contained fluorescent puncta where both proteins co-localised, but other puncta were positive for just CD63-GFP or Chaoptin (Figure 4.7A). These two markers showed some, but not complete co-localisation in the lumen of secondary cell Rab11-positive compartments (Appendix 8.1.2). These data support the hypothesis that Chaoptin could be secreted on exosomes derived from these compartments. In non-transgenic w^{1118} flies, Chaoptin also marked numerous puncta in the lumen of the glands, suggesting that exosome secretion was not simply super-physiologically induced by CD63-GFP overexpression (Figure 4.7B). This characterisation of Chaoptin showed that it might be a useful tool for the study of exosome secretion by secondary cells. However, fixation often

resulted in poor tissue quality, possibly because of the instability of secondary cells and their large compartments as fixative diffuses into tissue. Immunostaining in the gland's lumen was also somewhat inconsistent, perhaps for similar reasons. I therefore chose to perform most of my further research with living cells. The development of a *Chaoptin-GFP* gene trap line would prove valuable to future work.

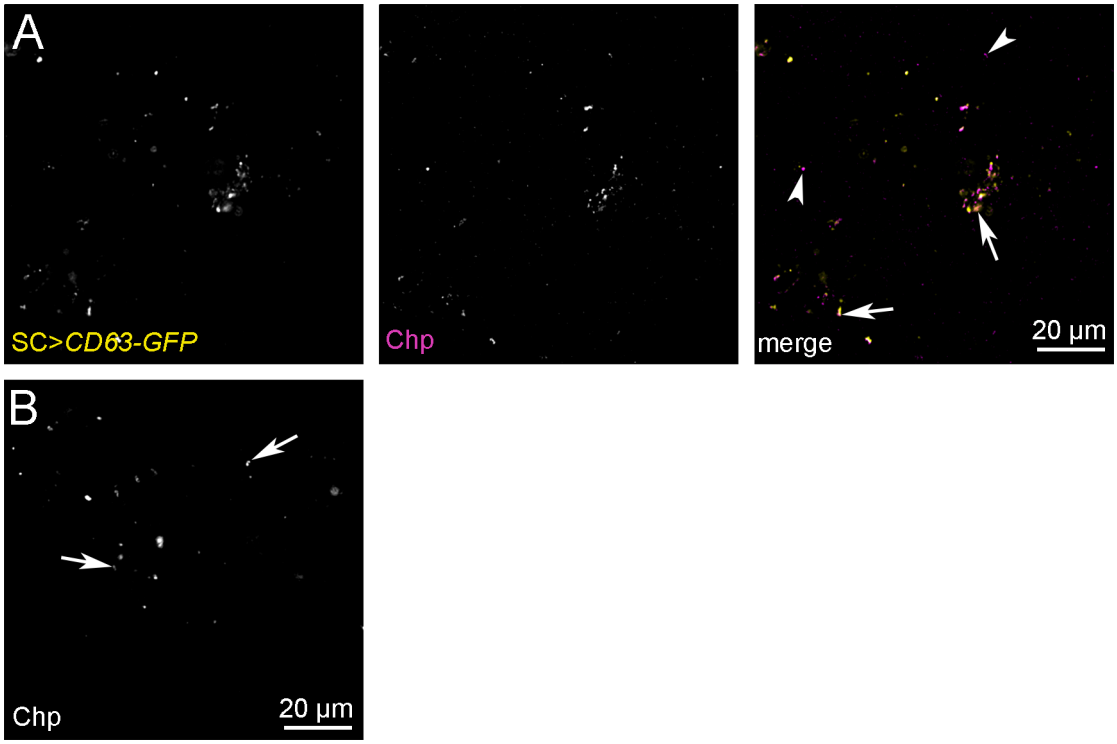


Figure 4.7 The GPI-anchored protein Chaoptin is secreted on exosomes

These panels display wide-field fluorescence images of the accessory gland lumen from fixed glands that were immunostained with anti-Chp antibodies. 6-day-old virgin males were incubated at 28.5°C following eclosion. These observations were made in collaboration with M. Wainwright, who first identified Chp in secondary cells.
(A) The accessory gland lumens from flies overexpressing CD63-GFP (yellow) contain numerous fluorescent puncta. Arrows highlight overlap between CD63-GFP- and Chp- (magenta) labelled puncta, and arrowheads highlight puncta only marked by Chp.
(B) The accessory gland lumens in non-transgenic w^{1118} flies also contain numerous Chp-labelled puncta (white).

The flies used in this figure are: *w; UAS-CD63-GFP, tub-GAL80ts / +; dsx-GAL4 /* + and w^{1118}.

4.2.1.5 breathless and branchless gene products are putative exosome cargos, specifically loaded onto ILVs within Rab11-positive compartments

Signalling molecules represent some of the most important cargos secreted within exosomes (Tkach & Théry, 2016). The stabilising properties of lipid encapsulated, cytosol-buffered exosomes are thought to enable the transport of signalling molecules over long distances before enacting their function. The localisation of important signalling proteins in secondary cells was studied here using GFP-tagged fusion proteins because of the potential functional roles they may play in exosome-mediated cell-cell signalling during *Drosophila* reproduction (Corrigan *et al*., 2014).

The localisation of a fluorescently tagged form of Breathless (Btl; Hayashi *et al*., 2002), a *Drosophila* Fibroblast Growth Factor Receptor (FGFR), was carefully analysed. When overexpressed in secondary cells, super-resolution 3D-SIM showed that GFP-tagged Btl (Sato & Kornberg, 2002) trafficked at high levels onto numerous ILVs specifically inside the non-acidic Rab11-positive compartments (Figure 4.8A-B''), and to the apical plasma membrane (data not shown). Like the fusion protein from the *YFP-Rab11* gene trap, and in contrast to overexpressed CD63-GFP, it was not detected on the limiting membranes of the acidic compartments (Figure 4.8A; Sections 3.2.2.4 and 4.2.1.3).

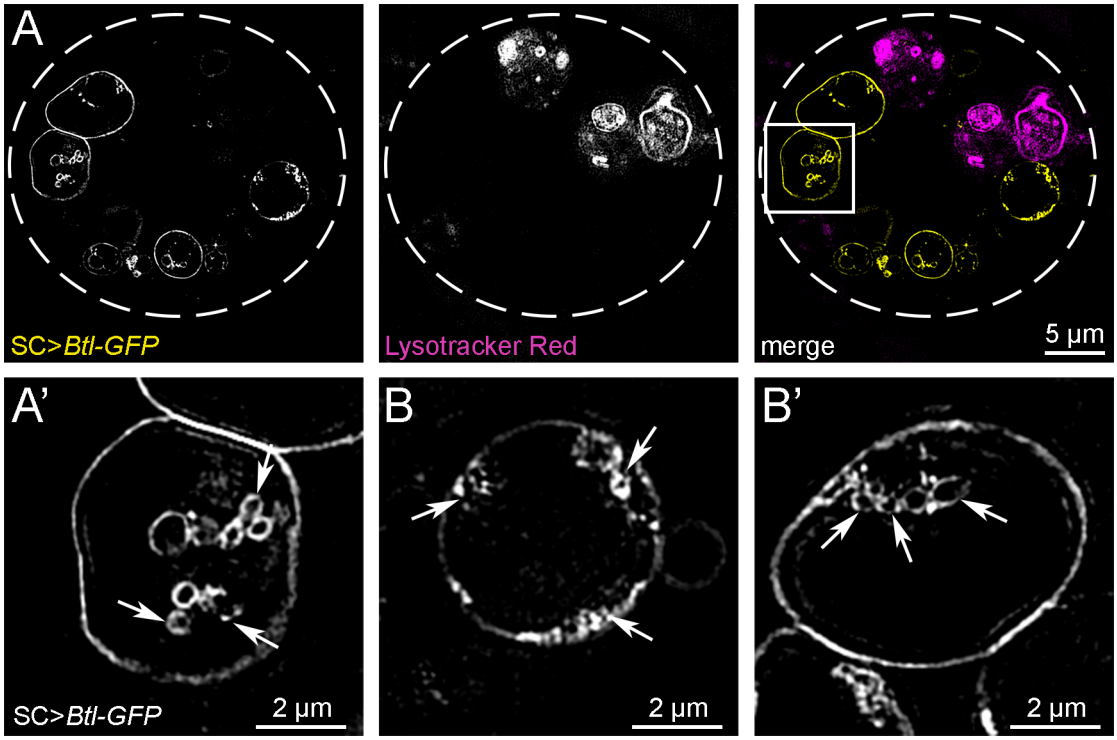


Figure 4.8 Btl-GFP is selectively localised on ILVs within non-acidic compartments

These panels show super-resolution 3D-SIM images of secondary cells from 6-day-old virgin transgenic males selectively overexpressing Btl-GFP. The flies were incubated at 28.5°C since eclosion to induce Btl-GFP expression using the GAL4-GAL80^{ts}-UAS system. Their accessory glands were stained with Lysotracker Red (magenta). Approximate cell outlines are shown using a dashed line.
(A) Btl-GFP (yellow) localises specifically on the limiting membranes of non-acidic compartments in this secondary cell. Box highlights the particular region enlarged in (A')
(A') Numerous Btl-GFP-labelled ILVs (white) are resolved within the non-acidic compartment lumen (arrows).
(B-B') Other example compartments of Btl-GFP marked ILVs.

The specific genotype of these males is: *w; tubGAL80ts / +; dsx-GAL4 / UAS-Btl-GFP*.

These distinctive localisations are common across most secondary cells in the accessory glands: compared to CD63-GFP (Figure 4.9A-A'), which localises to the limiting membrane of the acidic compartments, both Btl-GFP (Figure 4.9B-B') and YFP-Rab11 (Figure 4.9C-C') were found inside the large acidic compartment lumen in a subset of cells, but not on the limiting membrane, presumably because Rab11-labelled compartments sporadically fuse with the large acidic compartments within secondary cells (Figure 4.1; Corrigan *et al*., 2014). On the whole though, my data suggested that, unlike CD63-GFP, Btl-GFP preferentially localised to the limiting membrane of Rab11-positive non-acidic compartments. Furthermore, because overexpressed Btl-GFP localised to the ILVs within both acidic and non-acidic compartments, this clearly demonstrates for the first time that exosome cargos, other than compartment-specific Rab GTPases, can be preferentially localised within a specific compartment subtype.

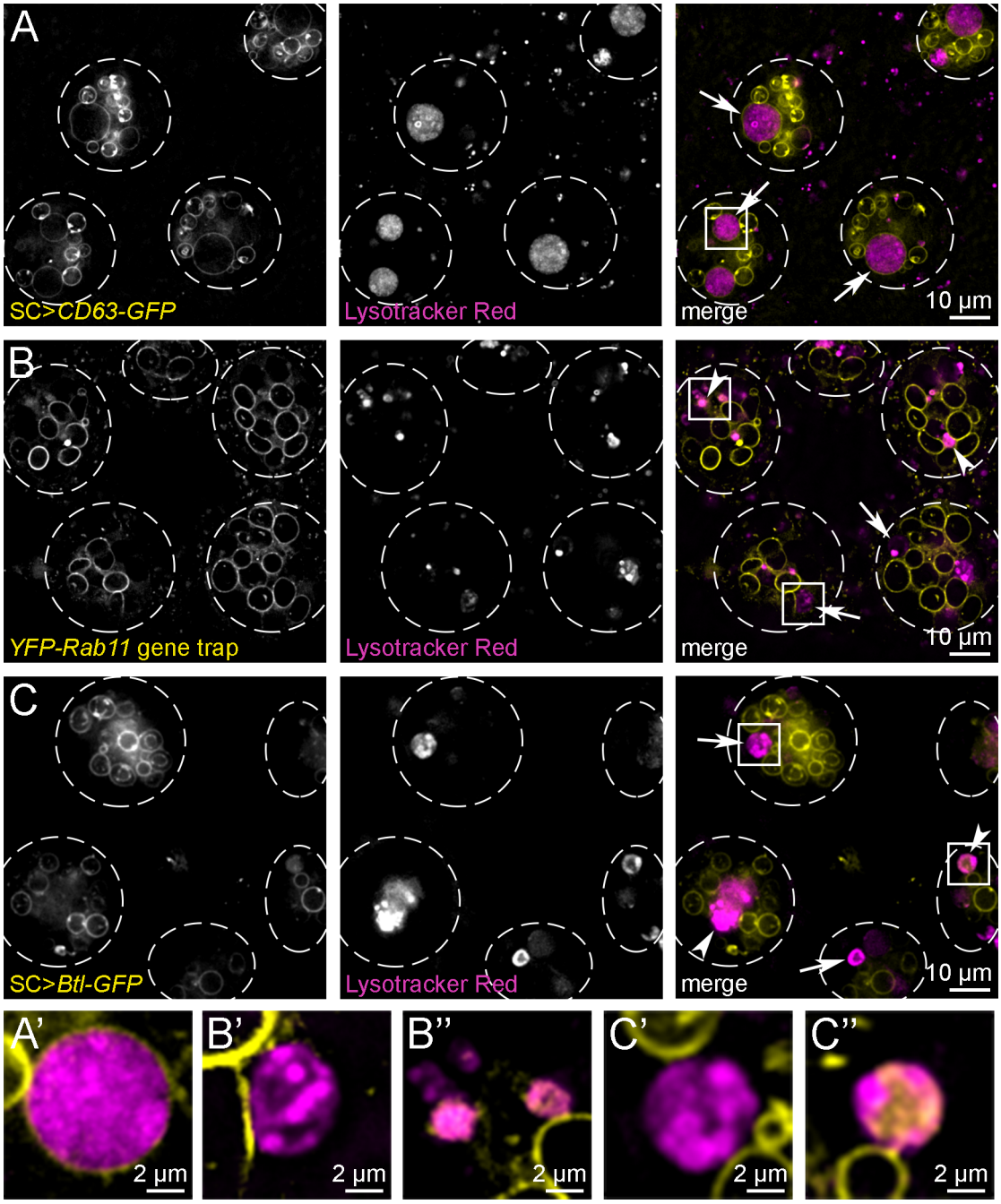

A
SC>CD63-GFP
Lysotracker Red
merge
10 µm
B
YFP-Rab11 gene trap
Lysotracker Red
merge
10 µm
C
SC>Btl-GFP
Lysotracker Red
merge
10 µm
A'
2 µm
B'
2 µm
B''
2 µm
C'
2 µm
C''
2 µm

Figure 4.9 YFP-Rab11 and Btl-GFP are not found on the limiting membranes of large acidic compartments

All panels show wide-field fluorescence images in an epithelial plane section through living secondary cells, from 6-day-old virgin transgenic males incubated at 28.5°C following eclosion. This permissive temperature drove secondary cell specific overexpression of CD63-GFP or Btl-GFP using the GAL4-GAL80^{ts}-UAS system. The accessary glands are stained with Lysotracker Red (magenta) to mark acidic compartments. Approximate cell outlines are shown with dashed lines.
(A) Overexpressed CD63-GFP (yellow) localises on the limiting membranes of all large acidic compartments in secondary cells (arrows; boxed region magnified in A').
(B) YFP-Rab11 (yellow) is not found on the limiting membranes of large acidic compartments. Furthermore, most acidic compartments from YFP-Rab11 gene trap males appear to contain no YFP fluorescence (arrows; example boxed region is magnified in B'). Sporadic compartments have fluorescent lumenal contents (arrowheads; boxed regions magnified in B'').
(C) Similarly to YFP-Rab11, overexpressed Btl-GFP (yellow) is not observed on the surface of large acidic compartments. Most acidic compartments in secondary cells that overexpress Btl-GFP also appear to contain no GFP fluorescence (arrows; boxed region is magnified in C'), but some sporadic compartments have fluorescent lumenal contents (arrowheads; boxed regions are magnified in C'').

The specific genotypes of the flies used here are: *w; UAS-CD63-GFP, tub-GAL80ts / +; dsx-GAL4 / +,* homozygous *YFP^{Myc}-Rab11* gene trap, and *w; tubGAL80ts / +; dsx-GAL4 / UAS-Btl-GFP.*

Importantly, overexpressed Btl-GFP was secreted on numerous extracellular vesicles into the accessory gland lumen, and at levels similar to glands that overexpressed CD63-GFP (Figure 4.10A-B). It remained difficult, however, to determine what proportion of the extracellular vesicles are exosomal, as Btl-GFP also localised to the plasma membrane, and may be shed from the cell surface. However, given that the non-acidic Rab11-positive compartments are readily secreted by secondary cells (Section 4.2.1.2), it seems likely that they make a significant contribution to the pool of secreted exosomes. When overexpression of *btl-GFP* was combined with *CD63-mCherry*, the fluorescently tagged proteins co-localised on many of their ILVs observed in non-acidic compartments carrying both markers (Figure 4.10C-C'), and on puncta in the lumen of the accessory gland (Figure 4.10D). These data suggested that overexpressed Btl-GFP might be a more ubiquitous exosome cargo derived from large non-acidic compartments than YFP-Rab11 expressed from a gene trap.

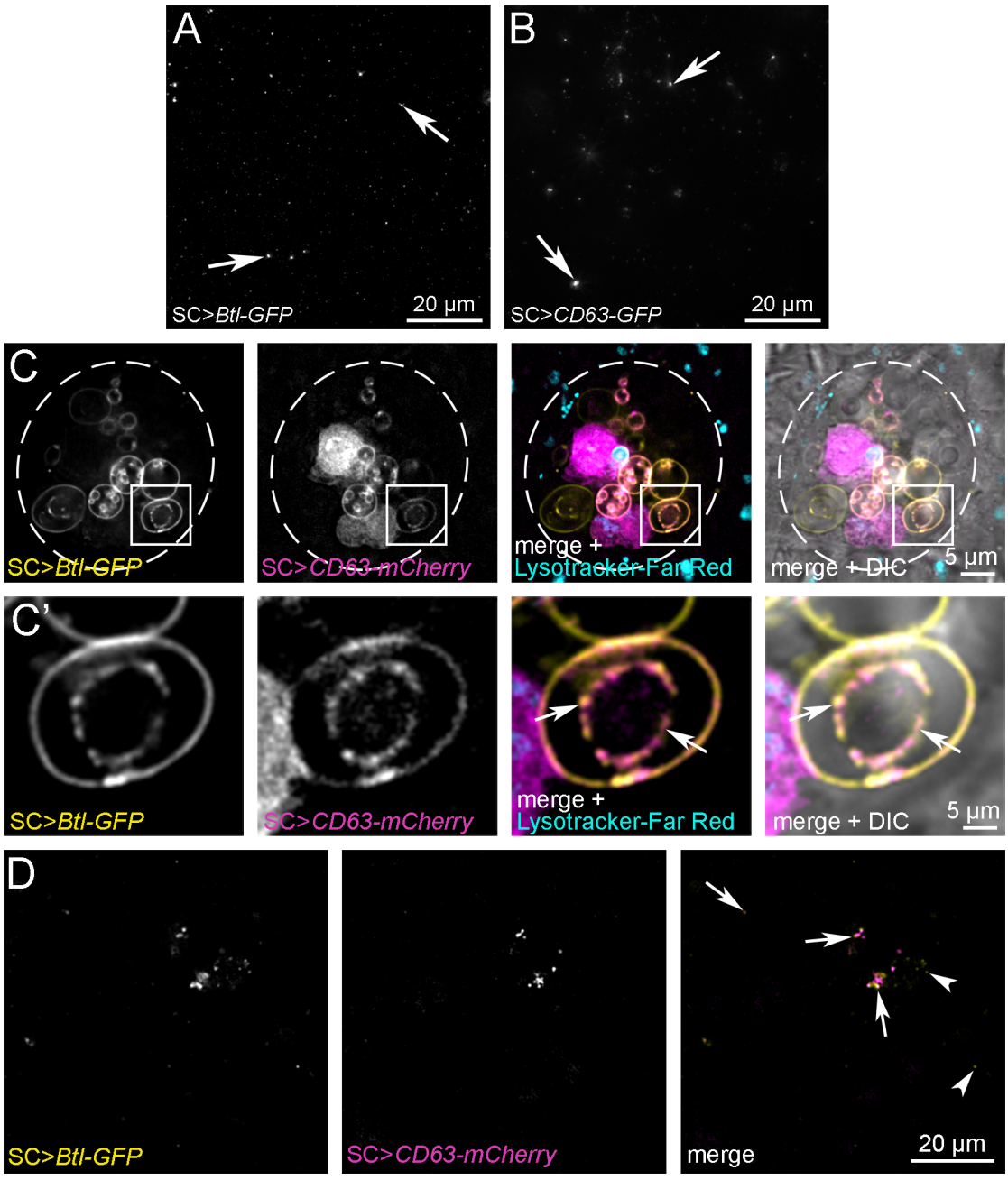

A
SC>Btl-GFP
20 µm
B
SC>CD63-GFP
20 µm
C
SC>Btl-GFP
SC>CD63-mCherry
merge +
Lysotracker-Far Red
merge + DIC
5 µm
C'
SC>Btl-GFP
SC>CD63-mCherry
merge +
Lysotracker-Far Red
merge + DIC
5 µm
D
SC>Btl-GFP
SC>CD63-mCherry
merge
20 µm

Figure 4.10 Btl-GFP is secreted into the accessory gland on numerous extracellular vesicles

These panels consist of wide-field fluorescent images of the accessory gland lumens from fixed glands (A, B, D) or living secondary cells (C-C'). All images are from 6-day-old virgin transgenic males incubated at 28.5°C following eclosion. This permissive temperature drove secondary cell specific overexpression of CD63-GFP, Btl-GFP, or combinations of Btl-GFP and CD63-mCherry, using the GAL4-GAL80^{ts}-UAS system. The accessory glands in (C-C') were stained with Lysotracker Far Red (cyan). The approximate cell outline in (C) is shown with a dashed line.
(A) Secondary cells overexpressing Btl-GFP secrete numerous Btl-GFP-positive puncta (arrows) into the accessory gland lumen. The level of secretion is comparable to when CD63-GFP is overexpressed in secondary cells (B).
(C) In secondary cells overexpressing both Btl-GFP (yellow) and CD63-mCherry (magenta), they co-localise on most of the large non-acidic compartments in secondary cells. CD63-mCherry is also localised at high levels within the Lysotracker Far Red-positive acidic compartments (cyan). The box highlights the region enlarged in (C').
(C') Btl-GFP and CD63-mCherry co-localise on the numerous ILVs (arrows) surrounding the dense-core granule.
(D) The accessory gland lumen from flies overexpressing both Btl-GFP (yellow) and CD63-mCherry contain numerous extracellular puncta, presumably extracellular vesicles, many of which carry both proteins (arrows). However, other puncta was positive only for Btl-GFP (arrowheads).

The specific genotypes of the flies used here are: *w; tubGAL80ts / +; dsx-GAL4 / UAS-Btl-GFP* (A), *w; UAS-CD63-GFP, tub-GAL80ts / +; dsx-GAL4 / +* (B), and *w; spi-GAL4, tubGAL80^{ts} / + ; UAS-CD63-mCherry / UAS-Btl-GFP* (C-D).

I also studied the localisation of a fluorescently tagged signal ligand, Branchless (bnl), a *Drosophila* Fibroblast Growth Factor (FGF) homologue. Using wide-field imaging, I showed that overexpressed Bnl-GFP localised specifically, and at high levels, to the limiting membranes of non-acidic compartments and their intraluminal puncta (Figure 4.11A-A'). Both this, and the finding that Bnl-GFP was also not observed on the limiting membrane of the large acidic compartments, mirrored the localisations of Btl-GFP and YFP-Rab11. Furthermore, Bnl-GFP was also secreted at high levels in numerous small extracellular vesicles (data not shown).

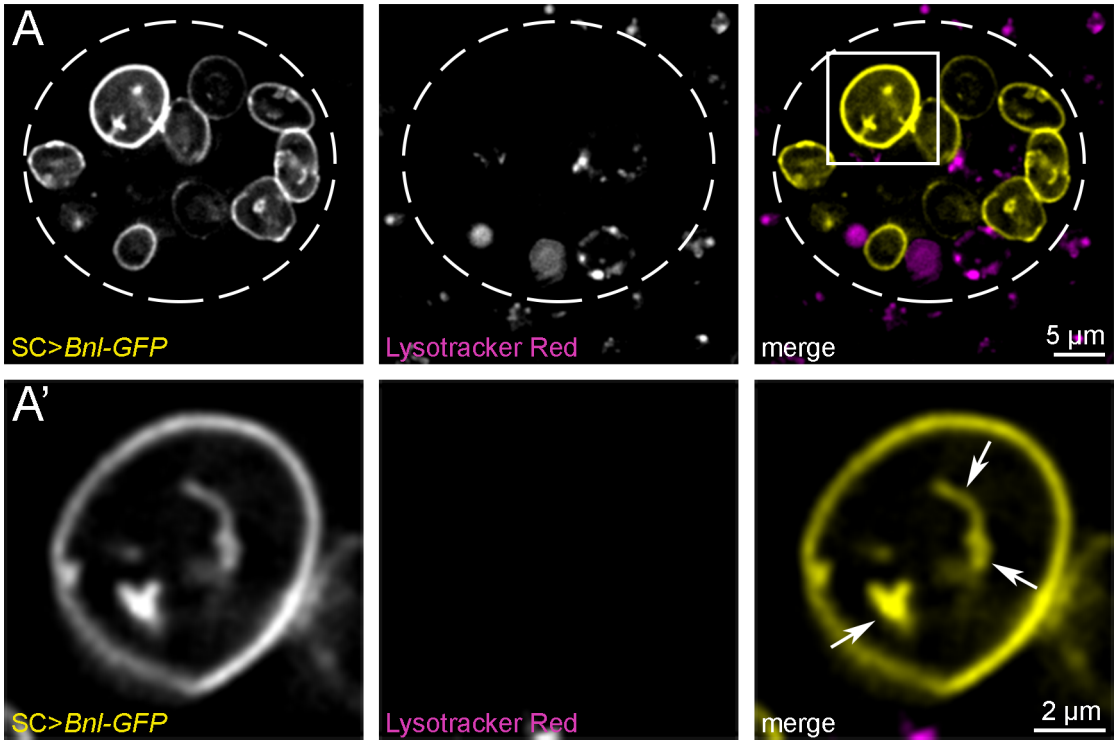


Figure 4.11 Bnl-GFP is selectively localised on intraluminal puncta within non-acidic compartments

These panels show wide-field fluorescence images of secondary cells from 6-day-old virgin transgenic males selectively overexpressing Bnl-GFP. The flies were incubated at 28.5°C since eclosion to induce Bnl-GFP expression using the GAL4-GAL80^{ts}-UAS system. Their accessory glands were stained with Lysotracker Red (magenta). Approximate cell outlines are shown using a dashed line.
(A) When overexpressed in secondary cells, Bnl-GFP (yellow) localises specifically on the limiting membranes of non-acidic compartments. The box highlights the particular region enlarged in (A')
(A') Bnl-GFP localises on intraluminal puncta in non-acidic compartments, presumably in a region surrounding the dense-core granule.

These flies carry the genetic combination of *tub-GAL80ts; dsx-GAL4* with *UAS-Bnl-GFP*.

A screen of over 30 different GAL4 enhancer trap insertions was recently undertaken in the Wilson lab to order to detect the types of signalling proteins expressed by secondary cells (Leiblich, 2015). Interestingly, the screen found that GAL4 enhancer trap insertions in either *btl* or *bnl* drove UAS-GFP^{NLS} expression specifically in secondary cells within the accessory glands. I confirmed this observation (Figure 4.12A-B), which strongly suggests that *Btl* and *Bnl* gene products are expressed by secondary cells. In addition, other reports show that modulating the Btl/Bnl signalling pathway in secondary cells impacts their subcellular organisation (Corrigan, 2014), suggesting that secondary cells normally express these molecules, and utilise them to control their biology, potentially in an autocrine fashion.

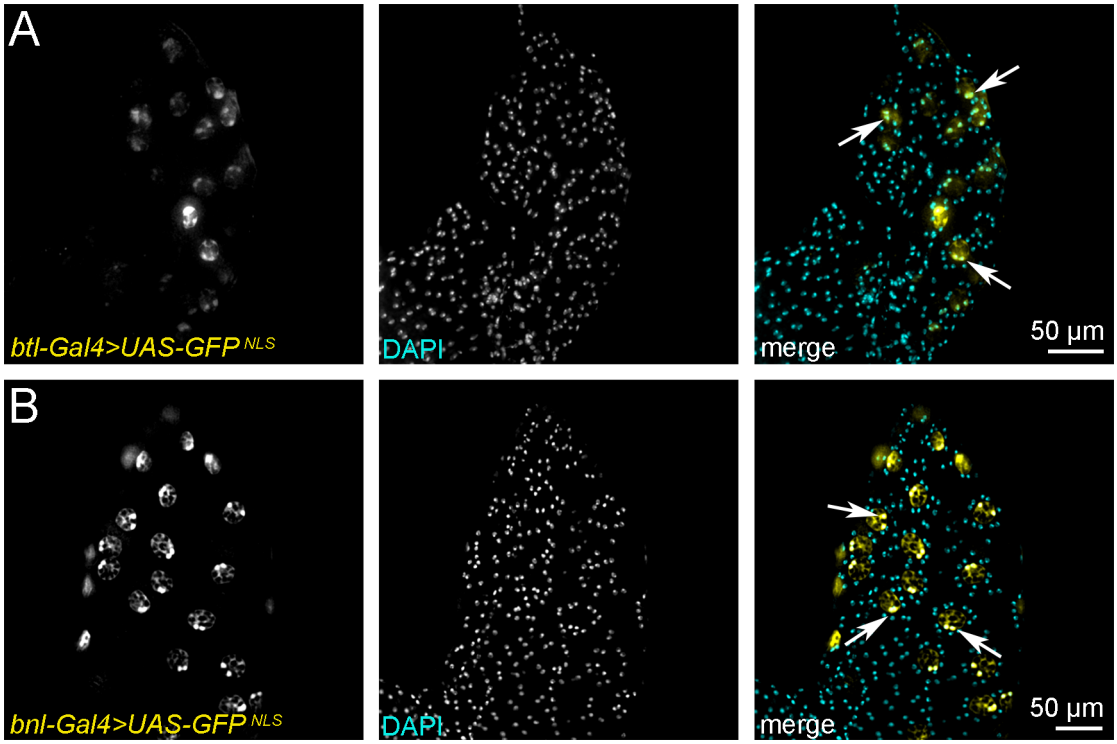


Figure 4.12 *btl-GAL4* and *bnl-GAL4* drive gene expression specifically in secondary cells within the accessory gland epithelium

These panels consist of wide-field fluorescence images of fixed accessory glands expressing nuclear localised GFP (yellow) under the control of characterised *btl-GAL4* and *bnl-GAL4* enhancer traps. The flies were incubated at 28.5°C following eclosion. Accessory glands were stained with DAPI (cyan) to mark nuclei prior to imaging.
(A-B) Within the accessory gland epithelium, secondary cells selectively express GFP^{NLS} (yellow) from both the btl-GAL4 and bnl-GAL4 drivers (arrows), suggesting that *btl* and *bnl* are normally expressed in secondary cells.

The specific genotypes used in this figure are: *bnl-GAL4* or *btl-GAL4* in combination with *UAS-GFP*^{NLS}

It is also possible that secondary cells normally secrete Btl and Bnl proteins on exosomes, and these may function elsewhere in the male reproductive tissues or in the female reproductive tract following mating. To further understand whether Btl/Bnl could play roles in the female, the *btl* and *bnl* GAL4 enhancer traps were used to drive expression of a *UAS-GFP*^{NLS} marker in the female reproductive tissues. These experiments suggested that Btl is expressed by neurons in close association with the uterus and spermathecae, (Figure 4.13A-B). *bnl*-GAL4, on the other hand, was expressed by a subset of cells in the spermathecae (Figure 4.13C). These data suggested that some key cell types in the female reproductive system are responsive to Btl signalling, and so secondary cell Btl and Bnl secretion on exosomes could cause responses after mating, possibly by activating Btl-signalling in neurons, or cell types of the reproductive tract.

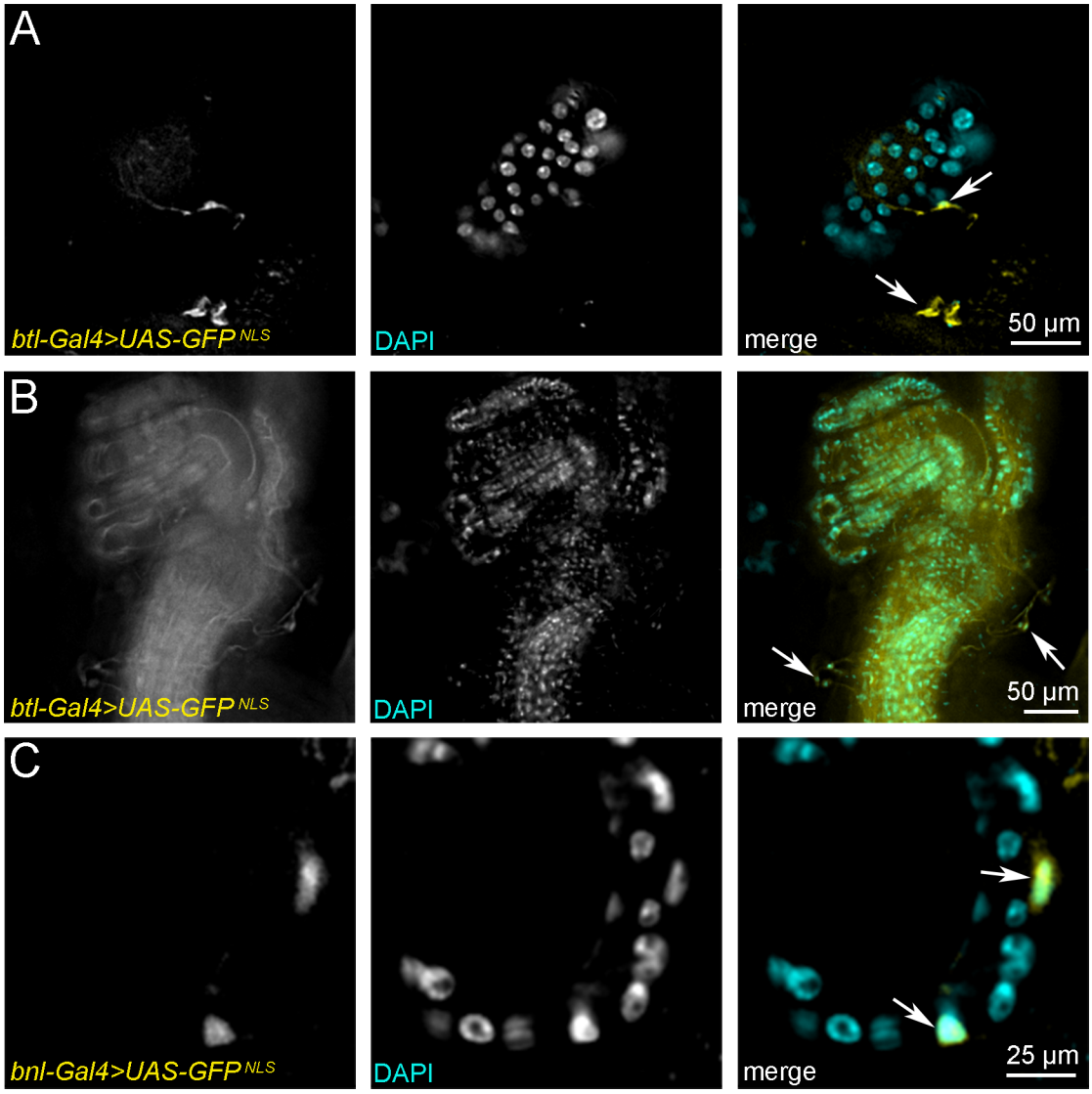


Figure 13. *btl-GAL4* and *bnl-GAL4* drive gene expression in different cell types within the female reproductive tract

These panels display wide-field fluorescence images of fixed female reproductive tracts expressing nuclear localised GFP (yellow) under the control of characterised *btl-GAL4* and *bnl-GAL4* enhancer traps. The flies were incubated at 28.5°C following eclosion. Reproductive tracts were stained with DAPI (cyan) to mark nuclei prior to imaging.
(A-B) *btl-GAL4* drives the expression of GFP^{NLS} (yellow) selectively in neurons, as distinguished by their characteristically long projections (arrows), in close association with the spermathecae (A) and uterus (B). High autofluorescent signal is also detected in the uterus.
(C) GFP^{NLS} is expressed in a subset of cells in the spermathecae (arrows), when under the control of *bnl-GAL4*.

The specific genotypes of the female flies used in this figure are: *bnl-GAL4* or *btl-GAL4* in combination with *UAS-*GFP^{NLS}

4.2.1.6 The effect of transgene expression on secondary cell biology

Having identified Btl-GFP and YFP-Rab11 as new markers for a specific exosome subtype, it was important to check whether expression of these transgenes affected the number and size of different compartments when compared to non-transgenic w^{1118} flies. Secondary cells expressing *YFP-Rab11* gene trap contained a normal number of non-acidic, but the acidic compartments were more numerous and considerably smaller (Figure 4.14A-C). Secondary cells overexpressing *btl-GFP* were very similar to controls; age- and temperature-matched transgenic flies were unaffected in the number of non-acidic compartments, or the size of the largest acidic compartment (Figure 4.14A,C). However, overexpression did slightly increase the number of acidic compartments when compared to w^{1118} cells (Figure 4.14B). These data suggest that Btl-GFP overexpression does not dramatically affect subcellular trafficking in secondary cells, and their behaviour is likely to be similar to 'wild type'. Overexpression of *CD63-GFP* by secondary cells impacted the average number of non-acidic compartments, almost trebling their number (Figure 4.14A). These data correlate well with previous reports (Redhai *et al*., 2016), which showed that the transgene also increased the size of the largest acidic compartment, while the number of acidic compartments remained the same (Figure 4.14B-C). Overall these data suggest that overexpressing CD63-GFP in secondary cells has a relatively high impact on trafficking pathways, and when utilised, should preferably only be compared to transgenic flies that are also overexpressing CD63-GFP.

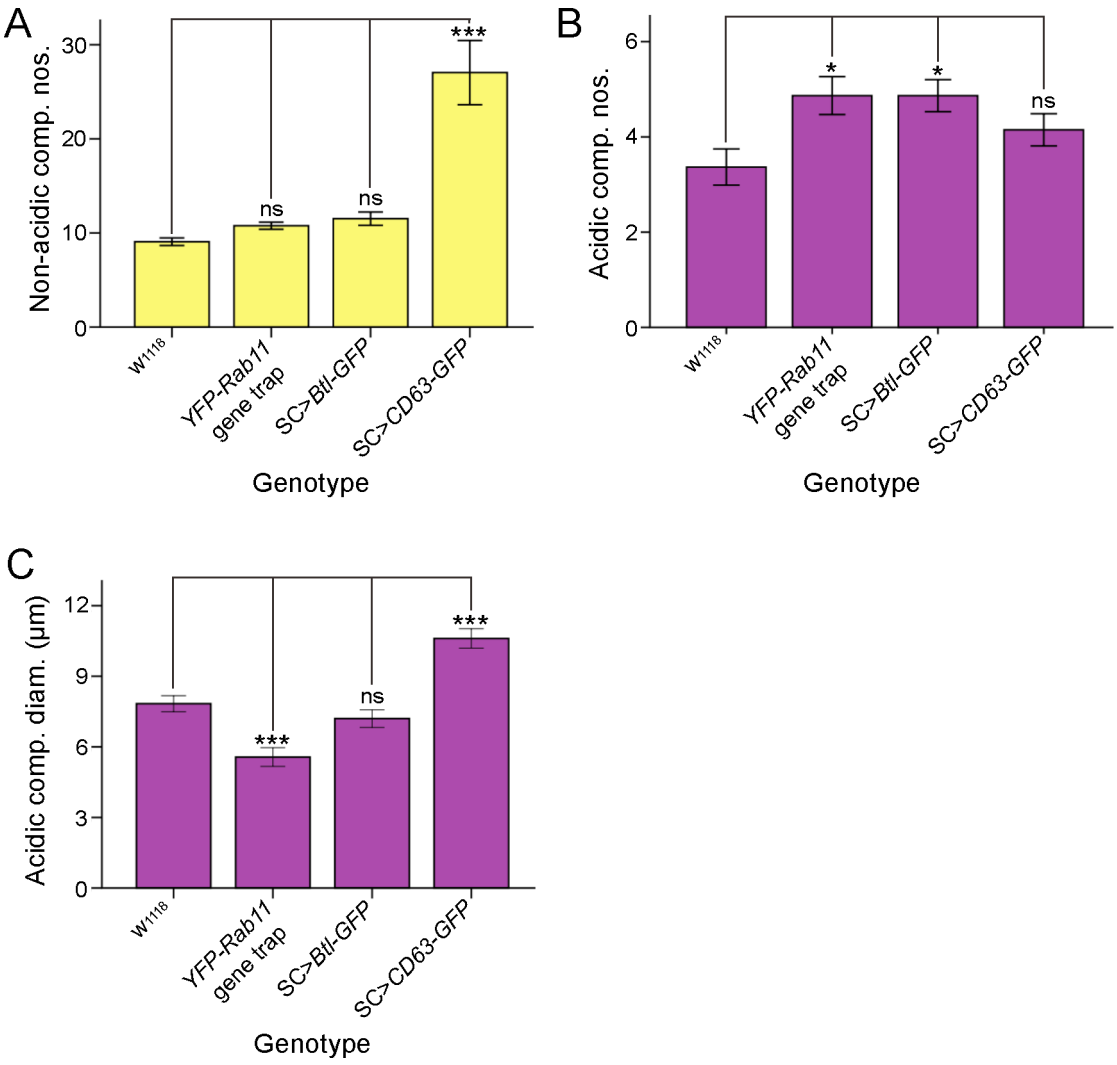

A
Non-acidic comp. nos.
30
20
10
0
***
ns
ns
w1118
YFP-Rab11 gene trap
SC>Btl-GFP
SC>CD63-GFP
Genotype
B
Acidic comp. nos.
6
4
2
0
*
*
ns
w1118
YFP-Rab11 gene trap
SC>Btl-GFP
SC>CD63-GFP
Genotype
C
Acidic comp. diam. (µm)
12
9
6
3
0
***
***
ns
w1118
YFP-Rab11 gene trap
SC>Btl-GFP
SC>CD63-GFP
Genotype

Figure 4.14 Quantification of the effects of transgene expression on large intracellular compartments in secondary cells

These data are generated from the secondary cells within six-day-old virgin males incubated at 28.5°C following eclosion.
(A) Bar chart showing average number of large (> 2 μm diameter), non-acidic compartments, identified using DIC microscopy, from w^{1118}, *YFP-Rab11* gene trap, *Btl-GFP*-overexpressing, and *CD63-GFP*-overexpressing secondary cells. The number of these compartments is increased by CD63-GFP expression, as previously reported (Redhai *et al*., 2016).
(B) Bar chart showing average number of large (> 2 μm diameter), acidic compartments in the same genetic backgrounds. The number of acidic compartments is slightly increased by the *YFP-Rab11* gene trap and Btl-GFP overexpression.
(C) Bar chart showing average size of largest acidic compartment in these genetic backgrounds. The YFP-Rab11 gene trap slightly reduces the size of the compartment, and CD63-GFP increases it.

The specific genotypes of the flies used here are: w^{11118}, homozygous YFP^{Myc}*-Rab11* gene trap, *w; UAS-CD63-GFP, tub-GAL80ts / +; dsx-GAL4 / +* and *w; tubGAL80ts / +; dsx-GAL4 / UAS-Btl-GFP.* Statistical comparisons are made between transgenic and w^{1118} flies as described in Section 2.23 (n=10 glands, with 3 cells analysed per gland). *P≤0.05; **P≤0.01; ***P≤0.001; ns = not significant.

4.2.2 Regulatory mechanisms of ILV formation in Rab11-positive compartments

4.2.2.1 ESCRTs localise onto the limiting membranes of Rab11-positive compartments

The formation of ILVs in mammalian cells is dependent on at least two mechanisms, one that requires the ESCRTs and their accessory proteins (Schöneburg *et al*., 2017; Colombo *et al*., 2014; Henne *et al*., 2011), and the other, ceremide (Trajkovic *et al*., 2008). The ESCRTs are highly conserved from yeast to humans and consist of five distinct subcomplexes (ESCRTs 0-III and the Vps4 ATPase; Schmidt & Teis, 2012). By forming ILVs, they play key roles in the generation of multivesicular endosomes, and have been localised to both early and late endosomal compartments in human cells (Welsch *et al*. 2006; Bache *et al*., 2003). During the formation of ILVs, they are thought to cluster ubiquitinated cargos, particularly transmembrane proteins, into the budding vesicles, before deubiquitinating the cargos and facilitating vesicle scission from the limiting membrane of the compartment (Teis *et al*., 2008). In secondary cells, a previous report has shown that knockdown of ESCRT-0 component *Hrs*, the ESCRT-I member *TSG101*, and the accessory protein *ALiX* (*Bro1*) affect the secretion of CD63-GFP-positive into the accessory gland lumen, providing evidence that they are linked to exosome biogenesis in *Drosophila*, too (Corrigan *et al*., 2014). Given these important roles as regulators of ILV formation in mammalian cells, and modulators of extracellular vesicle secretion in secondary cells, it was key to determine where the ESCRT complexes localised to in secondary cells.

The localisation of *Drosophila* ESCRT components was first studied in secondary cells by overexpressing a GFP-tagged fusion protein of the ESCRT-III subunit *shrb* (*shrub*, also known as *Vps32, Snf7 and Chmp4a-c*; Sweeney *et al*., 2006). *shrb* is a major constituent of the ESCRT-III complex, forming long filaments that wrap around the necks of budding ILVs, promoting their scission into the lumen of the compartment (Johnson *et al*., 2016; Wollert *et al*., 2009; Babst *et al*., 2002). It is the only ESCRT-III component absolutely required for membrane severing in yeast (Hurley & Hanson, 2010); however, it has not been previously been studied in the context of ILV formation in intracellular compartments using *Drosophila*. The *shrb-GFP* construct utilised here consisted of the full-length *shrb* gene fused to eGFP, and expressed under UAS control (Lone *et al*., 2010).

Due to the severe phenotypes caused by long-term overexpression of *shrb-GFP* (data not shown), its localisation was only studied following a transient pulse of expression. In these secondary cells, Shrb-GFP localised as puncta in subdomains on the surface of both large acidic and non-acidic compartments, supporting a model in which this scission-promoting ESCRT-III component may help to generate ILVs at specific loci within both types of compartment (Figure 4.15A-C). Shrb-GFP was absent from the apical plasma membrane, suggesting that it plays specific roles at the surfaces of subcellular compartments, and does not contribute to ectosome formation (data not shown). It was also localised non-specifically within the nuclei of the secondary cells, similar to previous localisation studies of the yeast homologue of shrb, Snf7 and two of the human homologues of shrb, CHMP4A and CHMP4B (Webster *et al*., 2014; Lee *et al*., 2011).

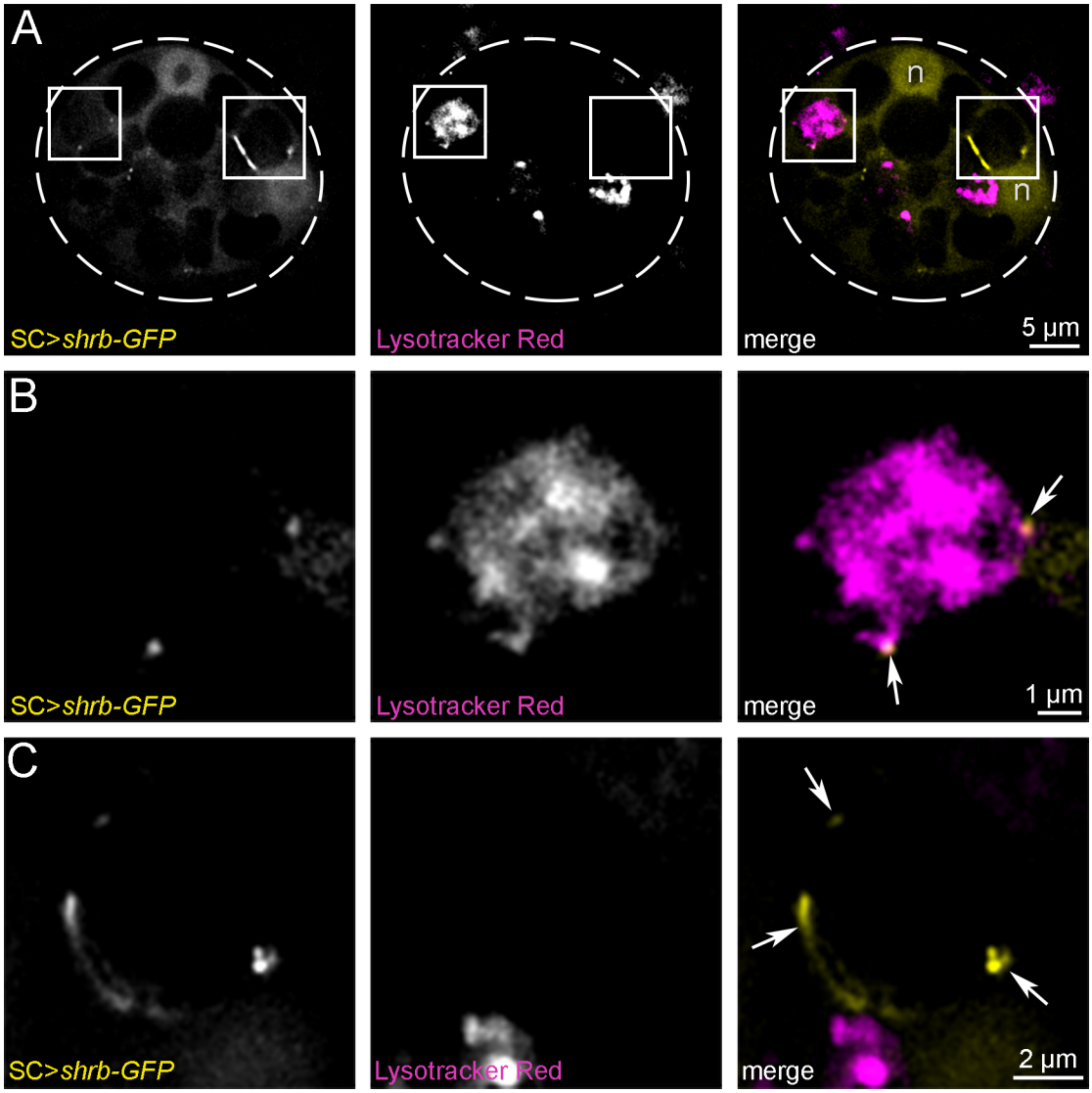


Figure 4.15 shrb-GFP accumulates on the surface of large non-acidic and acidic compartments in secondary cells

These panels show wide-field fluorescence images of secondary cells from 6-day-old virgin transgenic males selectively overexpressing Shrb-GFP. The flies were incubated at 17°C for 6 days since eclosion, before Shrb-GFP expression was induced with a 4 h pulse at 28.5°C, using the GAL4-GAL80^{ts}-UAS system. Their accessory glands were stained with Lysotracker Red (magenta). Approximate cell outlines are shown using a dashed line.
(A) Shrb-GFP (yellow) localises in a punctate manner on the surface of large intracellular compartments, and also accumulates in the two nuclei (n). Boxes highlight specific regions enlarged in (B) and (C).
(B) Large acidic compartments carry punctate regions of Shrb-GFP localisation on their surface (arrows).
(C) Shrb-GFP also localises on the surface of the large non-acidic compartments in a punctate manner (arrow).

The genotype of these males consisted of a combination between *tub-GAL80^{ts}; dsx-GAL4* and *UAS-shrb-GFP.*

The localisation of an overexpressed GFP-tagged form of the ESCRT-0 component *Hrs* (Lloyd *et al*., 2002) was also studied. *Hrs* is one of the two members of the ESCRT-0 complex. It functions to target the complex to endosomal membranes through binding of the endosomal lipid PI3P (Raiborg *et al*., 2001). Together with Stam, the other ESCRT-0 component, it binds clathrin and ubiquitinated cargos, concentrating ESCRT-0 in microdomains on the endosome surface, thereby facilitating cargo sorting. Finally, it recruits the ESCRT-I complex and thus triggers subsequent ILV formation steps at the appropriate subcellular locations (Christ *et al*., 2017). The *GFP-Hrs* transgene used in this study encoded a protein that consisted of eGFP linked to the N-terminus of full length *Drosophila* Hrs (developed in collaboration with S-J. Fan; see Methods), in a design similar to that used in transfected HeLa cells (Urbé *et al*., 2003).

When overexpressed in secondary cells, *GFP-Hrs* localised onto the limiting membranes of numerous large subcellular compartments (Figure 4.16A), and was enriched on several small non-acidic vesicles in close proximity to the larger compartments, possibly on early endosomes, as has been previously reported in HeLa cells (Figure 4.16E-E'; Bache *et al*., 2003). Similar to *shrb-GFP*, it was found in a punctate organisation on the surface of both large acidic and non-acidic compartments (Figure 4.16B-C). Interestingly, it was particularly enriched on acidic compartments that exhibited acidic microdomains only near their periphery, suggesting that it played a key role in these putative maturing late endosomes or lysosomes (Figure 14.6B). It was also occasionally observed as intraluminal puncta inside both acidic and non-

acidic compartments, suggesting that it may be packaged into a subset of ILVs within the compartments (Figure 4.16D).

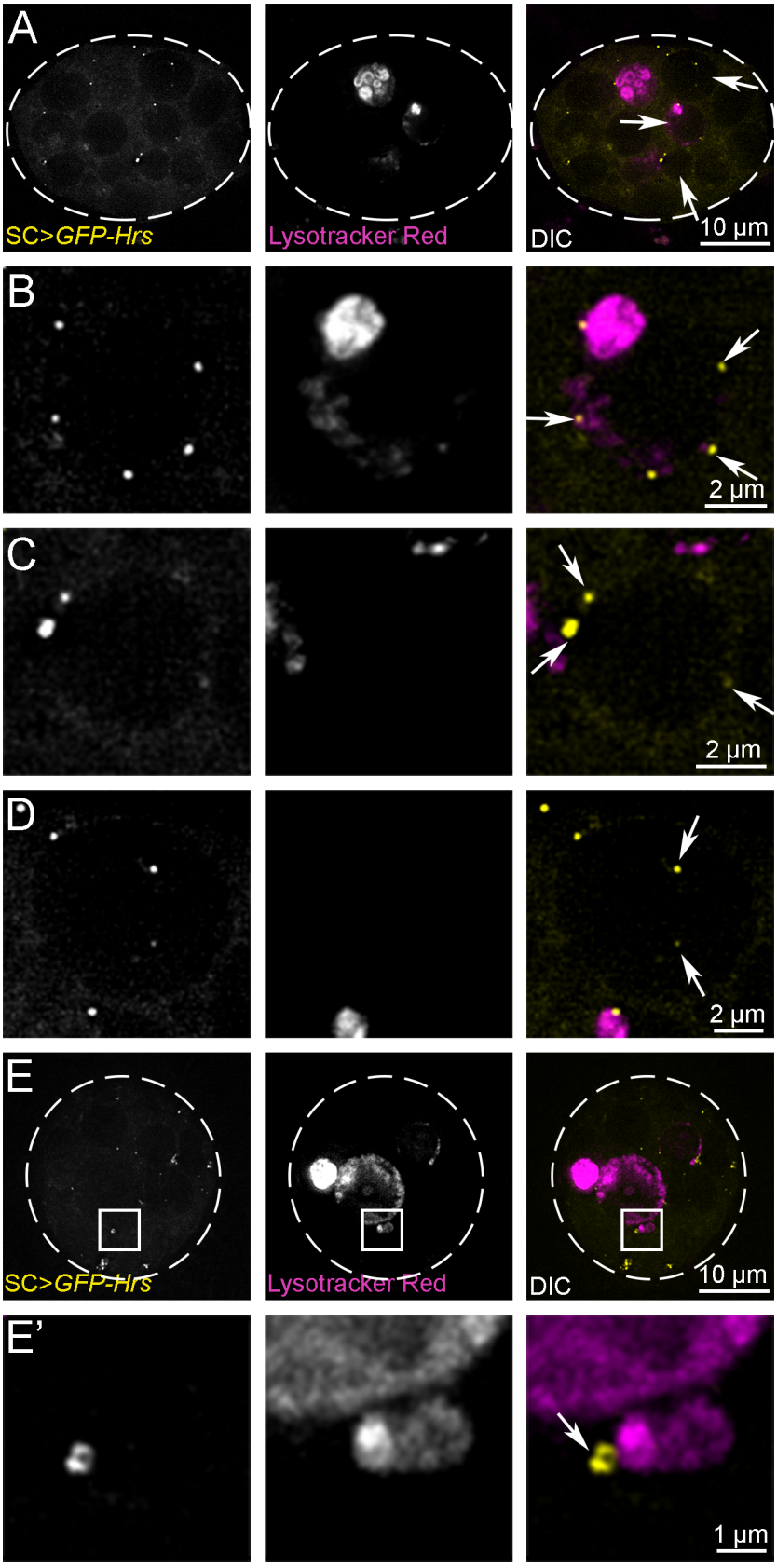

A
SC>GFP-Hrs
Lysotracker Red
DIC
10 µm
B
2 µm
C
2 µm
D
2 µm
E
SC>GFP-Hrs
Lysotracker Red
DIC
10 µm
E'
1 µm

Figure 4.16 GFP-Hrs localises on the surface of large intracellular compartments and other smaller vesicles in secondary cells

These panels display wide-field fluorescence images of living secondary cells from 6-day-old virgin transgenic males selectively overexpressing GFP-Hrs. The flies were incubated at 28.5°C since eclosion to induce GFP-Hrs expression using the GAL4-GAL80^{ts}-UAS system. Their accessory glands were stained with Lysotracker Red (magenta). Approximate cell outlines are shown using a dashed line.
(A) Overexpressed GFP-Hrs (yellow) in secondary cells localises in a punctate manner to the surfaces of both acidic and non-acidic subcellular compartments. Arrows highlight compartments enlarged in (B-D).
(B) GFP-Hrs puncta (arrows) localise on the surface of the large acidic compartment, several of which are in close association with acidic (magenta) microdomains on the interior of the compartment.
(C) The large non-acidic compartments, similarly, carry punctate GFP-Hrs-rich domains on their surface (arrows).
(D) GFP-Hrs is incorporated into some intraluminal puncta within non-acidic compartments (arrows).
(E-E') Small non-acidic vesicles in secondary cells are enriched in GFP-Hrs. The box region in (E) highlights enlarged area in (E'). Arrow highlights the small GFP-Hrs-labelled vesicle, in close proximity to an acidic compartment.

The genotype of these males consisted of a combination between *tub-GAL80^{ts}; dsx-GAL4* and *UAS-GFP-Hrs*.

To confirm that the subdomains of Hrs-GFP localisation were within the limiting membrane of Rab11-marked compartments, and not just on small closely associating vesicles, I analysed cells expressing GFP-Hrs and CD63-mCherry overexpressing cells (Figure 4.17A-A'). This demonstrated the close association of GFP-Hrs with the ILVs in the non-acidic compartments, as some of the GFP-Hrs enriched subdomains were adjacent to numerous ILVs, marked by CD63-mCherry (Figure 4.17B-B'). These data correlated well with similar observations of ESCRT localisation, which described them at the necks of budding ILVs within giant unilamellar vesicles, in a reconstituted *in vitro* system *(*Wollert *et al*., 2009*)*. However, to my knowledge this is the first time that an ESCRT has been observed in this location within a living cell, and *in vivo*.

GFP-Hrs was also localised to some small vesicles in the cytosol that lacked CD63-mCherry (Figure 4.17A', B'), many of which were non-acidic and are likely early endosomes (Riedel *et al.,* 2016). However, some of the small vesicles marked by GFP-Hrs contained acidic lumens (Figure 4.17C-C'), and may correspond to the small multivesicular bodies observed during electron microscopic analyses of these cells (Section 3.2.1.3). Co-localisation studies using Rab39 (Section 3.2.2.7) will be required to confirm this finding, which may indicate the presence of small late endosomal multivesicular bodies in these cells that are involved in secretion. Although primarily localised on subcellular compartments, GFP-Hrs was also observed at low levels on the plasma membrane, unlike Shrb-GFP (data not shown). It may be present in small clathrin-coated pits, as has been observed in other cells (Mayers *et al*., 2013).

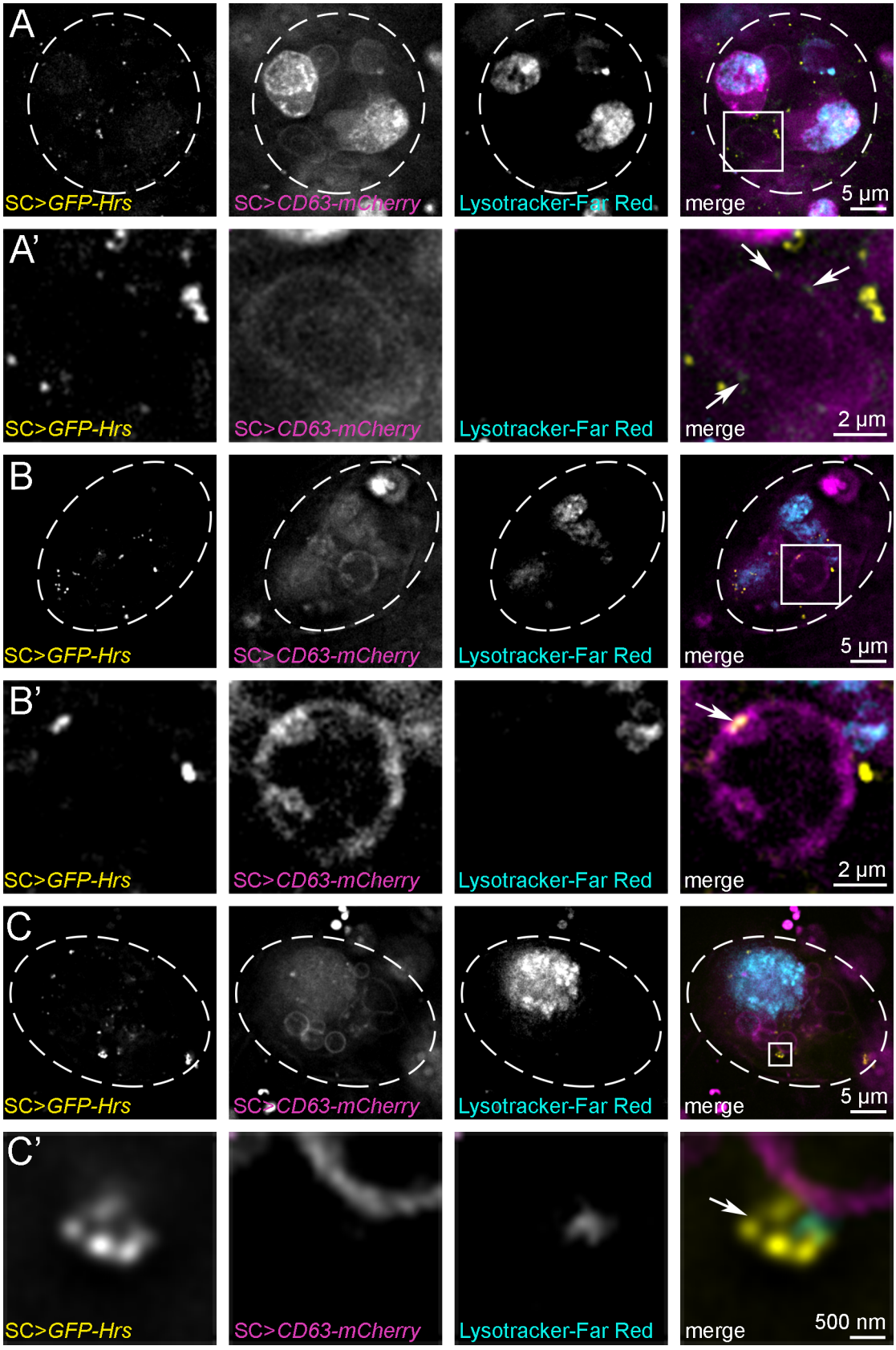

A
SC>GFP-Hrs
SC>CD63-mCherry
Lysotracker-Far Red
merge
5 µm
A'
SC>GFP-Hrs
SC>CD63-mCherry
Lysotracker-Far Red
merge
2 µm
B
SC>GFP-Hrs
SC>CD63-mCherry
Lysotracker-Far Red
merge
5 µm
B'
SC>GFP-Hrs
SC>CD63-mCherry
Lysotracker-Far Red
merge
2 µm
C
SC>GFP-Hrs
SC>CD63-mCherry
Lysotracker-Far Red
merge
5 µm
C'
SC>GFP-Hrs
SC>CD63-mCherry
Lysotracker-Far Red
merge
500 nm

Figure 4.17 GFP-Hrs co-localises with CD63-mCherry on the surface of non-acidic compartments and also marks smaller intracellular compartments

These panels display wide-field fluorescence images of living secondary cells from 6-day-old virgin transgenic males selectively overexpressing GFP-Hrs in combination with CD63-mCherry. The flies were incubated at 28.5°C following eclosion to induce transgene expression using the GAL4-GAL80^{ts}-UAS system. Their accessory glands were stained with Lysotracker Far Red (cyan). Approximate cell outlines are shown using a dashed line.
(A-A') GFP-Hrs (yellow) puncta colocalise with CD63-mCherry (magenta) on the surface of non-acidic compartments. Box in (A) highlights the region enlarged in (A'). Arrows mark the small punctate domains of Hrs localisation.
(B-B') GFP-Hrs localises at high levels in subdomains of the non-acidic compartment's limiting membrane, some of which are in close association with numerous CD63-mCherry-labelled ILVs (arrow). The box in (B) highlights the region enlarged in (B').
(C-C') Some small acidic vesicles are labelled with high levels of GFP-Hrs (arrow). Box in (C) highlights the enlarged region in (C').

The specific genotype of these flies is: *spi-GAL4, tubGAL80^{ts}; UAS-CD63-mCherry* in combination with *UAS-GFP-Hrs.*

Taken together, these data suggest that as previously reported in other cell types, the ESCRT complexes localise on endosomal compartments, such as early endosomes and late endosomal or lysosomal compartments in secondary cells. However, they also localise to the surface of other subcellular compartments, including Rab11-positive secretory compartments, where they may function in forming ILVs.

4.2.2.2 Exosome biogenesis in Rab11-positive compartments is ESCRT-dependent

The small size of endosomal and other subcellular compartments in many cell types has meant that previous studies of ESCRT function in ILV formation relied on electron microscopic analysis to compare mutant and control samples (Bache *et al*., 2003). However, this technique requires careful specimen preparation for reliable results, and quantification is challenging. The large size of secondary cell subcellular compartments, and relative ease of genetic knockdowns, provides a powerful new model for studying ESCRT functions during ILV biogenesis using fluorescence microscopy of living tissue.

By overexpressing the human exosome cargo *CD63-GFP* specifically in secondary cells that also expressed RNAi constructs targeting ESCRT components, I was able to determine whether they played essential roles inside non-acidic Rab11-marked compartments in forming ILVs. I screened a number of RNAi's directed against *ESCRT* components, including both members of the ESCRT-0 complex *Hrs* and *Stam*, the ESCRT-I subunits *Tsg101* and *Vps28*, the ESCRT-II members *Vps25* and *Vps36*, the ESCRT-III

components *shrb* and *Vps20*. In addition, I tested the accessory protein *ALIX*, and the regulatory ATPase, *Vps4*.

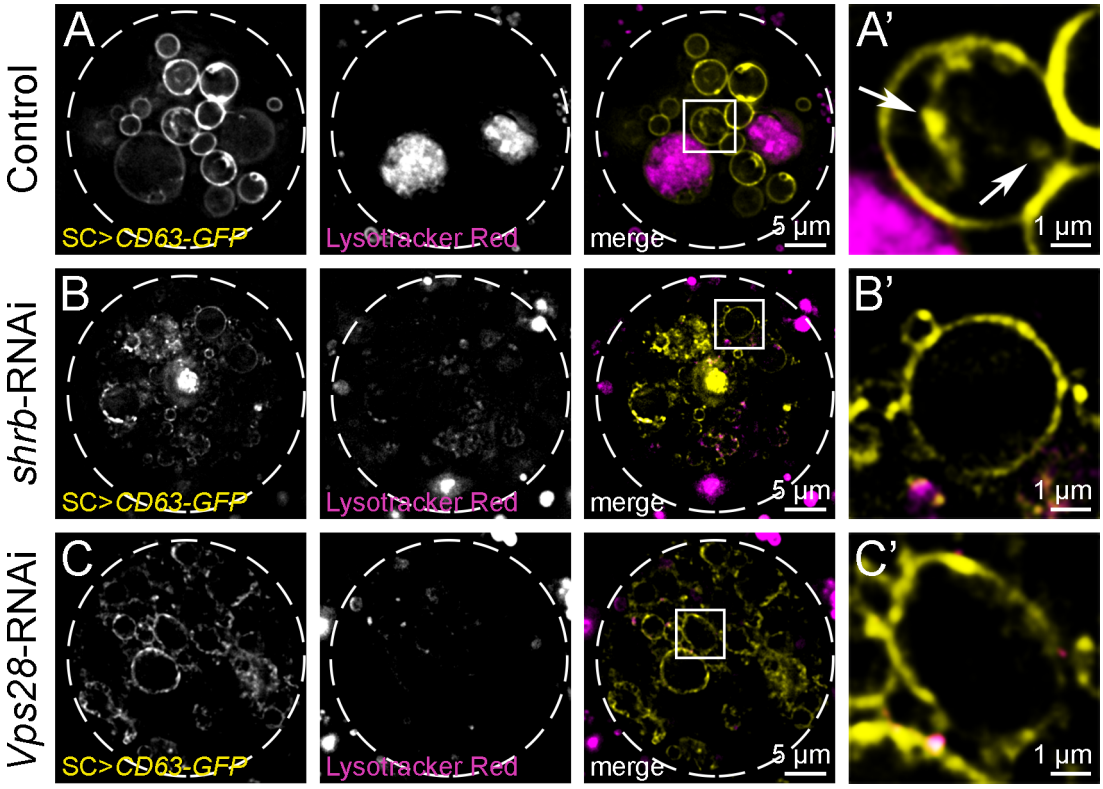
The most severe phenotypes were observed with knockdowns of the ESCRT-III gene *shrb* (Sweeney *et al*., 2006) and the ESCRT-I component *Vps28* (Sevrioukov *et al*., 2005). The large ESCRT-I complex binds ubiquitinated cargos, and is thought to play some roles in deforming the membrane into buds (Christ *et al*., 2017; Wollert & Hurley, 2010). Vps28 directly binds to Vps36 to recruit the ESCRT-II complex (Henne *et al*., 2011). The ESCRT-III complex is required for membrane scission, and *shrb* plays a central role in this process by forming filaments around the vesicle neck.

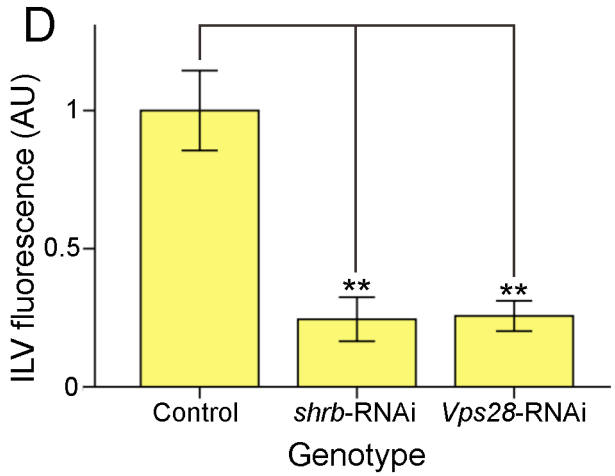
RNAi's targeted against both of these genes showed strong effects on the average intraluminal fluorescence (a proxy for ILVs), marked by CD63-GFP, inside the large non-acidic compartments in each secondary (Figure 4.18A-D). However, the compartments displayed enhanced fluorescence in subdomains at their limiting membranes, suggesting that cargos may still be clustered there, but cannot subsequently be loaded into ILVs.

I also utilised an established method in the lab to quantify the number of secreted CD63-GFP-labelled puncta in the accessory gland lumen (Corrigan et al., 2014; Redhai *et al*., 2016). Both *Vps28* and *shrb* knockdown strongly inhibited the secretion of CD63-GFP-positive puncta into the lumen (Figure 4.18E). The level of inhibition correlated well with the reduction in CD63-GFP-labelled intraluminal puncta fluorescence within the secretory Rab11-positive compartments (Figure 4.18D).

These data strongly implicate that CD63-positive ILVs within Rab11-positive compartments are generated using ESCRT-dependent mechanisms, and

indicate that vesicles within these compartments represent a novel exosome subtype.


Control
shrb-RNAi
Vps28-RNAi
A
A'
B
B'
C
C'
SC>CD63-GFP
Lysotracker Red
merge
5 µm
1 µm


D
ILV fluorescence (AU)
1
0.5
0
**
**
Control
shrb-RNAi
Vps28-RNAi
Genotype

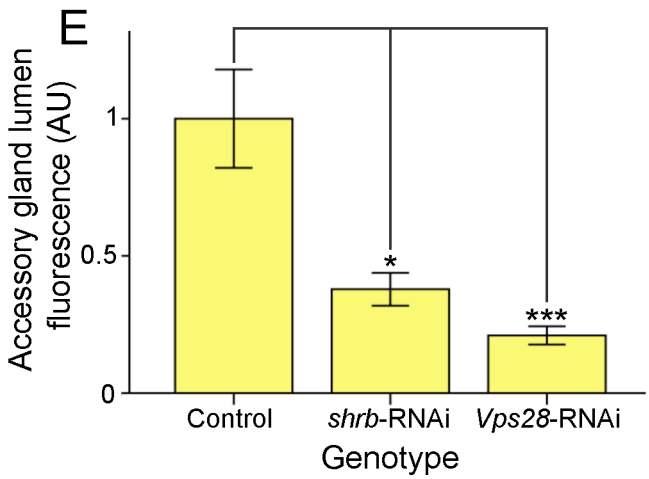

E
Accessory gland lumen fluorescence (AU)
1
0.5
0
*
***
Control
shrb-RNAi
Vps28-RNAi
Genotype

Figure 4.18 ESCRTs regulate exosome biogenesis from non-acidic Rab11 compartments

These panels display wide-field fluorescence images of secondary cells from 6-day-old virgin transgenic males selectively overexpressing CD63-GFP (yellow) in combination with different RNAi constructs targeting *shrb* and *Vps28*. The flies were incubated at 28.5°C following eclosion to induce CD63-GFP and RNAi expression using the GAL4-GAL80^{ts}-UAS system. All accessory glands were stained with Lysotracker Red (magenta). Representative secondary cell phenotypes are presented. Approximate secondary cell outlines are marked with a dashed line.
(A) Control secondary cell with no RNAi expressed. Arrows mark the CD63-GFP-positive ILV membranes within non-acidic compartments (A')
(B) In secondary cells also expressing an RNAi against ESCRT-III component shrb, ILVs are reduced (B').
(C) When *Vps28* is targeted by RNAi, ILV formation is reduced (C').
(D) Bar chart of mean fluorescence intensity inside the ten largest non-acidic secondary cell compartments (n=3 accessory glands, with 3 cells sampled per gland, for controls as well as *shrb and vps28* knockdown cells).
(E) Bar chart of the CD63-GFP fluorescent puncta density in the accessory gland lumen of controls vs the ESCRT knockdowns (n=10 accessory glands, with 3 areas sampled per gland).

The particular genotypes of these cells are combinations of *UAS-CD63-GFP, tub-GAL80ts; dsx-GAL4* with either *UAS-shrb*-RNAi (VDRC 106823) or *UAS-Vps28*-RNAi (VDRC 31894), or no other construct (as a control). Statistical tests are performed as described in Section 2.23. *P≤0.05; **P≤0.01; ***P≤0.001.

Careful quantification of the different subcellular compartments in these transgenic cells showed that although the numbers of large non-acidic compartments were reduced after *shrb* knockdown, they were unaffected by *Vps28* knockdown, suggesting a specific role for ESCRTs in ILV formation in these compartments (Figure 4.19A). I also found that the non-acidic compartments in cells that express *shrb*-RNAi remain Rab11-positive (Figure 4.19B-C'), despite being often smaller in size. Unfortunately, using the same approach for *Vps28*-RNAi with a *spi*-GAL4 driver, the driver was insufficiently strong to induce the 'reduced ILV' phenotype; so I could not confirm that the defective compartments previously observed using a *dsx*-GAL4 driver were Rab11-positive (data not shown).

For both *shrb* and *Vps28* knockdowns, the acidic compartments of secondary cells were also affected, becoming smaller and more numerous following knockdown of either *ESCRT* (Figure 4.19D-E). These effects on the large acidic compartments were expected, partly given the localisation of ESCRT molecules to their membranes, and also because of the known roles the ESCRTs in lysosome biogenesis in other cell types (Hurley *et al*., 2015; Bryant & Stevens, 1998).

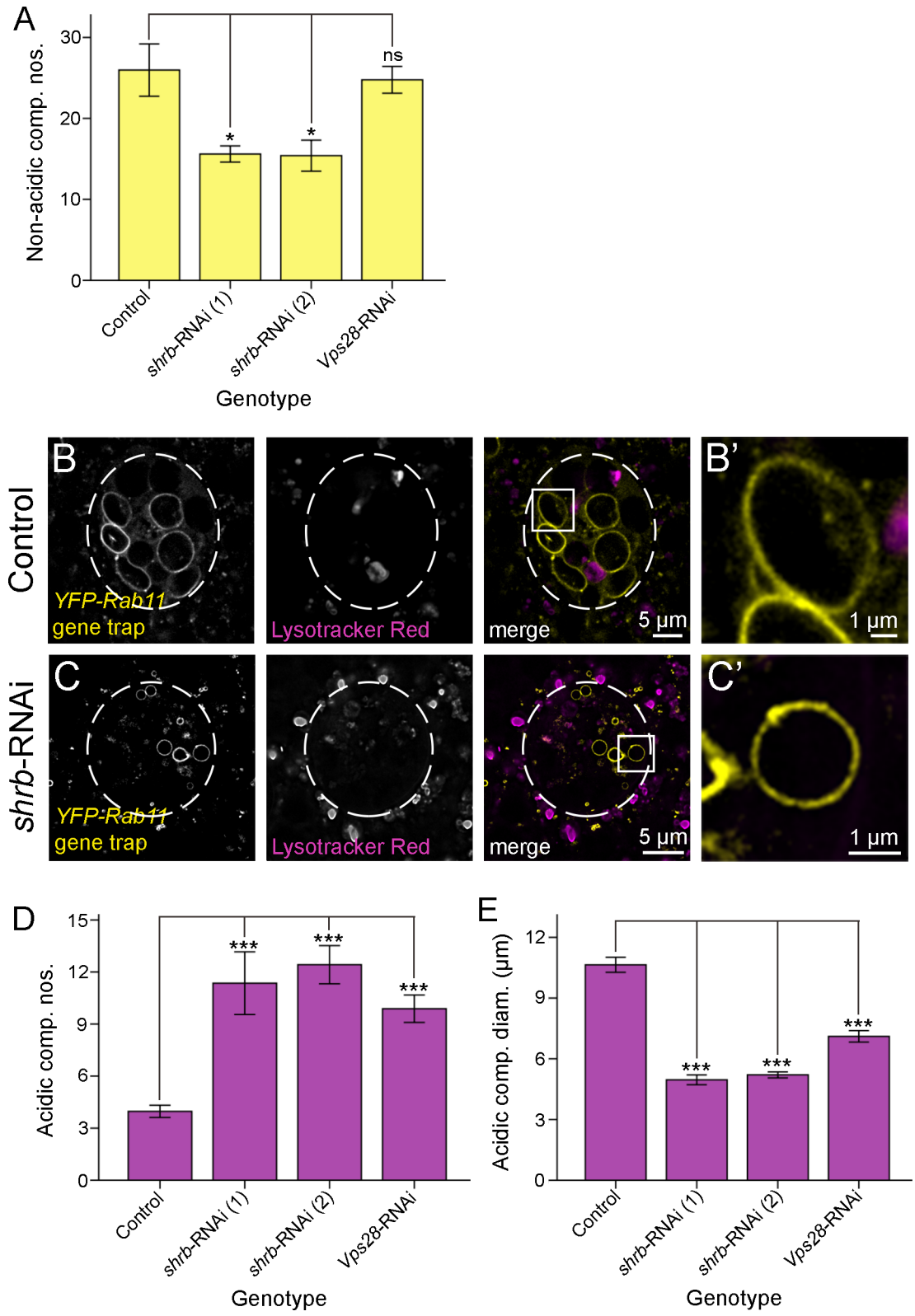

A
Non-acidic comp. nos.
30
20
10
0
*
*
ns
Control
shrb-RNAi (1)
shrb-RNAi (2)
Vps28-RNAi
Genotype
Control
B
YFP-Rab11
gene trap
Lysotracker Red
merge
5 µm
B'
1 µm
shrb-RNAi
C
YFP-Rab11
gene trap
Lysotracker Red
merge
5 µm
C'
1 µm
D
Acidic comp. nos.
15
12
9
6
3
0
***
***
***
Control
shrb-RNAi (1)
shrb-RNAi (2)
Vps28-RNAi
Genotype
E
Acidic comp. diam. (µm)
12
9
6
3
0
***
***
***
Control
shrb-RNAi (1)
shrb-RNAi (2)
Vps28-RNAi
Genotype

Figure 4.19 The effects of ESCRT knockdown on the large secondary cell compartments

Panels (A,C,D) consist of quantifications of the effects of RNAi constructs targeting *shrb* and *Vps28* in secondary cells overexpressing CD63-GFP. Panel (B) displays wide-field fluorescence images of a secondary cell from 6-day-old virgin transgenic males selectively expressing an RNAi construct targeting *shrb* in combination with *YFP-Rab11* gene trap. All flies were incubated for 6 days at 28.5°C since eclosion to induce CD63-GFP and/or RNAi expression using the GAL4-GAL80^{ts}-UAS system. Accessory glands were stained with Lysotracker Red (magenta) to mark and measure acidic compartments. In panel (B), the approximate secondary cell outline is marked with a dashed line.
(A) Bar chart showing average number of large (> 2 μm diameter), non-acidic CD63-GFP-positive compartments in CD63-GFP-expressing secondary cells also expressing RNAis targeting *shrb* or *Vps28*, or no construct (as a control). Two independent *shrb* knockdowns reduced the number of these types of compartment.
(B-C) Numerous non-acidic YFP-Rab11 (yellow) marked compartments are formed in control secondary cells or when *shrb* is silenced using RNAi.
(D) Bar chart showing average number of large (> 2 μm diameter), acidic compartments in these genetic backgrounds. All RNAi's targeting ESCRT components increased the numbers of acidic compartments.
(E) Bar chart showing average size of largest acidic compartment in these genetic backgrounds. ESCRT-knockdowns reduced the size of large acidic compartments.

The genotypes of the flies used in panels (A,C,D) are combinations of *UAS-CD63-GFP, tub-GAL80ts; dsx-GAL4* with either *UAS-shrb*-RNAi [VDRC 106823 = RNAi (1); HMS01767 = RNAi (2)] or *UAS-Vps28*-RNAi (VDRC 31894), or no other construct (as a control). The flies used in panel (B) are a combination of *spi-GAL4, tubGAL80^{ts}; YFP^{Myc}-Rab11* with *UAS-shrb*-RNAi (VDRC 106823) or no other construct (as a control). Statistical tests are performed as described in Section 2.23 (n=10 glands, with 3 cells analysed per gland). *P≤0.05; **P≤0.01; ***P≤0.001; ns = not significant.

4.2.3 Mechanisms of cargo selection for incorporation into ILVs within Rab11-positive compartments

Many of the fluorescent fusion proteins expressed in secondary cells that marked the limiting membranes of the large non-acidic compartments, were loaded onto their intraluminal puncta, likely within vesicles. This raised the question whether their loading was due to cargo-specific targeting, or whether the mechanism of loading in these compartments was non-specific, and in some overexpression cases, possibly due to the super-physiological levels of protein.

One important example that demonstrated that high levels of overexpressed protein did not necessarily load onto these intraluminal puncta was a myristoylated RFP (*myr-mRFP*) transgene. The construct comprised monomeric RFP with a myristoylation signal consisting of the first 90 amino acids of Src64B (Medina *et al*., 2008). When overexpressed specifically in secondary cells, myr-mRFP localised to the limiting membrane, but not the ILVs, of non-acidic Rab11-positive compartments (Figure 4.20A-A'). It was also found at high levels within the acidic compartments.

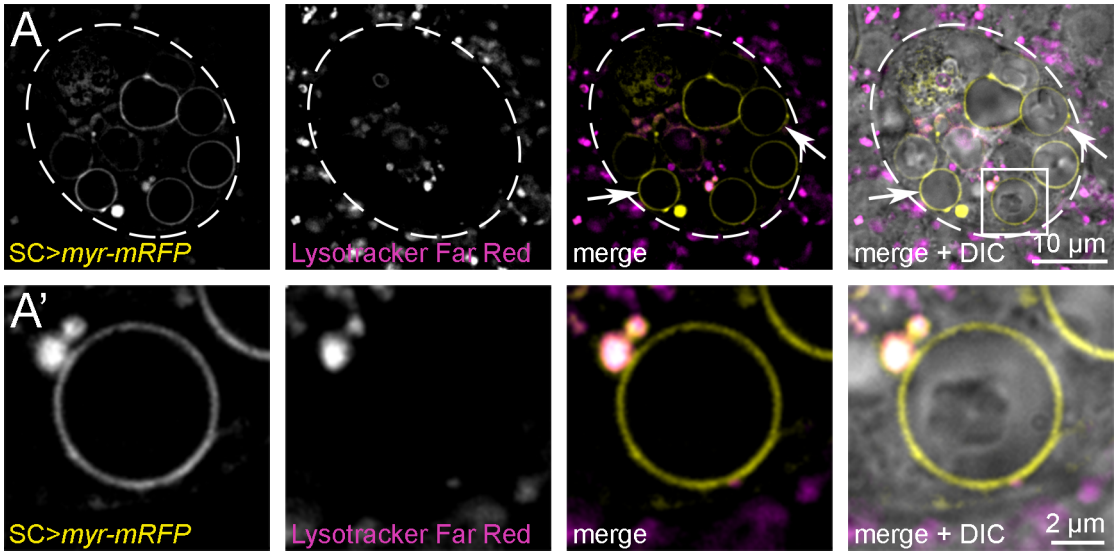


Figure 4.20 myr-mRFP localises to the surface, but not the intraluminal puncta inside non-acidic compartments

These panels show wide-field fluorescent and DIC images of secondary cells from 6-day-old virgin transgenic males selectively overexpressing a myristoylated form of RFP (myr-mRFP). The flies were incubated at 28.5°C following eclosion to induce myr-mRFP expression using the GAL4-GAL80^{ts}-UAS system. Their accessory glands were stained with Lysotracker Far Red (magenta). Approximate cell outlines are shown using a dashed line.
(A) myr-mRFP localises to the surface of numerous large non-acidic compartments in secondary cells (arrows). Box highlights the particular region enlarged in (A')
(A') Magnified view of a large non-acidic dense-core granule compartment shows that myr-mRFP does not mark ILVs.

The flies used here are a combination of *tub-GAL80ts; dsx-GAL4* with *UAS-myr-mRFP*.

A further set of experiments suggested that interaction of membrane-associated proteins with clathrin could regulate their incorporation into ILVs in non-acidic Rab11-positive compartments. This observation was made when two different GFP-tagged forms of the human transferrin receptor (hTFR) were overexpressed in secondary cells. The first construct was the full-length transferrin receptor fused to GFP at its C-terminus (hTFR-GFP; Henthorn *et al*., 2011). This receptor normally binds iron-associated transferrin at the cell surface, is endocytosed to allow iron uptake and then is recycled back to the plasma membrane. When overexpressed specifically in secondary cells, it localised within some of the large acidic compartments, and on the surface of several, but not all, of the large non-acidic compartments, and at the plasma membrane (Figure 4.21A-A'). However, despite localising to their limiting membranes, hTFR-GFP was not observed on intraluminal puncta within the non-acidic compartments. Importantly, this demonstrated that a GFP-tag alone was insufficient to drive cargo selection into ILVs. When a different construct consisting of a truncated form of the transferrin receptor which lacked its C-terminal clathrin-interacting region (hTFRΔC-GFP; Henthorn *et al*., 2011) was overexpressed in secondary cells, it localised at high levels on the surface and ILVs of the non-acidic compartments, but was mostly excluded from the acidic compartments and plasma membrane, in contrast to full length hTFR-GFP (Figure 4.21B-B'). These data suggest that the association of transmembrane receptors with trafficking molecules such as clathrin plays important roles regulating their incorporation into ILVs. Knockdown or overexpression experiments targeting the heavy or light chains of clathrin may provide further insight into these differences.

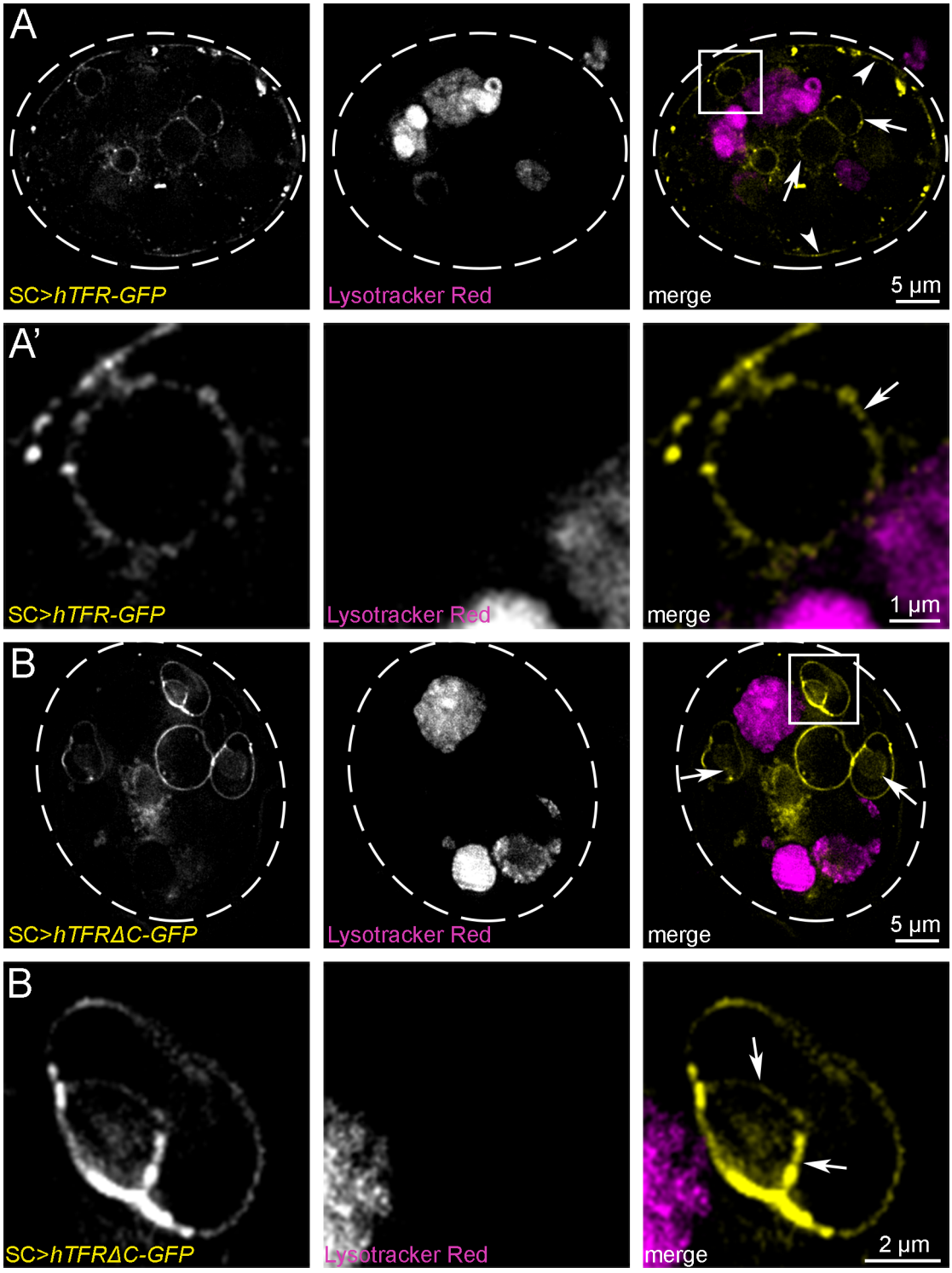

A
SC>hTFR-GFP
Lysotracker Red
merge
5 µm
A'
SC>hTFR-GFP
Lysotracker Red
merge
1 µm
B
SC>hTFRΔC-GFP
Lysotracker Red
merge
5 µm
B
SC>hTFRΔC-GFP
Lysotracker Red
merge
2 µm

Figure 4.21 Incorporation of the human Transferrin receptor into ILVs is regulated by interactions with Clathrin

These panels show wide-field fluorescence images of secondary cells from 6-day-old virgin transgenic males selectively overexpressing two different forms of the human transferrin receptor tagged with GFP. These consisted of a wild-type version (hTFR-GFP) and a mutant version, lacking its clathrin-interaction domain (hTFRΔC-GFP). The flies were incubated at 28.5°C following eclosion to induce transgene expression using the GAL4-GAL80^{ts}-UAS system. Their accessory glands were stained with Lysotracker Red (magenta). Approximate cell outlines are shown using a dashed line.
(A) Overexpressed hTFR-GFP (yellow) localises to the surface of several large non-acidic compartments (arrows), and onto the plasma membrane (arrowheads). The box highlights the region enlarged in (A').
(A') The hTFR-GFP-positive compartments lack fluorescent intraluminal puncta.
(B) hTFRΔC-GFP (yellow) localises to the surface of many large subcellular compartments and is incorporated into their intraluminal puncta (arrows). The box highlights the region enlarged in (B').
(B') Intraluminal puncta are in non-acidic compartments are clearly labelled by hTFRΔC-GFP.

The specific genotypes used here are combinations of *tub-GAL80ts; dsx-GAL4* with either *UAS-hTFR-GFP* or *UAS- hTFRΔC-GFP*.

4.2.4 Rab11-positive endosomal compartments are a novel source of exosomes in human cancer cells

4.2.4.1 Rab11a-positive endosomes contain ILVs labelled by Rab11a in human colorectal cancer cells

The novel observations in secondary cells that Rab11-positive compartments are a source of exosomes, whose formation was dependent on the ESCRT complexes, were paralleled by work done with collaborators in the Goberdhan lab, who were studying the exosome biology of human cells. They had evidence to suggest that exosome secretion from HCT116 cells may be redirected through Rab11a-positive compartments. Specifically, they found that the exosome cargos changed when the activity of mechanistic Target of Rapamycin Complex 1 (mTORC1) was decreased through the inhibition of the mTORC1 regulator, Proton-Assisted Amino Acid Transporter-4 (PAT4), or when extracellular glutamine was reduced (Perera *et al*., in preparation). When HCT116 cells were depleted of glutamine, their extracellular vesicles carried a variety of different exosome cargos to those secreted under normal conditions. For example, they packaged less CD63, but carried more Rab11a and Caveolin-1, a molecule that did not traffic to late endosomes and lysosomes, but was partly trafficked to Rab11a-positive compartments, as indicated by confocal analysis. These switched exosomes also enacted different functions; they promoted growth of other HCT116 cells, and supported stable capillary formation when applied to human umbilical vein endothelial cells (HUVECs).

S-J. Fan, who had undertaken a considerable proportion of this work in the Goberdhan lab, wanted to further investigate whether human Rab11a-positive

compartments might form ILVs marked by this specific Rab and Cav-1. We set out to test this using modifications of the super-resolution microscopy approaches I had established using secondary cells. If Rab11-positive compartments were the source of exosomes, this might help to explain the phenomenon of exosome switching discovered by the Goberdhan group. Dr Fan immunostained HCT116 cells and we examined these cells using super-resolution 3D-SIM. A GFP-Rab11a fusion protein was used to localise Rab11a at super-resolution, as the available antibodies to native Rab11a were not sensitive enough for the technique. Transfected HCT116 cells overexpressing *GFP-Rab11a* showed that the fusion protein localised on the limiting membranes of small clusters of compartments, some of which contained internal GFP-Rab11a puncta (Figure 4.22A-C). The other exosome cargo that was highly secreted in mTORC1-depleted conditions, Caveolin-1, was found in a more widely distributed punctate pattern around the cell, potentially including caveolae at the plasma membrane. However, some Cav-1 co-localised on parts of the limiting membrane of GFP-Rab11a compartments, and on intraluminal puncta (Figure 4.22C). Thus the Rab11a-positive exosomes produced by HCT116 cells under glutamine depletion are likely to be formed in Rab11a-positive compartments, just as secreted YFP-Rab11-marked extracellular puncta are produced in Rab11-positive compartments in secondary cells.

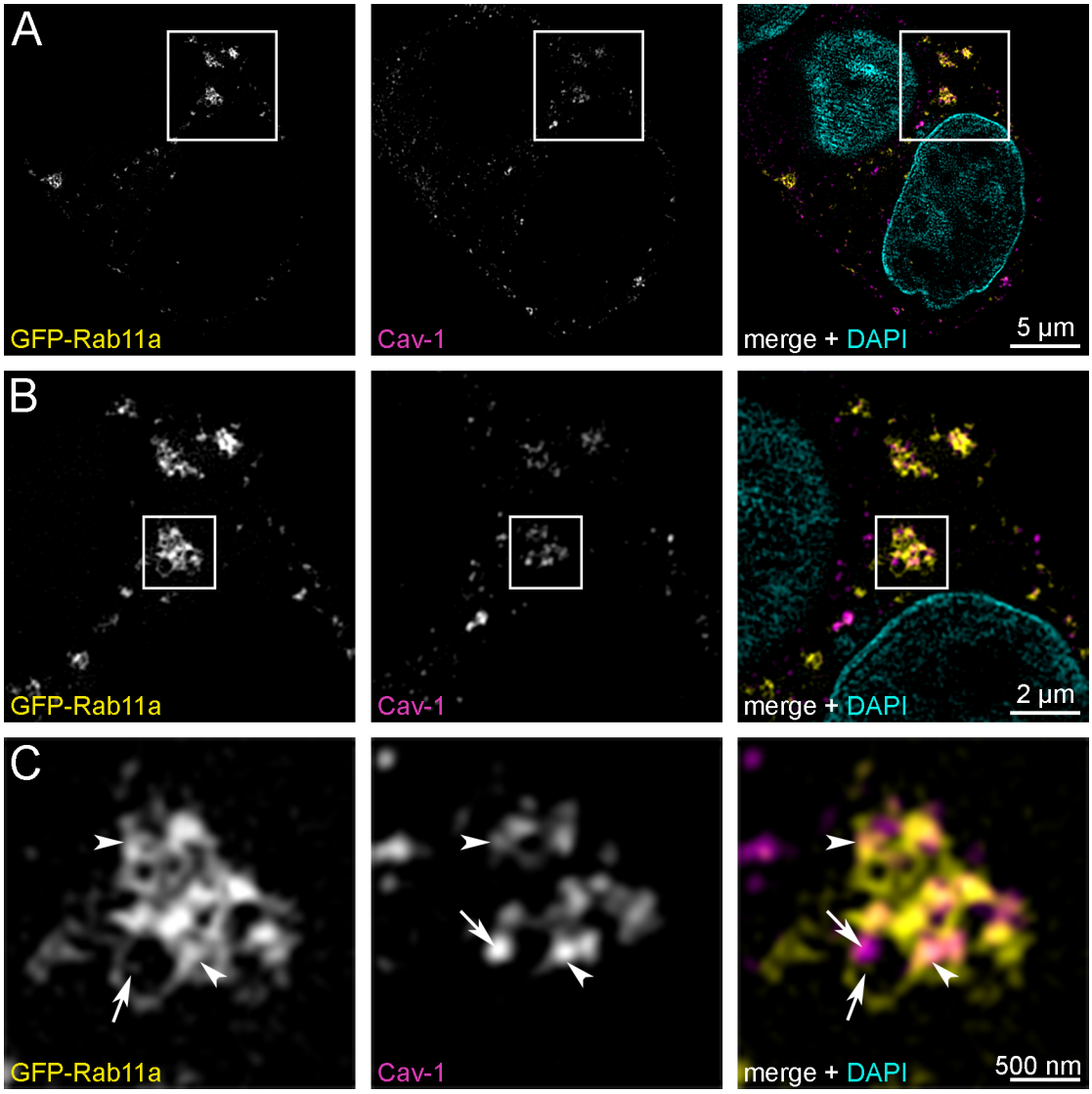


Figure 4.22 Rab11a-positive endosomes contain ILVs labelled by Rab11a and Caveolin-1 in HCT116 colorectal cancer cells

These panels display super-resolution 3D-SIM microscopy images of HCT-116 colorectal cancer cells, prepared in collaboration with S-J Fan. The HCT116 cells overexpress a *GFP-Rab11a* (yellow) construct and are immunostained with anti-Cav-1 (magenta) antibody and stained with DAPI (cyan) to mark nuclei.
(A-C) GFP-Rab11a-positive compartments often cluster together. Cav-1 shows more dispersed staining throughout the HCT116 cell, including putative caveolae at the plasma membrane. Box in (A) highlights several GFP-Rab11a-positive clusters that are enlarged in (B), one of which is further enlarged in (C). Both GFP-Rab11a and Cav-1 are observed as puncta within GFP-Rab11a-marked compartments (arrows, C), and colocalise on the limiting membrane (arrowheads, C).

4.2.4.2 Endosomal compartments in human cancer cells can produce ILVs carrying different Rab GTPases

To further confirm that human endosomal compartments could generate ILVs carrying Rab GTPases, HCT116 cells were transfected with a construct that encoded a constitutively active form of early endosomal Rab5 (*GFP-Rab5CA*), which inhibits the maturation of recycling and late endosomes, and drives the formation of large immature endosomes. Working collaboratively with S-J. Fan, immunostaining showed that Rab11a and Rab7 localised to subdomains on the limiting membranes of these GFP-Rab5CA-positive compartments, and were also trafficked into distinct intraluminal puncta (Figure 4.23A-A').

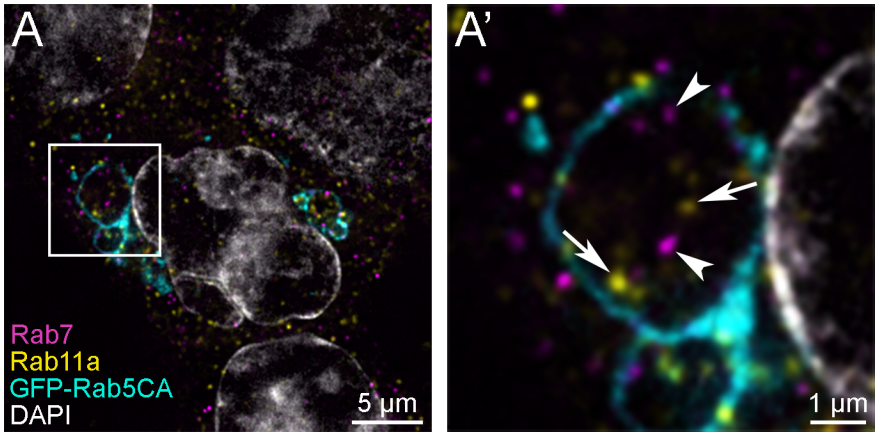


Figure 4.23 Enlarged endosomal compartments in HCT116 cells contain distinct populations of intraluminal vesicles labelled with Rab11 and Rab7

These panels display wide-field fluorescence images of HCT-116 colorectal cancer cells, prepared in collaboration with S-J Fan. The HCT116 cells overexpress a *GFP-Rab5CA* (cyan) construct and are immunostained with both anti-Rab11 (yellow) anti-Rab7 (magenta) antibody and stained with DAPI (white) to mark nuclei.
(A) Several enlarged endosomal compartments are formed in HCT116 cells overexpressing GFP-Rab5CA, which also display punctate staining with both Rab11 and Rab7. A box highlights a region that contains some of the enlarged endosomes, and is enlarged in (A').
(A') Rab11 (arrows) and Rab7 (arrowheads) localise on distinct pools of intraluminal vesicles within the GFP-Rab5CA compartments. Both Rab7 and Rab11 also localise on subdomains of the GFP-Rab5CA compartment's limiting membrane.

These data showed that like *Drosophila* secondary cells, in addition to late endosomal multivesicular bodies, HCT116 cells normally make Rab11a-positive multivesicular bodies, which contain Rab11a- and Caveolin-1-marked ILVs. Both Rab11a and Rab7 can be incorporated into ILVs, as was also found in secondary cells. A broad range of experiments in human cells have shown that these distinct populations of multivesicular endosomes appear to differentially secrete their ILVs as exosomes under the control of mTORC1 signalling.

4.3 Discussion

Within this chapter I have described how secondary cells generate and secrete exosomes, and how protein cargos are selectively loaded into or onto them. I have used super-resolution and time-lapse wide-field microscopy to reveal a novel source of exosomes produced by secondary cells, which derive from Rab11-positive compartments. I have determined that ESCRT components localise to these Rab11-positive compartments and are required to form ILVs within them. My work provides a new explanation for the heterogeneity observed in secreted exosomes and has shown that the Rab proteins, which are found as cargos in exosomes, can define their subcellular origin. In collaboration with the Goberdhan lab, I was able to show that Rab11 compartments are a conserved subcellular source of exosomes, as human cancer cells also produce them. The human Rab11-marked exosomes have distinct biological activities, which may mediate adaptation to metabolic stresses, such as glutamine depletion (Perera *et al*., in preparation).

4.3.1 Rab11-positive compartments contain ILVs, which can be secreted as exosomes, in both *Drosophila* and human cells

The work described in this chapter has highlighted a number of previously unrecognised processes involved in exosome biogenesis that appear to be conserved in *Drosophila* secondary cells and human cancer cell lines. I have shown that secondary cells secrete exosomes formed as ILVs within non-acidic Rab11-positive compartments, while their large late endosomal compartments probably do not secrete many exosomes, as had previously been assumed (Corrigan *et al*., 2014). Live cell imaging showed that the

contents of Rab11-positive compartments are released into the accessory gland lumen as exosomes upon fusion of these compartments with the apical plasma membrane (Section 4.2.1.2). The Rab11-positive compartments appear to be a major exosome secretory pathway for secondary cells, and may specifically carry important signalling cargos, such as Btl and Bnl that function in their target cells (Section 4.2.1.5). However, it remains possible that other exosome secretion pathways exist in secondary cells, involving small multivesicular endosomes, whose size is more typical of these compartments in other cell types (~400 nm diameter), which were also observed by electron microscopy (Section 3.2.1.3). These compartments require further classification, for example with specific Rab GTPase markers, to enable their future analysis. Potential candidates are the Rab39-positive compartments characterised in Section 3.2.2.7, which could be equivalent to the small GFP-Hrs-positive acidic compartments I have identified here (Section 4.2.2.1).

My super-resolution data also highlighted one other interesting feature of vesicles in *Drosophila* Rab11-positive compartments. Most of them appear to be less than 100 nm in diameter, consistent with typical exosome size (Section 4.2.1.2). However, some are more than 300 nm in diameter, which may only be possible because of the very large size of the compartment. This is notable because the determinants for ILV size *in vivo* are unknown (Hurley & Hanson 2010) and secondary cells may provide a powerful system to genetically dissect this process.

Overall, these findings appear to differ in some ways to human HCT116 colorectal cancer cells, where late endosomal, CD63-marked compartments

likely release the majority of exosomes under normal culture conditions (Perera *et al*., in preparation; Section 4.2.4). However, upon mTORC1 inhibition, for example by glutamine starvation, a different set of exosomes was secreted, with at least some of these being released from Rab11a-marked compartments. One other major difference is that although both secondary cells and human HCT116 cells produce Rab11-positive compartments containing ILVs, these compartments only have a dense core granule in secondary cells, which is indicative of regulated secretion in this and other cell types (Section 5.1.1). Interestingly, some studies have shown that recycling endosomes, which are commonly associated with Rab11, are a common site for cell-polarised sorting from both the endocytic and secretory pathways (Ang *et al*., 2004). Rab11-positive endosomes in human cancer cells are likely to have a recycling role, but it remains unclear whether this role is in any way linked to mechanisms involved in regulated secretion.

Rab11 has been implicated in exosome secretion in several previous knockdown studies in both human cells and *Drosophila* (Corrigan *et al*., 2014; Beckett *et al*., 2013; Koles *et al*., 2012; Savina *et al*., 2002). In fact, the first example of a Rab11-labelled multivesicular endosome was reported using overexpressed Rab11-GFP constructs in human myelogenous leukaemia (K562) cells (Savina *et al*., 2005). However, previous interpretations of this result were that Rab11 facilitated the docking and fusion of a classical multivesicular endosome to the plasma membrane in a calcium-dependent manner. Our observations suggest that Rab11 can in fact mark an alternative set of secretory subcellular compartments and their ILVs. Work by a previous DPhil student in the Wilson lab, S. Redhai, showed that in secondary cells,

Rab11 is essential for the maintenance of their large non-acidic compartments (Redhai, 2016). These results do not rule out the possibility that Rab11 carries out roles related to secretion, but they suggest that it is also required to define the identity or maintain the integrity of these compartments.

One important question for the future is how relevant the findings in *Drosophila* secondary cells will be to the exosome field in general, where *in vivo* studies and visualisation of exosome biogenesis in living cells has previously been so challenging. Below I discuss three new findings from my studies, the identification of Rabs as subtype-specific exosome markers, the differential loading of cargos into exosomes on single compartments and the role of ESCRTs in formation of exosomes in Rab11-positive compartments, that all seem to be relevant to fundamental processes in human exosome biogenesis. However, some of my data also suggest that we may learn from the fly model, even when considering specific exosome cargos.

Most notably, I have demonstrated that GFP-tagged forms of both the FGF receptor Btl and one of its FGF ligands Bnl are loaded selectively on to ILVs made in Rab11-positive compartments and secreted from secondary cells. Human homologues of FGFR, which include FGFR 1, 2, 3 and 4, have all been detected inside extracellular vesicles from numerous human cell types, as have several of the human FGF homologues, including FGF 2, 16, 18 and 19 (Exocarta.org – an online exosome database that provides the exosome contents identified from multiple organisms, though it is likely that some of these studies have not confirmed an exosomal origin). When overexpressed, both the Btl-GFP and Bnl-GFP cargos seem to be loaded on a large number of vesicles in Rab11-positive compartments, suggesting that they might be co-

loaded on the same vesicles (4.2.1.5). These data raise the possibility that exosomes may affect their target cells by delivering both ligand and receptor, in effect providing all the necessary cell surface elements to trigger a response. It also could permit signalling within the ILVs or exosomes themselves, another aspect that requires further investigation.

4.3.2 Rab GTPases may be useful markers of the subcellular compartments from which exosomes originate

The Rab GTPases have been implicated in the trafficking of multivesicular endosomes to the plasma membrane (Tkach & Théry, 2016). However, here I propose that they are also packaged within ILVs of the compartments that they specifically mark. For example, Rab11/Rab11a appear to provide specific markers of exosome secretion from their respectively marked compartments in both *Drosophila* and human cells (Sections 4.2.1.3 and 4.2.4). This may help to interpret previous studies, which have observed Rab11a in exosomes isolated from numerous cell types (Exocarta.org). The late endosomal or lysosomal Rab7 is also proposed here as an exosome cargo marker, as it localised specifically to the limiting membranes of Rab7-positive compartments and their intraluminal puncta (Section 3.2.2.7). Importantly, our collaborators have now shown that Rab7 is packaged on extracellular vesicles, presumably exosomes, secreted from HCT116 cells, consistent with previous findings in other human cell types (S-J. Fan, personal communication; Exocarta.org). Together, these data suggest that the Rab GTPases may act as conserved markers of exosomes that are indicative of their compartment of origin. It therefore seems possible that other Rabs

implicated in exosome secretion, such as Rab35, may also mark extracellular vesicles from a separate type of compartment. Indeed, Rab35 has already been reported in the extracellular vesicles isolated from numerous cell types (Exocarta.org), as have many other human Rabs.

Indeed, in Chapter 3, I showed that several other Rab GTPases, which have not been associated with exosome secretion yet, are loaded into ILVs within non-acidic compartments, including Rab6, 10, 19, 21 and 30 (Section 3.2.2). It is possible that these Rabs may in some cases distinguish subtypes of vesicles in Rab11-positive compartments, since several of them are associated with these compartments, and these differences may impart even further differences to the cargos included in their ILVs. In the case of Rab6, which marks non-cored, non-acidic compartments that are not Rab11-positive, it potentially labels a novel set of vesicles that are not made in Rab11-positive compartments. Furthermore, when CFP-tagged Rab6 was combined with other YFP-tagged Rab GTPases, the two proteins often highlighted mixed populations of intraluminal puncta within the marked compartments, supporting a model in which Rabs act as markers for different vesicle subpopulations. Importantly, these compartments released their contents into the accessory gland lumen. For example both CFP-Rab6 and YFP-Rab19 were detected on extracellular puncta (data not shown). However, it remains to be seen whether this applies to the other Rabs reported here.

4.3.3 Differential loading of exosome cargos within the same subcellular compartment

Although most of this chapter has focused on the generation of exosome diversity through differences in their subcellular compartment of origin, I also observed that some of the differences might arise due to differential loading of ILVs within the same compartment (Section 4.2.3). Secondary cells co-expressing CD63-mCherry and the YFP-Rab11 gene trap revealed a mixed ILV population within non-acidic Rab11-postive compartments (Section 4.2.1.3). However, the more numerous CD63-mCherry vesicles may be explained by CD63's reported roles in the induction of ILV formation (Edgar *et al*., 2014; van Niel *et al*., 2011), which perhaps produces abnormal vesicles do not recruit YFP-Rab11. Alternatively, the weakly expressed YFP-Rab11 gene trap may not produce sufficient fluorescent Rab11 to mark all the ILVs that incorporate it,

My observations using super-resolution microscopy also showed that GFP-Rab11a-positive compartments in HCT116 cells contain a heterogeneous mixture of ILVs when co-stained with Cav-1 (Section 4.2.4). And finally, secondary cells co-expressing the CFP-Rab6 and YFP-Rab11 gene traps carry puncta inside large non-acidic compartments with single Rab or mixed identity, again suggesting multiple loading mechanisms (Section 3.2.2.4). In the future, it will be important to back up these observations using immuno-electron microscopy to localise endogenous exosome markers within the subcellular compartments of non-transgenic cells.

My findings raised queries as to the molecular mechanisms driving this exosome heterogeneity and loading of specific cargos in particular

compartments. I undertook some initial studies to further understand the mechanisms of cargo selection within Rab11-positive compartments. It seems likely that inclusion into ILVs is cargo-specific, as some molecules, such as Myr-RFP were not readily packaged into ILVs in secondary cells (Section 4.2.3). My findings with the human transferrin receptor suggest that interaction with trafficking molecules such as clathrin, may be important for the inclusion or exclusion of certain molecules into vesicles Section 4.2.3). This is an area that now requires much more detailed investigation.

4.3.4 ESCRTs regulate ILV formation in Rab11-positive compartments

The ESCRT proteins have well described roles in exosome formation (Colombo *et al*., 2014), and their knockdown is often used to provide evidence that extracellular vesicle come from an endosomal source. In the Wilson lab, previous ESCRT knockdown experiments in secondary cells showed that the ESCRT-0 component Hrs, the ESCRT-I protein TSG101, and the accessory protein ALiX all affected exosome secretion (Corrigan *et al*., 2014). However, other mechanisms of exosome formation have been reported (Trajkovic *et al*., 2008). Indeed, these knockdown experiments did not appear to remove all vesicles from large endosomal compartments, though they did have major effects on secretion of CD63-positive puncta (Corrigan et al., 2014). Because ILVs were found in both acidic Rab7-positive compartments and non-acidic Rab11-positive compartments in secondary cells, it seemed plausible that different ILV formation pathways could operate on these different compartment subtypes. Alternatively, ESCRT complexes may be responsible for the formation of all or some ILVs in both. I showed that GFP-

tagged versions of the ESCRT-III component Shrb and the ESCRT-0 subunit Hrs localised to subdomains on both compartment membranes. GFP-Hrs was also sometimes observed in the ILVs, consistent with reports that it is present in exosome preparations (Beckler *et al*., 2013).

Using knockdown approaches, I demonstrated that the ESCRT-III component *shrb*, and the ESCRT-I member *Vps28* are required for ILV formation within the non-acidic Rab11-positive compartments in secondary cells. This correlated well with previous reports in Drosophila, where *shrb* has been reported to regulate the secretion of extracellular vesicles carrying hedgehog in the wing imaginal disc (Matusek *et al*., 2014). Other electron microscopic analysis confirmed that the *shrb* mutant cells failed to generate multivesicular endosomes, consistent with the findings we observe in secondary cells (Vaccari *et al*., 2009). In this latter study, vesicles are formed around the periphery of yolk granules that assemble inside intracellular compartments, suggesting an interesting parallel in the subcellular arrangement of these structures.

In contrast to our observations using a knockdown approach to affect ESCRT-I component *Vps28*, the initial mutational study of Vps28 function reported that it did not affect multivesicular endosome formation in *Drosophila* photoreceptor cells (Sevrioukov *et al*., 2005). However, subsequent analysis of the first mutant revealed that it was only a partial loss-of function allele (Vaccari *et al*., 2009) and three novel mutants in *Vps28* all had phenotypes typical of ESCRT-I members, for example the failure of the ubiquitin-dependent protein degradation pathway, which is involved in processes such as Notch degradation. However, the report did not show the phenotype of true

null *Vps28* mutants on multivesicular endosome formation, though other members of the ESCRT-I complex, such as *TSG101* and *vps22* (also known as *Larsen*) both caused dramatic phenotypes in ILV formation.

In screening through other *ESCRT* knockdowns (data not shown), I noticed that knocking down molecules like Hrs did not completely eliminate ILV formation in the same way as *shrb* or *Vps28* knockdown. Although a simple explanation is that this knockdown was less severe, it did have a major effect on CD63-GFP secretion (Corrigan *et al*., 2014), potentially as strong as *shrb* or *Vps28* (Section 4.2.2.2). In addition, secondary cells developed an enlarged acidic compartment, consistent with findings in other cell types (Lloyd *et al*., 2002). This raises the alternative possibility that ESCRT-0 proteins may not be required for all ILV formation that involves ESCRTs, a potential interpretation of a previous report in mammalian cells involving Hrs (Edgar *et al*., 2014).

Collaborators in the Goberdhan lab have now shown that knockdown of the ESCRT-0 component *Stam* blocked secretion of Rab11-positive exosomes from human colorectal cancer HCT116 cells (Perera *et al*., in preparation). These results suggest that the highly conserved ESCRT machinery can function in vesicle formation within compartments with recycling endosome identity as well as in late endosomes. These observations suggest that the different molecules trafficked to specific subcellular compartments may be sorted into distinct ILVs by the ESCRT machinery, and these differences would then be reflected in the heterogeneity of exosome cargos. This role expands the already numerous roles for ESCRTs in the literature (Christ *et al*., 2017; Hurley *et al*., 2015).

5.0 Regulation of dense-core granule compartment biogenesis and endolysosomal maturation in secondary Cells

5.1 Introduction

This chapter investigates the biogenesis of the large intracellular compartments of secondary cells. Specifically, I have studied the formation and maturation of the non-acidic dense-core granule compartments and the acidic lysosomes, important organelles that play multiple roles in both health and disease in humans. Building on observations made in Chapter 3, the significance of the Rab GTPase association with different types of compartment is investigated here. I also describe several novel markers of dense-core granules in secondary cells, which may be used during future studies of these cells. I characterise the genetic regulation of dense-core granule biogenesis and lysosome maturation, shedding light on the specific roles of known regulators, and identifying several novel regulators of these processes.

5.1.1 Dense-core granules are characteristic of regulated secretion

Specialised secretory organelles contain dense-core granules that are composed of highly concentrated bioactive proteins and peptides. In response to a specific stimulus, often mediated by an increase in intracellular Ca^{2+} levels, the dense-core granule constituents are released by compartmental fusion to the plasma membrane. The requirement for a stimulus for dense-core granule release has led to their association with ‘regulated secretion’ (Burgess & Kelly, 1987). Dense-core granules are especially prominent in endocrine, neuroendocrine and other secretory cell types, to the extent that

they are a considered a key ‘hallmark’ for the identification of these cells (Kim *et al*., 2006). However, the roles of dense-core granule secretion extend beyond specialist secretory cell types; for example they are utilised transiently by egg and sperm cells during their maturation (Burgoyne & Morgan, 2003). Regulated secretion is well demonstrated by endocrine cells, which package hormones at high levels into dense-core granules. For example, insulin is packaged inside the dense-core granules of pancreatic β-cells, and is released upon glucose-mediated Ca^{2+} stimulation (Prentki *et al*., 1987). They can be highly abundant organelles in these cells; for example, individual β-cells have been estimated to contain between 5000-6000 dense-core granules, each with a mean diameter of ~300 nm (Fava *et al*., 2012). However, they are not all released at once: *in vitro* studies using cultured mice islets have suggested that between 1 - 5% of each β-cell’s dense-core granules are released upon Ca^{2+} stimulation (Anello *et al*., 1999; Müller *et al*., 2017). Misregulation of insulin secretion in humans has been associated with some forms of diabetes type II (Gaisano, 2017). This and multiple other roles in physiology demonstrate that regulated secretion is not only a fundamental aspect of cell biology, but has important implications in human health and disease.

5.1.2 The biology of dense-core granule compartments in secondary cells

The ultrastructurally complex secretory compartments of secondary cells were first identified by electron microscopy (Bairati, 1968), and noted for their unusual contents, which included both a dense-core granule and numerous

fibrous structures. This led to their original description as ‘filamentous bodies’. A subsequent publication reported that the fibrous structures were microtubules, due to their diameter and subunit organisation (Perotti, 1972), though in Chapter 3, I was unable to confirm this identification, as fluorescently tagged alpha-tubulin did not localise to them (Section 3.2.1.6). Furthermore, cytosolic tubulin would not be expected to traffic to a dense-core granule compartment.

Using electron microscopy I presented novel ultrastructural details about these compartments, including the heterogeneous electron density across the dense-core granule and the presence of ILVs adjacent to the core (Section 3.2.1.3). Only a small number of endogenous secondary cell dense-core packaged proteins have been identified so far, the best characterised being Angiotensin Converting Enzyme (AnCE; Section 3.2.1.1). Once secreted into the accessory gland lumen, AnCE has been proposed to participate in peptide processing (Rylett *et al*., 2007). The first genetic analysis of a mutant in which dense-core granule biogenesis is defective utilised a mutant fly line that contained secondary cells without any of their normal large subcellular compartments. The mutant flies carried a deletion in a specific enhancer in the *Hox* gene, *Abd-B*, which drove gene expression specifically in secondary cells. These mutant flies failed to glycosylate several important accessory gland proteins, including Ovulin, and also exhibited impaired post-mating responses in the female (Gligorov *et al*., 2013). However, it is difficult to determine whether these functions were purely due to defects in secondary cell dense-core granule compartments, as the changes could involve

alternative exocytic pathways. It is also likely that the impairment of secondary cell secretions resulted in defective main cell functions.

A more recent report showed that overexpression of the BMP signalling ligand, *Dpp*, when tagged with GFP (*Dpp-GFP*), was specifically packaged into dense-core granules and secreted (Redhai *et al*., 2016). However, secondary cells proved highly responsive to its overexpression, which caused gross morphological changes within the cells, likely due to BMP's established functions in secondary cell biology (Corrigan *et al*., 2014; Redhai *et al*., 2016). Due to this limitation of *Dpp-GFP*, this study predominantly worked with an overexpressed GFP-GPI transgene (described in detail in Section 5.2.1.1), which localised within the dense-core granules, but which did not strongly impact their normal subcellular compartment organisation. Using GFP-GPI, Redhai *et al*., (2016) reported that mating stimulated the secretion of dense-core granules in a mechanism dependent on the conserved SNARE protein, SNAP24, which is involved in the fusion between lipid bilayers (Niemeyer & Schwartz, 2000). The secreted Dpp was thought to activate autocrine BMP-mediated signalling in secondary cells following mating, thus stimulating dense-core granule biogenesis *de novo*.

Although dense-core granules are an important aspect of secondary cell secretions, the mechanisms underlying their formation in secondary cells are not well understood.

5.1.3 Lysosomal growth in secondary cells

The giant lysosomal compartments of secondary cells, visualised in living cells with vital dye Lysotracker-Red staining (Section 3.2.1.4), are one of their

most striking subcellular features, and suggestive of their key roles in the functioning of these cells. Previous DPhil students in the Wilson lab have reported that as secondary cells age during adulthood, the number of large acidic compartments reduces, but the largest acidic compartment grows in size (Corrigan, 2014; Redhai, 2016). I showed in Chapter 4 that the largest acidic compartment likely grew at least in part driven by homotypic fusion between acidic compartments, and also through putative autophagic fusions with other large non-acidic compartments (Section 4.2.1.1). However, little is known about the genetic regulation that drives these processes.

I also reported several novel observations about the ultrastucture and molecular composition of the endolysosomal compartments in Chapter 3, including a detailed morphological characterisation using electron microscopy (Sections 3.2.1.2 and 3.2.1.3). Using immunological staining I confirmed that the Rab7 GTPase, which is known to be involved in endosome trafficking and lysosome fusion (Guerra & Bucci, 2016) localised to the surface of these large lysosomal compartments (Appendix 8.1.1). I also showed that the Arl8 GTPase, thought to function in lysosome motility in other cell types (Pu *et al*., 2016; Tuli *et al*., 2014), localised to the compartment's surface (Appendix 8.1.2). Finally, I identified two fluorescent fusion proteins expressed from their endogenous loci, *YFP-Rab7* and *YFP-Rab39* gene trap, that localised to the surface of acidic compartments in secondary cells (Section 3.2.2.7). These endogenous molecular markers and genetic tools provided novel ways in the work described here to visualise the formation of large acidic compartments, and help us to understand the genetic regulation underlying their biogenesis.

5.1.4 Chapter aims

In this chapter, I have utilised time-lapse microscopy to visualise the formation and maturation of different subcellular compartments in secondary cells for the first time. These descriptive findings informed my characterisation of the genetic regulatory mechanisms that underlie both dense-core granule biogenesis and lysosome growth and physiology in secondary cells. This permitted an *in vivo* analysis of processes that have to date primarily been investigated in cell culture systems and consequently highlighted several new processes, several of which are likely to be conserved in other cell types. My key aims were to:

- Describe in detail the cell biological processes underlying dense-core granule formation in secondary cells
- Characterise the roles of known and novel regulators of dense-core granule biogenesis in secondary cells
- Establish the secondary cell as a model for studying lysosome formation and maturation, and use the model to explore the mechanisms underpinning these processes

5.2 Results

5.2.1 Formation, maturation and secretion of dense-core granule-containing compartments

5.2.1.1 Dynamics of dense-core granule compartment formation and maturation in secondary cells

The visualisation of dense-core granule formation and maturation in living cells has been extremely challenging because of the small size of these compartments in most cells, which require electron microscopy for detailed analysis (Fava *et al*., 2012). However, the dense-core granule compartments of secondary cells overcome this limitation by reaching extraordinarily large sizes, of about 6-8 μm in diameter (Section 3.2.1.1). Furthermore, the diversity of genetic tools in *Drosophila*, including numerous GFP-tagged proteins that can be specifically expressed in secondary cells, enable the investigation of trafficking and packaging of dense-core-localised proteins *in vivo*.

In order to visualise dense-core granule formation within intracellular compartments, I carried out time-lapse imaging of secondary cells that overexpressed GFP-GPI, which localises at high levels on their dense-core granules (Redhai *et al*., 2016; Appendix 8.1.2), and used DIC microscopy to confirm the morphological features of the mature dense-core granules. GFP-GPI is a fusion protein produced from several protein fragments previously used in mammalian cells to follow apical secretory trafficking in polarised cells, and basolateral membrane secretion in *Drosophila* (Keller *et al*., 2001;

Greco *et al*., 2001). Its molecular organisation was characterised by another DPhil student in the lab, F. Castellanos (Castellanos, 2017). His analysis showed that GFP-GPI consists of an N-terminal ER-targeting signal sequence from rabbit lactase-phlorizin hydrolase linked to eGFP, and that it is anchored into lipid membranes through a C-terminal GPI anchor sequence from human lymphocyte function associated antigen 3 (LFA-3).

Careful observations showed that GFP-GPI-labelled dense-core granules formed within a large centrally located non-cored compartment over the course of ~2 hours (Figure 5.1A-D). This compartment constricted in size and migrated basally and to a more peripheral localisation. Whilst doing so, GFP-GPI began to diffusely mark the interior of the compartment, a change that initially did not correlate with any readily visible alterations by DIC microscopy (Figure 5B-C). The dense-core granule then condensed to become visible by DIC microscopy, and simultaneously very high levels of GFP-GPI rapidly accumulated within the dense-core granule (Figure 5B).

Both this and the other processes reported in this Chapter were observed with a high frequency during long-term time-lapse imaging, regardless of their genotype (In this case, n=6 individual glands, with ≥3 cells imaged each time).

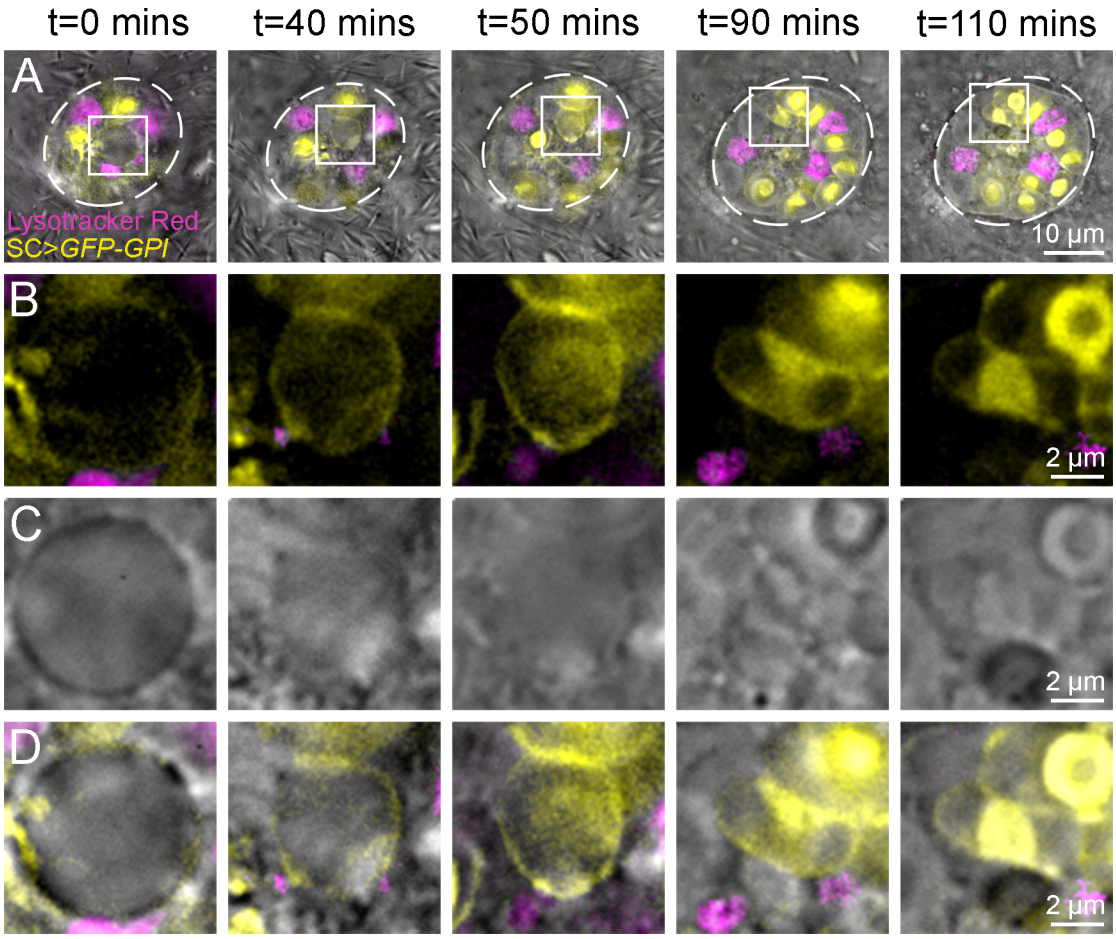


Figure 5.1 Dense-core granule formation occurs within the large rounded non-cored compartment

These panels display wide-field fluorescence and DIC images of a secondary cell from a 6-day-old virgin transgenic male selectively overexpressing GFP-GPI (yellow). The flies were incubated at 28.5°C following eclosion to induce GFP-GPI expression using the GAL4-GAL80^{ts}-UAS system. Their accessory glands are stained with Lysotracker Red (magenta).
(A-D) Time-lapse imaging shows the stages of dense-core granule formation within an individual subcellular compartment. The boxes in panel (A) highlight the regions enlarged in (B-D) at each time-point. The large rounded non-cored compartment reduces in size, and begins to migrate towards the basal portion of the cell between 0-50 minutes. At the same time, GFP-GPI begins to accumulate in the lumen of the non-cored compartment (B, D), but this is unclear from DIC imaging alone (C). The dense-core granule cargos condense between 50-90 mins, now visible by both DIC and GFP-GPI fluorescence, as the compartment moves towards a peripheral location in the basal portion of the cell. By 110 mins, a bright GFP-GPI-rich dense-core granule has formed inside the compartment.
The specific genotype of the flies used in this figure is: *w; spi-GAL4, tub-GAL80^{ts} / +; UAS-GFP-GPI / +*.

The large rounded central non-cored compartment was observed to form gradually from a vesicular structure, localised in the Golgi-rich central region of the cell, that enlarged over the course of an hour, possibly through fusion with neighbouring vesicles (Figure 5.2A-D). Initially, GFP-GPI was mostly found on small vesicles in close proximity to a non-cored and irregularly shaped central compartment, in the region known to include Golgi complexes and membranes marked by other Rabs, but this was transferred to the surface of irregularly shaped central compartment over time (Figure 5.2B). Whilst doing so, this compartment morphologically rearranged to become a smaller, but more rounded compartment.

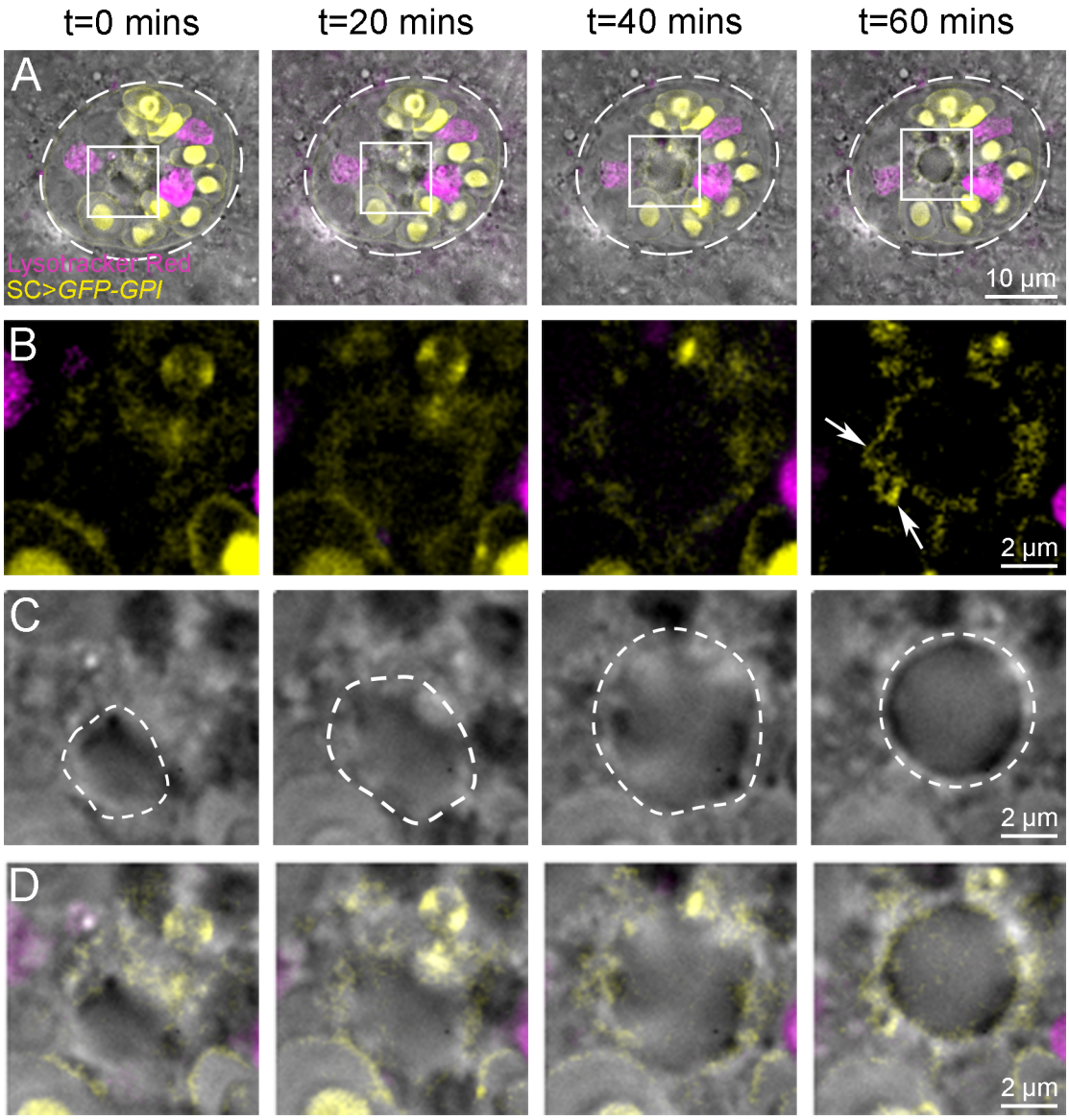

t=0 mins
t=20 mins
t=40 mins
t=60 mins
A
Lysotracker Red
SC>GFP-GPI
10 µm
B
2 µm
C
2 µm
D
2 µm

Figure 5.2. Formation of a rounded non-cored compartment occurs in the central region of secondary cells

These panels show wide-field fluorescence and DIC images of a secondary cell from a 6-day-old virgin transgenic male selectively overexpressing GFP-GPI (yellow). The flies were incubated at 28.5°C since eclosion to induce GFP-GPI expression using the GAL4-GAL80^{ts}-UAS system. Their accessory glands are stained with Lysotracker Red (magenta).
(A-D) Time-lapse imaging shows the stages of rounded non-cored compartment formation. The boxes in panel (A) highlight the regions enlarged in (B-D) at each time-point. Over the first 40 minutes, a large non-cored irregularly shaped compartment is formed in the central region of the secondary cell. At first, the growing compartment, identified using DIC (C, marked with a dashed line), is surrounded by small GFP-GPI-labelled vesicular structures (B, D). Some GFP-GPI appears to be gradually trafficked to the surface of the compartment between 20-40 mins. The compartment then changes in morphology between 40-60 mins, becoming more rounded, and higher levels of GFP-GPI can be observed on the limiting membrane of this resulting compartment. Some small vesicles are observed potentially fusing to the rounded compartment (B, arrows).

The specific genotype of the flies used in this figure is: *w; spi-GAL4, tub-GAL80^{ts} / +; UAS-GFP-GPI / +*.

To the best of my knowledge, these data are the most detailed observations of dense-core granule formation within an individual subcellular compartment in any cell type. They not only reveal morphological changes in the shape and size of compartments as they form dense-core granules, but they also suggest that during this process, the compartment moves away from its location adjacent to the central Golgi stacks, so that a new compartment can form in this position.

To ensure that similar processes took place in 'wild type' secondary cells, time-lapse DIC microscopy of non-transgenic w^{1118} flies was performed. Similar to GFP-GPI-overexpressing secondary cells, dense-core granule formation occurred inside a large non-cored compartment (Figure 5.3A-A'). Detailed DIC imaging, using more time-points than possible with fluorescence imaging, showed that dense-core condensation occurred in a morphologically distinctive manner (Figure 5.3B). Furthermore, the newly formed dense-core granule often moved around the interior of the compartment until stabilising (Figure 5.3A'). This suggested that physical forces, possibly exerted by the formation of fibrous structures or the ILV network I had identified, might function in the shaping and condensation of the dense-core granule material. Time-lapse imaging of w^{1118} cells also showed that the large non-cored precursor compartment could grow through fusions with other non-cored compartments (Figure 5.3D). These fusions resulted in extremely large irregularly shaped compartments, which constricted down in size to approximately the same as a typical dense-core granule compartment.

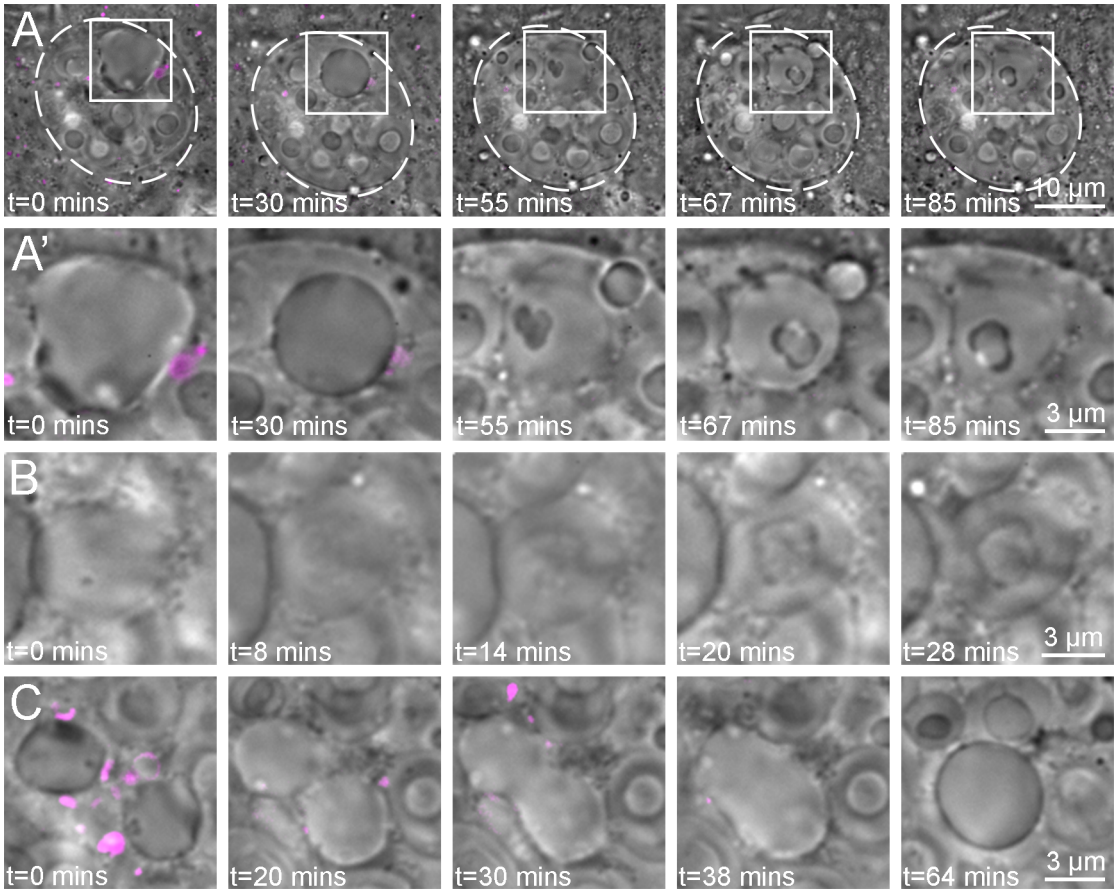


Figure 5.3 Live cell imaging of secondary cells from non-transgenic *w*^{1118} males shows a range of subcellular events during the formation of dense-core granules

These panels show wide-field fluorescence and DIC images of secondary cells from 6-day-old virgin non-transgenic *w*^{1118} males that were incubated at 28.5°C following eclosion. Their accessory glands were stained with Lysotracker Red (magenta).
(A-A') Time-lapse imaging shows that a very large irregularly shaped non-cored compartment rearranges in morphology to become more rounded over the first 30 mins of imaging. The contents within the compartment then condense to form a dense-core granule, which moves within the lumen of the compartment before stabilising in its position at approximately 85 mins. The boxes mark regions in (A) that are enlarged in (A').
(B) Distinct stages of dense-core granule condensation are observed within an individual compartment over the course of this time-lapse movie. The dense-core granule contents form a slight shadow by 8 mins, and then condense into a more visible structure by 20 mins, which then becomes smoother and rounder in appearance by 28 mins.
(C) Non-cored compartments sporadically fuse together to form very large irregularly shaped compartments, which then round up prior to dense-core granule condensation.

5.2.1.2 A novel Rab6 to Rab11 switch occurs during dense-core granule biogenesis

The striking inverted relationship between the localisations of Rab6 and Rab11 on the surface of non-acidic compartments, labelling the non-cored and dense-core granule compartments, respectively (Section 3.2.2.5), prompted me to study their dynamic association during dense-core granule formation. Long-term time-lapse observations of secondary cells from homozygous flies expressing the fusion proteins from *CFP-Rab6* and *YFP-Rab11* gene traps revealed that the CFP-Rab6-labelled non-cored compartment gradually acquired higher levels of YFP-Rab11 as it matured and formed a dense-core granule in its lumen (Figure 5.4A-D). Simultaneously to that, CFP-Rab6 localisation to the compartment's surface was reduced. These findings suggest that a Rab transition takes place as dense-core granules are formed, potentially reflecting the delivery of new components to the compartment via Rab11-mediated trafficking.

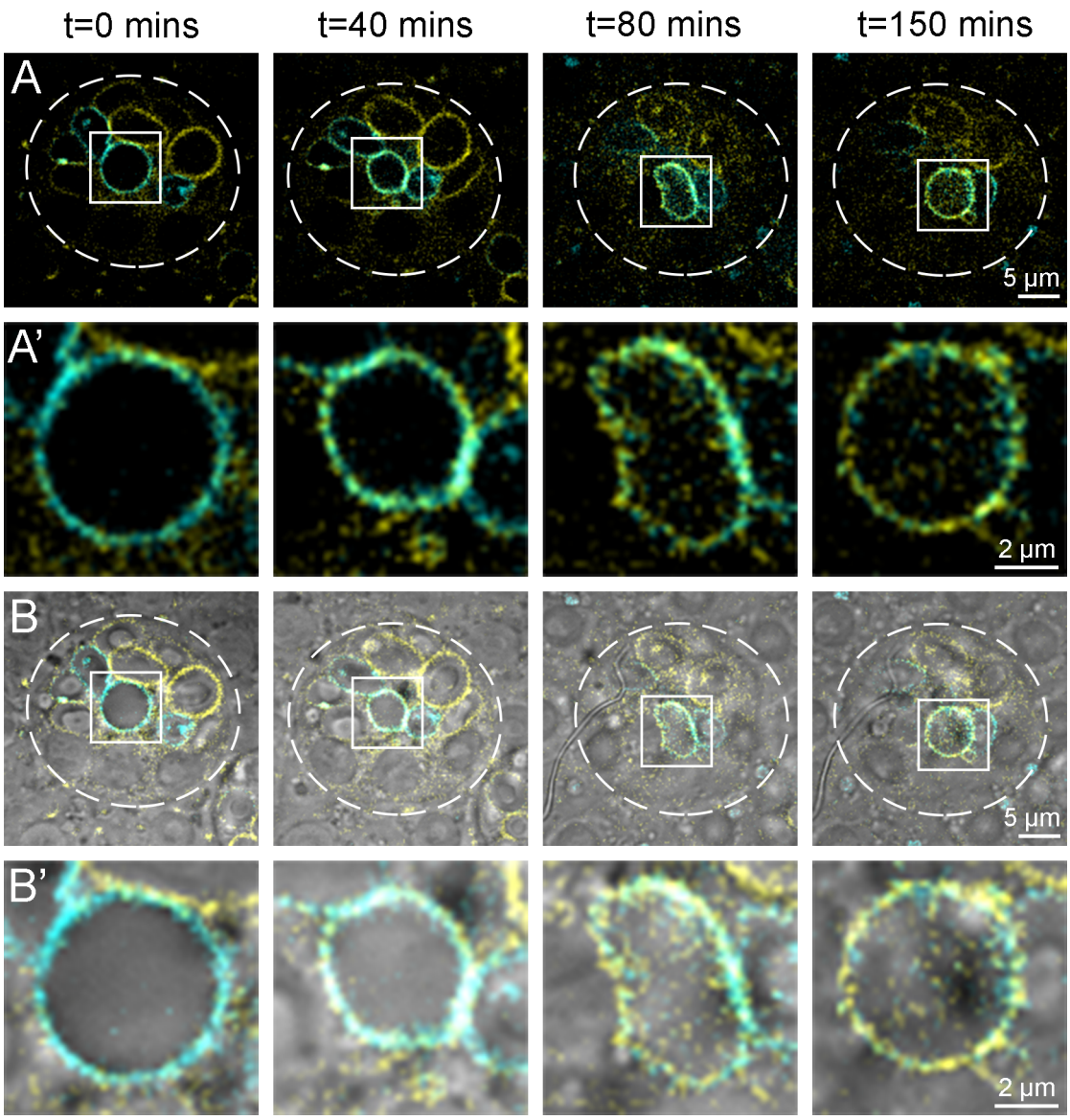

t=0 mins
t=40 mins
t=80 mins
t=150 mins
A
5 µm
A'
2 µm
B
5 µm
B'
2 µm

Figure 5.4 A novel Rab6 – Rab11 transition is observed on the surface of large compartments during dense-core granule biogenesis

These panels show wide-field fluorescence and DIC images from a six-day-old virgin male, kept at 28.5°C since eclosion, expressing both the *CFP-Rab6* and *YFP-Rab11* gene traps. Panels (A-A') are fluorescence microscopy images that are combined with DIC microscopy in (B-B'). The boxes in (A) and (B) highlight the specific region enlarged in (A') and (B').
(A-B') The central rounded non-cored compartment initially carries high levels of CFP-Rab6 (cyan) on its surface. This compartment constricts in size and begins to acquire higher levels of YFP-Rab11 (yellow) after 40 mins. Whilst doing so, the compartment starts to migrate towards the basal portion of the cell. YFP-Rab11 continues to accumulate on the surface of this large compartment as it passes between other compartments at 80 mins, and the level of CFP-Rab6 reduces. By 150 mins, the compartment occupies a very basal position, the outline of a dense-core granule can be seen, and it has switched its Rab association from being primarily CFP-Rab6-positive to YFP-Rab11-positive.

Homozygous *w; CFP^{Myc}-Rab6; YFP^{Myc}-Rab11* gene trap flies were used for all panels.

5.2.1.3 Secretion of dense-core granule compartments by secondary cells

Previous reports have suggested that the exocytosis of dense-core granule compartments by secondary cells is a regulated secretory process, though constitutive secretion may also take place (Redhai *et al*., 2016). However, the cellular mechanisms involved in regulated exocytosis are varied, with both complete collapse-fusion and kiss-and-run of vesicles with the plasma membrane being reported, and often both being employed by the same cell type (Wu *et al*., 2014; Harata *et al*., 2006; Hanna *et al*., 2009). Time-lapse microscopy was performed to better understand the forms of dense-core granule secretion by secondary cells. GFP-GPI-labelled dense-core granule compartments were occasionally observed to fuse directly to the apical plasma membrane, potentially depositing all of their contents into the lumen of the gland (Figure 5.5A-C'). Similar observations were reported in Chapter 4 using secondary cells that overexpressed CD63-GFP (Section 4.2.1.2).

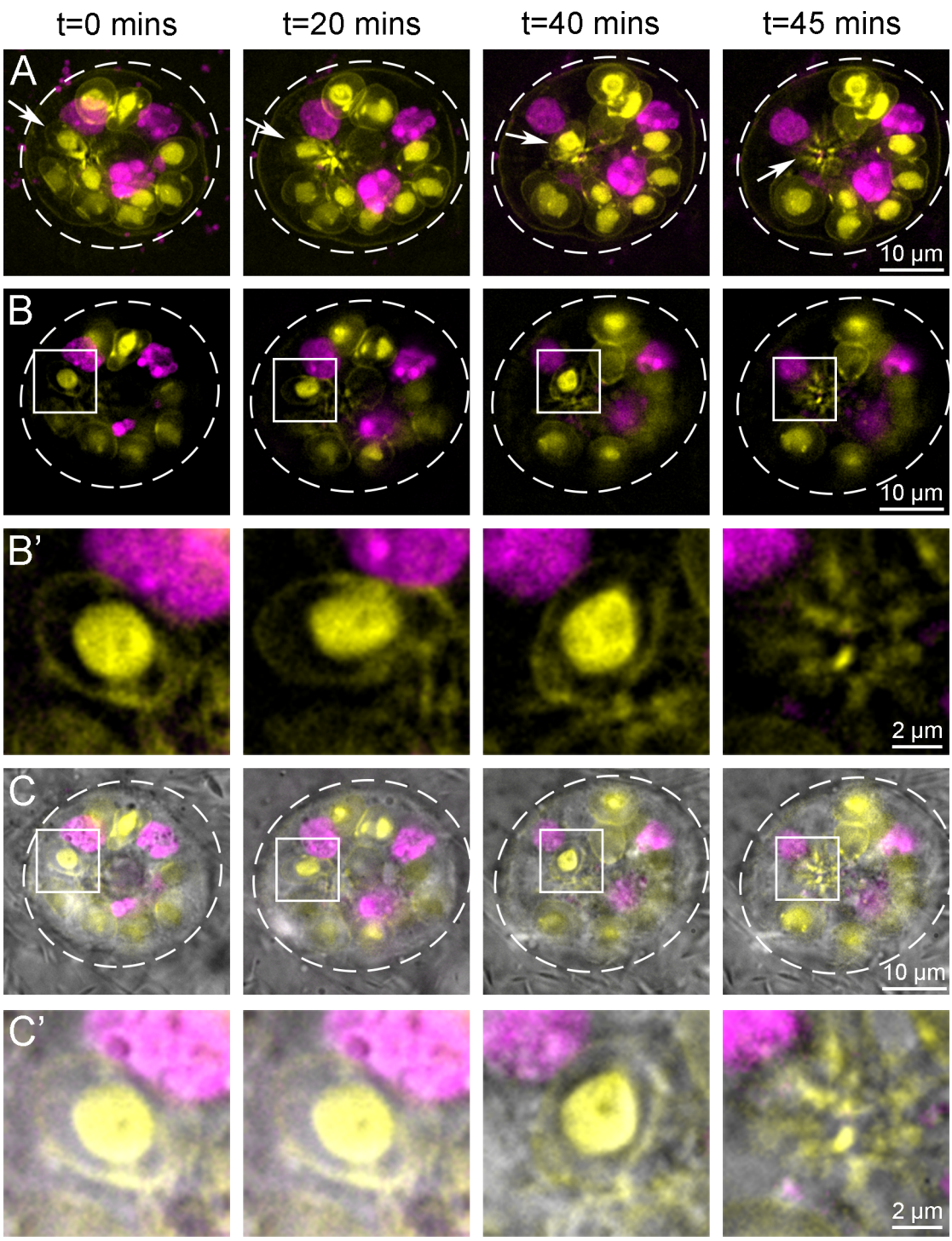

t=0 mins
t=20 mins
t=40 mins
t=45 mins
A
10 µm
B
10 µm
B'
2 µm
C
10 µm
C'
2 µm

Figure 5.5 Secretion of an entire dense-core granule compartment at the apical surface of the secondary cell

These panels show wide-field fluorescence and DIC images of a secondary cell from a 6-day-old virgin transgenic male selectively overexpressing GFP-GPI (yellow). The fly was incubated at 28.5°C since eclosion to induce GFP-GPI expression using the GAL4-GAL80^{ts}-UAS system and the accessory gland stained with Lysotracker Red (magenta) to mark the acidic compartments. Panel (A) is a maximum intensity projection image of 10 µm thickness, extending throughout the depth of a secondary cell, whilst panels (B-B') and (C-C') are individual z-planes through the same cell. In (C-C') the fluorescent images are combined with DIC. Boxes surrounding the secreted compartment in (B) and (C) highlight the regions enlarged in (B') and (C') (A) Time-lapse maximum intensity projection images show that a specific dense-core granule compartment (marked by GFP-GPI, arrows) migrates between other intracellular compartments and subsequently releases all of its contents during a secretion event, which occurs between 40- and 45 mins. (B-C') Individual z-planes through the same cell show that a basally located dense-core granule compartment migrates towards the apical portion of the cell over the first 40 minutes, and then subsequently releases all of its contents. DIC imaging (C-C') confirmed that the whole compartment was lost during the secretion event.

The specific genotype of the flies used in this figure is: *w; spi-GAL4, tub-GAL80^{ts} / +; UAS-GFP-GPI / +*.

Other dense-core granule compartments revealed a kiss-and-run interaction with the plasma membrane; GFP-GPI-labelled compartments released some, but not all, of their contents into the lumen, possibly via a fusion pore (Hanna *et al*., 2009), visualised by a reduction in GFP-GPI signal and a change in the dense-core granule's morphology, as observed by DIC microscopy (Figure 5.6A-A').

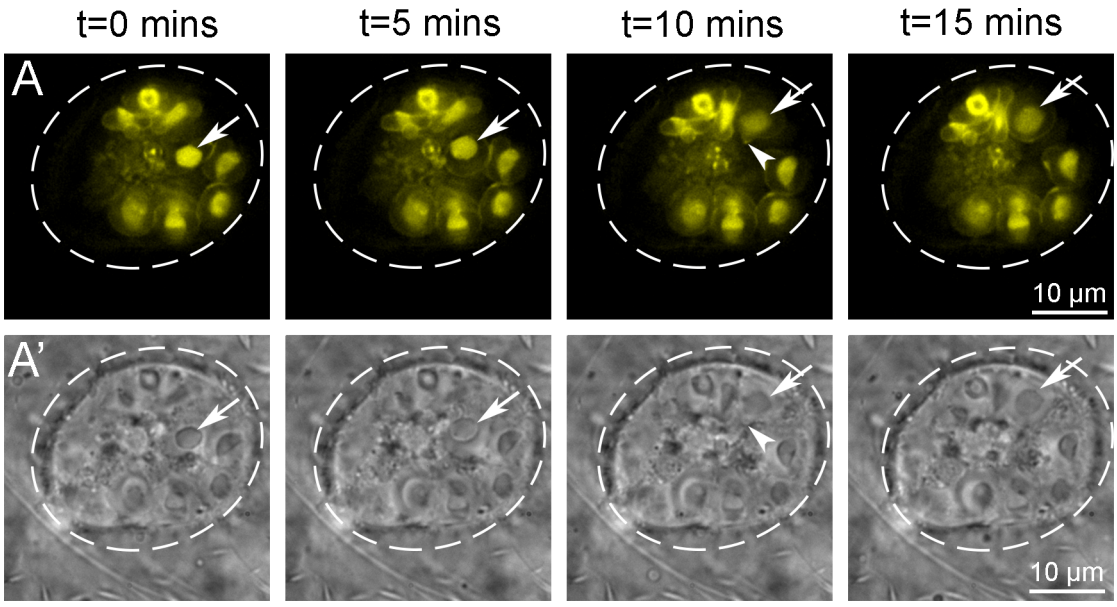


Figure 5.6 Secondary cells can release some of their dense-core granule contents through putative kiss-and-run interactions with the apical plasma membrane

These panels show wide-field fluorescence and DIC images of a secondary cell from a 6-day-old virgin transgenic male selectively overexpressing GFP-GPI (yellow). The flies were incubated at 28.5°C since eclosion to induce GFP-GPI expression using the GAL4-GAL80^{ts}-UAS system.
(A-A') Over the course of the time-lapse, a dense-core granule compartment containing high levels of GFP-GPI (yellow, arrows), migrates apically, where a portion of the compartment distorts and interacts with the apical plasma membrane, seen at 10 mins (arrowhead). Following this interaction, the GFP-GPI fluorescence within the compartment reduces as some of it is funnelled towards the apical distortion. By DIC microscopy (A'), the dense-core granule changes from being condensed, dark and clearly delimited prior to the interaction, to having a more diffuse morphology and less well-defined structure afterwards (15 mins).

The specific genotype of the flies used in this figure is: *w; spi-GAL4, tub-GAL80^{ts} / +; UAS-GFP-GPI / +*.

5.2.1.4 Secreted dense-core granule compartments in secondary cells appear to carry Rab19 on their limiting membrane

In Chapter 3, I found that several Rab GTPases decorated the limiting membranes of dense-core granule compartments in secondary cells, suggesting that they may work individually or co-operate to facilitate different trafficking events associated with the compartment's functions (Zhen & Stenmark, 2015; Section 3.2.2.4). Rab11 was observed at varied levels on all the dense-core granule compartments in secondary cells. However, time-lapse microscopy showed that only a small proportion of these were secreted over a period of a few hours, suggesting that it may mark both mature and immature compartments. It seemed likely that another Rab GTPase, which localised more specifically to the limiting membrane of the secreted compartments, might be involved in the their trafficking to the plasma membrane. In Chapter 3, I showed that 2-3 apically located dense-core granule compartments often carried the fusion protein from a *YFP-Rab19* gene trap at high levels on their limiting membrane (Section 3.2.2.4). Time-lapse imaging showed that YFP-Rab19-marked compartments fused to the plasma membrane, releasing their dense-core granule contents (Figure 5.7A-B'). These data suggested that Rab19 might regulate exocytic trafficking of dense-core granule compartments towards the apical plasma membrane.

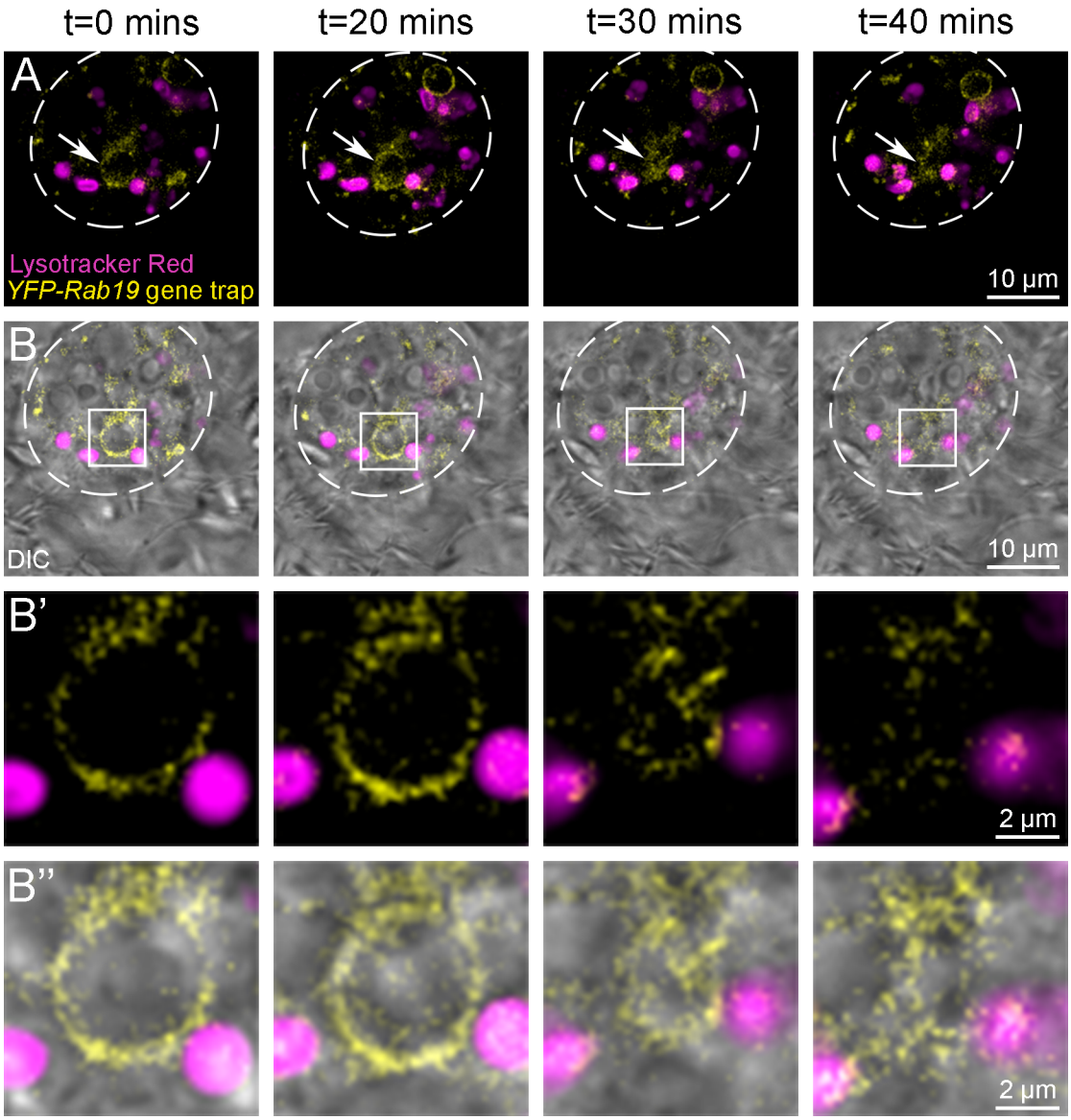


Figure 5.7 Dense-core granule compartments labelled with YFP-Rab19 are secreted at the apical cell surface

These panels consist of wide-field fluorescence and DIC images from a six-day-old virgin male, kept at 28.5°C following eclosion, that expressed *YFP-Rab19* from the gene's endogenous locus. Accessory glands were stained with Lysotracker Red (magenta). Panel (A) is a maximum intensity projection image of 5 µm thickness, and panels (B-B'') are individual z-slices through the same cell. The box region in panel (B) is enlarged in (B', only fluorescence) and (B'').

(A) Maximum intensity projection shows that a YFP-Rab19-delimited compartment (yellow; arrows) is lost between the 20-30 mins time points.

(B-B'') Individual z-slice from the same secondary cell highlights the particular YFP-Rab19-labelled dense-core granule compartment, which releases its contents at the apical plasma membrane.

Homozygous *YFP^{Myc}-Rab19* gene trap flies were used for these panels

5.2.1.5 Novel molecular markers of dense-core granules in secondary cells

Important signalling molecules are packaged inside dense-core granules within secretory cell types; for example, insulin is concentrated in the secretory granules of pancreatic β-cells, and neurotransmitters such as acetylcholine are packed inside the dense-core granules at neuronal synapses (Hou *et al*., 2009; Heeroma *et al*., 2003). In the dense-core granules of secondary cells, however, very few of the granule contents have been characterised. I have used newly developed fly lines to identify fluorescently tagged endogenous dense-core granule-localised proteins in living secondary cells.

Working collaboratively with F. Castellanos, I studied a GFP-tagged form of AnCE (*AnCE-GFP* gene trap; Nagarkar-Jaiswal *et al*., 2015), which had been generated by homologous recombination, so was expressed from its endogenous promoter. The fusion protein from this gene trap marked all of the secondary cell dense-core granules, as expected from the antibody staining of native AnCE protein (Figure 5.8A; Rylett *et al*., 2007). Unlike the immunological localisation of native AnCE, however, AnCE-GFP protein was not observed at the limiting membrane of the compartment (Appendix 8.1.2). A more comprehensive analysis of AnCE-GFP expression in secondary cells is reported elsewhere (Castellanos, 2017).

I found that AnCE-GFP protein is incorporated into forming dense-core granules within a CFP-Rab6-labelled compartment using time-lapse imaging (Figure 5.8B-B''). These data show that AnCE-GFP may be a useful marker for dense-core granule biogenesis. Unfortunately, however, its localisation

was affected by temperature, as surprisingly, it is not incorporated into dense-core granules when flies are maintained at 29°C (Castellanos, 2017), so it could not be readily combined with the GAL4/GAL80^{ts} gene expression system (McGuire *et al*., 2004), used elsewhere in my work.

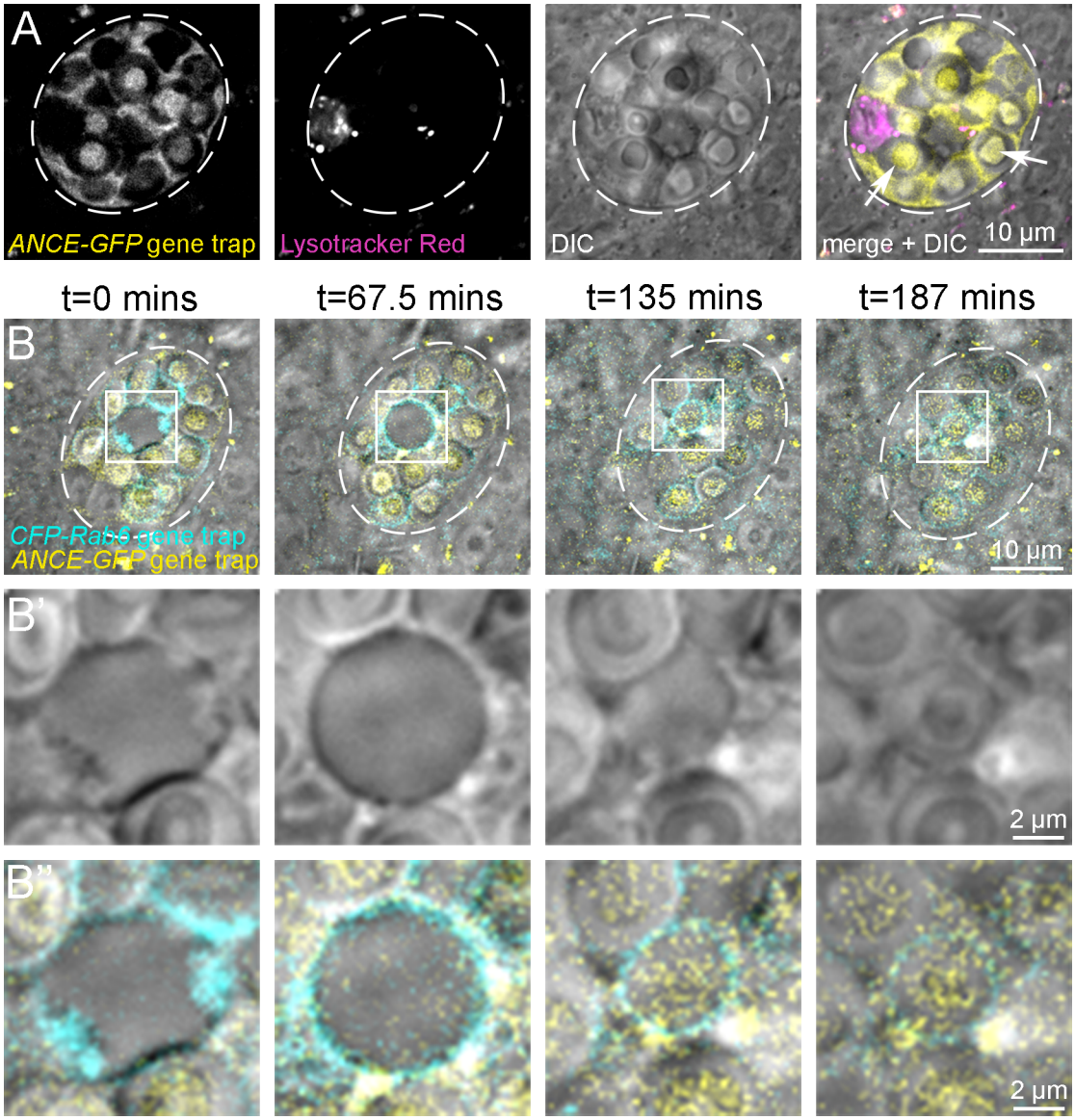

A
ANCE-GFP gene trap
Lysotracker Red
DIC
merge + DIC
10 µm
t=0 mins
t=67.5 mins
t=135 mins
t=187 mins
B
CFP-Rab6 gene trap
ANCE-GFP gene trap
10 µm
B'
2 µm
B"
2 µm

Figure 5.8 ANCE-GFP is packaged into forming dense-core granules in secondary cells

These panels consist of wide-field fluorescence and DIC images from six-day-old virgin males, kept at 18°C following eclosion. The images in panel (A) are from a fly that exclusively expressed the *ANCE-GFP* gene trap, whilst those in panel (B) expressed ANCE-GFP in combination with the *CFP-Rab6* gene trap. These lines were studied collaboratively with F. Castellanos, who has carried our further characterisations of this genotype. Accessory glands were stained with Lysotracker Red (magenta). Approximate secondary cell outlines are marked with a dashed line.
(A) ANCE-GFP (yellow) is localised within dense-core granules (arrows), and is also found throughout the cytosolic regions of the secondary cell, and in some small acidic compartments (magenta). Some dense-core granules carry higher levels of ANCE-GFP than others.
(B-B'') Time-lapse imaging of ANCE-GFP (yellow) shows how it is gradually packaged within the large CFP-Rab6- (cyan) marked compartment during dense-core granule formation. The box in (B) highlights the specific compartment, which is enlarged in (B') and (B''). At first, little ANCE-GFP is observed within the large non-cored CFP-Rab6-positive compartment (between 0-67.5 mins), but later it diffusely marks the interior of the compartment, particularly after its size reduces (135 mins). Finally, condensation takes place and most of the ANCE-GFP localises within the dense-core granule (187 mins).

The specific genotypes of the flies used in this figure are: homozygous *ANCE-GFP* gene trap flies, and *w; CFP^{Myc}-Rab6 / ANCE-GFP ; + / +*.

I have also characterised a GFP-tagged form of Cathepsin B1 (*CtsB1-GFP* gene trap; Flyprot.org – an online resource with annotated expression patterns for a number of CPTI lines in different tissues and during development; Lye *et al*., 2014; Lowe *et al*., 2014), expressed from its endogenous promoter. It had been shown to be expressed in secondary cells in a screen of such gene traps. I found that it localised within the dense-core granules (Figure 5.9A). However, unlike previously described dense-core-localised proteins, CtsB1-GFP localised unevenly within the dense-core granules, suggesting that the molecular make-up of these structures is not entirely homogeneous. Similar observations were made using a GFP-tagged form of the *Drosophila Perlecan* gene, *terribly reduced optic lobes* (*trol-GFP* gene trap; Voigt *et al*., 2002; Shannon *et al*., 1972; Flyprot.org; Lye *et al*., 2014; Lowe *et al*., 2014). Trol-GFP protein localised unevenly inside the dense-core granules (Figure 5.9B). This further supports the idea that the dense-core granules are non-homogeneous in their make-up and composition.

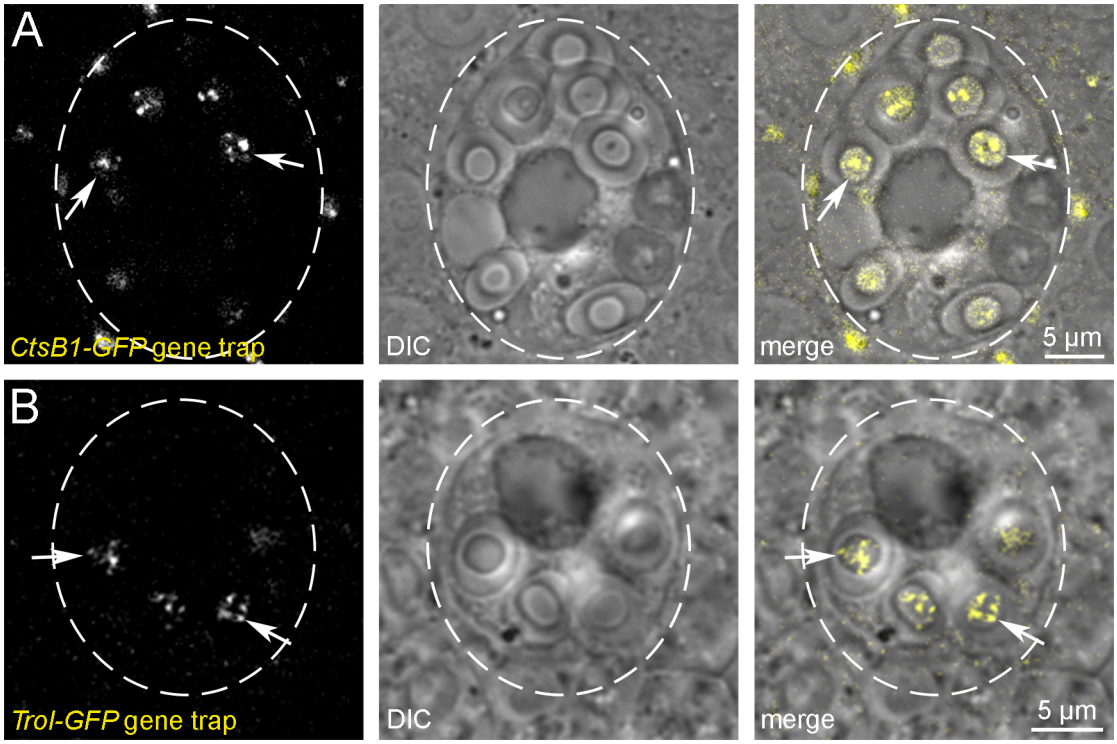


Figure 5.9 GFP-tagged Cathepsin B1 and Trol localise in subdomains of the secondary cell dense-core granules

These panels consist of wide-field fluorescence and DIC images from six-day-old virgin males, kept at 18°C following eclosion. The images in panel A are from flies that express the *Cathepsin-B1-GFP* (*CtsB1-GFP*) gene trap, and those in panel B are from flies that express the *Trol-GFP* gene trap. Approximate secondary cell outlines are marked with a dashed line.
(A) CtsB1-GFP (yellow) localises in an uneven punctate pattern within secondary cell dense-core granules (arrows).
(B) The fusion protein Trol-GFP localises within dense-core granules in a similar, uneven manner (arrows).

Flies homozygous for either the *CtsB1-GFP* gene trap or *Trol-GFP* gene trap were used for this figure.

A postdoctoral scientist in the Wilson lab, M. Wainwright, identified that GFP-tagged midline fasciclin (*mfas-GFP* fTRG line; Sarov *et al*., 2016), was localised specifically in secondary cells within the gland. Working collaboratively, I showed that this GFP-tagged fusion protein was specifically localised inside dense-core granules by DIC microscopy (Figure 5.10A). Interestingly, the level of *mfas-GFP* expression exceeded that of fluorescent proteins driven by the GAL4-UAS transcriptional machinery. This highly expressed gene was ideal for time-lapse microscopy, which I used to visualise dense-core granule packaging within individual subcellular compartments. Mfas-GFP protein localised into the lumen of the non-cored compartment prior to condensation (Figure 5.10B-B''). Like overexpressed GFP-GPI, this fusion protein localised at homogeneous levels across the dense-core granule. The localisation was confirmed using two different GFP-tagged Mfas lines. The first was a third chromosome insertion of 35kb containing most of *mfas* normal regulatory elements to drive the expression of the *mfas* coding sequence, which was tagged with GFP at its C terminus (Figure 5.10A-B''; Sarov *et al*., 2016). The other *mfas-GFP* gene trap contained all of its normal regulatory sequences, as it was inserted into its endogenous locus through homologous recombination towards its N-terminus (GFP-Mfas; Figure 5.10C; Nagarkar-Jaiswal *et al*., 2015).

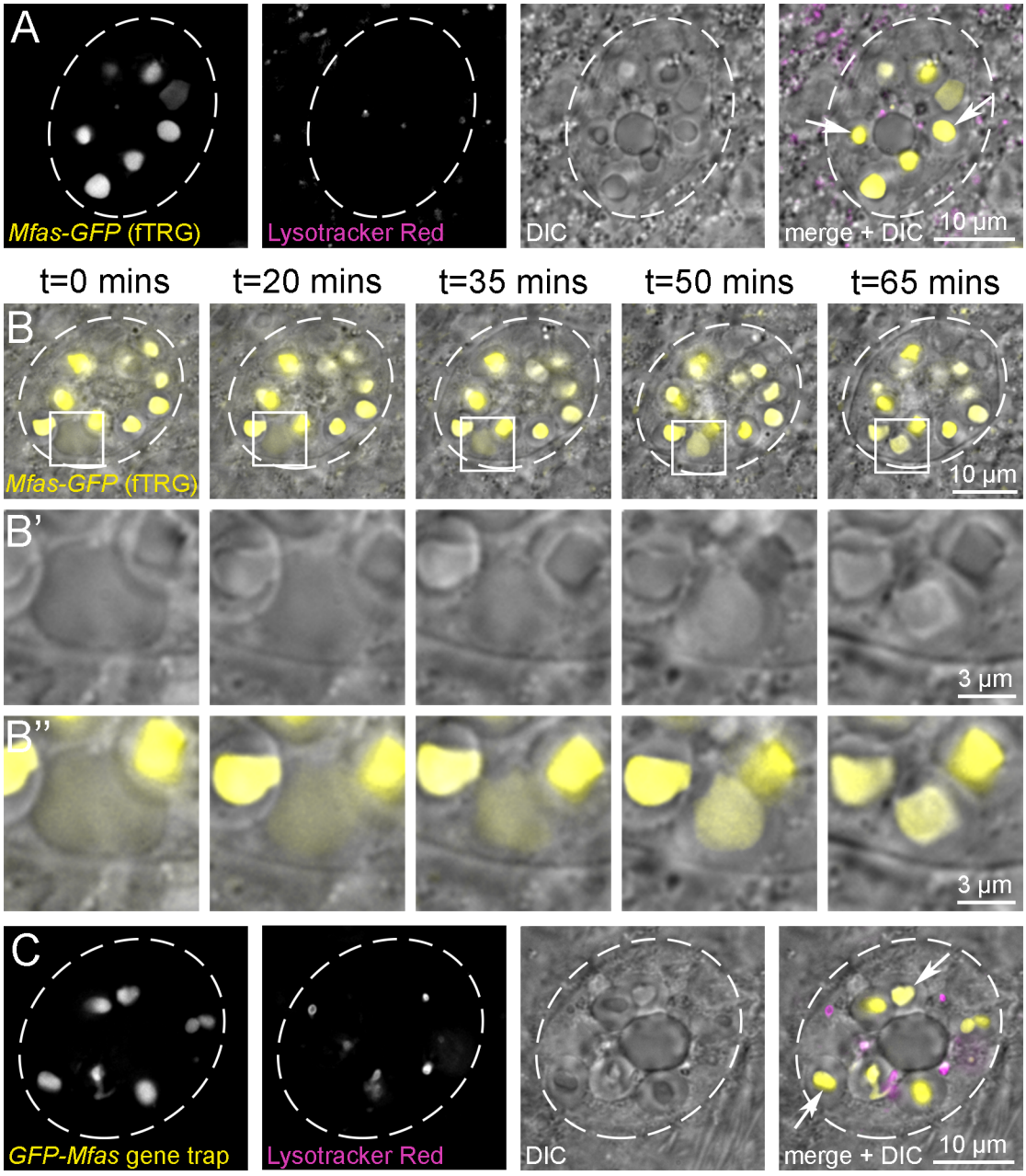

A
Mfas-GFP (fTRG)
Lysotracker Red
DIC
merge + DIC
10 µm
t=0 mins
t=20 mins
t=35 mins
t=50 mins
t=65 mins
B
Mfas-GFP (fTRG)
10 µm
B'
3 µm
B''
3 µm
C
GFP-Mfas gene trap
Lysotracker Red
DIC
merge + DIC
10 µm

Figure 5.10 Mfas-GFP localises at high levels within secondary cell dense-core granules

Panels A-B'' consist of wide-field fluorescence and DIC images from one-day-old virgin males, kept at 18°C following eclosion, that expressed *mfas-GFP* from a large genomic insertion containing *mfas* regulatory sequences (fTRG stock). The images in Panel C are from six-day-old virgin males kept at 28.5°C following eclosion, that expressed the *GFP-mfas* gene trap (MiMIC stock). Their accessory glands were stained with Lysotracker Red (magenta). Approximate secondary cell outlines are marked with a dashed line.
(A) Mfas-GFP (fTRG stock; C-terminal-GFP tag; yellow) localises at high levels in the dense-core granules of secondary cells (arrows).
(B-B'') Time-lapse imaging reveals how Mfas-GFP is packaged into dense-core granules. The box in (B) highlights the region enlarged in (B') and (B''). At first, Mfas-GFP diffusely marks the lumen of the non-cored compartment, but as it begins to reduce in volume (between 0-35 mins), Mfas-GFP is restricted to a more central region of the compartment. Finally, as the dense-core granule condenses further (50-65 mins), Mfas-GFP is also highly packaged within its interior with the levels of fluorescence increasing substantially during this time.
(C) A different fluorescently tagged GFP-Mfas protein (MiMIC stock; N-terminal GFP tag) also localises within the dense-core granules of secondary cells (arrows).

This analysis of Mfas-GFP localisation was undertaken in collaboration with M. Wainwright. Homozygous flies for either the *mfas-GFP* genomic construct (fTRG stock) or the *GFP-mfas* gene trap (MiMIC stock) were used for this figure.

5.2.2 Characterisation of the genetic regulation of dense-core granule biogenesis in secondary cells

5.2.2.1 Roles for Rab GTPases in dense-core granule biology

Rab proteins are key regulators of vesicular trafficking that mediate vesicle motility, tethering, and fusion within the secretory and endocytic pathways (Zhen & Stenmark, 2015). However, although several Rabs have been linked to the exocytic trafficking of dense-core granule compartments to the surface of the cell (Shirakawa *et al*., 2004; Yi *et al*., 2002), their roles in dense-core granule biogenesis are less well understood (Burgoyne & Morgan, 2006). In Chapter 3, I showed that a number of endogenously expressed YFP-tagged Rab GTPases were observed on the surface of dense-core granule compartments in secondary cells, suggesting that they may play some roles in their biology (Section 3.2.2). Interestingly, these Rabs included several that have not been implicated in dense-core granule biology previously, including Rab6 and Rab19.

In this chapter I study the roles of Rab6, Rab11 and Rab7 on secondary cell dense-core granule compartments, chosen partly because their localisations were confirmed using antibody staining of non-transgenic w^{1118} secondary cells (Appendix 8.1.1). Furthermore, the novel finding that Rab6 and Rab11 localise to precursor and mature dense-core granule compartments, respectively (Section 5.2.1.2), and that they label distinct phases during this process, suggested that they might play functional roles in dense-core granule biogenesis. I also showed in Chapter 3 that Rab7 was found at high levels on the surface of a subset of non-acidic dense-core granule compartments (Section 3.2.2.7), in addition to acidic compartments, suggesting that it may

regulate an aspect of their trafficking. The expression of *Rab6*, *Rab11* and *Rab7* was knocked down using an RNAi approach, and the effect on dense-core granule formation visualised using both DIC and GFP-GPI localisation (Figure 5.11).

Secondary cells that expressed RNAi transgenes targeting *Rab6* contained fewer large dense-core granule compartments, and also fewer large non-cored compartments compared to controls (Figure 5.11B, 5.12A). These data implicate *Rab6* in dense-core granule biogenesis for the first time. Taking into consideration the subcellular localisation of Rab6 protein (Section 3.2.2.2 and Appendix 8.1.1, 8.1.2), it seems likely that it is involved in the formation of the precursor compartment, possibly by regulating the fusion of trans-Golgi derived vesicles. However, Rab6 knockdown also dramatically affected their acidic compartments, which were more numerous and smaller (Figure 5.12B-C). This may be due to the redirection of cargos away from the secretory compartments towards the acidics. In the future it will be important to confirm that the RNAi specifically reduced Rab6 protein levels. However, given that the defective dense-core granule phenotype was observed using two different RNAi constructs (the second line has n=11 glands, each from an individual fly, with 5 cells imaged from each gland – although not thoroughly quantified, they present a very similar phenotype), it does suggest that the effect was specific.

Knockdown of *Rab11* also resulted in a dramatic loss of dense-core granule compartments compared to control cells; the few that formed contained dense-core granules with abnormal morphologies (Figure 5.11C, 5.12A). However, unlike the *Rab6* knockdown, these cells retained several large non-

cored compartments, some of which contained diffuse GFP-GPI in their interior.

The knockdown of *Rab7* specifically in secondary cells gave a converse phenotype, in which the number of dense-core granule compartments increased compared to controls (Figure 5.11D, 5.12A). The increased non-acidic compartment number, suggests that Rab7 may facilitate the trafficking of dense-core granule compartments for fusion with the acidic compartments (a process I identified in Section 4.2.1.1), or alternatively it may be involved in their secretion. This would fit well with the observation that there are fewer, and smaller large acidic compartments in these cells (Figure 5.11D, 5.12B-C). However, given its roles in other cells, where Rab7 has been implicated in the fusion of autophagosomes with late endosomes or lysosomes, the former seems likely to be part of the explanation (Szatmári & Sass, 2014). The results presented here correlate well with previous studies of *Rab7* knockdown in secondary cells overexpressing CD63-GFP, where the numbers of non-acidic compartments increased (Redhai, 2016). Furthermore, the RNAi line employed here was shown to specifically reduce Rab7 protein levels in secondary cells by antibody staining (Redhai, 2016).

These non-cored compartments carried YFP-Rab6 protein on their surface when *Rab11*-RNAi expression was combined with the *YFP-Rab6* gene trap (Figure 5.13A). This result suggests that Rab11 mediates important trafficking steps required for the maturation of dense-core granules from Rab6-labelled precursor compartments. The specificity of the *Rab11* knockdown was confirmed by combining it with the *YFP-Rab11* gene trap, which showed that YFP-Rab11 protein levels were dramatically reduced in secondary cells, but

at normal levels in neighbouring main cells (Figure 5.13B). This knockdown construct has also been previously confirmed to specifically affect Rab11 protein levels in secondary cells using antibody staining (Redhai, 2016). This finding also correlates well with previous observations that showed Rab11 knockdown in CD63-GFP overexpressing cells reduced the number of non-acidic compartments in secondary cells (Redhai, 2016).

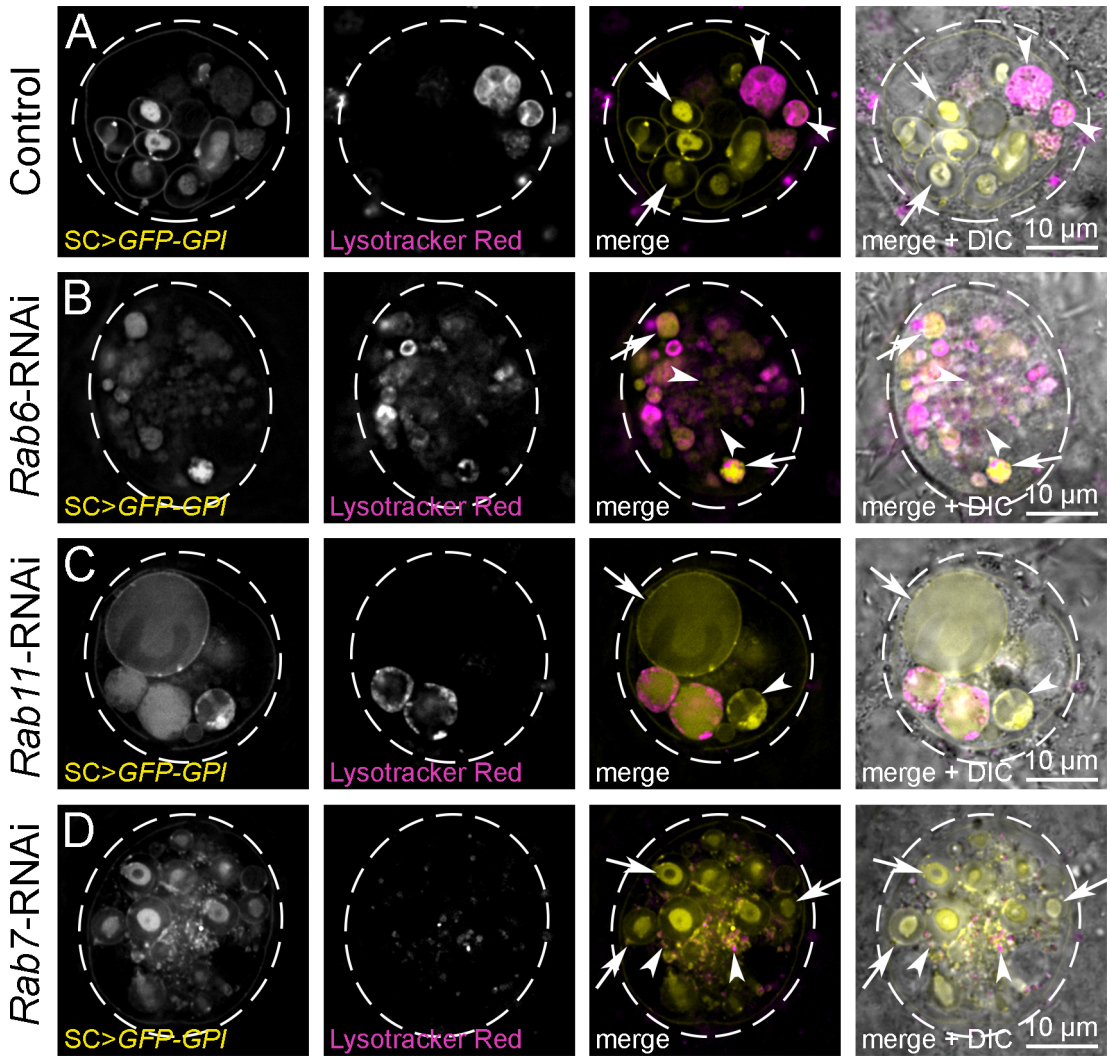

Control
Rab6-RNAi
Rab11-RNAi
Rab7-RNAi
A
B
C
D
SC>GFP-GPI
Lysotracker Red
merge
merge + DIC
10 µm

Figure 5.11 Rab6, Rab11 and Rab7 regulate different aspects of secondary cell dense-core granule biology

These panels display wide-field fluorescence and DIC images of secondary cells from 6-day-old virgin transgenic males selectively overexpressing GFP-GPI (yellow) in combination with different RNAi constructs targeting *Rab6*, *Rab11* and *Rab7*. The flies were incubated at 28.5°C following eclosion to induce GFP-GPI and RNAi expression using the GAL4-GAL80^{ts}-UAS system. All accessory glands were stained with Lysotracker Red (magenta). Representative secondary cell phenotypes are presented. Approximate secondary cell outlines are marked with a dashed line.
(A) Control secondary cells overexpressing GFP-GPI contain numerous dense-core granule compartments (arrows) and some large acidic compartments (arrowheads).
(B) In secondary cells expressing RNAi to target *Rab6*, the formation of large non-cored and dense-core granule compartments is disrupted. Most of the GFP-GPI traffics into the numerous acidic structures in the cell (arrows). In the central region of the cell, several small non-acidic GFP-GPI-labelled vesicles are observed (arrowheads).
(C) Secondary cells expressing RNAi to target *Rab11* contain large non-acidic compartments with diffuse GFP-GPI inside (arrow). Putative abnormal dense-core granules may also be present in some compartments (arrowhead).
(D) Secondary cells expressing RNAi to target Rab7 contain numerous dense-core granule compartments (arrows), but no large acidic compartments. Instead, the cells contain abundant small acidic compartments (arrowheads), many in close proximity to dense-core granule compartments.

The flies used in this figure consisted of combinations of *spi-GAL4, tub-GAL80^{ts}; UAS-GFP-GPI* with *UAS-Rab6*-RNAi (JF02640), *UAS-Rab11*-RNAi (JF02812), *UAS-Rab7*-RNAi (JF02377), or with no other construct (as a control).

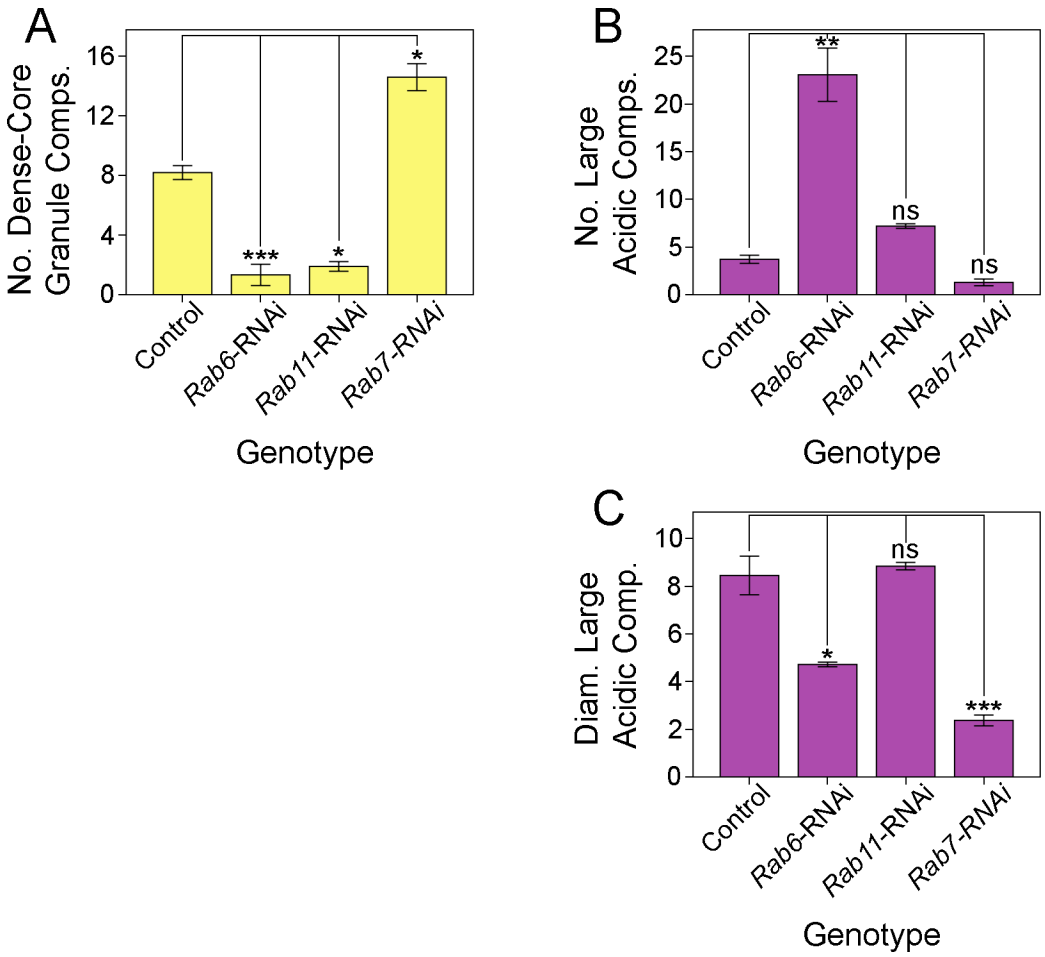

A
No. Dense-Core Granule Comps.
16
12
8
4
0
***
*
*
Control
Rab6-RNAi
Rab11-RNAi
Rab7-RNAi
Genotype
B
No. Large Acidic Comps.
25
20
15
10
5
0
**
ns
ns
Control
Rab6-RNAi
Rab11-RNAi
Rab7-RNAi
Genotype
C
Diam. Large Acidic Comp.
10
8
6
4
2
0
*
ns
***
Control
Rab6-RNAi
Rab11-RNAi
Rab7-RNAi
Genotype

Figure 5.12 Quantification of the effects of *Rab6*, *Rab11* and *Rab7* knockdown on dense-core granule compartments and large acidic compartments

These graphs highlight the differences between control secondary cells overexpressing GFP-GPI to those also expressing RNAi constructs targeting *Rab6*, *Rab11* and *Rab7*. Six-day-old male virgin flies were incubated at 28.5°C following eclosion to induce GFP-GPI and RNAi expression using the GAL4-GAL80^{ts}-UAS system. All accessory glands were stained with Lysotracker Red (magenta) to visualise and measure acidic compartments.
(A) Bar chart showing the average number of large (> 2 μm diameter) dense-core granule compartments, identified using both DIC microscopy and GFP-GPI localisation.
(B) Bar chart showing average number of large (> 2 μm diameter), Lysotracker Red-positive, acidic compartments in these backgrounds.
(C) Bar chart showing average size of largest acidic compartment in these genetic backgrounds.

The flies used for this figure consisted of combinations of *spi-GAL4, tub-GAL80^{ts}; UAS-GFP-GPI* with *UAS-Rab6*-RNAi (JF02640), *UAS-Rab11*-RNAi (JF02812), *UAS-Rab7*-RNAi (JF02377), or with no other construct (as a control). Statistical analysis is described in Section 2.23 (n=6 glands for all genotypes, with 5 cells per gland analysed). *P≤0.05; **P≤0.01; ***P≤0.001; ns = not significant.

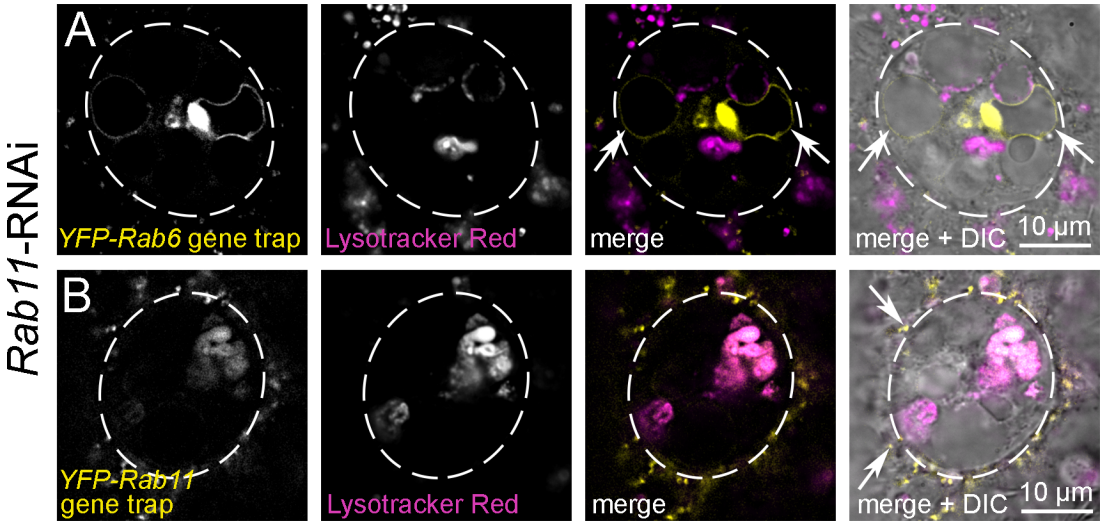


Figure 5.13 The large non-cored compartments in *Rab11*-knockdown secondary cells are Rab6-positive

These panels consist of wide-field fluorescence and DIC images of secondary cells from 6-day-old virgin transgenic males selectively expressing an RNAi construct targeting *Rab11* in combination with the *YFP-Rab6* or *YFP-Rab11* gene trap. The flies were incubated at 28.5°C following eclosion to induce RNAi expression using the GAL4-GAL80^{ts}-UAS system. Accessory glands were stained with Lysotracker Red (magenta). Approximate secondary cell outlines are marked with a dashed line.
(A) YFP-Rab6 (yellow) localises on the surface of the very large non-cored compartments within secondary cells expressing *Rab11*-RNAi.
(B) Main cells express YFP-Rab11 (yellow, arrows), but it is strongly silenced in secondary cells by *Rab11*-RNAi.

The specific genotypes used in this figure are *spi-GAL4, tub-GAL80^{ts}; YFP^{Myc}-Rab6* and *spi-GAL4, tub-GAL80^{ts}; YFP^{Myc}-Rab11* in combination with *UAS-Rab11*-RNAi (VDRC 22198).

The expression of several other Rab GTPases including *Rab10*, *Rab19* and *Rab21*, which had been localised to subsets of dense-core granule compartments in secondary cells (Section 3.2.2.4), was also knocked down using RNAi. However, none of these knockdowns resulted in phenotypes that were consistently dramatically different to controls when combined with GFP-GPI overexpression in secondary cells (Figure 5.14A-D). A more detailed quantitative analysis will likely be required to tease out more subtle roles in dense-core granule biology.

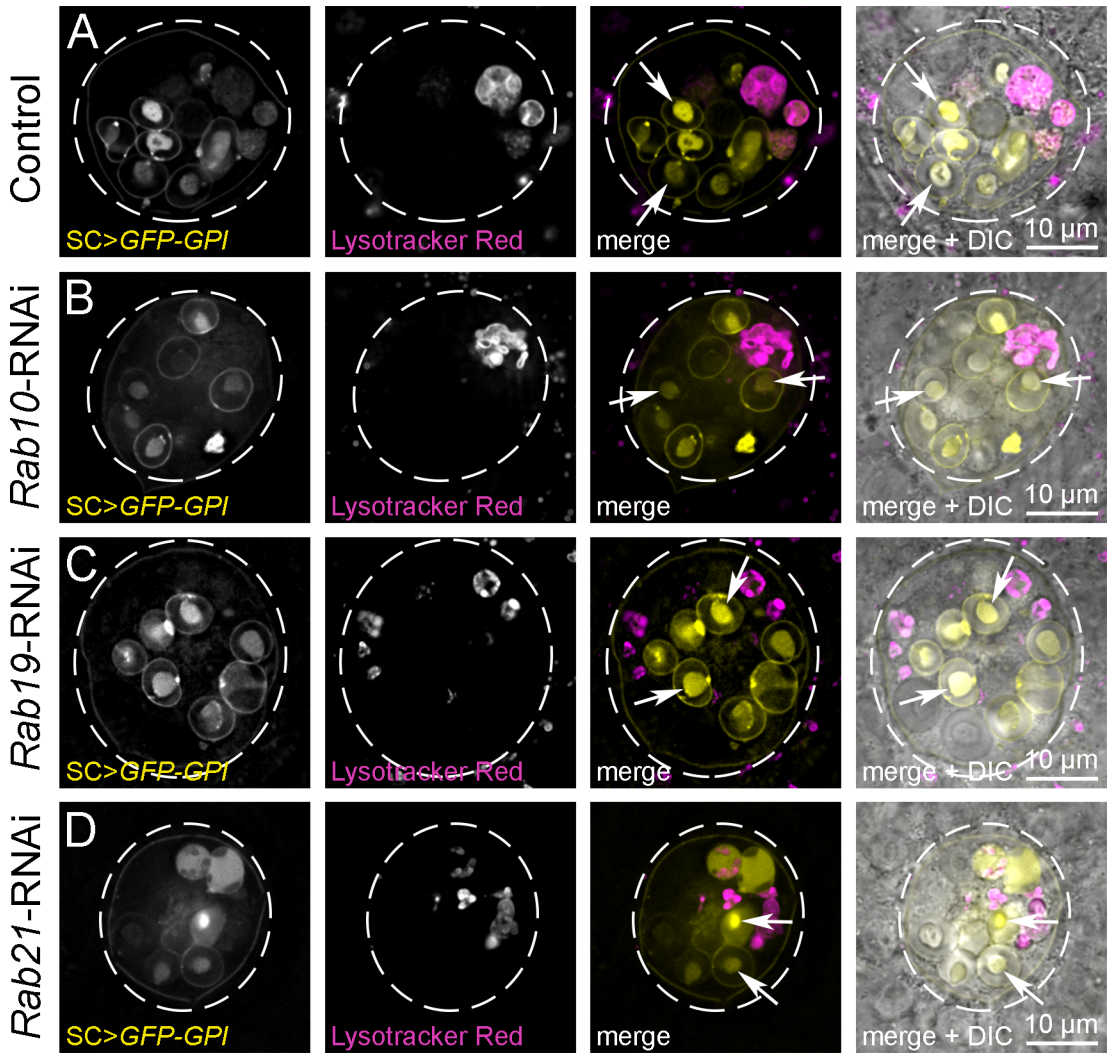


Figure 5.14 Preliminary analysis of the roles of Rab10, Rab19 and Rab21 in secondary cell dense-core granule compartments

These panels display wide-field fluorescence and DIC images of secondary cells from 6-day-old virgin transgenic males selectively overexpressing GFP-GPI (yellow) in combination with different RNAi constructs targeting *Rab10*, *Rab19* and *Rab21*. The flies were incubated at 28.5°C following eclosion to induce GFP-GPI and RNAi expression using the GAL4-GAL80^{ts}-UAS system. All accessory glands were stained with Lysotracker Red (magenta). Approximate secondary cell outlines are marked with a dashed line. (A-D) Compared with controls, secondary cells silenced for Rab10, Rab19 and Rab21 do not display gross changes in the morphology of dense-core granule compartments (arrows).

The flies used in this figure consisted of combinations of *spi-GAL4, tub-GAL80^{ts}; UAS-GFP-GPI* with *UAS-Rab10-RNAi* (JF02058), *UAS-Rab19-RNAi* (HMS00592), *UAS-Rab21-RNAi* (JF03338), or with no other transgene (as a control).

5.2.2.2 SNAREs regulate large dense-core granule compartment biogenesis in secondary cells

Previous studies have shown that the Qbc-SNARE, SNAP24, is involved in the secretion of large dense-core granules from secondary cells (Redhai *et al*., 2016). However, little was known about the SNARE complexes that mediate the formation of the large dense-core granule compartments. In neuroendocrine cells, the fusion between immature secretory granules near the trans-face of the Golgi is an important part of their maturation (Tooze *et al*., 2001). Previous studies have implicated the Qc-SNARE, Syntaxin 6 (*Syx6*; Wendler *et al*., 2001), in mediating these fusion events. When *Syx6* expression was knocked down in secondary cells, however, dense-core granule compartments were still formed normally (Figure 5.15A-B), suggesting that their formation may be dependent on a different fusion complex. Rather, when the expression of the Qa-SNARE, *Syntaxin 5* (*Syx5*; Banfield *et al*., 1994) was silenced using RNAi, the resulting secondary cells contained abnormally small YFP-Rab11-positive non-acidic compartments (Figure 5.15C). This suggested that fusion events involved in forming large compartments had been disrupted in these cells.

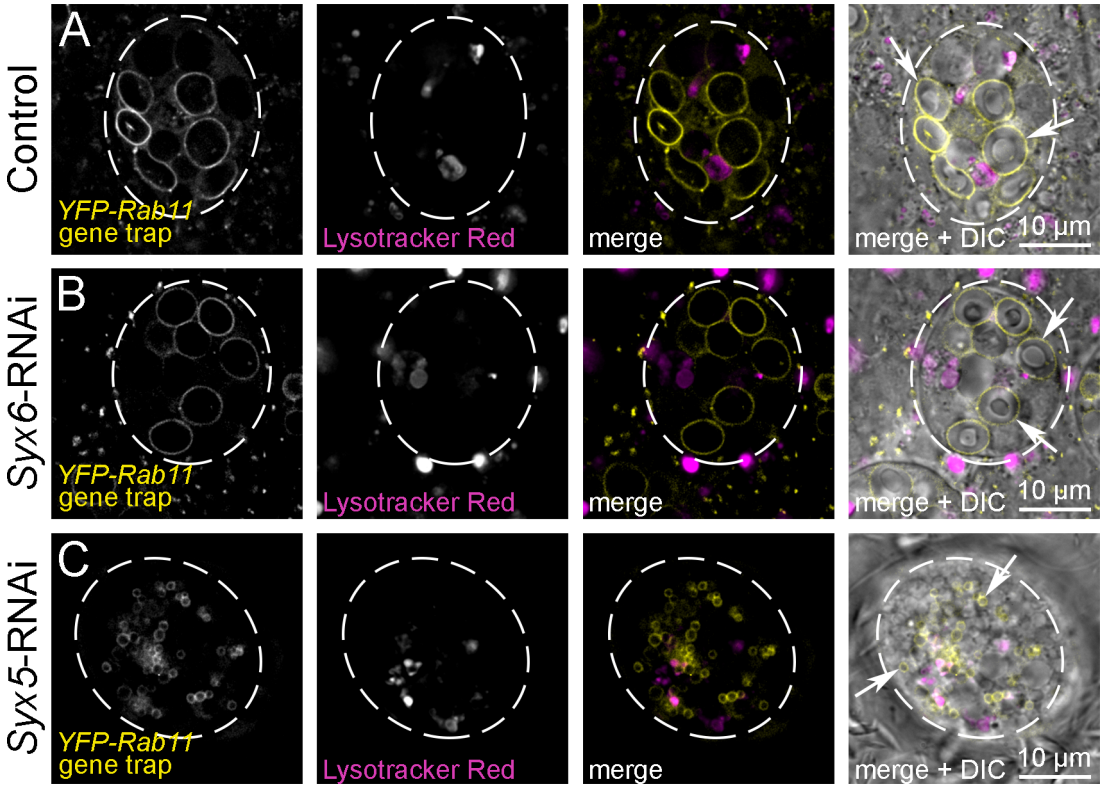


Figure 5.15 Syx5, but not Syx6, regulates the formation of large Rab11-positive compartments in secondary cells

These panels consist of wide-field fluorescence and DIC images of secondary cells from 6-day-old virgin transgenic males selectively expressing RNAi constructs targeting either *Syx6 or Syx5* in combination with the *YFP-Rab11* gene trap. The flies were incubated at 28.5°C following eclosion to induce RNAi expression using the GAL4-GAL80^{ts}-UAS system. All accessory glands were stained with Lysotracker Red (magenta). Approximate secondary cell outlines are marked with a dashed line.
(A) Control secondary cell with no RNAi expressed. Individual cells contain YFP-Rab11-positive dense-core granule compartments (yellow, arrows)
(B) Silencing of *Syx6* with RNAi in secondary cells does not affect the formation of large YFP-Rab11-positive compartments (arrows).
(C) Expression of an RNAi construct targeting *Syx5* results in the formation of many small YFP-Rab11 compartments (arrows). These cells also contain smaller acidic compartments (magenta), and numerous other non-acidic compartments that do not carry YFP-Rab11 on their surface.

The specific genotypes of the flies used in this figure are *spi-GAL4, tub-GAL80^{ts}; YFP^{Myc}-Rab11* in combination with *UAS-Syx6*-RNAi (JF03125) or *UAS-Syx5*-RNAi (VDRC 3859), or no other construct (as a control).

5.2.2.3 Conserved regulators of granule biogenesis, the AP-1 complex and the Arf79F GTPase regulate the maturation of dense-core granules

The large size of secondary cell dense-core granule compartments has enabled me to study the genetic mechanisms underlying their biogenesis in great detail. However, it was important to determine whether the formation of these unusually large compartments in secondary cells is similarly regulated to the formation of much smaller dense-core granule compartments, which are common in other secretory cell types from humans to nematodes. To this end, I studied the function of fundamental regulators of dense-core granule formation in these other cell types, including the Adaptor Protein complex 1 (AP-1) and the *ADP ribosylation factor at 79F* (*Arf79F*), a small Arl family GTPase homologous to mammalian *Arf1* (Bonnemaison *et al*., 2013; Kim *et al*., 2006). This work was done in collaboration with F. Castellanos, another DPhil student in the lab, who reports the functions of these genes in detail (Castellanos, 2017).

In *Drosophila*, the AP-1 complex consists of three different subunits, the γ, μ1 and ς1 adaptins (Boehm & Bonifacino, 2001), and is thought to participate in the maturation of immature secretory granules by facilitating the removal of non-specific proteins (Bonnemaison *et al*., 2013). The Arf79F GTPase, on the other hand, participates in the recruitment of the AP-1 complex onto the immature secretory granule membranes (Ren *et al*., 2013; Dittie *et al*., 1996; Austin *et al*., 2000). I found that knockdown of two different components of the AP-1 complex using multiple RNAi's targetting the adaptins γ and μ1, or Arf79F, with multiple RNAi's targeting either component, resulted in major defects in secondary cell dense-core granule formation (n=≥10 glands from

individual flies of each genotype, with 5 cells imaged within each gland; Figure 5.16A-D). Although the detailed characterisation of these RNAi phenotypes in living GFP-GPI overexpressing cells is reported elsewhere (Castellanos, 2017), I have independently carried out further research to supplement these observations. I have characterised the Rab GTPases that associate with the abnormal subcellular compartments formed within these cells. I have also used immunological techniques to identify the normal subcellular localisations of AP-1γ and Arf79F, to improve the interpretation of their loss-of-function phenotypes.

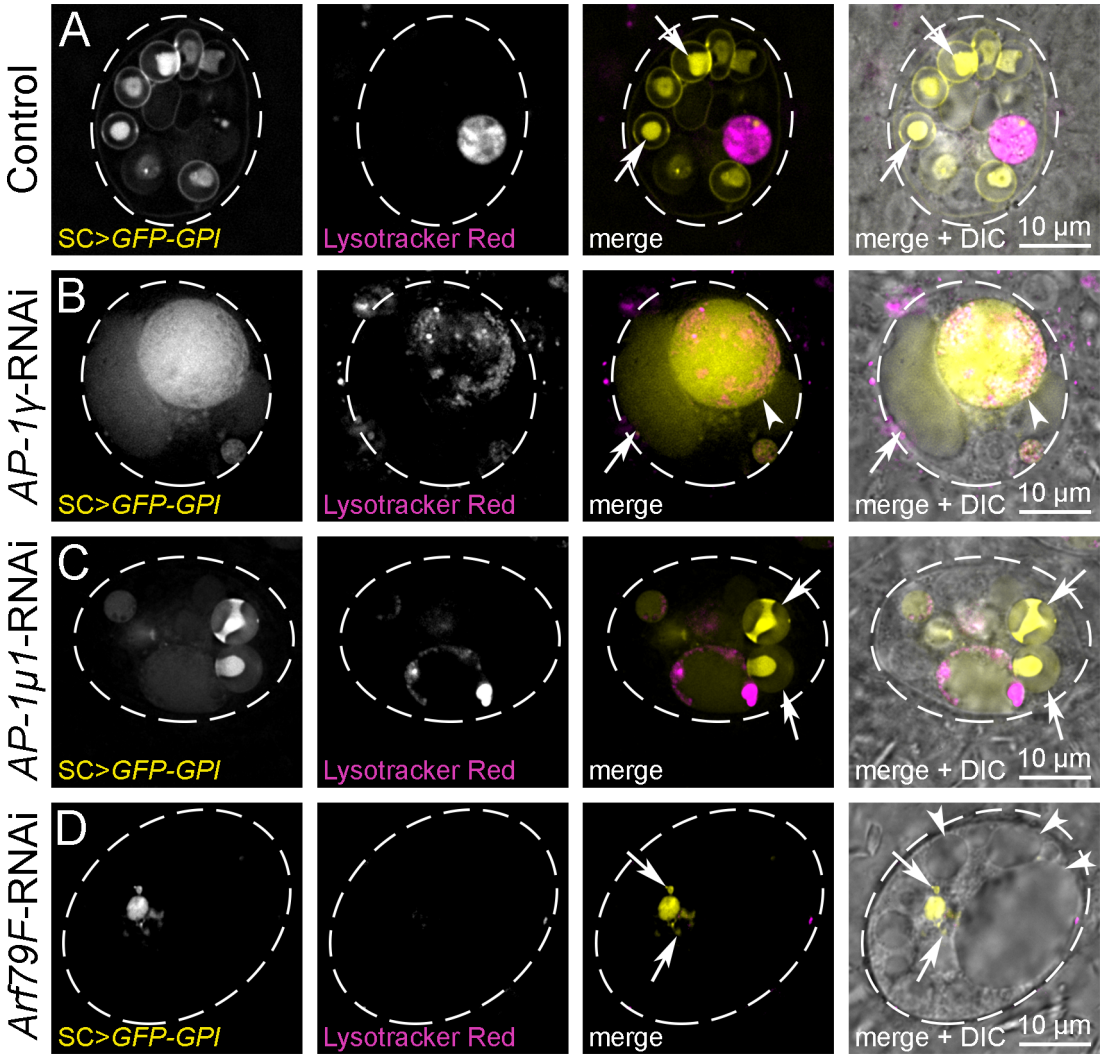

Control
A
SC>GFP-GPI
Lysotracker Red
merge
merge + DIC
10 µm
AP-1γ-RNAi
B
SC>GFP-GPI
Lysotracker Red
merge
merge + DIC
10 µm
AP-1µ1-RNAi
C
SC>GFP-GPI
Lysotracker Red
merge
merge + DIC
10 µm
Arf79F-RNAi
D
SC>GFP-GPI
Lysotracker Red
merge
merge + DIC
10 µm

Figure 5.16 The AP-1 complex and Arf79F regulate dense-core granule formation in secondary cells

These panels display wide-field fluorescence and DIC images of secondary cells from 6-day-old virgin transgenic males selectively overexpressing GFP-GPI (yellow) in combination with different RNAi constructs targeting *AP-1γ, AP-1μ1*, and *Arf79F.* The flies were incubated at 28.5°C following eclosion to induce GFP-GPI and RNAi expression using the GAL4-GAL80^{ts}-UAS system. All accessory glands were stained with Lysotracker Red (magenta). Approximate secondary cell outlines are marked with a dashed line
The functions of all these genes in secondary cells were studied in collaboration with F. Castellanos. The detailed analysis of the phenotypes with GFP-GPI-expressing cells is presented in his thesis, and the imaging data are presented here only as a reference for interpreting the analysis in Figures 5.17 and 5.18.
(A) Representative example of a secondary cell overexpressing GFP-GPI without any other transgene.
(B) Silencing of *AP-1γ* dramatically affects dense-core granule formation. GFP-GPI (yellow) localises diffusely within the lumen of a large non-acidic compartment (arrow) and a large acidic compartment (arrowhead), but is not concentrated at the limiting membrane of either.
(C) In secondary cells where the μ1 subunit of AP-1 is knocked down, fewer dense-core granules (arrows), some of them defective, are observed. Furthermore, GFP-GPI is absent from the limiting membrane of the non-acidic compartments, unlike controls.
(D) When *Arf79F* is knocked down in secondary cells, dense-core granules are not formed inside the large non-acidic compartments (arrowheads), some of which are highly expanded. GFP-GPI is not trafficked to these compartments and instead localises in a central region of the cell, inside some small vesicular structures (arrows).

The flies used in this figure consisted of combinations of *spi-GAL4, tub-GAL80^{ts}; UAS-GFP-GPI* with *UAS-AP-1γ*-RNAi (JF02684), *UAS-AP-1μ1*-RNAi (VDRC 24017), *UAS-Arf79F*-RNAi (VDRC 23082), or with no other transgene (as a control).

The localisation of the fusion proteins expressed from either *YFP-Rab6* or *YFP-Rab11* gene trap flies were examined in secondary cells that also expressed an RNAi construct targeting *AP-1γ*. The cells often contained a single very large non-acidic compartment, which carried relatively low levels of the precursor compartment marker, YFP-Rab6, on its limiting membrane, but no detectable YFP-Rab11 (Figure 5.17A-B). These data showed that, similar to when *Rab11* was knocked down by RNAi, the maturation of the dense-core precursor compartment was blocked. However, the very large size and irregular shape of the non-cored compartment suggested that AP-1 functions differently to Rab11, which produced a number of smaller spherical non-cored compartments when its expression was knocked down (Section 5.2.2.1). In support of this idea, relatively more GFP-GPI accumulated in the interior of the precursor compartment when *AP-1γ* expression was knocked down when compared to *Rab11* knockdown (Figure 5.11, 5.16). Both YFP-Rab6 and YFP-Rab11 were observed at high levels on small vesicles in a central region between the large acidic and non-acidic compartments, possibly on Golgi cisternae, a result that needs to be confirmed by immunological techniques (Figure 5.17A-B). It is possible that the concentration of these GTPases in this region reflects the emergence of defective secretory compartments from the trans-Golgi network in the absence of *AP-1γ*.

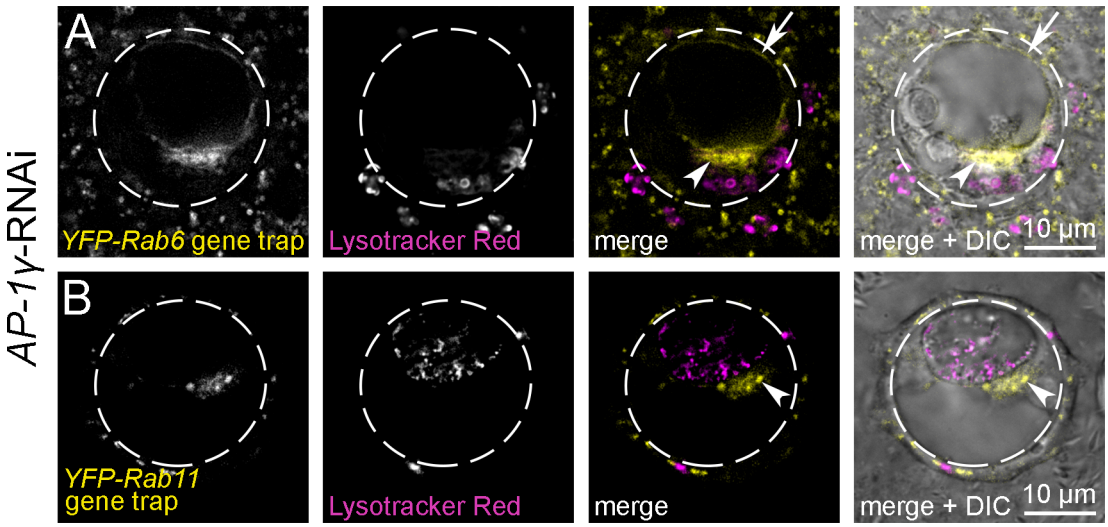


Figure 5.17 The association of YFP-Rab GTPases with the large non-cored, non-cored compartments in *AP-1* knockdown secondary cells

All panels consist of wide-field fluorescence and DIC images of secondary cells from 6-day-old virgin transgenic males. Panels (A-B) display secondary cells that selectively express an RNAi construct targeting *AP-1γ* in combination with the *YFP-Rab6* or *YFP-Rab11* gene traps. All flies were incubated at 28.5°C following eclosion to induce RNAi expression using the GAL4-GAL80^{ts}-UAS system, and their accessory glands were stained with Lysotracker Red (magenta). Approximate secondary cell outlines are marked with a dashed line.
(A-B) The very large non-cored compartment within *AP-1γ*-RNAi-expressing secondary cells carries YFP-Rab6 (arrow), but not YFP-Rab11 on its surface. Both YFP-tagged GTPases are also found on small non-acidic vesicles in a central region of the cell, in between the large non-acidic and acidic compartments (arrowheads).

The specific genotypes used in this figure included *UAS-AP-1γ*-RNAi (JF02684) in combination with either *spi-GAL4, tub-GAL80^{ts}; YFP^{Myc}-Rab6* or *spi-GAL4, tub-GAL80^{ts}; YFP^{Myc}-Rab11*.

In collaboration with F. Castellanos, the localisation of the AP-1 complex in secondary cells was studied using immunological staining of the AP-1γ subunit in cells overexpressing GFP-GPI. This showed that AP-1γ localised as puncta on subdomains of the central Rab6-positive compartment (Figure 5.18A-A'), and on several closely associating small vesicles in the Golgi-rich region, consistent with its proposed role in removing proteins that are not destined for the dense-core granule from the central compartment.

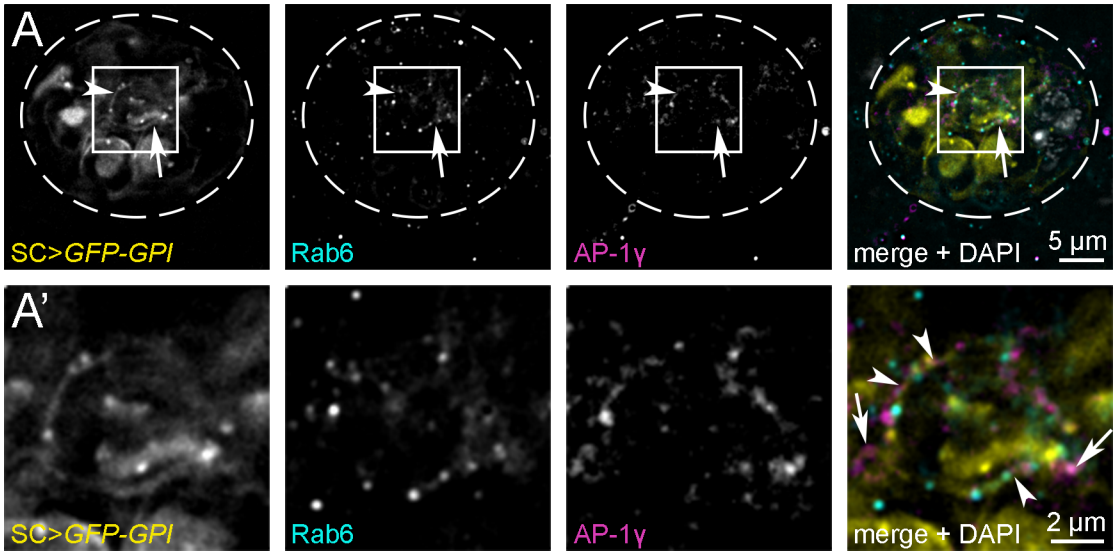


Figure 5.18 AP-1γ localises on and near the surface of the central Rab6-positive compartment in secondary cells overexpressing GFP-GPI

These panels show wide-field fluorescence images of a secondary cell from a 6-day-old virgin transgenic male selectively overexpressing GFP-GPI. The flies were incubated at 28.5°C following eclosion to induce GFP-GPI overexpression using the GAL4-GAL80^{ts}-UAS system. Their accessory glands were immunostained with anti-Rab6 and anti-AP-1γ antibodies, and nuclei were marked using DAPI staining. This analysis was performed in collaboration with F. Castellanos. Approximate cell outlines are shown using a dashed line.
(A) AP-1γ (magenta) staining in secondary cells overexpressing GFP-GPI (yellow) is primarily enriched around the central Rab6-marked (cyan) compartment (arrow). Box highlights this region, which is enlarged in (A').
(A') In addition to localising in subdomains on the surface of the centrally located GFP-GPI-marked compartment (arrowheads), AP-1γ is found on some closely associated vesicular structures (arrows).

The specific genotype of the flies used in this figure is: *w; spi-GAL4, tub-GAL80^{ts} / +; UAS-GFP-GPI / +*.

Given that Arf79F is thought to recruit the AP-1 complex to immature secretory granule compartments, it might have been expected to cause a similar phenotype upon knockdown. However, in contrast to the knockdown of AP-1 complex subunits, when RNAi knocked down *Arf79F* expression in secondary cells, numerous non-acidic compartments were formed, though they all lacked dense-core granules by DIC microscopy (Figure 5.16D). Furthermore, GFP-GPI was found inside small centrally located vesicles, possibly the Golgi apparatus, and was not observed on any of the many large non-cored compartments formed within the cell. Subsequent analysis of the large non-cored compartments showed that they carried neither YFP-Rab6 nor YFP-Rab11 on their surface (Figure 5.19A-B), suggesting that Arf79F activity may be required for their recruitment or to stabilise them on the surface of the forming compartments. Instead, YFP-Rab11 localised to a number of small vesicles scattered throughout the *Arf79F*-RNAi cells (Figure 5.19B). YFP-Rab6, on the other hand, localised to a central region of the cell, on a number of small vesicles, that might be Golgi-associated (5.19A). Given the absence of these important regulators of compartment biogenesis on the surface of the large non-acidic compartments, it is perhaps unsurprising that the dense-core granules failed to form.

Interestingly, YFP-Rab1, which localised on small cis-Golgi vesicles in normal cells (Section 3.2.2.1), was found on the surface of some of the large non-acidic compartments in the *Arf79F* knockdown cells (Figure 5.19C). However, the majority of these compartments were also YFP-Rab1-negative and therefore remain uncharacterised. Taken together, these data show that the normal secondary cell trafficking routes, and their overall subcellular

organisation, are severely disrupted in cells depleted of *Arf79F*. It also suggests that Arf79F may be functioning upstream of AP-1, possibly within the Golgi cisternae, as secretory cargos appear trapped there, to modify the trafficking or molecular composition of budding vesicles.

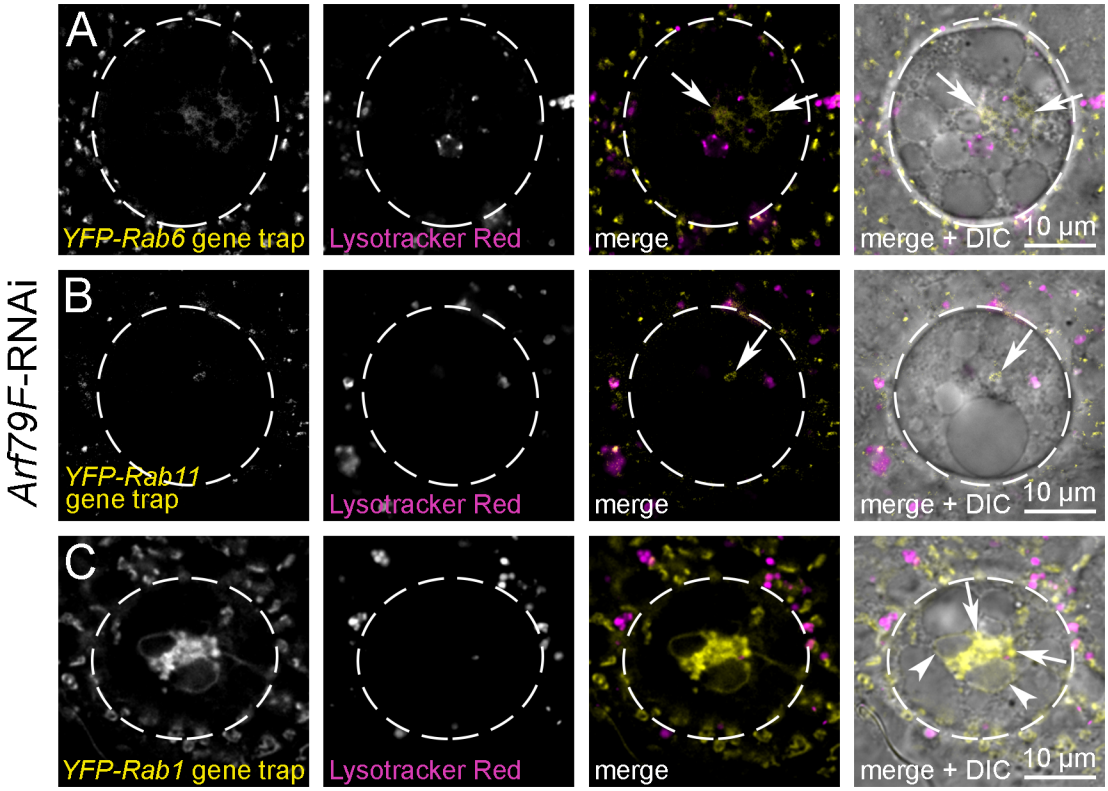


Figure 5.19 The association of YFP-Rab GTPases with the large non-cored, non-cored compartments in *AP-1* and *Arf79F* knockdown secondary cells

All panels consist of wide-field fluorescence and DIC images of secondary cells from 6-day-old virgin transgenic males. Panels (A-B) display secondary cells that selectively express an RNAi construct targeting *Arf79F* in combination with the *YFP-Rab6*, *YFP-Rab11* or *YFP-Rab1* gene traps. All flies were incubated at 28.5°C following eclosion to induce RNAi expression using the GAL4-GAL80^{ts}-UAS system, and their accessory glands were stained with Lysotracker Red (magenta). Approximate secondary cell outlines are marked with a dashed line.
(A-B) Neither YFP-Rab6 nor YFP-Rab11 (both yellow) localise on the surface of the large non-acidic compartments in *Arf79F*-RNAi-expressing cells. They are both found on some smaller non-acidic vesicles in the central region of the cells.
(C) Some of the large non-cored, non-acidic compartments in *Arf79F*-RNAi-expressing secondary cells carry YFP-Rab1 on their surface (arrowheads). YFP-Rab1 is also found at high levels on closely associated smaller vesicular structures (arrows). Acidic compartments are reduced in size.

The specific genotypes used in this figure included *UAS-Arf79F*-RNAi (VDRC 23082) in combination with either *spi-GAL4, tub-GAL80^{ts}; YFP^{Myc}-Rab6* or *spi-GAL4, tub-GAL80^{ts}; YFP^{Myc}-Rab11* or *spi-GAL4, tub-GAL80^{ts}; YFP^{Myc}-Rab1*.

5.2.2.4 Clathrin may regulate the trafficking of GFP-GPI in secondary cells

Clathrin is a highly conserved protein complex involved in the trafficking of subcellular vesicles, during both endocytosis and in the secretory pathway from the Golgi apparatus. It is a heterohexamer composed of three Clathrin light chains (*Clc*) and three Clathrin heavy chains (*Chc*). Clathrin is recruited to intracellular membranes by Adaptor Protein complexes, including the AP-1 complex, and is thought to facilitate removal of non-specific protein cargoes from immature secretory granules (Bonnemaison *et al*., 2013).

I studied the localisation of Clathrin in secondary cells by overexpressing a GFP-tagged form of *Clc* (*GFP-Clc*; Chang *et al*., 2002). I found that it localised on the surface of many, but not all, of the non-acidic compartments in secondary cells. Specifically, it localised in subdomains of both the large non-cored compartments, and a subset of the dense-core granule compartments (Figure 5.20A-A'). Within the non-acidic compartments, GFP-Clc was occasionally localised on intraluminal puncta, likely corresponding to ILVs (Figure 5.20B). It was also localised on a number of small vesicles throughout the cell, some of which were in close association with the apical and basolateral plasma membranes (Figure 5.20A), possibly coating endocytic vesicles, whilst others localised in between the large subcellular compartments (Figure 5.20A).

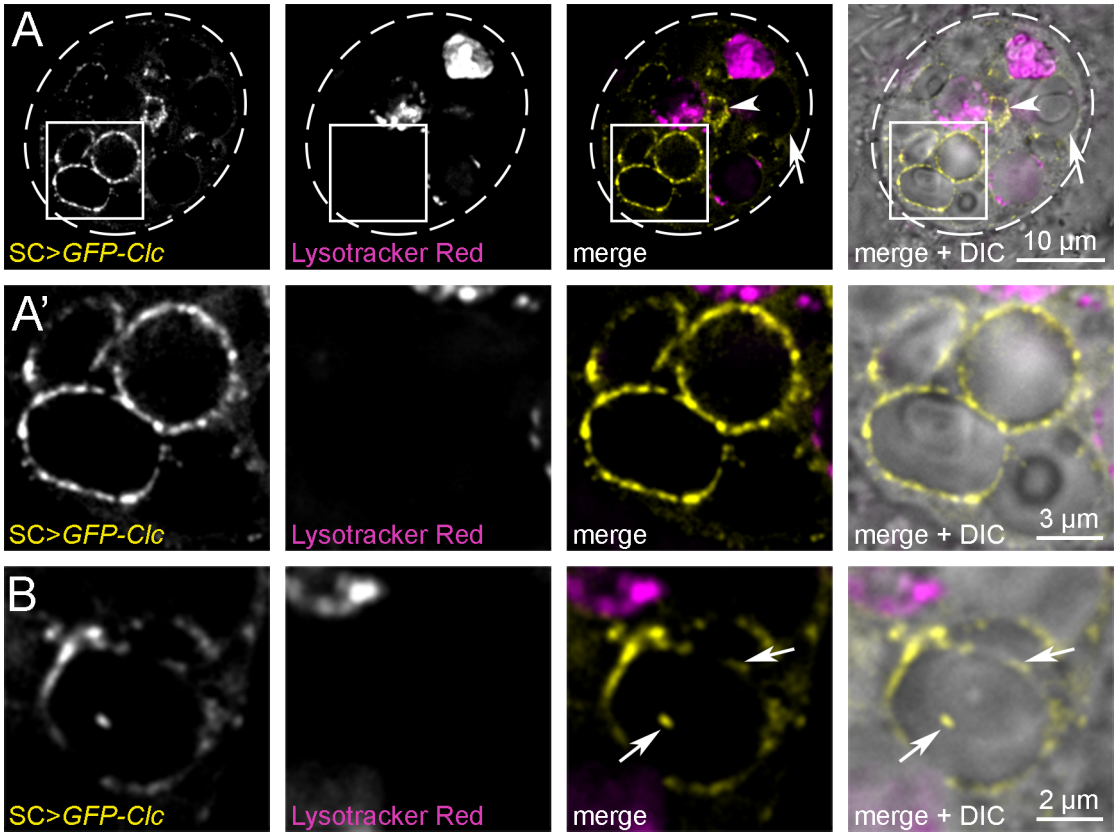


Figure 5.20 Clathrin light chain associates with the surface of large non-acidic compartments in secondary cells

These panels show wide-field fluorescence and DIC images of secondary cells from 6-day-old virgin transgenic males selectively overexpressing a GFP tagged form of Clc, one of the main subunits of Clathrin (yellow). The flies were incubated at 28.5°C following eclosion to induce GFP-Clc expression using the GAL4-GAL80^{ts}-UAS system. Accessory glands were stained with Lysotracker Red to mark acidic compartments (magenta). Approximate cell outlines are shown using a dashed line.
(A) Overexpressed GFP-Clc localises at high levels on the surface the large non-cored compartments in secondary cells. It is also present on a subset of dense-core granule compartments, but absent from others (arrow). In addition, Clc-GFP localises on numerous small vesicles throughout the cell, and in punctate regions at or near the plasma membrane. Some moderately sized irregular non-cored compartments also carry GFP-Clc at high levels on their surface (arrowhead). The box in (A) highlights the region enlarged in (A'). (A') GFP-Clc exhibits a punctate localisation pattern on the surface of the large non-acidic compartments in secondary cells.
(B) High magnification image showing that GFP-Clc localises on intraluminal puncta within dense-core granule compartments.
The specific genotype of the flies used in this figure is w; *w; tub-GAL80ts / +; dsx-GAL4 / UAS-GFP-Clc*.

This localisation study suggested that Clathrin may be playing roles in dense-core granule biology in secondary cells, and so a knockdown strategy was employed to better understand its function. *Chc* expression was silenced in secondary cells by expression of two different RNAi constructs, and the phenotypes studied in cells overexpressing GFP-GPI by wide-field fluorescence and DIC microscopy. Neither RNAi construct produced obvious defects in dense-core granule compartment number assessed by DIC microscopy, but one RNAi had a variable effect on GFP-GPI trafficking (Figure 5.21A-B). In a majority of the cells analysed, all of the GFP-GPI expressed in secondary cells was trafficked into the large acidic compartment or plasma membrane, rather than the dense-core granule compartments (Figure 5.21B), a phenotype never observed in wild type controls. Further analysis, in which knockdown is confirmed, is required to determine whether Clathrin plays a role in dense-core granule loading in secondary cells. Such a role might have been expected given the essential functions of Adaptor Protein complex AP-1 in dense-core granule assembly.

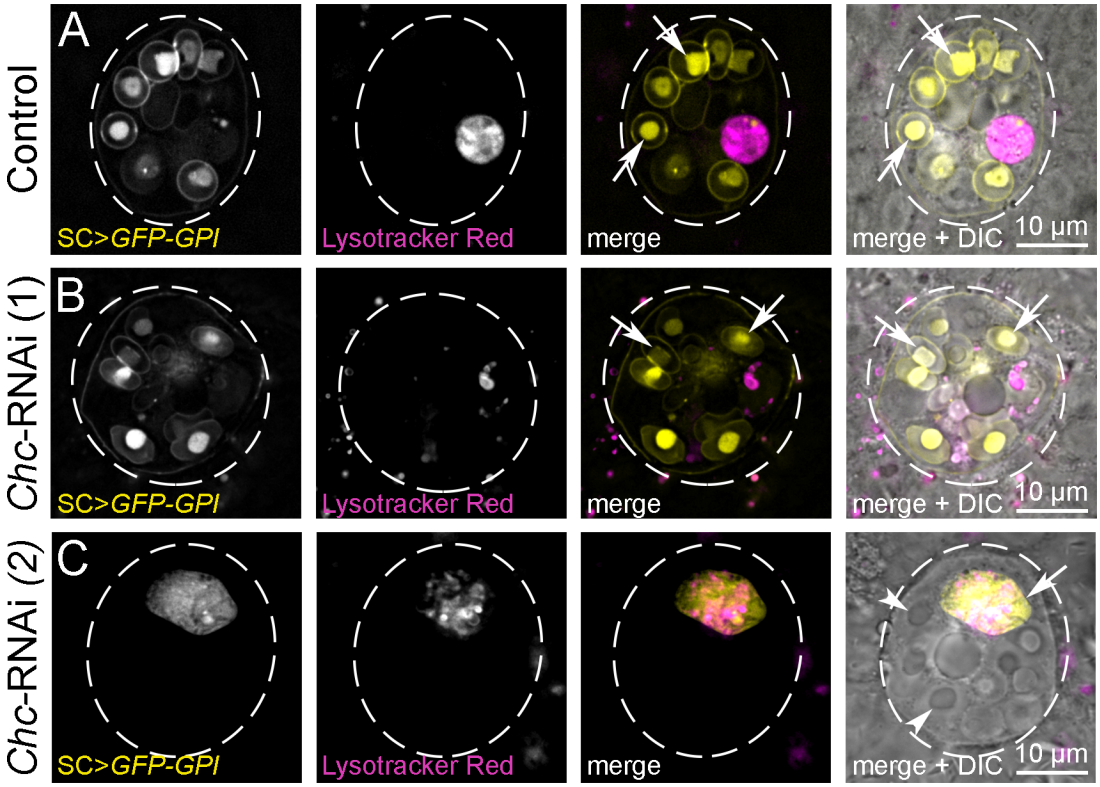


Figure 5.21 Knockdown of Clathrin components in secondary cells may affect trafficking of overexpressed GFP-GPI

These panels show wide-field fluorescence and DIC images of secondary cells from 6-day-old virgin transgenic males selectively overexpressing GFP-GPI (yellow) in combination with two different RNAi constructs targeting *Chc.* The flies were incubated at 28.5°C following eclosion to induce GFP-GPI and RNAi expression using the GAL4-GAL80^{ts}-UAS system. All accessory glands were stained with Lysotracker Red (magenta). Approximate cell outlines are shown using a dashed line.
(A-B) Expression of *Chc*-RNAi (1) in secondary cells does not majorly affect trafficking of GFP-GPI, which localises to dense-core granules (arrows) and the limiting membrane of large non-acidic compartments in a similar manner to controls.
(C) Silencing of *Chc* with a different RNAi construct causes GFP-GPI to accumulate in the large acidic compartment (arrow), whilst the dense-core granules (arrowheads) lack any GFP-GPI.

The flies used in this figure consisted of combinations of *spi-GAL4, tub-GAL80^{ts}; UAS-GFP-GPI* with *UAS-Chc*-RNAi lines 1 (JF02681) and 2 (HMS01222).

5.2.2.5 A novel role for the ESCRT components in dense-core granule biogenesis

In Chapter 4, I showed that the non-acidic dense-core granule compartments of secondary cells are filled with numerous ILVs, which are packaged with important signalling molecules and subsequently secreted as exosomes. I also showed that ILV formation within the secondary cell compartments is dependent on members of the *ESCRT* pathway, including *shrb* (Section 4.2.2). Interestingly, whilst undertaking live-cell imaging of secondary cells overexpressing GFP-GPI, I observed that small intraluminal puncta, presumably vesicles, appeared to transfer GFP-GPI into the dense-core granule (Figure 5.22A-B). This suggested that certain cargos might be delivered to the dense-core granules by ILVs.

To test this hypothesis, I used RNAi to silence the ESCRT-III component *shrb* in secondary cells that overexpressed GFP-GPI. These cells showed highly perturbed dense-core granule formation (Figure 5.22C-C'). Diffuse GFP-GPI was observed within the lumen of large non-acidic compartments, and was highly concentrated in membrane subdomains of the formed compartments. However, it was not packaged within a clear dense-core granule. Together, these data suggest that ILVs within these compartments play essential roles in dense-core granule biogenesis. However, it will be important to confirm this phenotype using electron microscopy.

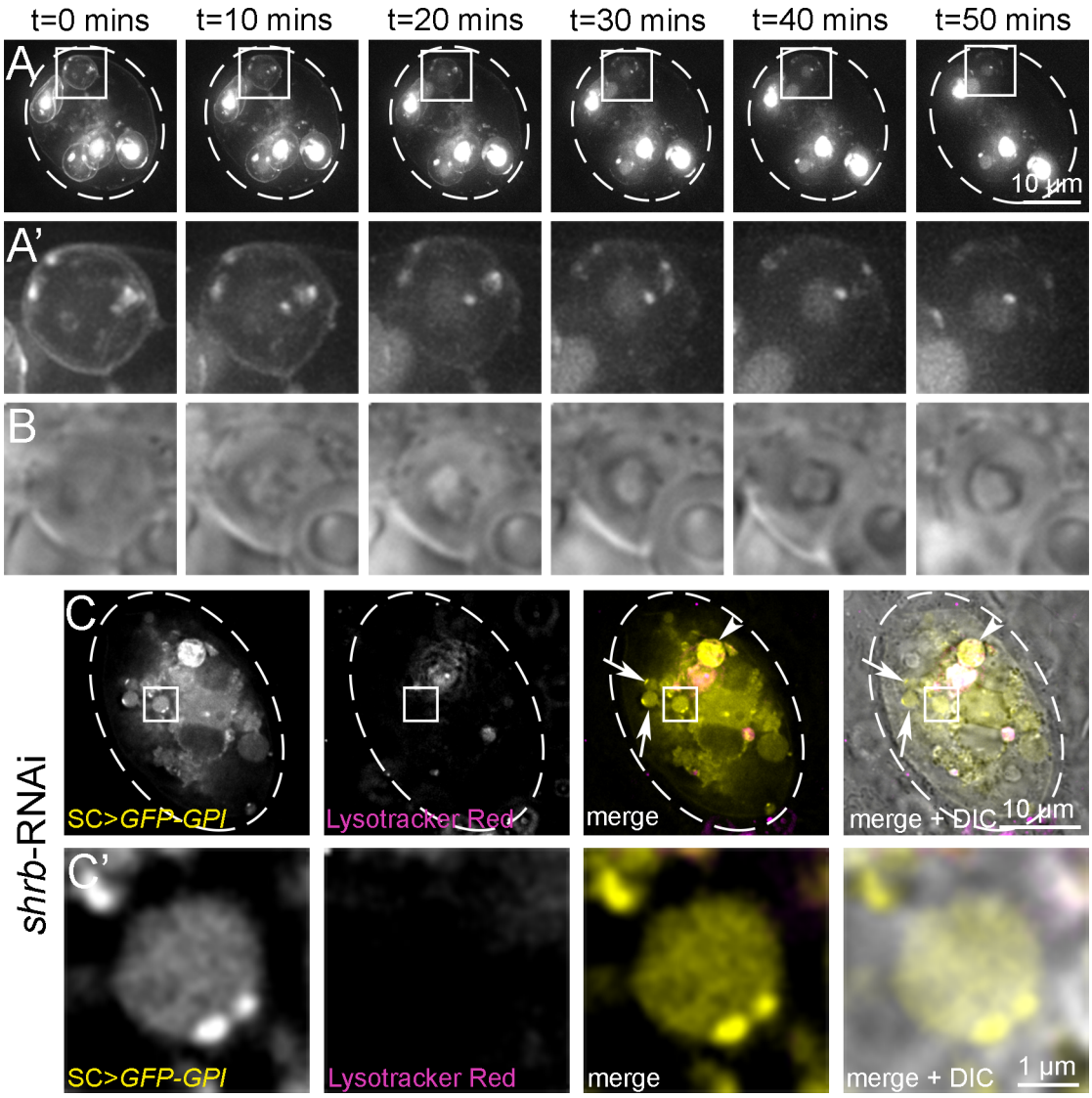

t=0 mins
t=10 mins
t=20 mins
t=30 mins
t=40 mins
t=50 mins
A
10 µm
A'
B
shrb-RNAi
C
SC>GFP-GPI
Lysotracker Red
merge
merge + DIC
10 µm
C'
SC>GFP-GPI
Lysotracker Red
merge
merge + DIC
1 µm

Figure 5.22 ILVs may facilitate dense-core granule formation

All panels display wide-field fluorescence and DIC images of secondary cells from 6-day-old virgin transgenic males selectively overexpressing GFP-GPI (yellow). The flies were incubated at 28.5°C following eclosion to induce GFP-GPI expression using the GAL4-GAL80^{ts}-UAS system. Panel (A-A') is a time-series of fluorescent microscopy images specifically of GFP-GPI (white). The images are maximum intensity projections of 4 µm thickness, extending the depth of an individual compartment in a secondary cell. Panel (B) is an individual z-plane through the same compartment highlighted in (A-A'), but imaged with DIC. Panels (C-C') show secondary cells that also express an RNAi constructs targeting *shrb*, in addition to overexpressing GFP-GPI (yellow). This gland was stained with Lysotracker Red (magenta). Approximate cell outlines are shown using a dashed line.
(A-A') Time-lapse imaging shows that bright GFP-GPI-positive (white) ILVs, observed as punctate structures in the lumen of the compartment highlighted with a box in (A) and enlarged in (A'), appear to transfer their fluorescence to the dense-core granule at the compartment's interior.
(B) Simultaneously to the observations in (A-A), a dense-core granule gradually becomes visible by DIC microscopy.
(C-C') In secondary cells overexpressing GFP-GPI (yellow), silencing of *shrb* with RNAi results in abnormal dense-core granule formation. GFP-GPI is observed diffusely throughout the lumen of non-acidic compartments (arrows), and in bright punctate regions near the limiting membrane. Some GFP-GPI is also observed inside the acidic compartments (magenta; arrowhead). The box highlights the region enlarged in (C').

The specific genotype of the flies used in Panel A-B is: *w; spi-GAL4, tub-GAL80^{ts} / +; UAS-GFP-GPI /* + and in panel (C) this was combined with *UAS-shrb*-RNAi (HMS01767).

5.2.2.6 Mfas regulates dense-core granule morphogenesis in secondary cells

midline fasciclin (*mfas*) was characterised by Hu et al., (1998) as a member of the conserved Fasciclin I family. These proteins are involved in cell adhesion and signalling. It was named on account of its expression in the midline central nervous system cells during *Drosophila* embryogenesis, and shown to be involved in axonogenesis, likely through the regulation of intracellular signalling pathways. However, a series of both genomic and proteomic studies have found that it is also highly expressed in the accessory glands of adult male flies, and contributes highly to the seminal fluid (FlyAtlas.org – an online database of tissue-specific *Drosophila* gene expression; Findlay *et al*., 2008; Mueller *et al*., 2005), though its specific roles there have not been explored previously. Working collaboratively with M. Wainwright, a postdoctoral scientist in the Wilson lab, I previously showed that Mfas-GFP expressed from a gene trap insertion localised at extremely high levels specifically within the dense-core granules of secondary cells (Section 5.2.1.5).

Interestingly, when *mfas* expression was knocked down in secondary cells using two independent RNAi constructs, the dense-core granules were dramatically disrupted by DIC microscopy (Figure 5.23A-C). This suggests that Mfas plays a critical role in dense-core granule formation in these cells. When GFP-GPI was co-expressed with *mfas*-RNAi in these cells, it localised to the surface of the non-acidic compartments and their small ILV-like puncta, suggesting that the normal trafficking of molecules in these cells was unperturbed (Figure 5.23D). Taken together, the results suggest that Mfas

plays an important assembly role in dense-core granule formation, which facilitates maturation. However, unlike other regulators such as the Rab GTPases, the organisation, number and size of the non-acidic compartments did not appear highly affected compared to controls.

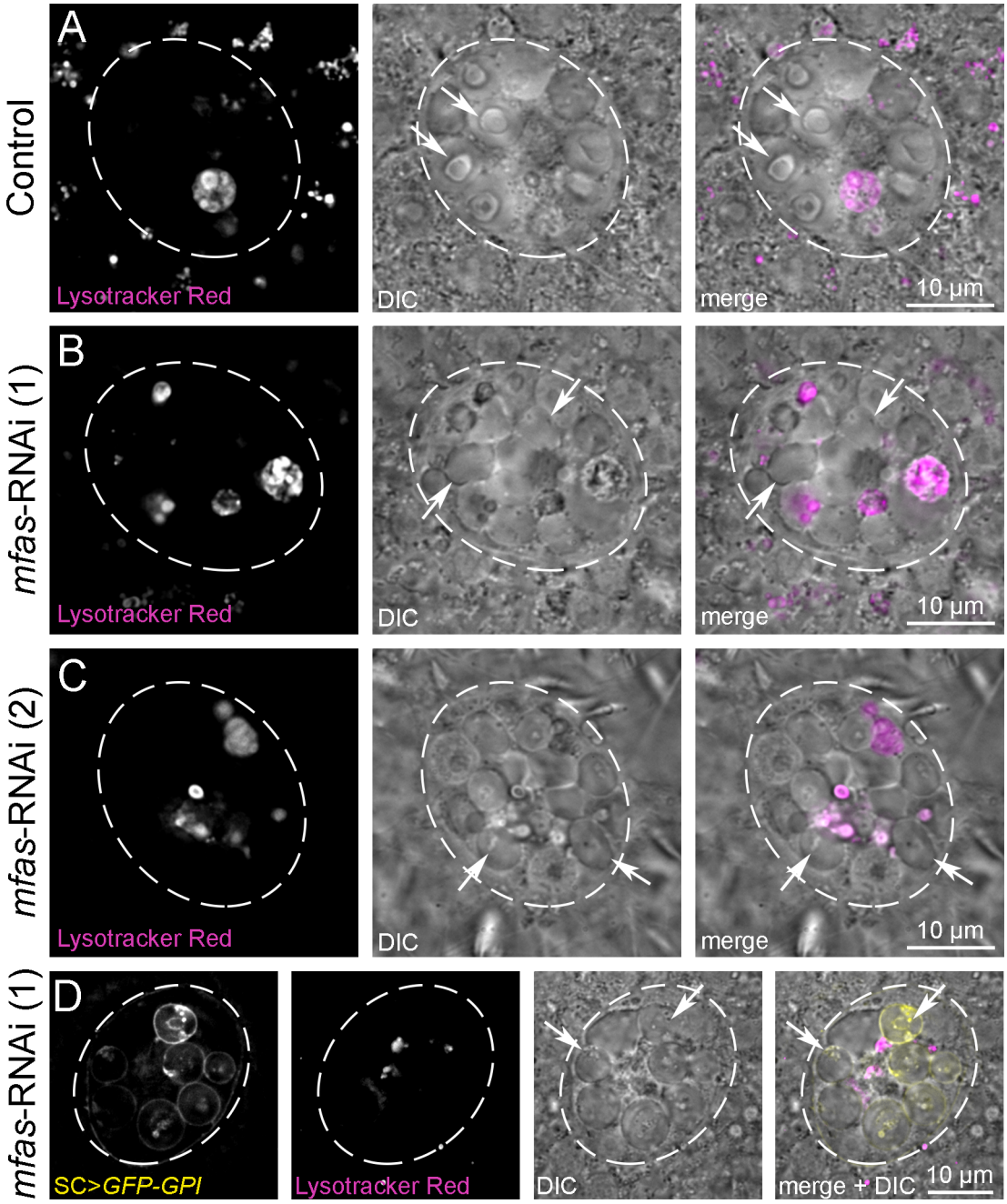

Control
A
Lysotracker Red
DIC
merge
10 µm
mfas-RNAi (1)
B
Lysotracker Red
DIC
merge
10 µm
mfas-RNAi (2)
C
Lysotracker Red
DIC
merge
10 µm
mfas-RNAi (1)
D
SC>GFP-GPI
Lysotracker Red
DIC
merge + DIC
10 µm

Figure 5.23 *mfas* regulates dense-core granule formation in secondary cells

These panels show wide-field fluorescence and DIC images of secondary cells from 6-day-old virgin males. Panels (B-C) show secondary cells selectively expressing two different RNAi constructs targeting *mfas*. Panel (D) shows a secondary cell selectively overexpressing GFP-GPI (yellow) in combination with one of the RNAi constructs targeting *mfas.* The flies were incubated at 28.5°C since eclosion to induce RNAi expression, or GFP-GPI and RNAi expression, using the GAL4-GAL80^{ts}-UAS system. All accessory glands were stained with Lysotracker Red (magenta). Approximate cell outlines are shown using a dashed line.
(A-C) Expression of *mfas*-RNAi (1) and *mfas*-RNAi (2) in secondary cells disrupts dense-core granule formation, shown using DIC imaging, in the large non-acidic compartments (arrows) compared to controls (A).
(D) Silencing of *mfas* with RNAi (1) in combination with GFP-GPI (yellow) overexpression revealed that most of the GFP-GPI was associated to the limiting membranes and ILVs within the non-acidic compartments (arrows).

The flies used in panels (A-C) consisted of combinations between *tub-GAL80ts; dsx-GAL4* with *UAS-mfas*-RNAi line 1 (HMC03645) or *UAS-mfas*-RNAi line 2 (VDRC 103621) or no other transgene (as a control). The flies used in (D) were *spi-GAL4, tub-GAL80^{ts}; UAS-GFP-GPI* crossed to *UAS-mfas*-RNAi line 1 (HMC03645).

5.2.3 Formation and maturation of large acidic compartments

5.2.3.1 Rab GTPases regulate the formation and maturation of large acidic compartments

Rab7 has been shown to play important roles in lysosome biology. It regulates multiple aspects including the maturation of endosomes, their transport along microtubules and fusion between endosomes and lysosomes (Guerra & Bucci, 2016; Bucci *et al*., 2000). Similarly, it is found on nascent autophagosomes, and is required for fusion of autophagosomes with lysosomes (Tooze *et al*., 2014). I studied the role of Rab7 in secondary cells using time-lapse microscopy of *YFP-Rab7* gene trap-expressing cells. The fusion protein localises on the surface of acidic compartments and a subset of non-acidic compartments (Section 3.2.2.7). Over the course of imaging, I observed that small YFP-Rab7-positive acidic compartments sporadically accumulated on the surface of a specific large dense-core granule compartment and subsequently fused with it (Figure 5.24A-A''). Alternatively, the dense-core granule compartments fused with the large acidic compartments (Figure 5.24B-B'). RNAi knockdown of *Rab7* in secondary cells overexpressing GFP-GPI caused a striking loss of large acidic compartments (Section 5.2.2.1), suggesting that *Rab7* is essential for their development. Taken together with the time-lapse imaging data, these results suggest that high Rab7 levels are likely required for the fusion of the large dense-core granule compartments with acidic compartments, which may directly or indirectly target them to fuse with lysosomes.

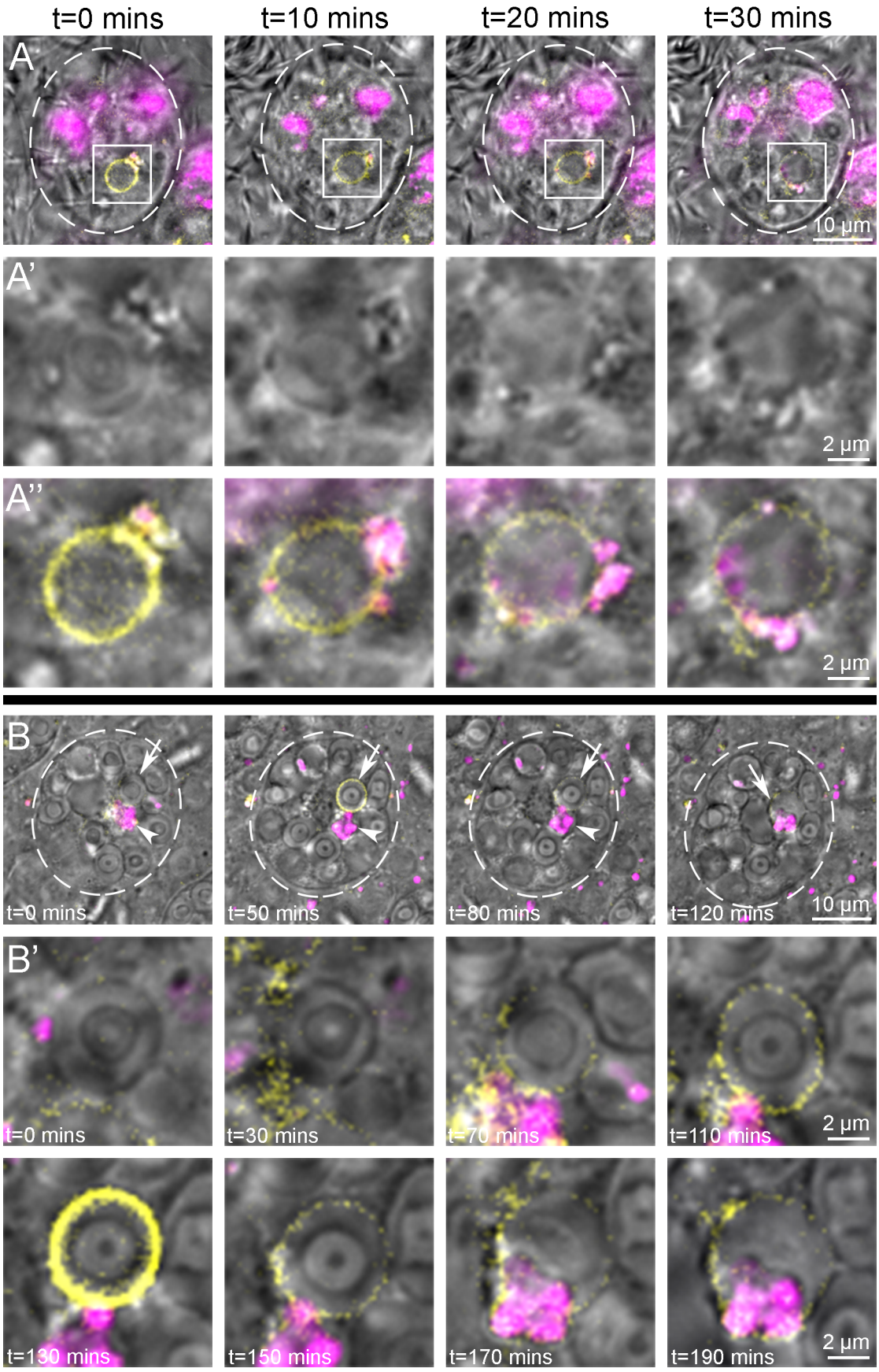

t=0 mins
t=10 mins
t=20 mins
t=30 mins
A
10 µm
A'
2 µm
A''
2 µm
B
t=0 mins
t=50 mins
t=80 mins
t=120 mins
10 µm
B'
t=0 mins
t=30 mins
t=70 mins
t=110 mins
2 µm
t=130 mins
t=150 mins
t=170 mins
t=190 mins
2 µm

Figure 5.24 YFP-Rab7 localises at high levels on non-acidic dense-core granule compartments that are targeted for degradation by fusing to acidic compartments

These panels show time-lapse wide-field fluorescence and DIC images from six-day-old virgin males, kept at 28.5°C since eclosion, that expressed the fusion protein from *YFP-Rab7* gene trap. Their accessory glands were stained with Lysotracker Red (magenta). Approximate cell outlines are shown using a dashed line.
(A-A'') Time-lapse imaging shows how an apically located non-acidic dense-core granule compartment fuses with surrounding small acidic compartments and eventually begins to form acidic microdomains (marked with Lysotracker) within its own lumen, as the dense-core granule structure within disintegrates. Initially, YFP-Rab7 (yellow) marks the surface of this compartment at high levels, but over time the levels of YFP-Rab7 reduces, particularly after fusion with surrounding small acidic compartments has taken place (30 mins onwards). Box region in (A) highlights the region enlarged in (A'-A''). Panel (A') shows DIC images only, and (A'') shows a merge of fluorescence and DIC images.
(B) Time-lapse images show how a large non-acidic dense-core granule compartment (arrows) acquires high levels of YFP-Rab7 (yellow) on its surface prior to fusing with a much larger acidic (magenta, arrowhead) compartment. The structure of the dense-core disintegrates following fusion.
(B') Higher magnification images including more time-points shows how the dense-core granule compartment in (B) gradually acquires higher YFP-Rab7 on its surface (between 70-130 mins). The levels of YFP-Rab7 drop following an initial interaction with the large acidic compartment (magenta), and whilst fusion takes place (170 mins), resulting in the disintegration of the large dense-core granule.

The genotype of the flies used in this figure is *w; + / +; YFP-Rab7 /* +.

5.2.3.2 ILVs may function as platforms for the acidification of endolysosomal compartments

Lysosomes play important roles in the endocytic pathway, digesting macromolecules and making the constituent parts available to the cell as nutrients. They contain many hydrolytic enzymes, specific to a wide range of targets, which are activated by the low pH (between 4.5 and 5.5; Perera & Zoncu, 2016). Acidification of the organelle is an essential aspect of endolysosomal maturation, required for the activity of its intralumenal hydolases. This low pH is generated and maintained through the activity of the V-ATPase proton pump (Mindell, 2012). Previous observations studying the lysosomes of secondary cells found that acidic microdomains were formed in close proximity to CD63-GFP-marked ILVs. This led to the hypothesis that the ILVs bud into the lumens of the large acidic compartments, where they may act as platforms for their acidification (Corrigan, 2014).

Using wide-field microscopy, I have confirmed these observations, resolving that the acidic microdomain surrounds some budding ILVs, rather than being encapsulated by the vesicle membrane (Figure 5.25A-A'). Interestingly, I found that the V-ATPase V_1 subunit Vha55, when tagged with GFP and expressed from its endogenous locus (*Vha55-GFP* gene trap; Lye *et al*., 2014), was localised on the ILVs within these compartments (Figure 5.25B).

In order to clarify the potential roles of ILVs in acidification, I worked collaboratively with a final year undergraduate student, Rosie Marshal, who was carrying out a summer project in the Wilson lab, to develop new quantitative methods to assess lysosome acidity using living secondary cells. A ratiometric pH dependent dye, LysoSensor Blue/Yellow, which has been

used to measure pH changes in other cell types (Diwu *et al*., 1999), was optimised for use in secondary cells. We confirmed the efficacy of the dye by imaging the large acidic compartments following knock down of either the V-ATPase V_1 subunit gene *VhaSFD* or the V_0 subunit gene *Vha100-1*. Both resulted in a significant reduction in yellow versus blue fluorescence in the large compartments compared to controls, consistent with a decrease in acidity (Figure 5.25C-E).

I then tested the role of the ESCRT-III component, *shrb*, which has well described roles in ILV formation (Wollert *et al*., 2009). I had already shown that it localises to the limiting membrane of large acidic and non-acidic compartments in secondary cells (Section 4.2.2.1) and is required for ILV formation, at least within non-acidic compartments. Similar to *V-ATPase* knockdowns, in *shrb*-RNAi cells, the pH of the acidic compartments was much higher than in controls (Figure 5.25G). Taken together, these data suggest that ILVs may function to promote acidification of large organelles, possibly by providing platforms for proton exchange via the V-ATPase on their surface (summarised in Figure 5.25H).

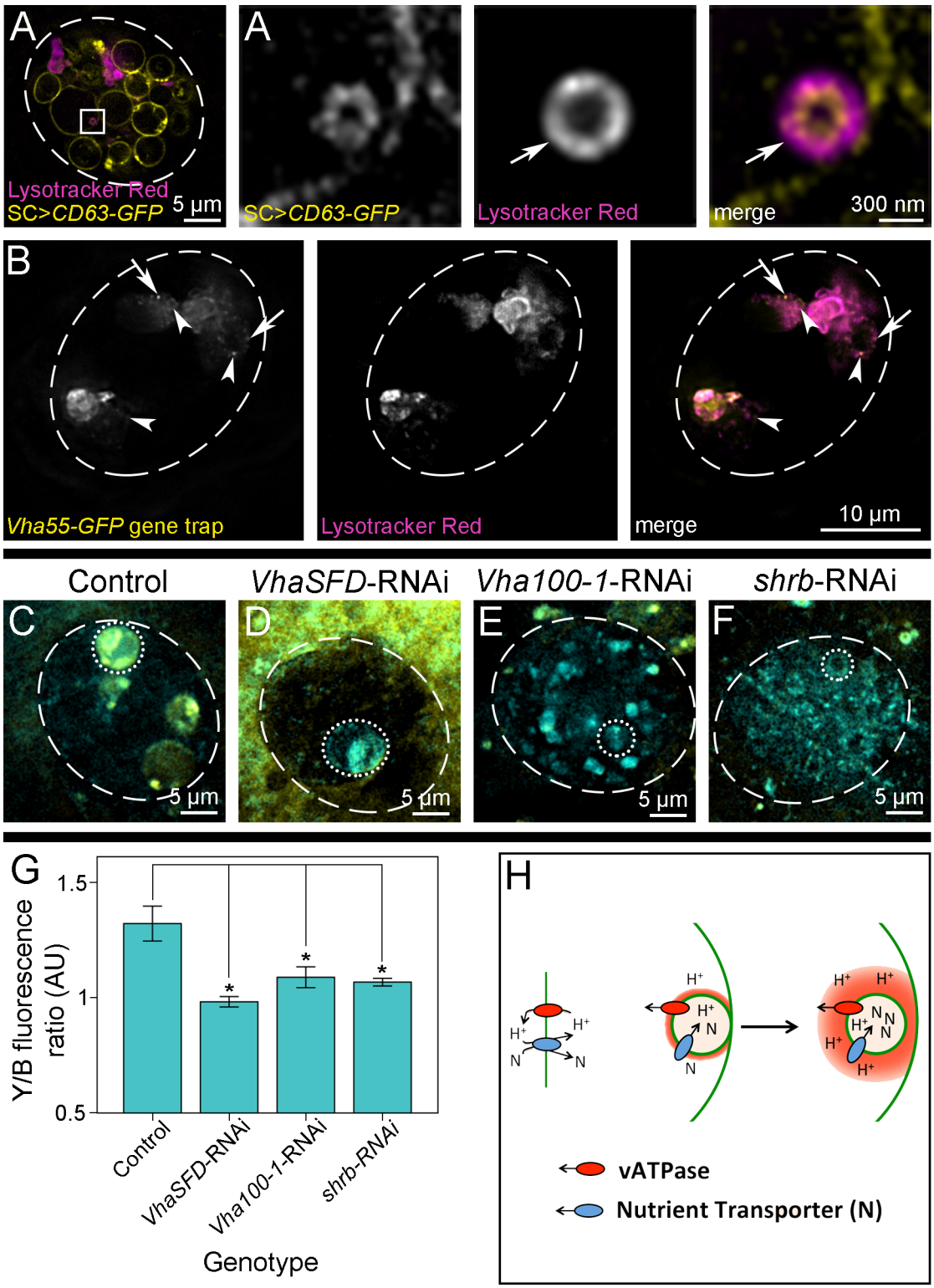

A
Lysotracker Red
SC>CD63-GFP
5 µm
A
SC>CD63-GFP
Lysotracker Red
merge
300 nm
B
Vha55-GFP gene trap
Lysotracker Red
merge
10 µm
Control
VhaSFD-RNAi
Vha100-1-RNAi
shrb-RNAi
C
D
E
F
5 µm
G
Y/B fluorescence ratio (AU)
1.5
1
0.5
Control
VhaSFD-RNAi
Vha100-1-RNAi
shrb-RNAi
Genotype
H
vATPase
Nutrient Transporter (N)

Figure 24. ILVs promote the acidification of large endosomal compartments

Panels (A-F) show wide-field fluorescence images of secondary cells from 6-day-old virgin males that have been kept at 28.5°C since eclosion. Approximate cell outlines are shown using a dashed line. Panels (A-A) consist of secondary cells selectively overexpressing CD63-GFP (yellow) and stained with Lysotracker Red (magenta). Panel (B) displays the localisation of the fusion protein from a *Vha55-GFP* gene trap line (yellow), which has also been stained with Lysotracker Red (magenta). The images in panels (C-E) are secondary cells that selectively express RNAi constructs targeting *Vha-SHD*, *Vha100-1, shrb,* or no target. These glands were stained with LysoSensor Yellow/Blue (yellow/cyan). Analysis was performed in collaboration with R. Marshall.
(A-A') In secondary cells overexpressing CD63-GFP (yellow), newly acidifying compartments occasionally contained ILVs that were surrounded by a ring of Lysotracker Red staining (magenta, arrow). The box in (A) highlights the region enlarged in (A').
(B) Vha55-GFP (yellow) localised on the surface of large acidic compartments (magenta; arrows) in secondary cells, and was also observed as intraluminal puncta and on the surface of larger membranous structures inside these compartments (arrowheads).
(C-F) All panels contain dotted circles around example acidic compartments.
(C) Control cell stained with LysoSensor Yellow/Blue dye contains large lysosomal compartments with high relative levels of yellow staining.
(D) Secondary cell expressing an RNAi targeting *VhaSFD* contained large lysosome-like compartments that are less acidic than controls.
(E) Knockdown of *Vha100-1* expression in secondary cells caused the formation of numerous smaller, but less acidic compartments.
(F) Secondary cells expressing an RNAi targeting the ESCRT-0 component *shrb*, required for ILV formation, resulted in smaller, and less acidic compartments with most of the LysoSensor staining observed at the periphery.
G) Bar chart showing the average ratio of Yellow/Blue fluorescence inside the lumens of the large lysosomal compartments of secondary cells (n=3 glands, with 5 cells analysed per gland).
(H) Model to explain how a proton gradient could be set up outside newly forming ILVs within the newly acidifying compartments. Green lines depict the limiting membrane and whose invagination results in the formation of ILVs, around which a concentration of proton builds up from the action of the vATPase residing in the ILV membrane. Nutrients accumulate inside the ILVs via proton-assisted transport

The genotypes of the flies used in this figure included: *w; UAS-CD63-GFP, tub-GAL80ts / +; dsx-GAL4 /* + as well as *w; + / +; Vha55-GFP /* + and combinations of *tub-GAL80ts; dsx-GAL4* with *UAS-VhaSFD*-RNAi (VDRC 47471), *UAS-Vha100-1*-RNAi (JF02059), *UAS-shrb*-RNAi (HMS01767) or no transgene (as a control). Statistical analysis is described in Section 2.23. *P≤0.05.

5.3 Discussion

In this Chapter I present a series of experiments that dissect out the genetic mechanisms regulating the formation and maturation of the large subcellular compartments within secondary cells. Using time-lapse microscopy, I describe in detail the formation of dense-core granules in secondary cells. I also have characterised several fluorescently tagged proteins that localise within the dense-core granules. I show how the Rab GTPases, particularly Rab6, Rab11 and Rab7, are essential for the morphogenesis of specific compartment types. Furthermore, I have observed a novel switch of Rab identity on compartments as dense-core granules are formed, changing from being primarily Rab6- to Rab11-positive. In addition to confirming that known regulators of dense-core granule formation, like the AP1 adaptor and Arf79F, control this process in secondary cells, I have also characterised novel roles for Mfas and ILVs, the latter perhaps by delivery of molecules to the dense-core granules. I have found that ILVs also appear to play a role in the acidification of large late endosomal and lysosomal compartments. Overall, my work establishes the secondary cell system as a unique model to genetically unpick the control of dense-core granule formation, endolysosomal maturation and other secretory events. Below I review how using this system has already provided several new insights into these processes.

5.3.1 Dense-core granules are formed within large Rab6-positive precursor compartments that undergo morphological and positional changes

Prior to this time-lapse microscopy study, it remained unclear exactly how the different types of Rab-associated compartments in secondary cells interacted with one another. In collaboration with F. Castellanos, a DPhil student in the lab, I performed pulse-chase experiments, which suggested that the centrally located Rab6-labelled compartment might play a central role in the trafficking of molecules, such as GFP-GPI and CD63-GFP, to the other large secretory organelles (Castellanos, 2017). Using time-lapse fluorescence and DIC imaging, I have now shown that dense-core granules are in fact formed within the large non-cored Rab6-positive compartments, which gradually acquire Rab11 on their surface at the same time (5.2.1.2). Initially this process involved morphological rearrangements of the limiting membrane from an irregularly shaped large Rab6-positive compartment, which often contained numerous tubular invaginations, to a smaller spherically structured compartment. The function of the invaginations, which do not appear to form vesicles (Section 3.2.1.3), is unclear. They may provide a greater surface area for binding of lumenal proteins that must be concentrated for granule biogenesis or removal. My previous electron microscopic analysis showed that the large central compartment contains a few fibers prior to core formation, suggesting that filament assembly may occur before the condensation of the dense-core granule (Section 3.2.1.3). Similar reports of reduction in compartment size during the maturation of immature secretory granules have been described in other cell types, including neuroendocrine

PC12 cells, though these events have not been directly observed in living cells (Tooze *et al*., 2001). These studies suggested that the reduction in size of the immature secretory granule compartments is mediated by the budding of small clathrin-coated vesicles, which remove non-specific cargos in a process mediated by AP-1 (Kim *et al*., 2006). This hypothesis is consistent with observations in secondary cells with reduced AP-1 expression, which form only a single large non-cored, non-acidic compartment (Castellanos, 2017).

Following this morphological transformation, specific protein cargos begin to concentrate within the interior of the compartment, and finally a dramatic condensation reaction forms a dense-core granule, observable with DIC microscopy (Section 5.2.1). Simultaneously, the compartment migrates basally, out of the Golgi-rich central region of the cell, to a more peripheral region, where it presumably undergoes further maturation events. It seems plausible that this migration out of the central region of the cell, which is closely associated with multiple Golgi complexes, may be required for the formation of new large secretory compartments. It will be interesting to determine whether other aspects of dense-core granule maturation in other cell types, such as the removal of water, as well as acidification and Ca^{2+} accumulation within the compartment's lumen (Kim *et al*., 2006), are conserved in secondary cells.

The biogenesis of new large Rab6-positive non-cored compartments is likely due to homotypic fusion of smaller vesicles, destined for the regulated secretory pathway, budding from the trans-Golgi cisternae. In accordance with my observations, previous electron microscopy studies of secondary cell

ultrastructure by Perotti (1972) also hypothesised that fusion of small vesicles budding from the trans- face of the Golgi was required to produce larger secretory vesicles. In a similar manner, the growth in size of neuroendocrine PC12 cell dense-core granule compartments is driven by fusion of immature secretory granule compartments (Tooze *et al*., 1991; Urbé *et al*., 1998; Wendler *et al*., 2001).

5.3.2 Novel dense-core granule cargos in secondary cells

Previous studies have furthered our understanding of dense-core granule biology in secondary cells through the identification and characterisation of molecules that localise within the cores (Redhai *et al*., 2016; Rylett *et al*., 2007). Similarly, here I have characterised several novel dense-core-localised proteins, including several GFP-tagged proteins: Cathepsin B1, Trol and mFas, expressed from their endogenous regulatory sequences (Section 5.2.1.5).

In contrast to other markers of dense-core granules in secondary cells, such as GFP-GPI and AnCE, both CtsB1-GFP and Trol-GFP were found unevenly distributed across the dense-core granules within every compartment. These localisation patterns are supported by my electron microscopic observations in Chapter 3, which showed that the electron density of the granule differed across its diameter (Section 3.2.1.3). Cathepsin B1 is a protease known to function within late endosomal or lysosomal compartments (Burleigh, 1974) but which has also been reported to enter the regulated secretory pathway (Kuliawat *et al*., 1997). For example, Cathepsin B has also been detected within secretory granules from rat juxtaglomerular epithelial cells and within

insulin granules, suggesting that the localisation may be conserved (Brunner *et al*., 2007; Taugner et al., 1985; Docherty *et al*., 1984). Within β-cells, Cathepsin B is thought to be predominantly trafficked out of the maturing insulin granules, perhaps because of its affinity with the mannose-6-phosphate receptor, a target of the AP-1 complex (Klumperman *et al*., 1998; Kuliawat *et al*., 1997; Taugner et al., 1985). Indeed, it has been proposed that the numerous lysosomal molecules found in the insulin granules of pancreatic β-cells are transferred to lysosomes, delivering enzymes and other molecules required for their function (Brunner *et al*., 2007).

By contrast, Cathepsin B is proposed to activate renin within the secretory granules of the juxtaglomerular epithelial cells. Similarly, in secondary cells, CtsB1-GFP was observed inside all dense-core granule compartments, suggesting that it is also retained in these compartments, assuming that the GFP tag does not affect its localisation. One important question that can now be addressed in our system is how the lysosomal enzymes traffic to the dense-core granule compartments. Could they arrive via Rab11-positive recycling endosomal compartments involved in the Rab transition I have observed? And is a proportion of this removed by AP-1/Clathrin-dependent mechanisms? It should be possible to answer these questions using some of the genetic tools I have characterised here.

In contrast to CtsB1, Trol is the fly orthologue of Perlecan, a secreted member of the heparin sulphate proteoglycans. These molecules are known to modulate growth factor signalling, including Hedgehog and Branchless signalling, in *Drosophila* (Lindner *et al*., 2007; Grigorian *et al*., 2013). Interestingly, an overexpressed, GFP-tagged form of Hedgehog has recently

been observed to localise within dense-core granules, suggesting that the two molecules may interact within this structure (Hellberg, 2017). It has already been reported that Dpp traffics to secondary cell dense-core granules, suggesting that these structures may act as a repository for developmental signalling molecules, which may then be released and act as an autocrine or paracrine fashion upon secretion (Redhai *et al*., 2016). To my knowledge, Perlecan has not previously been localised within the dense-core granules of other cell types, but its presence suggests a potential role in regulating the repository of growth factors in these structures.

Mfas-GFP, expressed from a gene trap or a genomic construct, localised throughout the dense-core granules at very high levels, and like AnCE-GFP, was more evenly distributed between compartments than overexpressed GFP-GPI. Interestingly, Mfas is one of the most highly expressed genes in the male accessory glands, and a major constituent of the male seminal fluid (FlyAtlas; Chintapalli *et al*., 2007; Findlay *et al*., 2008; Mueller *et al*., 2005). Much lower levels of gene trap expression were observed in main cells, but it is currently unclear whether this results from endocytosis of secondary cell-expressed Mfas or whether Mfas is also expressed in these cells. Whatever the answer, the *mfas* knockdown phenotype in secondary cells strongly suggests that most Mfas in these cells is not scavenged from adjacent main cells.

Based on its structure, Mfas is thought to multimerise (Sobota *et al*., 2006), a property that is thought to help facilitate protein incorporation into dense-core granules. Although never directly implicated in dense-core granule biology

previously, its potentially conserved roles in biogenesis are discussed later in Section 6.2.

5.3.3 Dense-core granules are secreted by more than one mechanism

The mechanisms of dense-core granule secretion by secondary cells were revealed for the first time using time-lapse imaging (Section 5.2.1.3). Two cellular mechanisms were observed: 1) complete fusion, where all or much of the compartment's contents were released into the lumen, and 2) kiss-and-run interactions with the plasma membrane, where only some of the compartment's contents were released. Interestingly, these two mechanisms have also been reported in other systems, including insulin granule exocytosis by pancreatic β-cells and in neurotransmitter release by neuroendocrine cells (Hanna *et al*., 2009; Rutter *et al*., 2006; Harata *et al*., 2006). However, the evidence for kiss-and-run was largely based on electrophysiological readings, rather than direct observational evidence (Wu *et al*., 2014).

My imaging data clearly demonstrate that kiss-and-run occurs *in vivo*, possibly through formation of a fusion pore. The molecular nature of fusion pores has only recently started to be explored in reconstituted systems (Bao *et al*., 2016). Secondary cells may prove a powerful *in vivo* model to further understand their molecular composition. These different secretory mechanisms provide a possible mechanism whereby individual secondary cells could modulate the levels of their secretion. It will be interesting to explore the physiological mechanisms that control the balance between

complete collapse and kiss-and-run interactions of these compartments with the plasma membrane.

These future studies would benefit from the classification of a secretogogue for dense-core granule secretion. Unlike Redhai *et al*., (2016), I was unable to stimulate dense-core granule exocytosis by mating (data not shown). This conflicting result requires further clarification, as it remains possible that after copulation, secretion may be stimulated to replenish the contents that are depleted, or alternatively that the compartments are secreted in a more constitutive manner than previously thought. It seems very likely that release will involve Ca^{2+} ions, and so further analysis of cells expressing photoactivatable Ca^{2+} channels or caged ions may provide one way of performing these experiments in cultured glands.

5.3.4 Rab GTPases play novel roles in dense-core granule maturation and may co-operate to perform different functions

I have also shown that both Rab6 and Rab11 play important roles in dense-core granule formation in secondary cells (Section 5.2.2.1). Rab6 is required for the formation of large non-acidic, secretory compartments, suggesting that it may regulate the homotypic fusion between trans-Golgi-derived vesicles. However, it will be important to investigate the *Rab6* knockdown phenotype further using electron microscopy and real-time imaging at earlier stages, as the morphology of these cells is deeply disrupted at six days after eclosion. Rab11, on the other hand, is required for dense-core granule formation within the large non-cored Rab6-positive compartments, possibly by facilitating the trafficking of important cargos into the compartment. Given Rab11's described

roles in the recycling of endocytic molecules, it is possible that cargos are recycled from the plasma membrane into these compartments (Lock & Stow, 2005; Kobayashi & Fukuda, 2013). Interestingly, Rab6 has been recently implicated in directing elements of the secretory system towards melanosomes, a type of lysosome-related organelle of endosomal origin (Patwardhan *et al*., 2017). It will be important to confirm using some of the genetic manipulations described here, that the large secondary cell dense-core granule compartments are composites of both the endocytic and secretory pathways.

Furthermore, it will be important to test whether Rab6 and Rab11 play similar roles in regulated secretion in other cell types. Some studies have suggested this may be the case: for example, both Rab11A and Rab6 have been identified by mass spectrometry in purified pancreatic acinar cell zymogen granule compartments (Chen *et al*., 2006). Furthermore, in mouse insulin-secreting MIN6 cells, Rab11B co-localised with insulin-containing secretory granules, and overexpression of a dominant negative Rab11B inhibited regulated exocytosis (Sugawara *et al*., 2009). However, this study did not report the cell biological phenotype of this manipulation, so it remains unclear if the reduced exocytosis was caused by an underlying defect in dense-core granule formation.

Although neither Rab6 nor Rab11 have been implicated in dense-core granule biogenesis previously, they play complementary roles in secretory trafficking pathways in other cell types. For instance, Rab6 and Rab11 have been implicated in the apical trafficking of Rhodopsin in *Drosophila* photoreceptor cells (Satoh *et al*., 2016; Satoh *et al*., 2005; Shetty *et al*., 1998). These

secretory functions involve specific effectors, which for Rab11 include Myosin V and dRip11 (Li *et al*., 2007), whilst for Rab6, Rich has been identified as an important effector (Iwanami *et al*., 2016). It will be important to investigate the roles of Rab6 and Rab11 effectors in dense-core granule biogenesis. Interestingly, both Rab6 and Rab11 have also been implicated in *Chlamydia trachomatis* infectivity of human cells (Lipinski *et al*., 2009). Furthermore, Rab6 and Rab11 have been implicated in the post-Golgi trafficking of Herpes simplex virus 1 (HSV1) envelope proteins to the plasma membrane, where virus envelopment occurs (Johns *et al*., 2013). Taken together, this suggests that the Rab6, Rab11-mediated secretory trafficking pathway not only plays important physiological roles, but may also be hijacked by infectious pathogens; studies in secondary cells may help to determine how these pathological processes could be blocked or modified.

I have also shown that Rab7 regulates dense-core granule number within secondary cells, likely by facilitating a programme of zymophagy (Vaccaro, 2012; Sections 5.2.2.1 and 5.2.3.1). This is a form of autophagy that targets secretory granules. Although Rab7 has not been directly reported to function in zymophagy, it has been implicated in multiple aspects of autophagy (Guerra & Bucci, 2016), for example it facilitates the fusion events between autophagosomes and lysosomes (Jager *et al*., 2004). It is likely that maintaining the flies as virgins for 6 days results in a build-up of secretions in the accessory gland lumen, which could potentially be harmful to the epithelium. This may activate a programme of autophagy that helps to reduce excess release of dense-core granule contents. Similar mechanisms have been reported in pancreatic β-cells, where insulin granules are degraded

upon starvation, to help keep insulin secretion low (Goginashvili *et al*., 2015). Failure of this process in the human exocrine pancreas results in improper release of pancreatic enzymes, causing acute pancreatitis (Helin *et al*., 1980). A closer characterisation of zymophagy in secondary cells would be an interesting avenue for further research, given the lack of genetic models available to study this process.

I also found that Rab19 is localised to a subset of apical Rab11-positive dense-core granule compartments, which seem to be targeted for exocytosis (Section 5.2.1.4). However, knockdown of *Rab19* did not reveal any obvious changes in secretory compartments of secondary cells (Section 5.2.2.1). Knockdown of other Rab GTPases, which localise to the surface of secondary cell compartments, including Rab10 and Rab21 also did not dramatically affect dense-core granule biogenesis or number (Section 5.2.2.1). This could be due to multiple reasons, for example their functions may be subtle or redundant, or alternatively, the degree of knockdown or sensitivity of my assays may have been insufficient. Nonetheless, the complex Rab GTPase associations on the surface of these compartments deserves further enquiry in the future.

5.3.5 Subcellular compartments undergo novel Rab transitions as they mature and interact with other compartments

During the formation of dense-core granules in secondary cells, Rab11 gradually replaces Rab6 on the limiting membrane of the maturing

compartment (Section 5.2.1.2). This novel ‘Rab switch’ is similar to a previously identified transition that occurs during endosome maturation from early endosomes, marked by Rab5, to late endosomes, marked by Rab7 (Rink et al, 2005; Vonderheit and Helenius, 2005). The molecular mechanisms behind the Rab5 to Rab7 switch have now been identified in some detail (Poteryaev et al., 2010). However, to the best of my knowledge, no other Rab switch has been demonstrated at the same level of detail. My knockdown experiments suggest that the Rab6 to Rab11 switch functions within the secretory pathway to facilitate intra-compartmental maturation.

It will now be important to understand how these two proteins interact and exchange. Based on the identified mechanisms from the Rab5 to Rab7 switch, the nature of this interaction is likely to be indirect. In human cells, Rab6 and Rab11 are coupled through Rab6 Interacting Protein 1 (R6IP1), which binds both Rab6 and Rab11A-GTP (Miserey-Lenkei *et al*., 2007; Janoueix-Lerosey *et al*., 1995). Rab6 is thought to recruit R6IP1 to Golgi membranes, forming Rab6-R6IP1 complexes that once formed, interact with Rab11-GTP. The *Drosophila* gene *pinstripe* (*pns*) shows homology with R6IP1, and has been previously identified as an effector molecule for Rab30 (Gillingham *et al*., 2014). However, silencing of *pns* expression by two independent RNAis did not cause any defect in dense-core granule formation (data not shown), suggesting that alternative molecular mechanisms may be responsible for the recruitment of Rab11.

Live-cell time-lapse imaging also suggested that a different Rab switch, from Rab11 to Rab7-positive occurs on the surface of selected non-acidic dense-core granule compartments that are targeted for degradation by zymophagy.

The development of more CFP-tagged *Rab* gene trap lines, which can be combined with the YFP-tagged lines, would likely enable a demonstration of these processes. Furthermore, it will be important to determine whether an autophagosomal membrane surrounds the compartment during this process, or whether the original limiting membrane of the compartment is simply modified to permit its fusion with late endosomes or lysosomes.

5.3.6 The conserved trafficking regulators, AP-1 and Arf79F block different steps of dense-core granule formation in secondary cells

The AP-1 complex is thought to play important roles during the maturation of immature secretory granules by facilitating the removal of non-specific proteins (Bonnemaison *et al*., 2013; Kim *et al*., 2006). For example, it is required for glue granule formation in the *Drosophila* salivary gland (Burgess *et al*., 2011). However, it has also been implicated in constitutive secretion from the trans-Golgi network to the plasma membrane (Chi *et al*., 2008) and in trafficking between the trans-Golgi network and endosomes (Bonnemaison *et al*., 2013; Waguri *et al*., 2003). In secondary cells, AP-1 depletion was shown to severely impact dense-core granule biogenesis (Castellanos, 2017). Here I have demonstrated that the extremely large non-acidic compartment in AP-1γ-depleted cells carries Rab6 on its surface, indicative of the immature non-cored secretory granule compartment (Section 5.2.2.3). I also report that AP-1γ localises predominantly on and around the non-cored Rab6 compartment, in the Golgi-rich region. Taken together, these data support the

hypothesis that the AP-1 complex plays roles during the maturation of the newly forming immature secretory granule compartments, likely by facilitating the removal of non-specific cargos and leaving essential molecules required for further compartment maturation. These events are likely required for the localisation of Rab11 to the surface of the maturing compartment.

The Arf79F GTPase is thought to function in dense-core granule biogenesis by recruiting AP-1 onto immature secretory granule compartment membranes (Ren *et al*., 2013; Kim *et al*., 2006). Although secondary cells with reduced *Arf79F* expression were unable to form dense-core granules, the phenotype was very different to when expression of AP-1 subunits was knocked down (Section 5.2.2.3). *Arf79F* appeared to be required for the appropriate transportation of dense-core cargos, which were trapped within small vesicles, likely within part of the Golgi apparatus (Castellanos, 2017). These data correlated well with previous studies of *Arf79F* function in secondary cells. Specifically, when Arf79F was knocked down in CD63-GFP overexpressing cells, the trafficking of CD63-GFP and AnCE was restricted to the Golgi-rich central region of the cell (Redhai, 2016). Interestingly, the *Arf79F* knockdown cells were still able to form large non-acidic compartments, but I show here that their Rab GTPase signatures were abnormal, lacking both Rab6 and Rab11. Furthermore, a subset of the large compartments carried Rab1, which is normally localised within the cis-Golgi cisternae of control cells. Arf79F is known to regulate the recruitment of several important proteins within the Golgi apparatus, for example COPI coated vesicles that mediate cis-Golgi to endoplasmic reticulum trafficking (Serafini *et al*., 1991; Donaldson *et al*., 1992), and other lipid-metabolising enzymes such as PKD (Christis & Munro,

2012). Taken together, it is likely that Arf79F's roles within the Golgi apparatus are essential to set up the regulated secretory pathway and that these functions are upstream of its interactions with AP-1.

5.3.7 Mfas, Syx5 and the ESCRT-III component shrb are novel regulators of dense-core granule formation and maturation

I have shown that Mfas is packaged at extremely high concentrations into secondary cell dense-core granules, and it plays essential roles in their formation (Sections 5.2.1.5 and 5.2.2.6). Based on its molecular structure, it is unclear what exact role Mfas is playing within the core: it contains a single N-terminal EMI domain, which is involved in multimerisation (Doliana *et al*., 2000), and four Fas1 domains, involved in cell-cell adhesion in other systems (Clout *et al*., 2003). The *mfas* knockdown phenotype suggests that it regulates the condensation or accumulation of dense-core granule cargos. Interestingly, in contrast to other regulators of the regulated secretory pathway that I have identified, such as the *Rab6* and *Rab11*, *mFas* knockdown cells remain relatively morphologically normal, except for their failure to form dense-core granules.

It will now be important to determine the Rab GTPase localisations on these compartments, to see whether they are unperturbed and to study how dense-core proteins are trafficked in the absence of dense-core granules. If compartment organisation is normal, *mFas*-RNAi may prove to be a powerful tool to unpick the specific roles of secondary cell dense-core granules in reproduction. It will also be important to determine whether Mfas's role in dense-core granule biogenesis is conserved in other cell types. The

homologue of *mfas* in humans, *transforming growth factor beta-induced* (*TGF-βI*), is an important extracellular protein, secreted via the Golgi apparatus, which has been implicated in corneal dystrophies (Han *et al*., 2016; Choi *et al*., 2015). Other studies have shown that SNPs in TGF-βI are associated with type 1 diabetes, which is characterised by the inability of the pancreas to produce insulin (Patry *et al*., 2015). The report showed that murine islet cells expressed TGF-βI, and that it co-localised extensively with insulin within some cells, possibly suggesting that it may play a role in its packaging. However, the study focused on the potential roles for TGF-βI, once secreted, so its roles inside beta cells remain unclear.

Using time-lapse imaging, I have shown that smaller compartments fuse together to generate the large non-acidic, non-cored compartments in secondary cells. Key mediators of membrane fusion, the SNARE complexes, are important candidate molecules that could facilitate this process (Hong and Lev, 2014; Jahn and Scheller, 2006). Work in PC12 cells has shown that Syx6 plays key roles in immature secretory granule compartment maturation by mediating homotypic fusion (Wendler *et al*., 2001). However, RNAi knockdown of *Syx6* in secondary cells showed no major defect in dense-core granule compartments, suggesting that other SNAREs may be involved in this process. Interestingly, depletion of *Syx5* by RNAi reduced the size of the large secretory compartments within secondary cells (Section 5.2.2.2). Like Rab6 and Rab11, Syx5 has been implicated in the trafficking of Rhodopsin in *Drosophila* photoreceptor cells (Satoh *et al*., 2016). The authors concluded that Syx5 functioned upstream of Rab6, mediating trafficking between the endoplasmic reticulum and cis-Golgi, similar to its roles in yeast (Hardwick &

Pelham, 1992). This is supported by its localisation, which is predominantly within the cis-Golgi (Banfield *et al*., 1994; Satoh *et al*., 2016). It is therefore possible that the abnormally small secretory compartments seen after knockdown in secondary cells are formed as a result of generally defective secretory trafficking.

In Chapter 4, I described in detail the numerous small ILVs within the large dense-core granule compartments of secondary cells (Section 4.2.1.2). Using time-lapse microscopy, I have now observed that ILVs carry dense-core granule cargos that can be transferred into the core. Furthermore, reducing ILV formation within these compartments by knocking down expression of the key ESCRT-III subunit, *shrb*, prevented the normal packaging of dense-core granules (Section 5.2.2.5). This novel role will require further elaboration in the future, for example by the examination of the roles of more ESCRT components, and careful electron microscopic analysis, as the general morphology of these cells is highly disrupted. Interestingly, ILVs have also been observed within yolk granule compartments in the *Drosophila* oocyte, though they are thought to derive from fusions with MVBs (Vaccari *et al*., 2009).

5.3.8 Rab-regulated trafficking pathways drive lysosome growth

I have used time-lapse microscopy to show that the giant lysosomes of secondary cells grow by homotypic fusion between acidic compartments, and also by heterotypic fusion with non-acidic compartments (Sections 4.2.1.1 and 5.2.3.1). Enlarged lysosomes can occur in human diseases such as

lysosomal storage disorders and neurodegenerative disease (Perera & Zoncu, 2016). In the case of lysosomal storage diseases, they are often driven by deficiencies in lysosomal enzymes, resulting in defective catabolism of important substrates such as sphingolipids (Platt *et al*., 2012; Platt, 2014). However, secondary cells from non-transgenic w^{1118} flies were shown to form large lysosomal compartments, suggesting that rather than a genetic malfunction, this growth is physiological, although growth levels can be strongly affected by some genetic manipulations.

I have shown that *Rab7* plays very important roles in the growth of lysosomes, as only very small acidic compartments were observed when it was depleted in secondary cells (Section 5.2.2.1). As previously stated, *Rab7* is likely involved in directing zymophagy, a form of autophagy where the large secretory dense-core granules are degraded (Vaccaro, 2012). It will be interesting to determine whether large acidic compartments develop in the same way as in virgins, when wild type male flies are allowed to mate frequently. One expectation would be that the dense-core granules are secreted more frequently in this context, rather than degraded, in order to replenish the accessory gland lumen. Thus zymophagy may be reduced. However, secretory trafficking is also likely to be increased in this scenario, which may mask these effects.

Given the small size of the acidic compartments in *Rab7* knockdown cells, it is likely that *Rab7* also regulates the formation of these compartments and the fusion between lysosomes and late endosomes, similar to findings using HeLa Cells (Vanlandingham *et al*., 2009; Hyttinen *et al*., 2013; Luzio *et al*., 2007). I also observed that knockdown of *Rab6* affected the formation of large

acidic compartments, although many smaller acidic compartments were formed. Given the localisation of *Rab6* in secondary cells, this is perhaps due to an indirect affect of reducing the formation of large secretory compartments, which are the target of zymophagy.

5.3.9 ILVs function as platforms for the acidification of large lysosomal compartments

Previous work in the Wilson lab used the pH-sensitive dye Lysotracker-Red to demonstrate the degree of acidity within subcellular organelles (Corrigan et al., 2014; Redhai, 2016). However, this method is not quantitative, so I employed a ratiometric LysoSensor Blue/Yellow dye to try to measure the pH within the large acidic compartments (Section 5.2.3.2). I first validated the efficacy of the new dye by detecting the change in ratiometric signal when subunits of the proton-pumping V-type ATPase, which is known to set up the low pH of lysosomal compartments, were knocked down (Mindell, 2012). Knockdown of two different V-ATPase subunits, the V_1 subunit *VhaSFD* and the V_0 subunit *Vha100-1* resulted in acidic compartments with higher pH when compared to controls. Interestingly, the acidic compartments in both knockdowns were smaller, suggesting that the V-ATPase may also regulate some aspects of lysosome fusion. However, this dye is known to have an alkalysing effect once inside compartments, so may downplay any potential phenotype, so is not suitable for a large scale study of novel acidification regulators.

Based on the observation that bright acidic microdomains were formed around ILVs within the large acidic compartments (Corrigan, 2014), and these

were maintained even as the vesicle moved through the compartment, it was hypothesised that the vesicles may perform functions to promote acidification of the organelle. Supporting this idea, I found that the V_1 subunit Vha55 localised to some of these intraluminal membranes, where it may be involved in these roles. To reduce ILV formation, the ESCRT machinery was targeted with RNAi, as it plays well-characterised roles in their biogenesis within late endosomes (Hurley, 2015). Furthermore, in Chapter 4 I showed that the ESCRT-III component shrb, when tagged with GFP, localised onto subdomains of the large lysosomal compartment membranes, consistent with its proposed function there (Section 4.2.2.1). Depletion of *shrb* caused the formation of smaller acidic compartments with higher pH than controls, similar to the V-ATPase knockdowns (Sections 4.2.2.2 and 5.2.3.2). Taken together, these data support a novel role for ILVs in regulating the physiology of the lysosome. It will be important to demonstrate whether other ESCRT components cause similar effects on acidification.

The mechanism by which acidic microdomains might be maintained remains a mystery. It may involve nutrient transporters acting in concert with the V-ATPase, as previously suggested (Corrigan, 2014; Section 5.2.3.2). Furthermore, given the limited volume of an ILV, it cannot provide a long-term source of protons. The vesicle must ultimately back fuse to the limiting membrane, a process that has been proposed in mammalian cells (Bissig & Gruenberg, 2014). It will of course be interesting to determine whether this mechanism of compartmental acidification is conserved. The larger the compartment, the more critical this mechanism may become because of the reduced surface to volume ratio. However, it seems unlikely this mechanism

would have specifically evolved for large endolysosomes. Investigating this question is important, because if the lysosome does not acidify appropriately, the lysosomal enzymes will not function optimally (Mindell, 2012). This may help to explain the presence of numerous ubiquitinated protein aggregates in neurodegenerative diseases such as Huntington's disease, frontotemporal dementia, Parkinson's disease, some of which are associated with mutations in the ESCRT-III homologue in humans, CHMP2B (Saksena & Emr, 2009; Skibinski *et al*., 2005).

In summary, the work in this chapter has opened up many new avenues in the areas of regulated secretion and endolysosomal trafficking, and identified several novel molecules that are involved in aspects of these processes.

6.0 Concluding remarks

In the preceding Results chapters, I have discussed a number of key implications of my work that are relevant to our understanding of the fundamental mechanisms regulating secretory and endolysosomal processes in eukaryotic cells. Here, I will present a summary of the overall conclusions from my research, and then put them into a wider research context and consider future directions.

My DPhil research built on the work of other members of the Wilson lab, who first established secondary cells as an *in vivo* model to study numerous different aspects of cell biology, including secretion, membrane trafficking and growth (Corrigan *et al*., 2014; Redhai *et al*., 2016; Leiblich *et al*., 2012). By using new techniques and technologies, I have delved deeper into the mechanisms driving these processes. In doing so, I have furthered our understanding of certain aspects of cell biology, particularly secretory compartment biogenesis, which may be relevant across the animal kingdom, particularly in different secretory cell types. I have worked collaboratively with the Goberdhan group to prepare a manuscript that crosses species boundaries, describing novel mechanisms of exosome biogenesis in both *Drosophila* and human cancer cells (Perera *et al*., in preparation), for which I am a joint first author. I plan to use some of my other findings, particularly the Rab-mediated regulation of dense-core granule biogenesis, to complete a second manuscript in collaboration with F. Castellanos in the Wilson lab, for which I will also be a joint first author (Kroeger *et al*., in preparation).

6.1 Summary of findings

My first results chapter (Section 3.0) contains a detailed characterisation of secondary cell intracellular compartments, obtained using powerful new imaging technologies and a plethora of new fly lines that have become available. Notably, I showed that large dense-core granule compartments in these cells contain a number of ILVs, an observation that I explored further in my second results chapter. I also identified a novel compartment subtype that is non-cored, carries Rab6 on its surface, and is likely a specialised post-Golgi compartment. By screening a set of YFP-tagged *Rab* gene traps, I discovered that this compartment acts as a trafficking hub, which might distinguish a complex series of Rab-mediated post-Golgi trafficking events, which in most cells cannot be separated from the Golgi. This screen also identified different populations of dense-core granule compartments that are likely at different stages of maturation and/or secretory trafficking. I visualised the processes underlying endolysosomal degradation of dense-core granule compartments, potentially establishing a first genetic model to study zymophagy. I show that some of the large acidic organelles involved in this process are morphologically similar to lysosomes. The distinctive localisation patterns characterised here, in particular those of Rab6, Rab11 and Rab7, informed several of my further studies in Chapters 4 and 5.

In my second results chapter (Section 4.0), I have characterised the mechanisms that secondary cells use to generate and secrete exosomes, and how protein cargos are selectively loaded into them. Importantly, I discovered ILVs inside Rab11-positive compartments and showed that they are released as exosomes, demonstrating for the first time that intracellular organelles

other than late endosomal MVBs are responsible for exosome secretion. I also showed that numerous cargos, including Rabs and signalling molecules, localise specifically on these intraluminal vesicles and are secreted into the accessory gland lumen. Interestingly, different subtypes of ILVs were observed within the same type of subcellular compartment, suggesting that exosome heterogeneity is generated by employing different compartments and from within individual compartments. I also showed that ESCRT components localise to the surface of these compartments, where they mediate ILV formation. Finally, I collaborated with researchers in the Goberdhan lab to show that Rab11a-positive compartments in human cells also contain ILVs. S-J. Fan has also demonstrated that Rab11a is released on exosomes, similar to *Drosophila* secondary cells, and that ESCRTs regulate exosome release from Rab11a-positive compartments in human cells, indicating that we have discovered a fundamental new mechanism in exosome biology.

My third results chapter (Section 5.0) explored the genetic regulation of intracellular compartment formation and maturation in secondary cells. This work primarily focussed on dense-core granule compartments, but also crossed paths with the large lysosomal compartments. I followed the entire process of dense-core granule biogenesis within individual non-cored compartments using live-cell imaging. This characterisation is, to the best of my knowledge, the clearest demonstration of dense-core granule biogenesis in any cell type. Interestingly, I observed a novel Rab transition between Rab6 and Rab11 on the surface of maturing compartments during this process. Using RNAi knockdowns, I showed how Rab6, Rab11 and Rab7 regulate

different stages of dense-core granule maturation and membrane trafficking. In addition, I used RNAi to confirm that previously characterised regulators of dense-core granule biogenesis in other systems perform similar roles in secondary cells, establishing these cells as a new genetic model to study this widely employed mechanism that has primarily been analysed in cell culture to date. I have also identified other novel regulators of dense-core granule biogenesis, including the fibrillar adhesion protein Mfas and propose that ILVs may deliver cargos to the forming core. The identification of these novel molecular regulators of dense-core granule formation may be relevant to several human diseases, most notably diabetes, cancer and neurodegenerative disorders. I also report that ILVs may help to promote the acidification of large late endosomal and lysosomal compartments. Overall this chapter implicates several novel proteins and cell biological processes in regulated secretion and endolysosomal biology.

6.2 Overall perspectives and future directions

6.2.1 Advantages of the secondary cell model to study membrane trafficking and secretion

The secondary cell system possesses several advantages as an *in vivo* model to study membrane trafficking and secretion. Most importantly, the large size of their subcellular compartments permits the study of intracompartmental biology using fluorescence microscopy, which can be used on living specimens and in real-time. Furthermore, the biogenesis of large compartments occurs one-by-one, making it possible to follow each

particular step, each labelled by a different vital marker, and to use mutant cells to pin-point the particular stage that each gene functions in this process. The work in my thesis has already illustrated how this approach can be used to dissect out new cell biological processes, whose evolutionary conservation can then be assessed by employing more standard approaches in other cell types. With the wide variety of RNAi knockdown tools available to Drosophilists, the secondary cell is well placed to characterise new genes with roles in compartment biogenesis and trafficking.

6.2.2 Implications for exosome biology

My work has helped to establish the idea that exosomes are made in a range of different endosomal compartments and that these different vesicles may be defined by their Rab signature, as well as carrying other specific cargoes. Thus, exosomes deriving from a particular type of subcellular compartment carry a particular Rab, which marks its origin, even after secretion. This is particularly important, since unlike transmembrane exosome proteins that are likely to reach the plasma membrane and could be shed from there in vesicles (eg., CD63-GFP, Btl-GFP), Rabs typically detach upon membrane fusion of compartments and are therefore likely to only be present in exosomes.
Given the challenges of identification of different exosome subtypes in the extracellular milieu (Maas *et al*., 2017), future human cell work could employ knockdowns for the Rabs identified here to identify their specific surface cargos, which could then be used for subtype-specific exosome pull-down and separation. Although my work has focused on Rab11 and Rab7, I have also identified Rab6- and Rab19-labelled ILVs, whose properties also need to be

studied. Indeed, proteomic analysis of mammalian extracellular vesicle preparations suggests that 20 or more Rabs may be incorporated as cargoes in exosomes, suggesting a remarkable complexity in these signalling moieties.

I have also demonstrated heterogeneous packaging of exosome cargos within the ILVs of the same compartments, which may help to explain further diversity seen in exosome isolations from mammalian cells (Willms *et al*., 2016). In the future, it will be important to determine if this is due to specialised sorting mechanisms or whether it reflects changes in the molecules that associate with a particular compartment over time, questions that can be addressed in the secondary cell system. Studies in mammalian cells have suggested different mechanisms for exosome production, eg. ESCRT-, ceramide- and CD63- (tetraspanin-) dependent (Christ et al., 2017; Trajkovic *et al*., 2008; Edgar *et al*., 2014), all of which can now be tested for each exosome population as it is formed inside specific compartments.

My work may help to understand how cancer cells utilise exosomes to manipulate their microenvironment in a variety of ways (Miller & Gunewald, 2015; Costa-Silva *et al*., 2015; Azmi *et al*., 2013), as they could potentially modulate the type of exosomes that they release, in response to specific stimuli. My collaborators in the Goberdhan lab have already identified that human colorectal cancer HCT116 cells respond to mTORC1 inhibition by releasing a different set of exosomes, which derive from Rab11a-positive compartments, and might drive tumour adaptation (Perera *et al*., in preparation).

6.2.3 Implications for dense-core granule biology

My studies of dense core granule biology demonstrated that known regulators of dense-core granule biogenesis also control formation of these structures in secondary cells. Indeed, even this 'me to' analysis has identified distinctions between the functions of regulators like AP-1 and Arf79F, which might have been predicted to give equivalent phenotypes. And some of the phenotypes I observe, for example with one of the *Chc* RNAi lines suggests remarkable specificity associated with the trafficking of GPI-anchored proteins that can now be probed in detail.

I have identified novel Rab transitions, where the predominant Rab on the surface of a particular compartment changes as it matures or undergoes particular trafficking events. These Rab transitions will now be further studied in the secondary cell model to identify the precise GEFs and GAPs that facilitate them (Barr, 2013), and also to characterise effector molecules for these Rabs. Several evolutionarily conserved candidates have been identified in other fly cell types or different organisms that could now be tested.

My work also strongly suggests that the endosomal system interacts with the secretory dense-core granule compartments, as they are enriched in endosome-associated Rabs and contain lumenal lysosomal hydrolases. Furthermore, ILVs, classically associated with late endosomes, are enriched inside these dense-core granule compartments. A closer characterisation of the interactions between these pathways may provide insight into the mechanisms of granule biogenesis and/or function. They certainly should help to explain some general observations made in other systems concerning changes in compartments during dense-core maturation, such as the fall in

pH and increase in Ca^{2+} levels. Again the secondary cell system is ideally suited for follow-up experiments in this area. The complex and evolving combinations of Rabs on maturing dense-core granule compartments also merit further investigation, since they may allow multiple steps in the process to be easily distinguished.

Interestingly, the dense-core granule compartments contain ILVs and an elaborate network of fibres. My analysis suggests that these appear before the dense core is formed and the vesicles are required for dense core biogenesis. Related processes have been reported in other types of dense-core granules, including the lysosome-related melanosomes (Patwardhan *et al*., 2007), where melanin is assembled on PMEL fibres. In this regard, the identification of the TGFBI homologue Mfas as a major component of the dense core in secondary cells required for its assembly is intriguing. The work suggests a potential re-evaluation of TGFBI's proposed roles in diabetes and corneal dystrophies. The presence of extracellular matrix components within dense-core granules may also have other roles, such as the regulation of growth factors like BMPs, which we already know are packaged within these structures.

It is notable that amyloid fibres have recently been reported to be primed on ILVs inside endosomal compartments (Morel *et al*., 2014). Since the endolysosomal and autophagic systems are increasingly being implicated in neurodegenerative diseases, it is possible that the fibres we observe in secondary cell dense-core granule compartments and high levels of Mfas are in some way linked to a physiological transition that leads to a rapid assembly of fibrous material and condensation of a dense-core upon this. As this

process is analysed in more detail, it will be possible to test whether the autophagy and endolysosomal genes that are linked to neurodegenerative disease might regulate fibre and dense-core assembly in secondary cells, which might them provide a completely new model to investigate the underlying biology.

6.2.4 Potential for the study of zymophagy

My studies also show that secondary cells may be well suited as a new genetic model to study zymophagy, a form of autophagy that involves the degradation of dense-core granules. Impairments in this process have been implicated in human diseases, such as acute pancreatitis (Helin *et al*., 1980), so a detailed cell biological and genetic characterisation of the mechanisms underlying these processes is likely to be valuable to future clinical studies. Furthermore this process may be critical in breaking down the fibrous material present in dense-core granule compartments, which could have positive or negative effects on the cell, depending on what forms of these fibrous proteins are potentially toxic. Important questions remain regarding the basic zymophagy-like process in secondary cells: especially to what extent it is occurring, and what physiological factors may control it. The flies used in my studies were not nutrient-starved; so classical autophagy is unlikely to have been activated (Russell *et al*., 2014).

6.2.5 Open questions and problems

The structural similarities between the secondary cell's large acidic compartment and those observed in human patients with lysosomal storage

disorders and certain neurodegenerative diseases further highlights the similarity in cell biological processes across evolution. To date, the lab has not investigated the system as a genetic model for these diseases, but it seems very likely that with the increased resolution in our system and the access to live imaging that a directed screen of the genes involved may allow phenotypes to be categorised in ways that have not been possible to date.
Despite the unique versatility of the secondary cell system, some limitations were noted. For example, using highly expressed fluorescent protein markers, such as GFP-GPI and CD63-GFP, affected the intracellular organisation and membrane trafficking of secondary cells. In fact, many of the *Rab* gene traps, presumably expressed at roughly endogenous levels, also had effects on cell morphology, even when some of them were heterozygous. Although it is possible that secondary cells are simply extremely sensitive to expression of transgenes, it is also plausible that they disrupt other cell types they are used in similarly, but it is less noticeable given the smaller size of subcellular compartments. The *Drosophila* community continues to generate new gene traps (eg. Flyprot; Morin *et al*., 2001) that will identify yet more fluorescently tagged fusion proteins that are expressed at physiological levels, and by screening through those implicated in secretion and trafficking, such as those linked to *mfas*, *Trol* and *CtsB1*, we are likely to build up an increasingly powerful set of tools to dissect out secondary cell biology.
To date, the focus of secondary cell studies has primarily been on the large compartments within these cells. Yet live imaging clearly illustrates the presence of vesicular tram-tracks and tubular extensions linking

compartments to each other and the plasma membrane, biological processes that also need to be investigated.

Currently the secondary cell system is powerful for candidate genetic screens, but setting up a whole genome screen would still be challenging given the tools available to us. Over the next few years, there will be attempts to design simpler assays, for example by trying to detect the effects of exosomes in females, which could then be employed in an exhaustive RNAi screen. Given the progress I have made with just a few candidate genes over the last three years in identifying highly specific phenotypes in secondary cells, this type of approach would allow a further step-change in our ability to dissect out the genetics of complex secretory processes in years to come.

7.0 Bibliography

- Adell, M. A., G. F. Vogel, M. Pakdel, M. Muller, H. Lindner, M. W. Hess and D. Teis (2014). "Coordinated binding of Vps4 to ESCRT-III drives membrane neck constriction during MVB vesicle formation." J Cell Biol **205**(1): 33-49.
- Alexandrov, K., H. Horiuchi, O. Steele-Mortimer, M. C. Seabra and M. Zerial (1994). "Rab escort protein-1 is a multifunctional protein that accompanies newly prenylated rab proteins to their target membranes." EMBO J **13**(22): 5262-5273.
- Ali, B. R., C. Wasmeier, L. Lamoreux, M. Strom and M. C. Seabra (2004). "Multiple regions contribute to membrane targeting of Rab GTPases." J Cell Sci **117**(Pt 26): 6401-6412.
- Alberts B., A. Johnson, J. Lewis, M. Raff, K. Roberts, and P. Walter (2002). "Molecular Biology of the Cell". 4th edition. New York: Garland Science. Chapter 12.
- Allan, B. B., B. D. Moyer and W. E. Balch (2000). "Rab1 recruitment of p115 into a cis-SNARE complex: programming budding COPII vesicles for fusion." Science **289**(5478): 444-448.
- Andres, D. A., M. C. Seabra, M. S. Brown, S. A. Armstrong, T. E. Smeland, F. P. Cremers and J. L. Goldstein (1993). "cDNA cloning of component A of Rab geranylgeranyl transferase and demonstration of its role as a Rab escort protein." Cell **73**(6): 1091-1099.
- Anello, M., P. Gilon and J. C. Henquin (1999). "Alterations of insulin secretion from mouse islets treated with sulphonylureas: perturbations of Ca2+ regulation prevail over changes in insulin content." Br J Pharmacol **127**(8): 1883-1891.
- Ang, A. L., T. Taguchi, S. Francis, H. Folsch, L. J. Murrells, M. Pypaert, G. Warren and I. Mellman (2004). "Recycling endosomes can serve as intermediates during transport from the Golgi to the plasma membrane of MDCK cells." J Cell Biol **167**(3): 531-543.
- Appelqvist, H., P. Waster, K. Kagedal and K. Ollinger (2013). "The lysosome: from waste bag to potential therapeutic target." J Mol Cell Biol **5**(4): 214-226.
- Armbruster, K. and S. Luschnig (2012). "The Drosophila Sec7 domain guanine nucleotide exchange factor protein Gartenzwerg localizes at the cis-Golgi and is essential for epithelial tube expansion." J Cell Sci **125**(Pt 5): 1318-1328.
- Ashcroft, F. M. and P. Rorsman (2012). "Diabetes mellitus and the beta cell: the last ten years." Cell **148**(6): 1160-1171.
- Asp, L., F. Kartberg, J. Fernandez-Rodriguez, M. Smedh, M. Elsner, F. Laporte, M. Barcena, K. A. Jansen, J. A. Valentijn, A. J. Koster, J. J. Bergeron and T. Nilsson (2009). "Early stages of Golgi vesicle and tubule formation require diacylglycerol." Mol Biol Cell **20**(3): 780-790.
- Austin, C., I. Hinners and S. A. Tooze (2000). "Direct and GTP-dependent interaction of ADP-ribosylation factor 1 with clathrin adaptor protein AP-1 on immature secretory granules." J Biol Chem **275**(29): 21862-21869.
- Azmi, A. S., B. Bao and F. H. Sarkar (2013). "Exosomes in cancer development, metastasis, and drug resistance: a comprehensive review." Cancer Metastasis Rev **32**(3-4): 623-642.
- Baba, M., K. Takeshige, N. Baba and Y. Ohsumi (1994). "Ultrastructural analysis of the autophagic process in yeast: detection of autophagosomes and their characterization." J Cell Biol **124**(6): 903-913.
- Babbey, C. M., N. Ahktar, E. Wang, C. C. Chen, B. D. Grant and K. W. Dunn (2006). "Rab10 regulates membrane transport through early endosomes of polarized Madin-Darby canine kidney cells." Mol Biol Cell **17**(7): 3156-3175.
- Babst, M. (2011). "MVB vesicle formation: ESCRT-dependent, ESCRT-independent and everything in between." Curr Opin Cell Biol **23**(4): 452-457.

- Babst, M., D. J. Katzmann, W. B. Snyder, B. Wendland and S. D. Emr (2002). "Endosome-associated complex, ESCRT-II, recruits transport machinery for protein sorting at the multivesicular body." Dev Cell **3**(2): 283-289.
- Babst, M., B. Wendland, E. J. Estepa and S. D. Emr (1998). "The Vps4p AAA ATPase regulates membrane association of a Vps protein complex required for normal endosome function." EMBO J **17**(11): 2982-2993.
- Bache, K. G., A. Brech, A. Mehlum and H. Stenmark (2003). "Hrs regulates multivesicular body formation via ESCRT recruitment to endosomes." J Cell Biol **162**(3): 435-442.
- Baietti, M. F., Z. Zhang, E. Mortier, A. Melchior, G. Degeest, A. Geeraerts, Y. Ivarsson, F. Depoortere, C. Coomans, E. Vermeiren, P. Zimmermann and G. David (2012). "Syndecan-syntenin-ALIX regulates the biogenesis of exosomes." Nat Cell Biol **14**(7): 677-685.
- Bainton, D. F. (1981). "The discovery of lysosomes." J Cell Biol **91**(3 Pt 2): 66s-76s.
- Bainton, D. F. and M. G. Farquhar (1966). "Origin of granules in polymorphonuclear leukocytes. Two types derived from opposite faces of the Golgi complex in developing granulocytes." J Cell Biol **28**(2): 277-301.
- Bairati. (1968). " Structure and ultrastructure of the male reproductive system in Drosophila melanogaster meig. 2. The genital duct and accessory glands." Monitore Zoologico Italiano-Italian Journal of Zoology, **2**(3-4), 105-182.
- Ball, G., R. M. Parton, R. S. Hamilton and I. Davis (2012). "A cell biologist's guide to high resolution imaging." Methods Enzymol **504**: 29-55.
- Ball, G., J. Demmerle, R. Kaufmann, I. Davis, I. Dobbie and L. Schermelleh (2015). "SIMcheck: a Toolbox for Successful Super-resolution Structured Illumination Microscopy." Scientific Reports **5**: 15915.
- Banfield, D. K., M. J. Lewis, C. Rabouille, G. Warren and H. R. Pelham (1994). "Localization of Sed5, a putative vesicle targeting molecule, to the cis-Golgi network involves both its transmembrane and cytoplasmic domains." J Cell Biol **127**(2): 357-371.
- Bao, H., M. Goldschen-Ohm, P. Jeggle, B. Chanda, J. M. Edwardson and E. R. Chapman (2016). "Exocytotic fusion pores are composed of both lipids and proteins." Nat Struct Mol Biol **23**(1): 67-73.
- Barr, F. and D. G. Lambright (2010). "Rab GEFs and GAPs." Curr Opin Cell Biol **22**(4): 461-470.
- Barr, F. A. (2013). "Review series: Rab GTPases and membrane identity: causal or inconsequential?" J Cell Biol **202**(2): 191-199.
- Bartfai, T., K. Iverfeldt, G. Fisone and P. Serfozo (1988). "Regulation of the release of coexisting neurotransmitters." Annu Rev Pharmacol Toxicol **28**: 285-310.
- Becker, A., B. K. Thakur, J. M. Weiss, H. S. Kim, H. Peinado and D. Lyden (2016). "Extracellular Vesicles in Cancer: Cell-to-Cell Mediators of Metastasis." Cancer Cell **30**(6): 836-848.
- Beckett, K., S. Monier, L. Palmer, C. Alexandre, H. Green, E. Bonneil, G. Raposo, P. Thibault, R. Le Borgne and J. P. Vincent (2013). "Drosophila S2 cells secrete wingless on exosome-like vesicles but the wingless gradient forms independently of exosomes." Traffic **14**(1): 82-96.
- Bellen, H. J., C. Tong and H. Tsuda (2010). "100 years of Drosophila research and its impact on vertebrate neuroscience: a history lesson for the future." Nat Rev Neurosci **11**(7): 514-522.
- Benhra, N., S. Lallet, M. Cotton, S. Le Bras, A. Dussert and R. Le Borgne (2011). "AP-1 controls the trafficking of Notch and Sanpodo toward E-cadherin junctions in sensory organ precursors." Curr Biol **21**(1): 87-95.

- Bertram, M. J., G. A. Akerkar, R. L. Ard, C. Gonzalez and M. F. Wolfner (1992). "Cell type-specific gene expression in the Drosophila melanogaster male accessory gland." Mech Dev **38**(1): 33-40.
- Beyenbach, K. W. and H. Wieczorek (2006). "The V-type H+ ATPase: molecular structure and function, physiological roles and regulation." J Exp Biol **209**(Pt 4): 577-589.
- Bissig, C. and J. Gruenberg (2014). "ALIX and the multivesicular endosome: ALIX in Wonderland." Trends Cell Biol **24**(1): 19-25.
- Blazquez, M., C. Thiele, W. B. Huttner, K. Docherty and K. I. Shennan (2000). "Involvement of the membrane lipid bilayer in sorting prohormone convertase 2 into the regulated secretory pathway." Biochem J **349 Pt 3**: 843-852.
- Blott, E. J., G. Bossi, R. Clark, M. Zvelebil and G. M. Griffiths (2001). "Fas ligand is targeted to secretory lysosomes via a proline-rich domain in its cytoplasmic tail." J Cell Sci **114**(Pt 13): 2405-2416.
- Blott, E. J. and G. M. Griffiths (2002). "Secretory lysosomes." Nat Rev Mol Cell Biol **3**(2): 122-131.
- Blumer, J., J. Rey, L. Dehmelt, T. Mazel, Y. W. Wu, P. Bastiaens, R. S. Goody and A. Itzen (2013). "RabGEFs are a major determinant for specific Rab membrane targeting." J Cell Biol **200**(3): 287-300.
- Boehm, M. and J. S. Bonifacino (2001). "Adaptins: the final recount." Mol Biol Cell **12**(10): 2907-2920.
- Bonifacino, J. S. and R. Rojas (2006). "Retrograde transport from endosomes to the trans-Golgi network." Nat Rev Mol Cell Biol **7**(8): 568-579.
- Bonnemaison, M. L., B. A. Eipper and R. E. Mains (2013). "Role of adaptor proteins in secretory granule biogenesis and maturation." Front Endocrinol (Lausanne) **4**: 101.
- Boucheix, C. and E. Rubinstein (2001). "Tetraspanins." Cell Mol Life Sci **58**(9): 1189-1205.
- Brand, A. H. and N. Perrimon (1993). "Targeted gene expression as a means of altering cell fates and generating dominant phenotypes." Development **118**(2): 401-415.
- Bright, N. A., M. J. Gratian and J. P. Luzio (2005). "Endocytic delivery to lysosomes mediated by concurrent fusion and kissing events in living cells." Curr Biol **15**(4): 360-365.
- Brown, W. J., J. Goodhouse and M. G. Farquhar (1986). "Mannose-6-phosphate receptors for lysosomal enzymes cycle between the Golgi complex and endosomes." J Cell Biol **103**(4): 1235-1247.
- Brunner, Y., Y. Coute, M. Iezzi, M. Foti, M. Fukuda, D. F. Hochstrasser, C. B. Wollheim and J. C. Sanchez (2007). "Proteomics analysis of insulin secretory granules." Mol Cell Proteomics **6**(6): 1007-1017.
- Bryant, N. J. and T. H. Stevens (1998). "Vacuole biogenesis in Saccharomyces cerevisiae: protein transport pathways to the yeast vacuole." Microbiol Mol Biol Rev **62**(1): 230-247.
- Bucci, C., P. Thomsen, P. Nicoziani, J. McCarthy and B. van Deurs (2000). "Rab7: a key to lysosome biogenesis." Mol Biol Cell **11**(2): 467-480.
- Burgess, J., M. Jauregui, J. Tan, J. Rollins, S. Lallet, P. A. Leventis, G. L. Boulianne, H. C. Chang, R. Le Borgne, H. Kramer and J. A. Brill (2011). "AP-1 and clathrin are essential for secretory granule biogenesis in Drosophila." Mol Biol Cell **22**(12): 2094-2105.
- Burgess, T. L. and R. B. Kelly (1987). "Constitutive and regulated secretion of proteins." Annu Rev Cell Biol **3**: 243-293.
- Burgoyne, R. D. and A. Morgan (2003). "Secretory granule exocytosis." Physiol Rev **83**(2): 581-632.

- Burleigh, M. C., A. J. Barrett and G. S. Lazarus (1974). "Cathepsin B1. A lysosomal enzyme that degrades native collagen." Biochem J **137**(2): 387-398.
- Cao, X., M. A. Surma and K. Simons (2012). "Polarized sorting and trafficking in epithelial cells." Cell Res **22**(5): 793-805.
- Castellanos, F. (2017). DPhil Thesis. In preparation.
- Chan, C. C., S. Scoggin, D. Wang, S. Cherry, T. Dembo, B. Greenberg, E. J. Jin, C. Kuey, A. Lopez, S. Q. Mehta, T. J. Perkins, M. Brankatschk, A. Rothenfluh, M. Buszczak and P. R. Hiesinger (2011). "Systematic discovery of Rab GTPases with synaptic functions in Drosophila." Curr Biol **21**(20): 1704-1715.
- Chang, A. J. D. Jamieson (1989). "Structural and secretory polarity in the pancreatic acinar cell". The gastrointestinal system, vol III, section 6 (Handbook of physiology). American Physiological Society, Bethesda, Md, pp 531–547
- Chang, H. C., S. L. Newmyer, M. J. Hull, M. Ebersold, S. L. Schmid and I. Mellman (2002). "Hsc70 is required for endocytosis and clathrin function in Drosophila." J Cell Biol **159**(3): 477-487.
- Chavrier, P., J. P. Gorvel, E. Stelzer, K. Simons, J. Gruenberg and M. Zerial (1991). "Hypervariable C-terminal domain of rab proteins acts as a targeting signal." Nature **353**(6346): 769-772.
- Chavrier, P., R. G. Parton, H. P. Hauri, K. Simons and M. Zerial (1990). "Localization of low molecular weight GTP binding proteins to exocytic and endocytic compartments." Cell **62**(2): 317-329.
- Chen. (1984). " The functional morphology and biochemistry of insect accessory glands and their secretions." Ann. Rev. Entomol. **29**:233-255
- Chen, P.S, E. Stumm-Zollinger, T. Aigaki, J. Balmer, M. Bienz and P. Bohlen (1988). "A male accessory gland peptide that regulates reproductive behavior of female D. melanogaster." Cell **54**(3): 291F298.
- Chen, W., Y. Feng, D. Chen and A. Wandinger-Ness (1998). "Rab11 is required for trans-golgi network-to-plasma membrane transport and a preferential target for GDP dissociation inhibitor." Mol Biol Cell **9**(11): 3241-3257.
- Chen, X., A. K. Walker, J. R. Strahler, E. S. Simon, S. L. Tomanicek-Volk, B. B. Nelson, M. C. Hurley, S. A. Ernst, J. A. Williams and P. C. Andrews (2006). "Organellar proteomics: analysis of pancreatic zymogen granule membranes." Mol Cell Proteomics **5**(2): 306-312.
- Chintapalli, V. R., J. Wang and J. A. Dow (2007). "Using FlyAtlas to identify better Drosophila melanogaster models of human disease." Nat Genet **39**(6): 715-720.
- Choi, S. I., Y. S. Maeng, T. I. Kim, Y. Lee, Y. S. Kim and E. K. Kim (2015). "Lysosomal trafficking of TGFBIp via caveolae-mediated endocytosis." PLoS One **10**(4): e0119561.
- Christ, L., C. Raiborg, E. M. Wenzel, C. Campsteijn and H. Stenmark (2017). "Cellular Functions and Molecular Mechanisms of the ESCRT Membrane-Scission Machinery." Trends Biochem Sci **42**(1): 42-56.
- Christis, C. and S. Munro (2012). "The small G protein Arl1 directs the trans-Golgi-specific targeting of the Arf1 exchange factors BIG1 and BIG2." J Cell Biol **196**(3): 327-335.
- Clout, N. J. and E. Hohenester (2003). "A model of FAS1 domain 4 of the corneal protein beta(ig)-h3 gives a clearer view on corneal dystrophies." Mol Vis **9**: 440-448.

- Cocucci, E. and J. Meldolesi (2015). "Ectosomes and exosomes: shedding the confusion between extracellular vesicles." Trends Cell Biol **25**(6): 364-372.
- Collins, R. N. (2003). ""Getting it on"--GDI displacement and small GTPase membrane recruitment." Mol Cell **12**(5): 1064-1066.
- Colombo, M., G. Raposo and C. Thery (2014). "Biogenesis, secretion, and intercellular interactions of exosomes and other extracellular vesicles." Annu Rev Cell Dev Biol **30**: 255-289.
- Cool, D. R., E. Normant, F. Shen, H. C. Chen, L. Pannell, Y. Zhang and Y. P. Loh (1997). "Carboxypeptidase E is a regulated secretory pathway sorting receptor: genetic obliteration leads to endocrine disorders in Cpe(fat) mice." Cell **88**(1): 73-83.
- Corrigan, L., S. Redhai, A. Leiblich, S. J. Fan, S. M. Perera, R. Patel, C. Gandy, S. M. Wainwright, J. F. Morris, F. Hamdy, D. C. Goberdhan and C. Wilson (2014). "BMP-regulated exosomes from Drosophila male reproductive glands reprogram female behavior." J Cell Biol **206**(5): 671-688.
- Corrigan, L. (2014) "Regulation and reproductive functions of membrane-bound vesicles secreted by the Drosophila male accessory gland." DPhil Thesis. University of Oxford.
- Costa-Silva, B., N. M. Aiello, A. J. Ocean, S. Singh, H. Zhang, B. K. Thakur, A. Becker, A. Hoshino, M. T. Mark, H. Molina, J. Xiang, T. Zhang, T. M. Theilen, G. Garcia-Santos, C. Williams, Y. Ararso, Y. Huang, G. Rodrigues, T. L. Shen, K. J. Labori, I. M. Lothe, E. H. Kure, J. Hernandez, A. Doussot, S. H. Ebbesen, P. M. Grandgenett, M. A. Hollingsworth, M. Jain, K. Mallya, S. K. Batra, W. R. Jarnagin, R. E. Schwartz, I. Matei, H. Peinado, B. Z. Stanger, J. Bromberg and D. Lyden (2015). "Pancreatic cancer exosomes initiate pre-metastatic niche formation in the liver." Nat Cell Biol **17**(6): 816-826.
- Cowland, J. B. and N. Borregaard (2016). "Granulopoiesis and granules of human neutrophils." Immunol Rev **273**(1): 11-28.
- Cox, S. (2015). "Super-resolution imaging in live cells." Dev Biol **401**(1): 175-181.
- Crivellato, E., B. Nico and D. Ribatti (2008). "The chromaffin vesicle: advances in understanding the composition of a versatile, multifunctional secretory organelle." Anat Rec (Hoboken) **291**(12): 1587-1602.
- Dannies, P. S. (1999). "Protein hormone storage in secretory granules: mechanisms for concentration and sorting." Endocr Rev **20**(1): 3-21.
- Day, R. and S. U. Gorr (2003). "Secretory granule biogenesis and chromogranin A: master gene, on/off switch or assembly factor?" Trends Endocrinol Metab **14**(1): 10-13.
- De Duve, C., B. C. Pressman, R. Gianetto, R. Wattiaux and F. Appelmans (1955). "Tissue fractionation studies. 6. Intracellular distribution patterns of enzymes in rat-liver tissue." Biochem J **60**(4): 604-617.
- Dehay, B., M. Martinez-Vicente, G. A. Caldwell, K. A. Caldwell, Z. Yue, M. R. Cookson, C. Klein, M. Vila and E. Bezard (2013). "Lysosomal impairment in Parkinson's disease." Mov Disord **28**(6): 725-732.
- Delevoye, C., S. Miserey-Lenkei, G. Montagnac, F. Gilles-Marsens, P. Paul-Gilloteaux, F. Giordano, F. Waharte, M. S. Marks, B. Goud and G. Raposo (2014). "Recycling endosome tubule morphogenesis from sorting endosomes requires the kinesin motor KIF13A." Cell Rep **6**(3): 445-454.
- Demmerle, J., C. Innocent, A. J. North, G. Ball, M. Muller, E. Miron, A. Matsuda, I. M. Dobbie, Y. Markaki and L. Schermelleh (2017). "Strategic and practical guidelines for successful structured illumination microscopy." Nat Protoc **12**(5): 988-1010.

- Demory Beckler, M., J. N. Higginbotham, J. L. Franklin, A. J. Ham, P. J. Halvey, I. E. Imasuen, C. Whitwell, M. Li, D. C. Liebler and R. J. Coffey (2013). "Proteomic analysis of exosomes from mutant KRAS colon cancer cells identifies intercellular transfer of mutant KRAS." Mol Cell Proteomics **12**(2): 343-355.
- DeNicola, G. M. and L. C. Cantley (2015). "Cancer's Fuel Choice: New Flavors for a Picky Eater." Mol Cell **60**(4): 514-523.
- DiBenedetto, A. J., H. A. Harada and M. F. Wolfner (1990). "Structure, cell-specific expression, and mating-induced regulation of a Drosophila melanogaster male accessory gland gene." Dev Biol **139**(1): 134-148.
- Diekmann, Y., E. Seixas, M. Gouw, F. Tavares-Cadete, M. C. Seabra and J. B. Pereira-Leal (2011). "Thousands of rab GTPases for the cell biologist." PLoS Comput Biol **7**(10): e1002217.
- Dittie, A. S., N. Hajibagheri and S. A. Tooze (1996). "The AP-1 adaptor complex binds to immature secretory granules from PC12 cells, and is regulated by ADP-ribosylation factor." J Cell Biol **132**(4): 523-536.
- Diwu, Z., C. S. Chen, C. Zhang, D. H. Klaubert and R. P. Haugland (1999). "A novel acidotropic pH indicator and its potential application in labeling acidic organelles of live cells." Chem Biol **6**(7): 411-418.
- Docherty, K., J. C. Hutton and D. F. Steiner (1984). "Cathepsin B-related proteases in the insulin secretory granule." J Biol Chem **259**(10): 6041-6044.
- Doliana, R., S. Bot, P. Bonaldo and A. Colombatti (2000). "EMI, a novel cysteine-rich domain of EMILINs and other extracellular proteins, interacts with the gC1q domains and participates in multimerization." FEBS Lett **484**(2): 164-168.
- Donaldson, J. G., D. Finazzi and R. D. Klausner (1992). "Brefeldin A inhibits Golgi membrane-catalysed exchange of guanine nucleotide onto ARF protein." Nature **360**(6402): 350-352.
- Dunst, S., T. Kazimiers, F. von Zadow, H. Jambor, A. Sagner, B. Brankatschk, A. Mahmoud, S. Spannl, P. Tomancak, S. Eaton and M. Brankatschk (2015). "Endogenously tagged rab proteins: a resource to study membrane trafficking in Drosophila." Dev Cell **33**(3): 351-365.
- Duve, C. (1975). "Exploring cells with a centrifuge." Science **189**(4198): 186-194.
- Edgar, J. R., E. R. Eden and C. E. Futter (2014). "Hrs- and CD63-dependent competing mechanisms make different sized endosomal intraluminal vesicles." Traffic **15**(2): 197-211.
- Evans, T. M., C. Ferguson, B. J. Wainwright, R. G. Parton and C. Wicking (2003). "Rab23, a negative regulator of hedgehog signaling, localizes to the plasma membrane and the endocytic pathway." Traffic **4**(12): 869-884.
- Fader, C. M., D. G. Sanchez, M. B. Mestre and M. I. Colombo (2009). "TI-VAMP/VAMP7 and VAMP3/cellubrevin: two v-SNARE proteins involved in specific steps of the autophagy/multivesicular body pathways." Biochim Biophys Acta **1793**(12): 1901-1916.
- Faust, F., M. Gomez-Lazaro, H. Borta, B. Agricola and M. Schrader (2008). "Rab8 is involved in zymogen granule formation in pancreatic acinar AR42J cells." Traffic **9**(6): 964-979.
- Fava, E., J. Dehghany, J. Ouwendijk, A. Muller, A. Niederlein, P. Verkade, M. Meyer-Hermann and M. Solimena (2012). "Novel standards in the measurement of rat insulin granules combining electron microscopy, high-content image analysis and in silico modelling." Diabetologia **55**(4): 1013-1023.

- Feliciano, W. D., S. Yoshida, S. W. Straight and J. A. Swanson (2011). "Coordination of the Rab5 cycle on macropinosomes." Traffic **12**(12): 1911-1922.
- Findlay, G. D., X. Yi, M. J. Maccoss and W. J. Swanson (2008). "Proteomics reveals novel Drosophila seminal fluid proteins transferred at mating." PLoS Biol **6**(7): e178.
- Gaisano, H. Y. (2017). "Recent new insights into the role of SNARE and associated proteins in insulin granule exocytosis." Diabetes Obes Metab **19 Suppl 1**: 115-123.
- Gan, Z., S. Ram, C. Vaccaro, R. J. Ober and E. S. Ward (2009). "Analyses of the recycling receptor, FcRn, in live cells reveal novel pathways for lysosomal delivery." Traffic **10**(5): 600-614.
- Gates, J., J. P. Mahaffey, S. L. Rogers, M. Emerson, E. M. Rogers, S. L. Sottile, D. Van Vactor, F. B. Gertler and M. Peifer (2007). "Enabled plays key roles in embryonic epithelial morphogenesis in Drosophila." Development **134**(11): 2027-2039.
- Gehart, H., A. Goginashvili, R. Beck, J. Morvan, E. Erbs, I. Formentini, M. A. De Matteis, Y. Schwab, F. T. Wieland and R. Ricci (2012). "The BAR domain protein Arfaptin-1 controls secretory granule biogenesis at the trans-Golgi network." Dev Cell **23**(4): 756-768.
- Geuze, H. J., J. W. Slot, G. J. Strous, H. F. Lodish and A. L. Schwartz (1983). "Intracellular site of asialoglycoprotein receptor-ligand uncoupling: double-label immunoelectron microscopy during receptor-mediated endocytosis." Cell **32**(1): 277-287.
- Gill, D. J., H. Teo, J. Sun, O. Perisic, D. B. Veprintsev, S. D. Emr and R. L. Williams (2007). "Structural insight into the ESCRT-I/-II link and its role in MVB trafficking." EMBO J **26**(2): 600-612.
- Gillingham, A. K., R. Sinka, I. L. Torres, K. S. Lilley and S. Munro (2014). "Toward a comprehensive map of the effectors of rab GTPases." Dev Cell **31**(3): 358-373.
- Gligorov, D., J. L. Sitnik, R. K. Maeda, M. F. Wolfner and F. Karch (2013). "A novel function for the Hox gene Abd-B in the male accessory gland regulates the long-term female post-mating response in Drosophila." PLoS Genet **9**(3): e1003395.
- Goginashvili, A., Z. Zhang, E. Erbs, C. Spiegelhalter, P. Kessler, M. Mihlan, A. Pasquier, K. Krupina, N. Schieber, L. Cinque, J. Morvan, I. Sumara, Y. Schwab, C. Settembre and R. Ricci (2015). "Insulin granules. Insulin secretory granules control autophagy in pancreatic beta cells." Science **347**(6224): 878-882.
- Gorvel, J. P., P. Chavrier, M. Zerial and J. Gruenberg (1991). "rab5 controls early endosome fusion in vitro." Cell **64**(5): 915-925.
- Goud, B., A. Zahraoui, A. Tavitian and J. Saraste (1990). "Small GTP-binding protein associated with Golgi cisternae." Nature **345**(6275): 553-556.
- Gould, G. W. and J. Lippincott-Schwartz (2009). "New roles for endosomes: from vesicular carriers to multi-purpose platforms." Nat Rev Mol Cell Biol **10**(4): 287-292.
- Greco, V., M. Hannus and S. Eaton (2001). "Argosomes: a potential vehicle for the spread of morphogens through epithelia." Cell **106**(5): 633-645.
- Griffiths, R. E., S. Kupzig, N. Cogan, T. J. Mankelow, V. M. Betin, K. Trakarnsanga, E. J. Massey, J. D. Lane, S. F. Parsons and D. J. Anstee (2012). "Maturing reticulocytes internalize plasma membrane in glycophorin A-containing vesicles that fuse with autophagosomes before exocytosis." Blood **119**(26): 6296-6306.

- Grigorian, M., T. Liu, U. Banerjee and V. Hartenstein (2013). "The proteoglycan Trol controls the architecture of the extracellular matrix and balances proliferation and differentiation of blood progenitors in the Drosophila lymph gland." Dev Biol **384**(2): 301-312.
- Grigoriev, I., D. Splinter, N. Keijzer, P. S. Wulf, J. Demmers, T. Ohtsuka, M. Modesti, I. V. Maly, F. Grosveld, C. C. Hoogenraad and A. Akhmanova (2007). "Rab6 regulates transport and targeting of exocytotic carriers." Dev Cell **13**(2): 305-314.
- Gross, J. C., V. Chaudhary, K. Bartscherer and M. Boutros (2012). "Active Wnt proteins are secreted on exosomes." Nat Cell Biol **14**(10): 1036-1045.
- Guerra, F. and C. Bucci (2016). "Multiple Roles of the Small GTPase Rab7." Cells **5**(3).
- Gustafsson, M. G. (2000). "Surpassing the lateral resolution limit by a factor of two using structured illumination microscopy." J Microsc **198**(Pt 2): 82-87.
- Gustafsson, M. G., L. Shao, P. M. Carlton, C. J. Wang, I. N. Golubovskaya, W. Z. Cande, D. A. Agard and J. W. Sedat (2008). "Three-dimensional resolution doubling in wide-field fluorescence microscopy by structured illumination." Biophys J **94**(12): 4957-4970.
- Han, K. E., S. I. Choi, T. I. Kim, Y. S. Maeng, R. D. Stulting, Y. W. Ji and E. K. Kim (2016). "Pathogenesis and treatments of TGFBI corneal dystrophies." Prog Retin Eye Res **50**: 67-88.
- Hanna, S. T., G. M. Pigeau, J. Galvanovskis, A. Clark, P. Rorsman and P. E. MacDonald (2009). "Kiss-and-run exocytosis and fusion pores of secretory vesicles in human beta-cells." Pflugers Arch **457**(6): 1343-1350.
- Hanson, P. I. and A. Cashikar (2012). "Multivesicular body morphogenesis." Annu Rev Cell Dev Biol **28**: 337-362.
- Haraszti, R. A., M. C. Didiot, E. Sapp, J. Leszyk, S. A. Shaffer, H. E. Rockwell, F. Gao, N. R. Narain, M. DiFiglia, M. A. Kiebish, N. Aronin and A. Khvorova (2016). "High-resolution proteomic and lipidomic analysis of exosomes and microvesicles from different cell sources." J Extracell Vesicles **5**: 32570.
- Harata, N. C., A. M. Aravanis and R. W. Tsien (2006). "Kiss-and-run and full-collapse fusion as modes of exo-endocytosis in neurosecretion." J Neurochem **97**(6): 1546-1570.
- Hardwick, K. G. and H. R. Pelham (1992). "SED5 encodes a 39-kD integral membrane protein required for vesicular transport between the ER and the Golgi complex." J Cell Biol **119**(3): 513-521.
- Hatefi, Y. (1985). "The mitochondrial electron transport and oxidative phosphorylation system." Annu Rev Biochem **54**: 1015-1069.
- Hayashi, S., K. Ito, Y. Sado, M. Taniguchi, A. Akimoto, H. Takeuchi, T. Aigaki, F. Matsuzaki, H. Nakagoshi, T. Tanimura, R. Ueda, T. Uemura, M. Yoshihara and S. Goto (2002). "GETDB, a database compiling expression patterns and molecular locations of a collection of Gal4 enhancer traps." Genesis **34**(1-2): 58-61.
- Heeroma, J. H., J. J. Plomp, E. W. Roubos and M. Verhage (2003). "Development of the mouse neuromuscular junction in the absence of regulated secretion." Neuroscience **120**(3): 733-744.
- Helin, H., M. Mero, H. Markkula and M. Helin (1980). "Pancreatic acinar ultrastructure in human acute pancreatitis." Virchows Arch A Pathol Anat Histol **387**(3): 259-270.
- Hellberg, J. E. (2017). DPhil Thesis. In preparation.
- Henne, W. M., N. J. Buchkovich and S. D. Emr (2011). "The ESCRT pathway." Dev Cell **21**(1): 77-91.

- Henthorn, K. S., M. S. Roux, C. Herrera and L. S. Goldstein (2011). "A role for kinesin heavy chain in controlling vesicle transport into dendrites in Drosophila." Mol Biol Cell **22**(21): 4038-4046.
- Hofmann, I. and S. Munro (2006). "An N-terminally acetylated Arf-like GTPase is localised to lysosomes and affects their motility." J Cell Sci **119**(Pt 8): 1494-1503.
- Hong, W. and S. Lev (2014). "Tethering the assembly of SNARE complexes." Trends Cell Biol **24**(1): 35-43.
- Horiuchi, H., R. Lippe, H. M. McBride, M. Rubino, P. Woodman, H. Stenmark, V. Rybin, M. Wilm, K. Ashman, M. Mann and M. Zerial (1997). "A novel Rab5 GDP/GTP exchange factor complexed to Rabaptin-5 links nucleotide exchange to effector recruitment and function." Cell **90**(6): 1149-1159.
- Hosaka, M., M. Suda, Y. Sakai, T. Izumi, T. Watanabe and T. Takeuchi (2004). "Secretogranin III binds to cholesterol in the secretory granule membrane as an adapter for chromogranin A." J Biol Chem **279**(5): 3627-3634.
- Hosaka, M., T. Watanabe, Y. Sakai, Y. Uchiyama and T. Takeuchi (2002). "Identification of a chromogranin A domain that mediates binding to secretogranin III and targeting to secretory granules in pituitary cells and pancreatic beta-cells." Mol Biol Cell **13**(10): 3388-3399.
- Hou, J. C., L. Min and J. E. Pessin (2009). "Insulin granule biogenesis, trafficking and exocytosis." Vitam Horm **80**: 473-506.
- Houy, S., C. Estay-Ahumada, P. Croise, V. Calco, A. M. Haeberle, Y. Bailly, P. Billuart, N. Vitale, M. F. Bader, S. Ory and S. Gasman (2015). "Oligophrenin-1 Connects Exocytotic Fusion to Compensatory Endocytosis in Neuroendocrine Cells." J Neurosci **35**(31): 11045-11055.
- Hsu, C., Y. Morohashi, S. Yoshimura, N. Manrique-Hoyos, S. Jung, M. A. Lauterbach, M. Bakhti, M. Gronborg, W. Mobius, J. Rhee, F. A. Barr and M. Simons (2010). "Regulation of exosome secretion by Rab35 and its GTPase-activating proteins TBC1D10A-C." J Cell Biol **189**(2): 223-232.
- Hu, S., M. Sonnenfeld, S. Stahl and S. T. Crews (1998). "Midline Fasciclin: a Drosophila Fasciclin-I-related membrane protein localized to the CNS midline cells and trachea." J Neurobiol **35**(1): 77-93.
- Huber, L. A., S. Pimplikar, R. G. Parton, H. Virta, M. Zerial and K. Simons (1993). "Rab8, a small GTPase involved in vesicular traffic between the TGN and the basolateral plasma membrane." J Cell Biol **123**(1): 35-45.
- Huotari, J. and A. Helenius (2011). "Endosome maturation." EMBO J **30**(17): 3481-3500.
- Hurley, J. H. (2015). "ESCRTs are everywhere." EMBO J **34**(19): 2398-2407.
- Hutagalung, A. H. and P. J. Novick (2011). "Role of Rab GTPases in membrane traffic and cell physiology." Physiol Rev **91**(1): 119-149.
- Hyttinen, J. M., M. Niittykoski, A. Salminen and K. Kaarniranta (2013). "Maturation of autophagosomes and endosomes: a key role for Rab7." Biochim Biophys Acta **1833**(3): 503-510.
- Ito, S., T. Ueda, A. Ueno, H. Nakagawa, H. Taniguchi, N. Kayukawa and T. Miki (2014). "A genetic screen in Drosophila for regulators of human prostate cancer progression." Biochem Biophys Res Commun **451**(4): 548-555.
- Iwanami, N., Y. Nakamura, T. Satoh, Z. Liu and A. K. Satoh (2016). "Rab6 Is Required for Multiple Apical Transport Pathways but Not the Basolateral Transport Pathway in Drosophila Photoreceptors." PLoS Genet **12**(2): e1005828.
- Jager, S., C. Bucci, I. Tanida, T. Ueno, E. Kominami, P. Saftig and E. L. Eskelinen (2004). "Role for Rab7 in maturation of late autophagic vacuoles." J Cell Sci **117**(Pt 20): 4837-4848.

- Jahn, R. and R. H. Scheller (2006). "SNAREs--engines for membrane fusion." Nat Rev Mol Cell Biol **7**(9): 631-643.
- Janoueix-Lerosey, I., F. Jollivet, J. Camonis, P. N. Marche and B. Goud (1995). "Two-hybrid system screen with the small GTP-binding protein Rab6. Identification of a novel mouse GDP dissociation inhibitor isoform and two other potential partners of Rab6." J Biol Chem **270**(24): 14801-14808.
- Johns, H. L., C. Gonzalez-Lopez, C. L. Sayers, M. Hollinshead and G. Elliott (2014). "Rab6 dependent post-Golgi trafficking of HSV1 envelope proteins to sites of virus envelopment." Traffic **15**(2): 157-178.
- Johnsen, K. B., J. M. Gudbergsson, M. N. Skov, L. Pilgaard, T. Moos and M. Duroux (2014). "A comprehensive overview of exosomes as drug delivery vehicles - endogenous nanocarriers for targeted cancer therapy." Biochim Biophys Acta **1846**(1): 75-87.
- Johnson, N., M. West and G. Odorizzi (2017). "Regulation of yeast ESCRT-III membrane scission activity by the Doa4 ubiquitin hydrolase." Mol Biol Cell **28**(5): 661-672.
- Juan, T. and M. Furthauer (2017). "Biogenesis and function of ESCRT-dependent extracellular vesicles." Semin Cell Dev Biol.
- Kalb, J. M., A. J. DiBenedetto and M. F. Wolfner (1993). "Probing the function of Drosophila melanogaster accessory glands by directed cell ablation." Proc Natl Acad Sci U S A **90**(17): 8093-8097.
- Kalluri, R. (2016). "The biology and function of exosomes in cancer." J Clin Invest **126**(4): 1208-1215.
- Keller, P., D. Toomre, E. Diaz, J. White and K. Simons (2001). "Multicolour imaging of post-Golgi sorting and trafficking in live cells." Nat Cell Biol **3**(2): 140-149.
- Kelly, E. E., F. Giordano, C. P. Horgan, F. Jollivet, G. Raposo and M. W. McCaffrey (2012). "Rab30 is required for the morphological integrity of the Golgi apparatus." Biol Cell **104**(2): 84-101.
- Kelly, R. B. (1993). "Loading synaptic vesicles with neurotransmitter." Curr Biol **3**(1): 59-61.
- Kim, T., M. C. Gondre-Lewis, I. Arnaoutova and Y. P. Loh (2006). "Dense-core secretory granule biogenesis." Physiology (Bethesda) **21**: 124-133.
- Kinchen, J. M. and K. S. Ravichandran (2010). "Identification of two evolutionarily conserved genes regulating processing of engulfed apoptotic cells." Nature **464**(7289): 778-782.
- Klinkert, K. and A. Echard (2016). "Rab35 GTPase: A Central Regulator of Phosphoinositides and F-actin in Endocytic Recycling and Beyond." Traffic **17**(10): 1063-1077.
- Klumperman, J., R. Kuliawat, J. M. Griffith, H. J. Geuze and P. Arvan (1998). "Mannose 6-phosphate receptors are sorted from immature secretory granules via adaptor protein AP-1, clathrin, and syntaxin 6-positive vesicles." J Cell Biol **141**(2): 359-371.
- Klumperman, J. and G. Raposo (2014). "The complex ultrastructure of the endolysosomal system." Cold Spring Harb Perspect Biol **6**(10): a016857.
- Knodler, A., S. Feng, J. Zhang, X. Zhang, A. Das, J. Peranen and W. Guo (2010). "Coordination of Rab8 and Rab11 in primary ciliogenesis." Proc Natl Acad Sci U S A **107**(14): 6346-6351.
- Kobayashi, H. and M. Fukuda (2013). "Arf6, Rab11 and transferrin receptor define distinct populations of recycling endosomes." Commun Integr Biol **6**(5): e25036.
- Koles, K., J. Nunnari, C. Korkut, R. Barria, C. Brewer, Y. Li, J. Leszyk, B. Zhang and V. Budnik (2012). "Mechanism of evenness interrupted (Evi)-exosome release at synaptic boutons." J Biol Chem **287**(20): 16820-16834.

- Kouranti, I., M. Sachse, N. Arouche, B. Goud and A. Echard (2006). "Rab35 regulates an endocytic recycling pathway essential for the terminal steps of cytokinesis." Curr Biol **16**(17): 1719-1725.
- Kourembanas, S (2015). "Exosomes: Vehicles of Intercellular Signalling, Biomarkers, and Vectors of Cell Therapy". Annual Review of Physiology **77**:13-27
- Kowal, J., G. Arras, M. Colombo, M. Jouve, J. P. Morath, B. Primdal-Bengtson, F. Dingli, D. Loew, M. Tkach and C. Thery (2016). "Proteomic comparison defines novel markers to characterize heterogeneous populations of extracellular vesicle subtypes." Proc Natl Acad Sci U S A **113**(8): E968-977.
- Kowal, J., M. Tkach and C. Thery (2014). "Biogenesis and secretion of exosomes." Curr Opin Cell Biol **29**: 116-125.
- Kramer-Albers, E. M., N. Bretz, S. Tenzer, C. Winterstein, W. Mobius, H. Berger, K. A. Nave, H. Schild and J. Trotter (2007). "Oligodendrocytes secrete exosomes containing major myelin and stress-protective proteins: Trophic support for axons?" Proteomics Clin Appl **1**(11): 1446-1461.
- Kuliawat, R., J. Klumperman, T. Ludwig and P. Arvan (1997). "Differential sorting of lysosomal enzymes out of the regulated secretory pathway in pancreatic beta-cells." J Cell Biol **137**(3): 595-608.
- Lee, J. A., L. Liu, R. Javier, A. C. Kreitzer, C. Delaloy and F. B. Gao (2011). "ESCRT-III subunits Snf7-1 and Snf7-2 differentially regulate transmembrane cargos in hESC-derived human neurons." Mol Brain **4**: 37.
- Leiblich, A., L. Marsden, C. Gandy, L. Corrigan, R. Jenkins, F. Hamdy and C. Wilson (2012). "Bone morphogenetic protein- and mating-dependent secretory cell growth and migration in the Drosophila accessory gland." Proc Natl Acad Sci U S A **109**(47): 19292-19297.
- Leiblich, A., (2015) "Cell biology and genetic regulation of secondary cells in the Drosophila accessory gland." DPhil Thesis. University of Oxford.
- Li, B. X., A. K. Satoh and D. F. Ready (2007). "Myosin V, Rab11, and dRip11 direct apical secretion and cellular morphogenesis in developing Drosophila photoreceptors." J Cell Biol **177**(4): 659-669.
- Li, H., H. F. Li, R. A. Felder, A. Periasamy and P. A. Jose (2008). "Rab4 and Rab11 coordinately regulate the recycling of angiotensin II type I receptor as demonstrated by fluorescence resonance energy transfer microscopy." J Biomed Opt **13**(3): 031206.
- Li, H., L. Ou, J. Fan, M. Xiao, C. Kuang, X. Liu, Y. Sun and Y. Xu (2017). "Rab8A regulates insulin-stimulated GLUT4 translocation in C2C12 myoblasts." FEBS Lett **591**(3): 491-499.
- Liegeois, S., A. Benedetto, J. M. Garnier, Y. Schwab and M. Labouesse (2006). "The V0-ATPase mediates apical secretion of exosomes containing Hedgehog-related proteins in Caenorhabditis elegans." J Cell Biol **173**(6): 949-961.
- Lim, J. A., L. Li and N. Raben (2014). "Pompe disease: from pathophysiology to therapy and back again." Front Aging Neurosci **6**: 177.
- Lindner, J. R., P. R. Hillman, A. L. Barrett, M. C. Jackson, T. L. Perry, Y. Park and S. Datta (2007). "The Drosophila Perlecan gene trol regulates multiple signaling pathways in different developmental contexts." BMC Dev Biol **7**: 121.
- Lloyd, T. E., R. Atkinson, M. N. Wu, Y. Zhou, G. Pennetta and H. J. Bellen (2002). "Hrs regulates endosome membrane invagination and tyrosine kinase receptor signaling in Drosophila." Cell **108**(2): 261-269.

- Lock, J. G. and J. L. Stow (2005). "Rab11 in recycling endosomes regulates the sorting and basolateral transport of E-cadherin." Mol Biol Cell **16**(4): 1744-1755.
- Lone, M., T. Kungl, A. Koper, W. Bottenberg, R. Kammerer, M. Klein, S. T. Sweeney, R. P. Auburn, C. J. O'Kane and A. Prokop (2010). "The nuclear protein Waharan is required for endosomal-lysosomal trafficking in Drosophila." J Cell Sci **123**(Pt 14): 2369-2374.
- Lowe, N., J. S. Rees, J. Roote, E. Ryder, I. M. Armean, G. Johnson, E. Drummond, H. Spriggs, J. Drummond, J. P. Magbanua, H. Naylor, B. Sanson, R. Bastock, S. Huelsmann, V. Trovisco, M. Landgraf, S. Knowles-Barley, J. D. Armstrong, H. White-Cooper, C. Hansen, R. G. Phillips, U. K. D. P. T. S. Consortium, K. S. Lilley, S. Russell and D. St Johnston (2014). "Analysis of the expression patterns, subcellular localisations and interaction partners of Drosophila proteins using a pigP protein trap library." Development **141**(20): 3994-4005.
- Lu, Q., L. W. Hope, M. Brasch, C. Reinhard and S. N. Cohen (2003). "TSG101 interaction with HRS mediates endosomal trafficking and receptor down-regulation." Proc Natl Acad Sci U S A **100**(13): 7626-7631.
- Luhtala, N. and G. Odorizzi (2004). "Bro1 coordinates deubiquitination in the multivesicular body pathway by recruiting Doa4 to endosomes." J Cell Biol **166**(5): 717-729.
- Luzio, J. P., Y. Hackmann, N. M. Dieckmann and G. M. Griffiths (2014). "The biogenesis of lysosomes and lysosome-related organelles." Cold Spring Harb Perspect Biol **6**(9): a016840.
- Luzio, J. P., P. R. Pryor and N. A. Bright (2007). "Lysosomes: fusion and function." Nat Rev Mol Cell Biol **8**(8): 622-632.
- Luzio, J. P., B. A. Rous, N. A. Bright, P. R. Pryor, B. M. Mullock and R. C. Piper (2000). "Lysosome-endosome fusion and lysosome biogenesis." J Cell Sci **113 (Pt 9)**: 1515-1524.
- Lye, C. M., H. W. Naylor and B. Sanson (2014). "Subcellular localisations of the CPTI collection of YFP-tagged proteins in Drosophila embryos." Development **141**(20): 4006-4017.
- Maas, S. L., X. O. Breakefield and A. M. Weaver (2017). "Extracellular Vesicles: Unique Intercellular Delivery Vehicles." Trends Cell Biol **27**(3): 172-188.
- MacDonald, C., J. A. Payne, M. Aboian, W. Smith, D. J. Katzmann and R. C. Piper (2015). "A family of tetraspans organizes cargo for sorting into multivesicular bodies." Dev Cell **33**(3): 328-342.
- Manning, A. (1962). "A sperm factor affecting the receptivity of *Drosophila melanogaster f*emales." Nature **194**(4825): 252-253.
- Marois, E., A. Mahmoud and S. Eaton (2006). "The endocytic pathway and formation of the Wingless morphogen gradient." Development **133**(2): 307-317.
- Martinez, O., A. Schmidt, J. Salamero, B. Hoflack, M. Roa and B. Goud (1994). "The small GTP-binding protein rab6 functions in intra-Golgi transport." J Cell Biol **127**(6 Pt 1): 1575-1588.
- Masumoto, N., T. Sasaki, M. Tahara, A. Mammoto, Y. Ikebuchi, K. Tasaka, M. Tokunaga, Y. Takai and A. Miyake (1996). "Involvement of Rabphilin-3A in cortical granule exocytosis in mouse eggs." J Cell Biol **135**(6 Pt 2): 1741-1747.
- Matias, N. R., J. Mathieu and J. R. Huynh (2015). "Abscission is regulated by the ESCRT-III protein shrub in Drosophila germline stem cells." PLoS Genet **11**(2): e1004653.

- Mattera, R., Y. C. Tsai, A. M. Weissman and J. S. Bonifacino (2006). "The Rab5 guanine nucleotide exchange factor Rabex-5 binds ubiquitin (Ub) and functions as a Ub ligase through an atypical Ub-interacting motif and a zinc finger domain." J Biol Chem **281**(10): 6874-6883.
- Matusek, T., F. Wendler, S. Poles, S. Pizette, G. D'Angelo, M. Furthauer and P. P. Therond (2014). "The ESCRT machinery regulates the secretion and long-range activity of Hedgehog." Nature **516**(7529): 99-103.
- Maxfield, F. R. and D. J. Yamashiro (1987). "Endosome acidification and the pathways of receptor-mediated endocytosis." Adv Exp Med Biol **225**: 189-198.
- Mayers, J. R., L. Wang, J. Pramanik, A. Johnson, A. Sarkeshik, Y. Wang, W. Saengsawang, J. R. Yates, 3rd and A. Audhya (2013). "Regulation of ubiquitin-dependent cargo sorting by multiple endocytic adaptors at the plasma membrane." Proc Natl Acad Sci U S A **110**(29): 11857-11862.
- Mayor, S. and R. E. Pagano (2007). "Pathways of clathrin-independent endocytosis." Nat Rev Mol Cell Biol **8**(8): 603-612.
- Mayorga, L. S., C. N. Tomes and S. A. Belmonte (2007). "Acrosomal exocytosis, a special type of regulated secretion." IUBMB Life **59**(4-5): 286-292.
- McDonald, M. M., P. Verkade, T. Muller-Reichart (2007). "Electron Microscopy: Methods and Protocold, Second Edition. Methods in Molecular Biology" Vol. 169. Humana Press Inc. Totowa, New Jersey.
- McGough, I. J. and J. P. Vincent (2016). "Exosomes in developmental signalling." Development **143**(14): 2482-2493.
- McGuire, S. E., P. T. Le, A. J. Osborn, K. Matsumoto and R. L. Davis (2003). "Spatiotemporal rescue of memory dysfunction in Drosophila." Science **302**(5651): 1765-1768.
- McGuire, S. E., Z. Mao and R. L. Davis (2004). "Spatiotemporal gene expression targeting with the TARGET and gene-switch systems in Drosophila." Sci STKE **2004**(220): pl6.
- Medina, P. M., R. J. Worthen, L. J. Forsberg and J. E. Brenman (2008). "The actin-binding protein capulet genetically interacts with the microtubule motor kinesin to maintain neuronal dendrite homeostasis." PLoS One **3**(8): e3054.
- Mellman, I. and W. J. Nelson (2008). "Coordinated protein sorting, targeting and distribution in polarized cells." Nat Rev Mol Cell Biol **9**(11): 833-845.
- Mesaki, K., K. Tanabe, M. Obayashi, N. Oe and K. Takei (2011). "Fission of tubular endosomes triggers endosomal acidification and movement." PLoS One **6**(5): e19764.
- Miller, I. V. and T. G. Grunewald (2015). "Tumour-derived exosomes: Tiny envelopes for big stories." Biol Cell **107**(9): 287-305.
- Mindell, J. A. (2012). "Lysosomal acidification mechanisms." Annu Rev Physiol **74**: 69-86.
- Miserey-Lenkei, S., F. Waharte, A. Boulet, M. H. Cuif, D. Tenza, A. El Marjou, G. Raposo, J. Salamero, L. Heliot, B. Goud and S. Monier (2007). "Rab6-interacting protein 1 links Rab6 and Rab11 function." Traffic **8**(10): 1385-1403.
- Monsma, S. A., H. A. Harada and M. F. Wolfner (1990). "Synthesis of two Drosophila male accessory gland proteins and their fate after transfer to the female during mating." Dev Biol **142**(2): 465-475.
- Montecalvo, A., A. T. Larregina, W. J. Shufesky, D. B. Stolz, M. L. Sullivan, J. M. Karlsson, C. J. Baty, G. A. Gibson, G. Erdos, Z. Wang, J. Milosevic, O. A. Tkacheva, S. J. Divito, R. Jordan, J. Lyons-Weiler, S. C. Watkins and A. E. Morelli (2012). "Mechanism of transfer of functional microRNAs between mouse dendritic cells via exosomes." Blood **119**(3): 756-766.

- Montero-Hadjadje, M., S. Elias, L. Chevalier, M. Benard, Y. Tanguy, V. Turquier, L. Galas, L. Yon, M. M. Malagon, A. Driouich, S. Gasman and Y. Anouar (2009). "Chromogranin A promotes peptide hormone sorting to mobile granules in constitutively and regulated secreting cells: role of conserved N- and C-terminal peptides." J Biol Chem **284**(18): 12420-12431.
- Morel, E., Z. Chamoun, Z. M. Lasiecka, R. B. Chan, R. L. Williamson, C. Vetanovetz, C. Dall'Armi, S. Simoes, K. S. Point Du Jour, B. D. McCabe, S. A. Small and G. Di Paolo (2013). "Phosphatidylinositol-3-phosphate regulates sorting and processing of amyloid precursor protein through the endosomal system." Nat Commun **4**: 2250.
- Morgan, T. H. (1910). "Sex Limited Inheritance in Drosophila." Science **32**(812): 120-122.
- Morin, X., R. Daneman, M. Zavortink and W. Chia (2001). "A protein trap strategy to detect GFP-tagged proteins expressed from their endogenous loci in Drosophila." Proc Natl Acad Sci U S A **98**(26): 15050-15055.
- Moyer, B. D., B. B. Allan and W. E. Balch (2001). "Rab1 interaction with a GM130 effector complex regulates COPII vesicle cis--Golgi tethering." Traffic **2**(4): 268-276.
- Mueller, J. L., K. Ravi Ram, L. A. McGraw, M. C. Bloch Qazi, E. D. Siggia, A. G. Clark, C. F. Aquadro and M. F. Wolfner (2005). "Cross-species comparison of Drosophila male accessory gland protein genes." Genetics **171**(1): 131-143.
- Muller, A., H. Mziaut, M. Neukam, K. P. Knoch and M. Solimena (2017). "A 4D view on insulin secretory granule turnover in the beta-cell." Diabetes Obes Metab **19 Suppl 1**: 107-114.
- Muller, H. J. (1946). "Thomas Hunt Morgan 1866-1945." Science **103**(2679): 550-551.
- Murray, J. M., P. L. Appleton, J. R. Swedlow and J. C. Waters (2007). "Evaluating performance in three-dimensional fluorescence microscopy." J Microsc **228**(Pt 3): 390-405.
- Nagarkar-Jaiswal, S., P. T. Lee, M. E. Campbell, K. Chen, S. Anguiano-Zarate, M. C. Gutierrez, T. Busby, W. W. Lin, Y. He, K. L. Schulze, B. W. Booth, M. Evans-Holm, K. J. Venken, R. W. Levis, A. C. Spradling, R. A. Hoskins and H. J. Bellen (2015). "A library of MiMICs allows tagging of genes and reversible, spatial and temporal knockdown of proteins in Drosophila." Elife **4**.
- Narasimha, M., A. Uv, A. Krejci, N. H. Brown and S. J. Bray (2008). "Grainy head promotes expression of septate junction proteins and influences epithelial morphogenesis." J Cell Sci **121**(Pt 6): 747-752.
- Niemeyer, B. A. and T. L. Schwarz (2000). "SNAP-24, a Drosophila SNAP-25 homologue on granule membranes, is a putative mediator of secretion and granule-granule fusion in salivary glands." J Cell Sci **113 (Pt 22)**: 4055-4064.
- Nixon, R. A., J. Wegiel, A. Kumar, W. H. Yu, C. Peterhoff, A. Cataldo and A. M. Cuervo (2005). "Extensive involvement of autophagy in Alzheimer disease: an immuno-electron microscopy study." J Neuropathol Exp Neurol **64**(2): 113-122.
- Novick, P., C. Field and R. Schekman (1980). "Identification of 23 complementation groups required for post-translational events in the yeast secretory pathway." Cell **21**(1): 205-215.
- Novikoff, A. B., H. Beaufay and C. De Duve (1956). "Electron microscopy of lysosomerich fractions from rat liver." J Biophys Biochem Cytol **2**(4 Suppl): 179-184.
- Nozawa, T., C. Aikawa, A. Goda, F. Maruyama, S. Hamada and I. Nakagawa (2012). "The small GTPases Rab9A and Rab23 function at distinct steps in

autophagy during Group A Streptococcus infection." Cell Microbiol **14**(8): 1149-1165.
- Nusslein-Volhard, C. and E. Wieschaus (1980). "Mutations affecting segment number and polarity in Drosophila." Nature **287**(5785): 795-801.
- Nusslein-Volhard, C., E. Wieschaus and H. Kluding (1984). "Mutations affecting the pattern of the larval cuticle inDrosophila melanogaster : I. Zygotic loci on the second chromosome." Wilehm Roux Arch Dev Biol **193**(5): 267-282.
- Odorizzi, G., D. J. Katzmann, M. Babst, A. Audhya and S. D. Emr (2003). "Bro1 is an endosome-associated protein that functions in the MVB pathway in Saccharomyces cerevisiae." J Cell Sci **116**(Pt 10): 1893-1903.
- Orci, L., M. Ravazzola, M. Amherdt, O. Madsen, A. Perrelet, J. D. Vassalli and R. G. Anderson (1986). "Conversion of proinsulin to insulin occurs coordinately with acidification of maturing secretory vesicles." J Cell Biol **103**(6 Pt 1): 2273-2281.
- Ortiz, D., M. Medkova, C. Walch-Solimena and P. Novick (2002). "Ypt32 recruits the Sec4p guanine nucleotide exchange factor, Sec2p, to secretory vesicles; evidence for a Rab cascade in yeast." J Cell Biol **157**(6): 1005-1015.
- Ostrowski, M., N. B. Carmo, S. Krumeich, I. Fanget, G. Raposo, A. Savina, C. F. Moita, K. Schauer, A. N. Hume, R. P. Freitas, B. Goud, P. Benaroch, N. Hacohen, M. Fukuda, C. Desnos, M. C. Seabra, F. Darchen, S. Amigorena, L. F. Moita and C. Thery (2010). "Rab27a and Rab27b control different steps of the exosome secretion pathway." Nat Cell Biol **12**(1): 19-30; sup pp 11-13.
- Palade, G. (1975). "Intracellular aspects of the process of protein synthesis." Science **189**(4206): 867.
- Panakova, D., H. Sprong, E. Marois, C. Thiele and S. Eaton (2005). "Lipoprotein particles are required for Hedgehog and Wingless signalling." Nature **435**(7038): 58-65.
- Parton, R. M., A. M. Valles, I. M. Dobbie and I. Davis (2010). "Live cell imaging in Drosophila melanogaster." Cold Spring Harb Protoc **2010**(4): pdb top75.
- Pataki, C., T. Matusek, E. Kurucz, I. Ando, A. Jenny and J. Mihaly (2010). "Drosophila Rab23 is involved in the regulation of the number and planar polarization of the adult cuticular hairs." Genetics **184**(4): 1051-1065.
- Patry, M., R. Teinturier, D. Goehrig, C. Zetu, D. Ripoche, I. S. Kim, P. Bertolino and A. Hennino (2015). "betaig-h3 Represses T-Cell Activation in Type 1 Diabetes." Diabetes **64**(12): 4212-4219.
- Patwardhan, A., S. Bardin, S. Miserey-Lenkei, L. Larue, B. Goud, G. Raposo and C. Delevoye (2017). "Routing of the RAB6 secretory pathway towards the lysosome related organelle of melanocytes." Nat Commun **8**: 15835.
- Pederson, T. (2011). "The nucleus introduced." Cold Spring Harb Perspect Biol **3**(5).
- Pellinen, T., A. Arjonen, K. Vuoriluoto, K. Kallio, J. A. Fransen and J. Ivaska (2006). "Small GTPase Rab21 regulates cell adhesion and controls endosomal traffic of beta1-integrins." J Cell Biol **173**(5): 767-780.
- Perera, R. M. and R. Zoncu (2016). "The Lysosome as a Regulatory Hub." Annu Rev Cell Dev Biol **32**: 223-253.
- Perera, S. M., S-J. Fan, B. Kroeger, C. Alves, H. Sheldon, M. Wainwright, I Stefana, J. F. Morris, A. L. Harris, C. Wilson, and D.C.I. Goberdhan. "A novel conserved exosome biogenesis pathway mediates adaptive responses to mTORC1-inhibitory microenvironmental stresses in cancer cells". In preparation.
- Perroti. (1972). " Microtubules as a secretion product." Boll. Zool., **39**: 249-254

- Pfeffer, S. R. (2005). "Structural clues to Rab GTPase functional diversity." J Biol Chem **280**(16): 15485-15488.
- Pfeffer, S. R. (2013). "Rab GTPase regulation of membrane identity." Curr Opin Cell Biol **25**(4): 414-419.
- Pineda-Molina, E., H. Belrhali, A. J. Piefer, I. Akula, P. Bates and W. Weissenhorn (2006). "The crystal structure of the C-terminal domain of Vps28 reveals a conserved surface required for Vps20 recruitment." Traffic **7**(8): 1007-1016.
- Platt, F. M. (2014). "Sphingolipid lysosomal storage disorders." Nature **510**(7503): 68-75.
- Platt, F. M., B. Boland and A. C. van der Spoel (2012). "The cell biology of disease: lysosomal storage disorders: the cellular impact of lysosomal dysfunction." J Cell Biol **199**(5): 723-734.
- Plutner, H., A. D. Cox, S. Pind, R. Khosravi-Far, J. R. Bourne, R. Schwaninger, C. J. Der and W. E. Balch (1991). "Rab1b regulates vesicular transport between the endoplasmic reticulum and successive Golgi compartments." J Cell Biol **115**(1): 31-43.
- Poteryaev, D., S. Datta, K. Ackema, M. Zerial and A. Spang (2010). "Identification of the switch in early-to-late endosome transition." Cell **141**(3): 497-508.
- Prentki, M. and F. M. Matschinsky (1987). "Ca2+, cAMP, and phospholipid-derived messengers in coupling mechanisms of insulin secretion." Physiol Rev **67**(4): 1185-1248.
- Properzi, F., M. Logozzi and S. Fais (2013). "Exosomes: the future of biomarkers in medicine." Biomark Med **7**(5): 769-778.
- Pu, J., C. Schindler, R. Jia, M. Jarnik, P. Backlund and J. S. Bonifacino (2015). "BORC, a multisubunit complex that regulates lysosome positioning." Dev Cell **33**(2): 176-188.
- Rabouille, C. (2017). "Pathways of Unconventional Protein Secretion." Trends Cell Biol **27**(3): 230-240.
- Raiborg, C., K. G. Bache, A. Mehlum, E. Stang and H. Stenmark (2001). "Hrs recruits clathrin to early endosomes." EMBO J **20**(17): 5008-5021.
- Raiborg, C., B. Bremnes, A. Mehlum, D. J. Gillooly, A. D'Arrigo, E. Stang and H. Stenmark (2001). "FYVE and coiled-coil domains determine the specific localisation of Hrs to early endosomes." J Cell Sci **114**(Pt 12): 2255-2263.
- Ram, K. R. and M. F. Wolfner (2007). "Sustained post-mating response in Drosophila melanogaster requires multiple seminal fluid proteins." PLoS Genet **3**(12): e238.
- Ramirez, A., A. Heimbach, J. Grundemann, B. Stiller, D. Hampshire, L. P. Cid, I. Goebel, A. F. Mubaidin, A. L. Wriekat, J. Roeper, A. Al-Din, A. M. Hillmer, M. Karsak, B. Liss, C. G. Woods, M. I. Behrens and C. Kubisch (2006). "Hereditary parkinsonism with dementia is caused by mutations in ATP13A2, encoding a lysosomal type 5 P-type ATPase." Nat Genet **38**(10): 1184-1191.
- Raposo, G. and M. S. Marks (2007). "Melanosomes--dark organelles enlighten endosomal membrane transport." Nat Rev Mol Cell Biol **8**(10): 786-797.
- Raposo, G., H. W. Nijman, W. Stoorvogel, R. Liejendekker, C. V. Harding, C. J. Melief and H. J. Geuze (1996). "B lymphocytes secrete antigen-presenting vesicles." J Exp Med **183**(3): 1161-1172.
- Raposo, G. and W. Stoorvogel (2013). "Extracellular vesicles: exosomes, microvesicles, and friends." J Cell Biol **200**(4): 373-383.
- Raymond, C. K., I. Howald-Stevenson, C. A. Vater and T. H. Stevens (1992). "Morphological classification of the yeast vacuolar protein sorting mutants:

evidence for a prevacuolar compartment in class E vps mutants." Mol Biol Cell **3**(12): 1389-1402.
- Reddy, A., E. V. Caler and N. W. Andrews (2001). "Plasma membrane repair is mediated by Ca(2+)-regulated exocytosis of lysosomes." Cell **106**(2): 157-169.
- Redhai, S., J. E. Hellberg, M. Wainwright, S. W. Perera, F. Castellanos, B. Kroeger, C. Gandy, A. Leiblich, L. Corrigan, T. Hilton, B. Patel, S. J. Fan, F. Hamdy, D. C. Goberdhan and C. Wilson (2016). "Regulation of Dense-Core Granule Replenishment by Autocrine BMP Signalling in Drosophila Secondary Cells." PLoS Genet **12**(10): e1006366.
- Redhai, S. (2016). "Genetic regulation of membrane trafficking, exosome secretion, growth and dense-core granule biogenesis in the Drosophila accessory gland" DPhil Thesis. University of Oxford.
- Rejman Lipinski, A., J. Heymann, C. Meissner, A. Karlas, V. Brinkmann, T. F. Meyer and D. Heuer (2009). "Rab6 and Rab11 regulate Chlamydia trachomatis development and golgin-84-dependent Golgi fragmentation." PLoS Pathog **5**(10): e1000615.
- Ren, M., G. Xu, J. Zeng, C. De Lemos-Chiarandini, M. Adesnik and D. D. Sabatini (1998). "Hydrolysis of GTP on rab11 is required for the direct delivery of transferrin from the pericentriolar recycling compartment to the cell surface but not from sorting endosomes." Proc Natl Acad Sci U S A **95**(11): 6187-6192.
- Ren, X., G. G. Farias, B. J. Canagarajah, J. S. Bonifacino and J. H. Hurley (2013). "Structural basis for recruitment and activation of the AP-1 clathrin adaptor complex by Arf1." Cell **152**(4): 755-767.
- Reynolds, E. S. (1963). "The use of lead citrate at high pH as an electron-opaque stain in electron microscopy." J Cell Biol **17**: 208-212.
- Rideout, E. J., A. J. Dornan, M. C. Neville, S. Eadie and S. F. Goodwin (2010). "Control of sexual differentiation and behavior by the doublesex gene in Drosophila melanogaster." Nat Neurosci **13**(4): 458-466.
- Riedel, F., A. K. Gillingham, C. Rosa-Ferreira, A. Galindo and S. Munro (2016). "An antibody toolkit for the study of membrane traffic in Drosophila melanogaster." Biol Open **5**(7): 987-992.
- Rink, J., E. Ghigo, Y. Kalaidzidis and M. Zerial (2005). "Rab conversion as a mechanism of progression from early to late endosomes." Cell **122**(5): 735-749.
- Roberts, M., S. Barry, A. Woods, P. van der Sluijs and J. Norman (2001). "PDGF-regulated rab4-dependent recycling of alphavbeta3 integrin from early endosomes is necessary for cell adhesion and spreading." Curr Biol **11**(18): 1392-1402.
- Rodriguez-Boulan, E. and I. G. Macara (2014). "Organization and execution of the epithelial polarity programme." Nat Rev Mol Cell Biol **15**(4): 225-242.
- Rojas, R., T. van Vlijmen, G. A. Mardones, Y. Prabhu, A. L. Rojas, S. Mohammed, A. J. Heck, G. Raposo, P. van der Sluijs and J. S. Bonifacino (2008). "Regulation of retromer recruitment to endosomes by sequential action of Rab5 and Rab7." J Cell Biol **183**(3): 513-526.
- Royer, C. and X. Lu (2011). "Epithelial cell polarity: a major gatekeeper against cancer?" Cell Death Differ **18**(9): 1470-1477.
- Russell, R. C., H. X. Yuan and K. L. Guan (2014). "Autophagy regulation by nutrient signaling." Cell Res **24**(1): 42-57.
- Rutter, G. A. and E. V. Hill (2006). "Insulin vesicle release: walk, kiss, pause ... then run." Physiology (Bethesda) **21**: 189-196.

- Rybin, V., O. Ullrich, M. Rubino, K. Alexandrov, I. Simon, M. C. Seabra, R. Goody and M. Zerial (1996). "GTPase activity of Rab5 acts as a timer for endocytic membrane fusion." Nature **383**(6597): 266-269.
- Rylett, C. M., M. J. Walker, G. J. Howell, A. D. Shirras and R. E. Isaac (2007). "Male accessory glands of Drosophila melanogaster make a secreted angiotensin I-converting enzyme (ANCE), suggesting a role for the peptide-processing enzyme in seminal fluid." J Exp Biol **210**(Pt 20): 3601-3606.
- Saksena, S. and S. D. Emr (2009). "ESCRTs and human disease." Biochem Soc Trans **37**(Pt 1): 167-172.
- Salminen, A. and P. J. Novick (1987). "A ras-like protein is required for a post-Golgi event in yeast secretion." Cell **49**(4): 527-538.
- Sancak, Y., L. Bar-Peled, R. Zoncu, A. L. Markhard, S. Nada and D. M. Sabatini (2010). "Ragulator-Rag complex targets mTORC1 to the lysosomal surface and is necessary for its activation by amino acids." Cell **141**(2): 290-303.
- Sano, H., W. G. Roach, G. R. Peck, M. Fukuda and G. E. Lienhard (2008). "Rab10 in insulin-stimulated GLUT4 translocation." Biochem J **411**(1): 89-95.
- Sarov, M., C. Barz, H. Jambor, M. Y. Hein, C. Schmied, D. Suchold, B. Stender, S. Janosch, J. V. K, R. T. Krishnan, A. Krishnamoorthy, I. R. Ferreira, R. K. Ejsmont, K. Finkl, S. Hasse, P. Kampfer, N. Plewka, E. Vinis, S. Schloissnig, E. Knust, V. Hartenstein, M. Mann, M. Ramaswami, K. VijayRaghavan, P. Tomancak and F. Schnorrer (2016). "A genome-wide resource for the analysis of protein localisation in Drosophila." Elife **5**: e12068.
- Sato, M. and T. B. Kornberg (2002). "FGF is an essential mitogen and chemoattractant for the air sacs of the drosophila tracheal system." Dev Cell **3**(2): 195-207.
- Satoh, A., F. Tokunaga, S. Kawamura and K. Ozaki (1997). "In situ inhibition of vesicle transport and protein processing in the dominant negative Rab1 mutant of Drosophila." J Cell Sci **110 (Pt 23)**: 2943-2953.
- Satoh, A., Y. Wang, J. Malsam, M. B. Beard and G. Warren (2003). "Golgin-84 is a rab1 binding partner involved in Golgi structure." Traffic **4**(3): 153-161.
- Satoh, A. K., J. E. O'Tousa, K. Ozaki and D. F. Ready (2005). "Rab11 mediates post-Golgi trafficking of rhodopsin to the photosensitive apical membrane of Drosophila photoreceptors." Development **132**(7): 1487-1497.
- Satoh, T., Y. Nakamura and A. K. Satoh (2016). "Rab6 functions in polarized transport in Drosophila photoreceptors." Fly (Austin) **10**(3): 123-127.
- Satoh, T., Y. Nakamura and A. K. Satoh (2016). "The roles of Syx5 in Golgi morphology and Rhodopsin transport in Drosophila photoreceptors." Biol Open **5**(10): 1420-1430.
- Savina, A., C. M. Fader, M. T. Damiani and M. I. Colombo (2005). "Rab11 promotes docking and fusion of multivesicular bodies in a calcium-dependent manner." Traffic **6**(2): 131-143.
- Savina, A., M. Furlan, M. Vidal and M. I. Colombo (2003). "Exosome release is regulated by a calcium-dependent mechanism in K562 cells." J Biol Chem **278**(22): 20083-20090.
- Savina, A., M. Vidal and M. I. Colombo (2002). "The exosome pathway in K562 cells is regulated by Rab11." J Cell Sci **115**(Pt 12): 2505-2515.
- Schindelin, J., I. Arganda-Carreras, E. Frise, V. Kaynig, M. Longair, T. Pietzsch, S. Preibisch, C. Rueden, S. Saalfeld, B. Schmid, J. Y. Tinevez, D. J. White, V. Hartenstein, K. Eliceiri, P. Tomancak and A. Cardona (2012). "Fiji: an open-source platform for biological-image analysis." Nat Methods **9**(7): 676-682.

- Schindelin, J., C. T. Rueden, M. C. Hiner and K. W. Eliceiri (2015). "The ImageJ ecosystem: An open platform for biomedical image analysis." Mol Reprod Dev **82**(7-8): 518-529.
- Schmidt, O. and D. Teis (2012). "The ESCRT machinery." Curr Biol **22**(4): R116-120.
- Schmidt, T., P. S. Chen and M. Pellegrini (1985). "The induction of ribosome biosynthesis in a nonmitotic secretory tissue." J Biol Chem **260**(12): 7645-7650.
- Schoneberg, J., I. H. Lee, J. H. Iwasa and J. H. Hurley (2017). "Reverse-topology membrane scission by the ESCRT proteins." Nat Rev Mol Cell Biol **18**(1): 5-17.
- Schuck, S., M. J. Gerl, A. Ang, A. Manninen, P. Keller, I. Mellman and K. Simons (2007). "Rab10 is involved in basolateral transport in polarized Madin-Darby canine kidney cells." Traffic **8**(1): 47-60.
- Serafini, T., L. Orci, M. Amherdt, M. Brunner, R. A. Kahn and J. E. Rothman (1991). "ADP-ribosylation factor is a subunit of the coat of Golgi-derived COP-coated vesicles: a novel role for a GTP-binding protein." Cell **67**(2): 239-253.
- Settembre, C., A. Fraldi, D. L. Medina and A. Ballabio (2013). "Signals from the lysosome: a control centre for cellular clearance and energy metabolism." Nat Rev Mol Cell Biol **14**(5): 283-296.
- Sevrioukov, E. A., N. Moghrabi, M. Kuhn and H. Kramer (2005). "A mutation in dVps28 reveals a link between a subunit of the endosomal sorting complex required for transport-I complex and the actin cytoskeleton in Drosophila." Mol Biol Cell **16**(5): 2301-2312.
- Shakya, R., T. Watanabe and F. Costantini (2005). "The role of GDNF/Ret signaling in ureteric bud cell fate and branching morphogenesis." Dev Cell **8**(1): 65-74.
- Shannon, M. P., T. C. Kaufman, M. W. Shen and B. H. Judd (1972). "Lethality patterns and morphology of selected lethal and semi-lethal mutations in the zeste-white region of Drosophila melanogaster." Genetics **72**(4): 615-638.
- Shetty, K. M., P. Kurada and J. E. O'Tousa (1998). "Rab6 regulation of rhodopsin transport in Drosophila." J Biol Chem **273**(32): 20425-20430.
- Shirakawa, R., T. Higashi, A. Tabuchi, A. Yoshioka, H. Nishioka, M. Fukuda, T. Kita and H. Horiuchi (2004). "Munc13-4 is a GTP-Rab27-binding protein regulating dense core granule secretion in platelets." J Biol Chem **279**(11): 10730-10737.
- Short, B., A. Haas and F. A. Barr (2005). "Golgins and GTPases, giving identity and structure to the Golgi apparatus." Biochim Biophys Acta **1744**(3): 383-395.
- Short, B., C. Preisinger, R. Korner, R. Kopajtich, O. Byron and F. A. Barr (2001). "A GRASP55-rab2 effector complex linking Golgi structure to membrane traffic." J Cell Biol **155**(6): 877-883.
- Siddhanta, A. and D. Shields (1998). "Secretory vesicle budding from the trans-Golgi network is mediated by phosphatidic acid levels." J Biol Chem **273**(29): 17995-17998.
- Simpson, J. C., G. Griffiths, M. Wessling-Resnick, J. A. Fransen, H. Bennett and A. T. Jones (2004). "A role for the small GTPase Rab21 in the early endocytic pathway." J Cell Sci **117**(Pt 26): 6297-6311.
- Sinka, R., A. K. Gillingham, V. Kondylis and S. Munro (2008). "Golgi coiled-coil proteins contain multiple binding sites for Rab family G proteins." J Cell Biol **183**(4): 607-615.
- Sitnik, J. L., D. Gligorov, R. K. Maeda, F. Karch and M. F. Wolfner (2016). "The Female Post-Mating Response Requires Genes Expressed in the

Secondary Cells of the Male Accessory Gland in Drosophila melanogaster." Genetics **202**(3): 1029-1041.
- Skibinski, G., N. J. Parkinson, J. M. Brown, L. Chakrabarti, S. L. Lloyd, H. Hummerich, J. E. Nielsen, J. R. Hodges, M. G. Spillantini, T. Thusgaard, S. Brandner, A. Brun, M. N. Rossor, A. Gade, P. Johannsen, S. A. Sorensen, S. Gydesen, E. M. Fisher and J. Collinge (2005). "Mutations in the endosomal ESCRTIII-complex subunit CHMP2B in frontotemporal dementia." Nat Genet **37**(8): 806-808.
- Snapp, E. L., T. Iida, D. Frescas, J. Lippincott-Schwartz and M. A. Lilly (2004). "The fusome mediates intercellular endoplasmic reticulum connectivity in Drosophila ovarian cysts." Mol Biol Cell **15**(10): 4512-4521.
- Sobota, J. A., F. Ferraro, N. Back, B. A. Eipper and R. E. Mains (2006). "Not all secretory granules are created equal: Partitioning of soluble content proteins." Mol Biol Cell **17**(12): 5038-5052.
- Sonnichsen, B., S. De Renzis, E. Nielsen, J. Rietdorf and M. Zerial (2000). "Distinct membrane domains on endosomes in the recycling pathway visualized by multicolor imaging of Rab4, Rab5, and Rab11." J Cell Biol **149**(4): 901-914.
- St Johnston, D. (2002). "The art and design of genetic screens: Drosophila melanogaster." Nat Rev Genet **3**(3): 176-188.
- Stefanis, L. (2012). "alpha-Synuclein in Parkinson's disease." Cold Spring Harb Perspect Med **2**(2): a009399.
- Stenmark, H. (2009). "Rab GTPases as coordinators of vesicle traffic." Nat Rev Mol Cell Biol **10**(8): 513-525.
- Stenmark, H. (2012). "The Rabs: a family at the root of metazoan evolution." BMC Biol **10**: 68.
- Stoorvogel, W., G. J. Strous, H. J. Geuze, V. Oorschot and A. L. Schwartz (1991). "Late endosomes derive from early endosomes by maturation." Cell **65**(3): 417-427.
- Stuffers, S., C. Sem Wegner, H. Stenmark and A. Brech (2009). "Multivesicular endosome biogenesis in the absence of ESCRTs." Traffic **10**(7): 925-937.
- Sugawara, K., T. Shibasaki, A. Mizoguchi, T. Saito and S. Seino (2009). "Rab11 and its effector Rip11 participate in regulation of insulin granule exocytosis." Genes Cells **14**(4): 445-456.
- Susic-Jung, L., C. Hornbruch-Freitag, J. Kuckwa, K. H. Rexer, U. Lammel and R. Renkawitz-Pohl (2012). "Multinucleated smooth muscles and mononucleated as well as multinucleated striated muscles develop during establishment of the male reproductive organs of Drosophila melanogaster." Dev Biol **370**(1): 86-97.
- Sweeney, N. T., J. E. Brenman, Y. N. Jan and F. B. Gao (2006). "The coiled-coil protein shrub controls neuronal morphogenesis in Drosophila." Curr Biol **16**(10): 1006-1011.
- Szatmari, Z., V. Kis, M. Lippai, K. Hegedus, T. Farago, P. Lorincz, T. Tanaka, G. Juhasz and M. Sass (2014). "Rab11 facilitates cross-talk between autophagy and endosomal pathway through regulation of Hook localization." Mol Biol Cell **25**(4): 522-531.
- Tanaka, S., T. Yora, K. Nakayama, K. Inoue and K. Kurosumi (1997). "Proteolytic processing of pro-opiomelanocortin occurs in acidifying secretory granules of AtT-20 cells." J Histochem Cytochem **45**(3): 425-436.
- Tanguy, E., O. Carmon, Q. Wang, L. Jeandel, S. Chasserot-Golaz, M. Montero-Hadjadje and N. Vitale (2016). "Lipids implicated in the journey of a secretory granule: from biogenesis to fusion." J Neurochem **137**(6): 904-912.

- Taniguchi, K., A. Kokuryo, T. Imano, R. Minami, H. Nakagoshi and T. Adachi-Yamada (2012). "Binucleation of Drosophila Adult Male Accessory Gland Cells Increases Plasticity of Organ Size for Effective Reproduction." Biological Systems **1**(1): 4.
- Taugner, R., C. P. Buhrle, R. Nobiling and H. Kirschke (1985). "Coexistence of renin and cathepsin B in epithelioid cell secretory granules." Histochemistry **83**(2): 103-108.
- Teis, D., S. Saksena and S. D. Emr (2008). "Ordered assembly of the ESCRT-III complex on endosomes is required to sequester cargo during MVB formation." Dev Cell **15**(4): 578-589.
- Thery, C. (2011). "Exosomes: secreted vesicles and intercellular communications." F1000 Biol Rep **3**: 15.
- Tisdale, E. J., J. R. Bourne, R. Khosravi-Far, C. J. Der and W. E. Balch (1992). "GTP-binding mutants of rab1 and rab2 are potent inhibitors of vesicular transport from the endoplasmic reticulum to the Golgi complex." J Cell Biol **119**(4): 749-761.
- Tkach, M. and C. Thery (2016). "Communication by Extracellular Vesicles: Where We Are and Where We Need to Go." Cell **164**(6): 1226-1232.
- Tooze, J. and M. Hollinshead (1991). "Tubular early endosomal networks in AtT20 and other cells." J Cell Biol **115**(3): 635-653.
- Tooze, S. A., A. Abada and Z. Elazar (2014). "Endocytosis and autophagy: exploitation or cooperation?" Cold Spring Harb Perspect Biol **6**(5): a018358.
- Tooze, S. A., T. Flatmark, J. Tooze and W. B. Huttner (1991). "Characterization of the immature secretory granule, an intermediate in granule biogenesis." J Cell Biol **115**(6): 1491-1503.
- Tooze, S. A., G. J. Martens and W. B. Huttner (2001). "Secretory granule biogenesis: rafting to the SNARE." Trends Cell Biol **11**(3): 116-122.
- Trajkovic, K., C. Hsu, S. Chiantia, L. Rajendran, D. Wenzel, F. Wieland, P. Schwille, B. Brugger and M. Simons (2008). "Ceramide triggers budding of exosome vesicles into multivesicular endosomes." Science **319**(5867): 1244-1247.
- Tsuchiya, M., M. Hosaka, T. Moriguchi, S. Zhang, M. Suda, H. Yokota-Hashimoto, K. Shinozuka and T. Takeuchi (2010). "Cholesterol biosynthesis pathway intermediates and inhibitors regulate glucose-stimulated insulin secretion and secretory granule formation in pancreatic beta-cells." Endocrinology **151**(10): 4705-4716.
- Tuli, A., J. Thiery, A. M. James, X. Michelet, M. Sharma, S. Garg, K. B. Sanborn, J. S. Orange, J. Lieberman and M. B. Brenner (2013). "Arf-like GTPase Arl8b regulates lytic granule polarization and natural killer cell-mediated cytotoxicity." Mol Biol Cell **24**(23): 3721-3735.
- Ullrich, O., S. Reinsch, S. Urbe, M. Zerial and R. G. Parton (1996). "Rab11 regulates recycling through the pericentriolar recycling endosome." J Cell Biol **135**(4): 913-924.
- Urbe, S., L. A. Huber, M. Zerial, S. A. Tooze and R. G. Parton (1993). "Rab11, a small GTPase associated with both constitutive and regulated secretory pathways in PC12 cells." FEBS Lett **334**(2): 175-182.
- Urbe, S., L. J. Page and S. A. Tooze (1998). "Homotypic fusion of immature secretory granules during maturation in a cell-free assay." J Cell Biol **143**(7): 1831-1844.
- Urbe, S., M. Sachse, P. E. Row, C. Preisinger, F. A. Barr, G. Strous, J. Klumperman and M. J. Clague (2003). "The UIM domain of Hrs couples receptor sorting to vesicle formation." J Cell Sci **116**(Pt 20): 4169-4179.
- Vaccari, T., T. E. Rusten, L. Menut, I. P. Nezis, A. Brech, H. Stenmark and D. Bilder (2009). "Comparative analysis of ESCRT-I, ESCRT-II and ESCRT-III

function in Drosophila by efficient isolation of ESCRT mutants." J Cell Sci **122**(Pt 14): 2413-2423.
- Vaccaro, M. I. (2012). "Zymophagy: selective autophagy of secretory granules." Int J Cell Biol **2012**: 396705.
- Valadi, H., K. Ekstrom, A. Bossios, M. Sjostrand, J. J. Lee and J. O. Lotvall (2007). "Exosome-mediated transfer of mRNAs and microRNAs is a novel mechanism of genetic exchange between cells." Nat Cell Biol **9**(6): 654-659.
- van Niel, G., S. Charrin, S. Simoes, M. Romao, L. Rochin, P. Saftig, M. S. Marks, E. Rubinstein and G. Raposo (2011). "The tetraspanin CD63 regulates ESCRT-independent and -dependent endosomal sorting during melanogenesis." Dev Cell **21**(4): 708-721.
- Van Vactor, D., Jr., D. E. Krantz, R. Reinke and S. L. Zipursky (1988). "Analysis of mutants in chaoptin, a photoreceptor cell-specific glycoprotein in Drosophila, reveals its role in cellular morphogenesis." Cell **52**(2): 281-290.
- Vanlandingham, P. A. and B. P. Ceresa (2009). "Rab7 regulates late endocytic trafficking downstream of multivesicular body biogenesis and cargo sequestration." J Biol Chem **284**(18): 12110-12124.
- Voigt, A., R. Pflanz, U. Schafer and H. Jackle (2002). "Perlecan participates in proliferation activation of quiescent Drosophila neuroblasts." Dev Dyn **224**(4): 403-412.
- Vonderheit, A. and A. Helenius (2005). "Rab7 associates with early endosomes to mediate sorting and transport of Semliki forest virus to late endosomes." PLoS Biol **3**(7): e233.
- Waguri, S., F. Dewitte, R. Le Borgne, Y. Rouille, Y. Uchiyama, J. F. Dubremetz and B. Hoflack (2003). "Visualization of TGN to endosome trafficking through fluorescently labeled MPR and AP-1 in living cells." Mol Biol Cell **14**(1): 142-155.
- Walther, R. F. and F. Pichaud (2010). "Crumbs/DaPKC-dependent apical exclusion of Bazooka promotes photoreceptor polarity remodeling." Curr Biol **20**(12): 1065-1074.
- Wandinger-Ness, A. and M. Zerial (2014). "Rab proteins and the compartmentalization of the endosomal system." Cold Spring Harb Perspect Biol **6**(11): a022616.
- Wang, Y., E. L. Ng and B. L. Tang (2006). "Rab23: what exactly does it traffic?" Traffic **7**(6): 746-750.
- Wang, Y., C. Thiele and W. B. Huttner (2000). "Cholesterol is required for the formation of regulated and constitutive secretory vesicles from the trans-Golgi network." Traffic **1**(12): 952-962.
- Webster, B. M., P. Colombi, J. Jager and C. P. Lusk (2014). "Surveillance of nuclear pore complex assembly by ESCRT-III/Vps4." Cell **159**(2): 388-401.
- Wegel, E., A. Gohler, B. C. Lagerholm, A. Wainman, S. Uphoff, R. Kaufmann and I. M. Dobbie (2016). "Imaging cellular structures in super-resolution with SIM, STED and Localisation Microscopy: A practical comparison." Sci Rep **6**: 27290.
- Welsch, S., A. Habermann, S. Jager, B. Muller, J. Krijnse-Locker and H. G. Krausslich (2006). "Ultrastructural analysis of ESCRT proteins suggests a role for endosome-associated tubular-vesicular membranes in ESCRT function." Traffic **7**(11): 1551-1566.
- Wendler, F., L. Page, S. Urbe and S. A. Tooze (2001). "Homotypic fusion of immature secretory granules during maturation requires syntaxin 6." Mol Biol Cell **12**(6): 1699-1709.
- Wernersson, S. and G. Pejler (2014). "Mast cell secretory granules: armed for battle." Nat Rev Immunol **14**(7): 478-494.

- Wilcox, G. (2005). "Insulin and insulin resistance." Clin Biochem Rev **26**(2): 19-39.
- Williams, J. A. (2010). "Regulation of acinar cell function in the pancreas." Curr Opin Gastroenterol **26**(5): 478-483.
- Willms, E., H. J. Johansson, I. Mager, Y. Lee, K. E. Blomberg, M. Sadik, A. Alaarg, C. I. Smith, J. Lehtio, S. El Andaloussi, M. J. Wood and P. Vader (2016). "Cells release subpopulations of exosomes with distinct molecular and biological properties." Sci Rep **6**: 22519.
- Wilson, C., A. Leiblich, D. C. Goberdhan and F. Hamdy (2017). "The Drosophila Accessory Gland as a Model for Prostate Cancer and Other Pathologies." Curr Top Dev Biol **121**: 339-375.
- Winchester, B. G. (2004). Primary Defects in Lysosomal Enzymes. In: Platt, FM and Walkley, SU, (eds.) "Lysosomal Disorders of the Brain: Recent Advances in Molecular and Cellular Pathogenesis and Treatment". (pp. 81-130). Oxford University Press: Oxford.
- Wolfner, M. F. (1997). "Tokens of love: functions and regulation of Drosophila male accessory gland products." Insect Biochem Mol Biol **27**(3): 179-192.
- Wolfner, M. F. (2002). "The gifts that keep on giving: physiological functions and evolutionary dynamics of male seminal proteins in Drosophila." Heredity (Edinb) **88**(2): 85-93.
- Wolfner, M. F. (2007). ""S.P.E.R.M." (seminal proteins (are) essential reproductive modulators): the view from Drosophila." Soc Reprod Fertil Suppl **65**: 183-199.
- Wollert, T. and J. H. Hurley (2010). "Molecular mechanism of multivesicular body biogenesis by ESCRT complexes." Nature **464**(7290): 864-869.
- Wollert, T., C. Wunder, J. Lippincott-Schwartz and J. H. Hurley (2009). "Membrane scission by the ESCRT-III complex." Nature **458**(7235): 172-177.
- Wu, L. G., E. Hamid, W. Shin and H. C. Chiang (2014). "Exocytosis and endocytosis: modes, functions, and coupling mechanisms." Annu Rev Physiol **76**: 301-331.
- Wucherpfennig, T., M. Wilsch-Brauninger and M. Gonzalez-Gaitan (2003). "Role of Drosophila Rab5 during endosomal trafficking at the synapse and evoked neurotransmitter release." J Cell Biol **161**(3): 609-624.
- Xue, L. and M. Noll (2002). "Dual role of the Pax gene paired in accessory gland development of Drosophila." Development **129**(2): 339-346.
- Yamashiro, D. J., B. Tycko, S. R. Fluss and F. R. Maxfield (1984). "Segregation of transferrin to a mildly acidic (pH 6.5) para-Golgi compartment in the recycling pathway." Cell **37**(3): 789-800.
- Yanez-Mo, M., P. R. Siljander, Z. Andreu, A. B. Zavec, F. E. Borras, E. I. Buzas, K. Buzas, E. Casal, F. Cappello, J. Carvalho, E. Colas, A. Cordeiro-da Silva, S. Fais, J. M. Falcon-Perez, I. M. Ghobrial, B. Giebel, M. Gimona, M. Graner, I. Gursel, M. Gursel, N. H. Heegaard, A. Hendrix, P. Kierulf, K. Kokubun, M. Kosanovic, V. Kralj-Iglic, E. M. Kramer-Albers, S. Laitinen, C. Lasser, T. Lener, E. Ligeti, A. Line, G. Lipps, A. Llorente, J. Lotvall, M. Mancek-Keber, A. Marcilla, M. Mittelbrunn, I. Nazarenko, E. N. Nolte-'t Hoen, T. A. Nyman, L. O'Driscoll, M. Olivan, C. Oliveira, E. Pallinger, H. A. Del Portillo, J. Reventos, M. Rigau, E. Rohde, M. Sammar, F. Sanchez-Madrid, N. Santarem, K. Schallmoser, M. S. Ostenfeld, W. Stoorvogel, R. Stukelj, S. G. Van der Grein, M. H. Vasconcelos, M. H. Wauben and O. De Wever (2015). "Biological properties of extracellular vesicles and their physiological functions." J Extracell Vesicles **4**: 27066.
- Yi, Z., H. Yokota, S. Torii, T. Aoki, M. Hosaka, S. Zhao, K. Takata, T. Takeuchi and T. Izumi (2002). "The Rab27a/granuphilin complex regulates

the exocytosis of insulin-containing dense-core granules." Mol Cell Biol **22**(6): 1858-1867.
- Yoo, S. H. and M. S. Lewis (1996). "Effects of pH and Ca2+ on heterodimer and heterotetramer formation by chromogranin A and chromogranin B." J Biol Chem **271**(29): 17041-17046.
- Yoshimura, S., J. Egerer, E. Fuchs, A. K. Haas and F. A. Barr (2007). "Functional dissection of Rab GTPases involved in primary cilium formation." J Cell Biol **178**(3): 363-369.
- Zeigerer, A., J. Gilleron, R. L. Bogorad, G. Marsico, H. Nonaka, S. Seifert, H. Epstein-Barash, S. Kuchimanchi, C. G. Peng, V. M. Ruda, P. Del Conte-Zerial, J. G. Hengstler, Y. Kalaidzidis, V. Koteliansky and M. Zerial (2012). "Rab5 is necessary for the biogenesis of the endolysosomal system in vivo." Nature **485**(7399): 465-470.
- Zerial, M. and H. McBride (2001). "Rab proteins as membrane organizers." Nat Rev Mol Cell Biol **2**(2): 107-117.
- Zhang, C. F., C. R. Snell and Y. P. Loh (1999). "Identification of a novel prohormone sorting signal-binding site on carboxypeptidase E, a regulated secretory pathway-sorting receptor." Mol Endocrinol **13**(4): 527-536.
- Zhang, J., K. L. Schulze, P. R. Hiesinger, K. Suyama, S. Wang, M. Fish, M. Acar, R. A. Hoskins, H. J. Bellen and M. P. Scott (2007). "Thirty-one flavors of Drosophila rab proteins." Genetics **176**(2): 1307-1322.
- Zhen, Y. and H. Stenmark (2015). "Cellular functions of Rab GTPases at a glance." J Cell Sci **128**(17): 3171-3176.
- Zitvogel, L., A. Regnault, A. Lozier, J. Wolfers, C. Flament, D. Tenza, P. Ricciardi-Castagnoli, G. Raposo and S. Amigorena (1998). "Eradication of established murine tumors using a novel cell-free vaccine: dendritic cell-derived exosomes." Nat Med **4**(5): 594-600.
- Zoncu, R., L. Bar-Peled, A. Efeyan, S. Wang, Y. Sancak and D. M. Sabatini (2011). "mTORC1 senses lysosomal amino acids through an inside-out mechanism that requires the vacuolar H(+)-ATPase." Science **334**(6056): 678-683.

8.0 Appendix

8.1.1 Characterisation of non-transgenic *w*^{1118} secondary cells using novel antibody markers for intracellular compartments

As a first step to further define the normal morphology of secondary cells, non-transgenic *w*^{1118} flies were immunostained to characterise the localisation of important trafficking molecules, such as the Rab GTPases, and organelles, such as the Golgi, in 'wild type' cells. The aim was not to precisely define how many compartments expressed each of these proteins or to determine their exact sub-compartmental expression patterns. I therefore did not seek to validate the staining patterns by knockdown, although all of the antibodies employed had previously been used in published work on *Drosophila* tissues, However, the antibodies, which sometimes produced relatively high levels of punctate staining outside of large secondary cell compartments, did provide a useful tool to characterise whether cells expressing various fluorescent fusion proteins had obvious defects in their compartmental organisation.

Rab11, which often regulates recycling endosomal trafficking pathways in mammalian cells (Lock & Stow, 2005), was observed as puncta on the surface of several large compartments (Figure 8.1A), with some differences in the level of staining between individual compartments. This confirmed previous localisation studies that used an overexpressed fluorescently tagged form of Rab11, *tubulin-YFP-Rab11*, to determine that it marked many secondary cell compartments (Corrigan *et al*., 2014). Rab11 antibody staining co-localised on the limiting membranes of compartments with a GPI-anchored adhesion protein, Chaoptin (Chp) – encoded by a fly gene highly expressed within the accessory gland (FlyAtlas.org; Chintapalli *et al*., 2007), and shown here to be specific to secondary cells (Figure 8.1A). The two molecules co-

localised on all but one centrally located compartment, which carried Chp, but not Rab11 on its limiting membrane. Rab11 was detected on some small puncta surrounding this compartment. Many of the Chp-positive compartments contained small intraluminal Chp-positive puncta, in addition to dense-core granules, which were stained using ANCE (Figure 8.1B).

The cis-Golgi matrix protein GM130 marked punctate structures scattered throughout the cell, but particularly in a central region, in between the Chp-positive compartments (Figure 8.1C). Rab6, a small GTPase known to localise to the Golgi in mammalian cells (Short *et al*., 2005), was observed on 1-2 centrally located compartments, and also on small vesicles in between other compartments (Figure 8.1D). These small vesicles associated closely with the Golgi resident protein, Golgin84 (Riedel *et al*., 2016; Satoh *et al*., 2003). Rab7, which localises to and regulates late endosomal and lysosomal functions in mammalian cells (Guerra & Bucci, 2016), was observed at high levels on the surface of 1-3 large subcellular compartments, and on some smaller vesicles (Figure 8.1E). By DIC microscopy, some of the large Rab7-positive compartments exhibited features characteristic of acidic compartments in living cells, such as numerous intraluminal structures, but others did not (Figure 8.1E'-E''). In contrast to previous reports (Corrigan *et al*., 2014), Rab11 and Rab7 did not overlap on a subset of compartments, though Rab11-positive puncta were observed inside Rab7-marked compartments (Figure 8.1F). However, this antibody produced a particularly high level of punctate staining throughout the cell, making it difficult to assess the specificity of the staining.

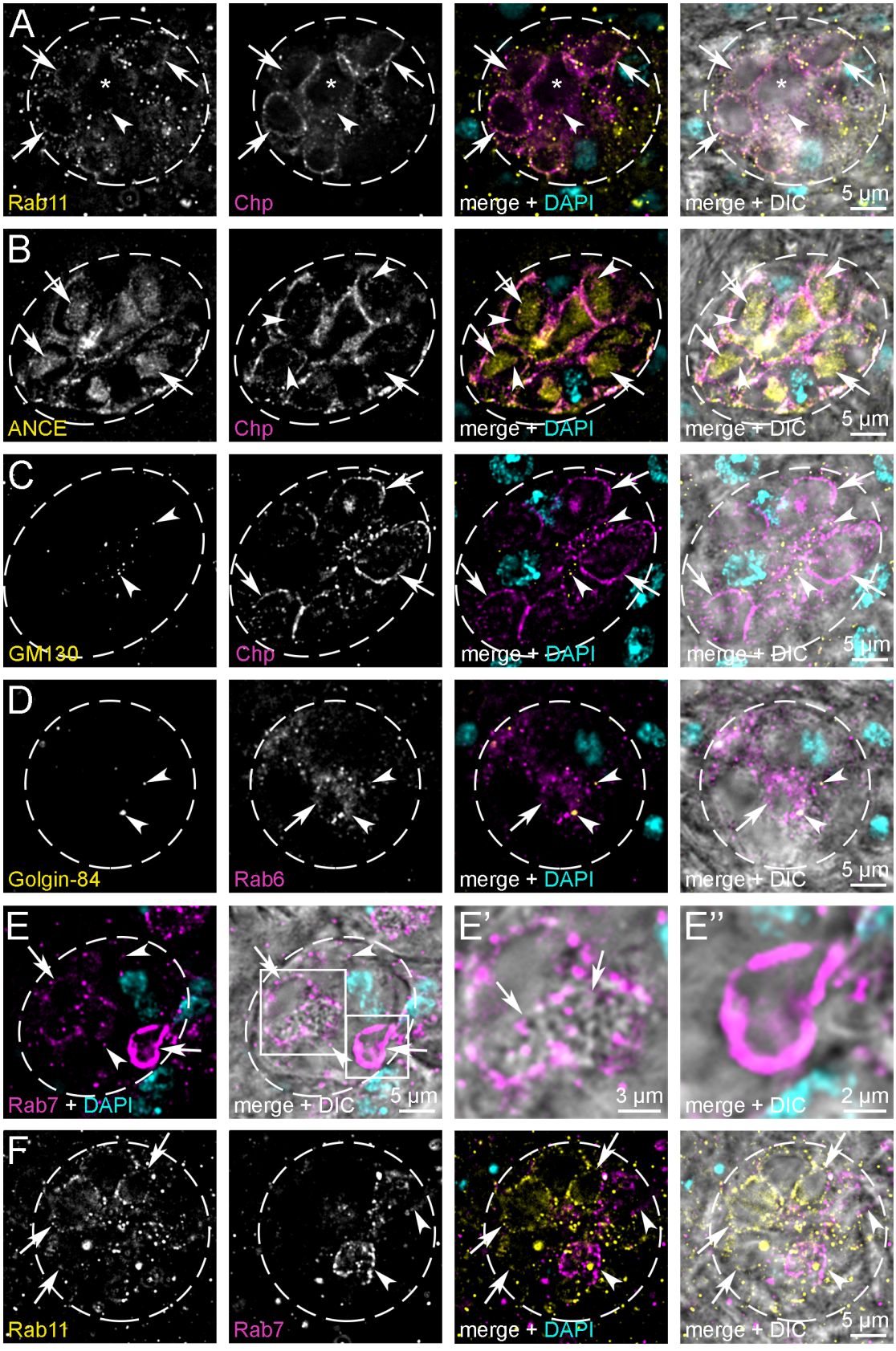

A
Rab11
Chp
merge + DAPI
merge + DIC
5 µm
B
ANCE
Chp
merge + DAPI
merge + DIC
5 µm
C
GM130
Chp
merge + DAPI
merge + DIC
5 µm
D
Golgin-84
Rab6
merge + DAPI
merge + DIC
5 µm
E
Rab7 + DAPI
merge + DIC
5 µm
E'
3 µm
E''
merge + DIC
2 µm
F
Rab11
Rab7
merge + DAPI
merge + DIC
5 µm

Figure 8.1 The subcellular compartments of secondary cells can be identified using specific protein markers.

All of these panels show wide-field fluorescence and DIC images of secondary cells from 6-day-old virgin w^{1118} males incubated at 28.5°C following eclosion. Their accessory glands were immunostained using a variety of antibodies including anti-Rab11, anti-Chp, anti-ANCE, anti-GM130, anti-Golgin-84, anti-Rab6 and anti-Rab7, and nuclei were marked using DAPI staining. Approximate cell outlines are shown using a dashed line.
A) The limiting membranes of several of the large intracellular compartments in secondary cells are marked by Rab11 (yellow; arrows), which colocalised extensively with Chaoptin (Chp; magenta). Rab11 was also observed on small vesicles in a central region of the cell (arrowhead), adjacent to a Chp-labelled, non-Rab11-positive compartment, marked by '*'.
B) Large subcellular compartments contain ANCE-rich dense-core granules (yellow; arrows) and numerous intraluminal puncta, marked by Chp (magenta; arrowheads). Both ANCE and Chp are also found on the limiting membrane of these compartments.
C) The cis-Golgi, marked by the cis-Golgi matrix protein GM130 (yellow; arrowheads), is predominantly found in the central region of the cell, in between the large compartments, which are marked by Chp (magenta; arrows).
D) Rab6 (magenta) localises primarily on the surface of the central compartment (arrow) and on small closely associating vesicles, a few of which colocalise with the Golgi-resident protein Golgin-84 (yellow; arrowheads).
E) Rab7 (magenta) localised on the surface of 2-3 large subcellular compartments (arrows) and on small vesicles scattered throughout the cell (arrowheads). The boxes highlight specific regions magnified and presented in panels E' and E''.
E') In addition to the surface of the large compartment, Rab7 localised on structures within its lumen (arrows). This compartment's mottled intra-compartmental appearance by DIC microscopy is similar to acidic compartments in living secondary cells.
E'') Rab7 localised on the surface of a large compartment with a more homogeneous appearance than other acidic compartments.
F) Immunostaining for Rab11 (yellow) and Rab7 (magenta) shows that they localised on the surface of different subsets of intracellular compartments (arrows and arrowheads, respectively).

Based on these observations, a more detailed model of secondary cell compartments in control w^{1118} cells was constructed, helping to interpret some of the subsequent analysis in my thesis, particularly where I used transgene overexpression and knockdown in secondary cells.

8.1.2 Characterisation of secondary cells overexpressing CD63-GFP and GFP-GPI by co-staining with compartment-specific antibodies

Some overexpressed transgenes have been used often throughout this study because they localise to important subcellular compartments or structures within secondary cells, or are markers for key secretory products. Two of these molecules, CD63-GFP and GFP-GPI were further characterised using immunofluorescence, employing the markers characterised in Section 3.2.4, in order to complement the analysis of w^{1118} cells.

8.1.2.1 CD63-GFP

Immunostaining showed that CD63-GFP co-localised with the GPI-anchored protein Chp on the surface of most, but not all, the large intracellular compartments (Figure 8.2A), and at the apical plasma membrane. By DIC morphology, it was determined that both CD63-GFP and Chp were present on non-acidic compartments, but only CD63-GFP localised to the limiting membrane of acidic compartments, one of which is enlarged in this genetic background, though Chp was sporadically found diffusely within its lumen (Figure 8.2B). Within the non-acidic compartments, CD63-GFP co-localised with Chp on most intraluminal puncta (Figure 8.2C). However, some heterogeneity in intraluminal puncta was observed, with some puncta marked

exclusively either by CD63-GFP or Chp (Figure 8.2C-C'). The CD63-GFP-labelled intraluminal puncta surrounded ANCE-marked dense-core granules, and co-localised with ANCE on some of the intraluminal puncta (Figure 8.2D). In some cells, ANCE was observed on the limiting membranes of CD63-GFP compartments, in addition to the dense-core granule localisation previously reported (data not shown; Rylett *et al*., 2007), suggesting that some of this peptidase is membrane-associated.

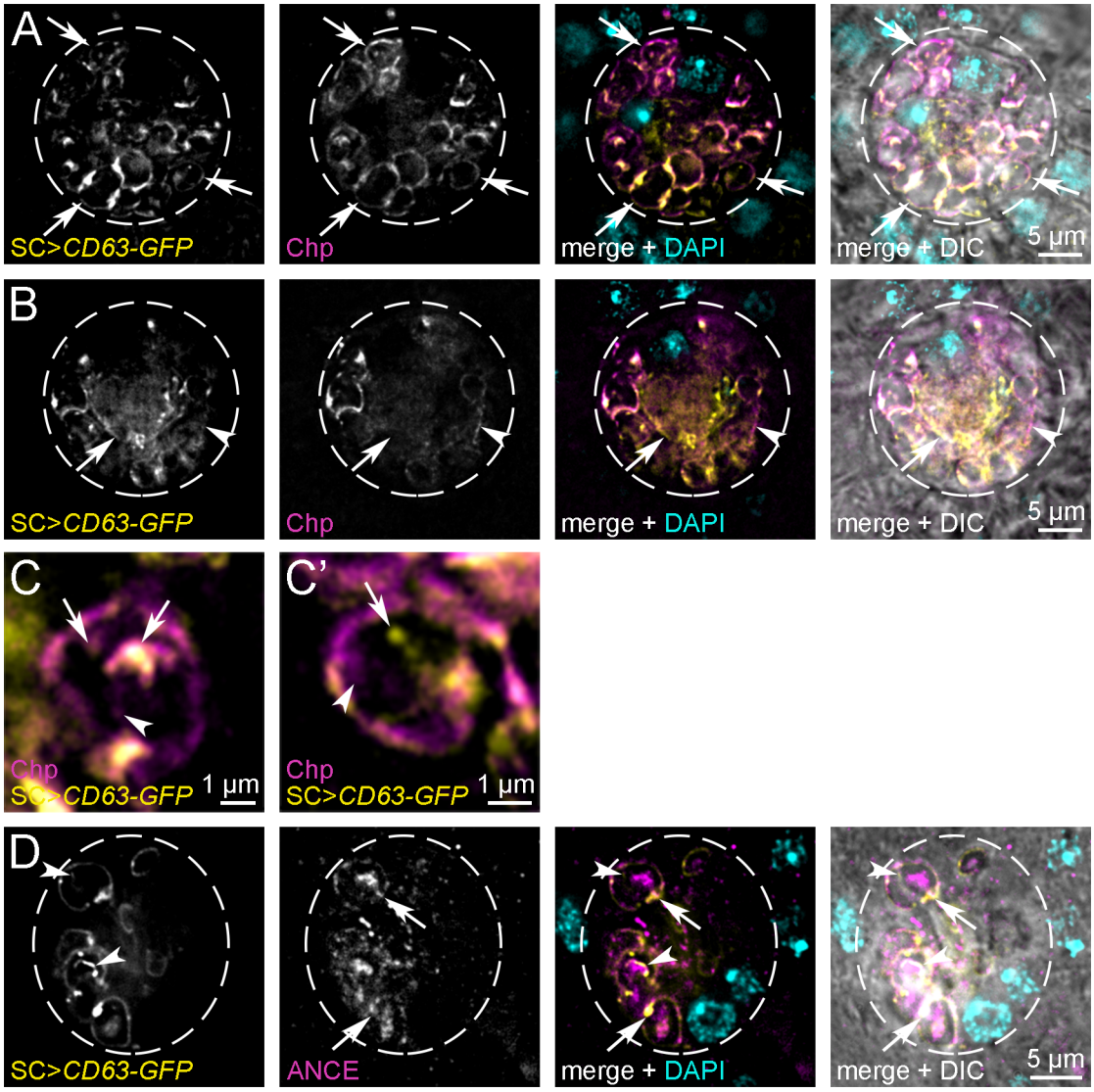

A
SC>CD63-GFP
Chp
merge + DAPI
merge + DIC
5 µm
B
SC>CD63-GFP
Chp
merge + DAPI
merge + DIC
5 µm
C
Chp
SC>CD63-GFP
1 µm
C'
Chp
SC>CD63-GFP
1 µm
D
SC>CD63-GFP
ANCE
merge + DAPI
merge + DIC
5 µm

Figure 8.2 Overexpressed CD63-GFP in secondary cells localises on the surface of many large compartments and their intraluminal puncta

These panels display wide-field fluorescence and DIC images of secondary cells from 6-day-old virgin transgenic males selectively overexpressing CD63-GFP. The flies were incubated at 28.5°C since eclosion to induce CD63-GFP expression using the GAL4-GAL80^{ts}-UAS system. Their accessory glands were immunostained with anti-Chp or anti-ANCE antibodies, and their nuclei were marked using DAPI staining. Approximate cell outlines are shown using a dashed line.
A) Overexpressed CD63-GFP (yellow) localises to the limiting membranes of numerous subcellular compartments, where it co-localises with Chp (magenta; arrows). DAPI staining (cyan) marks cell nuclei.
B) CD63-GFP localises to the surface of a particularly large compartment that is morphologically similar to large acidic compartments of living cells (arrow). This compartment does not carry Chp on its surface, though diffuse Chp staining is seen within its lumen. CD63-GFP and Chp colocalise on the apical plasma membrane (arrowhead).
C) High magnification image of a large CD63-GFP-labelled compartment that contains intraluminal puncta that colocalise with Chp (arrow), and some that are discretely Chp-marked (arrowhead).
C) High magnification image shows that CD63-GFP localises on intraluminal puncta without Chp (arrow), though Chp also labels some distinct intraluminal puncta (arrowhead).
D) Many of the CD63-GFP-labelled compartments contain dense-core granules, marked by ANCE (magenta). Some of the CD63-GFP intraluminal puncta co-localise with ANCE (arrows), but others do not (arrowheads).

The specific genotype of these males is: *w; UAS-CD63-GFP, tub-GAL80ts / +; dsx-GAL4 / +*.

Compared with non-transgenic w^{1118} cells, where Rab6 localised on just 1-2 compartments, in CD63-GFP expressing secondary cells, Rab6 localised on the surface of 2-4 compartments (Figure 8.3A). Consistent with w^{1118} cells, some of these were centrally located, however, some others were more peripheral and appeared to contain a dense-core granule by DIC morphology. Rab6 was also observed in the lumen of compartments that resemble acidic compartments by DIC morphology. Similarly, there were many more ANCE-stained compartments in the CD63-GFP expressing cells than in w^{1118} cells (Figure 8.3C). Together, this suggests that overexpression of CD63-GFP by secondary cells affected biogenesis rates or maintenance of these particular compartments. During my DPhil, I contributed to a paper (Redhai *et al*., 2016) that reported the effect of CD63-GFP overexpression on the numbers of large non-acidic and acidic compartments in secondary cells, though this did not specifically consider the numbers of non-cored, Rab6-positive compartments. CD63-GFP co-localised with Rab7 on the limiting membranes of several large subcellular compartments, most of which resembled acidic compartments in living secondary cells and at least one of which was larger than in non-CD63-GFP-expressing cells (Figure 8.3B). Antibody staining of the same cells for GFP showed that the compartments were often filled with CD63, even if the GFP fluorescence was quenched, likely caused by the acidic microenvironment (Figure 8.3B). These observations confirmed previous work with overexpressed *tubulin-YFP-Rab7* showing that Rab7 marks the large acidic compartments within the cell, and that CD63-GFP builds up to high levels inside large subcellular compartments (Corrigan *et al*., 2014). Rab7 was also observed as intraluminal puncta inside the compartments that it

localised to (Figure 8.3B). Interestingly Rab7 typically labelled one large apically located compartment containing an ANCE-marked dense-core granule (Figure 8.3C), which suggested that Rab7 also localised to a non-acidic compartment (see also Section 3.2.2.7). Arl8, a GTPase previously used to mark mature lysosomes in *Drosophila* (Riedel *et al*., 2016), was localised to the same large compartments as Rab7, suggesting that they may all be more lysosomal in identity, than late endosomal (Figure 8.3D). However, Arl8 was also observed inside other large compartments, frequently in the position of the dense-core granules, potentially suggesting that dense-core granule compartments might also receive an input from the endolysosomal system. This finding would require confirmation of antibody specificity using an *Arl8* knockdown.

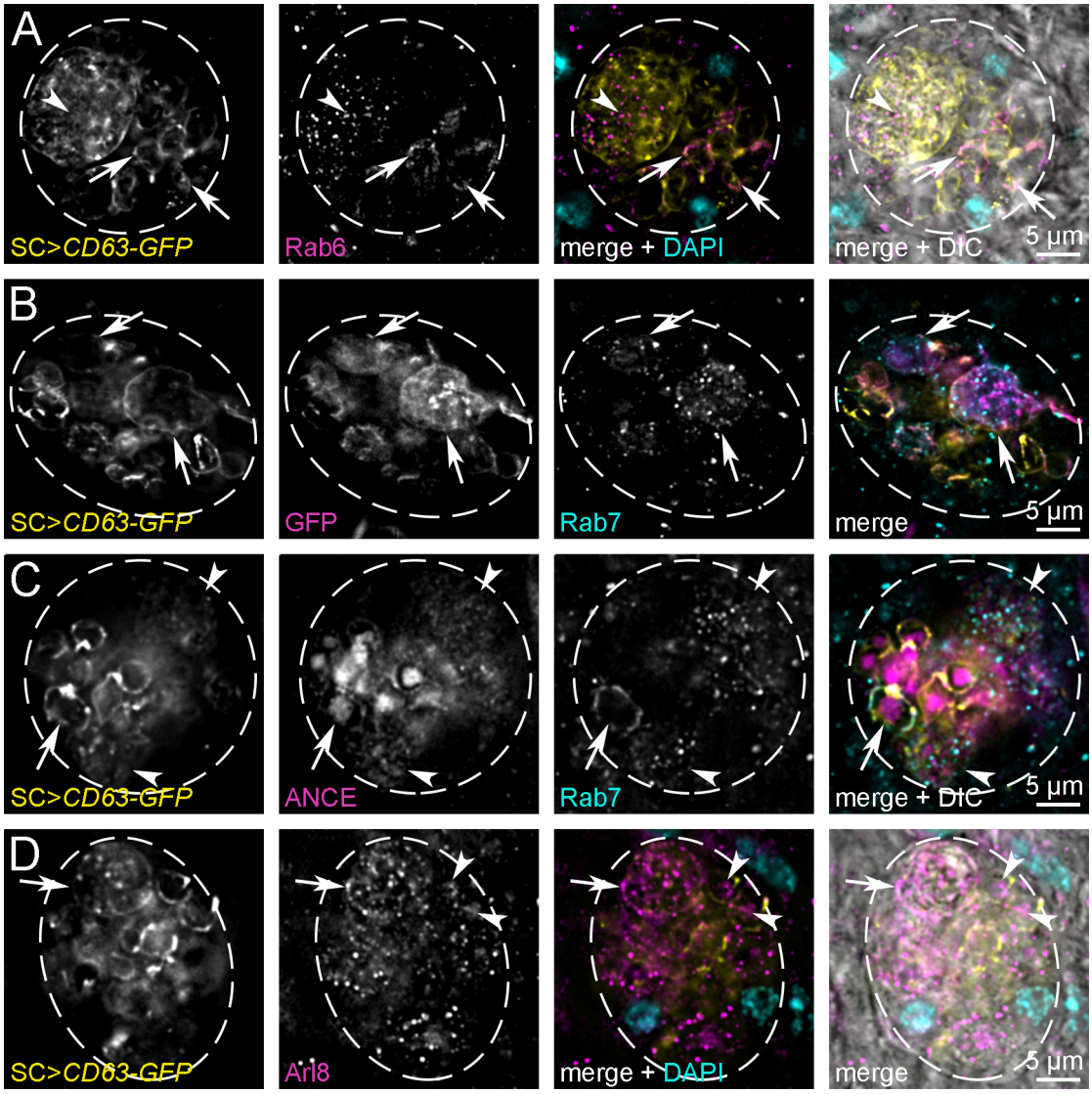

A
SC>CD63-GFP
Rab6
merge + DAPI
merge + DIC
5 µm
B
SC>CD63-GFP
GFP
Rab7
merge
5 µm
C
SC>CD63-GFP
ANCE
Rab7
merge + DIC
5 µm
D
SC>CD63-GFP
Arl8
merge + DAPI
merge
5 µm

Figure 8.3 Large secondary cell compartments marked by overexpression of CD63-GFP carry Rab GTPases at their surface

These panels contain wide-field fluorescence and DIC images of secondary cells from 6-day-old virgin transgenic males selectively overexpressing CD63-GFP. The flies were incubated at 28.5°C since eclosion to induce CD63-GFP expression using the GAL4-GAL80^{ts}-UAS system. Their accessory glands were immunostained with different combinations of anti-Rab7, anti-GFP, anti-Rab7, anti-ANCE and anti-Arl8 antibodies. Most of the glands were also stained with DAPI to mark their nuclei. Approximate cell outlines are shown using a dashed line.
A) Rab6 (magenta) co-localises on the surface of several CD63-GFP-labelled compartments (yellow; arrows). Punctate Rab6 was also observed within the particularly large CD63-GFP-positive acidic compartment (arrowhead).
B) A subset of the large CD63-GFP (yellow) compartments carries Rab7 (cyan) on their limiting membranes. The lumens of the largest Rab7-positive, CD63-GFP-marked compartments, which had a mottled DIC morphology suggestive of acidic compartments in living cells, also contained high levels of GFP (magenta; arrows), that is no longer fluorescent, likely quenched due to the acidic environment of the compartment.
C) CD63-GFP (yellow) and Rab7 (cyan) colocalise on the surface of a dense-core granule compartment (arrow), marked by ANCE staining (magenta). Punctate ANCE staining is also observed within the large Rab7/ CD63-GFP-marked compartments (arrowheads) that are presumably equivalent to the large acidic compartments seen in living cells.
D) The largest and presumably acidic CD63-GFP-labelled (yellow) compartments carry the lysosomal GTPase Arl8 (magenta) on their limiting membranes (arrows). However, Arl8 was also found within other subcellular compartments and frequently in a location that coincided with the central position of the dense-core granule (arrowheads).

The specific genotype of these flies is: *w; UAS-CD63-GFP, tub-GAL80ts / +; dsx-GAL4 / +*.

8.1.2.2 GFP-GPI

Immunostaining of secondary cells overexpressing GFP-GPI showed that it co-localised with Rab11 on the surface of many subcellular compartments (Figure 8.4A), and with ANCE inside the dense-core granules of most of these compartments (Figure 8.4B). Compared to CD63-GFP-overexpressing cells, the number of compartments in these cells was more similar to control w^{1118} cells, a result confirmed in my collaborative work in the lab (Redhai *et al*., 2016; Castellanos, 2017). Some cells showed an inverted relationship between the levels of GFP-GPI and ANCE inside their cores (Figure 8.4B'), whilst ANCE levels tended to be relatively homogeneous in w^{1118} cells, suggesting that the transgene can affect the incorporation of native secretory granule proteins or the accessibility of the anti-ANCE antibody. The dense-core granule localisation of GFP-GPI is not likely due to its GPI anchor, as the native GPI-anchored protein Chp does not localise inside the cores, but instead localises on small intraluminal puncta adjacent to the cores (Figure 8.4C). It may be that the high levels of overexpressed protein cannot be adequately GPI-anchored, so an alternative non-anchored form is deposited in the dense-core granules.

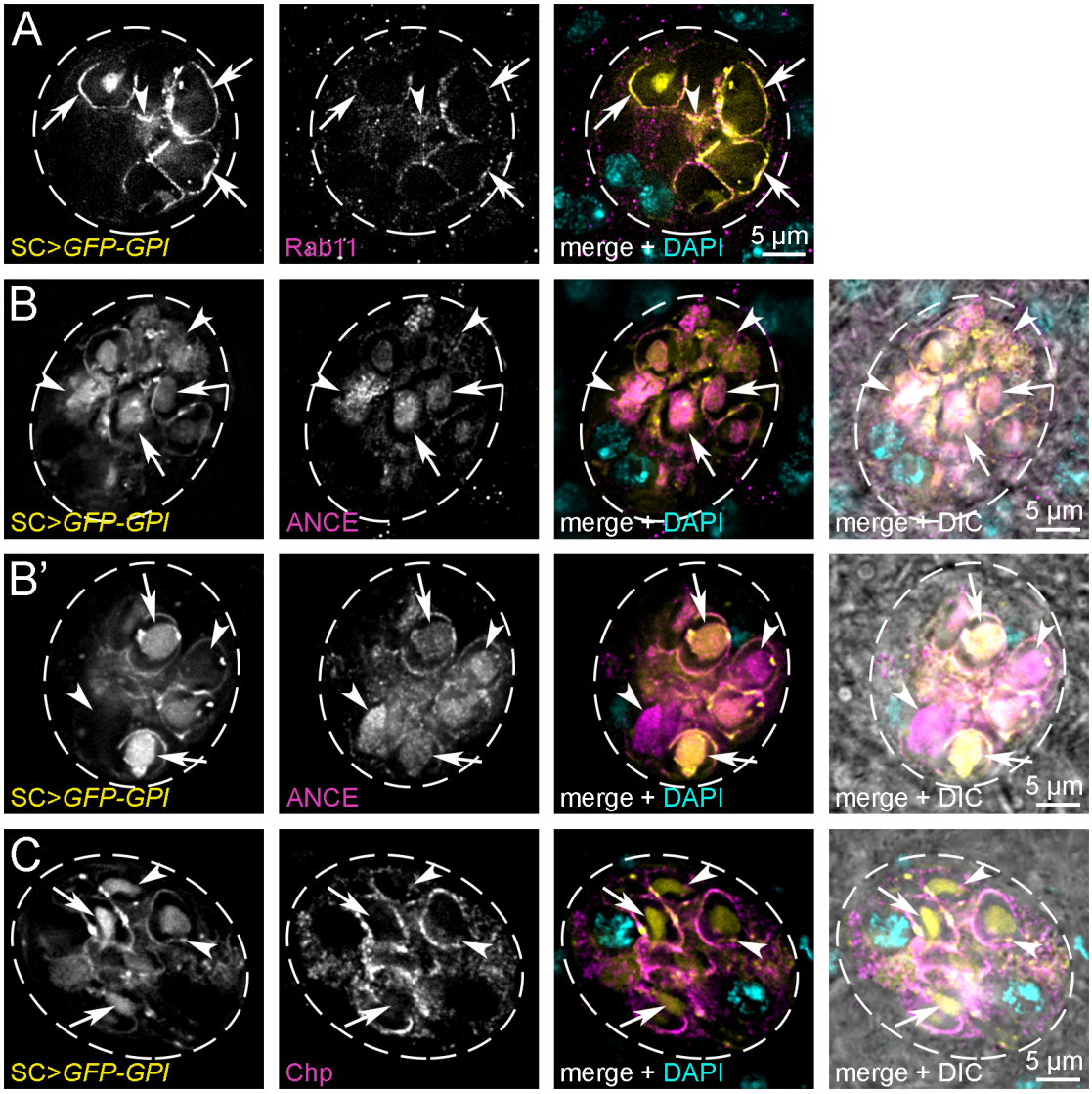

A
SC>GFP-GPI
Rab11
merge + DAPI
5 µm
B
SC>GFP-GPI
ANCE
merge + DAPI
merge + DIC
5 µm
B'
SC>GFP-GPI
ANCE
merge + DAPI
merge + DIC
5 µm
C
SC>GFP-GPI
Chp
merge + DAPI
merge + DIC
5 µm

Figure 8.4 Secondary cells package overexpressed GFP-GPI into Rab11- and Chp-positive dense-core granule compartments

These panels show wide-field fluorescence and DIC images of secondary cells from 6-day-old virgin transgenic males selectively overexpressing GFP-GPI. The flies were incubated at 28.5°C since eclosion to induce GFP-GPI expression using the GAL4-GAL80^{ts}-UAS system. Their accessory glands were immunostained with anti-Rab11, anti-ANCE or anti-Chp antibodies, and their nuclei were marked using DAPI staining. Approximate cell outlines are shown using a dashed line.
A) Overexpressed GFP-GPI (yellow) marks the limiting membranes and some dense-core granules of large Rab11-positive (magenta) secretory compartments in secondary cells. GFP-GPI also colocalises with Rab11 on some small structures in the central region of the cell (arrowhead).
B) In some cells overexpressing GFP-GPI (yellow), the dense-core granules could also be stained for ANCE (magenta). In this cell, both of these proteins were also found in the large compartment morphologically similar to the acidic compartment (arrowheads).
B') In other cells overexpressing GFP-GPI (yellow) and immunostained for ANCE, the two proteins segregated into distinct dense-core granules: some that were high in GFP-GPI and relatively low in ANCE (arrows), and vice versa (arrowheads).
C) The dense-core granule compartments labelled by GFP-GPI (yellow) carry Chp (magenta) on their limiting membranes. Chp localises on intraluminal puncta within the compartments (arrowheads), but not to the dense-core granules (arrows).

The specific genotype of the flies used in this figure is: *w; spi-GAL4, tub-GAL80ts / +; UAS-GFP-GPI / +*.

Importantly, this work identified that Rab6 localises to a large, centrally located compartment that carries GFP-GPI and Chaoptin at or near its limiting membrane, but contains no dense-core granules (Figure 8.5A-A'). However, these compartments often had a collapsed, irregular morphology, compared to equivalent compartments in living w^{1118} cells, potentially resulting from the fixation procedure (Figure 8.5D). Rab7 marked the limiting membranes of 2-3 large subcellular compartments in each cell, similar to w^{1118} cells (Figure 8.5B). These compartments were not all identical in morphology: some contained no detectable GFP-GPI, some were filled with GFP-GPI throughout their lumen, and others had Rab7 and GFP-GPI on their surface (Figure 8.5B). The cis-Golgi matrix protein GM130 co-localised with GFP-GPI on some small vesicles throughout the cell, in between the larger compartments (Figure 8.5C).

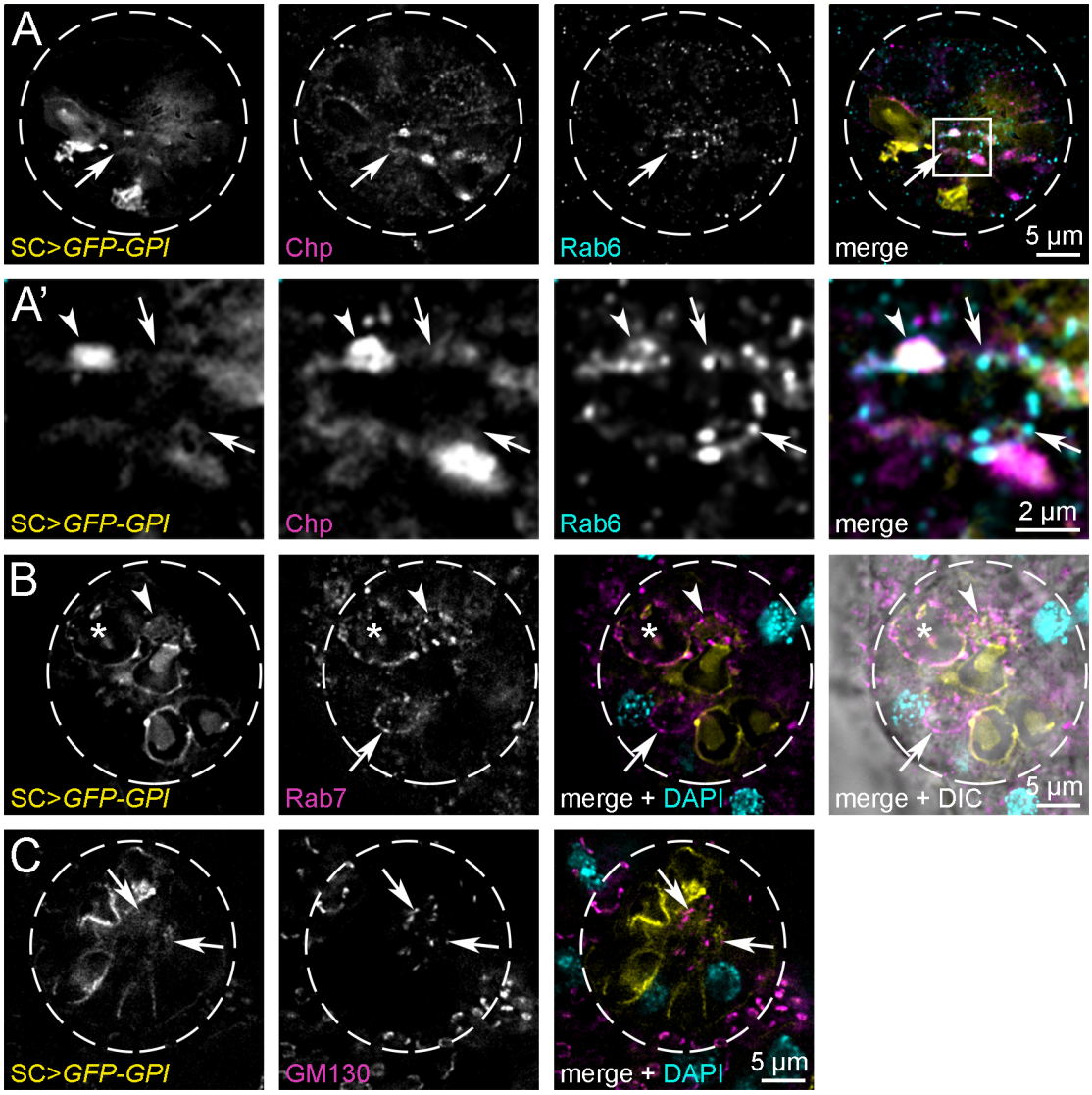

A
SC>GFP-GPI
Chp
Rab6
merge
5 µm
A'
SC>GFP-GPI
Chp
Rab6
merge
2 µm
B
SC>GFP-GPI
Rab7
merge + DAPI
merge + DIC
5 µm
C
SC>GFP-GPI
GM130
merge + DAPI
5 µm

Figure 8.5 Overexpressed GFP-GPI in secondary cells also localises to large compartments marked by Rab6 and Rab7 and small Golgi-associated vesicles

The accessory glands used for these panels are from six-day-old virgin transgenic males overexpressing GFP-GPI selectively in secondary cells. They were kept at 28.5°C since eclosion to induce GFP-GPI expression using the GAL4-GAL80^{ts}-UAS system, and then immunostained using different combinations of antibodies including anti-Chp, anti-Rab6, anti-Rab7 and anti-GM130. Most of these glands were also stained with DAPI to mark their nuclei. Wide-field fluorescence and DIC microscopy was performed to visualise the protein localisations in secondary cells.
(A) GFP-GPI (yellow) partially colocalises with Chp (magenta) in the region of a Rab6-positive (cyan), centrally located compartment, which lacks a clear dense-core granule (arrow). The box highlights the region magnified in (A'). (A') Higher magnification confirms that the limiting membrane of the central compartment potentially contains all three proteins, albeit at low levels for GFP-GPI (arrows). Other closely associating vesicles also carry all of these proteins (arrowhead).
(B) Rab7 (magenta) localises on 2-3 different compartments in GFP-GPI-overexpressing cells. Some of these Rab7-positive compartments lack GFP-GPI (yellow; arrow), but others contain GFP-GPI diffusely throughout the lumen of the compartment, in addition to some punctate Rab7-positive structures (arrowhead). Others carried both GFP-GPI and Rab7 on their surface, and are marked here by '*****'.
(C) Overexpressed GFP-GPI (yellow) colocalises with a limited proportion of small cis-Golgi structures, marked by GM130 (magenta), which are predominantly found in the central portion of the cell (arrows).

The specific genotype of the flies used in this figure is: *w; spi-GAL4, tub-GAL80ts / +; UAS-GFP-GPI / +*.

These immunofluorescent studies on fixed accessory gland tissue defined new markers for several different compartments in secondary cells, including, but not limited to, the observation of a large central Rab6-positive compartment in contact with Golgi structures, and a Rab7-positive dense-core granule-containing compartment. They also indicated that the CD63-GFP transgene affects secondary cell morphology, a finding confirmed by Redhai *et al*., (2016). However, some antibodies gave complex punctate staining patterns that might be partially explained by non-specific binding of the antibody, and the fixation often disrupted the morphology of secondary cells, particularly their subcellular compartments, when compared to living specimens. My findings therefore suggested that detailed analysis would, where possible, be best undertaken in living cells.